Mid- to Late Holocene climate variability and the 4.2 ka BP event on the Iberian Peninsula

Dissertation

zur Erlangung des Doktorgrades (Dr. rer. nat.)

der Mathematisch-Naturwissenschaftlichen Fakultät

der Christian-Albrechts-Universität zu Kiel

vorgelegt von

Julien Schirrmacher

Kiel, im Juni 2020

1. Gutachter und Betreuer:	Prof. Dr. Ralph R. Schneider
2. Gutachterin:	PD Dr. Mara Weinelt
Eingereicht am:	16.06.2020
Tag der Disputation:	24.07.2020
Zum Druck genehmigt:	24.07.2020
Der Dekan:	Prof. Dr. Frank Kempken

Erklärung

Hiermit versichere ich von Eides statt, dass ich die vorliegende Arbeit, abgesehen von der Beratung durch meine akademischen Lehrer, selbstständig und nur mit Hilfe der angegebenen Quellen angefertigt habe. Diese Arbeit ist unter Einhaltung der Regeln guter wissenschaftlicher Praxis der Deutschen Forschungsgemeinschaft entstanden und wurde weder ganz, noch in Teilen an anderer Stelle im Rahmen eines Prüfungsverfahrens eingereicht. Teile dieser Arbeit sind jedoch bereits in wissenschaftlichen Fachzeitschriften publiziert oder zur Publikation eingereicht. Darüber hinaus versichere ich, dass mir zum Zeitpunkt des Einreichens dieser Arbeit kein akademischer Grad entzogen worden ist.

Kiel, den

Julien Schirrmacher

Danksagung

Ohne eine Vielzahl von Kollegen und Freunden, die mir mit Rat und Tat zur Seite standen, wäre diese Dissertation in dieser Form nicht möglich gewesen. Bei allen möchte ich mich herzlich für die Unterstützung bedanken!

Zuerst und vor allem sei hier Mara erwähnt. Durch deine tolle Betreuung, unzählige hilfreiche Kommentare, tatkräftige Unterstützung beim Beproben der Sedimentkerne sowie dem Zählen und Picken der Foraminiferen hast Du zu einem wesentlichen Teil zu dieser Arbeit beigetragen. Vielen, vielen Dank dafür!

Darüberhinaus möchte ich Ralph ganz herzlich für die Betreuung und Bereitstellung des Arbeitsplatzes danken. Danke, dass Du es mir auch ermöglicht hast selbstständig zu arbeiten und so in vielen Dingen meinen eigenen Weg zu gehen!

Weiterhin bedanke ich mich bei meinen Co-Autoren und unzähligen Helfern, die mir bei den Papern, bei der Laborarbeit oder bei speziellen Fragen geholfen haben. Besondere Erwähnung sollen hier auch die Kollegen aus dem SFB1266 finden, die nicht nur meinen wissenschaftlichen Horizont durch maßgeblichen Input aus anderen Fachbereichen erweitert haben! Eine Aufzählung aller Namen würde vermutlich den Rahmen dieser Dissertation sprengen. Einige von Euch sind zudem in den Danksagungen der einzelnen Kapitel genannt. Trotzdem hier nochmal ein „Danke“ an Euch alle!

Des Weiteren möchte ich Wiebke und Martin danken, dass ihr euch dem Prüfungskomitee angeschlossen habt.

Außerdem gilt ein großes Dankeschön allen Freunden, die mich so oft moralisch unterstützt und meine Laune wieder gehoben haben, wenn diese mal schlecht war. Ob beim täglichen Mittagessen, bei einem Kaffee oder mal abends bei einem Bier, ohne Euch wäre diese Dissertation um einige Kapitel kürzer. Vielen, vielen Dank!

Zu guter Letzt möchte ich meiner Familie danken, die es mir ermöglicht hat, das Abenteuer „Dissertation und Familie“ erfolgreich zu meistern. Vor allem zum Ende der Dissertation während der Corona-Krise hätte es ohne eure Unterstützung und euer Wohlwollen nicht funktioniert. Danke an meine Liebsten!

Abstract

In light of the ongoing global warming, it is crucial to gain knowledge on the spatio-temporal manifestation on past climate events from local to supra-regional scales and their effect on ancient societies. This knowledge is needed to significantly improve local, regional, and global simulations of future climate change and its societal impacts. Following this aim, this thesis investigates the hydro-climatic and sea surface temperature variability on the Iberian Peninsula and its adjacent seas as well as its effect on ancient societies during the Mid- to Late Holocene, particularly focusing on the 4.2 ka BP event.

Paleo-climatic results are based on geochemical analysis of *n*-alkanes and alkenones from two marine sediment cores from the Gulf of Cádiz and the Alboran Sea as well as on a compilation of various paleo-climatic proxies, also from continental archives. The results show a long-term Holocene winter drying trend on the Iberian Peninsula as well as a winter cooling trend in the Atlantic realm. Both long-term trends were superimposed by pronounced seasonal sea surface temperature and precipitation events. For example, winter cooling events in the Gulf of Cádiz correlate with ice-rafted debris discharge during Bond Event 3, in particular. Instead, sea surface temperature variations in the Alboran Sea were local phenomena and could be related to the North Atlantic Oscillation. Moreover, the North Atlantic Oscillation was a major modulator of winter precipitation variability on the southern Iberian Peninsula with a positive mode of the North Atlantic Oscillation favouring dry events during winter and an increased proportion of local-sourced summer precipitation. However, the North Atlantic Oscillation likely did not modulate the 4.2 ka BP event on the Iberian Peninsula, because this event turned out to be a series of summer dry events between 4400 and 3800 cal. BP, which were restricted to the south-east of the Iberian Peninsula.

Despite of being a regional coherent event on the south-eastern Iberian Peninsula, the 4.2 ka BP event did not dramatically impact ancient societies in the area. Instead, people have been very much dependent on winter precipitation as suggested by two regional declines in settlement intensity, which were contemporaneous with winter dry events.

Zusammenfassung

Vor dem Hintergrund der aktuellen globalen Klimaerwärmung ist es wichtig mehr über vergangene klimatische Ereignisse bzw. Events und deren Einfluss auf vergangene Zivilisationen herauszufinden. Die räumlichen und zeitlichen Charakteristiken solcher vergangenen Klima-Events werden benötigt, um aktuelle Klimamodelle zu verbessern und deren Simulationen der globalen Klimaerwärmung auf unterschiedlichen räumlichen Skalen zu optimieren. Um zu einer Verbesserung der Klimamodelle beizutragen, werden in der vorliegenden Arbeit hydro-klimatische Veränderungen sowie Änderungen der Meeresoberflächentemperatur auf der Iberischen Halbinsel sowie der angrenzenden marinen Gebiete während des mittleren und späten Holozäns untersucht. Im Besonderen wird außerdem das 4.2 ka BP Ereignis betrachtet. Zusätzlich befasst sich die Arbeit mit den Auswirkungen der untersuchten Klimaereignisse auf die damaligen Zivilisationen auf der Iberischen Halbinsel.

Die paläo-klimatischen Ergebnisse basieren auf der geochemischen Analyse von *n*-Alkanen und Alkenonen von zwei marinen Sedimentkernen aus dem Golf von Cádiz sowie dem Alboranmeer. Zusätzlich wurden verschiedene paläo-klimatische Indikatoren aus dem Arbeitsgebiet zusammengetragen. Die Ergebnisse zeigen einen grundsätzlichen Trockenheitstrend sowie einen Abkühlungstrend seit dem mittleren Holozän in dem Arbeitsgebiet. Beide Entwicklungen sind primär im Winter nachweisbar und von kurzzeitigen saisonalen Klimaereignissen überlagert. Zum Beispiel wurden winterliche Abkühlungsereignisse im Golf von Cádiz nachgewiesen, welche zeitlich mit dem erhöhten Kalben von Eisbergen im Nordatlantik vor allem während Bond-Ereignis 3 einhergehen. Im Alboranmeer hingegen stellen Veränderungen in der Meeresoberflächentemperatur eher lokale Phänomene dar und sind mit der Nordatlantischen Oszillation verknüpft. Die Nordatlantische Oszillation erwies sich darüber hinaus als wichtige Treibkraft für Veränderungen der Winter-Niederschläge auf der südlichen Iberischen Halbinsel. So begünstigt beispielweise ein positiver Modus der Nordatlantischen Oszillation generell eine Abschwächung der Winter-Niederschläge und ein demnach einen erhöhten Anteil an Sommer-Niederschlägen lokalen Ursprungs im Jahresmittel. Allerdings stellte sich heraus, dass die Nordatlantische Oszillation keine oder nur geringe Auswirkungen auf das 4.2 ka BP Ereignis hatte. Das 4.2 ka BP Ereignis trat nämlich als eine Reihe mehrerer Dürre-Ereignisse zwischen 4400 und 3800 Jahren vor heute während des Sommers auf und war räumlich auf den Südosten der Iberischen Halbinsel begrenzt.

Trotz der ausgeprägten regionalen Dürre-Ereignisse während des 4.2 ka BP Ereignisses hat dieses Klimaereignis die damalige Zivilisation nicht sonderlich hart getroffen. Allerdings gibt es Hinweise, dass die damaligen Zivilisationen deutlich abhängiger von den Winter-Niederschlägen waren. So fallen beispielsweise zwei Reduktionen der Winterniederschläge jeweils mit einem Rückgang der Siedlungsintensitäten in den betroffenen Regionen zusammen.

Table of contents

Table of contents

Table of contents

Table of contents

List of figures

List of figures

List of tables

Abbreviations

$\sum C_{37}$ ..... *sum of alkenones with 2 and 3 double bonds*
AC ..... *Alboran Sea cold event*
ACL ..... *Average Chain Length*
aDNA ..... *ancient DNA*
AEMET ..... *Spanish State Meteorological Agency*
$AgNO_3$ ..... *silver nitrate*
AHP ..... *African Humid Period*
AMS ..... *Accelerator Mass Spectrometry*
AP ..... *arboreal pollen*
AzC ..... *Azores Current*
BCE ..... *before the common era*
BE ..... *Bond Event*
$C_{37:x}$ ..... *alkenone with x double bonds*
cal. BP ..... *calibrated years before present (1950)*
DCM ..... *dichloromethane*
EA ..... *East Atlantic*
EAG ..... *Eastern Alboran Gyre*
ENSO ..... *El Niño-Southern Oscillation*
FID ..... *flame ionization detector*
GC ..... *gas chromatography*
GC-IRMS ..... *gas chromatography - isotope ratio mass spectrometry*
GNIP ..... *Global Network of Isotopes in Precipitation*
HCl ..... *hydrochloric acid*
HSG ..... *hematite-stained grains*
HTM ..... *Holocene Thermal Maximum*
IDW ..... inverse distance weighted
IODP ..... *International Ocean Discovery Program*
IPC ..... *Iberian Poleward Current*
IRD ..... *ice-rafted debris*
ITCZ ..... *Intertropical Convergence Zone*
ka BP ..... *thousand years before present*
LDI ..... *long-chain diol index*
MAT ..... *Modern Analogue Technique*
MD-GC ..... *multi-dimensional double gas column chromatography*
MPP ..... *marine primary productivity*
NAO ..... *North Atlantic Oscillation*
NAO^- ..... *negative North Atlantic Oscillation mode*
NAO^+ ..... *positive North Atlantic Oscillation mode*
n-$C_{27\text{-}33}$ ..... *sum of odd-numbered n-alkanes with 27 to 33 carbon atoms*
n-C_x ..... *n-alkane with x carbon atoms*
Norm33 ..... *ratio of n-alkanes with 33 and 29 carbon atoms*

Abbreviations

NW ..... *north west*
PC ..... *Portugal Current*
PTV ..... *programmed temperature vaporizer*
QF ..... *quality flag*
SE ..... *south east*
SLP ..... *sea-level pressure*
SPD ..... *summed probability density*
SST ..... *sea surface temperature*
STG ..... *subtropical gyre*
SW ..... *south west*
$U^{K'}_{37}$ ..... *alkenone unsaturation index*
VPDB ..... *Vienna Pee Dee Belemnite*
VSMOW ..... *Vienna Standard Mean Ocean Water*
WAG ..... *Western Alboran Gyre*
WASM ..... *West African Summer Monsoon*
$\delta^{13}C$ ..... *ratio of stable carbon isotopes*
$\delta^{13}C_{Cx}$ ..... *ratio of carbon isotopes of the n-alkane with x carbon atoms*
δD ..... *ratio of stable hydrogen isotopes*
δD_{Cx} ..... *ratio of hydrogen isotopes of the n-alkane with x carbon atoms*
δD_{prec} ..... *ratio of hydrogen isotopes in precipitation*

Chapter 1

Motivation

1 Motivation

1.1 Motivation and research questions

The Mediterranean region including the Iberian Peninsula is considered a major hot spot of future climate change [*IPCC*, 2013]. According to the current predictions on future climate change, the Iberian Peninsula will likely experience an increase in duration and number of heat waves and dry spells particularly in its Mediterranean region [*Giorgi and Lionello*, 2008; *López-Franca et al.*, 2015]. Such dry spells likely will also occur during the wet winter season [*Raymond et al.*, 2019]. By 2050 regional climate models indicate a warming of the Iberian Peninsula of up to 2.5 °C and a reduction in precipitation between 5 and 25 % [*Turco et al.*, 2015]. Related to these developments, the risk of large fires on the Iberian Peninsula will significantly increase [*Turco et al.*, 2018]. Moreover, a decrease in wind speed across the Iberian Peninsula is proposed in response to global warming [*Gómez et al.*, 2016]. This is in line with the proposed trend towards a more stable positive mode of the North Atlantic Oscillation (NAO), an atmospheric circulation mode responsible for much of the westerly wind direction, temperature, and precipitation variability during winter in the Western Mediterranean [*Visbeck et al.*, 2001]. In contrast, other studies found no clear impact of modern anthropogenic emissions on NAO variability [*Cohen and Barlow*, 2005]. Thus, the impact of the ongoing global warming on potential driving forces of natural climate variability are still controversially debated.

Consequently, in order to forecast future climate change with less uncertainty, a much deeper understanding of the driving factors responsible for natural climate variability in the past is essential to better understand the climate system and improve climate modelling [*Lionello*, 2012]. This includes internal factors such as atmospheric and oceanic circulation patterns and also external factors such as concentration of greenhouse gases for example, responsible for past climate variability on global, regional, and local scales. This information is, further, essential to understand the implications of climate change for human communities. Regarding the predictions on future climate change, it is likely that due to the projected decrease in precipitation the agricultural production on the Iberian Peninsula will decrease significantly [*Kovats et al.*, 2014]. In addition, heat-related mortality on the Iberian Peninsula will likely increase as well [*Kovats et al.*, 2014]. Hence, more detailed reconstructions of the Holocene climate variability and climate events on the Iberian Peninsula are required in order to improve climate modelling, but also to investigate the impact of climate events on human society.

Up to now, many paleo-climatic studies revealed general cooling and drying trends on the Iberian Peninsula since the Mid- Holocene [*Cacho et al.*, 2001; *Fletcher and Sánchez Goñi*, 2008]. Between 3000 and 6000 calibrated years before present (cal. BP) – the temporal focus of this study – these trends are superimposed by natural climate events, namely the 4.2 ka BP (thousand years before present) event [*Bini et al.*, 2019] and Bond Events 2 to 4 [*Bond et al.*, 2001]. The so-called Bond Events are defined as periods of enhanced ice-rafted debris (IRD) discharge in the northern North Atlantic. These events occur roughly every 1500 years during the Holocene and three Bond Events are evident during the focus period of this study – namely Bond Event 2 centred at ca. 2800 cal. BP, Bond Event 3 centred at ca. 4200 cal. BP, and Bond Event 4 centred at ca. 5900 cal. BP [*Bond et al.*, 1997; *Bond et al.*, 2001]. These events were able to alter oceanic circulation possibly even on a global scale [*Bond et al.*, 2001] and thereby resulting in widespread cooling, particularly across the North Atlantic region [*Cacho et al.*, 2001; *Ramos-Román et al.*, 2018b]. Besides the observed cooling, these events are also associated with major dry spells in the Western Mediterranean and on the Iberian Peninsula [*Ramos-Román et al.*, 2018b; *Smith et al.*, 2016]. But controversially, a transition from "dry Bond Events" to "wet Bond Events" during the Mid- Holocene is indicated by a Moroccan lake record [*Zielhofer et al.*, 2019].

The 4.2 ka BP event, on the other hand, is associated with a marked dry phase between 3800 and 4400 cal. BP observed across much of the Mediterranean [*Cheng et al.*, 2015; *Kaniewski et al.*, 2018; *Ruan et al.*, 2016; *Zanchetta et al.*, 2016]. Dry conditions are also observed in the mid-latitudes of North America [*Booth et al.*, 2005] and Asia [*Giesche et al.*, 2019; *Kathayat et al.*, 2018; *Zhang et al.*, 2018]. However, on the Iberian Peninsula located at the interface of Atlantic and Mediterranean climate regimes the spatio-temporal manifestation of the 4.2 ka BP event is less clear [*Weinelt et al.*, 2015]. Similarly, potential drivers of the 4.2 ka BP event are not yet understood. Many paleo-climatic studies relate climate change during the 4.2 ka BP event to NAO variability [e.g. *Ramos-Román et al.*, 2018a; *Zielhofer et al.*, 2017], which also gains support from modelling studies [*Yan and Liu*, 2019]. However, dry conditions associated with the 4.2 ka BP event in Asia are related to a weakening of the summer monsoon systems [e.g. *Giesche et al.*, 2019; *Tan et al.*, 2018]. Additionally, the coincidence with Bond Event 3 points to a potential relation between both events [*Ruan et al.*, 2016; *Zielhofer et al.*, 2019]. An overarching force relating all these or an alternative explanation still remains to be found.

Apart from the spatio-temporal manifestation of climate change during the 4.2 ka BP event on the Iberian Peninsula and its potential forcing, also the impact of this event on past Iberian societies remains elusive. From the Near East transformations and collapses of various past

societies such as the Old Kingdom in Egypt, the Akkadian Empire, and the Indus civilization could be related to dry conditions during the 4.2 ka BP event [*Staubwasser et al.*, 2003; *Weiss et al.*, 1993; *Welc and Marks*, 2014]. A variety of archaeological transformations in for example pottery production, settlement activity, and economics during the period of the 4.2 ka BP event are known from societies of the Iberian Peninsula as well [*García Rivero et al.*, 2016; *Lull et al.*, 2015; *Valera*, 2015]. Their relation to a climate event, however, is still under debate [*Blanco-González et al.*, 2018].

This thesis aims to contribute to the open debate on the natural climate variability, the spatio-temporal manifestation of the 4.2 ka BP event, and its impact on past societies on the Iberian Peninsula. Therefore, two marine sedimentary archives from the Gulf of Cádiz and the Alboran Sea were explored for sea surface temperature (SST) and hydro-climatological changes between 3000 and 6000 cal. BP. Both archives provide a high temporal resolution of decadal to multi-decadal scale and are investigated through geochemical methods for alkenones and *n*-alkanes. Molecular proxies of land-derived *n*-alkanes serve as indicators of relative winter precipitation variability and its environmental impact. In constrast to continental archives, *n*-alkane proxies from marine archives allow to study hydro-climatological variations on a regional scale, and are thus, to a lesser extent influenced by local phenomena such as anthropogenic impact on the landscape. Alkenones, on the other hand, provide information on annual mean SST variability and, in addition, planktonic foraminiferal assemblages were studied for seasonal (summer and winter) SST variability. This enables the investigation of a potential link between hydro-climatological variations and surface ocean temperatures, eventually promoting precipitation change through varying evaporation intensity, in the same archive. In addition, potential spatially coherent patterns of climate events on the Iberian Peninsula are investigated through a compilation of various paleo-climatic archives and proxies.

This thesis also aims to help disentangling the complexity of the Holocene climate variability with many overlaying and interacting forces in the atmospheric (e.g. the NAO) and oceanic spheres (e.g. Bond Events) [*Rodrigo-Gámiz et al.*, 2018]. To do so, the Alboran Sea sedimentary archive has been additionally studied for compound-specific hydrogen and carbon isotopes within long-chain *n*-alkanes. The study of the hydrogen isotopic composition enables the investigation of Atlantic vs. Mediterranean influence in the study region and, together with the other studied paleo-climatic proxies, help to identify potential driving forces of climate variability.

Moreover, spatio-temporal settlement dynamics during the Chalcolithic and Bronze Age on the Iberian Peninsula were investigated by the summed probability density (SPD) of radiocarbon dates. In order to study the impact of climate change during the Mid- to Late Holocene and the 4.2 ka BP event, the reconstructed settlement dynamics were compared to the spatio-temporal variability of precipitation and temperature.

Altogether, the thesis draws a detailed picture of climate variability during the Mid- to Late Holocene and distinct events such as the 4.2 ka BP event on a seasonal scale. Together with the detection of coherent spatial patterns of climate events, this thesis allows an in-depth examination of the impact of climate change on past Iberian societies.

1.2 References

Bini, M., G. Zanchetta, A. Perşoiu, R. Cartier, A. Català, I. Cacho, J. R. Dean, F. Di Rita, R. N. Drysdale, M. Finnè, I. Isola, B. Jalali, F. Lirer, D. Magri, A. Masi, L. Marks, A. M. Mercuri, O. Peyron, L. Sadori, M.-A. Sicre, F. Welc, C. Zielhofer, and E. Brisset (2019), The 4.2 ka BP Event in the Mediterranean region: An overview, *Clim. Past*, *15*(2), 555–577, doi:10.5194/cp-15-555-2019.

Blanco-González, A., K. T. Lillios, J. A. López-Sáez, and B. L. Drake (2018), Cultural, Demographic and Environmental Dynamics of the Copper and Early Bronze Age in Iberia (3300–1500 BC): Towards an Interregional Multiproxy Comparison at the Time of the 4.2 ky BP Event, *J World Prehist*, *31*(1), 1–79, doi:10.1007/s10963-018-9113-3.

Bond, G., B. Kromer, J. Beer, R. Muscheler, M. N. Evans, W. Showers, S. Hoffmann, R. Lotti-Bond, I. Hajdas, and G. Bonani (2001), Persistent solar influence on North Atlantic climate during the Holocene, *Science (New York, N.Y.)*, *294*(5549), 2130–2136, doi:10.1126/science.1065680.

Bond, G., W. Showers, M. Cheseby, R. Lotti, P. Almasi, P. deMenocal, P. Priore, H. Cullen, I. Hajdas, and G. Bonani (1997), A Pervasive Millennial-Scale Cycle in North Atlantic Holocene and Glacial Climates, *Science*, *278*(5341), 1257–1266, doi:10.1126/science.278.5341.1257.

Booth, R. K., S. T. Jackson, S. L. Forman, J. E. Kutzbach, E. A. Bettis, J. Kreigs, and D. K. Wright (2005), A severe centennial-scale drought in midcontinental North America 4200 years ago and apparent global linkages, *The Holocene*, *15*(3), 321–328, doi:10.1191/0959683605hl825ft.

Cacho, I., J. O. Grimalt, M. Canals, L. Sbaffi, N. J. Shackleton, J. Schönfeld, and R. Zahn (2001), Variability of the western Mediterranean Sea surface temperature during the last 25,000 years and its connection with the Northern Hemisphere climatic changes, *Paleoceanography*, *16*(1), 40–52, doi:10.1029/2000PA000502.

Cheng, H., A. Sinha, S. Verheyden, F. H. Nader, X. L. Li, P. Z. Zhang, J. J. Yin, L. Yi, Y. B. Peng, Z. G. Rao, Y. F. Ning, and R. L. Edwards (2015), The climate variability in northern Levant over the past 20,000 years, *Geophysical Research Letters*, *42*(20), 8641–8650, doi:10.1002/2015GL065397.

Cohen, J., and M. Barlow (2005), The NAO, the AO, and Global Warming: How Closely Related?, *J. Climate*, *18*(21), 4498–4513, doi:10.1175/JCLI3530.1.

Fletcher, W. J., and M. F. Sánchez Goñi (2008), Orbital- and sub-orbital-scale climate impacts on vegetation of the western Mediterranean basin over the last 48,000 yr, *Quat. res.*, *70*(03), 451–464, doi:10.1016/j.yqres.2008.07.002.

García Rivero, D., J. M. Jurado Núñez, and R. Taylor (2016), Bell Beaker and the evolution of resource management strategies in the southwest of the Iberian Peninsula, *Journal of Archaeological Science*, *72*, 10–24, doi:10.1016/j.jas.2016.05.012.

Giesche, A., M. Staubwasser, C. A. Petrie, and D. A. Hodell (2019), Indian winter and summer monsoon strength over the 4.2 ka BP event in foraminifer isotope records from the Indus River delta in the Arabian Sea, *Clim. Past*, *15*(1), 73–90, doi:10.5194/cp-15-73-2019.

Giorgi, F., and P. Lionello (2008), Climate change projections for the Mediterranean region, *Global and Planetary Change*, *63*(2-3), 90–104, doi:10.1016/j.gloplacha.2007.09.005.

Gómez, G., W. D. Cabos, G. Liguori, D. Sein, S. Lozano-Galeana, L. Fita, J. Fernández, M. E. Magariño, P. Jiménez-Guerrero, J. P. Montávez, M. Domínguez, R. Romera, and M. Á. Gaertner (2016), Characterization of the wind speed variability and future change in the Iberian Peninsula and the Balearic Islands, *Wind Energy*, *19*(7), 1223–1237, doi:10.1002/we.1893.

IPCC, 2. (2013), Summary for Policymakers, in *Climate Change 2013: The Physical Science Basis*, Contribution of Working Group I to the Fifth Assessment Report of the Intergovernmental Penal on Climate Change, edited by T. F. Stocker et al., Cambridge University Press, Cambridge, United Kingdom and New York, NY, USA.

Kaniewski, D., N. Marriner, R. Cheddadi, J. Guiot, and E. van Campo (2018), The 4.2 ka BP event in the Levant, *Clim. Past*, *14*(10), 1529–1542, doi:10.5194/cp-14-1529-2018.

Kathayat, G., H. Cheng, A. Sinha, M. Berkelhammer, H. Zhang, P. Duan, H. Li, X. Li, Y. Ning, and R. L. Edwards (2018), Evaluating the timing and structure of the 4.2 ka event in the Indian summer monsoon domain from an annually resolved speleothem record from Northeast India, *Clim. Past*, *14*(12), 1869–1879, doi:10.5194/cp-14-1869-2018.

Kovats, R. S., R. Valentini, L. M. Bouwer, E. Georgopoulou, D. Jacob, E. Martin, M. Rounsevell, and J.-F. Soussana (2014), Europe, in *Climate Change 2014: Impacts, Adaptation, and Vulnerability. Part B: Regional Aspects.Contribution of Working Group II to the Fifth Assessment Report of the Intergovernmental Panel on Climate Change*, edited by V. R. Barros et al., pp. 1267–1326, Cambridge, United Kingdom and New York, NY, USA.

Lionello, P. (Ed.) (2012), *The climate of the Mediterranean region: From the past to the future*, 1st ed., 502 pp., *Elsevier insights*, Elsevier Science, Amsterdam.

López-Franca, N., E. Sánchez, T. Losada, M. Domínguez, R. Romera, and M. Á. Gaertner (2015), Markovian characteristics of dry spells over the Iberian Peninsula under present and future conditions using ESCENA ensemble of regional climate models, *Clim Dyn*, *45*(3-4), 661–677, doi:10.1007/s00382-014-2280-8.

Lull, V., R. Micó, C. Rihuete Herrada, and R. Risch (2015), Transition and conflict at the end of the 3rd millennium BC in south Iberia, in *2200 BC - ein Klimasturz als Ursache für den Zerfall der alten Welt?: 7. Mitteldeutscher Archäologentag vom 23. bis 26. Oktober 2014 in Halle (Saale)*, *Tagungen des Landesmuseums für Vorgeschichte Halle*, Band 12,1, edited by H. Meller et al., pp. 365–408, Landesamt für Denkmalpflege und Archäologie Sachsen-Anhalt, Landesmuseum für Vorgeschichte, Halle (Saale).

Ramos-Román, M. J., G. Jiménez-Moreno, J. Camuera, A. García-Alix, R. S. Anderson, F. J. Jiménez-Espejo, and J. S. Carrión (2018a), Holocene climate aridification trend and human impact interrupted by millennial- and centennial-scale climate fluctuations from a new sedimentary record from Padul (Sierra Nevada, southern Iberian Peninsula), *Clim. Past*, *14*(1), 117–137, doi:10.5194/cp-14-117-2018.

Ramos-Román, M. J., G. Jiménez-Moreno, J. Camuera, A. García-Alix, R. Scott Anderson, F. J. Jiménez-Espejo, D. Sachse, J. L. Toney, J. S. Carrión, C. Webster, and Y. Yanes (2018b), Millennial-scale cyclical environment and climate variability during the Holocene in the western Mediterranean region deduced from a new multi-proxy analysis from the Padul record (Sierra Nevada, Spain), *Global and Planetary Change*, *168*, 35–53, doi:10.1016/j.gloplacha.2018.06.003.

Raymond, F., A. Ullmann, Y. Tramblay, P. Drobinski, and P. Camberlin (2019), Evolution of Mediterranean extreme dry spells during the wet season under climate change, *Reg Environ Change*, *19*(8), 2339–2351, doi:10.1007/s10113-019-01526-3.

Rodrigo-Gámiz, M., F. Martínez-Ruiz, F. J. Rodríguez-Tovar, E. Pardo-Igúzquiza, and M. Ortega-Huertas (2018), Appraising timing response of paleoenvironmental proxies to the Bond cycle in the western Mediterranean over the last 20 kyr, *Clim Dyn*, *50*(7-8), 2925–2934, doi:10.1007/s00382-017-3782-y.

Ruan, J., F. Kherbouche, D. Genty, D. Blamart, H. Cheng, F. Dewilde, S. Hachi, R. L. Edwards, E. Régnier, and J.-L. Michelot (2016), Evidence of a prolonged drought ca. 4200 yr BP correlated with prehistoric settlement abandonment from the Gueldaman GLD1 Cave, Northern Algeria, *Climate of the Past*, *12*(1), 1–14, doi:10.5194/cp-12-1-2016.

Smith, A. C., P. M. Wynn, P. A. Barker, M. J. Leng, S. R. Noble, and W. Tych (2016), North Atlantic forcing of moisture delivery to Europe throughout the Holocene, *Scientific reports*, *6*, 24745, doi:10.1038/srep24745.

Staubwasser, M., F. Sirocko, P. M. Grootes, and M. Segl (2003), Climate change at the 4.2 ka BP termination of the Indus valley civilization and Holocene south Asian monsoon variability, *Geophysical Research Letters*, *30*(8), 155, doi:10.1029/2002GL016822.

Tan, L., Y. Cai, H. Cheng, L. R. Edwards, Y. Gao, H. Xu, H. Zhang, and Z. An (2018), Centennial- to decadal-scale monsoon precipitation variations in the upper Hanjiang River region, China over the past 6650 years, *Earth and Planetary Science Letters*, *482*, 580–590, doi:10.1016/j.epsl.2017.11.044.

Turco, M., J. J. Rosa-Cánovas, J. Bedia, S. Jerez, J. P. Montávez, M. C. Llasat, and A. Provenzale (2018), Exacerbated fires in Mediterranean Europe due to anthropogenic warming projected with non-stationary climate-fire models, *Nat Commun*, *9*(1), doi:10.1038/s41467-018-06358-z.

Turco, M., A. Sanna, S. Herrera, M.-C. Llasat, and J. M. Gutiérrez (2015), Evaluation of the ENSEMBLES Transient RCM Simulations Over Spain: Present Climate Performance and Future Projections, in *Engineering Geology for Society and Territory - Volume 1*, pp. 199–203, Springer, Cham.

Valera, A. C. (2015), Social change in the late 3rd millennium BC in Portugal: the twilight of enclosures, in *2200 BC - ein Klimasturz als Ursache für den Zerfall der alten Welt?: 7. Mitteldeutscher Archäologentag vom 23. bis 26. Oktober 2014 in Halle (Saale)*, *Tagungen des Landesmuseums für Vorgeschichte Halle*, Band 12,1, edited by H. Meller et al., pp. 409–428, Landesamt für Denkmalpflege und Archäologie Sachsen-Anhalt, Landesmuseum für Vorgeschichte, Halle (Saale).

Visbeck, M. H., J. W. Hurrell, L. Polvani, and H. M. Cullen (2001), The North Atlantic Oscillation: Past, present, and future, *Proceedings of the National Academy of Sciences*, *98*(23), 12876–12877, doi:10.1073/pnas.231391598.

Weinelt, M., C. Schwab, J. Kneisel, and M. Hinz (2015), Climate and societal change in the western Mediterranean area around 4.2 ka BP, in *2200 BC - ein Klimasturz als Ursache für den Zerfall der alten Welt?: 7. Mitteldeutscher Archäologentag vom 23. bis 26. Oktober 2014 in Halle (Saale)*, *Tagungen des Landesmuseums für Vorgeschichte Halle*, Band 12,1, edited by H. Meller et al., pp. 461–480, Landesamt für Denkmalpflege und Archäologie Sachsen-Anhalt, Landesmuseum für Vorgeschichte, Halle (Saale).

Weiss, H., M. A. Courty, W. Wetterstrom, F. Guichard, L. Senior, R. Meadow, and A. Curnow (1993), The genesis and collapse of third millennium north mesopotamian civilization, *Science (New York, N.Y.)*, *261*(5124), 995–1004, doi:10.1126/science.261.5124.995.

Welc, F., and L. Marks (2014), Climate change at the end of the Old Kingdom in Egypt around 4200 BP: New geoarchaeological evidence, *Quaternary International*, *324*, 124–133, doi:10.1016/j.quaint.2013.07.035.

Yan, M., and J. Liu (2019), Physical processes of cooling and mega-drought during the 4.2 ka BP event: Results from TraCE-21ka simulations, *Clim. Past*, *15*(1), 265–277, doi:10.5194/cp-15-265-2019.

Zanchetta, G., E. Regattieri, I. Isola, R. N. Drysdale, M. Bini, I. Baneschi, and J. C. Hellstrom (2016), The so-called "4.2 event" in the Central Mediterranean and its climatic teleconnections, *Alpine and Mediterranean Quaternary*, *29*(1), 5–17.

Zhang, H., H. Cheng, Y. Cai, C. Spötl, G. Kathayat, A. Sinha, R. L. Edwards, and L. Tan (2018), Hydroclimatic variations in southeastern China during the 4.2 ka event reflected by stalagmite records, *Clim. Past*, *14*(11), 1805–1817, doi:10.5194/cp-14-1805-2018.

Zielhofer, C., W. J. Fletcher, S. Mischke, M. de Batist, J. F.E. Campbell, S. Joannin, R. Tjallingii, N. El Hamouti, A. Junginger, A. Stele, J. Bussmann, B. Schneider, T. Lauer, K. Spitzer, M. Strupler, T. Brachert, and A. Mikdad (2017), Atlantic forcing of Western Mediterranean winter rain minima during the last 12,000 years, *Quaternary Science Reviews*, *157*, 29–51, doi:10.1016/j.quascirev.2016.11.037.

Zielhofer, C., A. Köhler, S. Mischke, A. Benkaddour, A. Mikdad, and W. J. Fletcher (2019), Western Mediterranean hydro-climatic consequences of Holocene ice-rafted debris (Bond) events, *Clim. Past*, *15*(2), 463–475, doi:10.5194/cp-15-463-2019.

1.3 Structure of the thesis

Chapter 1: Motivation

This chapter provides the scientific motivation and background of this thesis and mentions the main research questions, that were studied during this thesis. This chapter is based on the initial proposal of the project and on my own literature study. This chapter was written by myself.

Chapter 2: Introduction

This chapter introduces the study area with its present climatology and oceanography as well as the main paleo-climatological developments during the Holocene period. It further gives an overview of the main mechanisms of modern and past climate variability in the Western Mediterranean. This chapter relies on my own literature studies and synthesis.

Chapter 3: Materials and methods

This chapter summarizes and briefly explains the background of the main methods and proxies used in this thesis. This chapter relies on my own literature studies and synthesis. Methods applied by myself, co-authors, or third parties are outlined in the individual chapters.

Chapter 4: The Chalcolithic-Bronze Age transition in southern Iberia under the influence of the 4.2 ka BP event? A correlation of climatological and demographic proxies

This article describes the settlement patterns of the Iberian Peninsula from the Neolithic towards the end of the Bronze Age with a focus on the 4.2 ka BP event. It further discusses a potential correlation to dry conditions found in sediment core ODP-161-976A. Please note that this study relies on a meanwhile slightly modified age model (doi: 10.1594/PANGAEA.912673). The article was written by Martin Hinz, Julien Schirrmacher, Jutta Kneisel, Christoph Rinne, and Mara Weinelt. It has been published in the Journal of Neolithic Archaeology (JNA) on the 6th of December 2019 (doi: 10.12766/jna.2019.1).

I provided early versions of the paleo-climatological reconstructions, which are schematically shown, paleo-climatological background, and a methodological description of the paleo-climatological analysis for this article.

Chapter 5: Multi-decadal atmospheric and marine climate variability in southern Iberia during the Mid- to Late Holocene

This chapter provides new paleo-climatological data based on molecular *n*-alkane and alkenone proxies from marine sediment cores ODP-161-976A and GeoB5901-2. It further discusses seasonal SST changes based on planktonic foraminiferal assemblages from both sediment cores. Please note that this study relies on a meanwhile slightly modified age model of both sediment cores (doi: 10.1594/PANGAEA.912673 and doi: 10.1594/PANGAEA.912670). This

article was written by Julien Schirrmacher and co-authored by Mara Weinelt, Thomas Blanz, Nils Andersen, Emília Salgueiro, and Ralph R. Schneider. It has been published in Climate of the Past (Clim. Past) on the 2nd of April 2019 (doi: 10.5194/cp-15-617-2019).

I wrote the manuscript of this article based on my own interpretation of the paleo-climatic data with discussion contributions from all co-authors. Sediment core ODP-161-976A was sampled by C. Schwab and re-sampled by myself at the IODP (International Ocean Discovery Program) Core Repository at MARUM – Center for Marine Environmental Sciences, Bremen, supported by A. Wülbers. Sediment core GeoB5901-2 was sampled by myself and M. Weinelt in the GeoB Core Repository at MARUM – Center for Marine Environmental Sciences, Bremen, supported by J. Pätzold. I carried out the pre-treatment of all samples, partly with the help of student assistance, and the geochemical analysis of the *n*-alkanes and alkenones. I also measured and quantified the *n*-alkanes, while alkenones were measured by S. Koch under the direction of T. Blanz. I converted the alkenone raw data into SSTs. Planktonic foraminifera census data, sea surface temperature data based on SIMMAX transfer functions, and planktonic samples for Accelerator Mass Spectrometry (AMS) ^{14}C dating and calculation of seasonal SSTs have been provided by M. Weinelt. Planktonic foraminiferal counts have been transferred to seasonal SSTs by E. Salgueiro. AMS ^{14}C dating has been carried out under the direction of C. Hamann in the Leibniz Laboratory for Radiometric Dating and Stable Isotope Research, Kiel University.

Chapter 6: Spatial patterns of temperature, precipitation, and settlement dynamics on the Iberian Peninsula during the Chalcolithic and the Bronze Age

This chapter investigates spatial coherent patterns of seasonal and annual atmospheric temperature, SST, and precipitation variability on the Iberian Peninsula between 3000 and 6000 cal. BP. It is based on a comprehensive literature survey and compilation of various paleo-climatic archives including updated age models of the two main marine sediment cores of this thesis. This article was written by Julien Schirrmacher and co-authored by Jutta Kneisel, Daniel Knitter, Wolfgang Hamer, Martin Hinz, Ralph R. Schneider, and Mara Weinelt. It has been published in Quaternary Science Reviews (Quat. Sci. Rev.) on the 1st of April 2020 (doi: 10.1016/j.quascirev.2020.106220).

I wrote the manuscript of this article with contributions from all co-authors. The paleo-climatic compilation for this study was accomplished by myself and the resulting data was transformed, interpreted and displayed by myself as well. Planktonic foraminifera of ODP-161-976A and

GeoB5901-2 for AMS ^{14}C dating were sampled by M. Weinelt and dated under the direction of C. Hamann at the Leibniz Laboratory for Radiometric Dating and Stable Isotope Research, Kiel University. The archaeological database for this study was compiled by myself, M. Hinz, and a student assistant. The methodological analysis of the archaeological data was done by myself with input from M. Hinz and I. Feeser. The spatial interpolation of paleo-climatic data was done by myself with important input by D. Knitter and W. Hamer, who did the main programming of the computer code.

Chapter 7: Fossil leaf wax hydrogen isotopes reveal variability of North Atlantic climate forcing on the southeast Iberian Peninsula between 3000 to 6000 cal. BP

This chapter provides new compound-specific hydrogen and carbon isotope data from sediment core ODP-161-976A and discusses the interaction of Atlantic and Mediterranean climate forcing. This article was written by Julien Schirrmacher, Nils Andersen, Ralph R. Schneider, and Mara Weinelt. When handing in this thesis, it was planned to submit this chapter to PlosOne in summer 2020.

I wrote the manuscript of this article based on my own interpretation of the paleo-climatic data with discussion contributions from all co-authors. I did the *n*-alkane pre-treatment, analysis, and quantification, which form the basis for the isotope analysis. Compound-specific isotopes have been measured by K. Gramenz and P. Schindler under the direction of N. Andersen, who also did the quality control.

Chapter 8: Conclusion and outlook

This chapter summarises the main findings of this study based on the conclusions of the previous chapters and it further represents my personal perspectives on future research on the overall topic. In addition, potential research questions, which arose from this thesis are briefly discussed.

Chapter 2

Introduction

2 Introduction

2.1 Mechanisms of climate variability in the Western Mediterranean

Modern climate variability in the Western Mediterranean with regard to precipitation and air temperature change is related to various large-scale teleconnection patterns [*Lionello*, 2012]. Many of these atmospheric modes are interacting with each other and the surface ocean as well, resulting in a complex and dynamic system. For example, the North Atlantic Oscillation (NAO), which is considered the dominant mechanism driving winter precipitation variability in the Western Mediterranean [*Hurrell*, 1995], is closely coupled to the Arctic Oscillation – an atmospheric mode responsible for climate variability in the Arctic area [*Thompson and Wallace*, 1998]. Furthermore, the relationship between NAO and winter precipitation in the Western Mediterranean may be altered by different modes of the East Atlantic (EA) pattern [*Comas-Bru et al.*, 2016; *Hernández et al.*, 2015]. The EA pattern additionally influences winter air temperatures in the Western Mediterranean [*Comas-Bru et al.*, 2016]. The NAO also exerts an influence on the Mediterranean Oscillation – a dipole pattern between the Western and Eastern Mediterranean [*Maheras et al.*, 1999]. Another pattern influencing winter precipitation in the area, which is unrelated to the NAO, is the Scandinavian pattern with its centres of action close to the Scandinavian peninsula, the north-east Atlantic, and central Siberia [*Bueh and Nakamura*, 2007; *Lionello*, 2012].

Precipitation variability during spring and autumn in the Western Mediterranean is considered to be coupled to the El Niño-Southern Oscillation (ENSO) [*Mariotti et al.*, 2002; *Mariotti et al.*, 2005]. Moreover, summer precipitation in the area is also coupled to the variability of the West African Summer Monsoon (WASM) [*Alpert et al.*, 2006].

Many of these interacting teleconnections had also an impact on climate variability during the Holocene period [*Ausín et al.*, 2015; *Sánchez-López et al.*, 2016; *Wassenburg et al.*, 2016]. However, their influence, e.g. on Western Mediterranean climate, likely varied in relation to changing solar irradiation over the course of the Holocene [*Patricola and Cook*, 2007; *Walczak et al.*, 2015]. In addition, major surface ocean cooling, expressed as ice-rafted debris (IRD) discharge events in the northern North Atlantic represented an additional driver of Western Mediterranean climate variability during the Holocene [*Bond et al.*, 2001; *Zielhofer et al.*, 2019].

2.1.1 The North Atlantic Oscillation

The NAO is the dominant atmospheric mode responsible for modern winter climate in Europe [*Barnston and Livezey*, 1987; *Hurrell*, 1995; *Trigo et al.*, 2002]. Due to its northward contraction, the NAO loses impact across Europe during summer [*Barnston and Livezey*, 1987]. The NAO index is calculated from the sea-level pressure (SLP) difference between the subtropical Azores High and the subpolar Icelandic Low. A positive NAO index (NAO^+) refers to conditions when the SLP difference is larger than normal due to a higher SLP at the Azores High and a lower SLP at the Icelandic Low. Consequently, a negative NAO index (NAO^-) resembles conditions when the SLP difference is smaller than normal because of lower SLP at the Azores High and higher SLP at the Icelandic Low (Fig 2.1).

During NAO^+ conditions the main Atlantic storm track is directed more towards northern Europe, whereas NAO^- conditions favour a southerly direction of the Atlantic storm tracks (Fig 2.1) [*Gaetani et al.*, 2011; *Hurrell*, 1995]. The Atlantic storm track is associated with high precipitation amounts [*Gaetani et al.*, 2011; *Hurrell*, 1995; *Zorita et al.*, 1992]. Consequently, NAO^- (NAO^+) conditions are associated with above (below) normal winter precipitation in the Mediterranean (Fig 2.1) [*Trigo et al.*, 2002]. This is particular true for the Iberian Peninsula located at the Atlantic façade [*Fernández-González et al.*, 2012; *Hernández et al.*, 2015; *Trigo et al.*, 2004; *Zorita et al.*, 1992]. Related to these changes in Atlantic storm track orientation and precipitation, the NAO is also impacting European river discharges [*Shorthouse and Arnell*, 1997; *Trigo et al.*, 2004], Saharan dust mobilization and transport [*Moulin et al.*, 1997; *Sabatier et al.*, 2020], as well as vegetation growth [*Gouveia et al.*, 2008].

A correlation between the mode of the NAO and North Atlantic sea surface temperatures (SSTs) as well as European air temperatures during winter has also been proposed (Fig 2.1) [*Hurrell*, 1995]. More precisely, it has been demonstrated that persistent NAO^+ conditions are associated with slightly cooler winter SSTs across the North Atlantic between the equator and 30 °N as well as in the subpolar North Atlantic [*Visbeck et al.*, 2003]. Moreover, under such conditions slightly higher SSTs are recorded along the Atlantic coasts of North America as well as for European marginal seas (e.g. the North Sea) [*Visbeck et al.*, 2003]. Similarly, elevated winter air temperatures across northern and central Europe are associated with NAO^+ conditions [*Trigo et al.*, 2002]. For the Iberian Peninsula, *Hernandez et al.* [2015] showed a north – south gradient with warmer (cooler) winter air temperatures across northern (southern) Iberia during NAO^+ (NAO^-) conditions. These winter temperature patterns associated with a particular NAO mode

might be related to a northward shift of the heat-carrying Gulf Stream under NAO^+ conditions [*Joyce et al.*, 2000].

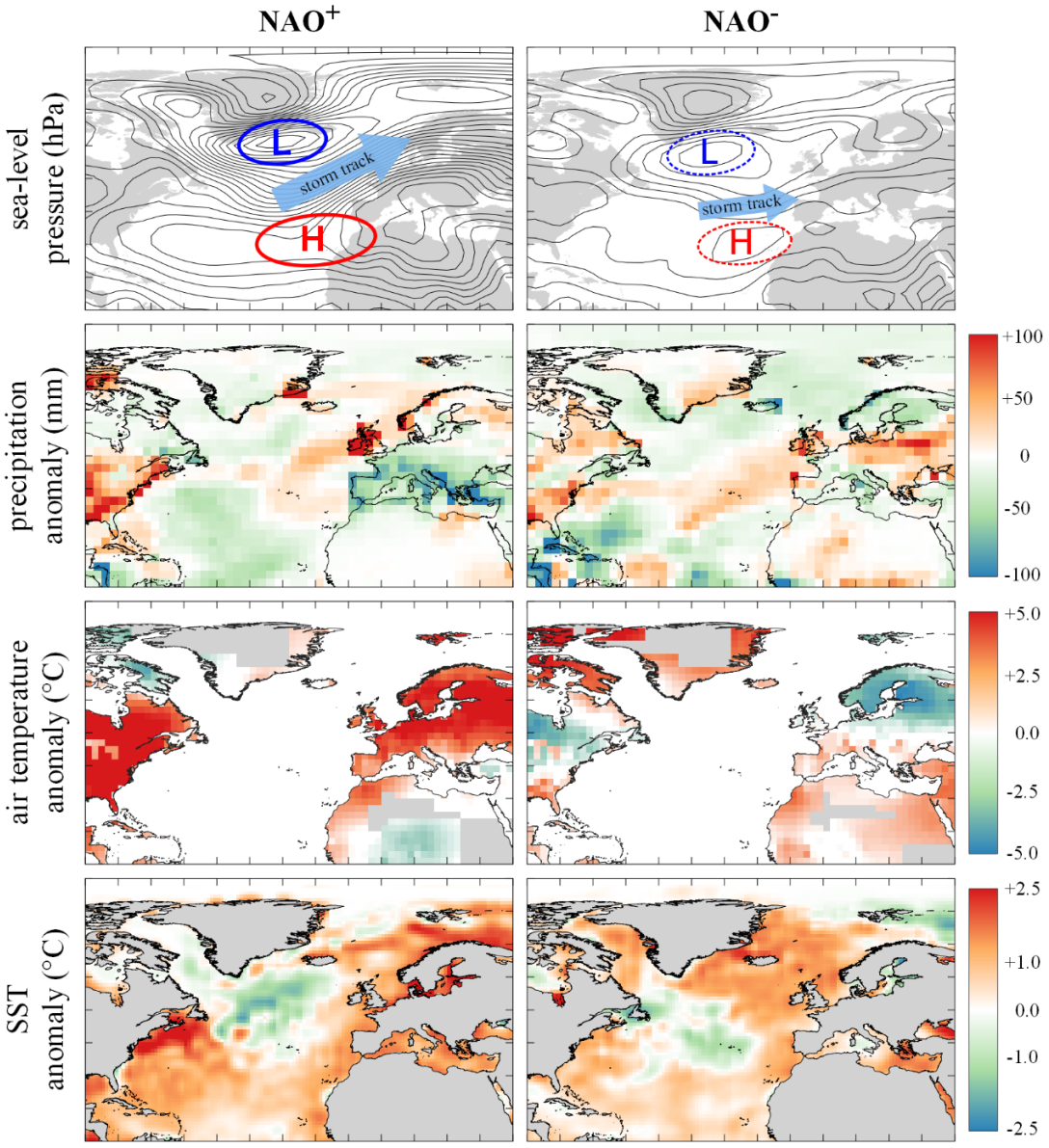

Figure 2.1 Impact of the North Atlantic Oscillation mode on chosen climatic parameters. *Left panel shows climatic conditions during an exemplary positive North Atlantic Oscillation mode (NAO^+) in December 2015 (NAO index = 2.24) and right panel shows the same during an exemplary negative North Atlantic Oscillation mode (NAO^-) in October 2002 (NAO index = -2.28). From top to bottom: Monthly average sea-level pressure based on a 2.5° grid provided by the NCEP/NCAR Reanalysis Project. Black lines indicate 2 hPa isobars. Positions of the Icelandic Low (blue circles) and Azores High (red circles) as well as the orientation of the Atlantic storm track (blue arrows) are indicated. Strong (weak) pressure cells are indicate through bold (dotted) circles and a strong (weak) storm track is indicated through a thick (thin) arrow, respectively. Monthly precipitation anomaly with respect to 1979-2000 based on a 2.5° grid provided by the NOAA NCEP Climate Prediction Center. Monthly surface air temperature anomaly with respect to 1971-2000 based on a 2.0° grid provided by the NOAA NCEP Climate Prediction Center. Regions with no data are coloured in grey. Monthly sea surface temperature (SST) anomaly with respect to 1971-2000 based on a 1.0° grid provided by the OISST V2 database.*

Accordingly, the NAO has a wide-ranging impact across the North Atlantic region and the European continent. Mechanisms driving its variability remain elusive, though [*Hurrell et al.*, 2003]. This is also because the NAO varies with no certain cyclicity. Large changes may occur at seasonal, annual, or decadal timescales [*Hurrell and Deser*, 2009; *Hurrell et al.*, 2003].

Many Holocene paleo-climatic studies explain their data with NAO-like variability [e.g. *Ausín et al.*, 2015; *Magny et al.*, 2013; *Zielhofer et al.*, 2019], but in fact NAO reconstructions are sparse. Probably, the most popular NAO reconstruction has been accomplished by *Olsen et al.* [2012] and extends back to 5200 cal. BP. Previously, a NAO reconstruction had been published for the last 950 years [*Trouet et al.*, 2009]. Moreover, based on reconstructions of storminess [*Goslin et al.*, 2018] or precipitation [*Deininger et al.*, 2017; *Wassenburg et al.*, 2016] in NAO sensitive areas, it has been accepted that the NAO was active at least since the Early Holocene.

2.2 Study area

The focus of this study is the Iberian Peninsula and its surrounding marginal seas, particularly the southern Iberian Peninsula as well as the Gulf of Cádiz and the Alboran Sea (Fig 2.2). The Iberian Peninsula comprises an area of about 596,740 km². The Mulhacén (3478 m) in the Sierra Nevada in south-east (SE) Iberia is the highest mountain of the peninsula. Two major river systems – the Guadiana and the Guadalquivir – are draining into the Gulf of Cádiz (Fig 2.2). While the Guadiana drains an area of approximately 68,000 km², the Guadalquivir drains an area of about 58,000 km². The Alboran Sea, instead, is just fed by small mountainous rivers.

2.2.1 Modern climate and vegetation of the Iberian Peninsula

The modern climate of the Iberian Peninsula is characterized by a large seasonality in atmospheric temperature and precipitation (Fig 2.3). The annual mean atmospheric temperature ranges between -1 and 20 °C [*Fick and Hijmans*, 2017]. Summer temperatures range between 6 and 31 °C and winter temperatures vary between -5 and 14 °C [*Fick and Hijmans*, 2017]. A north-south temperature gradient is common, with generally higher atmospheric temperatures across the southern part of the Iberian Peninsula.

Precipitation rather reveals a north-west (NW)-SE gradient, which is particularly evident in annual precipitation amount but also during the winter period (Fig 2.3). Generally, the northern and western Atlantic coasts experience more precipitation compared to the Mediterranean

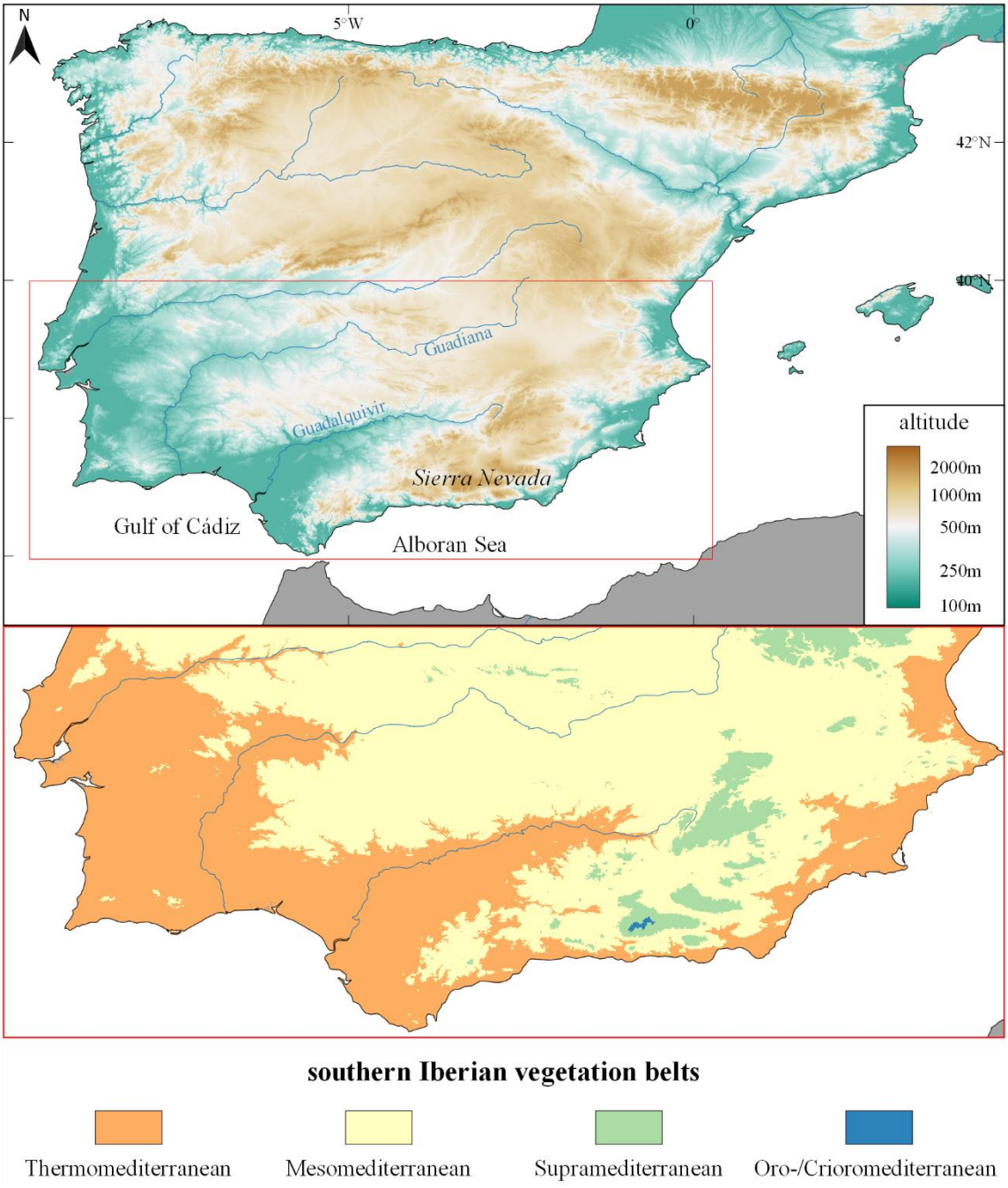

Figure 2.2 Overview of the Iberian Peninsula. *Top: Map showing the altitudinal range of the Iberian Peninsula and most important rivers, regions, and marine basins for this thesis. Bottom: Vegetation belts of the southern Iberian Peninsula are shown. These were calculated after [Loidi, 2017] based on 0.5° gridded climate data from WorldClim V2.0 [Fick and Hijmans, 2017].*

coasts. Consequently, the annual precipitation varies between 170 mm/month in the NW and 14 mm/month in the SE (Fig 2.3). This culminates in more than 2000 mm in the NW and only 170 mm in the SE annually [*Fick and Hijmans*, 2017] and is dominated by winter precipitation in most regions of the Iberian Peninsula (Fig 2.3). Accordingly, the winter rainfall reveals a spatial pattern similar to that on an annual basis, with more than 1400 mm of total precipitation (240 mm/month) in the NW and 100 mm (17 mm/month) in the SE [*Fick and Hijmans*, 2017].

The summer season is characterized by seasonal aridity, particularly in the southern and central Iberian Peninsula (Fig 2.3). Only along the northern coast, an average of up to 730 mm of total precipitation (122 mm/month) is registered. The southern part of the peninsula is experiencing significantly less precipitation averaging 9 mm/month from April to September [*Fick and Hijmans*, 2017].

While the temporal variability of overall precipitation on the Iberian Peninsula is mainly controlled by the NAO (see chapter 2.1.1 and Fig 2.1), the spatial distribution of precipitation on the Iberian Peninsula, on the other hand, is driven by the interaction of the Atlantic and Mediterranean atmospheric regimes with regions dominated by the Mediterranean regime experiencing significantly less precipitation. The scarce precipitation during the summer season is mainly driven by mesoscale synoptic patterns and local convective systems. These are responsible for short torrential rainfall events, which are particularly evident along the Mediterranean coast [*Araguas-Araguas and Diaz Teijeiro*, 2005].

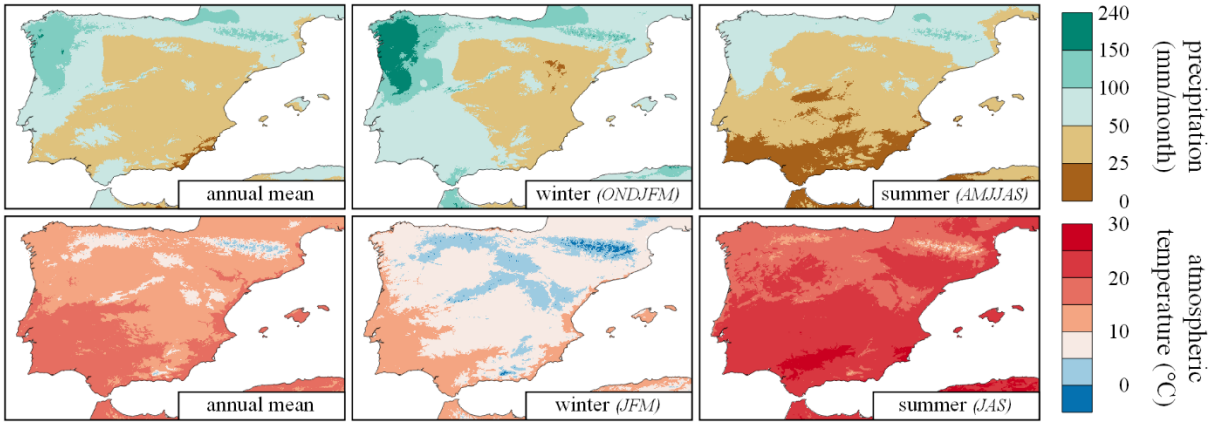

Figure 2.3 Climatology of the Iberian Peninsula. *Top: Average annual (left), monthly winter (center), and summer precipitation (right) are shown. Bottom: Annual mean (left), winter (center), and summer (right) surface air temperatures are displayed. The data reflects averages of the period 1970-2000 on a 0.5° spatial resolution. Climatological data has been provided by WorldClim V2.0 [Fick and Hijmans, 2017].*

The spatial distribution of temperature and precipitation is further associated with altitude and elevated mountain ranges, such as the Sierra Nevada and the Pyrenees, typically experiencing cooler and wetter conditions compared to the lowlands (Fig 2.3). Altogether, these three parameters (altitude, atmospheric temperature, and precipitation) define certain bioclimatic zones and, thus, control the natural distribution of plant taxa [*Loidi*, 2017]. These bioclimatic zones are associates with certain vegetation belts at the southern Iberian Peninsula (Fig 2.2) and are termed: Thermomediterranean (0 – 600/700 m), Mesomediterranean (600/700 –

1300/1400 m), Supramediterranean (1300/1400 – 1800 m), Oromediterranean (1800 – 2800 m), and Crioromediterranean (above 2800 m). Generally, the natural vegetation of the low altitude Thermo- and Mesomediterranean bioclimatic zones are dominated by a shrubby vegetation (*Fabaceae*, *Cistaceae*, *Pistaceae*, and *Olea*). Trees have a patchy distribution with the main trees being evergreen *Quercus* species and *Juniperus*. The density of trees increases in the Supramediterranean zone with deciduous *Quercus* and *Pinus* as the dominant species. Tree density reaches its maximum in the Oromediterranean zone, which is dominated by *Pinus*. *Juniperus* is also present in both bioclimatic zones. In the African mountains bordering the Alboran Sea the Oromediterranean is further characterized by *Cedrus* woods. The Crioromediterranean zone lies above the tree line and is, consequently, dominated by a steppe-like vegetation made up of *Poaceae* and other associated species.

2.2.2 Modern surface oceanography in the Gulf of Cádiz and the Alboran Sea

The overall circulation pattern south of the Iberian Peninsula is characterized by the surface inflow of Atlantic water masses from the North Atlantic into the Mediterranean Sea through the Strait of Gibraltar (Fig 2.4). The average annual mean SSTs in the entire region vary between 16 and 20 °C with cooler SSTs of below 17 °C at the western Atlantic coast and the north-western Alboran Sea [*Locarnini et al.*, 2019].

However, this general circulation pattern is highly dynamic on a seasonal scale with the most prominent features being the cold water tongues along the western Atlantic coast and in the north-western Alboran Sea (Fig 2.4) [*Locarnini et al.*, 2019]. These features are more dominant during the summer season, when summer SSTs are below 19 °C in both oceanic regions [*Locarnini et al.*, 2019]. During summer, the cold water tongue at the western Atlantic coast is associated with upwelling conditions favoured by the southward flowing Portugal Current (PC) [*Haynes et al.*, 1993; *Peliz et al.*, 2002]. These cool water masses occasionally also reach into the Gulf of Cádiz, where summer SSTs normally range between 21 and 22 °C [*Haynes et al.*, 1993; *Locarnini et al.*, 2019]. Also, a branch of the PC flows along the coast of the Gulf of Cádiz promoting two small-scale cyclonic gyres during summer [*García-Lafuente et al.*, 2006]. Parts of the PC further entrain the Alboran Sea through the Strait of Gibraltar (Fig 2.4). Here, water masses reach the Western Alboran Gyre (WAG) – a persistent anti-cyclonic circulation [*Peliz et al.*, 2013; *Sarhan et al.*, 2000]. The gyre circulation promotes year-round upwelling at the northern rim of the WAG [*Sarhan et al.*, 2000] responsible for the lowered SSTs of less than 20 °C (Fig 2.4) [*Locarnini et al.*, 2019]. During summer, the Atlantic water masses further entrain the East Alboran Gyre (EAG) and, subsequently, flow along the northern African coast

into the Mediterranean Sea (Fig 2.4) [*Peliz et al.*, 2013; *Sotillo et al.*, 2016]. On this route, summer SSTs progressively increase from 21 to 25 °C (Fig 2.4) [*Locarnini et al.*, 2019].

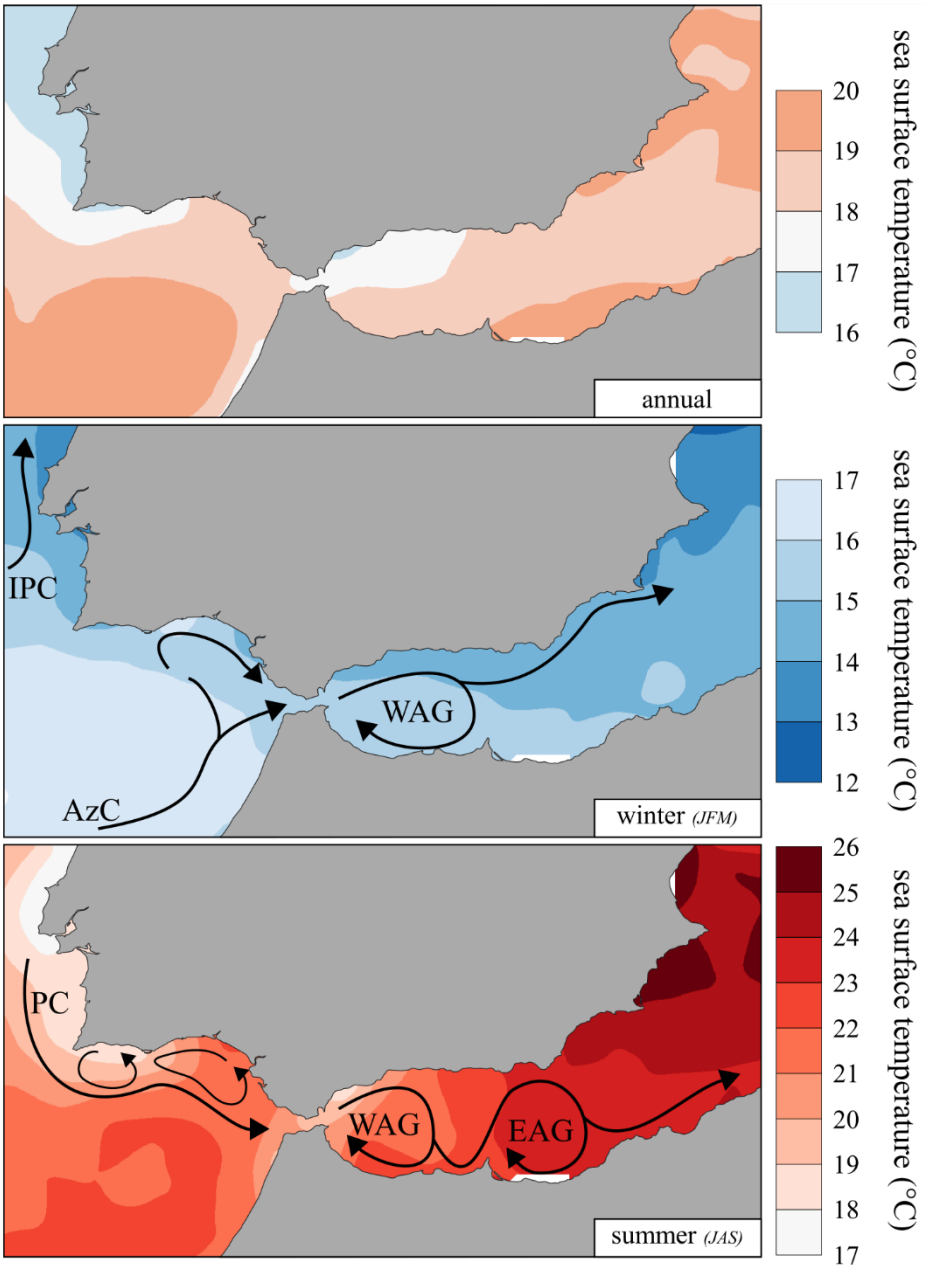

Figure 2.4 Oceanography of the Gulf of Cádiz and the Alboran Sea. *The coloured shadings display the annual (top), winter (center), and summer (bottom) sea surface temperatures (SSTs). SST data was provided by the World Ocean Atlas 18 [Locarnini et al., 2019] and represents averages of the period between 1981-2010 on a 0.25° spatial resolution. Seasonal ocean currents have been adopted from Criado-Aldeanueva et al. [2009], Garcia-Lafuente et al. [2006], Peliz et al. [2005], [2013], and Sotillo et al. [2016]. AzC – Azores Current; EAG – East Alboran Gyre; IPC – Iberian Poleward Current; PC – Portugal Current; WAG – West Alboran Gyre.*

Apart from the WAG this circulation pattern changes considerably during the winter period (Fig 2.4). Water masses at the western Atlantic coast are directed northwards with the Iberian

Poleward Current (IPC). In this scenario, the Gulf of Cádiz is influenced by a branch of the relatively warm (above 15 °C) Azores Current (AzC), which also enters the Alboran Sea [*Criado-Aldeanueva et al.*, 2009; *Locarnini et al.*, 2019; *Peliz et al.*, 2005]. After leaving the WAG, the Atlantic water masses flow along the southern Iberian coast into the Mediterranean Sea, because circulation within the EAG is limited during winter [*Peliz et al.*, 2013]. In contrast to the west-east SST gradient during summer, a north-south SST gradient from 14 to 17 °C is evident in the Alboran Sea during the winter period (Fig. 2.4) [*Locarnini et al.*, 2019].

2.2.3 Holocene climatic evolution and the 4.2 ka BP event

The Holocene period started at 11,700 cal. BP and reveals coherent trends across the northern hemisphere [*Leduc et al*., 2010; *Lorenz et al*., 2006; *Marsicek et al.*, 2018; *Wanner et al.*, 2015]. Generally, a warming trend during the Early Holocene (8200 – 11,700 cal. BP) leads into the Holocene Thermal Maximum (HTM) [*Marcott et al.*, 2013; *Renssen et al.*, 2012]. On the Iberian Peninsula the HTM is associated with warm and wet conditions favouring the maximum extension of the forest cover between 7600 and 9500 cal. BP (Fig 2.5) [*Jalut et al.*, 2009; *Ramos-Román et al.*, 2018b]. In relation to altered surface circulation in the North Atlantic and increased surface mixing the Mediterranean [*Cacho et al.*, 2002; *Repschläger et al.*, 2017], also SSTs in the Western Mediterranean have been relatively warm during this period [*Català et al.*, 2019]. Afterwards, during the Middle Holocene (4200 – 8200 cal. BP), a general cooling trend until the present pre-industrial period is observed [*Cacho et al.*, 2001; *Martrat et al.*, 2014]. Oceanic cooling is also related to an increased inflow of cooler Atlantic water masses into the Mediterranean Sea, increased water mass mixing, and the subsequent intensification of deep water formation in the Gulf of Lions [*Català et al.*, 2019; *Frigola et al.*, 2008]. In relation to the intensification of the oceanic circulation, at around 7700 cal. BP also the WAG established [*Ausín et al.*, 2015].

On the Iberian Peninsula this overall cooling trend coincides with aridification (Fig 2.5) [*Fletcher and Sánchez Goñi*, 2008; *Peyron et al.*, 2017; *Ramos-Román et al.*, 2018b]. The aridification trend becomes particularly apparent across the southern Iberian Peninsula after 5500 cal. BP [*Jalut et al.*, 2009; *Jiménez-Moreno et al.*, 2015]. At that time (between ca. 5000 and 7000 cal. BP) also the Mediterranean climate established, characterized by mild, humid winters and hot, dry summers at the Iberian Peninsula [*Pérez-Obiol et al.*, 2011]. Altogether, these trends (Fig 2.5) were likely driven by decreasing summer insolation [e.g. *Rimbu et al*., 2003], which mimics the southward movement of the Intertropical Convergence Zone (ITCZ) [*Cacho et al.*, 2001; *Peyron et al.*, 2017; *Ramos-Román et al.*, 2018b]. Due to the displacement

of the ITCZ also the wind systems and associated precipitation moved southward and, thus, were responsible for the end of the African Humid Period (AHP) in the Sahara and increasing aridity in the Mediterranean region including the Iberian Peninsula [*deMenocal et al.*, 2000; *Fletcher and Sánchez Goñi*, 2008].

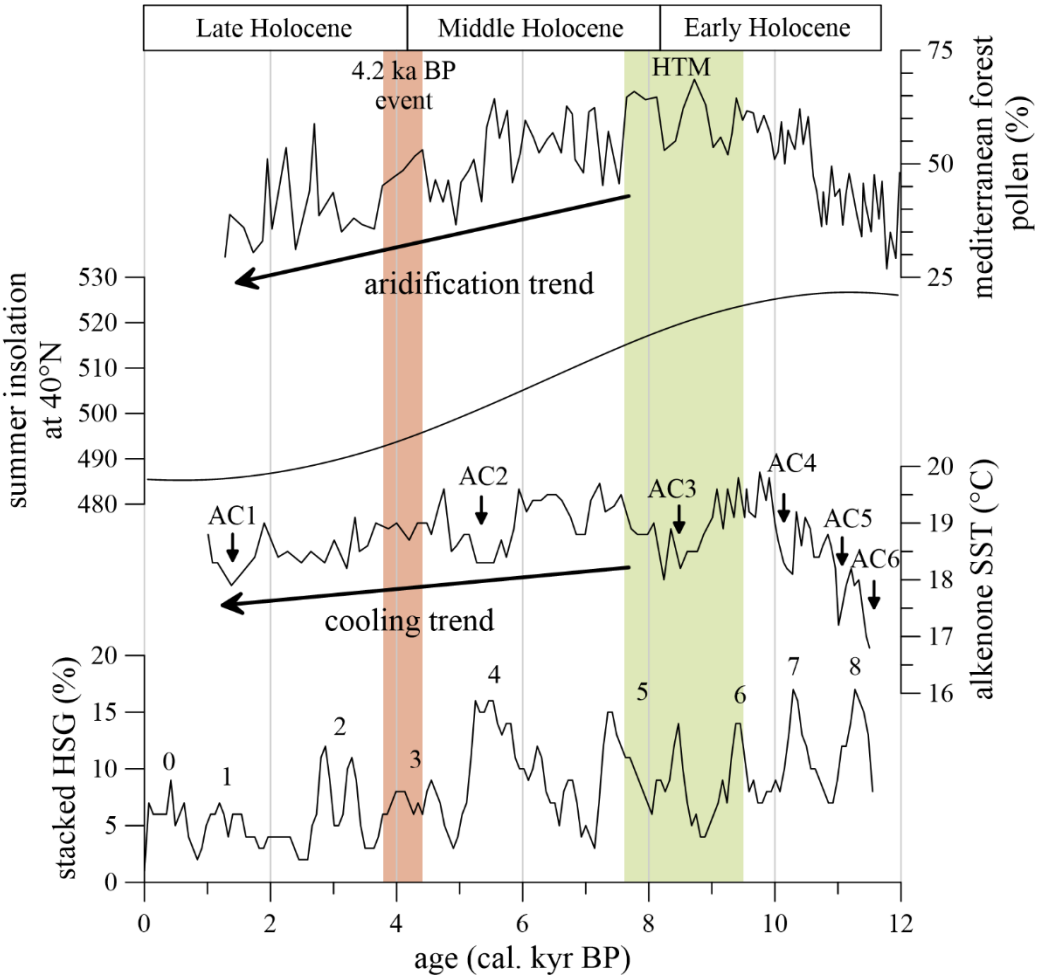

Figure 2.5 Holocene climate developments. *From top to bottom: Mediterranean forest percentages in sediment core MD95-2043 from the Alboran Sea [Fletcher and Sánchez Goñi, 2008], summer insolation (21st June) at 40°N [Laskar et al., 2004], alkenone-deduced sea surface temperature (SST) record from MD95-2043 [Cacho et al., 2001] and associated six Alboran Sea cold events (ACs) during the Holocene, stacked hematite-stained grains (HSG) from North Atlantic sediment cores [Bond et al., 2001] displaying the eight well-known periods of enhanced ice-rafted debris (IRD) discharge also known as Bond Events. The green bar indicates the period of the Holocene Thermal Maximum (HTM) on the Iberian Peninsula. The brown bar highlights the period of the 4.2 ka BP event.*

These overall trends are superimposed by abrupt short-term cooling and/or drying events on the northern hemisphere [*Mayewski et al.*, 2004; *Wanner et al.*, 2011] as well as on the Iberian Peninsula [*Jalut et al.*, 2009; *Ramos-Román et al.*, 2018b]. Many of these events are associated with increased IRD discharge to the North Atlantic from the northern hemisphere ice sheets –

the so-called Bond Events (Fig 2.5) [*Bond et al.*, 2001]. On the Iberian Peninsula some of the Bond Events are associated with cool and dry conditions (Fig 2.5) [*Ramos-Román et al.*, 2018b]. Similarly, a cooling during some Bond Events is noted in the Gulf of Cádiz and the Alboran Sea (Fig 2.5) [*Cacho et al.*, 2001].

Another particular climate event, which coincides roughly with Bond Event 3, is the 4.2 ka BP event, which is noted as a marked dry phase across much of the Mediterranean between 3800 and 4400 cal. BP [*Cheng et al.*, 2015; *Ruan et al.*, 2016; *Zanchetta et al.*, 2016]. On the Iberian Peninsula the spatio-temporal manifestation of the 4.2 ka BP event remains less clear [*Weinelt et al.*, 2015]. In northern Iberia, for example, a cessation of speleothem growth in multiple caves at around 4100 cal. BP points to regional dry conditions [*Stoll et al.*, 2013]. Contrastingly, wet conditions at that time were reported from Cova da Arcoia [*Railsback et al.*, 2011] and maximum forest development is indicated at Lake Sanabria [*Jambrina-Enríquez et al.*, 2016]. Similarly, contrasting evidence also emerges at the southern Iberian Peninsula. Abrupt dry conditions are reported from some pollen data associated with the 4.2 ka BP event [*Burjachs and Expósito*, 2015; *Ramos-Román et al.*, 2018a]. Instead, only a very brief dry event during rather stable humid conditions is indicated by records from Lake Medina [*Schröder et al.*, 2018] and El Refugio Cave [*Walczak et al.*, 2015]. Moreover, wet conditions during the 4.2 ka BP event are reported from the Alboran Sea (Fig 2.5) [*Fletcher and Sánchez Goñi*, 2008] and northern Moroccan archives [*Ait Brahim et al.*, 2019; *Wassenburg et al.*, 2016; *Zielhofer et al.*, 2019]. Accordingly, also potential driving mechanisms of the hemispheric or even global climatic anomaly remain elusive [*Bini et al.*, 2019].

2.3 References

Ait Brahim, Y., J. A. Wassenburg, L. Sha, F. W. Cruz, M. Deininger, A. Sifeddine, L. Bouchaou, C. Spötl, R. L. Edwards, and H. Cheng (2019), North Atlantic Ice-Rafting, Ocean and Atmospheric Circulation During the Holocene: Insights From Western Mediterranean Speleothems, *Geophys. Res. Lett.*, *4*, 150, doi:10.1029/2019GL082405.

Alpert, P., M. Baldi, R. Ilani, S. Krichak, C. Price, X. Rodó, H. Saaroni, B. Ziv, P. Kishcha, J. Barkan, A. Mariotti, and E. Xoplaki (2006), Chapter 2 Relations between climate variability in the Mediterranean region and the tropics: ENSO, South Asian and African monsoons, hurricanes and Saharan dust, in *Mediterranean Climate Variability*, 1st ed., edited by P. Lionello et al., pp. 149–177, Elsevier, Amsterdam.

Araguas-Araguas, L. J., and M. F. Diaz Teijeiro (2005), Isotope composition of precipitation and water vapour in the Iberian Peninsula, in *Isotopic composition of precipitation in the Mediterranean basin in relation to air circulation patterns and climate: Final report of a coordinated research project 2000-2004*, *IAEA-TECDOC*, vol. 1453, edited by International Atomic Energy Agency, pp. 173–190, IAEA, Vienna.

Ausín, B., J. A. Flores, F. J. Sierro, I. Cacho, I. Hernández-Almeida, B. Martrat, and J. O. Grimalt (2015), Atmospheric patterns driving Holocene productivity in the Alboran Sea (Western Mediterranean): A multiproxy approach, *The Holocene*, *25*(4), 583–595, doi:10.1177/0959683614565952.

Barnston, A. G., and R. E. Livezey (1987), Classification, Seasonality and Persistence of Low-Frequency Atmospheric Circulation Patterns, *Mon. Wea. Rev.*, *115*(6), 1083–1126, doi:10.1175/1520-0493(1987)115<1083:CSAPOL>2.0.CO;2.

Bini, M., G. Zanchetta, A. Perşoiu, R. Cartier, A. Català, I. Cacho, J. R. Dean, F. Di Rita, R. N. Drysdale, M. Finnè, I. Isola, B. Jalali, F. Lirer, D. Magri, A. Masi, L. Marks, A. M. Mercuri, O. Peyron, L. Sadori, M.-A. Sicre, F. Welc, C. Zielhofer, and E. Brisset (2019), The 4.2 ka BP Event in the Mediterranean region: An overview, *Clim. Past*, *15*(2), 555–577, doi:10.5194/cp-15-555-2019.

Bond, G., B. Kromer, J. Beer, R. Muscheler, M. N. Evans, W. Showers, S. Hoffmann, R. Lotti-Bond, I. Hajdas, and G. Bonani (2001), Persistent solar influence on North Atlantic climate during the Holocene, *Science (New York, N.Y.)*, *294*(5549), 2130–2136, doi:10.1126/science.1065680.

Bueh, C., and H. Nakamura (2007), Scandinavian pattern and its climatic impact, *Quarterly Journal of the Royal Meteorological Society*, *133*(629), 2117–2131, doi:10.1002/qj.173.

Burjachs, F., and I. Expósito (2015), Charcoal and pollen analysis: Examples of Holocene fire dynamics in Mediterranean Iberian Peninsula, *CATENA*, *135*, 340–349, doi:10.1016/j.catena.2014.10.006.

Cacho, I., J. O. Grimalt, M. Canals, L. Sbaffi, N. J. Shackleton, J. Schönfeld, and R. Zahn (2001), Variability of the western Mediterranean Sea surface temperature during the last 25,000 years and its connection with the Northern Hemisphere climatic changes, *Paleoceanography*, *16*(1), 40–52, doi:10.1029/2000PA000502.

Cacho, I., J. O. Grimalt, and M. Canals (2002), Response of the Western Mediterranean Sea to rapid climatic variability during the last 50,000 years: A molecular biomarker approach, *Journal of Marine Systems*, *33-34*, 253–272, doi:10.1016/S0924-7963(02)00061-1.

Català, A., I. Cacho, J. Frigola, L. D. Pena, and F. Lirer (2019), Holocene hydrography evolution in the Alboran Sea: A multi-record and multi-proxy comparison, *Clim. Past*, *15*(3), 927–942, doi:10.5194/cp-15-927-2019.

Cheng, H., A. Sinha, S. Verheyden, F. H. Nader, X. L. Li, P. Z. Zhang, J. J. Yin, L. Yi, Y. B. Peng, Z. G. Rao, Y. F. Ning, and R. L. Edwards (2015), The climate variability in northern Levant over the past 20,000 years, *Geophysical Research Letters*, *42*(20), 8641–8650, doi:10.1002/2015GL065397.

Comas-Bru, L., F. McDermott, and M. Werner (2016), The effect of the East Atlantic pattern on the precipitation δ18O-NAO relationship in Europe, *Clim Dyn*, *47*(7-8), 2059–2069, doi:10.1007/s00382-015-2950-1.

Criado-Aldeanueva, F., J. García-Lafuente, G. Navarro, and J. Ruiz (2009), Seasonal and interannual variability of the surface circulation in the eastern Gulf of Cadiz (SW Iberia), *J. Geophys. Res.*, *114*(C1), 1054, doi:10.1029/2008JC005069.

Deininger, M., F. McDermott, M. Mudelsee, M. Werner, N. Frank, and A. Mangini (2017), Coherency of late Holocene European speleothem $\delta^{18}O$ records linked to North Atlantic Ocean circulation, *Climate Dynamics*, *49*(1-2), 595–618, doi:10.1007/s00382-016-3360-8.

deMenocal, P., J. Ortiz, T. Guilderson, J. Adkins, M. Sarnthein, L. Baker, and M. Yarusinsky (2000), Abrupt onset and termination of the African Humid Period, *Quaternary Science Reviews*, *19*(1-5), 347–361, doi:10.1016/S0277-3791(99)00081-5.

Fernández-González, S., S. del Río, A. Castro, A. Penas, M. Fernández-Raga, A. I. Calvo, and R. Fraile (2012), Connection between NAO, weather types and precipitation in León, Spain (1948-2008), *Int. J. Climatol.*, *20*, 2181–2196, doi:10.1002/joc.2431.

Fick, S. E., and R. J. Hijmans (2017), WorldClim 2: New 1-km spatial resolution climate surfaces for global land areas, *Int. J. Climatol.*, *37*(12), 4302–4315, doi:10.1002/joc.5086.

Fletcher, W. J., and M. F. Sánchez Goñi (2008), Orbital- and sub-orbital-scale climate impacts on vegetation of the western Mediterranean basin over the last 48,000 yr, *Quat. res.*, *70*(03), 451–464, doi:10.1016/j.yqres.2008.07.002.

Frigola, J., A. Moreno, I. Cacho, M. Canals, F. J. Sierro, J. A. Flores, and J. O. Grimalt (2008), Evidence of abrupt changes in Western Mediterranean Deep Water circulation during the last 50kyr: A high-resolution marine record from the Balearic Sea, *Quaternary International*, *181*(1), 88–104, doi:10.1016/j.quaint.2007.06.016.

Gaetani, M., M. Baldi, G. A. Dalu, and G. Maracchi (2011), Jetstream and rainfall distribution in the Mediterranean region, *Nat. Hazards Earth Syst. Sci.*, *11*(9), 2469–2481, doi:10.5194/nhess-11-2469-2011.

García-Lafuente, J., J. Delgado, F. Criado-Aldeanueva, M. Bruno, J. del Río, and J. Miguel Vargas (2006), Water mass circulation on the continental shelf of the Gulf of Cádiz, *Deep Sea Research Part II: Topical Studies in Oceanography*, *53*(11-13), 1182–1197, doi:10.1016/j.dsr2.2006.04.011.

Goslin, J., M. Fruergaard, L. Sander, M. Gałka, L. Menviel, J. Monkenbusch, N. Thibault, and L. B. Clemmensen (2018), Holocene centennial to millennial shifts in North-Atlantic storminess and ocean dynamics, *Scientific reports*, *8*(1), 12778, doi:10.1038/s41598-018-29949-8.

Gouveia, C., R. M. Trigo, C. C. DaCamara, R. Libonati, and J. M. C. Pereira (2008), The North Atlantic Oscillation and European vegetation dynamics, *Int. J. Climatol.*, *28*(14), 1835–1847, doi:10.1002/joc.1682.

Haynes, R., E. D. Barton, and I. Pilling (1993), Development, persistence, and variability of upwelling filaments off the Atlantic coast of the Iberian Peninsula, *J. Geophys. Res.*, *98*(C12), 22681, doi:10.1029/93JC02016.

Hernández, A., R. M. Trigo, S. Pla-Rabes, B. L. Valero-Garcés, S. Jerez, M. Rico-Herrero, J. C. Vega, M. Jambrina-Enríquez, and S. Giralt (2015), Sensitivity of two Iberian lakes to North Atlantic atmospheric circulation modes, *Clim Dyn*, *45*(11-12), 3403–3417, doi:10.1007/s00382-015-2547-8.

Hurrell, J. W. (1995), Decadal trends in the north atlantic oscillation: regional temperatures and precipitation, *Science*, *269*(5224), 676–679, doi:10.1126/science.269.5224.676.

Hurrell, J. W., and C. Deser (2009), North Atlantic climate variability: The role of the North Atlantic Oscillation, *Journal of Marine Systems*, *78*(1), 28–41, doi:10.1016/j.jmarsys.2008.11.026.

Hurrell, J. W., Y. Kushnir, G. Ottersen, and M. Visbeck (2003), An Overview of the North Atlantic Oscillation, in *The North Atlantic Oscillation: Climate Significance and Environmental Impact*, edited by J. W. Hurrell et al., pp. 1–35, Geophysical Monograph Series, Washington DC.

Jalut, G., J. J. Dedoubat, M. Fontugne, and T. Otto (2009), Holocene circum-Mediterranean vegetation changes: Climate forcing and human impact, *Quaternary International*, *200*(1-2), 4–18, doi:10.1016/j.quaint.2008.03.012.

Jambrina-Enríquez, M., D. Sachse, and B. L. Valero-Garcés (2016), A deglaciation and Holocene biomarker-based reconstruction of climate and environmental variability in NW Iberian Peninsula: The Sanabria Lake sequence, *J Paleolimnol*, *56*(1), 49–66, doi:10.1007/s10933-016-9890-6.

Jiménez-Moreno, G., A. Rodríguez-Ramírez, J. N. Pérez-Asensio, J. S. Carrión, J. A. López-Sáez, J. Villarías-Robles, JR, S. Celestino-Pérez, E. Cerrillo-Cuenca, Á. León, and C. Contreras (2015), Impact of late-Holocene aridification trend, climate variability and geodynamic control on the environment from a coastal area in SW Spain, *The Holocene*, *25*(4), 607–617, doi:10.1177/0959683614565955.

Joyce, T. M., C. Deser, and M. A. Spall (2000), The Relation between Decadal Variability of Subtropical Mode Water and the North Atlantic Oscillation, *J. Climate*, *13*(14), 2550–2569, doi:10.1175/1520-0442(2000)013<2550:TRBDVO>2.0.CO;2.

Laskar, J., P. Robutel, F. Joutel, M. Gastineau, A. C. M. Correia, and B. Levrard (2004), A long-term numerical solution for the insolation quantities of the Earth, *A&A*, *428*(1), 261–285, doi:10.1051/0004-6361:20041335.

Leduc, G., R. Schneider, J.-H. Kim, and G. Lohmann (2010), Holocene and Eemian sea surface temperature trends as revealed by alkenone and Mg/Ca paleothermometry, Quaternary Science Reviews, 29(7-8), 989–1004, doi:10.1016/j.quascirev.2010.01.004.

Lionello, P. (Ed.) (2012), *The climate of the Mediterranean region: From the past to the future*, 1st ed., 502 pp., *Elsevier insights*, Elsevier Science, Amsterdam.

Locarnini, R. A., A. V. Mishonov, O. K. Baranova, T. P. Boyer, M. M. Zweng, H. E. Garcia, J. R. Reagan, D. Seidov, K. Weathers, C. R. Paver, and I. Smolyar (2019), World Ocean Atlas 2018, Volume 1: Temperature, 52 pp., NOAA Atlas NESDIS 81.

Loidi, J. (2017), *The Vegetation of the Iberian Peninsula*, vol. 13, Springer International Publishing, Cham.

Lorenz, S. J., J.-H. Kim, N. Rimbu, R. R. Schneider, and G. Lohmann (2006), Orbitally driven insolation forcing on Holocene climate trends: Evidence from alkenone data and climate modeling, Paleoceanography, 21(1), doi:10.1029/2005PA001152.

Magny, M., N. Combourieu-Nebout, J. L. de Beaulieu, V. Bout-Roumazeilles, D. Colombaroli, S. Desprat, A. Francke, S. Joannin, E. Ortu, O. Peyron, M. Revel, L. Sadori, G. Siani, M. A. Sicre, S. Samartin, A. Simonneau, W. Tinner, B. Vannière, B. Wagner, G. Zanchetta, F. Anselmetti, E. Brugiapaglia, E. Chapron, M. Debret, M. Desmet, J. Didier, L. Essallami, D. Galop, A. Gilli, J. N. Haas, N. Kallel, L. Millet, A. Stock, J. L. Turon, and S. Wirth (2013), North-south palaeohydrological contrasts in the central Mediterranean during the Holocene: Tentative synthesis and working hypotheses, *Climate of the Past*, *9*(5), 2043–2071, doi:10.5194/cp-9-2043-2013.

Maheras, P., E. Xoplaki, and H. Kutiel (1999), Wet and Dry Monthly Anomalies Across the Mediterranean Basin and their Relationship with Circulation, 1860-1990, *Theoretical and Applied Climatology*, *64*(3-4), 189–199, doi:10.1007/s007040050122.

Marcott, S. A., J. D. Shakun, P. U. Clark, and A. C. Mix (2013), A Reconstruction of Regional and Global Temperature for the Past 11,300 Years, *Science*, *339*(6124), 1198–1201, doi:10.1126/science.1228026.

Mariotti, A., J. Ballabrera-Poy, and N. Zeng (2005), Tropical influence on Euro-Asian autumn rainfall variability, *Clim Dyn*, *24*(5), 511–521, doi:10.1007/s00382-004-0498-6.

Mariotti, A., N. Zeng, and K.-M. Lau (2002), Euro-Mediterranean rainfall and ENSO—a seasonally varying relationship, *Geophys. Res. Lett.*, *29*(12), 2693, doi:10.1029/2001GL014248.

Marsicek, J., B. N. Shuman, P. J. Bartlein, S. L. Shafer, and S. Brewer (2018), Reconciling divergent trends and millennial variations in Holocene temperatures, *Nature*, *554*(7690), 92–96, doi:10.1038/nature25464.

Martrat, B., P. Jiménez-Amat, R. Zahn, and J. O. Grimalt (2014), Similarities and dissimilarities between the last two deglaciations and interglaciations in the North Atlantic region, *Quaternary Science Reviews*, *99*, 122–134, doi:10.1016/j.quascirev.2014.06.016.

Mayewski, P. A., E. E. Rohling, J. Curt Stager, W. Karlén, K. A. Maasch, L. D. Meeker, E. A. Meyerson, F. Gasse, S. van Kreveld, K. Holmgren, J. Lee-Thorp, G. Rosqvist, F. Rack, M. Staubwasser, R. R. Schneider, and E. J. Steig (2004), Holocene Climate Variability, *Quat. res.*, *62*(03), 243–255, doi:10.1016/j.yqres.2004.07.001.

Moulin, C., C. E. Lambert, F. Dulac, and u. Dayan (1997), Control of atmospheric export of dust from North Africa by the North Atlantic Oscillation, *Nature*, *387*(6634), 691–694.

Olsen, J., N. J. Anderson, and M. F. Knudsen (2012), Variability of the North Atlantic Oscillation over the past 5,200 years, *Nature Geoscience*, *5*(11), 808–812, doi:10.1038/ngeo1589.

Patricola, C. M., and K. H. Cook (2007), Dynamics of the West African Monsoon under Mid-Holocene Precessional Forcing: Regional Climate Model Simulations, *J. Climate*, *20*(4), 694–716, doi:10.1175/JCLI4013.1.

Peliz, A., D. Boutov, R. M. Cardoso, J. Delgado, and P. M.M. Soares (2013), The Gulf of Cadiz–Alboran Sea sub-basin: Model setup, exchange and seasonal variability, *Ocean Modelling*, *61*, 49–67, doi:10.1016/j.ocemod.2012.10.007.

Peliz, Á., J. Dubert, A. M. P. Santos, P. B. Oliveira, and B. Le Cann (2005), Winter upper ocean circulation in the Western Iberian Basin—Fronts, Eddies and Poleward Flows: An overview, *Deep Sea Research Part I: Oceanographic Research Papers*, *52*(4), 621–646, doi:10.1016/j.dsr.2004.11.005.

Peliz, Á., T. L. Rosa, A.M. P. Santos, and J. L. Pissarra (2002), Fronts, jets, and counter-flows in the Western Iberian upwelling system, *Journal of Marine Systems*, *35*(1-2), 61–77, doi:10.1016/S0924-7963(02)00076-3.

Pérez-Obiol, R., G. Jalut, R. Julià, A. Pèlachs, M. J. Iriarte, T. Otto, and B. Hernández-Beloqui (2011), Mid-Holocene vegetation and climatic history of the Iberian Peninsula, *The Holocene*, *21*(1), 75–93, doi:10.1177/0959683610384161.

Peyron, O., N. Combourieu-Nebout, D. Brayshaw, S. Goring, V. Andrieu-Ponel, S. Desprat, W. Fletcher, B. Gambin, C. Ioakim, S. Joannin, U. Kotthoff, K. Kouli, V. Montade, J. Pross, L. Sadori, and M. Magny (2017),

Precipitation changes in the Mediterranean basin during the Holocene from terrestrial and marine pollen records: A model–data comparison, *Climate of the Past*, *13*(3), 249–265, doi:10.5194/cp-13-249-2017.

Railsback, L. B., F. Liang, J. R. Vidal Romaní, A. Grandal-d'Anglade, M. Vaqueiro Rodríguez, L. Santos Fidalgo, D. Fernández Mosquera, H. Cheng, and R. L. Edwards (2011), Petrographic and isotopic evidence for Holocene long-term climate change and shorter-term environmental shifts from a stalagmite from the Serra do Courel of northwestern Spain, and implications for climatic history across Europe and the Mediterranean, *Palaeogeography, Palaeoclimatology, Palaeoecology*, *305*(1-4), 172–184, doi:10.1016/j.palaeo.2011.02.030.

Ramos-Román, M. J., G. Jiménez-Moreno, J. Camuera, A. García-Alix, R. S. Anderson, F. J. Jiménez-Espejo, and J. S. Carrión (2018a), Holocene climate aridification trend and human impact interrupted by millennial- and centennial-scale climate fluctuations from a new sedimentary record from Padul (Sierra Nevada, southern Iberian Peninsula), *Clim. Past*, *14*(1), 117–137, doi:10.5194/cp-14-117-2018.

Ramos-Román, M. J., G. Jiménez-Moreno, J. Camuera, A. García-Alix, R. Scott Anderson, F. J. Jiménez-Espejo, D. Sachse, J. L. Toney, J. S. Carrión, C. Webster, and Y. Yanes (2018b), Millennial-scale cyclical environment and climate variability during the Holocene in the western Mediterranean region deduced from a new multi-proxy analysis from the Padul record (Sierra Nevada, Spain), *Global and Planetary Change*, *168*, 35–53, doi:10.1016/j.gloplacha.2018.06.003.

Renssen, H., H. Seppä, X. Crosta, H. Goosse, and D. M. Roche (2012), Global characterization of the Holocene Thermal Maximum, *Quaternary Science Reviews*, *48*, 7–19, doi:10.1016/j.quascirev.2012.05.022.

Repschläger, J., D. Garbe-Schönberg, M. Weinelt, and R. Schneider (2017), Holocene evolution of the North Atlantic subsurface transport, *Climate of the Past*, *13*(4), 333–344, doi:10.5194/cp-13-333-2017.

Rimbu, N., G. Lohmann, J.-H. Kim, H. W. Arz, and R. Schneider (2003), Arctic/North Atlantic Oscillation signature in Holocene sea surface temperature trends as obtained from alkenone data, Geophys. Res. Lett., 30(6), 1939, doi:10.1029/2002GL016570.

Ruan, J., F. Kherbouche, D. Genty, D. Blamart, H. Cheng, F. Dewilde, S. Hachi, R. L. Edwards, E. Régnier, and J.-L. Michelot (2016), Evidence of a prolonged drought ca. 4200 yr BP correlated with prehistoric settlement abandonment from the Gueldaman GLD1 Cave, Northern Algeria, *Climate of the Past*, *12*(1), 1–14, doi:10.5194/cp-12-1-2016.

Sabatier, P., M. Nicolle, C. Piot, C. Colin, M. Debret, D. Swingedouw, Y. Perrette, M.-C. Bellingery, B. Chazeau, A.-L. Develle, M. Leblanc, C. Skonieczny, Y. Copard, J.-L. Reyss, E. Malet, I. Jouffroy-Bapicot, M. Kelner, J. Poulenard, J. Didier, F. Arnaud, and B. Vannière (2020), Past African dust inputs in the western Mediterranean area controlled by the complex interaction between the Intertropical Convergence Zone, the North Atlantic Oscillation, and total solar irradiance, *Clim. Past*, *16*(1), 283–298, doi:10.5194/cp-16-283-2020.

Sánchez-López, G., A. Hernández, S. Pla-Rabes, R. M. Trigo, M. Toro, I. Granados, A. Sáez, P. Masqué, J. J. Pueyo, M. J. Rubio-Inglés, and S. Giralt (2016), Climate reconstruction for the last two millennia in central Iberia: The role of East Atlantic (EA), North Atlantic Oscillation (NAO) and their interplay over the Iberian Peninsula, *Quaternary Science Reviews*, *149*, 135–150, doi:10.1016/j.quascirev.2016.07.021.

Sarhan, T., J. G. Lafuente, M. Vargas, J. M. Vargas, and F. Plaza (2000), Upwelling mechanisms in the northwestern Alboran Sea, *Journal of Marine Systems*, *23*(4), 317–331, doi:10.1016/S0924-7963(99)00068-8.

Schröder, T., J. van't Hoff, J. A. López-Sáez, F. Viehberg, M. Melles, and K. Reicherter (2018), Holocene climatic and environmental evolution on the southwestern Iberian Peninsula: A high-resolution multi-proxy study from Lake Medina (Cádiz, SW Spain), *Quaternary Science Reviews*, *198*, 208–225, doi:10.1016/j.quascirev.2018.08.030.

Shorthouse, C. A., and N. W. Arnell (1997), Spatial and temporal variability in European river flow and the North Atlantic oscillation, FRIEND'97-Regional Hydrology: Concepts and Models for Sustainable Water Resource Management, *International Association of Hydrological Sciences Publishing (IAHS Publ.)*, *246*, 77-85.

Sotillo, M. G., E. Garcia-Ladona, A. Orfila, P. Rodríguez-Rubio, J. C. Maraver, D. Conti, E. Padorno, J. A. Jiménez, E. Capó, F. Pérez, J. M. Sayol, F. J. de los Santos, A. Amo, A. Rietz, C. Troupin, J. Tintore, and E. Álvarez-Fanjul (2016), The MEDESS-GIB database: Tracking the Atlantic water inflow, *Earth System Science Data*, *8*(1), 141–149, doi:10.5194/essd-8-141-2016.

Stoll, H. M., A. Moreno, A. Mendez-Vicente, S. Gonzalez-Lemos, M. Jimenez-Sanchez, M. J. Dominguez-Cuesta, R. L. Edwards, H. Cheng, and X. Wang (2013), Paleoclimate and growth rates of speleothems in the northwestern Iberian Peninsula over the last two glacial cycles, *Quat. res.*, *80*(02), 284–290, doi:10.1016/j.yqres.2013.05.002.

Thompson, D. W. J., and J. M. Wallace (1998), The Arctic oscillation signature in the wintertime geopotential height and temperature fields, *Geophys. Res. Lett.*, *25*(9), 1297–1300, doi:10.1029/98GL00950.

Trigo, R. M., T. J. Osborn, and J. M. Corte-Real (2002), The North Atlantic Oscillation influence on Europe: Climate impacts and associated physical mechanisms, *Clim. Res.*, *20*, 9–17, doi:10.3354/cr020009.

Trigo, R. M., D. Pozo-Vázquez, T. J. Osborn, Y. Castro-Díez, S. Gámiz-Fortis, and M. J. Esteban-Parra (2004), North Atlantic oscillation influence on precipitation, river flow and water resources in the Iberian Peninsula, *Int. J. Climatol*, *24*(8), 925–944, doi:10.1002/joc.1048.

Trouet, V., J. Esper, N. E. Graham, A. Baker, J. D. SCOURSE, and D. C. Frank (2009), Persistent Positive North Atlantic Oscillation Mode Dominated the Medieval Climate Anomaly, *Science*, *324*(5923), 78–80, doi:10.1126/science.1166349.

Visbeck, M., E. Chassignet, R. Curry, T. Delworth, B. Dickson, and G. Krahmann (2003), The Ocean's Response to North Atlantic Oscillation Variability, in *The North Atlantic Oscillation: Climate Significance and Environmental Impact*, edited by J. W. Hurrell et al., pp. 113–146, Geophysical Monograph Series, Washington DC.

Walczak, I. W., J. U.L. Baldini, L. M. Baldini, F. McDermott, S. Marsden, C. D. Standish, D. A. Richards, B. Andreo, and J. Slater (2015), Reconstructing high-resolution climate using CT scanning of unsectioned stalagmites: A case study identifying the mid-Holocene onset of the Mediterranean climate in southern Iberia, *Quaternary Science Reviews*, *127*, 117–128, doi:10.1016/j.quascirev.2015.06.013.

Wanner, H., L. Mercolli, M. Grosjean, and S. P. Ritz (2015), Holocene climate variability and change; a data-based review, *Journal of the Geological Society*, *172*(2), 254–263, doi:10.1144/jgs2013-101.

Wanner, H., O. Solomina, M. Grosjean, S. P. Ritz, and M. Jetel (2011), Structure and origin of Holocene cold events, *Quaternary Science Reviews*, *30*(21-22), 3109–3123, doi:10.1016/j.quascirev.2011.07.010.

Wassenburg, J. A., S. Dietrich, J. Fietzke, J. Fohlmeister, K. P. Jochum, D. Scholz, D. K. Richter, A. Sabaoui, C. Spötl, G. Lohmann, M. O. Andreae, and A. Immenhauser (2016), Reorganization of the North Atlantic Oscillation during early Holocene deglaciation, *Nature Geoscience*, *9*(8), 602–605, doi:10.1038/ngeo2767.

Weinelt, M., C. Schwab, J. Kneisel, and M. Hinz (2015), Climate and societal change in the western Mediterranean area around 4.2 ka BP, in *2200 BC - ein Klimasturz als Ursache für den Zerfall der alten Welt?: 7. Mitteldeutscher Archäologentag vom 23. bis 26. Oktober 2014 in Halle (Saale)*, *Tagungen des Landesmuseums für Vorgeschichte Halle*, Band 12,1, edited by H. Meller et al., pp. 461–480, Landesamt für Denkmalpflege und Archäologie Sachsen-Anhalt, Landesmuseum für Vorgeschichte, Halle (Saale).

Zanchetta, G., E. Regattieri, I. Isola, R. N. Drysdale, M. Bini, I. Baneschi, and J. C. Hellstrom (2016), The so-called "4.2 event" in the Central Mediterranean and its climatic teleconnections, *Alpine and Mediterranean Quaternary*, *29*(1), 5–17.

Zielhofer, C., A. Köhler, S. Mischke, A. Benkaddour, A. Mikdad, and W. J. Fletcher (2019), Western Mediterranean hydro-climatic consequences of Holocene ice-rafted debris (Bond) events, *Clim. Past*, *15*(2), 463–475, doi:10.5194/cp-15-463-2019.

Zorita, E., V. Kharin, and H. von Storch (1992), The Atmospheric Circulation and Sea Surface Temperature in the North Atlantic Area in Winter: Their Interaction and Relevance for Iberian Precipitation, *Journal of Climate*, *5*(10), 1097–1108, doi:10.1175/1520-0442(1992)005<1097:TACASS>2.0.CO;2.

Chapter 3

Materials and methods

3 Materials and methods

3.1 Sediment cores and sampling

Paleo-climatological analyses during this thesis have been focused on two marine sediment cores: GeoB5901-2 from the Gulf of Cádiz (36°22.80´ N, 7°04.28´ W) and ODP-161-976A from the Alboran Sea (36°12.32´ N, 4°18.76´ W) (Fig 3.1).

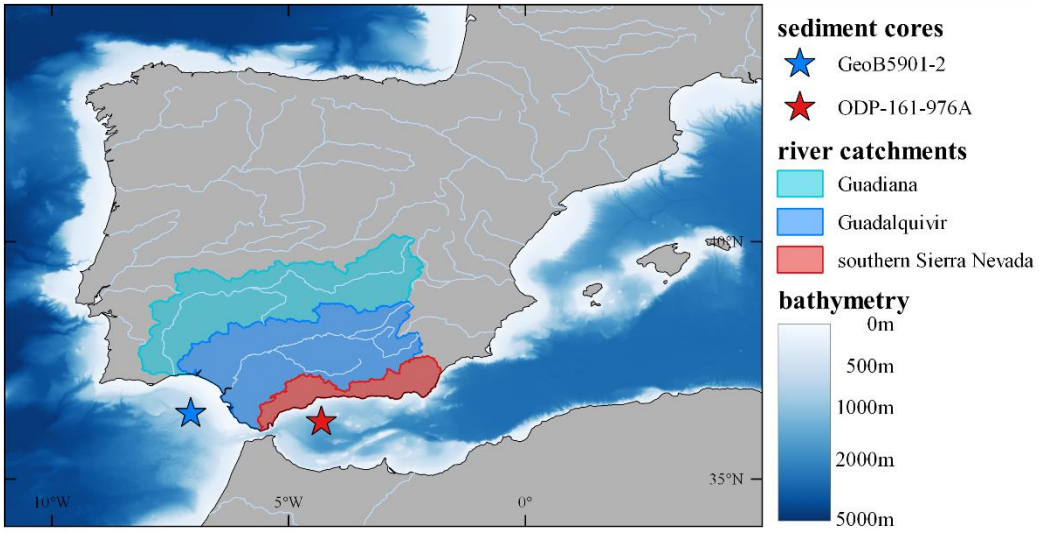

Figure 3.1 Core locations. *The core locations of GeoB5901-2 (blue star) and ODP-161-976A (red star) are indicated. Also, river catchments of the Guadiana (light blue shading), the Guadalquivir (blue shading), and catchments of various smaller rivers from the southern Sierra Nevada (red shading) are shown. Bathymetric data was obtained from the GEBCO bathymetric database [GEBCO Bathymetric Compilation Group, 2019].*

Sediment core GeoB5901-2 was retrieved from 574 m water depth during METEOR cruise M45 in 1999 [*Schott et al.*, 2000]. The recovery of the sediment core, containing undisturbed hemipelagic mud, was 3.26 m. The upper 1.50 m have been sampled at the GeoB Core Repository at MARUM, Bremen (Germany). Here, the upper 50 cm were sampled at 0.5 cm resolution, whereas the lower part down to 150 cm has been sampled on 1.0 cm resolution. Each sample was split into two separate parts for geochemical and planktonic foraminiferal analysis. Subsamples used for geochemical analysis have been freeze-dried at the Institute of Geosciences, Kiel University (Germany).

Sediment core ODP-161-976A was retrieved from 1108 m water depth during JOIDES RESOLUTION cruise Leg 161 in 1995 [*Comas et al.*, 1996]. The total recovery was 5.92 m. For this thesis the section between 100.0 and 149.0 cm have been continuously sampled at 0.5 cm resolution at the IODP Core Repository at MARUM, Bremen (Germany). Again,

subsamples used for geochemical analysis have been freeze-dried at the Institute of Geosciences, Kiel University (Germany). The analysed section consists of clayey and silty sediments. These appear slightly bioturbated, but no major depositional event (e.g. turbidite) or hiatus has been recognized.

3.2 Radiocarbon dating and age model

3.2.1 Radiocarbon dating

In order to improve and refine already existing age models for sediment core GeoB5901-2 [*Kim et al.*, 2004] and ODP-161-976A [*Combourieu Nebout et al.*, 2002], additional AMS (Accelerated Mass Spectrometry) ^{14}C dating was carried out on both sediment cores (Tab 3.1). All samples (including the existing ones) have been dated at the Leibniz Laboratory for Radiometric Dating and Stable Isotope Research at Kiel University (Germany).

Planktonic foraminifera for radiocarbon dating have been sampled by M. Weinelt. Each sample contained between 150 and 300 specimens of either *Globigerinoides ruber* (white and pink morphotypes) or *Globigerina bulloides*. Only specimens larger than 150 µm have been sampled. For sediment core GeoB5901-2 13 new samples have been radiocarbon dated. Altogether, the final age model is based on 19 radiocarbon dates during the last 8000 years including already existing ones from *Kim et al.* [2004] (Tab 3.1). No newly dated sample had to be rejected due to an age reversal. For sediment core ODP-161-976A 11 new radiocarbon dates have been accomplished. Since one sample at 100.25 cm had be to rejected due to an age reversal, the final age model for the last 8000 years is based on overall 13 age control points including the ones from *Combourieu Nebout et al.* [2002] (Tab 3.1).

Usually, the preferred species for radiometric dating was *G. ruber* (w+p) since it lives in the upper 10 m of the water column [*Lombard et al.*, 2011] and, thus, is hardly affected by intermediate or deep water masses containing aged carbon [*Hall et al.*, 2010; *Skinner et al.*, 2017]. The quality of radiocarbon dates from this species is validated by the good alinement with previous dates by *Kim et al.* [2004], which are based on a mix of planktonic foraminiferal species (Fig 3.2). But, for sediment core ODP-161-976A a big shift of about 700 years compared to the previous age model of *Combourieu Nebout et al.* [2002] was noticed. Planktonic foraminiferal samples dated by *Combourieu Nebout et al.* [2002] consists exclusively of *G. bulloides.* In order to validate the new radiocarbon dates based on *G. ruber* (w+p), additional samples containing *G. bulloides* from the same depth levels (120.25 and

132.75 cm) or similar depth levels (116.25 cm) have been radiocarbon dated. Overall, the radiocarbon dates of *G. bulloides* samples verified the previous dates based on *G. ruber* (w+p) (Tab 3.1).

Table 3.1 Results of the radiocarbon dating.

lab ID	depth (cm)	material	radiocarbon age (yrs BP)	error (yrs)	reference
			GeoB5901-2		
KIA-14522	2.00	planktonic mix	1840	±35	*Kim et al.* [2004]
KIA-53006	8.25	*G. ruber* (w+p)	2485	±25	*Schirrmacher et al.* [2019]
KIA-54011	9.25	*G. ruber* (w+p)	2833	±26	*Schirrmacher et al.* [2020]
KIA-53005	12.25	*G. ruber* (w+p)	3185	±27	*Schirrmacher et al.* [2019]
KIA-53002	14.75	*G. ruber* (w+p)	3545	±26	*Schirrmacher et al.* [2019]
KIA-14521	16.00	planktonic mix	3685	±35	*Kim et al.* [2004]
KIA-53003	16.75	*G. ruber* (w+p)	3789	±27	*Schirrmacher et al.* [2019]
KIA-53004	18.25	*G. ruber* (w+p)	3852	±27	*Schirrmacher et al.* [2019]
KIA-54012	20.75	*G. ruber* (w+p)	4138	±29	*Schirrmacher et al.* [2020]
KIA-54013	21.25	*G. ruber* (w+p)	4225	±28	*Schirrmacher et al.* [2020]
KIA-54014	21.75	*G. ruber* (w+p)	4384	±28	*Schirrmacher et al.* [2020]
KIA-14520	24.00	planktonic mix	4500	±40	*Kim et al.* [2004]
KIA-52665	26.25	*G. ruber* (w+p)	4820	±35	*Schirrmacher et al.* [2019]
KIA-14518	30.00	planktonic mix	5035	±40	*Kim et al.* [2004]
KIA-52666	30.75	*G. ruber* (w+p)	5130	±40	*Schirrmacher et al.* [2019]
KIA-54015	31.25	*G. ruber* (w+p)	5139	±29	*Schirrmacher et al.* [2020]
KIA-54016	49.75	*G. ruber* (w+p)	5680	±35	*Schirrmacher et al.* [2020]
KIA-14516	90.00	planktonic mix	7035	±55	*Kim et al.* [2004]
KIA-13704	120.00	planktonic mix	7495	±50	*Kim et al.* [2004]
			ODP-161-976A		
KIA-6435	61.00	*G. bulloides*	1710	±40	*Combourieu Nebout et al.* [2002]
KIA-54017*	100.25	*G. ruber* (w+p)	3930	±40	*Schirrmacher et al.* [2020]
KIA-6436	103.00	*G. bulloides*	3235	±30	*Combourieu Nebout et al.* [2002]
KIA-54210	108.75	*G. ruber* (w+p)	3590	±35	*Schirrmacher et al.* [2020]
KIA-54211	110.25	*G. ruber* w + p	3680	±30	*Schirrmacher et al.* [2020]
KIA-53326	116.25	*G. bulloides*	4435	±35	*Schirrmacher et al.* [2019]
KIA-54018	116.75	*G. ruber* (w+p)	4565	±35	*Schirrmacher et al.* [2020]
KIA-53235	120.25	*G. ruber* (w+p)	4435	±30	*Schirrmacher et al.* [2019]
KIA-53327	120.25	*G. bulloides*	4480	±40	*Schirrmacher et al.* [2019]
KIA-53236	124.75	*G. ruber* (w+p)	4435	±35	*Schirrmacher et al.* [2019]
KIA-53234	132.75	*G. ruber* (w+p)	4650	±35	*Schirrmacher et al.* [2019]
KIA-53325	132.75	*G. bulloides*	4700	±50	*Schirrmacher et al.* [2019]
KIA-54019	148.25	*G. ruber* (w+p)	5350	±55	*Schirrmacher et al.* [2020]
KIA-6437	214.00	*G. bulloides*	7010	±50	*Combourieu Nebout et al.* [2002]

** date not considered for the final age model due to an age reversal*

3.2.2 Age models

The final age models of both sediment cores (Fig 3.2) have been calculated using the Bacon package [*Blaauw and Christen*, 2011] in the R programming language [*R Core Team*, 2019]. All radiocarbon dates have been calibrated using the marine calibration curve (Marine13) [*Reimer et al.*, 2013] including the global average reservoir effect of 400 years. No local reservoir effect (ΔR) has been considered. For both sediment cores the default settings have

been used with the exception of the mean assumed accumulation rate (acc.mean), which has been set to 50 yrs/cm. Furthermore, a "boundary" at 30 cm depth was assumed for GeoB5901-2, since the accumulation rate changes significantly at this depth (Fig 3.2).

According to the final age model, the sedimentation rate of GeoB5901-2 varies between 2.7 and 41.7 cm/kyr with an average of 13.5 cm/kyr. Sedimentation rate in ODP-161-976A is on average 28.0 cm/kyr and varies between 4.5 and 62.5 cm/kyr. Thus, the average temporal resolution of the analysed sections of GeoB5901-2 and ODP-161-976A are 75 and 30 years per sample, respectively.

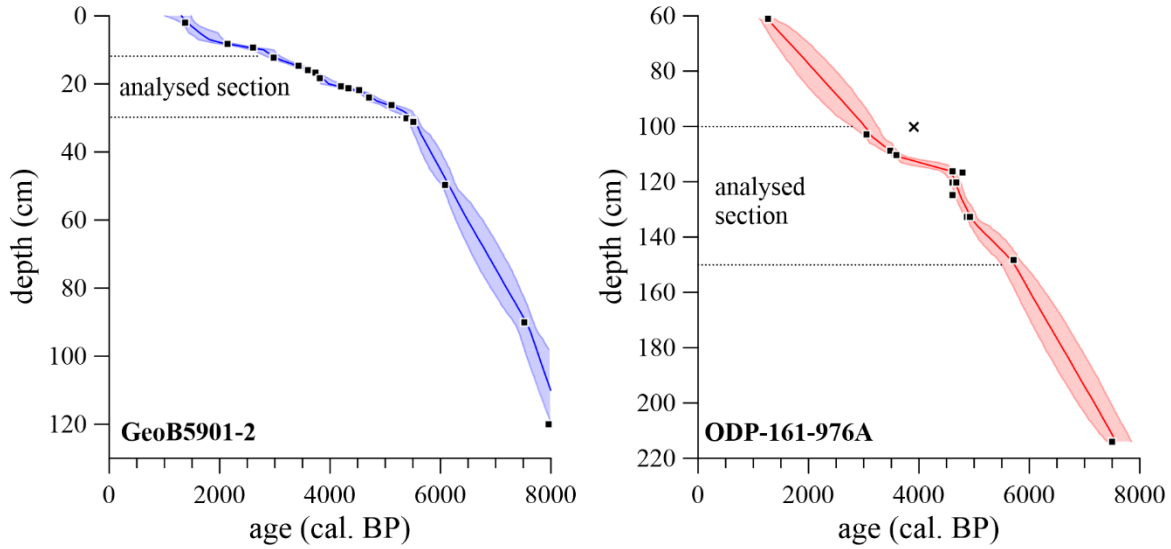

Figure 3.2 Age models. *The final age models of sediment cores GeoB5901-2 (left) and ODP-161-976A (right) of the last 8000 cal. BP are shown. Blue and red shaded areas display the probability (0.95) of each age model. Black squares denote the age control points. The cross marks the rejected age control point of ODP-161-976A. Dotted lines encompass the sections analysed with geochemical methods during this thesis.*

3.3 n-alkane biomarkers

3.3.1 Introduction

n-Alkanes are saturated hydrocarbons of varying chain length, part of which are synthesized as leaf waxes by higher terrestrial plants including grasses, shrubs, and trees in order to protect themselves against water loss due to transpiration [*Eglinton and Hamilton*, 1967]. Biogenic *n*-alkane distributions show a strong odd over even dominance [*Eglinton and Hamilton*, 1967]. Higher terrestrial plants typically synthesize long-chain *n*-alkanes of more than 25 carbon atoms (*n*-C_{27} – *n*-C_{35}) and, thus, can be discriminated from submerged aquatic macrophytes (*n*-C_{23} –

n-C_{25}) and algae (*n*-C_{17} – *n*-C_{21}) [*Castañeda and Schouten*, 2011; *Cranwell et al.*, 1987; *Ficken et al.*, 2000].

The *n*-alkanes from higher terrestrial plants can be either eroded by wind directly from the leaf surface or they are deposited in the soils [*Rogge et al.*, 1993]. Subsequently, *n*-alkanes are removed from the atmosphere or eroded from the soils by precipitation and are further transported by rivers into the marine environment [*Eglinton and Eglinton*, 2008; *Nelson et al.*, 2018; *Schreuder et al.*, 2018]. Once deposited in the sediments, *n*-alkanes are preserved on geological time scales [*Logan et al.*, 1995].

Due to the known processes of *n*-alkane formation and transport, sedimentary *n*-alkanes contain various paleo-environmental information [*Diefendorf and Freimuth*, 2017]. For example, within the higher terrestrial plants it can be discriminated between trees dominantly synthesizing *n*-alkane homologues with 29 and 31 carbon atoms (*n*-C_{29} and *n*-C_{31}) and grasses typically dominated by the *n*-C_{33} homologue [*Bush and McInerney*, 2013; *Diefendorf and Freimuth*, 2017]. However, the amount of synthesized *n*-alkanes varies across plant functional types, but also across individual species. Generally, gymnosperms (e.g. *Pinus*) synthesize lower amounts of *n*-alkanes compared to angiosperms [*Bush and McInerney*, 2013; *Diefendorf and Freimuth*, 2017].

Nevertheless, the total amount of terrestrial sourced *n*-alkanes can provide qualitative information on the terrestrial input [e.g. *Cortina et al.*, 2016; *Jalali et al.*, 2016]. Moreover, molecular ratios such as the Average Chain Length (ACL) can be used to discriminate between plant functional types [*Herrmann et al.*, 2016; *Vogts et al.*, 2009] or as temperature/ humidity proxy [*Eley and Hren*, 2018; *Leider et al.*, 2013].

Further paleo-environmental information is provided by compound-specific carbon ($\delta^{13}C$) and hydrogen isotopic (δD) analysis of individual *n*-alkane homologues. Whereas, $\delta^{13}C$ data allows to differentiate between C3 and C4 plant functional types [*Diefendorf and Freimuth*, 2017], the δD signal gives information on hydrological parameters such as precipitation source, the amount of precipitation, and atmospheric temperature [*Sachse et al.*, 2012; *Wirth and Sessions*, 2016].

3.3.2 Extraction and quantification of n-alkanes

An illustrative overview of the analytical procedure is depicted in Figure 3.3. During the entire analytical work, all pipettes were rinsed three times with the respective solvent. Lipids were extracted from freeze-dried and finely ground sediment samples with an accelerated solvent

extractor (ASE-200, Dionex) using a 9:1 (v/v) mixture of dichloromethane (DCM) and methanol as solvent. Prior to extraction each extraction cell was filled with maximum 3 g of the sediment sample on top of silica. Finally, the cell was filled with silica until the top. The ASE-200 system was operated at a pressure of 100 bar and a temperature of 100 °C. After preheating the extraction cell for 2 minutes, the solvent was pumped into the cell and heated for 5 minutes. Afterwards pressure and temperature conditions were kept stable for another 5 minutes. Subsequently, the cell was flushed with 8 ml of the solvent. These steps were repeated once more. Finally, the cell was purged with N_2 gas for 90 s. After extraction, the sample was dried by rotary evaporation and stored in the freezer.

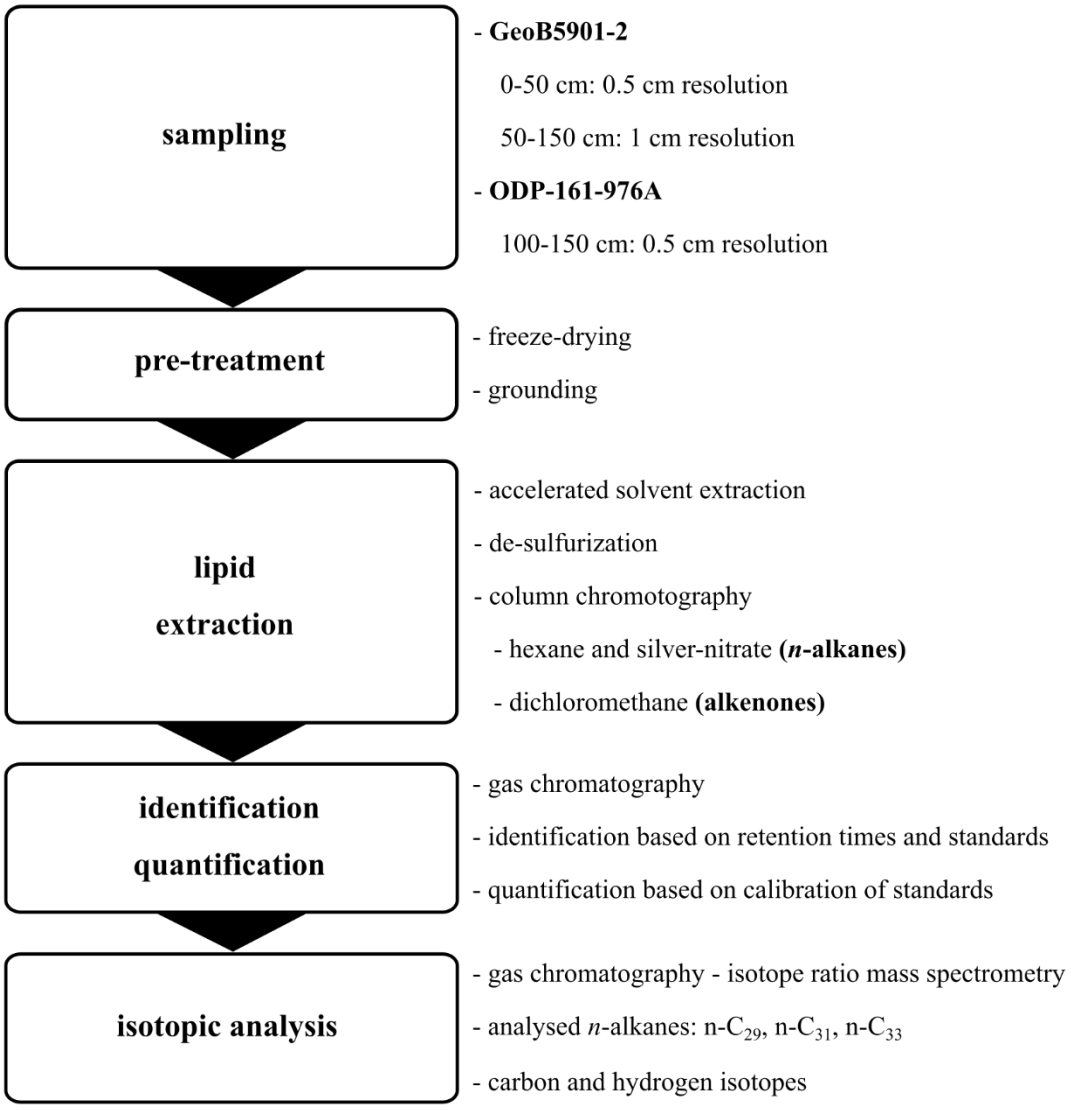

Figure 3.3 Workflow scheme. *Overview of the analytical procedure during geochemical analysis.*

Due to the overall low *n*-alkane concentrations within the sediment samples, all sample material was extracted. For GeoB5901-2 the total sample weight varies between 4.049 and 26.559 g, while ODP-161-976A samples range between 2.495 and 9.144 g (see Appendix). Because of the 3 g limit of the extraction cell, this results in up to 9 sub-samples, which were united prior to the de-sulfurization. To remove elemental sulfur from the samples, 2g of copper chips were activated with 15 ml of hydrochloric acid (HCl) (30% concentrated). These were stirred for 5 minutes using a Promax2020. Afterwards, the copper chips were neutralized using ten times 5 ml of destilled water, four times 5 ml of methanol, and five times 5 ml of DCM. Subsequently, each evaporated sample was rinsed into the activated copper using 10 ml DCM. Again, samples were stirred for 30 minutes on the Promax2020. Finally, the samples were moved into a separate vial and the solvent was removed by rotary evaporation.

In order to extract the *n*-alkanes from the de-sulfured sample, column chromatography was applied. The column was filled with 550 ng of activated silica gel (4 h at 450 °C) with a mesh size of 140 to 230. *n*-Alkanes were extracted by rinsing the sample vial with 10 ml of hexane onto the column. Afterwards, the samples were additionally given onto another column filled with 0.4 g of silver-nitrate ($AgNO_3$) impregnated silica gel (230 mesh) in order to remove aromatic and double-bonded compounds. Finally, the *n*-alkane containing sample was dried via rotary evaporation.

Before the measurement, the sample was rinsed with 100 µl hexane into a vial used for gas chromatography (GC) and kept at room temperature for 24 hours for homogenisation. *n*-Alkanes were analysed using an Agilent 6890N gas chromatograph equipped with a programmed temperature vaporizer (PTV) injector, a Restek XTI-5 capillary column (30 m x 320 µm x 0.25 µm) and a flame ionization detector (FID) at the Institute of Geosciences, Kiel University (Germany). The gas flow (helium) was held constant at 2.7 ml per minute. The PTV injector operated in splitless mode and rapidly heated from 70 °C to 330 °C. The GC oven temperature was increased by 10 °C per minute starting at 50 °C until 300 °C, which was kept for 10 minutes. Subsequently, the oven was heated up to 330 °C within a minute and, again, kept stable for another 10 minutes. Following this procedure, every sample was analysed 3 times.

Identification of the individual *n*-alkane homologues was based on their retention times by comparing with an internal standard containing eight *n*-alkane homologues (*n*-C_{18}, *n*-C_{20}, *n*-C_{24}, *n*-C_{28}, *n*-C_{32}, *n*-C_{36}, *n*-C_{38}, and *n*-C_{40}) of known concentration. Based on a peak area/

concentration calibration of the internal standard, the *n*-alkane concentrations of the samples were calculated.

3.3.3 Calculation of molecular proxies

In order to get *n*-alkane-based proxies sensitive to paleo-ecological and paleo-climatological changes, widely accepted concentrations and ratios of specific *n*-alkane homologues have been calculated. Relative changes of the input of terrestrial material into the marine realm can be investigated through the sum of long-chain *n*-alkanes of terrestrial source [e.g. *Cortina et al.*, 2016; *Jalali et al.*, 2016]. Here, the total concentration of chosen odd-numbered long-chain *n*-alkane homologues have been calculated after:

$$n\text{-}C_{27\text{-}33}\,(\text{ng/ g sediment}) = n\text{-}C_{27} + n\text{-}C_{29} + n\text{-}C_{31} + n\text{-}C_{33} \quad (1)$$

with n-C_x being the concentration of each *n*-alkane homologue in ng per g sediment. The mean analytical error (2σ) is 7.0 ng per g sediment based on replicate analysis.

Instead of calculating an ACL of the samples, the chain length distribution was evaluated with the Norm33 ratio [e.g. *Herrmann et al.*, 2016] after:

$$\text{Norm33} = n\text{-}C_{33} / (n\text{-}C_{29} + n\text{-}C_{33}) \quad (2)$$

with n-C_x being the peak area of the respective *n*-alkane homologue in the chromatogram. The mean analytical error (2σ) is 0.004 based on replicate analysis. This ratio has proven to be a more sensitive parameter to vegetation change concerning tree and grass distribution or plant water stress [*García-Alix et al.*, 2017].

3.3.4 Compound-specific hydrogen and carbon isotopic analysis

Following the *n*-alkane quantification, $\delta^{13}C$ and δD isotopes of selected odd-numbered long-chain *n*-alkanes (n-C_{29}, n-C_{31}, and n-C_{33}) have been analysed by gas chromatography – isotope ratio mass spectrometry (GC-IRMS) (Fig 3.3). Analysis were carried out at the Leibniz Laboratory for Radiometric Dating and Stable Isotope Research, Kiel University (Germany). The analytical setup consisted of an Agilent 6890 GC equipped with a Gerstel KAS 4 PTV injector and an Agilent DB-5 capillary column (30 m x 250 µm x 0.25 µm). This system was coupled to Thermo Scientific MAT 253 IRMS via a combustion interface and a pyrolysis oven. Depending on the *n*-alkane concentration, between 5 and 30 µl of each sample has been injected 2-4 times. The PTV injector was operated in split mode with solvent venting and its temperature increased from 30 °C rapidly to 600 °C. The gas flow (helium) was held constant at 2.0 ml per minute. The GC oven increased from 50 °C to 180 °C at 40 °C per minute, then to 300 °C at

20 °C per minute, and finally to 320 °C at 10 °C per minute where it was held constant for 15 minutes. The pyrolysis oven was operated at 1450 °C and the combustion unit at 940 °C, respectively. The δD and $\delta^{13}C$ values are reported relative to Vienna Standard Mean Ocean Water (‰ VSMOW) and Vienna Pee Dee Belemnite (‰ VPDB) scales, respectively. Long-term measurements of internal *n*-alkane standards yielded an analytical precision of ±3.0 ‰ for δD and ±0.3 ‰ for $\delta^{13}C$.

3.4 Alkenone biomarkers

3.4.1 Introduction

Alkenones are long-chain methyl ketones with 37 carbon atoms with a varying number of double-bonds, which are produced by haptophytic algae (Fig 3.4). The most abundant and distributed haptophytic algae in the marine realm, and thus the main alkenone producer, is the coccolithophore *Emiliania huxleyi* (Fig 3.4). *E. huxleyi* and other less abundant species live within the mixed layer near the sea surface [*Herbert*, 2014; *Kucera*, 2009]. In the Western Mediterranean, the highest density of coccolithophores is observed within the upper 50 m of the water column [*Oviedo et al.*, 2015]. Nonetheless, it has been shown that coccolithophores produce alkenones generally near the sea surface at 5 m depth [*Hamanaka et al.*, 2000].

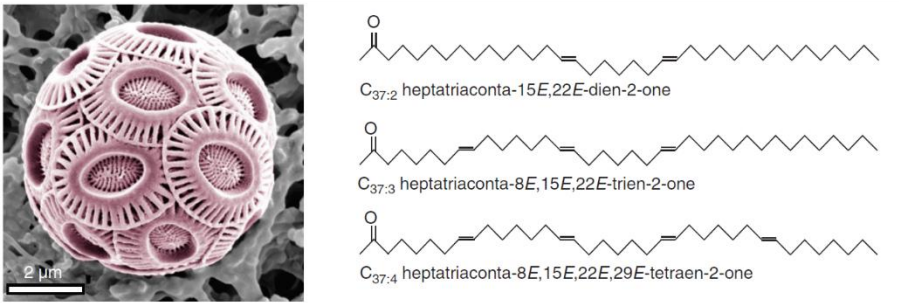

Figure 3.4 Alkenone producing coccolithophore. *On the left, a scanning electron micrograph of the species Emiliania huxleyi is shown. On the right, the three alkenone homologues are displayed. The picture was taken from Kucera [2009].*

Alkenones typically record a variety of paleo-environmental information. Since alkenones are produced constantly at high abundances by marine haptophytic algae, the most obvious paleo-environmental information they contain is a record of marine primary productivity (MPP) [*Prahl et al.*, 1988]. The more alkenones are produced, the more coccolithophores have been

present indicative of elevated MPP. But the most widespread application in paleo-climatology is the use of alkenones as paleo-thermometry of sea surface temperatures (SSTs) [e.g. *Cacho et al.*, 2001; *Jalali et al.*, 2016; *Martrat et al.*, 2007]. This application is based on the fact that the amount of alkenones with two double bonds ($C_{37:2}$) increases with increasing temperatures in relation to the homologues with three ($C_{37:3}$) or four double-bonds ($C_{37:4}$) and *vice versa* [*Prahl et al.*, 1988]. Based on this relationship, a number of SST calibrations emerged (see chapter 3.4.3). Related to the SST relationship of the alkenones, the $C_{37:4}$ homologue is usually restricted to cold polar waters [*Rosell-Melé et al.*, 1994]. In those regions, the amount of the $C_{37:4}$ homologue is also considered to record changes in sea surface salinity [*Chivall et al.*, 2014; *Rosell-Melé*, 1998].

3.4.2 Extraction and quantification of alkenones

The alkenones have been extracted parallel to the *n*-alkanes (described in chapter 3.3.2). Thus, the pre-treatment, liquid extraction with the accelerated solvent extractor, and the de-sulfurization was the same (Fig 3.3). After separating the *n*-alkanes with hexane during column chromatography, the alkenones were extracted into a separate vial using 10 ml of DCM. After drying the samples by rotary evaporation, the samples were diluted in 200 to 1500 µl DCM depending on the initial sample weight. Alkenones have subsequently been measured by multi-dimensional double gas column chromatography (MD-GC). The setup consisted of two Agilent 6890 GC systems, each one equipped with a FID and connected via a transfer line. The first GC was equipped with a Restek RXT-1 column and the second GC system with a Restek RTX-200 column. Both GCs were operated at different temperature programs. At the first one, temperatures increased at 15 °C per minute from 100 to 330 °C. The second oven increases its temperature stepwise from 0 to 100 °C, then to 210 °C at 15 °C per minute, where the temperature was kept stable for 10 minutes. Subsequently, the temperature increased by 5 °C per minute to 290 °C, where it was maintained again for 5 minutes. Finally, the temperature was increased to 330 °C. The part of the sample containing the alkenones was identified through the retention time and was then passed through a Dean Switch system into the second GC system. Quantification of the alkenone homologues was achieved through comparison of the peak areas in the chromatogram with internal standards (cholestane and hexatriacontane).

3.4.3 Calculation of paleo-environmental proxies

In order to analyse changes in MPP, the sum of the concentration of the individual compounds ($C_{37:2}$ and $C_{37:3}$) has been calculated after:

$$\sum C_{37}\ (\text{ng/ g sediment}) = C_{37:2\ conc} + C_{37:3\ conc} \quad (3)$$

with $C_{37:x\ conc}$ being the concentration of the respective alkenone homologue. The $C_{37:4}$ alkenone homologue has not been observed in the studied samples. Based on replicate analysis the mean analytical error (2σ) is 6.9 ng per g sediment.

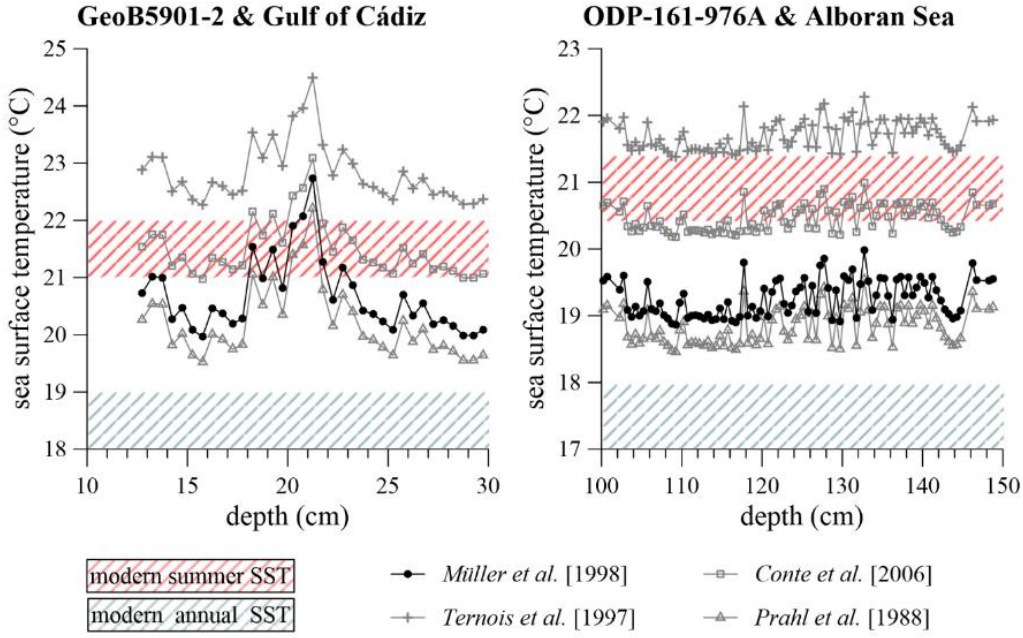

Figure 3.5 Sea surface temperature calibrations. *Chosen SST calibrations applied to alkenone data from sediment core GeoB5901-2 in the Gulf of Cádiz (left) and ODP-161-976A in the Alboran Sea (right). Red hatched areas indicate the modern mean summer SST in the respective oceanic basin, while green hatched areas display the modern mean annual SST. Black circles show the chosen global core-top calibration [Müller et al., 1998], grey crosses show Mediterranean sediment trap calibration [Ternois et al., 1997], grey squares indicate global surface water calibration [Conte et al., 2006], and grey triangles show a calibration based on cultures of E. huxleyi [Prahl et al., 1988].*

The SST of alkenone samples is typically studied through a relationship of the individual homologues. In this thesis the alkenone unsaturation index proposed by *Prahl and Wakeham* [1987] was applied:

$$U_{37}^{K'} = C_{37:2} / (C_{37:2} + C_{37:3}) \quad (4)$$

with $C_{37:x}$ being the peak area of the respective compound in the chromatogram. This unsaturation index can be transferred into SST by various calibrations. Several calibrations have been compared with the modern SST ranges in the Gulf of Cádiz and the Alboran Sea (Fig 3.5). Finally, the calibration of *Müller et al.* [1998] was chosen because it matches modern conditions best and, further, enables optimal comparison to other alkenone-based SST records since most of them applied the same calibration.

$$SST\ (°C) = (U^{K'}_{37} - 0.044)/\ 0.033 \quad (5)$$

The analytical error translates into 0.12 °C, while the error of the calibration is 1.5 °C. SSTs based on the calibration of *Müller et al.* [1998] refer to annual mean conditions and are valid for the 0 to 29 °C temperature range at a latitudinal range of 60 °N to 60 °S.

3.5 References

Blaauw, M., and J. A. Christen (2011), Flexible paleoclimate age-depth models using an autoregressive gamma process, *Bayesian Anal.*, *6*(3), 457–474, doi:10.1214/11-BA618.

Bush, R. T., and F. A. McInerney (2013), Leaf wax n-alkane distributions in and across modern plants: Implications for paleoecology and chemotaxonomy, *Geochimica et Cosmochimica Acta*, *117*, 161–179, doi:10.1016/j.gca.2013.04.016.

Cacho, I., J. O. Grimalt, M. Canals, L. Sbaffi, N. J. Shackleton, J. Schönfeld, and R. Zahn (2001), Variability of the western Mediterranean Sea surface temperature during the last 25,000 years and its connection with the Northern Hemisphere climatic changes, *Paleoceanography*, *16*(1), 40–52, doi:10.1029/2000PA000502.

Castañeda, I. S., and S. Schouten (2011), A review of molecular organic proxies for examining modern and ancient lacustrine environments, *Quaternary Science Reviews*, *30*(21-22), 2851–2891, doi:10.1016/j.quascirev.2011.07.009.

Chivall, D., D. M'Boule, D. Sinke-Schoen, J. S. Sinninghe Damsté, S. Schouten, and M. T.J. van der Meer (2014), Impact of salinity and growth phase on alkenone distributions in coastal haptophytes, *Organic Geochemistry*, *67*, 31–34, doi:10.1016/j.orggeochem.2013.12.002.

Comas, M. C., R. Zahn, and A. Klaus (Eds.) (1996), *Proceedings of the Ocean Drilling Program, 161 Initial Reports*, *Proceedings of the Ocean Drilling Program*, vol. 161, Ocean Drilling Program.

Combourieu Nebout, N., J. L. Turon, R. Zahn, L. Capotondi, L. Londeix, and K. Pahnke (2002), Enhanced aridity and atmospheric high-pressure stability over the western Mediterranean during the North Atlantic cold events of the past 50 k.y, *Geol*, *30*(10), 863, doi:10.1130/0091-7613(2002)030<0863:EAAAHP>2.0.CO;2.

Conte, M. H., M.-A. Sicre, C. Rühlemann, J. C. Weber, S. Schulte, D. Schulz-Bull, and T. Blanz (2006), Global temperature calibration of the alkenone unsaturation index (U K′37) in surface waters and comparison with surface sediments, *Geochem. Geophys. Geosyst.*, *7*(2), n/a-n/a, doi:10.1029/2005GC001054.

Cortina, A., J. O. Grimalt, A. Rigual-Hernández, A.-M. Ballegeer, B. Martrat, F. J. Sierro, and J. A. Flores (2016), The impact of ice-sheet dynamics in western Mediterranean environmental conditions during Terminations. An approach based on terrestrial long chain n-alkanes deposited in the upper slope of the Gulf of Lions, *Chemical Geology*, *430*, 21–33, doi:10.1016/j.chemgeo.2016.03.015.

Cranwell, P. A., G. Eglinton, and N. Robinson (1987), Lipids of aquatic organisms as potential contributors to lacustrine sediments—II, *Organic Geochemistry*, *11*(6), 513–527, doi:10.1016/0146-6380(87)90007-6.

Diefendorf, A. F., and E. J. Freimuth (2017), Extracting the most from terrestrial plant-derived n-alkyl lipids and their carbon isotopes from the sedimentary record: A review, *Organic Geochemistry*, *103*, 1–21, doi:10.1016/j.orggeochem.2016.10.016.

Eglinton, G., and R. J. Hamilton (1967), Leaf Epicuticular Waxes, *Science*, *156*(3780), 1322–1335, doi:10.1126/science.156.3780.1322.

Eglinton, T. I., and G. Eglinton (2008), Molecular proxies for paleoclimatology, *Earth and Planetary Science Letters*, *275*(1-2), 1–16, doi:10.1016/j.epsl.2008.07.012.

Eley, Y. L., and M. T. Hren (2018), Reconstructing vapor pressure deficit from leaf wax lipid molecular distributions, *Scientific reports*, *8*(1), 3967, doi:10.1038/s41598-018-21959-w.

Ficken, K. J., B. Li, D. L. Swain, and G. Eglinton (2000), An n-alkane proxy for the sedimentary input of submerged/floating freshwater aquatic macrophytes, *Organic Geochemistry*, *31*(7-8), 745–749, doi:10.1016/S0146-6380(00)00081-4.

García-Alix, A., F. J. Jiménez-Espejo, J. L. Toney, G. Jiménez-Moreno, M. J. Ramos-Román, R. S. Anderson, P. Ruano, I. Queralt, A. Delgado Huertas, and J. Kuroda (2017), Alpine bogs of southern Spain show human-induced environmental change superimposed on long-term natural variations, *Scientific reports*, *7*(1), 7439, doi:10.1038/s41598-017-07854-w.

GEBCO Bathymetric Compilation Group (2019), *The GEBCO_2019 Grid - a continuous terrain model of the global oceans and land.*, British Oceanographic Data Centre, National Oceanography Centre, NERC, UK.

Hall, B. L., G. M. Henderson, C. Baroni, and T. B. Kellogg (2010), Constant Holocene Southern-Ocean 14C reservoir ages and ice-shelf flow rates, *Earth and Planetary Science Letters*, *296*(1-2), 115–123, doi:10.1016/j.epsl.2010.04.054.

Hamanaka, J., K. Sawada, and E. Tanoue (2000), Production rates of C 37 alkenones determined by 13 C-labeling technique in the euphotic zone of Sagami Bay, Japan, *Organic Geochemistry*, *31*(11), 1095–1102, doi:10.1016/S0146-6380(00)00118-2.

Herbert, T. D. (2014), Alkenone Paleotemperature Determinations, in *Treatise on geochemistry*, 2nd ed., edited by H. D. Holland, pp. 399–433, Elsevier, Amsterdam.

Herrmann, N., A. Boom, A. S. Carr, B. M. Chase, R. Granger, A. Hahn, M. Zabel, and E. Schefuß (2016), Sources, transport and deposition of terrestrial organic material: A case study from southwestern Africa, *Quaternary Science Reviews*, *149*, 215–229, doi:10.1016/j.quascirev.2016.07.028.

Jalali, B., M.-A. Sicre, M.-A. Bassetti, and N. Kallel (2016), Holocene climate variability in the North-Western Mediterranean Sea (Gulf of Lions), *Climate of the Past*, *12*(1), 91–101, doi:10.5194/cp-12-91-2016.

Kim, J.-H., N. Rimbu, S. J. Lorenz, G. Lohmann, S.-I. Nam, S. Schouten, C. Rühlemann, and R. R. Schneider (2004), North Pacific and North Atlantic sea-surface temperature variability during the Holocene, *Quaternary Science Reviews*, *23*(20-22), 2141–2154, doi:10.1016/j.quascirev.2004.08.010.

Kucera, M. (2009), Determination of Past Sea Surface Temperatures, in *Encyclopedia of ocean sciences*, 2nd ed., edited by J. H. Steele, pp. 98–113, Elsevier, Amsterdam.

Leider, A., K.-U. Hinrichs, E. Schefuß, and G. J.M. Versteegh (2013), Distribution and stable isotopes of plant wax derived n-alkanes in lacustrine, fluvial and marine surface sediments along an Eastern Italian transect and their potential to reconstruct the hydrological cycle, *Geochimica et Cosmochimica Acta*, *117*, 16–32, doi:10.1016/j.gca.2013.04.018.

Logan, G. A., C. J. Smiley, and G. Eglinton (1995), Preservation of fossil leaf waxes in association with their source tissues, Clarkia, northern Idaho, USA, *Geochimica et Cosmochimica Acta*, *59*(4), 751–763, doi:10.1016/0016-7037(94)00362-P.

Lombard, F., L. Labeyrie, E. Michel, L. Bopp, E. Cortijo, S. Retailleau, H. Howa, and F. Jorissen (2011), Modelling planktic foraminifer growth and distribution using an ecophysiological multi-species approach, *Biogeosciences*, *8*(4), 853–873, doi:10.5194/bg-8-853-2011.

Martrat, B., J. O. Grimalt, N. J. Shackleton, L. de Abreu, M. A. Hutterli, and T. F. Stocker (2007), Four climate cycles of recurring deep and surface water destabilizations on the Iberian margin, *Science (New York, N.Y.)*, *317*(5837), 502–507, doi:10.1126/science.1139994.

Müller, P. J., G. Kirst, G. Ruhland, I. von Storch, and A. Rosell-Melé (1998), Calibration of the alkenone paleotemperature index $U^{K'}_{37}$ based on core-tops from the eastern South Atlantic and the global ocean (60°N-60°S), *Geochimica et Cosmochimica Acta*, *62*(10), 1757–1772, doi:10.1016/S0016-7037(98)00097-0.

Nelson, D. B., S. N. Ladd, C. J. Schubert, and A. Kahmen (2018), Rapid atmospheric transport and large-scale deposition of recently synthesized plant waxes, *Geochimica et Cosmochimica Acta*, *222*, 599–617, doi:10.1016/j.gca.2017.11.018.

Oviedo, A., P. Ziveri, M. Álvarez, and T. Tanhua (2015), Is coccolithophore distribution in the Mediterranean Sea related to seawater carbonate chemistry?, *Ocean Science*, *11*(1), 13–32, doi:10.5194/os-11-13-2015.

Prahl, F. G., L. A. Muehlhausen, and D. L. Zahnle (1988), Further evaluation of long-chain alkenones as indicators of paleoceanographic conditions, *Geochimica et Cosmochimica Acta*, *52*(9), 2303–2310, doi:10.1016/0016-7037(88)90132-9.

Prahl, F. G., and S. G. Wakeham (1987), Calibration of unsaturation patterns in long-chain ketone compositions for palaeotemperature assessment, *Nature*, *330*(6146), 367–369, doi:10.1038/330367a0.

R Core Team (2019), *R: A Language and Environment for Statistical Computing*, R Foundation for Statistical Computing, Vienna, Austria.

Reimer, P. J., E. Bard, A. Bayliss, J. W. Beck, P. G. Blackwell, C. B. Ramsey, C. E. Buck, H. Cheng, R. L. Edwards, M. Friedrich, P. M. Grootes, T. P. Guilderson, H. Haflidason, I. Hajdas, C. Hatté, T. J. Heaton, D. L. Hoffmann, A. G. Hogg, K. A. Hughen, K. F. Kaiser, B. Kromer, S. W. Manning, M. Niu, R. W. Reimer, D. A. Richards, E. M. Scott, J. R. Southon, R. A. Staff, C. S. M. Turney, and J. van der Plicht (2013), IntCal13 and Marine13 Radiocarbon Age Calibration Curves 0–50,000 Years cal BP, *Radiocarbon*, *55*(04), 1869–1887, doi:10.2458/azu_js_rc.55.16947.

Rogge, W. F., L. M. Hildemann, M. A. Mazurek, G. R. Cass, and B. R. T. Simoneit (1993), Sources of fine organic aerosol. 4. Particulate abrasion products from leaf surfaces of urban plants, *Environ. Sci. Technol.*, *27*(13), 2700–2711, doi:10.1021/es00049a008.

Rosell-Melé, A. (1998), Interhemispheric appraisal of the value of alkenone indices as temperature and salinity proxies in high-latitude locations, *Paleoceanography*, *13*(6), 694–703, doi:10.1029/98PA02355.

Rosell-Melé, A., J. Carter, and G. Eglinton (1994), Distributions of long-chain alkenones and alkyl alkenoates in marine surface sediments from the North East Atlantic, *Organic Geochemistry*, *22*(3-5), 501–509, doi:10.1016/0146-6380(94)90122-8.

Sachse, D., I. Billault, G. J. Bowen, Y. Chikaraishi, T. E. Dawson, S. J. Feakins, K. H. Freeman, C. R. Magill, F. A. McInerney, M. T.J. van der Meer, P. Polissar, R. J. Robins, J. P. Sachs, H.-L. Schmidt, A. L. Sessions, J. W.C. White, J. B. West, and A. Kahmen (2012), Molecular Paleohydrology: Interpreting the Hydrogen-Isotopic Composition of Lipid Biomarkers from Photosynthesizing Organisms, *Annual Review of Earth and Planetary Sciences*, *40*(1), 221–249, doi:10.1146/annurev-earth-042711-105535.

Schirrmacher, J., J. Kneisel, D. Knitter, W. Hamer, M. Hinz, R. R. Schneider, and M. Weinelt (2020), Spatial patterns of temperature, precipitation, and settlement dynamics on the Iberian Peninsula during the Chalcolithic and the Bronze Age, *Quaternary Science Reviews*, *233*, doi:10.1016/j.quascirev.2020.106220.

Schirrmacher, J., M. Weinelt, T. Blanz, N. Andersen, E. Salgueiro, and R. R. Schneider (2019), Multi-decadal atmospheric and marine climate variability in southern Iberia during the mid- to late-Holocene, *Clim. Past*, *15*(2), 617–634, doi:10.5194/cp-15-617-2019.

Schott, F., J. Meincke, G. Meinecke, S. Neuer, and W. Zenk (2000), North Atlantic 1999 - Cruise No. M45 - May 18 - November 4, 1999 - Malaga (Spain) - Las Palmas (Spain).

Schreuder, L. T., J.-B. W. Stuut, L. F. Korte, J. S. Sinninghe Damsté, and S. Schouten (2018), Aeolian transport and deposition of plant wax n -alkanes across the tropical North Atlantic Ocean, *Organic Geochemistry*, *115*, 113–123, doi:10.1016/j.orggeochem.2017.10.010.

Skinner, L. C., F. Primeau, E. Freeman, M. de La Fuente, P. A. Goodwin, J. Gottschalk, E. Huang, I. N. McCave, T. L. Noble, and A. E. Scrivner (2017), Radiocarbon constraints on the glacial ocean circulation and its impact on atmospheric CO2, *Nat Commun*, *8*(1), 1129, doi:10.1038/ncomms16010.

Ternois, Y., M.-A. Sicre, A. Boireau, M. H. Conte, and G. E (1997), Evaluation of long-chain alkenones as paleo-temperature indicators in the Mediterranean Sea, *Deep Sea Research Part I: Oceanographic Research Papers*, *44*(2), 271–286, doi:10.1016/S0967-0637(97)89915-3.

Vogts, A., H. Moossen, F. Rommerskirchen, and J. Rullkötter (2009), Distribution patterns and stable carbon isotopic composition of alkanes and alkan-1-ols from plant waxes of African rain forest and savanna C_3 species, *Organic Geochemistry*, *40*(10), 1037–1054, doi:10.1016/j.orggeochem.2009.07.011.

Wirth, S. B., and A. L. Sessions (2016), Plant-wax D/H ratios in the southern European Alps record multiple aspects of climate variability, *Quaternary Science Reviews*, *148*, 176–191, doi:10.1016/j.quascirev.2016.07.020.

Chapter 4

The Chalcolithic-Bronze Age transition in southern Iberia under the influence of the 4.2 ka BP event?

A correlation of climatological and demographic proxies

Martin Hinz, **Julien Schirrmacher**, Jutta Kneisel, Christoph Rinne, and Mara Weinelt, (2019): The Chalcolithic–Bronze Age transition in southern Iberia under the influence of the 4.2 ka BP event? A correlation of climatological and demographic proxies, JNA 21, 1–26, doi: 10.12766/jna.2019.1

Please note that this study relies on meanwhile updated age model of sediment core ODP-161-976A.
The formatting of the original article has been changed.
Spelling mistakes have been corrected.

4 The Chalcolithic–Bronze Age transition in southern Iberia under the influence of the 4.2 ka BP event? A correlation of climatological and demographic proxies

4.1 Abstract

The end of the third millennium BCE represents (not only) on the Iberian Peninsula the time of transition to the Bronze Age. At the same time this is the time of a general climatic event, the so-called 4.2 ka BP event, which can be observed (in different manifestations) in different regions of the northern hemisphere. By synchronizing cultural and climatic developments and above all by assessing demographic developments and their spatial development, a much-discussed connection between the two phenomena can be made plausible and opens the perspective for further, more detailed research on the interdependence between cultural, demographic and climatological processes. For this purpose, the results of aoristics, ^{14}C sum calibration and the evaluation of the concentration of long-chain *n*-alkane homologues of terrestrial origin as precipitation predictor are combined, their correlation is presented and possible responses are interpreted from the mapping of the settlement system development. This article provides an initial overview of the current results.

4.2 Introduction

The turn to the third millennium BCE on the Iberian Peninsula is a period of a dynamic development characterized by regional differences. It is mainly represented by the Copper Age and the transition to the Bronze Age.

In the last three decades, the Iberian Copper Age or Chalcolithic (ca. 3200 – 2200 cal. BCE) and the transition to the Bronze Age (ca. 2200 – 900 cal. BCE) was probably the most controversial period in the discourse on Iberian prehistory [*García Sanjuán and Murillo-Barosso*, 2013, *119*]. Key issues were early social stratification and state formation. The peninsula is indeed a good laboratory for the study of these phenomena [*Cruz Berrocal et al.*, 2013, *3*].

Research today is dominated above all by the narrative that economic activity and social inequality intensified during the Copper Age [*Chapman*, 1990; *Díaz-del-Río*, 2004; *García Sanjuán*, 1999; *Gilman*, 1987; *Hutado*, 1997], and that these tendencies would have been strongly reinforced in the course of the Early Bronze Age, especially in the south-eastern area

of the peninsula. In contrast, the other regions seem to show signs of disintegration and collapse at the time of transition and thereafter. This observation inevitably raises questions about demography and possible migration movements, which are currently increasingly discussed on the basis of aDNA analyses [*Günther et al.*, 2015; *Martiniano et al.*, 2017; *Szécsényi-Nagy et al.*, 2017; critical e.g. *Furholt*, 2018; *Vander Linden*, 2017]. From an archaeological point of view, this perspective has so far received relatively little critical appreciation [*García Rivero and Escacena Carrasco*, 2015; *Lillios*, 2015; *Lillios et al.*, 2016; contrary e.g. *Chapman*, 2008, *205*].

Following a general trend, the climatic changes on the Iberian Peninsula in connection with the 4.2 ka BP event have recently been examined in more detail, from an archaeological [*Cardoso*, 2005; *García et al.*, 2006; *Lillios*, 1997; *Lillios et al.*, 2016] and a natural science approach [*Carrión et al.*, 2007; *Jalut et al.*, 2009; *Magny et al.*, 2009; *Waterman et al.*, 2016]. The former approach often cannot argue with a local climate signal, the latter often lacks a connection to cultural-historical development. In addition, these are often small-scale studies that can hardly trace an overall development.

In general, human-environment relations have an important role in the archaeological interpretation on the Iberian Peninsula, especially against the background of the in part marginal conditions with regard to agricultural potential. However, a stable climatic situation was widely assumed [*Gilman and Thornes*, 1985], climate change and its relations to cultural changes have hardly been focused on so far, perhaps with the exception of the archaeology of the southeast of the peninsula. Climatic influences are also partly explicitly rejected there [*Risch et al.*, 2015].

4.2.1 The CRC Project

The Collaborative Research Centre (CRC) ’Scales of Transformation: Human-Environmental Interaction in Prehistoric and Archaic Societies’ of the German Research Foundation (DFG) investigates transformation processes in a key period of human history (15,000 to 1 BCE) in a long-term perspective.

Within the framework of the CRC, the subproject F1 ‘Supra-regional Crises: Abrupt Climate Change and Responses of (Multi-cultural) Ancient Societies in the Western Mediterranean Area and in Southern Central Europe around 4200 years BP’ investigates the interdependence between climatic and socio-cultural changes in connection with the 4.2 ka BP event.

The project aims to unravel complex socio-ecological transformation processes from a supra-regional and supra-cultural perspective and, in particular, to evaluate the role of abrupt climate

changes and socio-ecological crises in shaping archaeological transformations. In the first phase of this project (2016–2020), this will be done on the basis of two areas of activity in southern Portugal and south-western Spain. The temporal focus is on the time between 2700 and 1700 cal. BCE (4650–3650 BP) in order to cover the 4.2 ka BP event, but at the same time also the preconditions and the consequences of the archaeologically tangible change in the material culture and social configuration of the societies under consideration.

In the quantitative framework of our approach, scenarios of both climatic and social variables are quantitatively reconstructed in relation to the 4.2 ka BP event (i.e. time slices before, during and after the event). Time series of climate and population reconstructions will be produced on the basis of refined chronologies to assess the timing and extent of ecological and social changes and to evaluate the relationships between them. The magnitude of possible social, cultural and technological/innovative responses to these external constraints will be analysed. In the course of the project, archaeological variables reflecting transformation processes (indications of changes in material culture, subsistence and settlement patterns and social organization) are identified that indicate the susceptibility or resilience to external disturbances.

In two work packages, a broad approach is taken to obtain information on the role of archaeological and environmental variables. Both research areas will compile and process existing data from literature and regional archives in order to reconstruct scenarios of climate and social variables.

In the climatological part, climate change in connection with the 4.2 ka BP event in the western Mediterranean is reconstructed from marine archives relevant for the Iberian Peninsula. New high-resolution time series are created on the basis of multi-proxy reconstructions at key locations, e.g. in the Alboran Sea. In this way, the extent and speed of the hydro-climatic, temperature related and seasonal changes in connection with the 4.2 ka BP event can be quantitatively assessed. The precipitation estimates are derived from the *n*-alkane concentrations of the plant waxes. Since plant waxes are mainly introduced into the marine sediments via river systems and/or wind transport, the data on the catchment area of the river systems integrate and thus reconstruct the regional rather than the local climate.

The archaeological work package will examine the patterns of archaeological changes associated with the 4.2 ka BP event in the western Mediterranean and identify its possible links with Central Europe with the aim of quantitatively evaluating the intensity and extent of the transformations from the archaeological record. Information on settlements, architecture, material culture and archaeological data on the environment and subsistence is collected and

evaluated. These allow in particular quantitative proxy reconstructions for settlement patterns, continuity, population density and other derived variables such as the stability of a society, integration into exchange networks and changes in material culture at the regional level.

In the following, we would like to present some first results of our work. Here, we limit ourselves to the evaluation of supra-regionally available indicators. Aspects such as cultural changes based on material culture and individual site biographies also play a non-subordinate role in the project. These detailed studies will be presented elsewhere.

4.2.2 Presentation of the working area

In the first phase of the project underlying this contribution, on the study of human-environmental relations and the assessment of the climatic influence on socio-cultural development, the work focuses on two areas 1: southern Portugal including the Spanish borderland (catchment of river Tejo and Guadiana) and south-western Spain (catchment of river Guadalquivir). These two areas were selected because they have different trajectories from an archaeological point of view, and because they represent the catchment areas of the Guadiana and Guadalquivir river systems from a climatological perspective, for which the rainfall development is to be reconstructed with the help of plant waxes (*n*-alkanes).

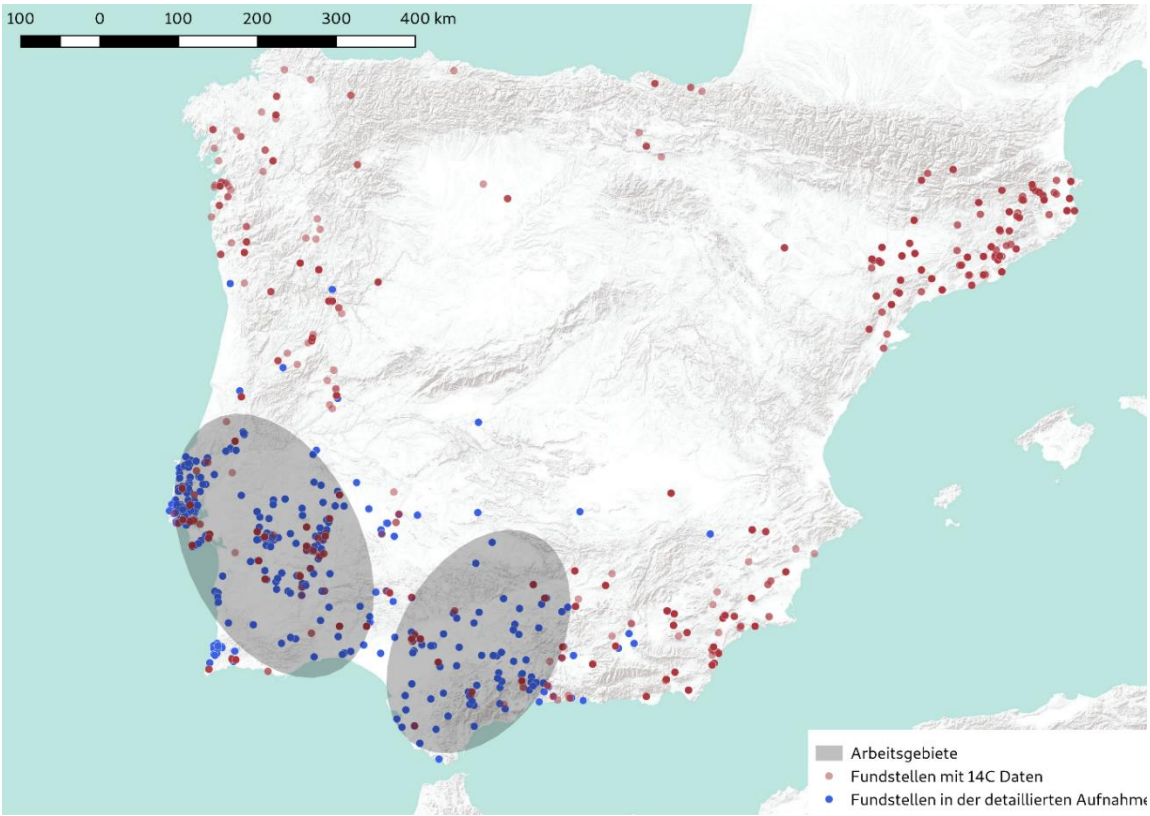

Figure 4.1 Map of the working areas

Today, the Mediterranean coastal regions are characterised by a dry to semi-arid climate, with some regions receiving less than 200 mm of precipitation per year [*Lionello et al.*, 2006]. The border areas of the Mediterranean, including the southern Iberian Peninsula, are therefore vulnerable to desertification and drought, and the climate has a strong impact on local society and economies. This is particularly true since the environment and the way of farming depend heavily on winter precipitation [*Lionello et al.*, 2006]. In general, the climate zones of the Middle and Late Holocene (from the 6th century BCE) in the Mediterranean region show a tendency towards gradual warming that is more pronounced in south-western Europe than in south-eastern Europe [*Davis et al.*, 2003], while the Atlantic region of medium latitude, including the Iberian margin, has an opposite trend.

Long-term Holocene tendencies were interrupted by short drought episodes [*Finné et al.*, 2011]. During the Holocene these episodes changed in frequency and character [*Fletcher et al.*, 2007]. The more serious of these episodes, including the 4.2 ka BP event, are probably related to the Bond cycles in the North Atlantic [e.g. *Bond et al.*, 1997; *Bond et al.*, 2001; *Marino et al.*, 2009] and are therefore considered to be driven and/or modulated by large-scale oceanic and atmospheric circulation changes. According to the current state of climate research, however, the Bond cycles themselves are probably not the actual, hitherto unknown trigger of the climatic shifts, more likely are changes in solar activity in connection with changes in atmospheric circulation and volcanic activities affecting a complex chaotic system [e.g. *Ruan et al.*, 2016; *Wanner et al.*, 2008].

4.2.3 The 4.2 ka BP event

The so-called 4.2 ka BP event represents an aridification event that probably lasted the entire 22nd century BCE (or longer) [*Magny et al.*, 2009; *Ruan et al.*, 2016]. This climate event marks the transition from the Middle to the Late Holocene and in many regions of the northern hemisphere also the beginning of almost modern (pre-industrial) climate and environmental conditions [*Walker et al.*, 2012]. It is often cited as an analogue of current socio-ecological change under rapid global warming [e.g. *Booth et al.*, 2005; *deMenocal*, 2001; *Riehl*, 2008], which poses a threat to social, economic, and environmental stability, and as a predictor for aggravating the existing problems of poverty, conflict, health, and escalating food and water shortages in crises [*IPCC*, 2013]. The 4.2 ka BP event at the transition from the Middle to the Late Holocene affected the climatic stability of the entire northern hemisphere.

The widespread accompaniment of major social upheavals and abrupt climate changes in geographically and culturally distant regions makes it plausible that the regional developments

of the 4.2 ka BP event are linked and reinforced by complex socio-ecological processes, including large-scale climate processes, social responses to changing environmental conditions, and internal social and intercultural processes. On the other hand, the emergence of early Bronze Age cultures throughout Europe can point to resistance strategies that enable transformation into new cultural phenomena and lay the foundations for later developments.

The abrupt onset of drought is considered to be one of the main causes of or at least in favour of widespread social instability in the monsoon area. The synchronicity of regionally related drought events is well limited at 4.2 – 4.1 ka BP. The effects affect large areas in Asia e.g. the Indus region [*Staubwasser et al.*, 2003], and Central China [*Wenxiang and Tungsheng*, 2004], Mesopotamia and North Africa [e.g. *deMenocal et al.*, 2000; *Kaniewski et al.*, 2017; *Ruan et al.*, 2016; *Welc and Marks*, 2014]. Recent high-resolution reconstructions using marine deuterium recordings [*Tierney and deMenocal*, 2013] and high-resolution terrestrial reconstructions of speleothems, paleo-river valleys, and sea levels have further narrowed the extent and magnitude of the dramatic monsoon failure [*Dixit et al.*, 2014], leading to massive changes in the precipitation rate [e.g. *Bar-Matthews et al.*, 1997; *Gupta et al.*, 2003].

In the Eastern Mediterranean and the Middle East, the 4.2 ka BP event manifests itself as an episode of barely 300 years (22nd to 19th century BCE) [e.g. *Weiss*, 2013], after a general long-term shift from humid to drier conditions [*Rohling and Rijk*, 1999].

Unfortunately, the available climate data sets of the Middle and Late Holocene in the Western Mediterranean mostly lack the multi-decadal resolution that is necessary to document a short episode of several hundred years in detail [*Weinelt et al.*, 2015]. Some speleothem data records [e.g. *Cruz et al.*, 2015] are exceptions. Accordingly, reconstructed patterns based on different proxies are still fragmentary and need to be revised to examine the potential extent of a supra-regional drought period in the Western Mediterranean.

On the south-eastern Iberian Peninsula and in the Mediterranean region of France, where pollen/terrestrial climate data are mainly available from the mountain ranges, an irreversible change in vegetation dates back to about 4.2 – 4.0 ka BP [e.g. *Brisset et al.*, 2013; *Carrión et al.*, 2003]. On the south-eastern Iberian Peninsula, from 4.2 ka BP an increase in fire events [*Jalut et al.*, 2000; *Jalut et al.*, 2009; *López-Sáez et al.*, 2014] accompanied the vegetation changes [*Carrión et al.*, 2003]. These changes were probably a consequence of the intensification of agriculture and/or the climate, whereby the climatological explanation is the more likely one [*Burjachs and Expósito*, 2015]. Dust layers of Sahara origin are described in the records of the Central Italian lakes and indicate prevailing southern wind directions at

4.2 ka BP [*Magri and Parra*, 2002]. In contrast to these indications of hotter and drier conditions, some marine records based on biomarker proxies suggest a cooling during the 4.2 ka BP event in the Alboran Sea [*Cacho et al.*, 2001].

Climate patterns and socio-ecological implications of the 4.2 ka BP event are well researched in the Eastern Mediterranean and the Middle East, especially in the area of written sources, which testify to a series of declines in early thriving and fast-growing societies that lead to 'collapses' under the influence of severe drought. By contrast, little is known about the impact and possible effects of this event on societies in the Western Mediterranean and possible long-term effects on Central Europe. Its role in the Late Neolithic/Chalcolithic and Early Bronze Age transformations at the transition to the Late Middle Holocene (Late Atlantic) is still to be explored.

4.2.4 Archaeological transformations

In the Western Mediterranean and Central Europe in general, a broad transition horizon from the Neolithic/Chalcolithic to the Bronze Age can be observed, which is reflected in an overwhelming amount of literature on the strong regional cultural changes that characterize this period (e.g. the Bell Beaker phenomenon). This transition is most often dated around 4.2 ka BP and indicates widespread and (within the dating accuracy) synchronous upheavals, so that a common trigger and mutual influences appear likely. However, despite striking convergence and coincidences, social change in Western and Central Europe has so far hardly been viewed from the perspective of a socio-ecological crisis on a supra-regional scale.

In the Mediterranean region in France [*Cauliez*, 2015], but also on the Greek mainland discontinuities and hiatuses are reported [*van Andel et al.*, 1990, *Fig 10*; *Maran*, 1998]. They give the impression that in large parts of Southern Europe with a formerly continuous development of several centuries settlements were abandoned towards the end of the 3rd millennium BCE.

On the Iberian Peninsula there is a significant transition working at different levels in temporal relation to the 4.2 ka BP event: the disappearance of the Chalcolithic and the emergence of new cultural units of the Early Bronze Age, changes in regional population, changes in settlement structures and patterns, in demography, in material culture, in subsistence and resource management, and in changes in social practices. This transition marks a period of increasing social complexity on the way to the development and hierarchisation of Bronze Age societies

[*Benítez de Lugo Enrich and Mejías*, 2017, *1933*; *Chapman*, 1982; *Chapman*, 1990; *Lull et al.*, 2014].

Although the respective natural conditions and cultural development can be very different locally, the Copper Age Iberian Peninsula can be roughly divided into two zones. In the north the human activities resulted in a significantly lower archaeological evidence and must therefore also be considered as less well investigated [*Ontañón*, 2013, *207*]. The (semi-permanent) settlements, which are scattered mainly in flat areas, reach an extent of up to 1–2 ha, an amount that will not be reached again until Roman times. These are mainly found in the form of 'pit fields' (campos de hoyos), which are generally the most common form of settlement on the Iberian Peninsula until the Bronze Age [*Lull et al.*, 2013a, *605*]. Livestock seems to dominate economically [*Ontañón*, 2013, *212*]. There are some signs of supra-regional contacts, and the burial tradition suggests abandoning the existing megalithic tradition. A few small enclosures as ritual places complete the picture [*Parcero Oubiña and Criado Boado*, 2013, *244-255*]. Copper mines such as Picos de Europa (El Milagro in Asturias) are unique due to their size and complexity [*Lull et al.*, 2013a].

This picture does not change fundamentally in the transition to the Bronze Age, even if the archaeological evidence is even more scarce. Settlement evidence remains rare and can be found in zones similar to those of the Chalcolithic. Furthermore, a temporary or seasonal use of the sites by a few (dozen) people seems to predominate. The finds indicate a broad spectrum of economic activities and a high degree of self-sufficiency. Economically, agriculture seems to gain in importance, which is also indicated by an increase in storage capacity [*Lull et al.*, 2013a, *605*]. On the other hand, a certain shift of the settlement areas to higher areas suggests a focus on cattle breeding, which may result in a diversified farming method [*Bettencourt et al.*, 2007, *152-153*; *Valcarce and Priego*, 1994, *148*]. The burials remain in the Chalcolithic tradition and show a great variety, whereby individual burials are more prominent [*Lull et al.*, 2013a, *606-607*].

The southern Iberian Peninsula, on the other hand, has been a hot spot of archaeological research for decades, due to its partly permanent character and the good preservation conditions for settlement structures and the rich funeral archaeology. In particular, the investigation of early complexity and the hypothesis of the emergence of a state based on archaeological finds in the course of the Chalcolithic and the Early Bronze Age El Argar phenomenon [*Chapman*, 1990, 2008; *Lull et al.*, 2011, 2013b; *Nocete et al.*, 2010] have caused a completely different kind of archaeological activity here. To what extent such an interpretation is justified, however,

remains controversial [*Bartelheim*, 2012; *García Sanjuán and Murillo-Barosso*, 2013; *Gilman*, 2001].

In general, a significant increase in settlement evidence in areas with good agricultural conditions can be observed in this region during the Copper Age. This applies, on the one hand, to the unfortified settlements, but especially to the emergence of extraordinarily large fortifications such as Zambujal, Los Millares, or Valencina de la Concepción, which are connected with metal objects, beakers, and the depositing of the deceased in extramural megalithic tombs [*Chapman*, 2008, *201-202*].

Direct evidence of agricultural production shows the use of cereals, legumes, and wild plants, and predominantly domesticated animals (mainly cattle and sheep/goats). The knowledge of the water and nutritional needs of the exploited plant and animal species suggests that agricultural production was stable within the relatively marginal environment. A system of dry agriculture with fallow periods and stubble grazing, coupled with the cultivation of legumes along watercourses in valley bottoms, can be considered realistic [*Chapman*, 2008, *201-202*].

In the first half of the third millennium a continuous process of social expansion took place. However, around 2200 cal. BCE, taking into account regional diversity, there were significant discontinuities which either intensified some of the previous trends or slowed or interrupted them. In any case, new forms of social organization emerged, which according to traditional chronology are usually attributed to the Early Bronze Age (2200 – 1600 cal. BCE) [*García Sanjuán and Murillo-Barosso*, 2013, *120*].

With the transition to the Bronze Age, different trajectories became apparent within the southern region. In some parts elements of the Bell Beaker phenomenon are at least partially and temporarily continued, in others (especially in the southeast) there is a clear break with them [*Lull et al.*, 2013b]. Especially in the domain of settlement structures, however, a clear change is generally perceptible, which is accompanied by the abandonment of collective burial customs and possibly associated with the emergence of a new symbolic system [*Senna-Martinez*, 2014].

In the southwest there is a widespread abandonment of settlements and discontinuity. Where stratigraphic continuity is evident, there is a clear change in the archaeological remains within a complex [*García Rivero and Escacena Carrasco*, 2015]. The settlement system is now more dispersed, concentrations are found in artificially terraced settlements in higher, more defensible locations and further away from cultivable soils [*Chapman*, 2008, *244*]. The settlement tradition is also being discontinued in the southeast, but in a different way. The rapid

spread of Early Bronze Age cultures on the south-eastern Iberian Peninsula seems to be accompanied by a demographic growth [*Lull et al.*, 2011; *Risch et al.*, 2015], as predicted from regional land use reconstructions [*Lull et al.*, 2011] and supported by estimations of grain production [*Delgado-Raack and Risch*, 2015]. New settlements are emerging even more prominently than in the west in well-protected and inaccessible locations, either on steep slopes, or on elevated plains with steep cliffs, such as the eponymous settlement El Argar [*Chapman*, 2008, *205*; *Risch et al.*, 2015]. This is accompanied by signs of a strongly stratifying society with control over resources and food production [*Chapman*, 2008, *210*; *Lull et al.*, 2011]. The standard model here is a 'vertical' production system [*Lull et al.*, 2011, *390-398*], in which the raw materials were exclusively collected and further processed in the controlling, fortified hilltop settlements. A barley monoculture seems to have developed [*Chapman*, 2008, *205*; *Delgado-Raack and Risch*, 2015, *27*], which is cautiously related to drought [*Stika*, 1988, 2001; for late El Argar *Lull et al.*, 2013b]. In the west as well as in the east the burial tradition is changing to individual (or double) burials, even though the choice of grave goods shows a certain continuity. In the west, extramural burials are more common [*Chapman*, 2008, *245*; *Lull et al.*, 2013a, *607*], in the east, however, burials typically take place within the houses [*Risch et al.*, 2015, *386*]. Also in the catchment area of the Guadalquivir there are clear indications of settlement discontinuities, where the Chalcolithic settlements at the lower reaches are abandoned and settlement activity shifts to the upper ones. Here archaeo-zoological findings from the long-term populated Úbeda site also point to a shift in domestic animal husbandry towards sheep/goats, indicating changes in subsistence strategies [*Nocete et al.*, 2010]. Not least, climatic influences and the resulting population shifts are also taken into account for these changes [*Cardoso*, 2005].

Widespread settlement discontinuities are also evident in Portugal, where about 4200 years BP the ditch and wall enclosures that characterise the Late Neolithic/Chalcolithic were largely abandoned in the south and survived only sporadically in the north [*Valera*, 2015, *417*]. The partly monumental and fortified Chalcolithic settlements are abandoned, leaving smaller settlements in the lowlands without any monumentality, which are preserved in the form of 'pit fields' and as 'negative structures'. Monumentality is also disappearing in relation to funeral architecture, in ceramics the proportion of closed forms is increasing, and the previously blade-based lithic industry is now becoming a flaking industry. The iconographically rich symbolic world of the Chalcolithic disappears completely, so that this change is referred to as an iconoclasm [*Valera*, 2015, *418*]. These significant cultural and settlement changes were apparently accompanied by major demographic changes: a continuous population growth is

assumed for the Chalcolithic, but this process abruptly breaks off with the transition to the 2nd millennium cal. BCE [*Valera*, 2015, *422*].

4.3 Materials and methods

4.3.1 Data acquisition and proxy development

In the following, two data sources for recording the change in settlement intensity at different scaling levels are presented: aoristics and evaluation of sum-calibrated ^{14}C data. The results of these independent data sources both complement and confirm each other, as far as their data basis overlaps spatially. For a more in-depth discussion of the methodology of sum calibration [*Contreras and Meadows*, 2014; *Hinz et al.*, 2012a; *Shennan et al.*, 2013; *Williams*, 2012] and aoristics [*Crema*, 2012; *Kolář et al.*, 2016; *Mischka*, 2004; *Palmisano et al.*, 2017; *Ratcliffe*, 2000] we refer to the relevant literature and two methodological contributions from the project, which are currently in progress (aoristics: *Hinz and Müller-Scheeßel*, [n.d.]; sum-calibration: *Hinz*, [n.d.]).

Aoristic is a method that was originally used to investigate crimes [*Ratcliffe*, 2000]. As with these, the exact (absolute) dating is often unknown, but can be limited to a phase of a certain duration by marginal information, indicating the start and end of the period within which the event must have taken place. By means of aoristics, the probability that the event took place (100 %) is distributed over this time interval in such a way that each temporal subunit (e.g. one year) receives the total probability divided by the number of subunits.

If there are several objects belonging to such events, describing the same facts (e.g. several settlements indicate the settlement density), the respective probabilities are summed up for each temporal subunit, and in this special case an expectation value is obtained, which describes how many simultaneous settlements most likely existed. A disadvantage of this method is that no uncertainty range can be given. Derived Monte Carlo-based methods [*Crema*, 2012; *Kolář et al.*, 2016] make this possible in a certain sense, although they can also quantify only the internal, not the external, uncertainty. For this reason, the original procedure was used here, as it is much simpler and more comprehensible.

Summed ^{14}C data from archaeological contexts are increasingly used to reveal changes in population density and/or human activities in the broader sense. This approach has now been applied in a large number of studies on different temporal settings [*Hinz et al.*, 2012a; *Lillios et al.*, 2016; *Shennan et al.*, 2013; *Weinelt et al.*, 2015; *Whitehouse et al.*, 2014] to name just a

few recent examples. Admittedly, there are a number of problems associated with this approach, such as: the ambiguity of the archaeological contexts of dated materials, the uneven distribution of sampling in space and time, possible differences between burial and settlement contexts, sensitivity to differential preservation and selective material loss and, perhaps most importantly, its dependence on regional and temporal research intensity (critical voices for example [*Contreras and Meadows*, 2014; *Williams*, 2012], both with further literature). A desirable random distribution is per se unattainable and, accordingly, the underlying database is inevitably distorted.

These uncertainties require careful verification and filtering of the data sets, including merging the data per site (i.e. each site then contributes with the weight of 1 to the final sum calibration, regardless of the number of ^{14}C samples taken) and cross-checking with independent quantitative population data. The main advantage of the approach is clearly the constantly increasing availability and quality of archaeological ^{14}C data and the statistical robustness of large data sets, the resulting absolute chronologies and the continuity of the data sets, with each individual sample representing a three-dimensional variable in space and time.

Furthermore, the inherent independence of this proxy from regional archaeological circumstances (e.g. chronology systems) allows the comparison of regional patterns for different cultural units over long distances and the synchronisation of these patterns with reconstructions of environmental changes. It is therefore particularly suitable for investigating transitions in the archaeological remains and in past social-ecological developments at regional to supra-regional level.

4.3.2 Aoristics

The basis for the aoristic analysis consists of 4084 sites with Neolithic, Chalcolithic, and/or Bronze Age date from southern Portugal (Algarve, Alentejo, and Lisbon). Of these sites taken from the ‘Portal do Arqueólogo’ of the ‘Direção Geral do Património Cultural’, 1437 sites remained for evaluation after filtering, as exclusively settlement sites were chosen in order to ensure comparability.

The temporal resolution of the data, which was taken directly from the database, is relatively low: Neolithic, Chalcolithic, and Bronze Age each break down into three phases, thus adding up to nine phases altogether.

4.3.3 Sum calibration

For the south-eastern Iberian Peninsula, it is certainly true that a strong focus on the El Argar phenomenon distorts the data basis. However, given the scale of this study over several hundred years, such distortion is of secondary importance. Spatially, the scope was extended beyond the work area, since at the time of the analysis (summer 2017) the data basis for the work areas themselves was too small for statistically significant results to be achievable. Therefore, all data in the databases RADON and RADON B [*Hinz et al.*, 2012b; *Kneisel et al.*, 2013] of relevant time settings available for the Iberian Peninsula were included. At the same time, however, the analysis was limited to sites with settlement character, again with the premise that distortions due to time-dependent deposition and detection probabilities can be largely avoided in this site category [*Hinz et al.*, 2012a, 3332]. Thus, 1895 ^{14}C dates of 302 settlement sites remained to be included in the sum calibration. Each site was given a weight of 1 to compensate for different dating frequencies at individual sites.

The software package oxcAAR [*Hinz et al.*, 2018] for the statistical environment R [*R Core Team*, 2017] was used for the actual calibration of the sums. This enables the utilization of the calibration program OxCal [*Bronk Ramsey*, 2009], which is widely used in archaeology as a quasi-standard, in conjunction with the automation and programming possibilities offered by R which are indispensable for checking the statistical significance of the sum-calibrated results. The software package oxcAAR is open source and can be downloaded for free.

To check the significance of the result, a Monte Carlo-based simulation approach was chosen. Unlike comparable studies, we assume an equal distribution of ^{14}C data as a null model, not an estimation of a general trend based on a generalized linear model [e.g. *Lillios et al.*, 2016; *Shennan et al.*, 2013]. The reason is that we look for significant local variations within a given time window and not, as there, for significant over- or underruns of a population growth assumed as given. Within a time window, the same number of ^{14}C data as in the actual data set was uniformly distributed, this simulation was repeated 1000 times and the 95 % interval of random effects was extracted from this. Where the curve of the real data leaves the envelope of the simulation (in the figure these areas are highlighted in red), with 5 % error probability the observed effect (over- or undershot) is not random or induced by the calibration curve, and the interpretation as event of interest can then be regarded as robust.

4.3.4 Climatological examinations: methodology

The climate reconstruction is based on the marine sediment core ODP-161-976A from the Alboran Sea (36°12.32' N; 4°18.76' W; 1108 m water depth). The age model of this sediment core is taken from a published source [*Jiménez-Amat and Zahn*, 2015]. The sediment core was sampled in the range of 103 cm to 145 cm depth in 0.5 cm resolution. The samples had already been freeze-dried and for the organic-geochemical analysis initially mortared to a homogeneous sediment powder. The lipids were then extracted at 100 bar pressure and 100 °C using an accelerated solvent extractor (ASE-200, Dionex). A solution mixture consisting of dichloromethane (DCM) and methanol (MeOH) in a ratio of 9:1 v/v was used. After extraction, the samples were desulfurized with activated copper chips for 30 minutes. The neutral fraction (using hexane) was separated from the desulfurized samples by liquid chromatography with activated silica gel (pre-treated for 4 hours at 450 °C). The neutral fraction containing the *n*-alkanes was also passed through a liquid chromatographic column of silver nitrate treated silica gel to separate aromatics and unsaturated fatty acids to purify the *n*-alkane fraction. The samples were then left for homogenization at room temperature for about 24 hours.

Subsequently, the *n*-alkanes were measured with a gas chromatograph (GC) at the Christian-Albrechts-University in Kiel. An Agilent 6890N GC equipped with a flame ionization detector and a Restek XTI-5 capillary column (30 m × 320 µm × 0.25 µm) was used. The *n*-alkanes were identified and quantified using a standard mixture of *n*-alkanes of known chain length and concentration. The retention time was used as the basis for identification and the peak areas of the respective components were integrated for quantification.

4.3.5 Proxy

In the context of this publication, we unfortunately cannot go into details of the climatological proxies. Details can be found elsewhere [*Schirrmacher et al.*, 2019]. In short: The concentration of long-chain *n*-alkane homologues of terrestrial origin is taken as a precipitation proxy. Since the concentration of these *n*-alkanes in marine sediments is strongly dependent on the river flow, low concentrations are interpreted as low river flow or dry phase. The data are presented here in a roughly simplified form to avoid pre-empting a separate publication. In the raw data, several phases of relatively stable conditions – delimited by rapid changes – were identified. These are roughly represented here. Small values represent a low *n*-alkane concentration in the raw data and are therefore indicative for dry climatic conditions.

4.4 Results

4.4.1 Aoristics

If we consider the result of the aoristic sum for work area (Fig 4.2), it becomes clear that a relatively well represented Neolithic phase is followed by a further significant increase in settlement activity in the Chalcolithic. In the transition to the Bronze Age, an abrupt decline in settlement intensity becomes apparent. Only in the late Bronze Age a slight recovery phase can be derived.

The changes in the spatial structure become apparent when the settlements of the individual phases are mapped. In the Neolithic (Fig 4.3) three intensive settlement clusters are recognizable: in the western Algarve, as well as two clusters in the Evora region, of which the western one concentrates west of today's city Evora, the eastern one in the concelho Reguengos de Monsaraz. This concentration intensifies during the course of the Chalcolithic, where the Algarve region is clearly less represented, and an even stronger clustering in Evora becomes apparent.

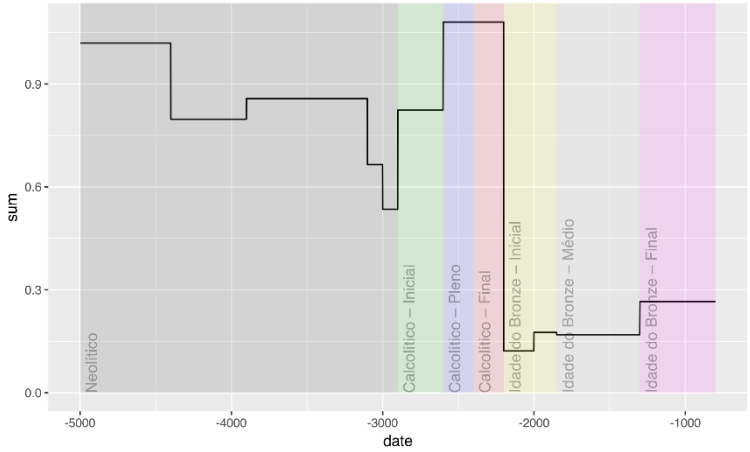

Figure 4.2 The aoristic sum of the 1437 settlement sites within southern Portugal

With the transition to the Bronze Age, the settlement of the Evora region largely ceased, and there are hardly any Bronze Age settlement sites preserved here. Rather, the region southeast of Beja and again the Algarve are more prominent now, but above all because the northern regions are disappearing. Overall, the settlement is significantly thinner (as can already be seen from the aoristic sum) and more dispersed than in previous periods.

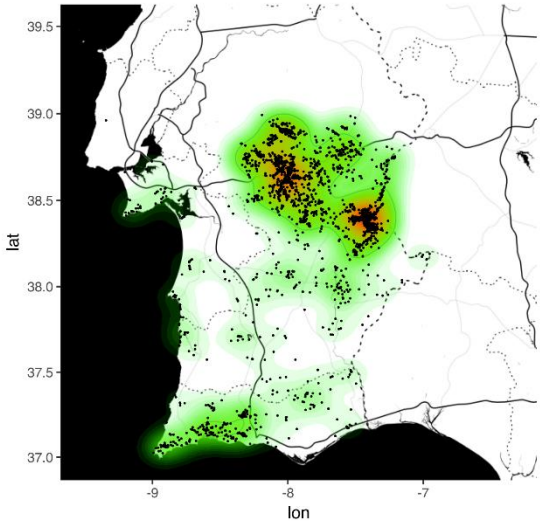

Figure 4.3 Map of the aoristic evidence from the Neolithic settlement sites of southern Portugal

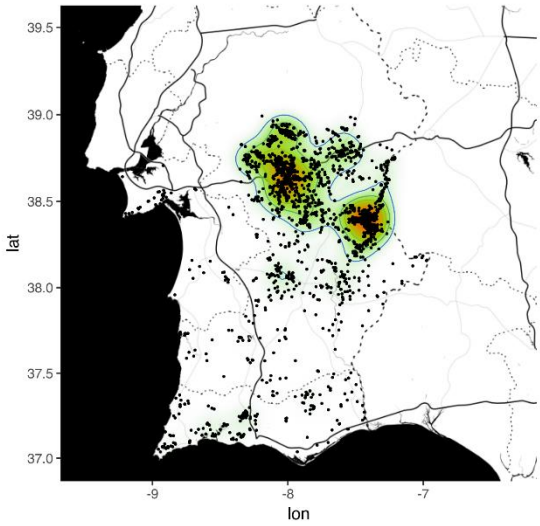

Figure 4.4 Map of the aoristic evidence from the Chalcolithic settlement sites of southern Portugal

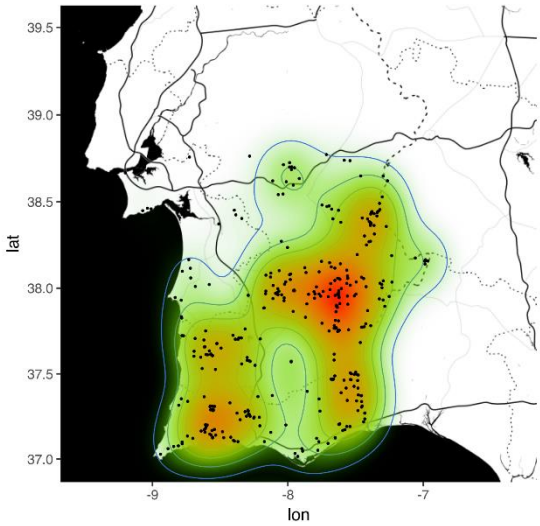

Figure 4.5 Map of the aoristic evidence from the Bronze Age settlement sites of southern Portugal

4.4.2 Sum calibration

Figure 4.6 shows the result of the sum calibration for the entire Iberian Peninsula. While the Neolithic represents a more or less constant plateau, the settlement intensity documented by the ^{14}C data increases significantly by 3000 cal. BCE in the transition to the Chalcolithic. If the probability values of the sum calibration are taken literally (which, however, is risky due to the possible distortions caused by research), the population density would have quadrupled. Shortly after 2500 cal. BCE, and thus after the maximum of the curve, a decrease in intensity is again apparent, which forms a minimum between 2300 – 2100 cal. BC. Shortly after the beginning of the Early Bronze Age, the curve rises again, in contrast to the (aoristic) observation of the southern Portuguese area. This difference is certainly due to different trajectories in the individual southern Iberian regions, as they are already apparent in *Lillios et al.* [2016], and as they will be described in detail in a later study [*Schirrmacher et al.*, submitted].

The result of the significance analysis shows on the one hand (Fig 4.7) that the Chalcolithic and parts of the (early) Bronze Age are significantly overrepresented within the time window between 4000 and 500 cal. BCE, and that on the other hand (Fig 4.8) within the plateau between 2900 and 1600 cal. BCE the decrease at 2200 cal. BCE represents a significant anomaly.

Overall, it can be stated here that around the canonical date of the 4.2 ka BP event (~2200 cal. BCE) a minimum of settlement activity can be determined.

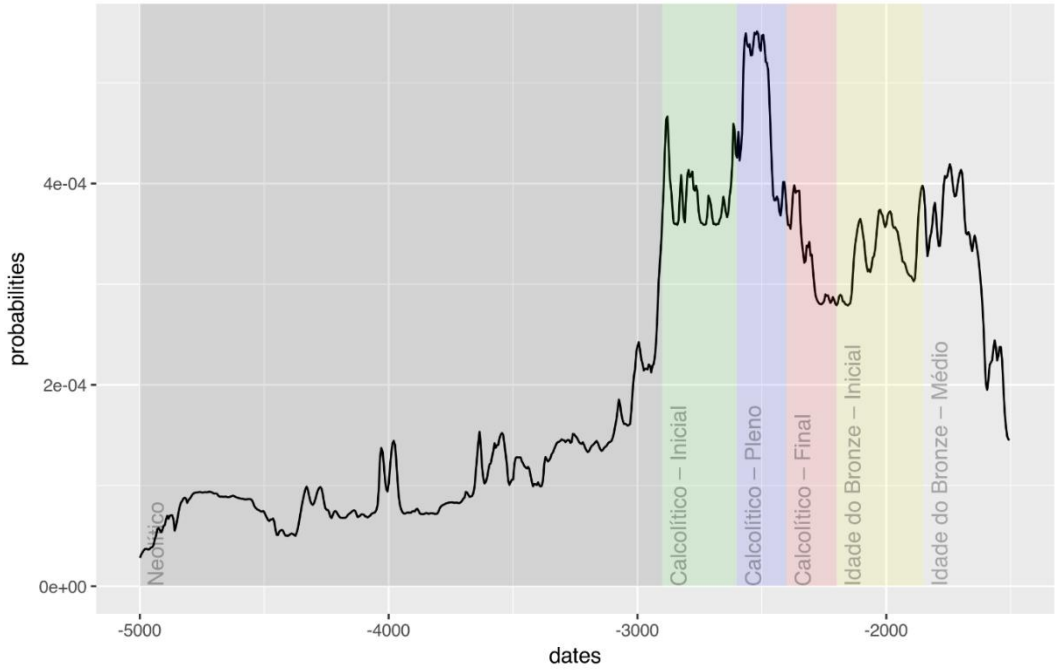

Figure 4.6 Sum calibration of 1895 ^{14}C dates (from 302 settlement sites) of the whole Iberian Peninsula

4.4.3 Climatology

For the detailed evaluation of the climatological investigations and their results, the reader must be referred to another publication [*Schirrmacher et al.*, 2019]. Very briefly summarized, the corresponding analyses result in the following picture: In general, according to the proxy used, the climate between 2800 and 1100 cal. BCE is rather stable and relatively humid. The precipitation reconstruction shows two rapidly occurring, pronounced dryness phases from 2350 to 2200 cal. BCE (4.3 – 4.15 ka BP) and from 2100 to 2000 cal. BCE (4.05 – 3.95 ka BP), standing out from this background. These two dry phases are interrupted by a return to more humid conditions.

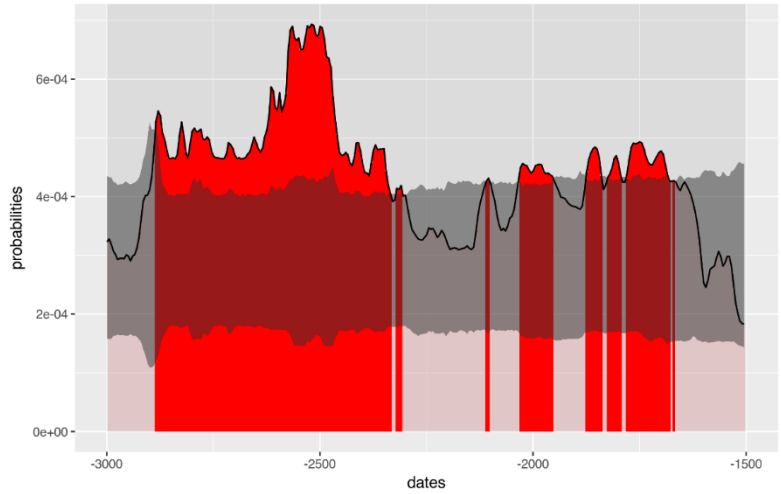

Figure 4.7 Significance test for the sum calibration within the time window of 4000-500 cal. BCE. *Null hypothesis is a uniform distribution of the site evidence within this time frame. Number of dates for this time window: 1394 dates from 254 sites.*

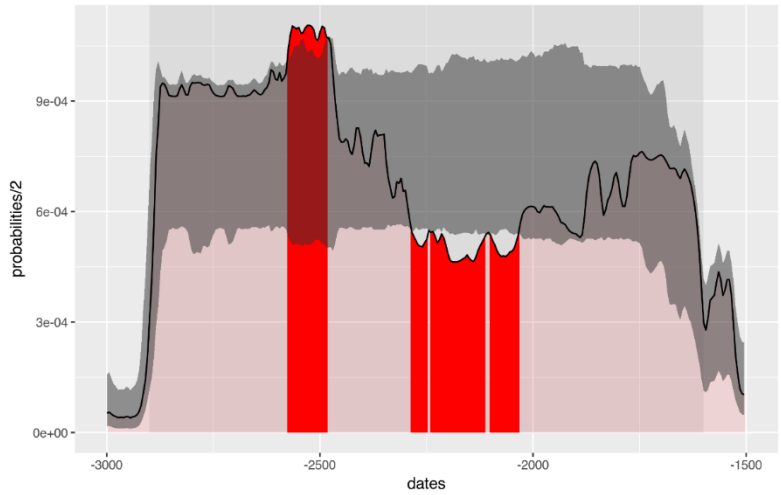

Figure 4.8 Significance test for the sum calibration within the time window of 2900-1600 cal. BCE. *Null hypothesis is a uniform distribution of the site evidence within this time frame. Number of dates for this time window: 969 dates from 176 sites.*

4.5 Discussion

4.5.1 Climate linkage and correlation

By comparing regional and supra-regional proxies for population development with local climate change around the period of the 4.2 ka BP event, new insights and interpretations of the inter-relationship of the two developments can be formulated. With regard to the overall development between 4000 and 500 cal. BCE, it can be stated that the Chalcolithic period is clearly overrepresented compared to an equal distribution of settlement and thus population evidence. This also applies to some parts of the (Early) Bronze Age, which are certainly due to the expansion of the El Argar phenomenon. The Copper Age on the Iberian Peninsula certainly represents a heyday in settlement terms, even if this is not always easy to grasp in individual cases due to the specific type of occupation and the resulting preservation conditions. Only in the synopsis does this development become clear.

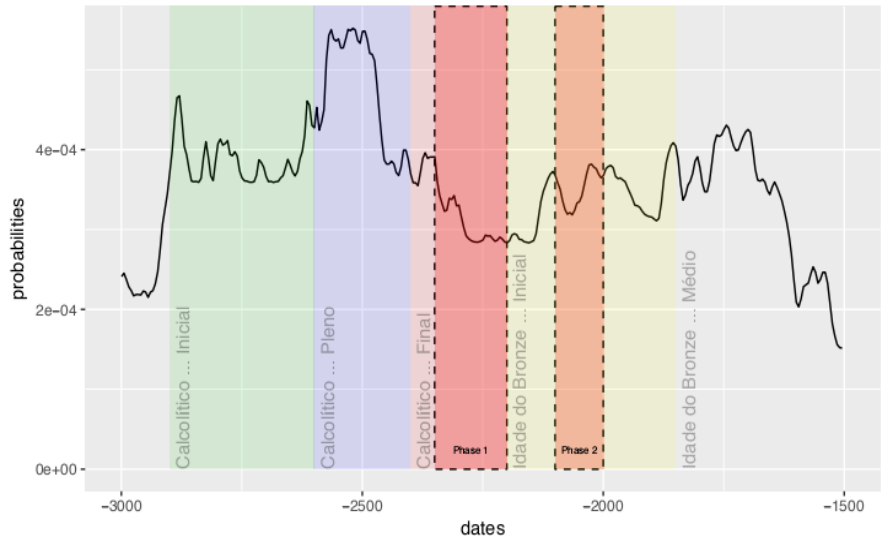

Figure 4.9 Sum calibration of the settlement sites of whole Iberian Peninsula with periods of drought. *Details see Fig 4.6.*

Within these Chalcolithic and Early Bronze Age expansion and climax phases, the decline in the period between roughly 2500 and 2100 cal. BCE represents a significant decrease, which culminates in a significantly under-represented settlement frequency between 2300 and 2100 cal. BCE. From approx. 2000 cal. BCE we can see a gradual recovery of settlement intensity, which, however, remains significantly below that of the Copper Age. A partial explanation may be an increased concentration of the settlement structure, since our method essentially analyses the number of settlements over time and is therefore 'blind' to differences in the size of

individual settlements and their temporal dynamics. However, if we look at the results of aoristics (based on the same measure), it becomes apparent that, at least in individual regions, there are clear tendencies towards decentralisation that prevent such an explanatory approach from being generally valid.

If we parallelize the climatic and the derived demographic development (Fig 4.9) and take into account the smoothing effects of the ^{14}C proxy, it becomes clear that the second decline in settlement intensity can well be associated with the first drought phase in connection with a two-part and 'prolonged' 4.2 ka BP event. In reality, a lag of forcing and effect is very likely, but due to the mentioned smoothing effect and the general temporal uncertainty, this is not apparent here. The minimum in the ^{14}C cumulative curve touches the margins of the second dryness phase, but is itself in the range of returning to more humid conditions. The described synchronism becomes even clearer if one compares the curve of the climatic signal directly with the ^{14}C sum curves and takes into account the regionally different characteristic of the dynamics. For reasons of publication policy (the climatological studies within our project take place within the framework of a natural scientific dissertation), however, reference must unfortunately be made to a later paper for such a detailed presentation. However, the figure shown here and the data presented already indicate that there are good reasons to postulate a connection between the drought events and the decrease in settlement evidence. The fact that the first decline in settlement intensity cannot be linked to a climatic signal is a reminder that socio-economic changes cannot and must not always be attributed to external factors, but may very well be the result of internal, more difficult to identify or unknown factors.

4.5.2 Spatial shift

As the aoristics have shown, very different trends can be seen in the different regions of the Iberian Peninsula, as they have already been shown elsewhere [*Lillios et al.*, 2016]. If we concentrate on the southern region, there is a very clear decline in the southwest in connection with the first drought phase, which is equivalent to the interruption of settlement activity, and in which the settlement indicators remain at a very low level in the Early Bronze Age. In the Andalusian region there has also been a significant decline, but there has been a strong recovery during the return to more humid conditions, which continues into the Early Bronze Age and only decreases to a level equal to that of the settlement minimum during the first drought phase with the advent of the El Argar phenomenon. The second drought phase does not appear to have a significant effect here. The south-eastern region is quite different: the first drought phase does not seem to have a significant influence here, but rather a decline in the course of the more

humid intermediate phase and the second drought phase can be derived, which leads to a boom after the drier conditions have eased, which can be associated with the El Argar expansion of the Early Bronze Age. For the reasons mentioned, no raw data of these trends can be presented here, but from the mappings of the ^{14}C based settlement evidence the alluded shifts can be derived (Fig 4.10).

Overall, a general shift in settlement activity from the Copper Age to the Early Bronze Age from the west to the east can be observed, which can be linked to climatic developments, their effects on agricultural conditions, and the associated evasion and adaptation strategies via intermediate stages. At the end of the development is the El Argar phenomenon, within which people were able to create a flourishing and expanding socio-economical complex in the economically non-optimal areas of south-eastern Spain by means of adapted and (not least on drought) optimized farming methods. It is precisely these regions, namely Almeria and Murcia, which today are among the driest in Europe and one of the most mountainous on the peninsula.

4.6 Conclusions and outlook

As has been shown, the transition from the Chalcolithic to the Early Bronze Age on the southern Iberian Peninsula, which primarily represents a cultural and technical innovation, is taking place in the course of a demographic transformation and is accompanied by a climatic development in which two rapidly occurring, pronounced periods of drought are likely to have influenced the environmental conditions and thus also the economic basis of the societies in this region. The aim of the project presented here is, and will continue to be, to establish the connection between these different levels. A first step in this direction is to determine to what extent these developments can actually be parallelized. According to the available results, this seems very well possible.

The next step will be to ask whether causal relationships can also be established here, and how the mechanisms of change present themselves in detail. We were able to show that the drought phases can be linked not only in general to the overall dynamics of population development on the southern Iberian Peninsula, but that spatial shifts of population centres are also connected with the drought phases. This makes a causal relationship beyond a mere correlation likely. In the first drought phase, for example, the result appears to have been the abandonment of areas that were no longer economically viable, while the second phase may have necessitated new

adaptation strategies that may have been the driving force behind the further development and the emergence of the El Argar complex.

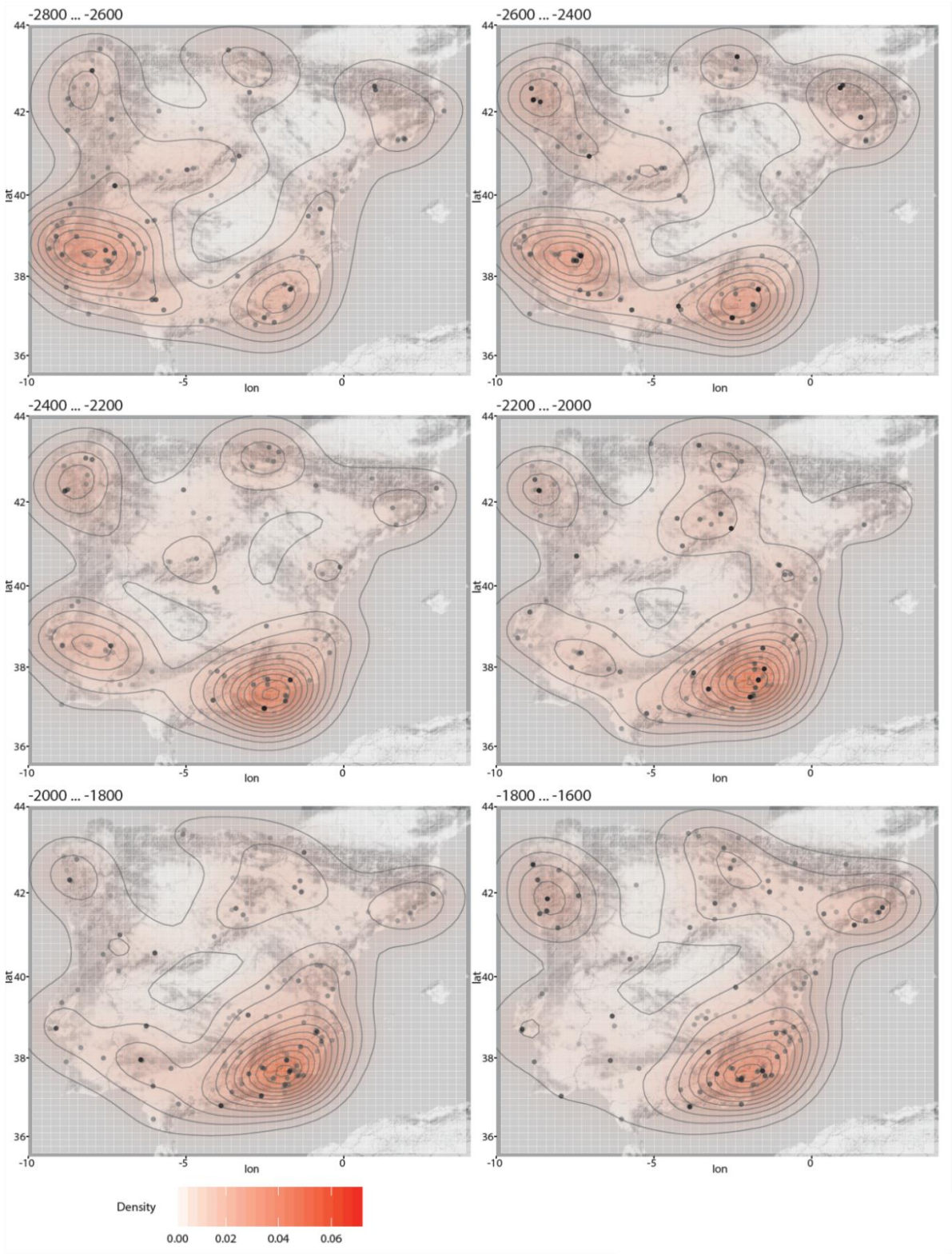

Figure 4.10 The ^{14}C evidence of the Iberian Peninsula between 2800 and 1600 cal. BCE in 200 year time slices. *The transparency of the sites represents probability from the ^{14}C data, the shading and contour lines represent density of sites.*

However, it must be noted that a complex social event cannot be explained by monocausal reasons and that, despite the obvious relationships, it is not our intention to formulate here a simple equation from climate to economy and demography to socio-cultural change.

Reinforcement, feedback and consequential effects are likely to have culminated in regional crises, up to a supra-regional scale. Such supra-regional socio-ecological crisis can threaten social and environmental stability equally, and the resulting social pressures could have played an important role in the spread, acceleration and shaping of general transformations at the end of the 3rd millennium BCE in the Western Mediterranean and through far-reaching effects also on the development of contemporary societies in central and northern Europe. Potential crisis drivers, whose role must be assessed beyond external triggers and amplifiers such as drought or other abrupt climate deteriorations are social inequality, overexploitation and competition for resources, demographic change due to increased mobility and possibly large population shifts, and violent conflicts.

Nevertheless, all these influences on the course of human history are interrelated, which is one more reason not to lose sight of climatic development. The investigation of the situation of the southern Iberian Peninsula has shown on an overarching level that general trends converged at a certain point in time in the second half of the 3rd millennium BCE, and influenced the trajectories of further development in this area and beyond. In the further process of the investigations, smaller-scale and more detailed analyses will now have to be carried out, which will make it possible to focus more strongly on local characteristics. This will be the work of the next three years. However, it should already be noted that the close cooperation between the humanities and the natural sciences that we are striving for in our project, which goes beyond simple interdisciplinarity, opens up new perspectives and investigation possibilities with regard to human-environment relations and their historical role.

4.7 Acknowledgements

This research was carried out in the framework of the CRC 1266 “Scales of transformation” (project number: 2901391021 – SFB 1266) funded by the DFG (German Research Foundation). We are also grateful for help with the archaeological data collection by Jan-Eric Schlicht and Merle Oehlbüttel. Additionally, we thank Eileen Kücükkaraca for editing and improving the English language, and the unknown reviewers for their helpful comments that improved the paper significantly.

4.8 References

Bar-Matthews, M., A. Ayalon, and A. Kaufman (1997), Late Quaternary Paleoclimate in the Eastern Mediterranean Region from Stable Isotope Analysis of Speleothems at Soreq Cave, Israel, *Quaternary Research*, *47*(02), 155–168, doi:10.1006/qres.1997.1883.

Bartelheim, M. (2012), Detecting social structures in the Bronze Age of southeastern Spain, in *Beyond elites: Alternatives to hierarchical systems in modelling social formations ; international conference at the Ruhr-Universität Bochum, Germany, October 22 - 24, 2009*, *Universitätsforschungen zur prähistorischen Archäologie Aus dem Institut für Archäologische Wissenschaften an der Universität Bochum, Fach Ur- und Frühgeschichte*, vol. 215, edited by T. L. Kienlin and A. Zimmermann, pp. 339–354, Habelt, Bonn.

Benítez de Lugo Enrich, L., and M. Mejías (2017), The hydrogeological and paleoclimatic factors in the Bronze Age Motillas Culture of La Mancha (Spain): The first hydraulic culture in Europe, *Hydrogeol J*, *25*(7), 1931–1950, doi:10.1007/s10040-017-1607-z.

Bettencourt, A., A. Dinis, I. Figueiral, A. Rodrigues, C. Cruz, I. Silva, M. Azevedo, and R. Barbosa (2007), A ocupação do território e a exploração dos recursos durante a Pré-História Recente do Noroeste de Portugal, in *A concepção das paisagens e dos espaços na arqueologia da Península Ibérica: Actas do IV Congresso de Arqueologia Peninsular (Faro, 14 a 19 Setembro de 2004)*, *Promontoria Monográfica*, vol. 8, edited by S. O. Jorge, pp. 149–164, Universidade do Algarve Departamento de História Arqueologia e Património, Faro.

Bond, G., B. Kromer, J. Beer, R. Muscheler, M. N. Evans, W. Showers, S. Hoffmann, R. Lotti-Bond, I. Hajdas, and G. Bonani (2001), Persistent solar influence on North Atlantic climate during the Holocene, *Science (New York, N.Y.)*, *294*(5549), 2130–2136, doi:10.1126/science.1065680.

Bond, G., W. Showers, M. Cheseby, R. Lotti, P. Almasi, P. deMenocal, P. Priore, H. Cullen, I. Hajdas, and G. Bonani (1997), A Pervasive Millennial-Scale Cycle in North Atlantic Holocene and Glacial Climates, *Science*, *278*(5341), 1257–1266, doi:10.1126/science.278.5341.1257.

Booth, R. K., S. T. Jackson, S. L. Forman, J. E. Kutzbach, E. A. Bettis, J. Kreigs, and D. K. Wright (2005), A severe centennial-scale drought in midcontinental North America 4200 years ago and apparent global linkages, *The Holocene*, *15*(3), 321–328, doi:10.1191/0959683605hl825ft.

Brisset, E., C. Miramont, F. Guiter, E. J. Anthony, K. Tachikawa, J. Poulenard, F. Arnaud, C. Delhon, J.-D. Meunier, E. Bard, and F. Suméra (2013), Non-reversible geosystem destabilisation at 4200 cal. BP: Sedimentological, geochemical and botanical markers of soil erosion recorded in a Mediterranean alpine lake, *The Holocene*, *23*(12), 1863–1874, doi:10.1177/0959683613508158.

Bronk Ramsey, C. (2009), Bayesian Analysis of Radiocarbon Dates, *Radiocarbon*, *51*(1), 337–360, doi:10.1017/S0033822200033865.

Burjachs, F., and I. Expósito (2015), Charcoal and pollen analysis: Examples of Holocene fire dynamics in Mediterranean Iberian Peninsula, *CATENA*, *135*, 340–349, doi:10.1016/j.catena.2014.10.006.

Cacho, I., J. O. Grimalt, M. Canals, L. Sbaffi, N. J. Shackleton, J. Schönfeld, and R. Zahn (2001), Variability of the western Mediterranean Sea surface temperature during the last 25,000 years and its connection with the Northern Hemisphere climatic changes, *Paleoceanography*, *16*(1), 40–52, doi:10.1029/2000PA000502.

Cardoso, J. (2005), Visibilidade e invisibilidade do Património Arqueológico: O caso do Bronze Pleno da Estremadura, *DISCURSOS. Língua, Cultura e Sociedade*, *III SÉRIE, Nº 6*, 7–27.

Carrión, J. S., N. Fuentes, P. González-Sampériz, L. Sánchez Quirante, J. C. Finlayson, S. Fernández, and A. Andrade (2007), Holocene environmental change in a montane region of southern Europe with a long history of human settlement, *Quaternary Science Reviews*, *26*(11-12), 1455–1475, doi:10.1016/j.quascirev.2007.03.013.

Carrión, J. S., P. Sánchez-Gómez, J. F. Mota, R. Yll, and C. Chaín (2003), Holocene vegetation dynamics, fire and grazing in the Sierra de Gádor, southern Spain, *The Holocene*, *13*(6), 839–849, doi:10.1191/0959683603hl662rp.

Cauliez, J. (2015), The Bell Beaker Complex: A vector of transformations? Stabilities and changes of the indigenous cultures in south-east France at the end of the Neolithic Period, in *The Bell beaker transition in Europe: Mobility and local evolution during the 3rd millennium BC*, edited by L. Salanova and M. P. Prieto Martínez, pp. 88–112, Oxbow Books, Philadelphia.

Chapman, R. (1982), Autonomy, ranking and resources in Iberian prehistory, in *Ranking, resource and exchange: Aspects of the archaeology of early European society: symposium ... offered to the Society for American*

Archaeology, for its 45. Annual Meeting, New directions in archeology, edited by C. Renfrew and S. Shennan, pp. 46–51, Cambridge Univ. Press, Cambridge.

Chapman, R. (1990), *Emerging complexity: The later prehistory of south-east Spain, Iberia and the west Mediterranean*, 304 pp., *New studies in archaeology*, Cambridge Univ. Pr, Cambridge.

Chapman, R. (2008), Producing Inequalities: Regional Sequences in Later Prehistoric Southern Spain, *J World Prehist*, *21*(3-4), 195–260, doi:10.1007/s10963-008-9014-y.

Contreras, D. A., and J. Meadows (2014), Summed radiocarbon calibrations as a population proxy: A critical evaluation using a realistic simulation approach, *Journal of Archaeological Science*, *52*, 591–608, doi:10.1016/j.jas.2014.05.030.

Crema, E. R. (2012), Modelling Temporal Uncertainty in Archaeological Analysis, *J Archaeol Method Theory*, *19*(3), 440–461, doi:10.1007/s10816-011-9122-3.

Cruz, J. A., M. J. Turrero, J. O. Cáceres, A. Marín-Roldán, A. I. Ortega, A. Garralón, L. Sánchez, P. Gómez, M. B. Muñoz-García, R. L. Edwards, and J. Martín-Chivelet (2015), Long-term hydrological changes in northern Iberia (4.9–0.9 ky BP) from speleothem Mg/Ca ratios and cave monitoring (Ojo Guareña Karst Complex, Spain), *Environmental Earth Sciences*, *74*(12), 7741–7753, doi:10.1007/s12665-015-4687-x.

Cruz Berrocal, M., L. G. Sanjuán, and A. Gilman (Eds.) (2013), *The Prehistory of Iberia*, 834 pp., *Routledge Studies in Archaeology*, Taylor and Francis, Hoboken.

Davis, B.A.S., S. Brewer, A. C. Stevenson, and J. Guiot (2003), The temperature of Europe during the Holocene reconstructed from pollen data, *Quaternary Science Reviews*, *22*(15-17), 1701–1716, doi:10.1016/S0277-3791(03)00173-2.

Delgado-Raack, S., and R. Risch (2015), Social Change and Subsistence Production on the Iberian Peninsula during the 3rd and 2nd Millennia BCE, in *The Third Food Revolution?: Setting the Bronze Age table : common trends in economic and subsistence strategies in Bronze Age Europe : proceedings of the International Workshop "Socio-Environmental Dynamics over the Last 12,000 Years: the Creation of Landscapes III (15th-18th April 2013)" in Kiel*, edited by J. Kneisel et al., pp. 21–46, Verlag Dr. Rudolph Habelt GmbH, Bonn.

deMenocal, P., J. Ortiz, T. Guilderson, J. Adkins, M. Sarnthein, L. Baker, and M. Yarusinsky (2000), Abrupt onset and termination of the African Humid Period, *Quaternary Science Reviews*, *19*(1-5), 347–361, doi:10.1016/S0277-3791(99)00081-5.

deMenocal, P. B. (2001), Cultural Responses to Climate Change During the Late Holocene, *Science*, *292*(5517), 667–673, doi:10.1126/science.1059287.

Díaz-del-Río, P. (2004), Factionalism and collective labor in Copper Age Iberia, *Trabajos de Prehistoria*, *61*(2), 85–98.

Dixit, Y., D. A. Hodell, R. Sinha, and C. A. Petrie (2014), Abrupt weakening of the Indian summer monsoon at 8.2 kyr B.P, *Earth and Planetary Science Letters*, *391*, 16–23, doi:10.1016/j.epsl.2014.01.026.

Finné, M., K. Holmgren, H. S. Sundqvist, E. Weiberg, and M. Lindblom (2011), Climate in the eastern Mediterranean, and adjacent regions, during the past 6000 years – A review, *Journal of Archaeological Science*, *38*(12), 3153–3173, doi:10.1016/j.jas.2011.05.007.

Fletcher, W. J., T. Boski, and D. Moura (2007), Palynological evidence for environmental and climatic change in the lower Guadiana valley, Portugal, during the last 13 000 years, *The Holocene*, *17*(4), 481–494, doi:10.1177/0959683607077027.

Furholt, M. (2018), Massive Migrations?: The Impact of Recent aDNA Studies on our View of Third Millennium Europe, *Eur. j. archaeol.*, *21*(2), 159–191, doi:10.1017/eaa.2017.43.

García, J. F. F., A. B. González, and J. A. L. Sáez (2006), La transición del Calcolítico-Bronce Antiguo desde una perspectiva arqueológica y ambiental: El Valle Amblés (Ávila) como referencia, *Arqueología especial* (26), 37–56.

García Rivero, D., and J. L. Escacena Carrasco (2015), Del Calcolítico al Bronce antiguo en el Guadalquivir inferior. El Cerro de San Juan (Coria del Río, Sevilla) y el 'modelo de reemplazo', *Zephyrvs*, *76*(0), 15, doi:10.14201/zephyrus2015761538.

García Sanjuán, L. (1999), *Los orígenes de la estratificación social: Patrones de desigualdad en la Edad del Bronce del suroeste de la Península Ibérica; (Sierra Morena Occidental c. 1700 - 1100 a.n.e./2100 - 1300 A.N.E.)*, 307 pp., *BAR international series*, vol. 823, Archeopress, Oxford.

García Sanjuán, L., and M. Murillo-Barosso (2013), Social complexity in Copper Age Southern Iberia (ca. 3200 – 2200 cal. B.C.): Reviewing the "State" Hypothesis at Valencina de la Conception (Seville, Spain), in *The Prehistory of Iberia*, *Routledge Studies in Archaeology*, edited by M. Cruz Berrocal et al., pp. 119–140, Taylor and Francis, Hoboken.

Gilman, A. (1987), Unequal development in copper age Iberia., in *Specialization, exchange and complex societies*, *New directions in archaeology*, edited by E. M. Brumfiel and T. Earle, pp. 22–29, Cambridge Univ. Pr, Cambridge.

Gilman, A. (2001), Assessing Political Development in Copper and Bronze Age Southeast Spain, in *From Leaders to Rulers*, *Fundamental Issues in Archaeology*, edited by J. Haas, pp. 59–81, Springer, Boston, MA.

Gilman, A., and J. B. Thornes (1985), *Land-use and prehistory in South-East Spain*, 217 pp., *London research series in geography*, vol. 8, Allen & Unwin, London.

Günther, T., C. Valdiosera, H. Malmström, I. Ureña, R. Rodriguez-Varela, Ó. O. Sverrisdóttir, E. A. Daskalaki, P. Skoglund, T. Naidoo, E. M. Svensson, J. M. Bermúdez de Castro, E. Carbonell, M. Dunn, J. Storå, E. Iriarte, J. L. Arsuaga, J.-M. Carretero, A. Götherström, and M. Jakobsson (2015), Ancient genomes link early farmers from Atapuerca in Spain to modern-day Basques, *Proceedings of the National Academy of Sciences of the United States of America*, *112*(38), 11917–11922, doi:10.1073/pnas.1509851112.

Gupta, A. K., D. M. Anderson, and J. T. Overpeck (2003), Abrupt changes in the Asian southwest monsoon during the Holocene and their links to the North Atlantic Ocean, *Nature*, *421*(6921), 354–357, doi:10.1038/nature01340.

Hinz, M., I. Feeser, K.-G. Sjögren, and J. Müller (2012a), Demography and the intensity of cultural activities: An evaluation of Funnel Beaker Societies (4200–2800 cal BC), *Journal of Archaeological Science*, *39*(10), 3331–3340, doi:10.1016/j.jas.2012.05.028.

Hinz, M., M. Furholt, J. Müller, D. Raetzel-Fabian, C. Rinne, K.-G. Sjögren, and H.-P. Wotza (2012b), RADON - Radiocarbon dates online 2012: Central European database of 14C dates for the Neolithic and Early Bronze Age.

Hinz, M., C. Schmid, D. Knitter, and C. Tietze (2018), *OxcAAR: Interface to 'oxcal' radiocarbon calibration*.

Hutado, V. (1997), The dynamics of the occupation of the middle basin of the river Guadiana between the fourth and second millennia BC, in *The archaeology of Iberia: the dynamics of change*, edited by M. Díaz-Andreu García and S. J. Keay, Routledge, London, New York.

IPCC (2013), *Climate Change 2013: The Physical Science Basis. Contribution of Working Group I to the Fifth Assessment Report of the Intergovernmental Panel on Climate Change*, Cambridge, United Kingdom and New York, NY, USA.

Jalut, G., J. J. Dedoubat, M. Fontugne, and T. Otto (2009), Holocene circum-Mediterranean vegetation changes: Climate forcing and human impact, *Quaternary International*, *200*(1-2), 4–18, doi:10.1016/j.quaint.2008.03.012.

Jalut, G., A. Esteban Amat, L. Bonnet, T. Gauquelin, and M. Fontugne (2000), Holocene climatic changes in the Western Mediterranean, from south-east France to south-east Spain, *Palaeogeography, Palaeoclimatology, Palaeoecology*, *160*(3-4), 255–290, doi:10.1016/S0031-0182(00)00075-4.

Jiménez-Amat, P., and R. Zahn (2015), Offset timing of climate oscillations during the last two glacial-interglacial transitions connected with large-scale freshwater perturbation, *Paleoceanography*, *30*(6), 768–788, doi:10.1002/2014PA002710.

Kaniewski, D., N. Marriner, D. Ilan, C. Morhange, Y. Thareani, and E. van Campo (2017), Climate change and water management in the biblical city of Dan, *Science advances*, *3*(11), e1700954, doi:10.1126/sciadv.1700954.

Kneisel, J., M. Hinz, and C. Rinne (2013), Radon-B, http://radon-b.ufg.uni-kiel.de.

Kolář, J., M. Macek, P. Tkáč, and P. Szabó (2016), Spatio-temporal modelling as a way to reconstruct patterns of past human activities, *Archaeometry*, *58*(3), 513–528, doi:10.1111/arcm.12182.

Lillios, K. T. (1997), The Third Millennium BC in Iberia: Chronometric Evidence for Settlement Histories and Socio-cultural Change, in *Third Millennium BC Climate Change and Old World Collapse*, edited by H. N. Dalfes et al., pp. 173–191, Springer Berlin Heidelberg.

Lillios, K. T. (2015), Crossing Borders: Death and Life in Second Millennium BC Southern Iberia and North Africa, in *The Cambridge Prehistory of the Bronze and Iron Age Mediterranean*, edited by A. B. Knapp and P. van Dommelen, pp. 554–570, Cambridge University Press.

Lillios, K. T., A. Blanco-González, B. L. Drake, and J. A. López-Sáez (2016), Mid-late Holocene climate, demography, and cultural dynamics in Iberia: A multi-proxy approach, *Quaternary Science Reviews*, *135*, 138–153, doi:10.1016/j.quascirev.2016.01.011.

Lionello, P., P. Malanotte-Rizzoli, and R. Boscolo (Eds.) (2006), *Mediterranean climate variability*, 421 pp., *Developments in earth & environmental sciences*, vol. 4, Elsevier, Amsterdam.

López-Sáez, J. A., D. Abel-Schaad, S. Pérez-Díaz, A. Blanco-González, F. Alba-Sánchez, M. Dorado, B. Ruiz-Zapata, M. J. Gil-García, C. Gómez-González, and F. Franco-Múgica (2014), Vegetation history, climate and human impact in the Spanish Central System over the last 9000 years, *Quaternary International*, *353*, 98–122, doi:10.1016/j.quaint.2013.06.034.

Lull, V., R. Micó, C. Rihuete Herrada, and R. Risch (2011), El Argar and the Beginning of Class Society in the Western Mediterranean, in *Sozialarchäologische Perspektiven: Gesellschaftlicher Wandel 5000 - 1500 v. Chr. zwischen Atlantik und Kaukasus: Internationale Tagung, 15. - 18. Oktober 2007 in Kiel*, *Archäologie in Eurasien*, vol. 24, edited by S. Hansen and J. Müller, pp. 381–414, von Zabern, Mainz.

Lull, V., R. Micó, C. Rihuete Herrada, and R. Risch (2013a), Bronze Age Iberia, in *The Oxford Handbook of the European Bronze Age*, edited by H. Fokkens and A. Harding, Oxford University Press.

Lull, V., R. Micó, C. Rihuete Herrada, and R. Risch (2013b), Political collapse and social change at the end of El Argar, in *1600 - Kultureller Umbruch im Schatten des Thera-Ausbruchs?: 4. Mitteldeutscher Archäologentag vom 14. bis 16. Oktober 2011 in Halle (Saale)*, Band 9, edited by H. Meller et al., pp. 283–302, Landesamt für Denkmalpflege und Archäologie Sachsen-Anhalt, Landesmuseum für Vorgeschichte, Halle (Saale).

Lull, V., R. Micó, C. Rihuete-Herrada, and R. Risch (2014), The La Bastida fortification: New light and new questions on Early Bronze Age societies in the western Mediterranean, *Antiquity*, *88*(340), 395–410, doi:10.1017/S0003598X00101073.

Magny, M., B. Vannière, G. Zanchetta, E. Fouache, G. Touchais, L. Petrika, C. Coussot, A.-V. Walter-Simonnet, and F. Arnaud (2009), Possible complexity of the climatic event around 4300—3800 cal. BP in the central and western Mediterranean, *The Holocene*, *19*(6), 823–833, doi:10.1177/0959683609337360.

Magri, D., and I. Parra (2002), Late Quaternary western Mediterranean pollen records and African winds, *Earth and Planetary Science Letters*, *200*(3-4), 401–408, doi:10.1016/S0012-821X(02)00619-2.

Maran, J. (1998), *Kulturwandel auf dem griechischen Festland und den Kykladen im späten 3. Jahrtausend v. Chr: Studien zu den kulturellen Verhältnissen in Südosteuropa und dem zentralen sowie östlichen Mittelmeerraum in der späten Kupfer- und frühen Bronzezeit*, Zugl.: Bonn, Univ., Habil.-Schr., 1994, *Universitätsforschungen zur prähistorischen Archäologie*, Bd. 53, Habelt, Bonn.

Marino, G., E. J. Rohling, F. Sangiorgi, A. Hayes, J. L. Casford, A. F. Lotter, M. Kucera, and H. Brinkhuis (2009), Early and middle Holocene in the Aegean Sea: Interplay between high and low latitude climate variability, *Quaternary Science Reviews*, *28*(27-28), 3246–3262, doi:10.1016/j.quascirev.2009.08.011.

Martiniano, R., L. M. Cassidy, R. Ó'Maoldúin, R. McLaughlin, N. M. Silva, L. Manco, D. Fidalgo, T. Pereira, M. J. Coelho, M. Serra, J. Burger, R. Parreira, E. Moran, A. C. Valera, E. Porfirio, R. Boaventura, A. M. Silva, and D. G. Bradley (2017), The population genomics of archaeological transition in west Iberia: Investigation of ancient substructure using imputation and haplotype-based methods, *PLoS genetics*, *13*(7), e1006852, doi:10.1371/journal.pgen.1006852.

Mischka, D. (2004), Aoristische Analyse in der Archäologie, *Archäologische Informationen: Mitteilungen zur Ur- und Frühgeschichte*, *27*(2), 233–243, doi:10.11588/ai.2004.2.12685.

Nocete, F., R. Lizcano, A. Peramo, and E. Gómez (2010), Emergence, collapse and continuity of the first political system in the Guadalquivir Basin from the fourth to the second millennium BC: The long-term sequence of Úbeda (Spain), *Journal of Anthropological Archaeology*, *29*(2), 219–237, doi:10.1016/j.jaa.2010.03.001.

Ontañón, R. (2013), Social dynamics in the recent prehistory of Northern Iberia: Examining the margins of the Mediterranean regions, in *The Prehistory of Iberia*, *Routledge Studies in Archaeology*, edited by M. Cruz Berrocal et al., pp. 203–230, Taylor and Francis, Hoboken.

Palmisano, A., A. Bevan, and S. Shennan (2017), Comparing archaeological proxies for long-term population patterns: An example from central Italy, *Journal of Archaeological Science*, *87*, 59–72, doi:10.1016/j.jas.2017.10.001.

Parcero Oubiña, C., and F. Criado Boado (2013), Social Change, Social Resistance.: A Long-Term Approach to the Processes of Transformation of Social Landscapes in the Northwest Iberian Peninsula, in *The Prehistory of Iberia*, *Routledge Studies in Archaeology*, edited by M. Cruz Berrocal et al., pp. 249–266, Taylor and Francis, Hoboken.

R Core Team (2017), *R: A Language and Environment for Statistical Computing*, R Foundation for Statistical Computing, Vienna, Austria.

Ratcliffe, J. H. (2000), Aoristic analysis: The spatial interpretation of unspecific temporal events, *International Journal of Geographical Information Science*, *14*(7), 669–679, doi:10.1080/136588100424963.

Riehl, S. (2008), Climate and agriculture in the ancient Near East: A synthesis of the archaeobotanical and stable carbon isotope evidence, *Veget Hist Archaeobot*, *17*(S1), 43–51, doi:10.1007/s00334-008-0156-8.

Risch, R., V. Lull, R. Micó, and C. Rihuete (2015), Transitions and conflict at the end of the 3rd millennium BC in south Iberia, in *2200 BC - ein Klimasturz als Ursache für den Zerfall der alten Welt?: 7. Mitteldeutscher Archäologentag vom 23. bis 26. Oktober 2014 in Halle (Saale)*, *Tagungen des Landesmuseums für Vorgeschichte Halle*, Band 12,1, edited by H. Meller et al., pp. 365–407, Landesamt für Denkmalpflege und Archäologie Sachsen-Anhalt, Landesmuseum für Vorgeschichte, Halle (Saale).

Rohling, E. J., and S. de Rijk (1999), Holocene Climate Optimum and Last Glacial Maximum in the Mediterranean: The marine oxygen isotope record, *Marine Geology*, *153*(1-4), 57–75, doi:10.1016/S0025-3227(98)00020-6.

Ruan, J., F. Kherbouche, D. Genty, D. Blamart, H. Cheng, F. Dewilde, S. Hachi, R. L. Edwards, E. Régnier, and J.-L. Michelot (2016), Evidence of a prolonged drought ca. 4200 yr BP correlated with prehistoric settlement abandonment from the Gueldaman GLD1 Cave, Northern Algeria, *Climate of the Past*, *12*(1), 1–14, doi:10.5194/cp-12-1-2016.

Schirrmacher, J., M. Weinelt, T. Blanz, N. Andersen, E. Salgueiro, and R. R. Schneider (2019), Multi-decadal atmospheric and marine climate variability in southern Iberia during the mid- to late-Holocene, *Clim. Past*, *15*(2), 617–634, doi:10.5194/cp-15-617-2019.

Senna-Martinez, J. C. (2014), Death as "life's mirror"?: Funerary practices and trajectories of complexity in the prehistory of peasant societies of Iberia, in *Rendering death: Ideological and archaeological narratives from recent prehistory (Iberia) : proceedings of the conference held in Abrantes, Portugal, 11 May 2013*, *BAR international series*, vol. 2648, edited by A. R. Cruz et al., pp. 35–44, Archaeopress, Oxford.

Shennan, S., S. S. Downey, A. Timpson, K. Edinborough, S. Colledge, T. Kerig, K. Manning, and M. G. Thomas (2013), Regional population collapse followed initial agriculture booms in mid-Holocene Europe, *Nat Commun*, *4*, 2486, doi:10.1038/ncomms3486.

Staubwasser, M., F. Sirocko, P. M. Grootes, and M. Segl (2003), Climate change at the 4.2 ka BP termination of the Indus valley civilization and Holocene south Asian monsoon variability, *Geophysical Research Letters*, *30*(8), 155, doi:10.1029/2002GL016822.

Stika, H. P. (1988), Botanische Untersuchungen in der bronzezeitlichen Höhensiedlung Fuente Álamo, *Madrider Mitteilungen* (29), 21–76.

Stika, H. P. (2001), Fuente álamo-Botanische Ergebnisse der Grabungskampagne 1988 in der bronzezeitlichen Höhensiedlung (Prov. Almería, Südostspanien), in *Die Grabungen von 1977 bis 1991 in einer bronzezeitlichen Höhensiedlung Andalusiens*, *Madrider Beiträge*, vol. 25, edited by H. Schubart et al., pp. 263–336, von Zabern, Mainz am Rhein.

Szécsényi-Nagy, A., C. Roth, G. Brandt, C. Rihuete-Herrada, C. Tejedor-Rodríguez, P. Held, Í. García-Martínez-de-Lagrán, H. Arcusa Magallón, S. Zesch, C. Knipper, E. Bánffy, S. Friederich, H. Meller, P. Bueno Ramírez, R. Barroso Bermejo, R. de Balbín Behrmann, A. M. Herrero-Corral, R. Flores Fernández, C. Alonso Fernández, J. Jiménez Echevarria, L. Rindlisbacher, C. Oliart, M.-I. Fregeiro, I. Soriano, O. Vicente, R. Micó, V. Lull, J. Soler Díaz, J. A. López Padilla, C. Roca de Togores Muñoz, M. S. Hernández Pérez, F. J. Jover Maestre, J. Lomba Maurandi, A. Avilés Fernández, K. T. Lillios, A. M. Silva, M. Magalhães Ramalho, L. M. Oosterbeek, C. Cunha, A. J. Waterman, J. Roig Buxó, A. Martínez, J. Ponce Martínez, M. Hunt Ortiz, J. C. Mejías-García, J. C. Pecero Espín, R. Cruz-Auñón Briones, T. Tomé, E. Carmona Ballestero, J. L. Cardoso, A. C. Araújo, C. Liesau von Lettow-Vorbeck, C. Blasco Bosqued, P. Ríos Mendoza, A. Pujante, J. I. Royo-Guillén, M. A. Esquembre Beviá, V. M. Dos Santos Goncalves, R. Parreira, E. Morán Hernández, E. Méndez Izquierdo, J. Vega y Miguel, R. Menduiña García, V. Martínez Calvo, O. López Jiménez, J. Krause, S. L. Pichler, R. Garrido-Pena, M. Kunst, R. Risch, M. A. Rojo-Guerra, W. Haak, and K. W. Alt (2017), The maternal genetic make-up of the Iberian Peninsula between the Neolithic and the Early Bronze Age, *Scientific reports*, *7*(1), 3459, doi:10.1038/s41598-017-15480-9.

Tierney, J. E., and P. B. deMenocal (2013), Abrupt shifts in Horn of Africa hydroclimate since the Last Glacial Maximum, *Science (New York, N.Y.)*, *342*(6160), 843–846, doi:10.1126/science.1240411.

Valcarce, R. F., and M. R.-G. Priego (1994), Ámbitos funerario y doméstico en la Prehistoria de NO. de la Península Ibérica, *Zephyrus: Revista de prehistoria y arqueología* (46), 143–160.

Valera, A. C. (2015), Social change in the late 3rd millennium BC in Portugal: the twilight of enclosures, in *2200 BC - ein Klimasturz als Ursache für den Zerfall der alten Welt?: 7. Mitteldeutscher Archäologentag vom 23. bis 26. Oktober 2014 in Halle (Saale)*, *Tagungen des Landesmuseums für Vorgeschichte Halle*, Band 12,1, edited by H. Meller et al., pp. 409–428, Landesamt für Denkmalpflege und Archäologie Sachsen-Anhalt, Landesmuseum für Vorgeschichte, Halle (Saale).

van Andel, T. H., E. Zangger, and A. Demitrack (1990), Land Use and Soil Erosion in Prehistoric and Historical Greece, *Journal of Field Archaeology*, *17*(4), 379, doi:10.2307/530002.

Vander Linden, M. (2017), Population history in third-millennium-BC Europe: Assessing the contribution of genetics, *World Archaeology*, *48*(5), 714–728, doi:10.1080/00438243.2016.1209124.

Walker, M. J. C., M. Berkelhammer, S. Björck, L. C. Cwynar, D. A. Fisher, A. J. Long, J. J. Lowe, R. M. Newnham, S. O. Rasmussen, and H. Weiss (2012), Formal subdivision of the Holocene Series/Epoch: A Discussion Paper by a Working Group of INTIMATE (Integration of ice-core, marine and terrestrial records) and the Subcommission on Quaternary Stratigraphy (International Commission on Stratigraphy), *J. Quaternary Sci.*, *27*(7), 649–659, doi:10.1002/jqs.2565.

Wanner, H., J. Beer, J. Bütikofer, T. J. Crowley, U. Cubasch, J. Flückiger, H. Goosse, M. Grosjean, F. Joos, J. O. Kaplan, M. Küttel, S. A. Müller, I. C. Prentice, O. Solomina, T. F. Stocker, P. Tarasov, M. Wagner, and M. Widmann (2008), Mid- to Late Holocene climate change: An overview, *Quaternary Science Reviews*, *27*(19-20), 1791–1828, doi:10.1016/j.quascirev.2008.06.013.

Waterman, A. J., K. T. Lillios, R. H. Tykot, and M. Kunst (2016), Environmental change and economic practices between the third and second millennia BC using isotope analyses of ovicaprid remains from the archeological site of Zambujal (Torres Vedras), Portugal, *Journal of Archaeological Science: Reports*, *5*, 181–189, doi:10.1016/j.jasrep.2015.11.017.

Weinelt, M., C. Schwab, J. Kneisel, and M. Hinz (2015), Climate and societal change in the western Mediterranean area around 4.2 ka BP, in *2200 BC - ein Klimasturz als Ursache für den Zerfall der alten Welt?: 7. Mitteldeutscher Archäologentag vom 23. bis 26. Oktober 2014 in Halle (Saale)*, *Tagungen des Landesmuseums für Vorgeschichte Halle*, Band 12,1, edited by H. Meller et al., pp. 461–480, Landesamt für Denkmalpflege und Archäologie Sachsen-Anhalt, Landesmuseum für Vorgeschichte, Halle (Saale).

Weiss, H. (2013), The Northern Levant During the Intermediate Bronze Age, in *The Oxford Handbook of the Archaeology of the Levant: c. 8000-332 BCE*, edited by A. E. Killebrew and M. Steiner, Oxford.

Welc, F., and L. Marks (2014), Climate change at the end of the Old Kingdom in Egypt around 4200 BP: New geoarchaeological evidence, *Quaternary International*, *324*, 124–133, doi:10.1016/j.quaint.2013.07.035.

Wenxiang, W., and L. Tungsheng (2004), Possible role of the "Holocene Event 3" on the collapse of Neolithic Cultures around the Central Plain of China, *Quaternary International*, *117*(1), 153–166, doi:10.1016/S1040-6182(03)00125-3.

Whitehouse, N. J., R. J. Schulting, M. McClatchie, P. Barratt, T. R. McLaughlin, A. Bogaard, S. Colledge, R. Marchant, J. Gaffrey, and M. J. Bunting (2014), Neolithic agriculture on the European western frontier: The boom and bust of early farming in Ireland, *Journal of Archaeological Science*, *51*, 181–205, doi:10.1016/j.jas.2013.08.009.

Williams, A. N. (2012), The use of summed radiocarbon probability distributions in archaeology: A review of methods, *Journal of Archaeological Science*, *39*(3), 578–589, doi:10.1016/j.jas.2011.07.014.

Chapter 5

Multi-decadal atmospheric and marine climate variability in southern Iberia during the Mid- to Late Holocene

Julien Schirrmacher, Mara Weinelt, Thomas Blanz, Nils Andersen, and Ralph R. Schneider, (2019): Multi-decadal atmospheric and marine climate variability in southern Iberia during the mid- to late-Holocene, Clim. Past 15, 617–634, doi: 10.5194/cp-15-617-2019

Please note that this study relies on meanwhile updated age models of both sediment cores.
The formatting of the original article has been changed.
Spelling mistakes have been corrected.

5 Multi-decadal atmospheric and marine climate variability in southern Iberia during the Mid- to Late Holocene

5.1 Abstract

To assess the regional multi-decadal to multi-centennial climate variability along the southern Iberian Peninsula during the Mid- to Late Holocene records of paleo-environmental indicators from marine sediments were established for two sites in the Alboran Sea (ODP-161-976A) and the Gulf of Cádiz (GeoB5901-2). High-resolution records of organic geochemical properties and planktonic foraminiferal assemblages are used to decipher precipitation and vegetation changes as well as hydrological conditions with respect to sea surface temperature (SST) and marine primary productivity (MPP). As a proxy for precipitation change records of plant derived *n*-alkane composition suggest a series of five distinct dry episodes in southern Iberia at 5.4 ± 0.3, from 5.1 to 4.9 ± 0.1, from 4.8 to 4.7 ± 0.1, from 4.4 to 4.3 ± 0.1 and, at 3.7 ± 0.1 cal. ka BP. During each dry episode the vegetation suffered from reduced water availability. Interestingly, the dry phase from 4.4 to 4.3 ± 0.1 cal. ka BP is followed by a rapid shift towards wetter conditions revealing a more complex pattern in terms of its timing and duration than was described for the 4.2 ka BP event in other regions. The series of dry episodes as well as closely connected hydrological variability in the Alboran Sea were probably driven by North Atlantic Oscillation (NAO)-like variability. In contrast, surface waters in the Gulf of Cádiz appear to have responded more directly to North Atlantic cooling associated with Bond Events. In particular, during Bond Events 3 and 4 a pronounced increase in seasonality with summer warming and winter cooling is found.

5.2 Introduction

Holocene climate has been considered to be fairly stable in comparison with the large and abrupt climatic changes during the last glacial and deglacial [*Martrat et al.*, 2007; *Rasmussen et al.*, 2014]. For the Mediterranean realm, generally long-term trends in sea surface temperature (SST) cooling [*Kim et al.*, 2004; *Martrat et al.*, 2014] and continental aridification [*Fletcher and Sánchez Goñi*, 2008; *Ramos-Román et al.*, 2018a] are described, superimposed by several short cold and dry perturbations, for example the 8.2 ka BP event or the North Atlantic Bond Events [*Alley et al.*, 1997; *Bond et al.*, 1997; *Mayewski et al.*, 2004]. Another prominent Holocene climate perturbation is the 4.2 ka BP event. This event, considered to have had global

impact, is associated with generally colder and wetter conditions over the North Atlantic as well as Northern and Central Europe and is broadly coincident with the onset of Neoglacial glacier advances in Scandinavia and the Alps [*Bakke et al.*, 2010; *Le Roy et al.*, 2017]. Additionally, intense droughts have been ascribed to this event for the mid-latitudes in Northern America and Eurasia including the Eastern and Central Mediterranean [*Booth et al.*, 2005; *Cheng et al.*, 2015; *Jalut et al.*, 2000; *Magny et al.*, 2013]. In the Western Mediterranean the 4.2 ka BP event is so far insufficiently resolved in existing marine and terrestrial archives. Several marine archives reveal even contrasting (dry vs. wet) signals [*Weinelt et al.*, 2015]. Concerning terrestrial records, a dry event at 4.2 cal. ka BP is suggested for southern Iberia [*Schröder et al.*, 2018; *Walczak et al.*, 2015] while relatively wet conditions were inferred for northern Morocco [*Zielhofer et al.*, 2019].

Similar to the manifestation of the 4.2 ka BP event in the Western Mediterranean region, the driving mechanism(s) for it are not well understood. Many studies suggest North Atlantic Oscillation (NAO)-like atmospheric variability as potential driver of climatic change during the Mid- to Late Holocene in the area [e.g. *Deininger et al.*, 2017; *Wassenburg et al.*, 2016]. The NAO is the dominant driver for the modern precipitation distribution in the Western Mediterranean and particularly active during winter [*Hurrell*, 1995]. Another potential driving mechanism not only of the oceanic variability are the cyclical Bond Events [*Bond et al.*, 1997], which are believed to weaken the thermohaline oceanic circulation and associated northward heat transport, thus, responsible for cooling of the northern hemisphere [*Bond et al.*, 2001; *Wanner et al.*, 2011].

Here, we explore the Mid- to Late Holocene climate development in southern Iberia on the basis of two marine sediment cores from the Gulf of Cádiz (GeoB5901-2) and the Alboran Sea (ODP-161-976A). Both sites are analysed for changes in terrestrial vegetation and precipitation as well as for changes in seasonal and annual SST and marine primary productivity (MPP). For that purpose, terrestrial *n*-alkane concentrations and the Norm33 *n*-alkane ratio from higher plant leaf-waxes are used to decipher the continental climate change. For the marine conditions, analyses of the alkenone-derived SST index ($U^{K'}_{37}$) and planktonic foraminiferal assemblages applying the modern analogue technique (MAT) were used to reconstruct annual mean and seasonal changes in SST. Changes in MPP are based on fluctuations in the content of alkenones in the bulk sediment. Altogether, this study aims to provide new insights into the temporal and spatial manifestation of the 4.2 ka BP event as well as to discuss potential driving mechanisms by linking terrestrial and marine surface climate variability in southern Iberia and adjacent oceans.

5.2.1 Study area

The Iberian Peninsula is influenced by the major Atlantic and Mediterranean atmospheric regimes [*Lionello*, 2012]. Today, the Atlantic climate is typically marked by relatively cool annual air temperatures and evenly distributed precipitation throughout the year. In contrast, the Mediterranean climate is characterized by pronounced seasonal contrasts with a rainy winter season and a dry and hot summer season. In general, most of the precipitation at the Iberian Peninsula occurs during the winter season (Fig 5.1) [*Lionello*, 2012]. The spatial pattern of winter precipitation clearly reflects the two atmospheric regimes (Fig 5.1). The Atlantic regime, which spans along the western and northern coasts, is characterized by high precipitation of more than 800 mm during winter. It is associated with the westerly wind belt at the Iberian Peninsula [*Zorita et al.*, 1992] and to a large extent controlled by the NAO winter conditions [*Hernández et al.*, 2015; *Hurrell*, 1995]. During positive NAO conditions (i.e. a high pressure difference between the Azores High and the Icelandic Low) North Atlantic storm tracks and associated precipitation are directed towards northern Europe, while Iberia receives less rainfall. On the other hand, during negative NAO conditions (i.e. a low pressure difference) storm tracks are directed towards the Iberian Peninsula, which then experiences wetter winters. The pronounced difference in precipitation is also evident in the seasonal variability of the river discharges in southern Iberia. For example, the average discharge of the Guadalquivir is below about 100 hm^3 per month from April to October and peaks during December and January with values above 400 hm^3 per month [*Fernández-Delgado et al.*, 2007]. Nonetheless, the central parts of the Iberian Peninsula as well as the eastern and southern coasts under influence of the Mediterranean climate remain relatively dry on average with precipitation less than 600 mm during winter (Fig 5.1).

A strong seasonal contrast is also evident in the surface ocean in the Gulf of Cádiz, which receives warm waters with the eastward Azores Current (AzC) that turns into a poleward surface current (Iberian Poleward Current; IPC) along the western Iberian coast during winter [*Peliz et al.*, 2005]. During summer, however, the surface current is directed southward and favours coastal upwelling along the western continental margin limiting the influence of the AzC and, thus, causing relatively low SSTs (Fig 5.1) [*Haynes et al.*, 1993; *Peliz et al.*, 2002]. These opposite oceanographic currents limit the seasonality recognized in the SSTs in the Gulf of Cádiz. The seasonal difference at the core location of GeoB5901-2 is typically ~6 °C during modern times [*Locarnini et al.*, 2013]. Atlantic surface water passes the Strait of Gibraltar and enters the Alboran Sea. Within the Alboran Sea it circulates in two anti-cyclonic gyres – the West Alboran Gyre (WAG) and the East Alboran Gyre (EAG) [*Lionello*, 2012]. At the WAG

relatively warm and fresh waters become upwelled almost continuously throughout the year [*Sarhan et al.*, 2000]. This upwelling is accompanied by an elevated MPP at the northern rim of the gyre [*Minas et al.*, 1991]. The modern seasonality in the Alboran Sea is very similar to the one in the Gulf of Cádiz (~6 °C).

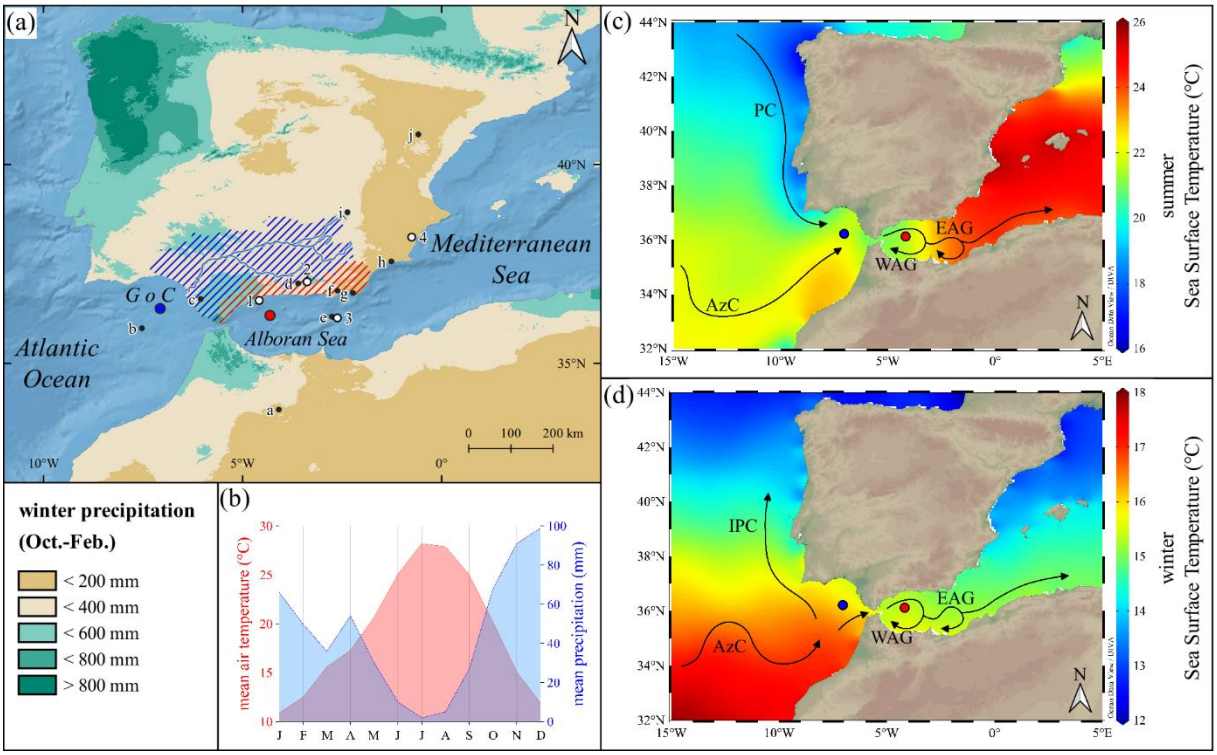

Figure 5.1 Overview maps. *(a) overview with discussed (black dots) and shown (white dots) references at the Iberian Peninsula and studied sediment cores. Cores of this study: GeoB5901-2 (blue dot) and ODP-161-976A (red dot). Shown references: 1: El Refugio Cave [Walczak et al., 2015], 2: Borreguil de la Virgen and Borreguil de la Caldera [García-Alix et al., 2018], 3: MD95-2043 [Cacho et al., 2001; Fletcher and Sánchez Goñi, 2008; Martrat et al., 2014; Pérez-Folgado et al., 2003], 4: Elx [Burjachs and Expósito, 2015]. Discussed references: a: Grotte de Piste [Wassenburg et al., 2016], b: MD99-2339 [Salgueiro et al., 2014], c: Lake Medina [Schröder et al., 2018], d: Padul [Ramos-Román et al., 2018a], e: TTR-293G [Rodrigo-Gámiz et al., 2014], f: San Rafael [Pantaléon-Cano et al., 2003], g: Cabo de Gata [Burjachs and Expósito, 2015], h: Mazarrón [Navarro-Hervás et al., 2014], i: Villaverde [Carrión et al., 2003] and, j: Ejulve cave [Moreno et al., 2017]. The main river system and associated catchment of the Guadalquivir (hatched blue area) is shown as well as the river catchments of various small-scale rivers draining the southern Sierra Nevada area (hatched red area). The river catchments have been downloaded from the website of the European Environmental Agency. The colour shading indicates the mean winter precipitation (October to February) from 1970 to 2000 in the area. The data was provided by WorldClim V2 [Fick and Hijmans, 2017]. (b) Annual average precipitation (blue) and air temperature (red) at Sevilla airport (1981-2010) show the high seasonality with rainy and cold winters and hot and dry summers. Data was provided by the Spanish State Meteorological Agency (AEMET). Mean summer (c) and winter (d) SSTs for the period 1955 – 2012 are shown. The data was provided by the World Ocean Atlas 2013 [Locarnini et al., 2013] and processed with Ocean Data View 5.1.2 [Schlitzer, 2016]. Black arrows indicate the surface currents in the area including the gyres in the Alboran Sea. Blue and red dot mark locations of sediment cores GeoB5901-2 and ODP-161-976A, respectively. AzC – Azores Current, IPC – Iberian Poleward Current, PC – Portugal Current, EAG – East Alboran Gyre, WAG – West Alboran Gyre.*

5.3 Materials and methods

5.3.1 Sediment cores and sampling

For this study two marine sediment cores from the Alboran Sea and the Gulf of Cádiz were analysed. Sediment core ODP-161-976A (36°12.32' N; 4°18.76' W; 1108 m water depth) was retrieved in the Alboran Sea during JOIDES RESOLUTION cruise in 1995 [*Comas et al.*, 1996]. To achieve multi-decadal resolution, the section from 100.0 cm to 149.0 cm was continuously sampled at 0.5 cm distances in the IODP Core Repository at MARUM in Bremen (Germany). The analysed section consists of homogenous clayey and silty sediments, which appear slightly bioturbated. No hiatus or depositional event (e.g. turbidite) has been recognized throughout the section [*Comas et al.*, 1996]. Sediment core GeoB5901-2 (36°22.80' N; 7°04.28' W; 574 m water depth) was retrieved during METEOR cruise in 1999 in the Gulf of Cádiz [*Schott et al.*, 2000]. This sediment core, containing hemipelagic mud, was sampled on 0.5 cm resolution from 1.0 cm to 50.0 cm in the GeoB Core Repository at MARUM in Bremen (Germany). The samples used for organic geochemical analysis were freeze-dried and homogenized prior to analysis.

5.3.2 Age model

Age models of both cores are based on existing and new AMS ^{14}C dates, all measured at Leibniz Laboratory at Kiel University (Tab 5.1). Published data of cores ODP-161-976A and GeoB5901-2 were taken from *Combourieu Nebout et al.* [2002] and *Kim et al.* [2004], respectively. In addition, we measured six new AMS ^{14}C dates on monospecific planktonic foraminiferal samples of *Globigerinoides ruber* white + pink or *Globigerina bulloides* larger than 150 µm from sediment core ODP-161-976A as well as seven new dates from sediment core GeoB5901-2. A section from 116.25 cm to 124.75 cm in ODP-161-976A included three samples yielding the same AMS ^{14}C age (see Tab 5.1). Since there is no evidence for strong bioturbation, hiatuses or, turbidites we assume a rather continuous sedimentation rate throughout the core and, thus, decided to take the date at 120.25 cm as the only age control point for this depth interval since it has been dated twice on two different planktonic foraminifera. The dates at 116.25 cm and 124.75 cm were not considered for the final age model in order to avoid artificially induced calculations of extraordinary high sedimentations rates in this thin sediment increment. The final age models have been calculated using Bacon [*Blaauw and Christen*, 2011]. During age model processing all AMS ^{14}C dates have been calibrated

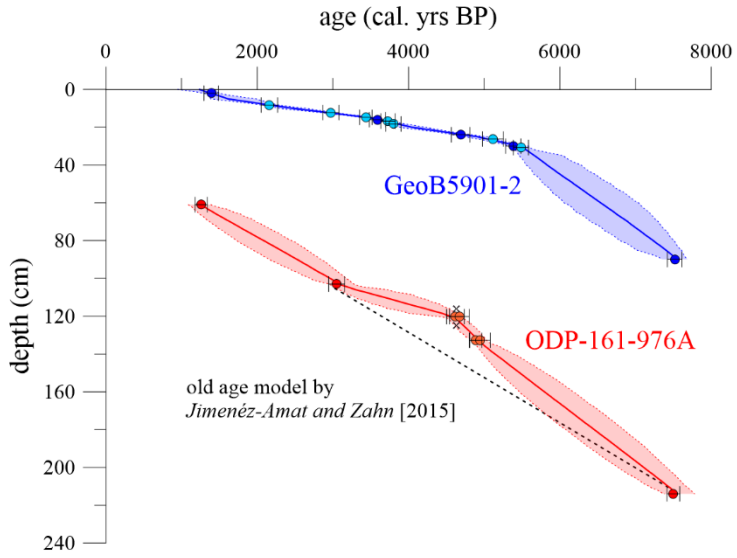

Figure 5.2 Age model. *The age model from ODP-161-976A (red) is based on AMS ^{14}C dates (red dots) from [Combourieu Nebout et al., 2002] and new AMS ^{14}C dates from this study (orange dots). Black crosses mark AMS ^{14}C dates considered as outliers. Black dotted line indicates the shift of the previous age model from Jiménez-Amat and Zahn [2015]. The Age model of GeoB5901-2 (blue) is based on AMS ^{14}C datings done by Kim et al. [2004] (dark blue dots) and new AMS ^{14}C dates accomplished during this study (light blue dots). The red and blue shaded area indicates the 95% probability of the age model for ODP-161-976A and GeoB5901-2, respectively. All AMS ^{14}C dates are listed in Tab 5.1.*

using the marine13 calibration curve including a global mean reservoir correction of 400 years [*Reimer et al.*, 2013]. Based on the AMS ^{14}C dates, we assume a relatively high accumulation rate for ODP-161-976A. Accordingly, we set the mean accumulation parameter of the model to 50 yr/cm and run the model for 2.5 cm thick sections to allow for a certain variability of the accumulation rates throughout the section. The accumulation rate of GeoB5901-2 is expected to be lower in the analysed section based on AMS ^{14}C data. Thus, the model parameters have been set to 100 yr/cm and 5 cm thick sections. In the case of sediment core ODP-161-976A the initial age model of *Jiménez-Amat and Zahn* [2015] was shifted significantly within the studied section by about 700 years. The reason for this shift are the new AMS ^{14}C dates accomplished during this study emphasizing the need of a dense dating strategy. According to the final age model, sedimentation rates range between 9.8 and 50.0 cm/kyr in core ODP-161-976A and between 4.8 and 33.3 cm/kyr in core GeoB5901-2, respectively. With 0.5 cm sampling intervals decadal to multi-decadal resolution is achieved. The studied section of sediment core ODP-161-976A dates between approximately 5.4 to 3.0 cal. ka BP exhibiting a temporal resolution between 10 to 57 years per sample with continuous high resolution between 5.4 and 4.6 cal. ka BP. The analysed section of sediment core GeoB5901-2 dates between approximately 6.2 and 1.8 cal. ka BP resulting in a temporal resolution between 15 and 104 years per sample. Age

models and sedimentation rates for both sediment cores are shown in Figs 5.2 and 5.3, respectively.

Table 5.1 Age model of sediment cores ODP-161-976A and GeoB5901-2. *All dates from previous studies have been re-calibrated. Not considered dates are shown in grey.*

sediment core	lab No.	depth (cm)	AMS^{14}C age (yr BP) ±σ	cal. age (yr BP) ±2σ	dated material	reference
GeoB5901-2	KIA-14522	2.00	1840 ± 35	1392 ± 96	planktic mix	[*Kim et al.*, 2004]
GeoB5901-2	KIA-53006	8.25	2485 ± 25	2162 ± 110	*G. ruber* w+p	this study
GeoB5901-2	KIA-53005	12.25	3185 ± 27	2973 ± 106	*G. ruber* w+p	this study
GeoB5901-2	KIA-53002	14.75	3545 ± 26	3436 ± 82	*G. ruber* w+p	this study
GeoB5901-2	KIA-14521	16.00	3685 ± 35	3590 ± 108	planktic mix	[*Kim et al.*, 2004]
GeoB5901-2	KIA-53003	16.75	3789 ± 27	3730 ± 95	*G. ruber* w+p	this study
GeoB5901-2	KIA-53004	18.25	3852 ± 27	3801 ± 100	*G. ruber* w+p	this study
GeoB5901-2	KIA-14520	24.00	4500 ± 40	4689 ± 123	planktic mix	[*Kim et al.*, 2004]
GeoB5901-2	KIA-52665	26.25	4820 ± 35	5116 ± 138	*G. ruber* w+p	this study
GeoB5901-2	KIA-14518	30.00	5035 ± 40	5384 ± 101	planktic mix	[*Kim et al.*, 2004]
GeoB5901-2	KIA-52666	30.75	5130 ± 40	5486 ± 99	*G. ruber* w+p	this study
GeoB5901-2	KIA-14516	90.00	7035 ± 55	7518 ± 97	planktic mix	[*Kim et al.*, 2004]
GeoB5901-2	KIA-13704	120.00	7495 ± 50	7955 ± 121	planktic mix	[*Kim et al.*, 2004]
ODP-161-976C	KIA-6435	61.00	1710 ± 40	1259 ± 82	*G. bulloides*	[*Combourieu Nebout et al.*, 2002]
ODP-161-976C	KIA-6436	103.00	3235 ± 30	3050 ± 106	*G. bulloides*	[*Combourieu Nebout et al.*, 2002]
ODP-161-976A	KIA-53326	116.25	4435 ± 35	4636 ± 138	*G. bulloides*	this study
ODP-161-976A	KIA-53235	120.25	4435 ± 30	4619 ± 117	*G. ruber* w+p	this study
ODP-161-976A	KIA-53327	120.25	4480 ± 40	4671 ± 130	*G. bulloides*	this study
ODP-161-976A	KIA-53236	124.75	4435 ± 35	4636 ± 138	*G. ruber* w+p	this study
ODP-161-976A	KIA-53234	132.75	4650 ± 35	4885 ± 84	*G. ruber* w+p	this study
ODP-161-976A	KIA-53325	132.75	4700 ± 50	4945 ± 134	*G. bulloides*	this study
ODP-161-976C	KIA-6437	214.00	7010 ± 50	7500 ± 84	*G. bulloides*	[*Combourieu Nebout et al.*, 2002]

5.3.3 Organic geochemical analysis and calculations

Lipids were extracted from the freeze-dried and finely ground sediment samples with an Accelerated Solvent Extractor (ASE-200, Dionex) at 100 bar and 100 °C using a 9:1 (v/v) mixture of dichloromethane (DCM) and methanol. After extraction samples were de-sulphured by stirring for 30 minutes with activated copper. The de-sulphured lipids were subsequently separated by silica gel column chromatography using activated silica gel (450 °C for 4 h) into neutral (hexane) and polar (DCM) fractions containing *n*-alkanes and alkenones, respectively.

The neutral fraction was further separated using silver-nitrate ($AgNO_3$) coated silica gel. Samples were then left at room temperature for approximately 24 hours for homogenisation.

Afterwards, *n*-alkanes were analysed by gas chromatography (GC) using an Agilent 6890N gas chromatograph equipped with a Restek XTI-5 capillary column (30 m x 320 µm x 0.25 µm) and a Flame Ionization Detector (FID) at the Institute of Geosciences, Kiel University. Example chromatograms are provided in the supplement of this paper. *n*-Alkanes were identified by comparison of their retention times with an external standard containing a series of *n*-alkane homologues of known concentration. On this basis, *n*-alkanes were also quantified using the FID peak areas calibrated against the external standard. For environmental interpretation the sum of terrestrial sourced, odd *n*-alkane homologues *n*-C_{27} to *n*-C_{33} is used. The mean analytical error (2σ) is 7.0 ng/ g sediment based on replicate analyses (n = 62).

Various studies used ratios among individual *n*-alkane homologues as environmental sensitive parameter, for example the Norm33 ratio [e.g. *Herrmann et al.*, 2016]. The Norm33 ratio was calculated by the following equation:

$$\text{Norm33} = n\text{-}C_{33} / (n\text{-}C_{29} + n\text{-}C_{33}) \quad (1)$$

where *n*-C_X is the peak area of the *n*-alkane with x carbon atoms in the chromatogram. The mean analytical error (2σ) is 0.004 based on replicate analyses (n = 62).

Alkenones were analysed on a multi-dimensional, double gas column chromatography (MD-GC) set up with two Agilent 6890 gas chromatographs. The compounds ($C_{37:2}$ and $C_{37:3}$) were quantified by calibration to an external standard. The alkenone concentration is derived from the sum of the $C_{37:2}$ and $C_{37:3}$ isomers with a mean analytical error (2σ) of 6.9 ng/g sediment. The alkenone unsaturation index ($U_{37}^{K'}$) was obtained by using the peak areas of the aforementioned compounds applying the equation of *Prahl and Wakeham* [1987]:

$$U_{37}^{K'} = C_{37:2} / (C_{37:2} + C_{37:3}) \quad (2)$$

where $C_{37:X}$ represents the respective peak area in the chromatogram. The $U_{37}^{K'}$ index was subsequently transferred into annual mean SST using the calibration of *Müller et al.* [1998]:

$$\text{SST (°C)} = (U_{37}^{K'} - 0.044)/ 0.033 \quad (3)$$

The laboratory internal analytical error is approximately 0.12 °C, while the error of the calibration is 1.5 °C.

5.3.4 Planktonic foraminiferal analysis and modern analogue technique

For foraminiferal analysis sediment samples of approximately 10 cc were washed over 63 μm sieves, dried at 40 °C and, subsequently dry sieved for larger fractions. Planktonic foraminifera assemblages were analysed in the size fractions >150 μm enabling the application of commonly used transfer techniques for SST reconstructions based on relative abundances of 26 taxonomic categories within the assemblage, following concept by *Pflaumann et al.* [1996]. For reliable assemblage counts samples were dry split into aliquots of at least 300 specimens with a Kiel dry sample splitter. For SST estimates we used SIMMAX non-distance-weighted modern analogue technique, using a similarity index of >0.963 and based on 10 closest analogues [*Pflaumann et al.*, 2003]. Because the study sites are influenced by Atlantic and Mediterranean ocean circulation, we combined an updated North Atlantic core top database [*Kucera et al.*, 2005a; *Kucera et al.*, 2005b; *Salgueiro et al.*, 2014] and the Mediterranean database [*Hayes et al.*, 2005] with modern temperature at 10 m water depth taken from the World Ocean Atlas 1998 [*Salgueiro et al.*, 2014]. Seasonal temperatures are averaged for northern hemisphere summer (July to September) and winter (December to February). This method applied on overall 1212 core top samples from the Atlantic and the Mediterranean yields a root-mean square error predicted accuracy of ± 1.3 °C for summer and winter seasons.

5.4 Results

5.4.1 ODP-161-976A

Terrestrial proxies. The terrestrial *n*-alkane concentration varies between 67 and 714 ng/g sediment exhibiting no long-term trend across the covered time period from 5.4 to 3.0 cal. ka BP (Fig 5.3). Three distinct concentration minima below 200 ng/g sediment can be observed at 5.4 cal. ka BP, from 5.0 to 4.9 cal. ka BP and, from about 4.8 to 4.7 cal. ka BP. Less distinct minima are observed between 4.4 and 4.3 cal. ka BP and at about 3.7 cal. ka BP. A sharp increase towards high concentrations of up to 617 ng/g sediment is evident at about 4.2 cal. ka BP. *n*-Alkane concentrations appear to remain generally above 450 ng/g sediment until 3.8 cal. ka BP, when concentrations sharply decrease towards 209 ng/g sediment at 3.7 cal. ka BP. Afterwards, *n*-alkane concentrations reveal a slightly increasing trend towards 3.0 cal. ka BP. The Norm33 ratio exhibits no trends and varies between 0.29 and 0.49 (Fig 5.3). Four sharp increases towards values greater than 0.42 can be recognized at about 5.4 cal. ka BP, from 5.0

to 4.9 cal. ka BP, from 4.8 to 4.7 cal. ka BP and, at about 4.6 cal. ka BP. Apparently, the Norm33 maxima parallel the *n*-alkane concentration minima between 5.4 and 4.7 cal. ka BP.

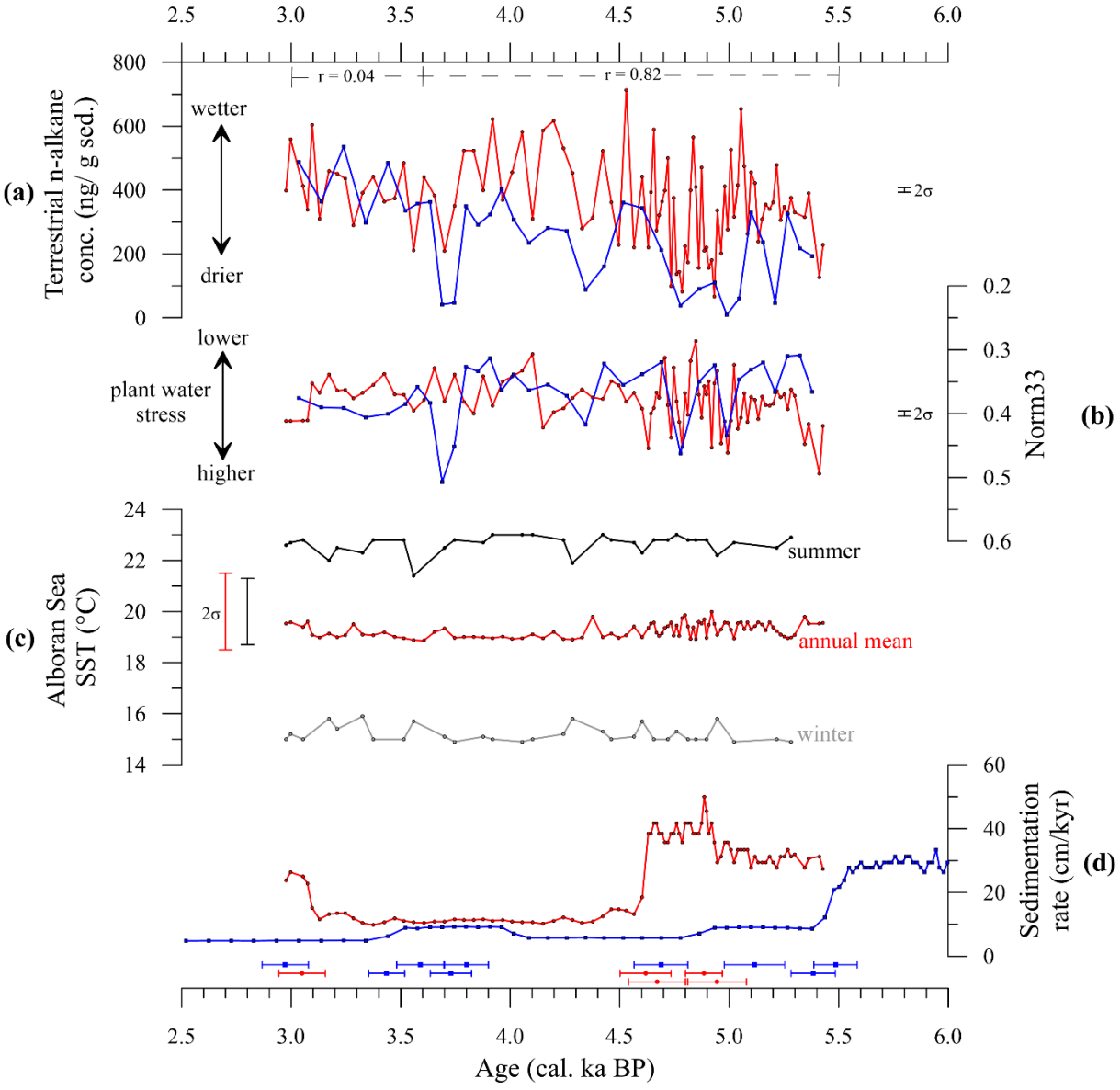

Figure 5.3 Data of marine sediment cores ODP-161-976A (red) and GeoB5901-2 (blue). *(a) Terrestrial n-alkane concentration (n-C_{27-33}) indicative of precipitation change. Pearson's correlation coefficient has been calculated based on 100-year time slices for two periods (see supplement for further information). (b) Norm33 n-alkane ratio showing plant water stress. (c) Alkenone and planktonic foraminifera based sea surface temperature (SST) reconstruction from ODP-161-976A (black – summer; grey – winter; red – annual mean). Error bars indicate the uncertainty of the calibration for the annual mean (red) and seasonal (black) reconstructions. (d) Sedimentation rate of both cores are shown for comparison. Coloured dots at the bottom show AMS ^{14}C age control points and associated 2σ errors.*

Marine proxies. The alkenone-derived annual mean SST remains quite stable between 18.9 °C and 20.0 °C (Fig 5.3). No trends are visible in the analysed time period. Only weak maxima in the annual mean SST of 0.5 to 1.0 °C in amplitude are apparent at about 5.4, 3.3 and, 3.0 cal.

ka BP as well as between 5.1 and 4.6 cal. ka BP at about 100 year intervals (Fig 5.4). All foraminifera-derived seasonal SST reconstructions suggest similar stable temperature conditions without any obvious trends between 5.4 and 3.0 cal. ka BP. Summer SSTs vary around 22.8 ± 0.1 °C with several cooling episodes of up to 1 °C at about 5.0, 4.6, 4.3, 3.6, 3.3 and, 3.2 cal. ka BP. Winter SST generally vary around 15.0 ± 0.1 °C with weak warming episodes of up to 1 °C at about 5.0, 4.6, 4.3, 3.6, 3.3 and, 3.2 cal. ka BP. Thus, the winter SST maxima and summer SST minima are contemporaneous and result in a decreasing seasonal SST difference during these periods. Notably, the seasonal SST maxima or minima, respectively, do not parallel the SST maxima observed in the annual mean reconstruction. The alkenone concentration varies between about 224 and 440 ng/ g sediment and shows an increasing trend from 5.4 to 4.0 cal. ka BP followed by a decreasing trend towards 3.0 cal. ka BP (Fig 5.4). These trends are superimposed by several minima from 5.4 to 5.3 cal. ka BP, around 5.2, 5.0, 4.8 cal. ka BP, from 4.7 to 4.6 cal. ka BP, at 3.8 cal. ka BP and, from 3.1 to 3.0 cal. ka BP. The alkenone concentration is to some degree correlated (r = 0.61) to the annual mean SST across the studied time period (see supplement) with warmer annual mean SSTs paralleled by decreased alkenones content at about 5.4, 5.2, 4.9, 4.7, 4.6 cal. ka BP and, from 3.1 to 3.0 cal. ka BP (Fig 5.4).

5.4.2 GeoB5901-2

Terrestrial proxies. The terrestrial *n*-alkane concentration varies between 9 and 535 ng/g sediment and has an increasing trend towards younger ages between 5.4 and 3.0 cal. ka BP (Fig 5.3). During the studied time period at least three periods of decreasing *n*-alkane concentration below 100 ng/g sediment are found from 5.1 to 4.7 cal. ka BP, from 4.4 to 4.3 cal. ka BP and, at about 3.7 cal. ka BP. The oldest concentration minimum reveals a “W”-shaped pattern with increasing concentrations of up to 110 ng/g sediment at about 4.9 cal. ka BP. An additional concentration minimum (46 ng/g sediment) at 5.2 cal. ka BP is only corroborated by a single data point and, thus, not robust. The Norm33 varies without any trends between 0.31 and 0.51 showing high amplitude maxima with values above 0.42 at about 5.0, 4.8, 4.3 and, 3.7 cal. ka BP (Fig 5.3). Notably, the Norm33 reveals maxima during periods of low terrestrial *n*-alkane concentration.

Marine proxies. Alkenone-derived annual mean SST vary without any trends between 5.5 and 3.0 cal. ka BP and reveal SSTs around 20.4 ± 0.3 °C with the exception of a period from about 4.3 to 3.9 cal. ka BP, where SST vary around 21.6 ± 0.6 °C with maximum SST being 22.7 °C

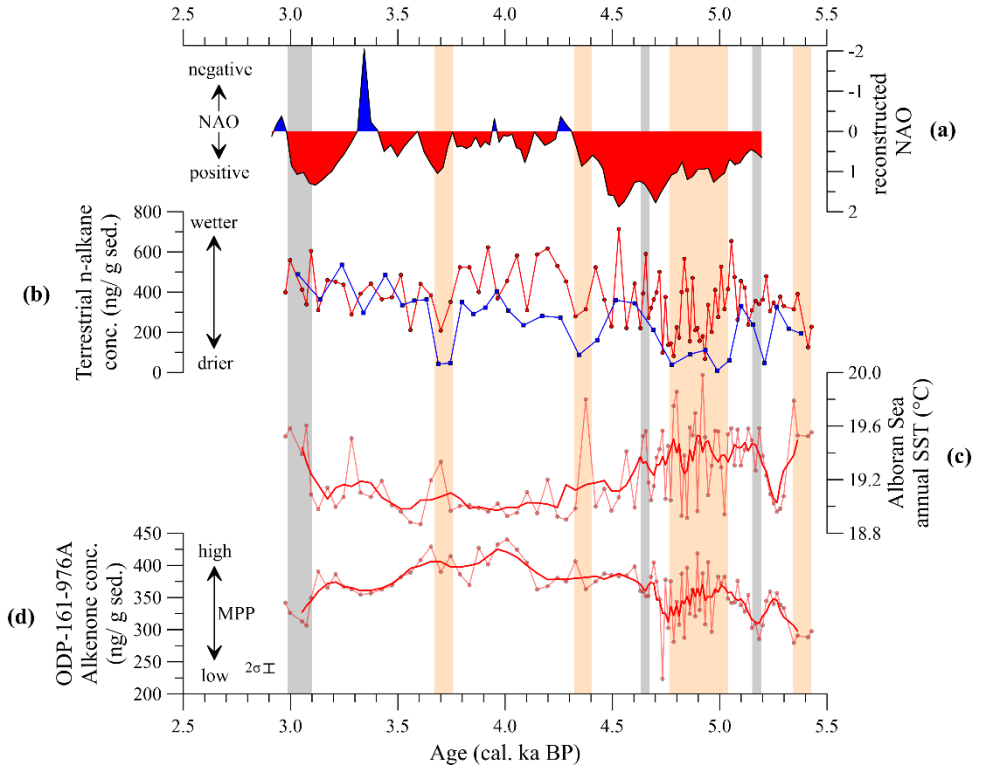

Figure 5.4 Potential driver of atmospheric and Alboran Sea climate variability. *(a) NAO reconstruction [Olsen et al., 2012]. (b) Terrestrial n-alkane concentrations from ODP-161-976A (red) and GeoB5901-2 (blue) (this study). (c) Annual mean SST from ODP-161-976A (this study). (d) Alkenone concentration from ODP-161-976A indicative of MPP variability (this study). Thick red lines show the 5-point running means. Orange bars indicate dry phases observed in this study, while grey bars indicate periods of annual mean SST maxima and MPP minima at the core location of ODP-161-976A.*

(Fig 5.5). Foraminifera-derived summer SST reveal a slight decreasing trend towards the present between 6.2 and 1.8 cal. ka BP. Notably, between about 6.2 and 4.0 cal. ka BP the variability in summer SST is quite high with a mean of 22.4 ± 0.7 °C superimposed by several warm events of up to 23.9 °C that occur at 6.0, 5.8, 5.5, 4.7 and, 4.1 cal. ka BP. Also, the variability and the amplitudes of the warm events decrease towards the present. After 4.0 cal. ka BP summer SST vary around 21.7 ± 0.2 °C. Winter SST reveal a very similar pattern compared to the summer SST with high variability (16.0 ± 0.7 °C) until 4.0 cal. ka BP and less (16.8 ± 0.2 °C) afterwards. Overall, there is a warming trend from about 16 to 17 °C towards younger ages with major cooling episodes at 6.0, 5.8, 5.5, 4.7 and, 4.1 cal. ka BP. Winter SST decrease below 15.0 °C during most of these periods. The observed SST events in the seasonal reconstructions (summer and winter) are contemporaneous and result in an increasing seasonal difference of up to 9.3 °C during these events (Fig 5.5). Overall, the seasonal difference is decreasing towards younger ages from 6.4 to 4.7 °C. SST events within the seasonal reconstructions do not parallel any events in the alkenone derived annual mean SST. The warm period observed in the annual mean data between 4.3 and 3.9 cal. ka BP is not visible in the

seasonal data. Also, the annual mean SST is very close to summer conditions, even exceeding those around 4.2 cal. ka BP.

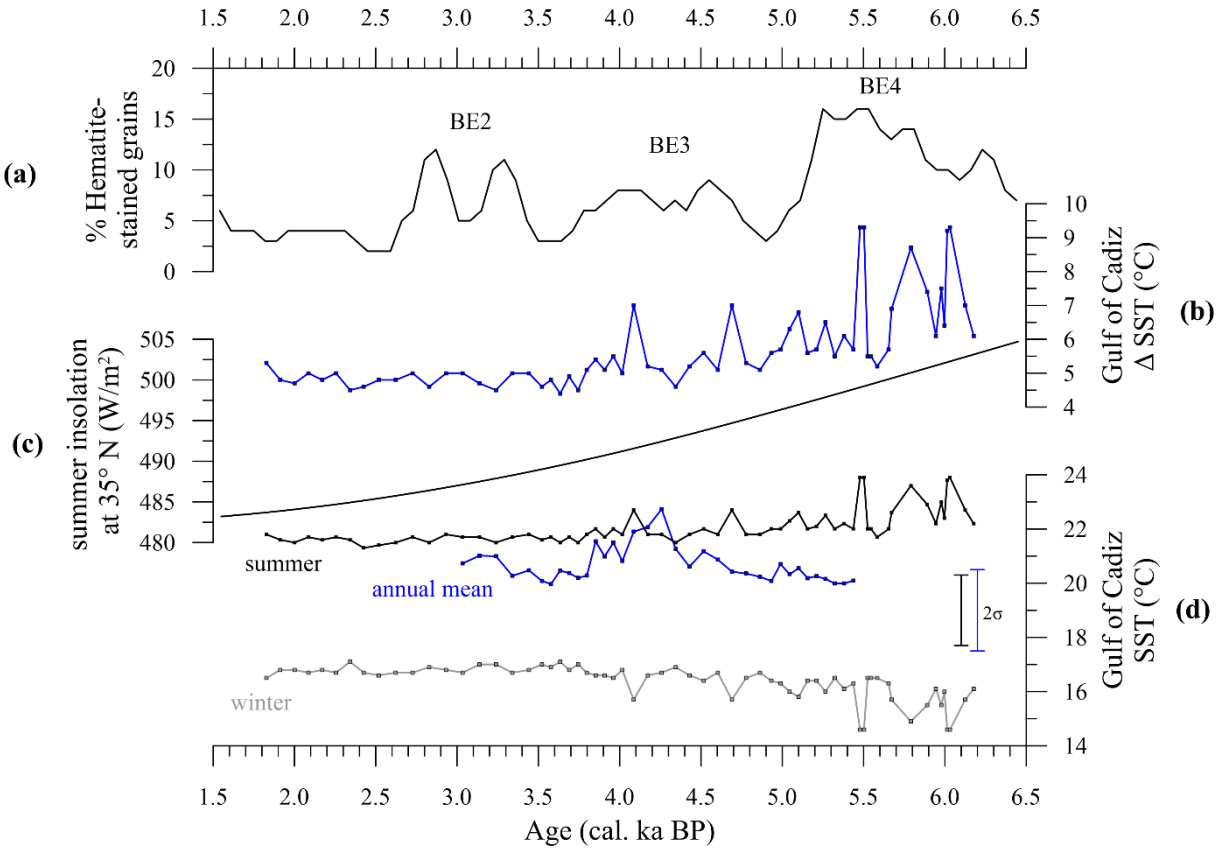

Figure 5.5 Oceanic variability in the Gulf of Cádiz. *(a) Stacked hematite-stained grain percentages from marine sediment cores in the North Atlantic showing Bond Events (BEs) 2 to 4 [Bond et al., 2001]. (b) Seasonal SST difference (winter – summer) deduced from the GeoB5901-2 foraminiferal data. (c) Summer insolation at 35° N [Laskar et al., 2004]. (d) Alkenone and planktonic foraminifera based SST reconstruction from GeoB5901-2 (black – summer; grey – winter; blue – annual mean). Error bars indicate the uncertainty of the calibration for the annual mean (blue) and seasonal (black) reconstructions.*

5.4.3 Comparison of both sediment cores

In general, a good agreement between the *n*-alkane concentration in both sediment cores is apparent (Fig 5.3). This is corroborated by the high correlation coefficient (r = 0.82) for the period between 5.5 and 3.6 cal. ka BP. Since the correlation calculation is based on 100-year time slices (see supplement), there is not such a robust correlation in the younger part between 3.6 and 3.0 cal. ka BP (r = 0.04). Nonetheless, visual inspection implies a good agreement between both records when only the more pronounced minima and maxima are considered for this younger interval. The *n*-alkane concentration minima observed at about 4.3 and 3.7 cal. ka BP appear to be contemporaneous in both regions. Also, the two events from about 5.0 to 4.9 cal. ka BP and from 4.8 to 4.7 cal. ka BP in ODP-161-976A as well as the “W”-shaped event

between 5.1 and 4.7 cal. ka BP in GeoB5901-2 correspond to a large extent. Only the drop towards low *n*-alkane concentrations between 5.1 and 5.0 cal. ka BP is offset by about 100 years (Fig 5.3). Bearing in the mind the chronological uncertainties around 5.0 cal. ka BP of ±110 years and ±160 years in the age model of GeoB5901-2 and ODP-161-976A, respectively, this offset likely is chronological bias. The Norm33 maxima of both sediment cores correspond well between 5.4 and 4.7 cal. ka BP (Fig 5.3).

With respect to absolute SST values and trends in the temperature reconstructions, differences between both cores are larger than for the terrestrial biomarker records. The alkenone-based as well as the foraminifera-derived winter SST were about 1 °C warmer in the Gulf of Cádiz, while summer SST were about 1 °C warmer in the Alboran Sea. The most apparent difference between both regions is noticeable in the seasonal warm/cold events, which do not agree in their timing, as is the same for the much more moderate events observed in the alkenone-based SST records. Also, the overall trend in the difference in seasonal SST estimates is not similar in both regions. While in the Gulf of Cádiz (GeoB5901-2) the seasonal difference increases (i.e. summer warming and winter cooling), the seasonal difference in the Alboran Sea record (ODP-161-976A) record does not change significantly.

5.5 Discussion

5.5.1 Terrestrial climate conditions in southern Iberia

Terrestrial plants synthesize long-chain *n*-alkanes in their leaves as coating for protection against water loss [*Eglinton and Hamilton*, 1967]. These long-chain *n*-alkanes are either eroded directly from the leaves by wind or deposited in the soils in autumn. Afterwards, *n*-alkanes are removed from the atmosphere or eroded from the soils by rain and are further transported into the marine realm via aeolian and riverine transport [e.g. *Bird et al.*, 1995; *Conte and Weber*, 2002; *Schreuder et al.*, 2018]. The fraction of the riverine input in coastal areas is usually much higher compared to the aeolian input. Therefore, terrestrial *n*-alkane concentrations have already been successfully applied to study the riverine input in marine settings in the Mediterranean [*Abrantes et al.*, 2017; *Cortina et al.*, 2016; *Jalali et al.*, 2016; *Jalali et al.*, 2017]. More specifically, *Rodrigo-Gámiz et al.* [2015] have shown from radiogenic isotopes that in the Alboran Sea the riverine dominates the aeolian input during the studied time period. Because of the dominant riverine transport mechanism, it is assumed that both proxies integrate spatially over the river catchment areas shown in Fig 5.1 and, thus, indicate climate conditions

for the entire southernmost Iberian Peninsula. The dominant catchment for sediment core GeoB5901-2 is the one of the Guadalquivir river draining into the Gulf of Cádiz. The smaller mountainous rivers draining the southern Sierra Nevada area are considered as more relevant for sediment core ODP-161-976A. A delivery of material from the Guadalquivir with the inflow of the Atlantic water through the Strait of Gibraltar cannot be excluded, though. Since the river discharge and also the plant growing season is strongly coupled to precipitation and the rainy season at the Iberian Peninsula is in winter (Fig 5.1) [*Lionello*, 2012], the *n*-alkane proxies are probably biased towards the winter season.

Consequently, intervals of very low *n*-alkane concentration in the studied cores are interpreted as periods of dry winters, which occurred in southern Iberia at 5.4 ± 0.3, from 5.1 to 4.9 ± 0.1, from 4.8 to 4.7 ± 0.1, from 4.4 to 4.3 ± 0.1 and, at 3.7 ± 0.1 cal. ka BP (Fig 5.3). Drier conditions at about 5.5 cal. ka BP well in phase with the end of the African Humid Period [*deMenocal et al.*, 2000]. This transition appears to be marked by an aridity event as evidenced by speleothem data from El Refugio Cave and Grotte de Piste [*Walczak et al.*, 2015; *Wassenburg et al.*, 2016] and high charcoal concentration in Cabo de Gata between about 5.4 and 5.3 cal. ka BP. Also, a contemporaneous remarkable decrease in Mediterranean forest was noticed by *Ramos-Román et al.* [2018b] from 5.5 to 5.4 cal. ka BP. *Schröder et al.* [2018] describe a drought event centred at about 5.3 cal. ka BP in Lake Medina (SW Iberia). The dry phases between about 5.1 and 4.9 and from 4.8 to 4.7 cal. ka BP observed in this study are corroborated by regional speleothem records [*Moreno et al.*, 2017; *Wassenburg et al.*, 2016]. A dramatic forest decline occurred between 5.0 and 4.5 cal. ka BP in SE Iberia [*Pantaléon-Cano et al.*, 2003] along with high charcoal concentrations at Cabo de Gata indicating more frequent wild fires [*Burjachs and Expósito*, 2015]. Moderate forest declines are found in pollen records from the Alboran Sea and Elx sequence (Fig 5.6) [*Burjachs and Expósito*, 2015; *Fletcher and Sánchez Goñi*, 2008]. The following period between 4.4 and 3.8 cal. ka BP comprising the 4.2 ka BP event is discussed in more detail in chapter 5.5.2. The youngest dry phase found in this study at about 3.7 cal. ka BP has also been inferred from pollen data at Elx and Villaverde [*Burjachs and Expósito*, 2015; *Carrión et al.*, 2001], while pollen data from the Alboran Sea indicate a moderate forest decline [*Fletcher and Sánchez Goñi*, 2008]. Additional evidence for a severe dry phase around 3.7 cal. ka BP again stems from speleothem data [*Moreno et al.*, 2017; *Walczak et al.*, 2015].

Notably, in the GeoB5901-2 data all dry episodes are paralleled by Norm33 maxima, while in the ODP-161-976A record the dry phases at about 5.4, 4.9 and, 4.7 cal. ka BP coincide with Norm33 maxima (Fig 5.3). A tendency towards higher *n*-alkane chain lengths, as revealed by

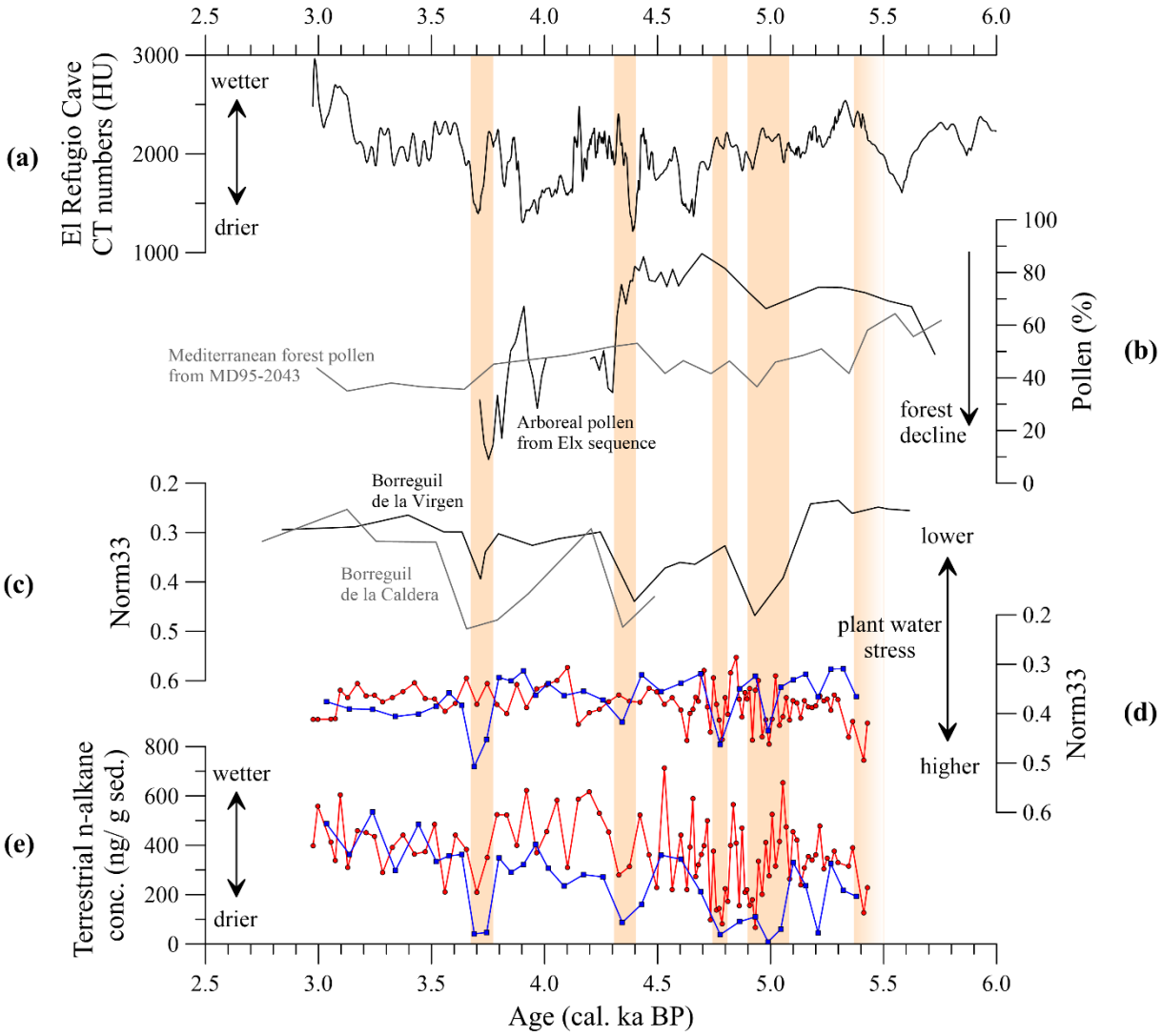

Figure 5.6 Proxy data from the Iberian Peninsula. *(a) Speleothem density data from El Refugio Cave [Walczak et al., 2015]. (b) Pollen data from Elx sequence [Burjachs and Expósito, 2015; Burjachs et al., 1997] and marine sediment core MD95-2043 [Fletcher and Sánchez Goñi, 2008]. (c) Norm33 n-alkane ratios from Borreguil de la Caldera and Borreguil de la Virgen. These data have been calculated on the basis of n-alkane raw data from [García-Alix et al., 2018]. (d) Norm33 n-alkane ratios from ODP-161-976A (red) and GeoB5901-2 (blue) (this study). (e) Terrestrial n-alkane concentrations from ODP-161-976A (red) and GeoB5901-2 (blue) (this study). The orange bars indicate dry phases observed in this study. The locations of all the references are shown in Fig 5.1.*

increasing Norm33 values, is an indication for warmer and/or drier environmental conditions [*Bush and McInerney*, 2013; *Leider et al.*, 2013; *Rommerskirchen et al.*, 2006]. A local study from southern Iberia further shows that increasing chain lengths are a function of decreasing water availability [*García-Alix et al.*, 2017]. Consequently, the Norm33 maxima observed in this study indicate high water stress for the plants in relation to the dry climate episodes. This is supported by Sierra Nevada bog sediments Borreguil de la Virgen and Borreguil de la Caldera (Fig 5.6) [*García-Alix et al.*, 2018], which also show Norm33 maxima during such dry episodes. It has further been shown that Mediterranean forests declined while scrubs expanded in

southern Iberia during the respective dry phases [*Fletcher et al.*, 2007; *Ramos-Román et al.*, 2018a; *Ramos-Román et al.*, 2018b]. Accordingly, the dry episodes caused a noticeable response in the vegetation, which suffered from decreasing water availability. This further implies that the vegetation in southern Iberia at that time was very sensitive to winter precipitation changes.

5.5.2 The 4.2 ka BP event

The manifestation of the 4.2 ka BP event across the Mediterranean is currently intensively debated with a particular focus on the western part. In the Eastern and Central Mediterranean many studies suggest a dry phase in the time window between 4.4 and 3.8 cal. ka BP [e.g. *Calò et al.*, 2012; *Cheng et al.*, 2015; *Finné et al.*, 2017; *Zanchetta et al.*, 2016]. In the Western Mediterranean evidence for a dry phase associated with the 4.2 ka BP event comes from northern Algeria [*Ruan et al.*, 2016] and pollen data from southern Iberia [*Ramos-Román et al.*, 2018a]. Furthermore, a drastic forest opening in SE Iberia is indicated from pollen sequences at Cabo de Gata around 4.4 cal. ka BP and at Elx at about 4.3 cal. ka BP (Fig 5.6) [*Burjachs and Expósito*, 2015]. Additional indications for a dry phase coinciding with the 4.2 ka BP event come from lithological analyses in SE Iberia [*Navarro-Hervás et al.*, 2014], a hiatus in pollen data from SW Iberia [*Schröder et al.*, 2018], and speleothem data [*Moreno et al.*, 2017; *Walczak et al.*, 2015; *Wassenburg et al.*, 2016].

Compared to the prolonged dry phase between about 4.4 and 3.8 cal. ka BP recorded in speleothems from the Italian Peninsula and Algeria [*Ruan et al.*, 2016; *Zanchetta et al.*, 2016], our data indicate a more complex environmental pattern around the 4.2 ka BP event. The terrestrial *n*-alkane concentrations suggest a brief dry period from about 4.4 to 4.3 cal. ka BP followed by a rapid return to relatively moister conditions after about 4.2 cal. ka BP, which lasted until approximately 3.8 cal. ka BP. The Norm33 data, further, shows a peak in the GeoB5901-2 at about 4.3 cal. ka BP indicating that plants in the Guadalquivir basin were suffering from water stress. Contrastingly, the intermediate drop in *n*-alkane concentration in ODP-161-976A from the Alboran Sea is not paralleled by a Norm33 maximum. This might imply that the dry episode between about 4.4 and 4.3 cal. ka BP was more severely manifested in the lowlands of the Guadalquivir basin compared to the high altitudes of the Sierra Nevada. Altogether, our reconstructions show that the onset of the dry phase at about 4.4 cal. ka BP is in line with proxy data from the Central Mediterranean, while the rapid return to relatively moister conditions at about 4.2 cal. ka BP lasting until about 3.8 cal. ka BP highlights regional differences in the duration of the 4.2 ka BP event compared to the prolonged dry phase

associated with the 4.2 ka BP event in Italian and Algerian speleothems [*Ruan et al.*, 2016; *Zanchetta et al.*, 2016]. This interpretation is corroborated by dry conditions at 4.4 cal. ka BP and wet conditions at 4.2 cal. ka BP found in ostracod shells from northern Morocco [*Zielhofer et al.*, 2017; *Zielhofer et al.*, 2019].

5.5.3 Hydrological conditions in the Gulf of Cádiz and the Alboran Sea

In contrast to the terrestrial climate variability our marine reconstructions suggest fairly stable conditions between 5.4 and 3.0 cal. ka BP in the Alboran Sea and between 6.2 and 1.8 cal. ka BP the Gulf of Cádiz. The maximum range in the annual mean values based on alkenones is about 1 °C and, thus, within the calibration uncertainty. The low temporal resolution of previously studied cores from the area (below about 115 and 250 years for annual mean and seasonal data, respectively) further hampers the comparison with here observed SST events. Therefore, a careful interpretation of the alkenone-based SST results is required.

Alkenone-derived SSTs from sediment core ODP-161-976A suggest annual mean temperatures between 18.9 and 20.0 °C (Fig 5.4), which exceed the modern values of about 18.0 °C [*Locarnini et al.*, 2013]. An overall cooling trend over the course of the Mid- to Late Holocene in response to decreasing insolation (Fig 5.5) is known on regional as well as on global scale [e.g. *Cacho et al.*, 2001; *NGRIP-Members*, 2004], thus corroborating warmer SSTs during the Mid- Holocene compared to modern SSTs. Annual mean SST values around 19 °C at that time were also reconstructed by other studies from the Alboran Sea [*Ausín et al.*, 2015; *Cacho et al.*, 2001; *Martrat et al.*, 2014; *Pérez-Folgado et al.*, 2003; *Rodrigo-Gámiz et al.*, 2014]. Moreover, *Cacho et al.* [2001] described a cold SST event of about 1.5 °C in the Alboran Sea between 5.94 and 4.75 cal. ka BP. Our data from the Alboran Sea shows no cooling event of similar magnitude between 5.4 and 4.7 cal. ka BP. Bearing in mind the error of the calibration there might be a cooling at about 5.3 cal. ka BP in the order of just 0.5 °C, but surface water conditions between 5.4 and 4.7 cal. ka BP appear to have even been warmer compared to the period afterwards. In the Gulf of Cádiz alkenone-based SST values vary between 20.0 to 22.7 °C and are warmer compared to recent annual mean temperatures (18.7 °C) [*Locarnini et al.*, 2013]. Higher SSTs during the Mid- Holocene might be partly a consequence of higher insolation during this period. However, previous alkenone analyses of *Kim et al.* [2004] on the same sediment core yielded SST values between 19 and 20 °C using a different SST calibration of *Prahl et al.* [1988], which would result in slightly cooler SSTs for our data as well. Additionally, annual mean SSTs around 20 °C in Gulf of Cádiz were also found by *Cacho et al.* [2001].

Summer temperatures. Reconstructed summer SST based on foraminiferal assemblage variations vary around 22.8 °C in the Alboran Sea and around 22.4 and 21.7 °C before and after approximately 4.0 cal. ka BP, respectively, in the Gulf of Cádiz. Alboran Sea summer SSTs are exceeding modern ones (21.4 °C) [*Locarnini et al.*, 2013] likely due to higher insolation forcing during the Mid- Holocene. This is even better demonstrated by the summer SST record in the Gulf of Cádiz. Here, summer SST estimates are progressively cooling towards mean summer SSTs around 21.7 °C, which perfectly agree with modern summer temperatures in the Gulf of Cádiz (21.7 °C) [*Locarnini et al.*, 2013]. Reconstructed Alboran Sea summer SSTs are supported by *Rodrigo-Gámiz et al.* [2014], who estimated summer SSTs varying around 22 °C between 5.5 and 3.0 cal. ka BP. *Pérez-Folgado et al.* [2003] found even warmer summer SSTs between 24 and 25 °C in the Alboran Sea. This difference may be a result of the *Pérez-Folgado et al.* [2003] data calibrated against August temperatures only, while our method used the mean of the summer season (July – September). These authors also found a 0.5 °C cooling between about 5.0 and 4.5 cal. ka BP, when our data implies two cold events of approximately 1 °C at about 5.0 and 4.6 cal. ka BP. In the Gulf of Cádiz, in sediment core MD99-2339 [*Salgueiro et al.*, 2014], summer SSTs vary between approximately 22 and 24 °C, exhibiting a cooling trend towards the present, which is in harmony with our summer SST reconstructions deduced from GeoB5901-2.

Winter temperatures. Winter SSTs in the Alboran Sea vary around ca. 15.0 °C between 5.4 and 3.0 cal. ka BP and agree with modern conditions (15.4 °C) [*Locarnini et al.*, 2013]. Moreover, winter SSTs (February) around 14.5 °C during the Mid- to Late Holocene reported by *Pérez-Folgado et al.* [2003] support our results. Winter SSTs between 16 and 17 °C between 6.2 and 1.8 cal. ka BP in the Gulf of Cádiz are also in good agreement with the modern winter SSTs of 16.0 °C [*Locarnini et al.*, 2013]. Slightly colder winter SSTs between 15 and 16 °C were reconstructed from dinocyst assemblages in the neighbouring core MD99-2339 [*Penaud et al.*, 2016].

5.5.4 Potential drivers of terrestrial and oceanic climate variability

Under modern conditions the NAO is responsible for much of the variability in winter precipitation at the Iberian Peninsula [*Hurrell*, 1995; *Zorita et al.*, 1992]. Many paleo-climatic studies provide evidence for NAO-like climate variability since the Mid- Holocene [*Abrantes et al.*, 2017; *Deininger et al.*, 2017; *Olsen et al.*, 2012]. We, thus, compare the observed sequence of dry climate episodes to a reconstruction of NAO-like variability from Lake SS1220 in Greenland (Fig 5.4) [*Olsen et al.*, 2012]. All dry phases observed in this study can be

associated with positive excursions in the NAO reconstruction. Moreover, it is evident that a wetter period between about 4.2 and 3.8 cal. ka BP coincides with a period of more stable, less positive NAO-like conditions. Accordingly, we conclude that the dry phases observed between 5.4 and 3.0 cal. ka BP in southern Iberia were caused by more dominant positive NAO-like conditions. Yet, other atmospheric circulation patterns like the Scandinavian and the East Atlantic patterns also influence precipitation variability at the Iberian Peninsula [*Abrantes et al.*, 2017; *Hernández et al.*, 2015]. This may explain, why our records do not reveal dry episodes between 4.7 and 4.5 cal. ka BP and at about 3.1 cal. ka BP despite the NAO reconstruction suggests a strong positive circulation mode for these times. Interestingly, at around 5.2, 4.6, and 3.0 cal. ka BP we found contemporaneous minima in the MPP and maxima in annual mean SSTs in the Alboran Sea (Fig 5.6). This linkage is also visible in the dry phases at about 5.4 cal. ka BP and between 5.0 and 4.8 cal. ka BP, while during those at about 4.3 and 3.7 cal. ka BP the warming of the annual mean SSTs was more pronounced. This linkage has previously been described by *Ausín et al.* [2015] since 7.7 cal. ka BP in the Alboran Sea and can also be related to NAO forcing. Currently, the inflow of the Atlantic Waters through the Strait of Gibraltar is strong under negative NAO conditions and, thereby, its flow within the Alboran Sea is shifted southwards. This promotes intensified upwelling of cold and nutrient rich waters, which also result in higher MPP [*Sarhan et al.*, 2000]. During positive NAO conditions, on the other hand, the inflow of the Atlantic Waters is weakened resulting in a more stable water column with limited upwelling and, thus, low MPP [*Sarhan et al.*, 2000]. Despite the calibration uncertainty of the annual mean SST reconstructions a similar mechanism is also indicated by our data during the Mid- to Late Holocene. Accordingly, we conclude that a NAO-like variability was coupled to the terrestrial variability in southern Iberia as well as for the surface water variability in the Alboran Sea between 5.4 and 3.0 cal. ka BP.

It has further been suggested that NAO-like variability in the past was responsible for oceanic changes in the subtropical Atlantic such as the position of the Azores Front [*Goslin et al.*, 2018; *Repschläger et al.*, 2017] as well as for increased upwelling and related SST changes along the western Iberian margin [*Abrantes et al.*, 2017]. In more detail, *Abrantes et al.* [2017] suggest that warm winters and cool summers during the Medieval Climate Anomaly were related to positive NAO-like conditions. For the time interval between 6.2 and 1.8 cal. ka BP we cannot confirm a general link between the NAO and the hydrological conditions in the Gulf of Cádiz. Interestingly, we observe two notable differences between the hydrological conditions in the Gulf of Cádiz and the Alboran Sea: (1) the summer/winter SST variability in the Gulf of Cádiz is opposite resulting in a greater seasonality during seasonal SST events, while seasonality

appears to decrease during summer/winter events in the Alboran Sea within methodological error and (2) the observed seasonal warming/cooling events in both adjacent basins are not contemporaneous. This suggests different mechanisms driving the hydrological variability in the Gulf of Cádiz and the Alboran Sea. The pronounced seasonal SST variability in the Gulf of Cádiz is in general agreement with the stacked ice-rafted debris (IRD) records for the North Atlantic (Fig 5.5) [*Bond et al.*, 2001]. This implies that larger seasonal SST contrasts in the Gulf of Cádiz relate to periods of enhanced iceberg discharge in the North Atlantic during Bond Events 3 and 4. During Bond Events cold polar water masses have been advected as far south as the latitude of Britain [*Bond et al.*, 1997]. Our data suggests that this regime resulted in colder winter temperatures in the Gulf of Cádiz as well. Moreover, the Bond Events likely weakened the deep water formation in the North Atlantic by limiting the oceanic heat transport towards the north [*Bond et al.*, 2001; *Wanner et al.*, 2011]. *Repschläger et al.* [2017] further proposed that Early Holocene freshwater forcing from the Laurentide ice sheet may have resulted in a weak subsurface heat transport from the Subtropical Gyre (STG) towards the North Atlantic and, subsequently, in a subsurface heat storage within the STG. Following these mechanisms, we hypothesize that during Bond Events 3 and 4 the northward heat transport was blocked due to freshwater forcing in the North Atlantic, which in turn results in a heat storage within the STG. During summer, when the Intertropical Convergence Zone (ITCZ) moved northwards, these heated water masses probably reached the Gulf of Cádiz via the Azores Current resulting in warmer summer temperatures. These warmer water masses could also reach the Alboran Sea through the Strait of Gibraltar, but are not recorded within our data because summer temperatures in the Alboran Sea were generally warmer by about 1 °C during the studied period. Interestingly, it seems that annual mean SSTs in the Gulf of Cádiz warmed by up to 2 °C during Bond Event 3 (Fig 5.5). This might imply rather a growing season shift of the alkenone-producing coccolithophores from spring to summer rather than a warming of the annual mean SSTs. Such a reaction of the coccolithophores might be also indicated to a lesser extent during Bond Event 2 when annual mean SSTs warmed by approximately 1 °C at about 3.2 cal. ka BP. Our data does not cover the whole interval, though. Also, Bond Event 4 is not entirely covered so that this interpretation remains hypothetical. But all in all, the influence of cold water from the North Atlantic during winter along with the influence of warmer subtropical water masses during summer likely resulted in a pronounced seasonality during Bond Events 3 and 4 (Fig 5.5). Notably, the amplitude of the seasonal events and their according high seasonality as well as the overall seasonality in the Gulf of Cádiz were decreasing towards the present. It is, moreover, interesting to note that Bond Event 2 is not visible in our seasonal SST records at all

(Fig 5.5). The general decrease in seasonality in the Gulf of Cádiz can be attributed to decreasing summer insolation. We hypothesize that this is also true for the decreasing amplitude of the seasonal SST events. During Bond Event 4, when summer insolation was high, the more northward position of the ITCZ during summer allowed for a stronger inflow of warmer subtropical water masses into the Gulf of Cádiz. On the other hand, during winter the ITCZ was much further south compared to its present position, allowing enhanced southward flow of the colder water masses from the north. During Bond Event 3 the summer and winter positions of the ITCZ were already less extreme, thus, weakening the influence of either warm and cold water masses during summer or winter, respectively. Later, during Bond Event 2 seasonal movements of the ITCZ were even more limited that no influence of either cold water masses during winter or warm subtropical water masses during summer are recognizable by a pronounced seasonal temperature difference in the Gulf of Cádiz.

5.6 Conclusion

Two marine sediment cores from the Gulf of Cádiz and the Alboran Sea have been studied aiming at exploring the climatic variability with respect to precipitation and vegetation change in southern Iberia as well as resolving seasonal hydrological conditions during the Mid- to Late Holocene. The following conclusions can be drawn from this study:

- Based on terrestrial *n*-alkane concentrations we found five major dry climate episodes in southern Iberia at 5.4 ± 0.3, from 5.1 to 4.9 ± 0.1, from 4.8 to 4.7 ± 0.1, from 4.4 to 4.3 ± 0.1, and at 3.7 ± 0.1 cal. ka BP. These dry phases also impacted the vegetation, which suffered from environmental stress due to reduced water availability.
- The manifestation of the 4.2 ka BP event in southern Iberia appears to be shorter compared to the prolonged dry episode observed in other regions. Instead, our data suggests a distinct dry phase from 4.4 to 4.3 ± 0.1 cal. ka BP followed by a rapid shift towards relatively moister conditions at about 4.2 cal. ka BP, which lasted until approximately 3.8 cal. ka BP.
- SST reconstructions suggest fairly stable annual mean temperature conditions in the Alboran Sea and the Gulf of Cádiz with estimates values varying within the range of uncertainty of the calibration. Based on summer and winter SST estimates the new records imply different mechanisms driving the seasonal variability in these two oceanic basins. While in the Gulf of Cádiz opposite seasonal SST events (i.e. summer warming and winter

cooling) of up to 2 °C amplitude enhanced the seasonal SST difference, only slight seasonal SST variations (i.e. summer cooling and winter warming) within the methodological uncertainty have been found in the Alboran Sea at different times.

- The new records further suggest that variability in precipitation and vegetation in southern Iberia and probably the hydrological variability in the Alboran Sea can be well explained by a NAO-like atmospheric circulation. Dominant positive NAO-like conditions appear contemporaneous with the observed dry phases over southern Iberia associated with slightly warmer annual mean SSTs and decreased MPP in the Alboran Sea.
- The variability of the seasonal SST contrasts in the Gulf of Cádiz seems to be closely related to North Atlantic Bond Events. We observe increasing seasonality with summer warming and winter cooling during Bond Events 3 and 4. We propose that during winter the southward transport of cold water masses from the North Atlantic affected the Gulf of Cádiz, while during summer warm water masses originating from the STG reached our study site. Bond Event 2 is not reflected by a larger difference in our seasonal SST reconstructions. This is likely due to decreasing summer insolation that also influences the seasonal movements of the subtropical Azores Front, which in the Gulf of Cádiz can also limit either the inflow of cold or warm water masses during winter and summer, respectively.

5.7 Acknowledgments

This research was performed in the framework of the CRC 1266 “Scales of transformation” (project number: 2901391021) funded by the DFG (German Research Foundation). E. Salgueiro was funded by Fundação para a Ciência e Tecnologia (fellowship: SFRH/BPD/26525/2006 & SFRH/BPD/111433/2015). Sample material has been provided by the GeoB Core Repository and the IODP Core Repository at the MARUM – Center for Marine Environmental Sciences, University of Bremen, Germany. In this respect, kind support is acknowledged provided by J. Pätzold, V. B. Bender, and A. Wülbers. The authors acknowledge F. Burjachs for his kind data supply. We are also very grateful for enormous support from S. Koch with the geochemical analyses. Additionally, we thank I. Feeser for assistance with the Bayesian age modelling and W. Hamer for helping with the statistical analyses. We also thank the four anonymous referees as well as A. García-Alix for their helpful comments on improving the manuscript.

5.8 Supplement

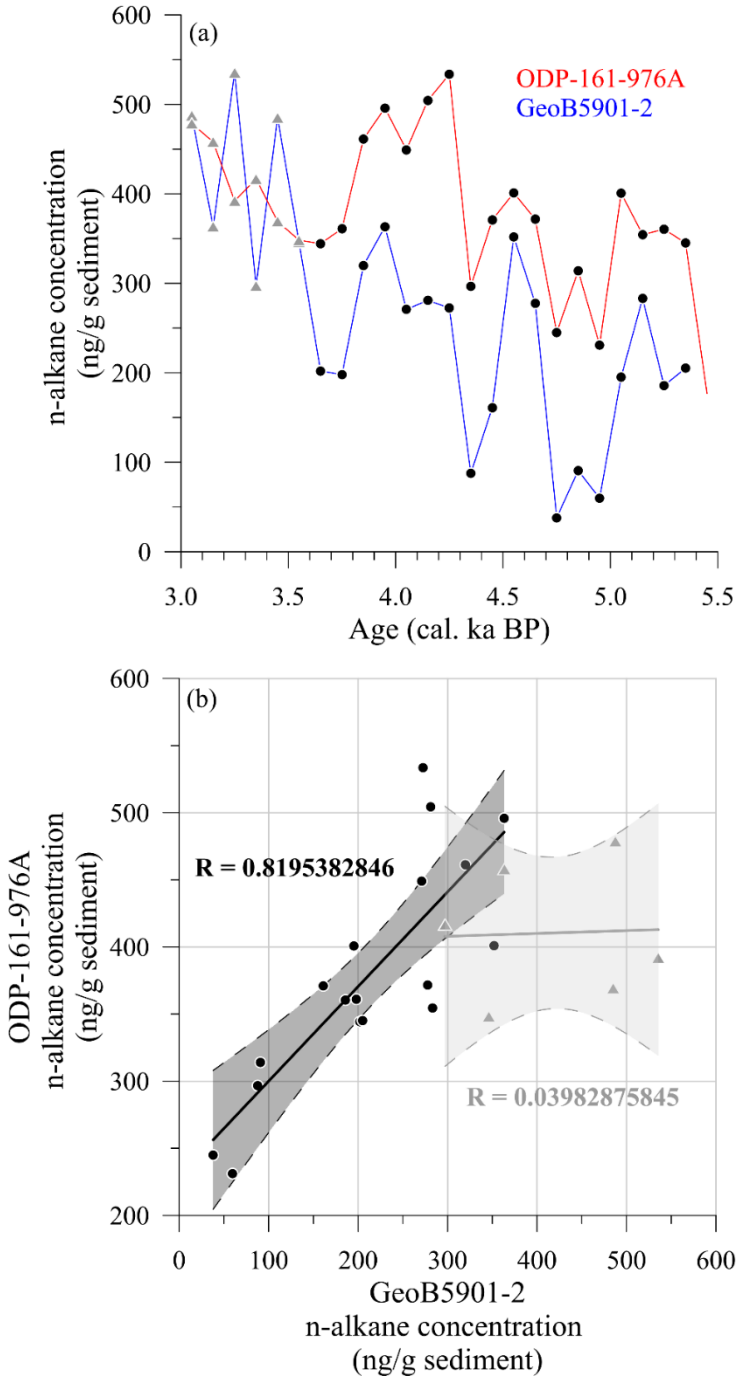

Figure 5.7 Supplementary figure S5.1 . *(a) 100 yr-means of the n-alkane concentration of sediment cores ODP-161-976A (red) and GeoB5901-2 (blue) calculated from the raw data. Black dots and grey triangles indicate the subdivision of two periods with large differences in the correlation. (b) scatter plot for the period from 3.0 to 3.6 cal. ka BP (grey triangle) and from 3.6 to 5.4 cal. ka BP (black dots) and the according correlation factors (R).*

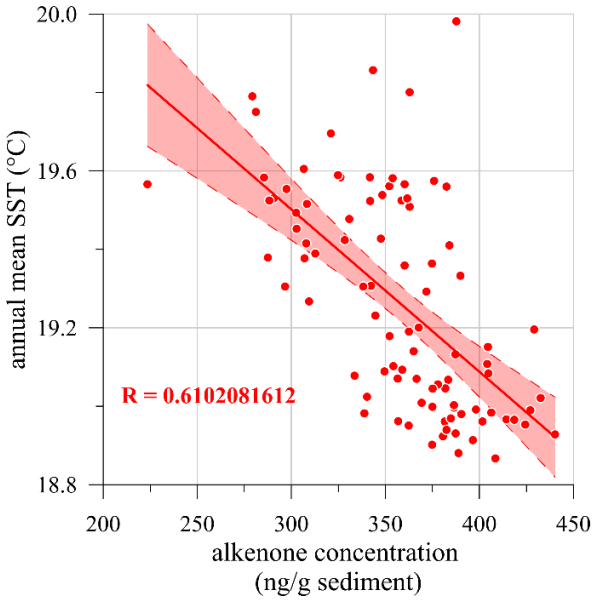

Figure 5.8 Supplementary figure S5.2. *Scatter plot for annual mean SST and MPP from sediment core ODP-161-976A and the according correlation factor (R).*

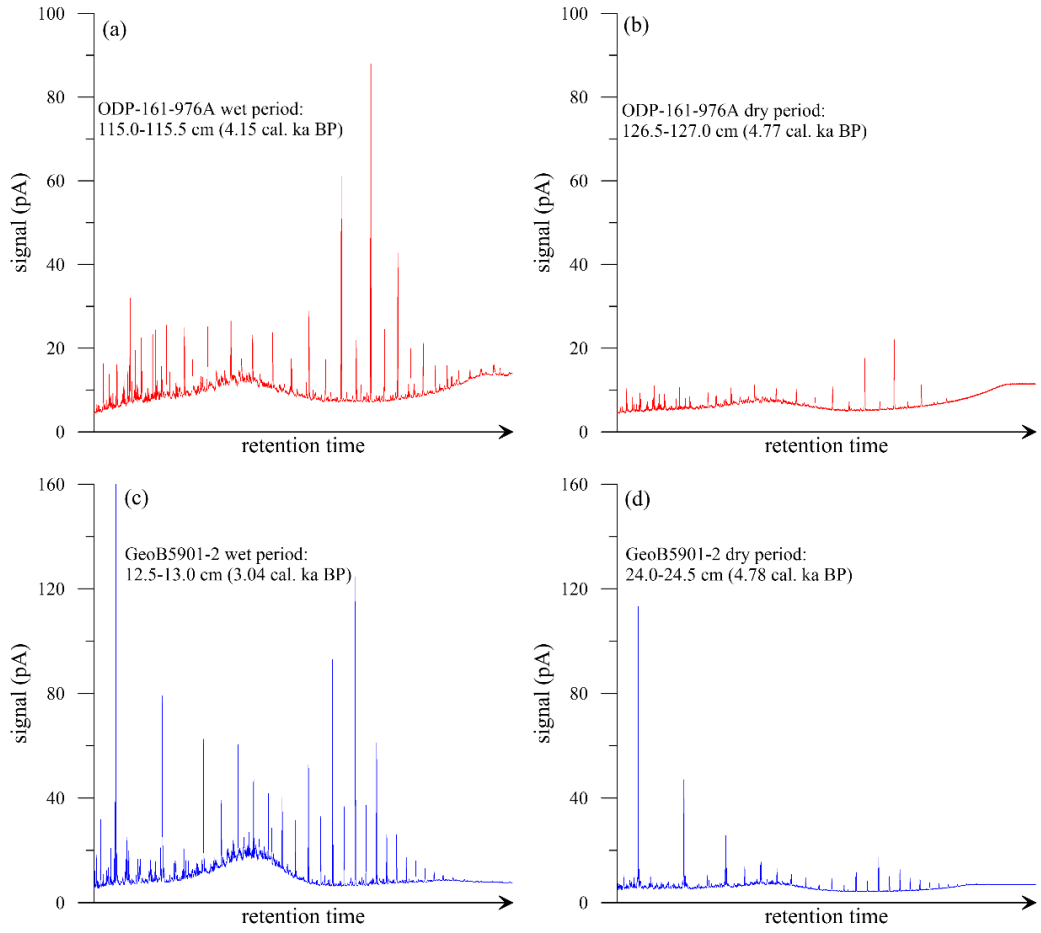

Figure 5.9 Supplementary figure S5.3. *Example chromatograms showing the n-alkane distribution for high terrestrial n-alkane concentrations interpreted as wet periods (a and c) and low terrestrial n-alkane concentrations interpreted as dry periods (b and d) in sediment cores ODP-161-976A (red) and GeoB5901-2 (blue), respectively.*

5.9 References

Abrantes, F., T. Rodrigues, M. Rufino, E. Salgueiro, D. Oliveira, S. Gomes, P. Oliveira, A. Costa, M. Mil-Homes, T. Drago, and F. Naughton (2017), The Climate of the Common Era off the Iberian Peninsula, *Climate of the Past Discussions*, 1–42, doi:10.5194/cp-2017-84.

Alley, R. B., P. A. Mayewski, T. Sowers, M. Stuiver, K. C. Taylor, and P. U. Clark (1997), Geology: Holocene climatic instability: A prominent, widespread event 8200 yr ago, *Geol*, *25*(6), 483–486.

Ausín, B., J. A. Flores, F. J. Sierro, I. Cacho, I. Hernández-Almeida, B. Martrat, and J. O. Grimalt (2015), Atmospheric patterns driving Holocene productivity in the Alboran Sea (Western Mediterranean): A multiproxy approach, *The Holocene*, *25*(4), 583–595, doi:10.1177/0959683614565952.

Bakke, J., S. O. Dahl, Ø. Paasche, J. Riis Simonsen, B. Kvisvik, K. Bakke, and A. Nesje (2010), A complete record of Holocene glacier variability at Austre Okstindbreen, northern Norway: An integrated approach, *Quaternary Science Reviews*, *29*(9-10), 1246–1262, doi:10.1016/j.quascirev.2010.02.012.

Bird, M. I., R. E. Summons, M. K. Gagan, Z. Roksandic, L. Dowling, J. Head, L. Keith Fifield, R. G. Cresswell, and D. P. Johnson (1995), Terrestrial vegetation change inferred from n-alkane σ13C analysis in the marine environment, *Geochimica et Cosmochimica Acta*, *59*(13), 2853–2857, doi:10.1016/0016-7037(95)00160-2.

Blaauw, M., and J. A. Christen (2011), Flexible paleoclimate age-depth models using an autoregressive gamma process, *Bayesian Anal.*, *6*(3), 457–474, doi:10.1214/11-BA618.

Bond, G., B. Kromer, J. Beer, R. Muscheler, M. N. Evans, W. Showers, S. Hoffmann, R. Lotti-Bond, I. Hajdas, and G. Bonani (2001), Persistent solar influence on North Atlantic climate during the Holocene, *Science (New York, N.Y.)*, *294*(5549), 2130–2136, doi:10.1126/science.1065680.

Bond, G., W. Showers, M. Cheseby, R. Lotti, P. Almasi, P. deMenocal, P. Priore, H. Cullen, I. Hajdas, and G. Bonani (1997), A Pervasive Millennial-Scale Cycle in North Atlantic Holocene and Glacial Climates, *Science*, *278*(5341), 1257–1266, doi:10.1126/science.278.5341.1257.

Booth, R. K., S. T. Jackson, S. L. Forman, J. E. Kutzbach, E. A. Bettis, J. Kreigs, and D. K. Wright (2005), A severe centennial-scale drought in midcontinental North America 4200 years ago and apparent global linkages, *The Holocene*, *15*(3), 321–328, doi:10.1191/0959683605hl825ft.

Burjachs, F., and I. Expósito (2015), Charcoal and pollen analysis: Examples of Holocene fire dynamics in Mediterranean Iberian Peninsula, *CATENA*, *135*, 340–349, doi:10.1016/j.catena.2014.10.006.

Burjachs, F., S. Giralt, J. R. Roca, G. Seret, and R. Julià (1997), Palinología holocénica y desertización en el Mediterráneo occidental., in *El paisaje mediterráneo a través del espacio y del tiempo.: Implicaiones en la desertificación.*, edited by J. J. Ibañez et al., pp. 379–394, Geoforma Editores, Logroño.

Bush, R. T., and F. A. McInerney (2013), Leaf wax n-alkane distributions in and across modern plants: Implications for paleoecology and chemotaxonomy, *Geochimica et Cosmochimica Acta*, *117*, 161–179, doi:10.1016/j.gca.2013.04.016.

Cacho, I., J. O. Grimalt, M. Canals, L. Sbaffi, N. J. Shackleton, J. Schönfeld, and R. Zahn (2001), Variability of the western Mediterranean Sea surface temperature during the last 25,000 years and its connection with the Northern Hemisphere climatic changes, *Paleoceanography*, *16*(1), 40–52, doi:10.1029/2000PA000502.

Calò, C., P. D. Henne, B. Curry, M. Magny, E. Vescovi, T. La Mantia, S. Pasta, B. Vannière, and W. Tinner (2012), Spatio-temporal patterns of Holocene environmental change in southern Sicily, *Palaeogeography, Palaeoclimatology, Palaeoecology*, *323-325*, 110–122, doi:10.1016/j.palaeo.2012.01.038.

Carrión, J. S., A. Andrade, K. D. Bennett, C. Navarro, and M. Munuera (2001), Crossing forest thresholds: inertia and collapse in a Holocene sequence from south-central Spain, *The Holocene*, *11*(6), 635–653.

Carrión, J. S., P. Sánchez-Gómez, J. F. Mota, R. Yll, and C. Chaín (2003), Holocene vegetation dynamics, fire and grazing in the Sierra de Gádor, southern Spain, *The Holocene*, *13*(6), 839–849, doi:10.1191/0959683603hl662rp.

Cheng, H., A. Sinha, S. Verheyden, F. H. Nader, X. L. Li, P. Z. Zhang, J. J. Yin, L. Yi, Y. B. Peng, Z. G. Rao, Y. F. Ning, and R. L. Edwards (2015), The climate variability in northern Levant over the past 20,000 years, *Geophysical Research Letters*, *42*(20), 8641–8650, doi:10.1002/2015GL065397.

Comas, M. C., R. Zahn, and A. Klaus (Eds.) (1996), *Proceedings of the Ocean Drilling Program, 161 Initial Reports*, *Proceedings of the Ocean Drilling Program*, vol. 161, Ocean Drilling Program.

Combourieu Nebout, N., J. L. Turon, R. Zahn, L. Capotondi, L. Londeix, and K. Pahnke (2002), Enhanced aridity and atmospheric high-pressure stability over the western Mediterranean during the North Atlantic cold events of the past 50 k.y, *Geol*, *30*(10), 863, doi:10.1130/0091-7613(2002)030<0863:EAAAHP>2.0.CO;2.

Conte, M. H., and J. C. Weber (2002), Long-range atmospheric transport of terrestrial biomarkers to the western North Atlantic, *Global Biogeochem. Cycles*, *16*(4), 89-1-89-17, doi:10.1029/2002GB001922.

Cortina, A., J. O. Grimalt, A. Rigual-Hernández, A.-M. Ballegeer, B. Martrat, F. J. Sierro, and J. A. Flores (2016), The impact of ice-sheet dynamics in western Mediterranean environmental conditions during Terminations. An approach based on terrestrial long chain n-alkanes deposited in the upper slope of the Gulf of Lions, *Chemical Geology*, *430*, 21–33, doi:10.1016/j.chemgeo.2016.03.015.

Deininger, M., F. McDermott, M. Mudelsee, M. Werner, N. Frank, and A. Mangini (2017), Coherency of late Holocene European speleothem $\delta^{18}O$ records linked to North Atlantic Ocean circulation, *Climate Dynamics*, *49*(1-2), 595–618, doi:10.1007/s00382-016-3360-8.

deMenocal, P., J. Ortiz, T. Guilderson, J. Adkins, M. Sarnthein, L. Baker, and M. Yarusinsky (2000), Abrupt onset and termination of the African Humid Period, *Quaternary Science Reviews*, *19*(1-5), 347–361, doi:10.1016/S0277-3791(99)00081-5.

Eglinton, G., and R. J. Hamilton (1967), Leaf Epicuticular Waxes, *Science*, *156*(3780), 1322–1335, doi:10.1126/science.156.3780.1322.

Fernández-Delgado, C., F. Baldó, C. Vilas, D. García-González, J. A. Cuesta, E. González-Ortegón, and P. Drake (2007), Effects of the river discharge management on the nursery function of the Guadalquivir river estuary (SW Spain), *Hydrobiologia*, *587*(1), 125–136, doi:10.1007/s10750-007-0691-9.

Fick, S. E., and R. J. Hijmans (2017), WorldClim 2: New 1-km spatial resolution climate surfaces for global land areas, *Int. J. Climatol.*, *37*(12), 4302–4315, doi:10.1002/joc.5086.

Finné, M., K. Holmgren, C.-C. Shen, H.-M. Hu, M. Boyd, and S. Stocker (2017), Late Bronze Age climate change and the destruction of the Mycenaean Palace of Nestor at Pylos, *PloS one*, *12*(12), e0189447, doi:10.1371/journal.pone.0189447.

Fletcher, W. J., T. Boski, and D. Moura (2007), Palynological evidence for environmental and climatic change in the lower Guadiana valley, Portugal, during the last 13 000 years, *The Holocene*, *17*(4), 481–494, doi:10.1177/0959683607077027.

Fletcher, W. J., and M. F. Sánchez Goñi (2008), Orbital- and sub-orbital-scale climate impacts on vegetation of the western Mediterranean basin over the last 48,000 yr, *Quat. res.*, *70*(03), 451–464, doi:10.1016/j.yqres.2008.07.002.

García-Alix, A., F. J. Jiménez-Espejo, G. Jiménez-Moreno, J. L. Toney, M. J. Ramos-Román, J. Camuera, R. S. Anderson, A. Delgado-Huertas, F. Martínez-Ruiz, and I. Queralt (2018), Holocene geochemical footprint from Semi-arid alpine wetlands in southern Spain, *Scientific data*, *5*, 180024, doi:10.1038/sdata.2018.24.

García-Alix, A., F. J. Jiménez-Espejo, J. L. Toney, G. Jiménez-Moreno, M. J. Ramos-Román, R. S. Anderson, P. Ruano, I. Queralt, A. Delgado Huertas, and J. Kuroda (2017), Alpine bogs of southern Spain show human-induced environmental change superimposed on long-term natural variations, *Scientific reports*, *7*(1), 7439, doi:10.1038/s41598-017-07854-w.

Goslin, J., M. Fruergaard, L. Sander, M. Gałka, L. Menviel, J. Monkenbusch, N. Thibault, and L. B. Clemmensen (2018), Holocene centennial to millennial shifts in North-Atlantic storminess and ocean dynamics, *Scientific reports*, *8*(1), 12778, doi:10.1038/s41598-018-29949-8.

Hayes, A., M. Kucera, N. Kallel, L. Sbaffi, and E. J. Rohling (2005), Glacial Mediterranean sea surface temperatures based on planktonic foraminiferal assemblages, *Quaternary Science Reviews*, *24*(7-9), 999–1016, doi:10.1016/j.quascirev.2004.02.018.

Haynes, R., E. D. Barton, and I. Pilling (1993), Development, persistence, and variability of upwelling filaments off the Atlantic coast of the Iberian Peninsula, *J. Geophys. Res.*, *98*(C12), 22681, doi:10.1029/93JC02016.

Hernández, A., R. M. Trigo, S. Pla-Rabes, B. L. Valero-Garcés, S. Jerez, M. Rico-Herrero, J. C. Vega, M. Jambrina-Enríquez, and S. Giralt (2015), Sensitivity of two Iberian lakes to North Atlantic atmospheric circulation modes, *Clim Dyn*, *45*(11-12), 3403–3417, doi:10.1007/s00382-015-2547-8.

Herrmann, N., A. Boom, A. S. Carr, B. M. Chase, R. Granger, A. Hahn, M. Zabel, and E. Schefuß (2016), Sources, transport and deposition of terrestrial organic material: A case study from southwestern Africa, *Quaternary Science Reviews*, *149*, 215–229, doi:10.1016/j.quascirev.2016.07.028.

Hurrell, J. W. (1995), Decadal trends in the north atlantic oscillation: regional temperatures and precipitation, *Science*, *269*(5224), 676–679, doi:10.1126/science.269.5224.676.

Jalali, B., M.-A. Sicre, M.-A. Bassetti, and N. Kallel (2016), Holocene climate variability in the North-Western Mediterranean Sea (Gulf of Lions), *Climate of the Past*, *12*(1), 91–101, doi:10.5194/cp-12-91-2016.

Jalali, B., M.-A. Sicre, N. Kallel, J. Azuara, N. Combourieu-Nebout, M.-A. Bassetti, and V. Klein (2017), High-resolution Holocene climate and hydrological variability from two major Mediterranean deltas (Nile and Rhone), *The Holocene*, *27*(8), 1158–1168, doi:10.1177/0959683616683258.

Jalut, G., A. Esteban Amat, L. Bonnet, T. Gauquelin, and M. Fontugne (2000), Holocene climatic changes in the Western Mediterranean, from south-east France to south-east Spain, *Palaeogeography, Palaeoclimatology, Palaeoecology*, *160*(3-4), 255–290, doi:10.1016/S0031-0182(00)00075-4.

Jiménez-Amat, P., and R. Zahn (2015), Offset timing of climate oscillations during the last two glacial-interglacial transitions connected with large-scale freshwater perturbation, *Paleoceanography*, *30*(6), 768–788, doi:10.1002/2014PA002710.

Kim, J.-H., N. Rimbu, S. J. Lorenz, G. Lohmann, S.-I. Nam, S. Schouten, C. Rühlemann, and R. R. Schneider (2004), North Pacific and North Atlantic sea-surface temperature variability during the Holocene, *Quaternary Science Reviews*, *23*(20-22), 2141–2154, doi:10.1016/j.quascirev.2004.08.010.

Kucera, M., A. Rosell-Melé, R. Schneider, C. Waelbroeck, and M. Weinelt (2005a), Multiproxy approach for the reconstruction of the glacial ocean surface (MARGO), *Quaternary Science Reviews*, *24*(7-9), 813–819, doi:10.1016/j.quascirev.2004.07.017.

Kucera, M., M. Weinelt, T. Kiefer, U. Pflaumann, A. Hayes, M. Weinelt, M.-T. Chen, A. C. Mix, T. T. Barrows, E. Cortijo, J. Duprat, S. Juggins, and C. Waelbroeck (2005b), Reconstruction of sea-surface temperatures from assemblages of planktonic foraminifera: Multi-technique approach based on geographically constrained calibration data sets and its application to glacial Atlantic and Pacific Oceans, *Quaternary Science Reviews*, *24*(7-9), 951–998, doi:10.1016/j.quascirev.2004.07.014.

Laskar, J., P. Robutel, F. Joutel, M. Gastineau, A. C. M. Correia, and B. Levrard (2004), A long-term numerical solution for the insolation quantities of the Earth, *A&A*, *428*(1), 261–285, doi:10.1051/0004-6361:20041335.

Le Roy, M., P. Deline, J. Carcaillet, I. Schimmelpfennig, and M. Ermini (2017), 10 Be exposure dating of the timing of Neoglacial glacier advances in the Ecrins-Pelvoux massif, southern French Alps, *Quaternary Science Reviews*, *178*, 118–138, doi:10.1016/j.quascirev.2017.10.010.

Leider, A., K.-U. Hinrichs, E. Schefuß, and G. J.M. Versteegh (2013), Distribution and stable isotopes of plant wax derived n-alkanes in lacustrine, fluvial and marine surface sediments along an Eastern Italian transect and their potential to reconstruct the hydrological cycle, *Geochimica et Cosmochimica Acta*, *117*, 16–32, doi:10.1016/j.gca.2013.04.018.

Lionello, P. (Ed.) (2012), *The climate of the Mediterranean region: From the past to the future*, 1st ed., 502 pp., *Elsevier insights*, Elsevier Science, Amsterdam.

Locarnini, R. A., A. V. Mishonov, J. I. Antonov, T. P. Boyer, H. E. Garcia, O. K. Baranova, M. M. Zweng, C. R. Paver, J. R. Reagan, D. R. Johnson, M. Hamilton, and D. Seidov (2013), World Ocean Atlas 2013: Volume 1: Temperature, 40 pp., NOAA Atlas NESDIS 73.

Magny, M., N. Combourieu-Nebout, J. L. de Beaulieu, V. Bout-Roumazeilles, D. Colombaroli, S. Desprat, A. Francke, S. Joannin, E. Ortu, O. Peyron, M. Revel, L. Sadori, G. Siani, M. A. Sicre, S. Samartin, A. Simonneau, W. Tinner, B. Vannière, B. Wagner, G. Zanchetta, F. Anselmetti, E. Brugiapaglia, E. Chapron, M. Debret, M. Desmet, J. Didier, L. Essallami, D. Galop, A. Gilli, J. N. Haas, N. Kallel, L. Millet, A. Stock, J. L. Turon, and S. Wirth (2013), North-south palaeohydrological contrasts in the central Mediterranean during the Holocene: Tentative synthesis and working hypotheses, *Climate of the Past*, *9*(5), 2043–2071, doi:10.5194/cp-9-2043-2013.

Martrat, B., J. O. Grimalt, N. J. Shackleton, L. de Abreu, M. A. Hutterli, and T. F. Stocker (2007), Four climate cycles of recurring deep and surface water destabilizations on the Iberian margin, *Science (New York, N.Y.)*, *317*(5837), 502–507, doi:10.1126/science.1139994.

Martrat, B., P. Jiménez-Amat, R. Zahn, and J. O. Grimalt (2014), Similarities and dissimilarities between the last two deglaciations and interglaciations in the North Atlantic region, *Quaternary Science Reviews*, *99*, 122–134, doi:10.1016/j.quascirev.2014.06.016.

Mayewski, P. A., E. E. Rohling, J. Curt Stager, W. Karlén, K. A. Maasch, L. D. Meeker, E. A. Meyerson, F. Gasse, S. van Kreveld, K. Holmgren, J. Lee-Thorp, G. Rosqvist, F. Rack, M. Staubwasser, R. R. Schneider, and E. J. Steig (2004), Holocene Climate Variability, *Quat. res.*, *62*(03), 243–255, doi:10.1016/j.yqres.2004.07.001.

Minas, H. J., B. Coste, P. Le Corre, M. Minas, and P. Raimbault (1991), Biological and geochemical signatures associated with the water circulation through the Strait of Gibraltar and in the western Alboran Sea, *J. Geophys. Res.*, *96*(C5), 8755, doi:10.1029/91JC00360.

Moreno, A., C. Pérez-Mejías, M. Bartolomé, C. Sancho, I. Cacho, H. Stoll, A. Delgado-Huertas, J. Hellstrom, R. L. Edwards, and H. Cheng (2017), New speleothem data from Molinos and Ejulve caves reveal Holocene hydrological variability in northeast Iberia, *Quat. res.*, *88*(02), 223–233, doi:10.1017/qua.2017.39.

Müller, P. J., G. Kirst, G. Ruhland, I. von Storch, and A. Rosell-Melé (1998), Calibration of the alkenone paleotemperature index U37K′ based on core-tops from the eastern South Atlantic and the global ocean (60°N-60°S), *Geochimica et Cosmochimica Acta*, *62*(10), 1757–1772, doi:10.1016/S0016-7037(98)00097-0.

Navarro-Hervás, F., M.-M. Ros-Salas, T. Rodríguez-Estrella, E. Fierro-Enrique, J.-S. Carrión, J. García-Veigas, J.-A. Flores, M. Á. Bárcena, and M. S. García (2014), Evaporite evidence of a mid-Holocene (c . 4550–4400 cal. yr BP) aridity crisis in southwestern Europe and palaeoenvironmental consequences, *The Holocene*, *24*(4), 489–502, doi:10.1177/0959683613520260.

NGRIP-Members (2004), High-resolution record of Northern Hemisphere climate extending into the last interglacial period, *Nature*, *431*(7005), 147–151, doi:10.1038/nature02805.

Olsen, J., N. J. Anderson, and M. F. Knudsen (2012), Variability of the North Atlantic Oscillation over the past 5,200 years, *Nature Geoscience*, *5*(11), 808–812, doi:10.1038/ngeo1589.

Pantaléon-Cano, J., E.-I. Yll, R. Pérez-Obiol, and J. M. Roure (2003), Palynological evidence for vegetational history in semi-arid areas of the western Mediterranean (Almería, Spain), *The Holocene*, *13*(1), 109–119, doi:10.1191/0959683603hl598rp.

Peliz, Á., J. Dubert, A. M. P. Santos, P. B. Oliveira, and B. Le Cann (2005), Winter upper ocean circulation in the Western Iberian Basin—Fronts, Eddies and Poleward Flows: An overview, *Deep Sea Research Part I: Oceanographic Research Papers*, *52*(4), 621–646, doi:10.1016/j.dsr.2004.11.005.

Peliz, Á., T. L. Rosa, A.M. P. Santos, and J. L. Pissarra (2002), Fronts, jets, and counter-flows in the Western Iberian upwelling system, *Journal of Marine Systems*, *35*(1-2), 61–77, doi:10.1016/S0924-7963(02)00076-3.

Penaud, A., F. Eynaud, A. H. L. Voelker, and J.-L. Turon (2016), Palaeohydrological changes over the last 50 ky in the central Gulf of Cadiz: Complex forcing mechanisms mixing multi-scale processes, *Biogeosciences*, *13*(18), 5357–5377, doi:10.5194/bg-13-5357-2016.

Pérez-Folgado, M., F. J. Sierro, J. A. Flores, I. Cacho, J. O. Grimalt, R. Zahn, and N. Shackleton (2003), Western Mediterranean planktonic foraminifera events and millennial climatic variability during the last 70 kyr, *Marine Micropaleontology*, *48*(1-2), 49–70, doi:10.1016/S0377-8398(02)00160-3.

Pflaumann, U., J. Duprat, C. Pujol, and L. D. Labeyrie (1996), SIMMAX: A modern analog technique to deduce Atlantic sea surface temperatures from planktonic foraminifera in deep-sea sediments, *Paleoceanography*, *11*(1), 15–35, doi:10.1029/95PA01743.

Pflaumann, U., M. Sarnthein, M. Chapman, L. d'Abreu, B. Funnell, M. Huels, T. Kiefer, M. Maslin, H. Schulz, J. Swallow, S. van Kreveld, M. Vautravers, E. Vogelsang, and M. Weinelt (2003), Glacial North Atlantic: Sea-surface conditions reconstructed by GLAMAP 2000, *Paleoceanography*, *18*(3), n/a-n/a, doi:10.1029/2002PA000774.

Prahl, F. G., L. A. Muehlhausen, and D. L. Zahnle (1988), Further evaluation of long-chain alkenones as indicators of paleoceanographic conditions, *Geochimica et Cosmochimica Acta*, *52*(9), 2303–2310, doi:10.1016/0016-7037(88)90132-9.

Prahl, F. G., and S. G. Wakeham (1987), Calibration of unsaturation patterns in long-chain ketone compositions for palaeotemperature assessment, *Nature*, *330*(6146), 367–369, doi:10.1038/330367a0.

Ramos-Román, M. J., G. Jiménez-Moreno, J. Camuera, A. García-Alix, R. S. Anderson, F. J. Jiménez-Espejo, and J. S. Carrión (2018a), Holocene climate aridification trend and human impact interrupted by millennial- and centennial-scale climate fluctuations from a new sedimentary record from Padul (Sierra Nevada, southern Iberian Peninsula), *Clim. Past*, *14*(1), 117–137, doi:10.5194/cp-14-117-2018.

Ramos-Román, M. J., G. Jiménez-Moreno, J. Camuera, A. García-Alix, R. Scott Anderson, F. J. Jiménez-Espejo, D. Sachse, J. L. Toney, J. S. Carrión, C. Webster, and Y. Yanes (2018b), Millennial-scale cyclical environment and climate variability during the Holocene in the western Mediterranean region deduced from a new multi-

proxy analysis from the Padul record (Sierra Nevada, Spain), *Global and Planetary Change*, *168*, 35–53, doi:10.1016/j.gloplacha.2018.06.003.

Rasmussen, S. O., M. Bigler, S. P. Blockley, T. Blunier, S. L. Buchardt, H. B. Clausen, I. Cvijanovic, D. Dahl-Jensen, S. J. Johnsen, H. Fischer, V. Gkinis, M. Guillevic, W. Z. Hoek, J. J. Lowe, J. B. Pedro, T. Popp, I. K. Seierstad, J. P. Steffensen, A. M. Svensson, P. Vallelonga, B. M. Vinther, M. J.C. Walker, J. J. Wheatley, and M. Winstrup (2014), A stratigraphic framework for abrupt climatic changes during the Last Glacial period based on three synchronized Greenland ice-core records: Refining and extending the INTIMATE event stratigraphy, *Quaternary Science Reviews*, *106*, 14–28, doi:10.1016/j.quascirev.2014.09.007.

Reimer, P. J., E. Bard, A. Bayliss, J. W. Beck, P. G. Blackwell, C. B. Ramsey, C. E. Buck, H. Cheng, R. L. Edwards, M. Friedrich, P. M. Grootes, T. P. Guilderson, H. Haflidason, I. Hajdas, C. Hatté, T. J. Heaton, D. L. Hoffmann, A. G. Hogg, K. A. Hughen, K. F. Kaiser, B. Kromer, S. W. Manning, M. Niu, R. W. Reimer, D. A. Richards, E. M. Scott, J. R. Southon, R. A. Staff, C. S. M. Turney, and J. van der Plicht (2013), IntCal13 and Marine13 Radiocarbon Age Calibration Curves 0–50,000 Years cal BP, *Radiocarbon*, *55*(04), 1869–1887, doi:10.2458/azu_js_rc.55.16947.

Repschläger, J., D. Garbe-Schönberg, M. Weinelt, and R. Schneider (2017), Holocene evolution of the North Atlantic subsurface transport, *Climate of the Past*, *13*(4), 333–344, doi:10.5194/cp-13-333-2017.

Rodrigo-Gámiz, M., F. Martínez-Ruiz, M. Chiaradia, F. J. Jiménez-Espejo, and D. Ariztegui (2015), Radiogenic isotopes for deciphering terrigenous input provenance in the western Mediterranean, *Chemical Geology*, *410*, 237–250, doi:10.1016/j.chemgeo.2015.06.004.

Rodrigo-Gámiz, M., F. Martínez-Ruiz, S. W. Rampen, S. Schouten, and J. S. Sinninghe Damsté (2014), Sea surface temperature variations in the western Mediterranean Sea over the last 20 kyr: A dual-organic proxy (U K′37 and LDI) approach, *Paleoceanography*, *29*(2), 87–98, doi:10.1002/2013PA002466.

Rommerskirchen, F., A. Plader, G. Eglinton, Y. Chikaraishi, and J. Rullkötter (2006), Chemotaxonomic significance of distribution and stable carbon isotopic composition of long-chain alkanes and alkan-1-ols in C_4 grass waxes, *Organic Geochemistry*, *37*(10), 1303–1332, doi:10.1016/j.orggeochem.2005.12.013.

Ruan, J., F. Kherbouche, D. Genty, D. Blamart, H. Cheng, F. Dewilde, S. Hachi, R. L. Edwards, E. Régnier, and J.-L. Michelot (2016), Evidence of a prolonged drought ca. 4200 yr BP correlated with prehistoric settlement abandonment from the Gueldaman GLD1 Cave, Northern Algeria, *Climate of the Past*, *12*(1), 1–14, doi:10.5194/cp-12-1-2016.

Salgueiro, E., F. Naughton, A.H.L. Voelker, L. de Abreu, A. Alberto, L. Rossignol, J. Duprat, V. H. Magalhães, S. Vaqueiro, J.-L. Turon, and F. Abrantes (2014), Past circulation along the western Iberian margin: A time slice vision from the Last Glacial to the Holocene, *Quaternary Science Reviews*, *106*, 316–329, doi:10.1016/j.quascirev.2014.09.001.

Sarhan, T., J. G. Lafuente, M. Vargas, J. M. Vargas, and F. Plaza (2000), Upwelling mechanisms in the northwestern Alboran Sea, *Journal of Marine Systems*, *23*(4), 317–331, doi:10.1016/S0924-7963(99)00068-8.

Schlitzer, R. (2016), *Ocean Data View*.

Schott, F., J. Meincke, G. Meinecke, S. Neuer, and W. Zenk (2000), North Atlantic 1999 - Cruise No. M45 - May 18 - November 4, 1999 - Malaga (Spain) - Las Palmas (Spain).

Schreuder, L. T., J.-B. W. Stuut, L. F. Korte, J. S. Sinninghe Damsté, and S. Schouten (2018), Aeolian transport and deposition of plant wax n -alkanes across the tropical North Atlantic Ocean, *Organic Geochemistry*, *115*, 113–123, doi:10.1016/j.orggeochem.2017.10.010.

Schröder, T., J. van‘t Hoff, J. A. López-Sáez, F. Viehberg, M. Melles, and K. Reicherter (2018), Holocene climatic and environmental evolution on the southwestern Iberian Peninsula: A high-resolution multi-proxy study from Lake Medina (Cádiz, SW Spain), *Quaternary Science Reviews*, *198*, 208–225, doi:10.1016/j.quascirev.2018.08.030.

Walczak, I. W., J. U.L. Baldini, L. M. Baldini, F. McDermott, S. Marsden, C. D. Standish, D. A. Richards, B. Andreo, and J. Slater (2015), Reconstructing high-resolution climate using CT scanning of unsectioned stalagmites: A case study identifying the mid-Holocene onset of the Mediterranean climate in southern Iberia, *Quaternary Science Reviews*, *127*, 117–128, doi:10.1016/j.quascirev.2015.06.013.

Wanner, H., O. Solomina, M. Grosjean, S. P. Ritz, and M. Jetel (2011), Structure and origin of Holocene cold events, *Quaternary Science Reviews*, *30*(21-22), 3109–3123, doi:10.1016/j.quascirev.2011.07.010.

Wassenburg, J. A., S. Dietrich, J. Fietzke, J. Fohlmeister, K. P. Jochum, D. Scholz, D. K. Richter, A. Sabaoui, C. Spötl, G. Lohmann, M. O. Andreae, and A. Immenhauser (2016), Reorganization of the North Atlantic Oscillation during early Holocene deglaciation, *Nature Geoscience*, *9*(8), 602–605, doi:10.1038/ngeo2767.

Weinelt, M., C. Schwab, J. Kneisel, and M. Hinz (2015), Climate and societal change in the western Mediterranean area around 4.2 ka BP, in *2200 BC - ein Klimasturz als Ursache für den Zerfall der alten Welt?: 7. Mitteldeutscher Archäologentag vom 23. bis 26. Oktober 2014 in Halle (Saale)*, *Tagungen des Landesmuseums für Vorgeschichte Halle*, Band 12,1, edited by H. Meller et al., pp. 461–480, Landesamt für Denkmalpflege und Archäologie Sachsen-Anhalt, Landesmuseum für Vorgeschichte, Halle (Saale).

Zanchetta, G., E. Regattieri, I. Isola, R. N. Drysdale, M. Bini, I. Baneschi, and J. C. Hellstrom (2016), The so-called "4.2 event" in the Central Mediterranean and its climatic teleconnections, *Alpine and Mediterranean Quaternary*, *29*(1), 5–17.

Zielhofer, C., W. J. Fletcher, S. Mischke, M. de Batist, J. F.E. Campbell, S. Joannin, R. Tjallingii, N. El Hamouti, A. Junginger, A. Stele, J. Bussmann, B. Schneider, T. Lauer, K. Spitzer, M. Strupler, T. Brachert, and A. Mikdad (2017), Atlantic forcing of Western Mediterranean winter rain minima during the last 12,000 years, *Quaternary Science Reviews*, *157*, 29–51, doi:10.1016/j.quascirev.2016.11.037.

Zielhofer, C., A. Köhler, S. Mischke, A. Benkaddour, A. Mikdad, and W. J. Fletcher (2019), Western Mediterranean hydro-climatic consequences of Holocene ice-rafted debris (Bond) events, *Clim. Past*, *15*(2), 463–475, doi:10.5194/cp-15-463-2019.

Zorita, E., V. Kharin, and H. von Storch (1992), The Atmospheric Circulation and Sea Surface Temperature in the North Atlantic Area in Winter: Their Interaction and Relevance for Iberian Precipitation, *Journal of Climate*, *5*(10), 1097–1108, doi:10.1175/1520-0442(1992)005<1097:TACASS>2.0.CO;2.

Chapter 6

Spatial patterns of temperature, precipitation, and settlement dynamics on the Iberian Peninsula during the Chalcolithic and the Bronze Age

Julien Schirrmacher, Jutta Kneisel, Daniel Knitter, Wolfgang Hamer, Martin Hinz, Ralph R. Schneider, and Mara Weinelt (2020): Spatial patterns of temperature, precipitation, and settlement dynamics on the Iberian Peninsula during the Chalcolithic and the Bronze Age, Quaternary Science Reviews 223, 106220, doi: 10.1016/j.quascirev.2020.106220

The formatting of the original article has been changed.

Spelling mistakes have been corrected.

6 Spatial patterns of temperature, precipitation, and settlement dynamics on the Iberian Peninsula during the Chalcolithic and the Bronze Age

6.1 Abstract

In light of recent climate changes, it is important to also gain knowledge about the spatial manifestation of past climate events and their potential impact on ancient societies across a wide range of different scenarios. Following this approach, we compare compilations of seasonal (winter and summer) as well as annual precipitation and temperature changes to a measure of human activity based on AMS ^{14}C data of settlement sites from the Iberian Peninsula during the Chalcolithic and the Bronze Age – a period of major social turnover. Paleo-climatic reconstructions show a long-term decrease in winter precipitation between 6000 and 3000 cal. BP (4050 – 1050 BCE). Superimposed to this long-term trend in aridification was the 4.2 ka BP climate event, which manifested itself as a period of abrupt decrease in summer precipitation and/or an elongation of the summer dry period, but probably with constant winter precipitation from 4000 to 3800 cal. BP (2050 – 1850 BCE), particularly affecting the southeast of the Iberian Peninsula. Additionally, a winter cooling event across the Iberian Peninsula and its marginal seas occurred between 4400 and 4000 cal. BP (2450 – 2050 BCE) coinciding with Bond Event 3. By comparing human activities to the changes in seasonal and annual precipitation, new insight is gained into the causal relationships between climatic and social dynamics in the past. We show that winter precipitation potentially played a major role for the societies during the Chalcolithic and the Bronze Age of the southern Iberian Peninsula. While the El Argar culture at the south-eastern Iberian Peninsula boomed in spite of enhanced summer drought associated to the 4.2 ka BP climate event, decreasing winter precipitation was potentially contributing to a demographic decline in the southwest after 4800 cal. BP (2850 BCE) as well as to the bust of the El Argar culture in the southeast after 3600 cal. BP (1650 BCE) by limiting the agricultural strategies.

6.2 Introduction

The current climate change is considered to severely affect people living on the Iberian Peninsula by reducing precipitation and increasing the duration and number of heat waves and dry spells particularly in its Mediterranean region [*Giorgi and Lionello*, 2008]. As a

consequence, people likely will increasingly suffer from bad crop yields and bad health status [*Kovats et al.*, 2014]. A better understanding of how climate change affected people in the past in marginal environments, which are characterized by large-scale seasonal precipitation and temperature changes, may contribute to the current climate change debate. Such a marginal environment with particular challenges for human societies can be found on the Iberian Peninsula with the spatial and seasonal distribution of precipitation varying considerably. Recently, the south-eastern region, for instance, is the driest area of Europe with an annual average precipitation of less than 400 mm, while the north-western region receives a great amount of annual precipitation (> 1500 mm) [*Fick and Hijmans*, 2017].

Studying past abrupt climate events in such marginal environments and their potential impact on societies can provide crucial information on the long-term impact of current climate change. In this regard, one of the prime targets for this study is the 4.2 ka BP event, which manifested itself across the Eastern and Central Mediterranean as a prolonged dry episode between 4300 and 3800 cal. BP (calibrated years before present) corresponding to 2350 – 1850 years before the Common Era (BCE) [*Cheng et al.*, 2015; *Ruan et al.*, 2016; *Zanchetta et al.*, 2016]. On the Iberian Peninsula a variety of climate records including the 4.2 ka BP event have been published over the last years. These include botanical records in particular, in which discrete climate signals are often masked by variable and highly local land use signals [*Fyfe et al.*, 2019; *López-Sáez et al.*, 2014; *Schneider et al.*, 2016]. In this respect, the study of marine archives turns out to be an important tool for regional paleo-climatic reconstructions as local land use signals are diluted in such archives, which incorporate large-scale regional signals [*Faust and Wolf*, 2017]. Recent studies based on marine archives suggest that the Western Mediterranean area likely experienced stable winter precipitation along with dry summer conditions during the 4.2 ka BP event [*Bini et al.*, 2019; *Schirrmacher et al.*, 2019]. Parallel to the precipitation changes, the Western Mediterranean area is also considered by some authors to have experienced a major cooling between 4300 and 3800 cal. BP (2350 – 1850 BCE) [*Bini et al.*, 2019; *Català et al.*, 2019; *Zielhofer et al.*, 2019]. However, due to the limited availability of high-resolution and well-dated regional archives, the spatio-temporal manifestation of the 4.2 ka BP event on the Iberian Peninsula remains less clear [*Bini et al.*, 2019; *Weinelt et al.*, 2015].

The climatic deteriorations associated with the 4.2 ka BP event have been shown to have had a large impact on societies in the Near East, where an array of social collapses has been reported along with large-scale population displacements [*Weiss*, 2017; *Welc and Marks*, 2014]. However, the potential impact of poorly defined climate constraints related to this event on ancient societies of the Iberian Peninsula is still under debate [*Lillios et al.*, 2016]. The rich and

well-explored Chalcolithic and Bronze Age archaeological record with many well-dated settlement sites provides a unique archive to explore past social dynamics. Accordingly, an array of studies using summed probability densities (SPDs) of AMS ^{14}C dates as a proxy for human activities and population density in a broader sense have been carried out for the Iberian Peninsula investigating either the role of climate change on societies or the human impact on the environment [*Blanco-González et al.*, 2018; *Drake et al.*, 2017; *Fyfe et al.*, 2019; *Lillios et al.*, 2016; *Walsh et al.*, 2019]. Yet, these data are often generalized over a sub-region of the Iberian Peninsula, e.g. the entire Atlantic coast, limiting the detection of the true/full spatial variability within this sub-region. In addition, many studies include data from burial contexts, which likely biases the results towards ritual behaviour [*Hinz et al.*, 2012a]. Regarding climatic data, many of the above-mentioned studies just rely on a limited number of single-proxy paleo-climatic datasets. Considering only a small number of single-proxy data results in potentially large uncertainty questioning their representativeness on a regional scale.

Hence, despite the intense research carried out during the last few years, many crucial questions remain unanswered. These are particularly related to the spatial manifestation of the 4.2 ka BP event on the Iberian Peninsula, which is hampered due to the lack of a coherent data base and the difficult distinction between local anthropogenic and regional climatic signals in many archives. Aiming to address the spatial manifestation of the 4.2 ka BP event on the Iberian Peninsula and trace coherent regional patterns, we compiled a variety of paleo-climatic proxies from terrestrial and marine archives on the Iberian Peninsula including some sites from northern Africa and its adjacent seas along the Iberian margin, respectively (Fig 6.1). Based on this paleo-climatic multi-proxy compilation, we compare the demographic development of the Iberian Peninsula, which is based on a compilation of AMS ^{14}C data from archaeological settlement contexts, with the seasonal (summer and winter) and annual temperature and precipitation history between 6000 and 3000 cal. BP – corresponding to 4050 – 1050 BCE – encompassing the late Neolithic, Chalcolithic, and Bronze Age in the area.

6.2.1 Climate of the Iberian Peninsula

While during recent times, temperatures across the entire Iberian Peninsula are marked by pronounced seasonal contrasts with more than 20 °C during summer and around 7 °C in winter [*Fick and Hijmans*, 2017], the distribution of precipitation reveals a marked regional pattern, which is mainly driven by the Atlantic and Mediterranean atmospheric regimes [*Lionello*, 2012]. Today, precipitation on the Iberian Peninsula in general is associated with the westerly

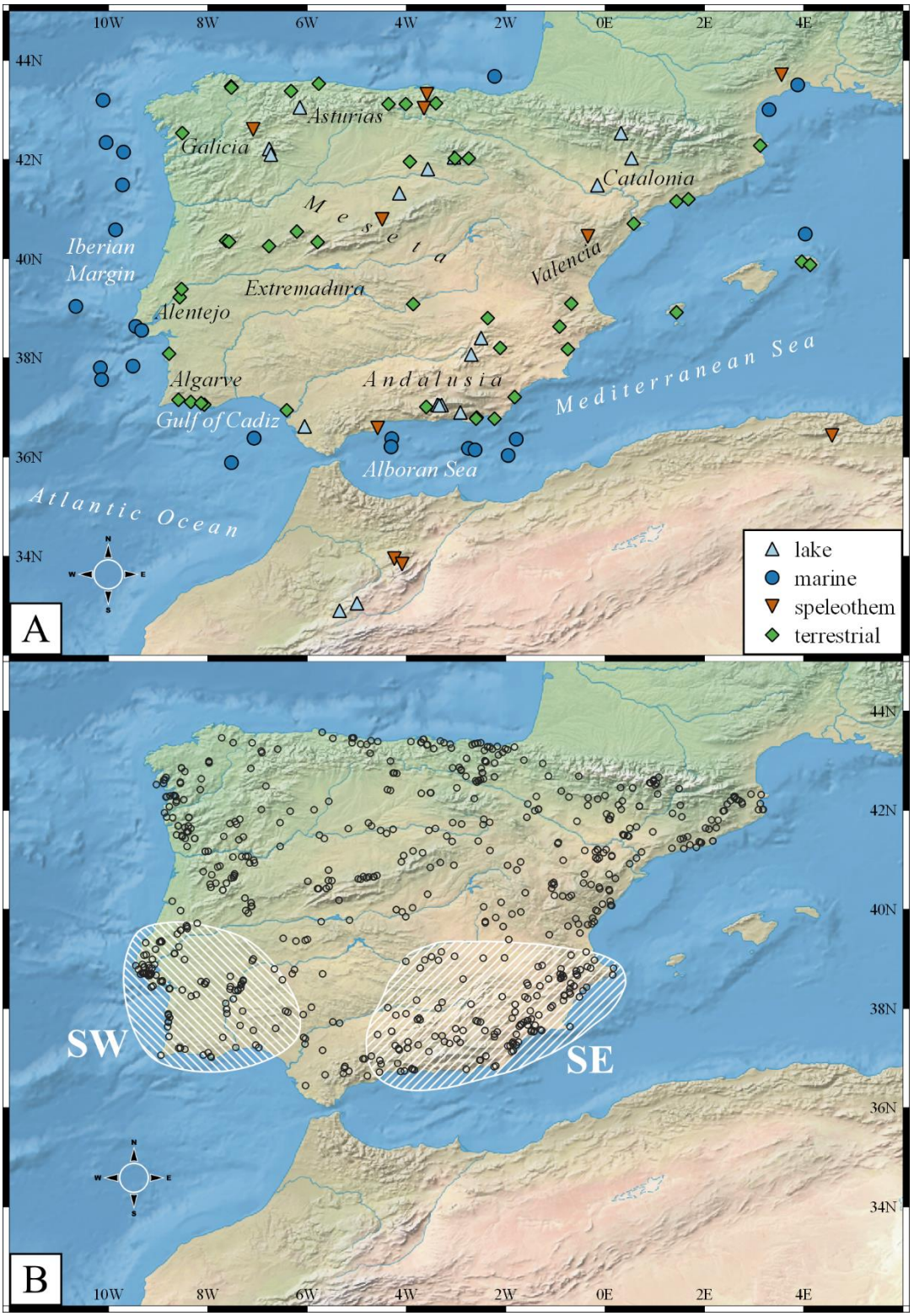

Figure 6.1 Overview of the study areas on the Iberian Peninsula and adjacent marine regions *showing A) locations of compiled climatic proxies as well as major geographic regions referred to in the text and B) locations of archaeological settlements with AMS ^{14}C dates between 6000 and 3000 cal. BP (4050 – 1050 BCE). Hatched areas indicate geographic regions in the southwest (SW) and the southeast (SE) of similar developments in settlement intensity referred to in the text. For further information on the paleo-climatic archives see Tab 6.1.*

wind belt [*Zorita et al.*, 1992] and to a large extent controlled by the North Atlantic Oscillation [*Hernández et al.*, 2015; *Hurrell*, 1995; *Trigo et al.*, 2004]. However, the Atlantic climate is bounded to the northern and western coasts and typically marked by high precipitation of 400 mm to more than 1000 mm during the rainy season from October to February and between 300 mm and 700 mm from March to September [*Fick and Hijmans*, 2017]. In contrast, the Mediterranean climate, which is most pronounced at the southern and eastern coasts as well as in the Meseta area, is characterized by significantly drier conditions with a rainy winter season (up to 500 mm) and a dry summer season barely exceeding 200 mm [*Fick and Hijmans*, 2017].

Given that the variability of sea surface temperatures (SSTs) and atmospheric temperatures at Iberian coasts are tightly coupled (Fig 6.6), the marine conditions with respect to temperature, in particular, are of major importance for the climate system across the Iberian Peninsula. Regarding the SSTs, a strong seasonal contrast is evident at the western coast, which receives warm waters with the Iberian Poleward Current from the south during the winter season [*Peliz et al.*, 2005]. During the summer, however, the surface current is directed southward and favours coastal upwelling along the western continental margin, thus, causing relatively low SSTs [*Haynes et al.*, 1993; *Peliz et al.*, 2002]. At the southern coast in the Alboran Sea Atlantic water masses circulate in two anti-cyclonic gyres [*Lionello*, 2012]. These gyres promote local upwelling and, thus, also modulate the regional temperature variability in the Alboran Sea [*Sarhan et al.*, 2000].

Over the course of the Holocene, climatic conditions on the Iberian Peninsula and adjacent marine areas were modulated by long-term trends as well as by superimposed abrupt events. In relation to decreasing solar forcing from the beginning of the Holocene, the Iberian Peninsula faced a trend towards cooler and drier conditions [*Cacho et al.*, 2001; *Peyron et al.*, 2017; *Ramos-Román et al.*, 2018]. The overall cooling trend is questioned by [*Davis et al.*, 2003], though, who based on pollen data found a warming trend since ca. 8000 cal. BP (6050 BCE) across southwest Europe. Nonetheless, the Holocene Climatic Optimum between ca. 9500 and 7600 cal. BP (7550 – 5650 BCE) is associated with maximum extension of the forest cover at the Iberian Peninsula suggesting intense winter precipitation and high temperatures [*Jalut et al.*, 2009; *Ramos-Román et al.*, 2018]. Afterwards, a trend towards increasing aridity is particularly evident since around 5500 cal. BP (3550 BCE) [*Jalut et al.*, 2009; *Jiménez-Moreno et al.*, 2015]. Also, between 7000 and 5000 cal. BP (5050 – 3050 BCE) the Mediterranean climate characterized by mild winters as well as hot and dry summers gradually established on the Iberian Peninsula [*Pérez-Obiol et al.*, 2011]. Seasonality in sea surface temperatures, on the other hand, became smaller, i.e. cooler summers and warmer winters, during the Holocene,

which is particularly evident in the Atlantic realm [*Schirrmacher et al.*, 2019]. These long-term trends are amplified by several dry and cool episodes [*Cacho et al.*, 2001; *Chabaud et al.*, 2014; *Ramos-Román et al.*, 2018; *Schirrmacher et al.*, 2019; *Zielhofer et al.*, 2019]. These dry and cool episodes are modulated by the interference of North Atlantic (subpolar) and Mediterranean (subtropical) climatic regimes. For instance, the North Atlantic Oscillation controlled winter precipitation variability on the Iberian Peninsula since the Mid- Holocene [*Ausín et al.*, 2015; *Schirrmacher et al.*, 2019; *Wassenburg et al.*, 2016; *Zielhofer et al.*, 2017]. Holocene cooling events on the Iberian Peninsula, on the other hand, were related to the so-called Bond Events [*Bond et al.*, 2001], a series of iceberg discharge events in the North Atlantic [*Ramos-Román et al.*, 2018; *Schirrmacher et al.*, 2019; *Smith et al.*, 2016; *Zielhofer et al.*, 2019].

6.2.2 Archaeological background

Detailed reviews of the prehistoric developments on the Iberian Peninsula are beyond the scope of this study and can be found elsewhere [*Blanco-González et al.*, 2018; *Chapman*, 2008; *Lull et al.*, 2013a]. The following summary intends to provide an overview of the most important cultural developments during the Chalcolithic (c. 5300 – 4200 cal. BP; 3300 – 2200 BCE) and Bronze Age (c. 4200 – 2900 cal. BP; 2200 – 900 BCE).

The Chalcolithic or Copper Age marks the beginning of metallurgy, namely copper metalworking [*Bartelheim and Pearce*, 2015]. Whereas people in Galicia, Asturias, and the northern Meseta mainly lived in small farmsteads [*Blanco-González et al.*, 2018], in the southern part of the Iberian Peninsula in Alentejo and Andalusia people nucleated and major sites such as Zambujal and Los Millares emerged [*Kunst and Lutz*, 2008; *Molina González et al.*, 2004]. As suggested from different trade networks [*Schuhmacher*, 2017], both sites likely reflect two distinct social systems: a society close to the site of Zambujal in the southwest (SW) at the Atlantic coast and the Los Millares culture in the southeast (SE) at the Mediterranean coast. Furthermore, defensive structures associated with many sites and specialized manufacture of arrowheads in both regions indicate that violent conflicts were prominent features between rivalling societies at that time [*Lull et al.*, 2015]. Apart from these notable differences, both societies share numerous similarities, for example, the use of Bell Beaker pottery [*Müller and van Willigen*, 2001], a megalithic burial tradition [*Schulz Paulsson*, 2019], or participation in long-distance exchange networks [*Schuhmacher*, 2017]. Moreover, settlement sites share similarities with the occurrence of major sites including ditched and walled enclosures (sometimes on hilltops), or pit complexes [*Blanco-González et al.*, 2018; *Lull et al.*, 2015; *Valera*, 2015], which are perhaps the most prominent and best explored settlement

features from that time. So-called mega-sites, for instance, Valencina de la Concepción or Marroquíes Bajos encompassed an area of up to 450 and 113 hectares, respectively [*García Sanjuán et al.*, 2017]. Apart from these, also small sites in the lowlands associated with increased agricultural production, whose frequencies are likely underestimated due to their low visibility in the field, were settled in the south at that time [*Chapman*, 2008; *García Sanjuán et al.*, 2016].

The period around c. 4200 cal. BP (2250 BCE) marks a time of major societal turnover and transformation on the Iberian Peninsula, particularly in the south spanning economic, ritual, and traditional practises as well as settlement patterns. In the SW, including the Alentejo and Algarve regions, the majority of sites – also those with ditched enclosures and large walled sites – were abandoned and also many traditions (e.g. material culture and burial customs) vanished [*Lull et al.*, 2015; *Soares et al.*, 2007; *Valera*, 2015]. The rapidity of these transformations, which occurred within some decades [*García Sanjuán et al.*, 2018; *Lull et al.*, 2015], imply a social collapse in the area. Subsequently, a semi-nomadic lifestyle was established in the Alentejo, Algarve, and Extremadura regions [*Lull et al.*, 2013a; *Valera*, 2015]. In the Meseta, agricultural activity sharply dropped between 4200 and 4000 cal. BP (2250 – 2050 BCE) and people increasingly relied on pastoralism [*López Saez et al.*, 2017]. Furthermore, the site of Los Millares in Andalusia decreased significantly between 4500 and 4200 cal. BP (2550 – 2250 BCE) and probably ended violently by fire [*Lull et al.*, 2015].

In the beginning of the Bronze Age, bronze and later silver metallurgy were introduced to the Iberian Peninsula [*Comendador Rey et al.*, 2014]. Nonetheless, in Galicia and Asturias social developments are considered to be marked by relative stability in terms of subsistence strategies (i.e. small number of lowland sites mainly dependent on agriculture). Andalusia and the southern parts of the Meseta and Valencia, in contrast, featured the rise of the El Argar civilization, which is regarded as the first political and hierarchical society on the Iberian Peninsula with broad control of specialized metallurgy and agricultural practises [*Delgado-Raack et al.*, 2014; *Delgado-Raack and Risch*, 2015; *Lull et al.*, 2011]. Based on differential endowments of grave goods, [*Lull et al.*, 2011] have defined five to six distinct social classes underlining the hierarchical system of the Argaric culture. The Argaric culture spread from the south-eastern coast along the Valencian coast and extended into the southern Meseta within about 300 years and is also associated with a demographic boom in these areas [*Aranda et al.*, 2008; *Chapman*, 2008; *Lull et al.*, 2011]. Prominent settlement types were hilltop sites in the mountains [*Chapman*, 2008] and fortified settlements (*motillas*) in the upper Guadalquivir and Guadiana river basins [*Aranda et al.*, 2008]. The *motillas* were used for groundwater extraction

supplying the intense agriculture practised at that time [*Aranda et al.*, 2008; *Benítez de Lugo Enrich and Mejías*, 2017]. Overall, irrigation techniques were known in the Argaric culture and spread westwards during the following centuries [*Mora-González et al.*, 2016; *Mora-González et al.*, 2018]. While the Argaric people were not engaged in trans-regional trade, highly specialized manufacturing processes are documented [*Delgado-Raack and Risch*, 2015]. Starting from the hilltop settlements, where the elites and, thus, the political power was situated, intense agricultural production took place in the lowlands [*Aranda et al.*, 2008; *Castro et al.*, 1999]. Processing of cereals took place in specialized workshops at the hilltop sites, while the food was stored in different areas within the sites where it was redistributed by the elites [*Delgado-Raack and Risch*, 2015]. It has been proposed that the end of the Argaric culture by c. 3500 cal. BP (1550 BCE) is characterized by environmental over-exploitation due to intense agriculture [*Chapman*, 2008]. At that time, 50 to 100 per cent of Argaric settlements, among them hilltop sites and the *motillas*, were abandoned and replaced by small sites based on subsistence [*Lull et al.*, 2013a]. Along with the collapse of the Argaric culture, its political system also disappeared [*Chapman*, 2008].

6.3 Methods

6.3.1 Paleo-climatological compilation and approach

In this paper, we compiled climate data from various archives (Fig 6.1) including multiple proxies to limit potential biases from single-proxy approaches and to identify coherent regional climatic patterns on the Iberian Peninsula. Temperature and precipitation compilations based on own data [*Schirrmacher et al.*, 2019] and other published data have been accomplished from various databases such as SISAL [*Atsawawaranunt et al.*, 2019], PANGAEA WDC-Mare, NOAA, and European Pollen Database (Tab 6.1). Temperature and precipitation have been chosen as main climatic variables confining agricultural activities and abrupt changes of those variables are considered as hazardous, and thus, as crucial for the subsistence/economies of ancient societies. The database compiled for this study contains 157 datasets from 95 sites between 12 °W and 6 °E and 32 °N to 45 °N (Fig 6.1; Tab 6.1). Altogether, the database comprises records from 18 lake archives, 25 marine sites, 10 speleothems, and 42 other terrestrial archives (e.g. peat deposits), and is based on 18 different quantitative or qualitative proxies. While 111 datasets reflect precipitation changes, 46 datasets are indicative of sea surface and/or atmospheric temperature variability. With 97 datasets pollen represent the majority of the compiled proxies.

The compiled temperature data from marine sediment archives are based on a suite of biomarker and other semi-quantitative and quantitative proxies that enable to assess the variability of precipitation and temperature at seasonal or annual scale. These include long-chain diol indexes (LDI), alkenones, TEX_{86}, and planktonic foraminiferal assemblages transferred to temperatures via modern analogue technique (MAT), all reflecting sea surface temperatures (SSTs). A tight coupling between SST and atmospheric temperature variability along the Iberian coasts is suggested from observational data (Fig 6.6) and justifies the use of SST data for a comparative study with archaeological data. To assess seasonality as a variable potentially highly influential to agrarian production, the compiled climatic proxy data were assigned to individual seasons wherever possible. Following [*Gouveia et al.*, 2008], we considered decreasing arboreal pollen (AP) percentages on the Iberian Peninsula as reflecting a decrease in winter precipitation. This is in harmony with interpretations in previous paleo-climatic studies from the Iberian Peninsula [*Ramos-Román et al.*, 2018; *Fletcher et al.*, 2010; *Chabaud et al.*, 2014]. Contrastingly, xerophytic species such as Chenopodiaceae, Amaranthaceae, and *Artemisia* are adapted to seasonal dry conditions and, thus, are indicative of prolonged annual dry periods [*Cariñanos et al.*, 2004]. Accordingly, an increase in xerophytic pollen percentage – either within a single of the above mentioned species or the sum of all three – was considered as reflecting annual dry conditions. Concerning the data of all non-pollen proxies, we follow the original interpretation of the authors. This also includes the interpretation of *Cedrus* pollen percentages in northern Africa, where an increase indicates decreasing summer temperatures [*Lamb and van der Kaars*, 1995; *Campbell et al.*, 2017].

Age models for the new marine records of cores ODP-161-976A and GeoB5901-2 [*Schirrmacher et al.*, 2019] were updated with 5 and 6 new AMS ^{14}C dates, respectively, and have been calculated using the Bacon package [*Blaauw and Christen*, 2011] in the R programming language [*R Core Team*, 2019]. The new AMS ^{14}C dates were measured at the Leibniz Laboratory at Kiel University (Tab 6.3).

For the analysis only paleo-climatic data between 6000 and 3000 cal. BP (4050 – 1050 BCE) have been compiled. For each dataset the z-score [*Clark-Carter*, 2014] has been calculated to achieve comparability among all proxies. Depending on the variable, a positive (negative) score indicates relatively humid (dry) or warm (cool) conditions, respectively, in relation to the average conditions of each record between 6000 and 3000 cal. BP (4050 – 1050 BCE). The higher (positive or negative) the score, the more pronounced the respective climatic conditions. Afterwards, medians of 200-year time slices within the interval have been calculated for each proxy. For an illustration of the methodological approach please see Fig 6.2.

Table 6.1 Paleo-climatic proxies compiled for this study. *[a] The age model for this archive has been re-calculated for this study. The individual age-depth models are shown in Fig 6.7. [b]The data has been digitized from the original reference. The assignment of the final quality flag (QF) based on the number of datings, the temporal coverage, and the average temporal resolution is explained in Tab 6.2. Parameter-based QFs for number of datings, temporal coverage, and temporal resolution are shown in brackets. preWin = 2000 – 3000 cal. BP (50 – 1050 BCE); Win = 3000 – 6000 cal. BP (1050 – 4050 BCE); postWin = 6000 – 7000 cal. BP (4050 – 5050 BCE)*

Name	Latitude	Longitude	Archive	Proxy	No. of datings preWin/Win/postWin (parameter-based QF)	Temporal coverage in Win (parameter-based QF)	Temporal resolution (parameter-based QF)	Final QF	References
Precipitation									
annual									
Monte Areo	43.528889	-5.768889	terrestrial	pollen WAPLS	1/1/2 (2)	85 % (1)	427 yrs (3)	3	[*Ilvonen et al.*, 2019]
PB06	43.506604	3.875170	marine	XRD data	6/7/2 (1)	99 % (1)	20 yrs (1)	1	[*Sabatier et al.*, 2012]
Alto de la Espina	43.381111	-6.327222	terrestrial	pollen WAPLS	2/3/0 (1)	95 % (1)	178 yrs (2)	2	[*Ilvonen et al.*, 2019]
Zalama	43.135000	-3.409722	terrestrial	pollen WAPLS	0/6/3 (1)	97 % (1)	72 yrs (1)	1	[*Ilvonen et al.*, 2019]
Alsa	43.117778	-4.016667	terrestrial	Chenopodiaceae	1/1/0 (2)	40 % (3)	101 yrs (2)	3	[*Mariscal*, 1993]
Lago de Ajo[a,b]	43.050000	-6.150000	lake	pollen MAT	0/1/0 (3)	94 % (1)	201 yrs (3)	3	[*Allen et al.*, 1996]
KGSC-31[b]	43.006389	3.298889	marine	*n*-alkane concentration	1/4/2 (1)	99 % (1)	15 yrs (1)	1	[*Jalali et al.*, 2016]
Basa de la Mora[b]	42.533333	0.316667	lake	*Artemisia*	2/3/1 (1)	100 % (1)	125 yrs (2)	2	[*Pérez-Sanz et al.*, 2013]
Laguna de la Roya[a,b]	42.216667	-6.766667	lake	pollen MAT	0/1/1 (2)	90 % (1)	209 yrs (3)	3	[*Allen et al.*, 1996]
Sanabria[a,b]	42.100000	-6.733333	lake	pollen MAT	0/0/0 (3)	94 % (1)	177 yrs (2)	3	[*Allen et al.*, 1996]
Las Pardillas	42.045556	-3.045278	lake	Xerophytes	0/1/0 (3)	86 % (1)	184 yrs (2)	3	[*Sánchez Goñi and Hannon*, 1999]
Estanya	42.027139	0.5304340	lake	PCA2 XRF data	0/1/2 (2)	93 % (1)	15 yrs (1)	2	[*Morellón et al.*, 2009]
Quintanar de la Sierra	42.025278	-3.026111	terrestrial	pollen WAPLS	0/1/0 (3)	69 % (2)	347 yrs (3)	3	[*Ilvonen et al.*, 2019]
Espinosa de Cerrato[b]	41.956667	-3.935000	terrestrial	*Artemisia*	1/2/0 (2)	99 % (1)	68 yrs (1)	2	[*Franco-Múgica et al.*, 2001]
Hoya del Castillo	41.481944	-0.158333	lake	Xerophytes	0/0/1 (3)	44 % (3)	187 yrs (2)	3	[*Davis and Stevenson*, 2007]
Amposta[b]	40.706669	0.574036	terrestrial	*Artemisia*	1/3/0 (2)	90 % (1)	208 yrs (3)	3	[*Pérez-Obiol et al.*, 2011]
El Maíllo	40.546667	-6.209722	terrestrial	pollen WAPLS	0/2/0 (2)	95 % (1)	130 yrs (2)	2	[*Ilvonen et al.*, 2019]
MD99-2343	40.497333	4.028167	marine	potassium/ aluminium ratio	1/1/2 (2)	98 % (1)	140 yrs (2)	2	[*Frigola et al.*, 2008]
Algendar	39.940556	3.958611	terrestrial	Xerophytes	0/2/1 (2)	99 % (1)	65 yrs (1)	2	[*Yll et al.*, 1997]
Hort Timoner	39.875000	4.126389	terrestrial	Xerophytes	0/0/0 (3)	98 % (1)	118 yrs (2)	3	[*Yll et al.*, 1997]
Navarrés	39.093333	-0.683333	terrestrial	pollen WAPLS	0/1/1 (2)	98 % (1)	113 yrs (2)	2	[*Ilvonen et al.*, 2019]
MD03-2699	39.036700	-10.660500	marine	*n*-alkane concentration	0/2/0 (2)	92 % (1)	154 yrs (2)	2	[*Palumbo et al.*, 2013]
Villaverde[b]	38.800000	-2.366667	terrestrial	Xerophytes	2/2/0 (2)	96 % (1)	57 yrs (1)	2	[*Carrión et al.*, 2001a]
D13882	38.634500	-9.454200	marine	*n*-alkane concentration	1/1/1 (2)	97 % (1)	112 yrs (2)	2	[*Rodrigues et al.*, 2009]
D13902	38.554000	-9.335500	marine	*n*-alcohol concentation	0/0/1 (3)	36 % (3)	271 yrs (3)	3	[*Rodrigues et al.*, 2009]
Siles[b]	38.400000	-2.500000	lake	Xerophytes	1/3/0 (2)	97 % (1)	162 yrs (2)	2	[*Carrión*, 2002]
El Sabinar[a,b]	38.200000	-2.116667	terrestrial	Xerophytes	2/4/1 (1)	97 % (1)	81 yrs (1)	1	[*Carrión et al.*, 2004]
Elx	38.174444	-0.752778	terrestrial	Xerophytes	0/2/1 (2)	75 % (2)	45 yrs (1)	2	[*Burjachs et al.*, 1997]
Santo Andre[a,b]	38.083333	-8.783333	terrestrial	Chenopodiaceae	0/2/1 (2)	74 % (2)	369 yrs (3)	3	[*Santos and Sánchez Goñi*, 2003]
Cañada de la Cruz[a,b]	38.066667	-2.700000	lake	Xerophytes	3/3/1 (1)	96 % (1)	206 yrs (3)	3	[*Carrión et al.*, 2001b]
MD95-2042[b]	37.799833	-10.166500	marine	Chenopodiaceae	1/2/1 (2)	90 % (1)	180 yrs (2)	2	[*Chabaud et al.*, 2014]
Antas	37.208333	-1.823611	terrestrial	Xerophytes	0/0/0 (3)	86 % (1)	369 yrs (3)	3	[*Pantaléon-Cano et al.*, 2003]
P01-5[b]	37.085105	-8.138509	terrestrial	*Artemisia*	4/4/0 (1)	68 % (2)	156 yrs (2)	2	[*Schneider et al.*, 2010; *Schneider et al.*, 2016]

Name	Latitude	Longitude	Archive	Proxy	No. of datings preWin/Win/postWin (parameter-based QF)	Temporal coverage in Win (parameter-based QF)	Temporal resolution (parameter-based QF)	Final QF	References
Borreguil de la Virgen[b]	37.054167	-3.377778	lake	*Artemisia*	0/3/1 (2)	95 % (1)	72 yrs (1)	2	[*Jiménez-Moreno and Anderson*, 2012]
Laguna Hondera[b]	37.048000	-3.294333	lake	calcium/titanium ratio	1/1/2 (2)	94 % (1)	118 yrs (2)	2	[*Mesa-Fernández et al.*, 2018]
Laguna de Río Seco[b]	37.040500	-3.342833	lake	*Artemisia*	1/3/2 (1)	97 % (1)	139 yrs (2)	2	[*Anderson et al.*, 2011]
Padul[b]	37.011047	-3.603906	terrestrial	Xerophytes	2/4/2 (1)	98 % (1)	55 yrs (1)	1	[*Ramos-Román et al.*, 2018]
Donana[b]	36.941667	-6.413333	terrestrial	Amaranthaceae	1/4/0 (1)	68 % (2)	120 yrs (2)	2	[*Jiménez-Moreno et al.*, 2015]
Sierra de Gádor[a,b]	36.900000	-2.916667	lake	Xerophytes	0/1/2 (2)	98 % (1)	65 yrs (1)	2	[*Carrión et al.*, 2003]
Roquetas de Mar	36.794444	-2.588889	terrestrial	Xerophytes	0/1/1 (2)	97 % (1)	162 yrs (2)	2	[*Pantaléon-Cano et al.*, 2003]
San Rafael	36.773611	-2.601389	terrestrial	Xerophytes	0/1/0 (3)	86 % (1)	90 yrs (1)	3	[*Pantaléon-Cano et al.*, 2003]
San Rafael	36.773611	-2.601389	terrestrial	pollen WAPLS	0/1/0 (3)	86 % (1)	90 yrs (1)	3	[*Ilvonen et al.*, 2019]
Lake Medina[b]	36.617778	-6.053611	lake	ostracod assemblages	3/5/3 (1)	99 % (1)	74 yrs (1)	1	[*Schröder et al.*, 2018]
El Refugio Cave	36.583333	-4.583333	speleothem	CT density	0/6/0 (1)	100 % (1)	3 yrs (1)	1	[*Walczak et al.*, 2015]
Gueldaman Cave	36.433300	4.566700	speleothem	stalagmite $\delta^{18}O$	0/8/0 (1)	87 % (1)	13 yrs (1)	1	[*Ruan et al.*, 2016]
TTR14-300G[b]	36.358867	-1.791783	marine	lanthanum/ lutetium ratio	0/0/1 (3)	90 % (1)	244 yrs (3)	3	[*Cortés-Sánchez et al.*, 2011]
ODP-161-976A[a,b]	36.205333	-4.312667	marine	pollen MAT	0/11/0 (1)	86 % (1)	259 yrs (3)	3	[*Combourieu Nebout et al.*, 2009]
MD95-2043	36.143333	-2.621167	marine	pollen MAT	0/2/1 (2)	94 % (1)	117 yrs (2)	2	[*Bini et al.*, 2019]; [*Fletcher et al.*, 2010]; [*Peyron et al.*, 2017]
MD95-2043	36.143333	-2.621167	marine	Xerophytes	0/2/1 (2)	94 % (1)	117 yrs (2)	2	[*Fletcher and Sánchez Goñi*, 2008]
summer									
ODP-161-976A[a,b]	36.205333	-4.312667	marine	pollen MAT	0/11/0 (1)	86 % (1)	259 yrs (3)	3	[*Combourieu Nebout et al.*, 2009]
MD95-2043	36.143334	-2.621168	marine	pollen MAT	0/2/1 (2)	94 % (1)	117 yrs (2)	2	[*Bini et al.*, 2019]; [*Fletcher et al.*, 2010]; [*Peyron et al.*, 2017]
winter									
Cuadramón	43.474167	-7.534722	terrestrial	arboreal pollen	0/0/0 (3)	74 % (2)	442 yrs (3)	3	[*González and Saa*, 2000]
Pedrido	43.450278	-7.529167	terrestrial	arboreal pollen	8/9/0 (1)	76 % (2)	79 yrs (1)	2	[*Stefanini et al.*, 2018]
Cueva de Asiul	43.316842	-3.591200	speleothem	stalagmite $\delta^{18}O$	2/3/1 (1)	100 % (1)	15 yrs (1)	1	[*Smith et al.*, 2016]
Alsa	43.117778	-4.016667	terrestrial	arboreal pollen	1/1/0 (2)	40 % (3)	101 yrs (2)	3	[*Mariscal*, 1993]
Avellanosa	43.116667	-4.364167	terrestrial	arboreal pollen	1/0/1 (2)	92 % (1)	184 yrs (2)	2	[*Mariscal Álvarez*, 1983]
Cova da Arcoia	42.610000	-7.090000	speleothem	stalagmite $\delta^{13}C$	1/7/1 (1)	89 % (1)	65 yrs (1)	1	[*Railsback et al.*, 2011]
Basa de la Mora[b]	42.533333	0.316667	lake	arboreal pollen	2/3/1 (1)	100 % (1)	125 yrs (2)	2	[*Pérez-Sanz et al.*, 2013]
PRD-4	42.533333	-8.516667	terrestrial	arboreal pollen	0/2/1 (2)	91 % (1)	248 yrs (3)	3	[*López-Merino et al.*, 2012]
Castelló d'Empúries[b]	42.281389	3.120278	terrestrial	arboreal pollen	1/0/1 (2)	96 % (1)	240 yrs (3)	3	[*Burjachs and Expósito*, 2015]
Las Pardillas	42.045556	-3.045278	lake	arboreal pollen	0/1/0 (3)	86 % (1)	184 yrs (2)	3	[*Sánchez Goñi and Hannon*, 1999]
Hoyos de Iregua[a,b]	42.023889	-2.750000	terrestrial	arboreal pollen	0/0/1 (3)	94 % (1)	257 yrs (3)	3	[*Gil García et al.*, 2002]
Espinosa de Cerrato[b]	41.956667	-3.935000	terrestrial	arboreal pollen	1/2/0 (2)	99 % (1)	68 yrs (1)	2	[*Franco-Múgica et al.*, 2001]
Tubilla del Lago	41.808417	-3.572675	lake	arboreal pollen	1/4/2 (1)	99 % (1)	80 yrs (1)	1	[*Morales-Molino et al.*, 2017]
Hoya del Castillo	41.481944	-0.158333	lake	arboreal pollen	0/0/1 (3)	44 % (3)	187 yrs (2)	3	[*Davis and Stevenson*, 2007]
El Carrizal[a,b]	41.320028	-4.146972	lake	arboreal pollen	0/1/0 (3)	91 % (1)	227 yrs (3)	3	[*Franco-Múgica et al.*, 2005]
Cubelles[b]	41.200278	1.675000	terrestrial	arboreal pollen	1/1/0 (2)	95 % (1)	167 yrs (2)	2	[*Burjachs and Expósito*, 2015]
Creixell[b]	41.155556	1.433889	terrestrial	arboreal pollen	0/1/1 (2)	89 % (1)	223 yrs (3)	3	[*Burjachs and Expósito*, 2015]
Molinos Cave	40.792500	-4.492000	speleothem	stalagmite $\delta^{13}C$	1/3/1 (1)	90 % (1)	31 yrs (1)	1	[*Muñoz et al.*, 2015]
Amposta[b]	40.706669	0.574036	terrestrial	arboreal pollen	1/3/0 (2)	90 % (1)	208 yrs (3)	3	[*Pérez-Obiol et al.*, 2011]

Name	Latitude	Longitude	Archive	Proxy	No. of datings preWin/Win/postWin (parameter-based QF)	Temporal coverage in Win (parameter-based QF)	Temporal resolution (parameter-based QF)	Final QF	References
El Maíllo	40.546667	-6.209722	terrestrial	arboreal pollen	0/2/0 (2)	89 % (1)	121 yrs (2)	2	[*Morales-Molino et al.*, 2013]
Ejulve Cave	40.450000	-0.350000	speleothem	stalagmite $\delta^{13}C$	4/15/2 (1)	100 % (1)	13 yrs (1)	1	[*Moreno et al.*, 2017]
Lagoa Comprida[a]	40.362778	-7.636111	terrestrial	arboreal pollen	0/2/0 (2)	93 % (1)	117 yrs (2)	2	[*van den Brink and Janssen*, 1985]
Charco de Candieira[a]	40.341667	-7.576389	terrestrial	arboreal pollen	3/5/2 (1)	97 % (1)	56 yrs (1)	1	[*van der Knaap and van Leeuwen*, 1995]
Peña Negra	40.334722	-5.792222	terrestrial	arboreal pollen	1/1/0 (2)	34 % (3)	92 yrs (1)	3	[*Abel-Schaad and López-Sáez*, 2013]
El Payo	40.253333	-6.771111	terrestrial	arboreal pollen	0/1/0 (3)	25 % (3)	150 yrs (2)	3	[*Abel Schaad et al.*, 2009]
Algendar	39.940556	3.958611	terrestrial	arboreal pollen	0/2/1 (2)	99 % (1)	65 yrs (1)	2	[*Yll et al.*, 1997]
Hort Timoner	39.875000	4.126389	terrestrial	arboreal pollen	0/0/0 (3)	98 % (1)	118 yrs (2)	3	[*Yll et al.*, 1997]
0501.029[b]	39.387519	-8.532257	terrestrial	arboreal pollen	1/2/2 (2)	94 % (1)	202 yrs (3)	3	[*Vis et al.*, 2010]
ALP III[b]	39.221083	-8.568478	terrestrial	arboreal pollen	1/1/2 (2)	96 % (1)	80 yrs (1)	2	[*Vis et al.*, 2010]
CC-17[a,b]	39.083333	-3.866667	terrestrial	arboreal pollen	0/0/0 (3)	91 % (1)	228 yrs (3)	3	[*Dorado Valiño et al.*, 2002]
Eivissa[b]	38.915833	1.435000	terrestrial	arboreal pollen	1/2/0 (2)	89 % (1)	178 yrs (2)	2	[*Burjachs and Expósito*, 2015]
Villaverde[b]	38.800000	-2.366667	terrestrial	arboreal pollen	2/2/0 (2)	96 % (1)	57 yrs (1)	2	[*Carrión et al.*, 2001a]
Villena[a,b]	38.629667	-0.919889	terrestrial	aridity ratio	0/3/0 (2)	83 % (1)	146 yrs (2)	2	[*Jones et al.*, 2018]
Elx	38.174444	-0.752778	terrestrial	arboreal pollen	0/2/1 (2)	75 % (2)	45 yrs (1)	2	[*Burjachs et al.*, 1997]
Santo Andre[a,b]	38.083333	-8.783333	terrestrial	arboreal pollen	0/2/1 (2)	74 % (2)	369 yrs (3)	3	[*Santos and Sánchez Goñi*, 2003]
Cañada de la Cruz[a,b]	38.066667	-2.700000	lake	arboreal pollen	3/3/1 (1)	96 % (1)	206 yrs (3)	3	[*Carrión et al.*, 2001b]
MD95-2042[b]	37.799833	-10.166500	marine	arboreal pollen	1/2/1 (2)	90 % (1)	180 yrs (2)	2	[*Chabaud et al.*, 2014]
Antas	37.208333	-1.823611	terrestrial	arboreal pollen	0/0/0 (3)	86 % (1)	369 yrs (3)	3	[*Pantaléon-Cano et al.*, 2003]
ABI 05/07[b]	37.152416	-8.594227	terrestrial	arboreal pollen	1/6/1 (1)	97 % (1)	121 yrs (2)	2	[*Trog et al.*, 2013; *Schneider et al.*, 2016]
ADP 01/06[b]	37.110503	-8.345146	terrestrial	arboreal pollen	1/2/0 (2)	98 % (1)	419 yrs (3)	3	[*Trog et al.*, 2013]; [*Schneider et al.*, 2016]
P01-5[b]	37.085105	-8.138509	terrestrial	arboreal pollen	4/4/0 (1)	68 % (2)	156 yrs (2)	2	[*Schneider et al.*, 2010; *Schneider et al.*, 2016]
VDL PB2[b]	37.055965	-8.074490	terrestrial	arboreal pollen	3/1/3 (2)	16 % (3)	32 yrs (1)	3	[*Schneider et al.*, 2016; *Schneider et al.*, 2010]
Borreguil de la Virgen[b]	37.054167	-3.377778	lake	arboreal pollen	0/3/1 (2)	95 % (1)	72 yrs (1)	2	[*Jiménez-Moreno and Anderson*, 2012]
Laguna de Río Seco[b]	37.040500	-3.342833	lake	arboreal pollen	1/3/2 (1)	97 % (1)	139 yrs (2)	2	[*Anderson et al.*, 2011]
Padul[b]	37.011047	-3.603906	terrestrial	arboreal pollen	2/4/2 (1)	98 % (1)	55 yrs (1)	1	[*Ramos-Román et al.*, 2018]
Donana[b]	36.941667	-6.413333	terrestrial	arboreal pollen	1/4/0 (1)	68 % (2)	120 yrs (2)	2	[*Jiménez-Moreno et al.*, 2015]
Sierra de Gádor[a,b]	36.900000	-2.916667	lake	arboreal pollen	0/1/2 (2)	98 % (1)	65 yrs (1)	2	[*Carrión et al.*, 2003]
Roquetas de Mar	36.794444	-2.588889	terrestrial	arboreal pollen	0/1/1 (2)	97 % (1)	162 yrs (2)	2	[*Pantaléon-Cano et al.*, 2003]
San Rafael	36.773611	-2.601389	terrestrial	arboreal pollen	0/1/0 (3)	86 % (1)	90 yrs (1)	3	[*Pantaléon-Cano et al.*, 2003]
Cabo de Gata[b]	36.771389	-2.228611	terrestrial	arboreal pollen	0/1/1 (2)	97 % (1)	103 yrs (2)	2	[*Burjachs and Expósito*, 2015]
GeoB5901-2[a]	36.380000	-7.071333	marine	*n*-alkane concentration	3/12/1 (1)	78 % (2)	69 yrs (1)	2	[*Schirrmacher et al.*, 2019]
ODP-161-976A[a]	36.205333	-4.312667	marine	*n*-alkane concentration	0/11/0 (1)	91 % (1)	29 yrs (1)	1	[*Schirrmacher et al.*, 2019]
ODP-161-976A[a,b]	36.205333	-4.312667	marine	pollen MAT	0/11/0 (1)	86 % (1)	259 yrs (3)	3	[*Combourieu Nebout et al.*, 2009]
MD95-2043	36.143333	-2.621167	marine	pollen MAT	0/2/1 (2)	94 % (1)	117 yrs (2)	2	[*Bini et al.*, 2019]; [*Fletcher et al.*, 2010]; [*Peyron et al.*, 2017]
MD95-2043	36.143333	-2.621167	marine	arboreal pollen	0/2/1 (2)	94 % (1)	117 yrs (2)	2	[*Fletcher and Sánchez Goñi*, 2008]

Name	Latitude	Longitude	Archive	Proxy	No. of datings preWin/Win/postWin (parameter-based QF)	Temporal coverage in Win (parameter-based QF)	Temporal resolution (parameter-based QF)	Final QF	References
Chaara Cave 1	33.950000	-4.246000	speleothem	stalagmite $\delta^{18}O$	3/6/4 (1)	100 % (1)	9 yrs (1)	1	[*Ait Brahim et al.*, 2019]
Chaara Cave 2	33.950000	-4.246000	speleothem	stalagmite $\delta^{18}O$	3/10/3 (1)	98 % (1)	12 yrs (1)	1	[*Ait Brahim et al.*, 2019]
Grotte de Piste	33.840000	-4.090000	speleothem	stalagmite $\delta^{18}O$	1/6/4 (1)	99 % (1)	14 yrs (1)	1	[*Wassenburg et al.*, 2016]
Lake Sidi Ali	33.050000	-5.000000	lake	ostracod $\delta^{18}O$	2/5/1 (1)	98 % (1)	89 yrs (1)	1	[*Zielhofer et al.*, 2019]
Tigalmamine[b]	32.900000	-5.350000	lake	shallow water diatom-species	1/1/0 (2)	96 % (1)	107 yrs (2)	2	[*Lamb and van der Kaars*, 1995]
Temperature									
annual									
Grotte de Clamouse	43.710000	3.550000	speleothem	stalagmite $\delta^{18}O$	2/2/0 (2)	99 % (1)	47 yrs (1)	2	[*McDermott et al.*, 1999]
PP10-07	43.677000	-2.228000	marine	MAT on planktonic foraminifera	1/1/1 (2)	98 % (1)	59 yrs (1)	2	[*Mary et al.*, 2017]
Monte Areo[b]	43.528889	-5.768889	terrestrial	pollen PCA	1/1/2 (2)	96 % (1)	480 yrs (3)	3	[*López-Merino et al.*, 2010]
Kaite Cave	43.033333	-3.650000	speleothem	stalagmite $\delta^{13}C$	6/3/0 (1)	30 % (3)	10 yrs (1)	3	[*Martín-Chivelet et al.*, 2011]
KGSC-31	43.006389	3.298889	marine	alkenones	1/4/2 (1)	99 % (1)	16 yrs (1)	1	[*Jalali et al.*, 2016]
Cova da Arcoia	42.610000	-7.090000	speleothem	stalagmite $\delta^{18}O$	1/7/1 (1)	89 % (1)	67 yrs (1)	1	[*Railsback et al.*, 2011]
Molinos Cave	40.792500	-4.492000	speleothem	stalagmite $\delta^{18}O$	1/3/1 (1)	90 % (1)	31 yrs (1)	1	[*Muñoz et al.*, 2015]
MD03-2699	39.036700	-10.660500	marine	alkenones	0/2/0 (2)	92 % (1)	154 yrs (2)	2	[*Rodrigues et al.*, 2010]
D13882	38.634500	-9.454200	marine	alkenones	1/1/1 (2)	97 % (1)	112 yrs (2)	2	[*Rodrigues et al.*, 2009]
D13902	38.554000	-9.335500	marine	alkenones	0/0/1 (3)	36 % (3)	271 yrs (3)	3	[*Rodrigues et al.*, 2009]
MD01-2444	37.561333	-10.142167	marine	alkenones	0/0/0 (3)	96 % (1)	169 yrs (2)	3	[*Martrat et al.*, 2007]
GeoB5901-2[a]	36.380000	-7.071333	marine	alkenones	3/12/1 (1)	79 % (2)	68 yrs (1)	2	[*Schirrmacher et al.*, 2019]
M39008-3	36.380000	-7.071667	marine	alkenones	1/2/1 (2)	76 % (2)	456 yrs (3)	3	[*Cacho et al.*, 2001]
HER_GC_T1	36.370146	-4.299015	marine	alkenones	0/1/1 (2)	95 % (1)	135 yrs (2)	2	[*Ausín et al.*, 2015]
ODP-161-976A[a]	36.205333	-4.312667	marine	alkenones	0/11/0 (1)	91 % (1)	29 yrs (1)	1	[*Schirrmacher et al.*, 2019]
ODP-161-976A[a,b]	36.205333	-4.312667	marine	pollen MAT	0/11/0 (1)	86 % (1)	259 yrs (3)	3	[*Combourieu Nebout et al.*, 2009]
TTR-17_434G	36.205220	-4.312250	marine	alkenones	0/2/0 (2)	92 % (1)	129 yrs (2)	2	[*Rodrigo-Gámiz et al.*, 2014]
TTR-12_293G	36.173567	-2.754667	marine	alkenones	0/1/0 (3)	83 % (1)	312 yrs (3)	3	[*Rodrigo-Gámiz et al.*, 2014]
TTR-12_293G	36.173567	-2.754667	marine	TEX86	0/1/0 (3)	83 % (1)	312 yrs (3)	3	[*Kim et al.*, 2015]
MD95-2043	36.143333	-2.621167	marine	alkenones	0/2/1 (2)	98 % (1)	117 yrs (2)	2	[*Cacho et al.*, 1999]
ODP-161-977	36.031700	-1.955283	marine	alkenones	0/1/0 (3)	74 % (2)	553 yrs (3)	3	[*Martrat et al.*, 2007]
summer									
PP10-07	43.677000	-2.228000	marine	MAT on planktonic foraminifera	1/1/1 (2)	98 % (1)	59 yrs (1)	2	[*Mary et al.*, 2017]
SU92-03	43.195800	-10.113000	marine	MAT on planktonic foraminifera	1/0/0 (3)	83 % (1)	827 yrs (3)	3	[*Salgueiro et al.*, 2014]
Basa de la Mora[b]	42.533333	0.316667	lake	chironomid assemblage	2/3/1 (1)	90 % (1)	300 yrs (3)	3	[*Tarrats et al.*, 2018]
OMEXII-9K	42.343000	-10.051000	marine	MAT on planktonic foraminifera	0/1/0 (3)	83 % (1)	415 yrs (3)	3	[*Salgueiro et al.*, 2014]
MD03-2697	42.150000	-9.700000	marine	MAT on planktonic foraminifera	1/1/0 (2)	71 % (2)	713 yrs (3)	3	[*Salgueiro et al.*, 2014]
PO200-10-28-1	41.488000	-9.721000	marine	MAT on planktonic foraminifera	1/0/0 (3)	80 % (2)	803 yrs (3)	3	[*Salgueiro et al.*, 2014]
MD95-2040	40.581833	-9.861167	marine	MAT on planktonic foraminifera	0/0/0 (3)	97 % (1)	242 yrs (3)	3	[*Salgueiro et al.*, 2014]
MD95-2041	37.833333	-9.510833	marine	MAT on planktonic foraminifera	0/0/0 (3)	77 % (2)	463 yrs (3)	3	[*Salgueiro et al.*, 2014]
MD95-2042	37.799833	-10.166500	marine	MAT on planktonic foraminifera	1/2/1 (2)	89 % (1)	332 yrs (3)	3	[*Salgueiro et al.*, 2014]
GeoB5901-2[a]	36.380000	-7.071333	marine	MAT on planktonic foraminifera	3/12/1 (1)	100 % (1)	64 yrs (1)	1	[*Schirrmacher et al.*, 2019]
ODP-161-976A[a]	36.205333	-4.312667	marine	MAT on planktonic foraminifera	0/11/0 (1)	84 % (1)	76 yrs (1)	1	[*Schirrmacher et al.*, 2019]
ODP-161-976A[a,b]	36.205333	-4.312667	marine	pollen MAT	0/11/0 (1)	86 % (1)	259 yrs (3)	3	[*Combourieu Nebout et al.*, 2009]
TTR-17_434G	36.205220	-4.312250	marine	LDI	0/2/0 (2)	95 % (1)	129 yrs (2)	2	[*Rodrigo-Gámiz et al.*, 2014]

Name	Latitude	Longitude	Archive	Proxy	No. of datings preWin/Win/postWin (parameter-based QF)	Temporal coverage in Win (parameter-based QF)	Temporal resolution (parameter-based QF)	Final QF	References
TTR-12_293G	36.173567	-2.754667	marine	LDI	0/1/0 (3)	83 % (1)	312 yrs (3)	3	[*Rodrigo-Gámiz et al.*, 2014]
MD99-2339	35.885500	-7.527833	marine	MAT on planktonic foraminifera	0/1/0 (3)	94 % (1)	401 yrs (3)	3	[*Salgueiro et al.*, 2014]
Lake Sidi Ali[b]	33.050000	-5.000000	lake	*Cedrus*	2/5/1 (1)	94 % (1)	63 yrs (1)	1	[*Campbell et al.*, 2017]
Tigalmamine	32.900000	-5.350000	lake	*Cedrus*	1/1/0 (2)	96 % (1)	107 yrs (2)	2	[*Lamb and van der Kaars*, 1995]
winter									
PP10-07	43.677000	-2.228000	marine	MAT on planktonic foraminifera	1/1/1 (2)	98 % (1)	59 yrs (1)	2	[*Mary et al.*, 2017]
Lago de Ajo[a,b]	43.050000	-6.150000	lake	pollen MAT	0/1/0 (3)	94 % (1)	201 yrs (3)	3	[*Allen et al.*, 1996]
Laguna de la Roya[a,b]	42.216667	-6.766667	lake	pollen MAT	0/1/1 (2)	90 % (1)	209 yrs (3)	3	[*Allen et al.*, 1996]
Sanabria[a,b]	42.100000	-6.733333	lake	pollen MAT	0/0/0 (3)	94 % (1)	177 yrs (2)	3	[*Allen et al.*, 1996]
MD95-2042[b]	37.799833	-10.166500	marine	MAT on planktonic foraminifera	1/2/1 (2)	90 % (1)	180 yrs (2)	2	[*Chabaud et al.*, 2014]
GeoB5901-2[a]	36.380000	-7.071333	marine	MAT on planktonic foraminifera	3/12/1 (1)	100 % (1)	64 yrs (1)	1	[*Schirrmacher et al.*, 2019]
ODP-161-976A[a]	36.205333	-4.312667	marine	MAT on planktonic foraminifera	0/11/0 (1)	84 % (1)	76 yrs (1)	1	[*Schirrmacher et al.*, 2019]
ODP-161-976A[a,b]	36.205333	-4.312667	marine	pollen MAT	0/11/0 (1)	86 % (1)	259 yrs (3)	3	[*Combourieu Nebout et al.*, 2009]

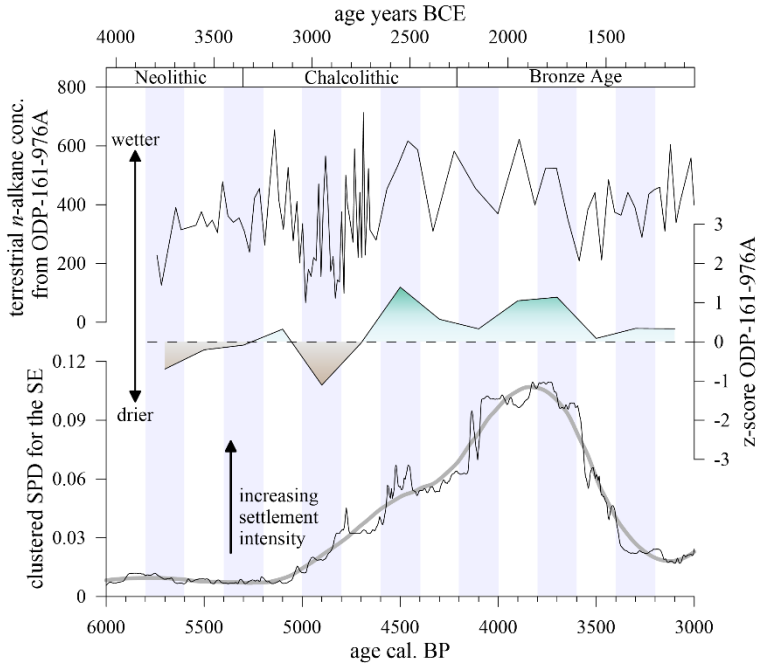

Figure 6.2 Illustration of the methodological approach. *At the top the concentration of terrestrial n-alkanes (n-C_{27-33}) of marine sediment core ODP-161-976A from the Alboran Sea [Schirrmacher et al., 2019] with the updated age model (see Fig 6.7) is shown. In the centre the according medians of the z-transformed data are shown for the 200-year time slices (blue vertical bars). The green and brown shadings indicate the intensity of wetter or drier conditions, respectively. At the bottom raw data of clustered summed probability densities (SPDs) for the southeast (SE) of the Iberian Peninsula are displayed in black together with a LOESS smooth in grey (see Fig 6.1 for location).*

Considering the wide range of important parameters within the compiled paleo-climatic data, such as temporal resolution, coverage of the studied time period, and number of datings, we assigned a quality flag (QF) to each record based on the above mentioned parameters. The QF ranges from 1 to 3 and was calculated separately for every parameter (number of datings, temporal resolution, and temporal coverage). The thresholds for every parameter are shown in Table 6.2. The final QF is then based on the lowest QF of all parameters. For example, a well-dated record with decadal resolution (QFs of 1 for number of datings and temporal resolution), which covers less than half of the studied period (QF of 3 for temporal coverage), received a final QF of 3. Given the relatively high spatial coverage of annual and winter precipitation data, we interpolated the data in order to highlight areas of coherent regional developments. This was done by inverse distance weighting interpolation of the individual z-scores using packages gstat [*Pebesma*, 2004] and raster [*Hijmans*, 2019] within R software [*R Core Team*, 2019]. Thereby, we weighted the data according to its final QF to account for the different quality of each record during interpolation. Records with a QF of 1 were taken into account with a factor of 3, while records with a QF of 2 received a factor of 2. During interpolation we used a power value of 1.5 while the search radius was not limited. Unfortunately, the spatial coverage of all other

variables was insufficient for reasonable interpolations. Animations showing the development of all six paleo-climatic reconstructions for the whole time period can be found in the supplement of this article (Videos S1 – S6).

Table 6.2 Quality flag parameters. *The assignment of the final quality flag (QF) is described in the text. preWin = 2000 – 3000 cal. BP (50 – 1050 BCE); Win = 3000 – 6000 cal. BP (1050 – 4050 BCE); postWin = 6000 – 7000 cal. BP (4050 – 5050 BCE)*

QF	Average temporal resolution	Number of datings in 2000 – 7000 cal. BP (50 – 5050 BCE)	Temporal coverage (3000 – 6000 cal. BP/ 1050 – 4050 BCE)
1	> 100 years	≥ 5 with at least 3 in Win	> 80 %
2	≥ 200 years	≥ 2 with either at least 1 in Win or 1/1 in preWin and postWin	≥ 50 %
3	< 200 years	< 2	< 50 %

6.3.2 Archaeological approach

In this paper, we use summed probability densities (SPDs) of AMS ^{14}C dates from archaeological contexts to infer past human activity on the Iberian Peninsula (Fig 6.1). SPDs are used as a preferred proxy for the past human activity as it provides a high temporal and spatial resolution, and allows for supra-regional comparison. Due to potential (and inevitable) biases related to the shape of the ^{14}C calibration curve and the focus of archaeological research, the use of this proxy is critically debated [*Contreras and Meadows*, 2014; *Weninger et al.*, 2015; *Williams*, 2012]. Nonetheless, its successful and intensive use, which is paralleled by a rapidly growing AMS ^{14}C database, is well documented in recent literature and enables increasingly robust reconstructions and safer interpretations [*Blanco-González et al.*, 2018; *Drake et al.*, 2017; *Hinz et al.*, 2012a; *Lillios et al.*, 2016; *Warden et al.*, 2017]. In order to avoid biases from changes in the cultural behaviour of the societies samples from funeral and ritual contexts were left out, and only samples from settlement context were retained in the database [*Hinz et al.*, 2012a]. Iberian AMS ^{14}C data have been compiled from existing datasets [*Hinz et al.*, 2012b; *IDEArq; Kneisel et al.*, 2013] and complemented with other published data [*Lillios et al.*, 2016]. The data have been carefully checked for duplicate dates before analysis to avoid over-representation of well-researched sites. For further analysis, AMS ^{14}C dates between 7000 and 2000 uncalibrated (uncal.) BP (5050 – 50 uncal. BCE) have been taken into account in order to ensure that the calibrated dates fall within the analysed period between 6000 and 3000 cal. BP (4050 – 1050 BCE). In this (uncalibrated) timeframe, our database contains 4710 dates from 880 settlements covering the entire Iberian Peninsula. Calibration of AMS ^{14}C data and SPD

computation was done using INTCAL13 calibration curve [*Reimer et al.*, 2013] and the rcarbon package [*Bevan and Crema*, 2018; *Crema et al.*, 2017], and using the R programming language [*R Core Team*, 2019]. Prior to sum-calibration the calibrated data were binned by site and the resulting site-SPDs have then been normalized to unity, in order to achieve comparability between all sites, and to minimize bias potentially resulting from different research intensity [*Hinz et al.*, 2012a]. Nonetheless, biases introduced into the reconstructed spatial patterns by different archaeological research intensities cannot be fully eliminated and, thus, unavoidably affect the outcome.

After computing the site-SPDs, medians of each site were calculated for 200-year time slices between 6000 and 3000 cal. BP (4050 – 1050 BCE) to match the resolution of the climate compilations (Fig 6.2). The advantage of medians is that their calculation is not as dependent on outlier (or minima and maxima) as the calculation of mean values. Hence, this also minimizes an effect pointed out by *Weninger et al.* [2015] where the normalization of sum-calibrated dates may produce false peaks related to the calibration curve and, thus, increases the reliability of our results. For each time slice a heat map based on the distances between settlements and the respective SPD of each site was calculated. An animation showing the development of the settlement density within the whole time period can be found in the supplement of this article (Video S7).

6.4 Results and discussion

6.4.1 Settlement intensity variability during the Chalcolithic and Bronze Age on the Iberian Peninsula

The settlement pattern during the Chalcolithic and the Bronze Age as reconstructed from spatial SPD analyses reveal new insights into the spatio-temporal developments of specific regions of the Iberian Peninsula. Overall, our results imply high human activities in the southern part of the peninsula during the analysed period, which agree well with the development of major archaeological cultures of the time. Thus, this further enables the use of SPDs as indicator for demographic and settlement developments on the southern Iberian Peninsula at that time.

A high settlement density developed after 5600 cal. BP (3650 BCE) in the Alentejo and Algarve near the Atlantic coast (Fig 6.3) and lasted until 4200 cal. BP (2250 BCE) (Fig 6.4; Video S7). Nucleation of settlements during this phase is well supported by aoristic analysis of settlement patterns in the Alentejo and Algarve regions [*Hinz et al.*, 2019]. In this late Chalcolithic phase,

the walled site of Zambujal has been constructed in the area [*Kunst and Lutz*, 2008] contemporaneous with the overall increasing settlement density in the SW. After 4800 cal. BP (2850 BCE) settlement intensity gradually shifted towards the SE, where the Los Millares culture had already emerge since 5150 cal. BP (3200 BCE) [*Molina González et al.*, 2004]. According to our SPD data, both societies in the SW and the SE were co-existing until ca. 4200 cal. BP (2250 BCE), when SPDs sharply dropped in the SW and settlements in the Alentejo and Algarve virtually disappeared (Fig 6.4). Yet, this final "collapse" was preceded by a gradual decline in SPD values starting from 4400 cal. BP (2450 BCE) onwards (Video S7) in line with archaeological studies from Zambujal and Perdigões [*Kunst and Lutz*, 2008; *Valera*, 2015]. Based on regional-clustered SPDs from settlement and burial contexts, *Lillios et al.* [2016] have argued previously that the decrease in demographic signals in the SW started around 4500 cal. BP (2550 BCE) and considered the possibility of demic migration towards the east. But, also in the SE various settlement sites have been abandoned, among them well investigated mega-sites like Los Millares, Valencina de la Concepción, or Marroquíes Bajos coinciding with the disappearance of the Los Millares culture [*García Sanjuán et al.*, 2018; *Lull et al.*, 2015]. Jointly, the large-scale abandonment of settlement sites and the vanishing of traditions in material culture and burial rites implies that the southern part of the Iberian Peninsula featured a regional-wide social collapse around 4200 cal. BP (2250 BCE).

Nonetheless, the settlement intensity in the SE intensified and spread northward along the Mediterranean coast and into the southern Meseta area after 4200 cal. BP (2250 BCE) (Fig 6.4). This development is associated with the boom of the El Argar culture [*Lull et al.*, 2011]. Human activity in the southern Meseta area is, further, associated with the construction of the *motillas* in the floodplains of the Guadiana and Guadalquivir river basins [*Aranda et al.*, 2008; *Benítez de Lugo Enrich and Mejías*, 2017]. In line with *Lull et al.* [2011], our data suggest that the Argaric territory reached its maximum between 3800 and 3600 cal. BP (1850 – 1650 BCE) and its bust started after ca. 3600 cal. BP (1650 BCE) with the majority of settlement sites in the area being abandoned by 3400 cal. BP (1450 BCE) (Fig 6.4 and Video S7).

According to our SPD analyses two periods of interesting settlement patterns stand out and are discussed in the following chapters. The first period ranges from 5200 to 4600 cal. BP (3250 – 2650 BCE) and comprised the development of the co-existing societies in the SW and the SE. The second period from 4400 to 3400 cal. BP (2450 – 1450 BCE) featured the collapse in the SW and the boom and bust of the El Argar culture in the SE. Comparing these settlement patterns with the compiled paleo-climatic data, we explore whether the subsequent development of the societies in the SW and the SE during the Chalcolithic, which potentially featured a

population migration [*Lillios et al.*, 2016], was favoured by more pleasant climatic conditions in the SE. Also, after resolving the spatio-temporal manifestation of the 4.2 ka BP climate event across the Iberian Peninsula we explore its potential impact on the social collapse at that time in the SW and the following demographic boom associated with the El Argar culture in the SE.

6.4.2 Development of two settlement hotspots between 5200 – 4600 cal. BP (3250 – 2650 BCE)

The development of the society in the SW after 5600 cal. BP (3650 BCE) and the subsequent rise of the Los Millares culture after 4800 cal. BP (2850 BCE) were accompanied by profound climatic changes between 5000 and 4800 cal. BP (3050 – 2850 BCE) (Fig 6.3). Although likely not dramatic, the majority of annual temperature records in this time slice suggests a peninsular-wide cooling. The few seasonal temperature records available suggest that people had to deal rather with a winter cooling (Videos S2 and S3). Regarding the hydro-climatic conditions, it has been relatively moist in the annual mean between 5200 and 4600 cal. BP (3250 – 2650 BCE) with the exception of a regional drying across the northern Iberian Peninsula at the end of this phase (Fig 6.3). The overall relatively moist annual and winter conditions during that period reflect the long-term Holocene drying trend towards the present, rather than a particular wet event (Videos S4 and S5). Nonetheless, while annual conditions were relatively moist from 5000 to 4800 cal. BP (3050 – 2850 BCE), winter precipitation likely decreased during this phase as for example indicated by marine core GeoB5901-2 from the Gulf of Cádiz [*Schirrmacher et al.*, 2019]. This decrease in winter precipitation was more pronounced along the Atlantic coast including the SW area (Fig 6.3).

Accordingly, it is interesting to note that the rise of the Los Millares culture in the SE was preceded by a cool and dry winter event, which was particularly manifested in the SW. At this time, economies across the southern Iberian Peninsula were highly dependent on agriculture and, consequently, arable land [*García Sanjuán et al.*, 2016; *López-Sáez et al.*, 2018; *Schneider et al.*, 2016]. Moreover, irrigation was likely not practised before 4300 cal. BP (2350 BCE) in the area, highlighting the importance of natural water resources [*Benítez de Lugo Enrich and Mejías*, 2017; *Mora-González et al.*, 2016; *Mora-González et al.*, 2018].

Thus, following the idea that this cool and dry winter event between 5000 and 4800 cal. BP (3050 – 2850 BCE) hampered the agricultural production in the SW, it appears plausible that the rise of the Los Millares culture in the SE after 4800 cal. BP (2850 BCE) was favoured by climatic-induced migration from the SW. *Lillios et al.* [2016] already suggested a potential migration after ca. 4500 cal. BP (2550 BCE) from the SW towards the SE. Strontium isotopic

analysis ($^{87/86}$Sr) of human teeth indeed suggest that a variable amount of non-local population at the Andalusian mega-sites Marroquíes Bajos and Valencina de la Concepción entered existing social networks [*Díaz-Zorita Bonilla*, 2013; *Díaz-Zorita Bonilla et al.*, 2018]. The provenance of such groups remain an open question, though. While it is unlikely that people moved eastwards for metals and related economic reasons [*Bartelheim and Pearce*, 2015], it might be possible that the establishment of trade networks as evidenced by the arrival of Asian ivory favoured migration towards the SE [*Schuhmacher*, 2017].

Following these lines of evidence, climatic-induced migration related to a cool and dry winter event, particularly evident in the SW, likely contributed to the observed gradual displacement of settlement intensities from the SW towards the SE after 4800 cal. BP (2850 BCE).

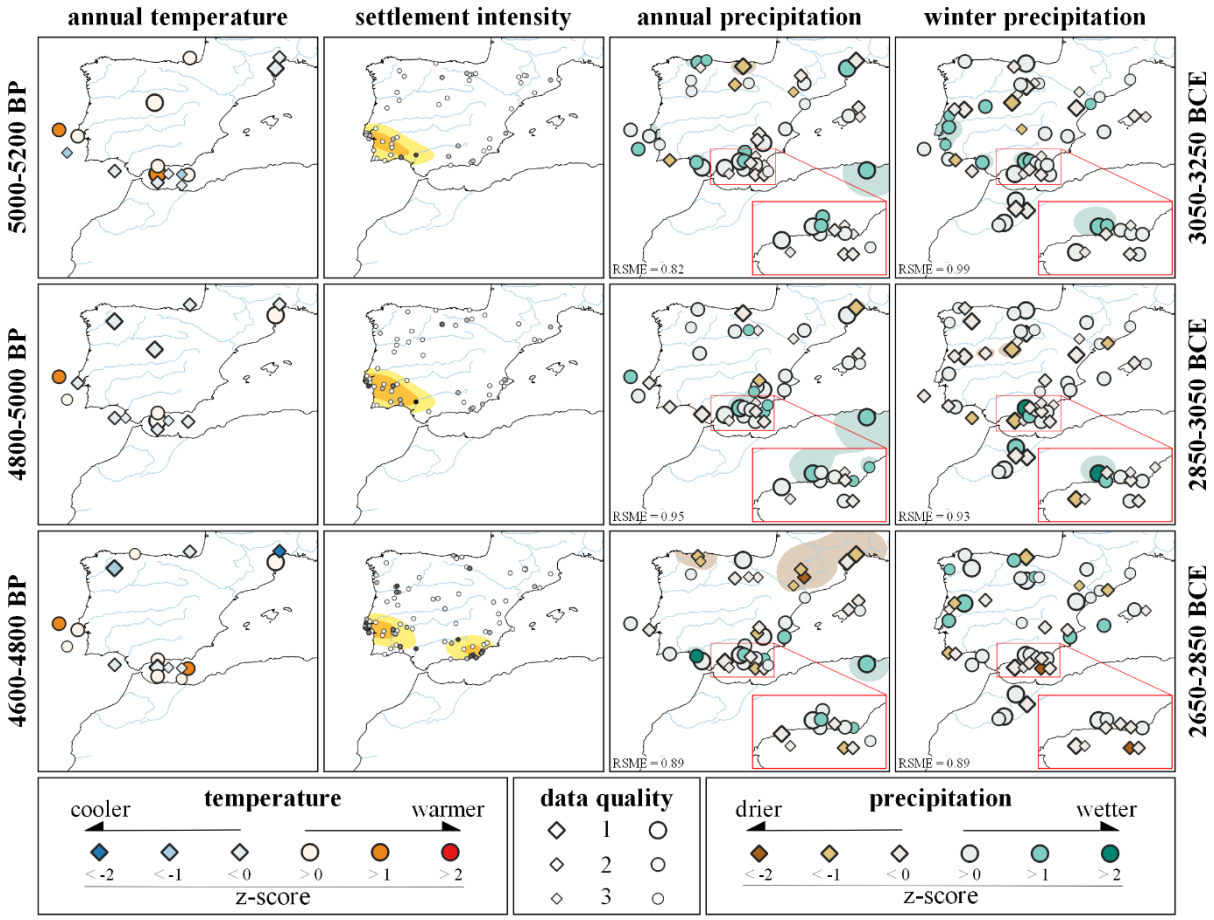

Figure 6.3 Climatic and archaeological proxy data for the time slices between 5200 to 4600 cal. BP (3250 – 2650 BCE). *From left to right: annual temperatures, settlement intensities, annual precipitation and winter precipitation reconstructions. The heatmap in the settlement intensity column (from yellow to red colours) were calculated using the settlement density as well as the SPD data of each settlement. The brown and green shadings in the annual and winter precipitation data highlight areas of regional change towards drier or wetter conditions, respectively, based on inverse distance weighted interpolation of the z-score data.*

6.4.3 Boom and bust on the southern Iberian Peninsula between 4400 – 3400 cal. BP (2450 – 1450 BCE)

The period between 4400 and 3400 cal. BP (2450 – 1450 BCE) is characterized by two distinct climatic events, which superimpose the general drying and cooling trends. Particularly, we observe increasingly drier conditions across the southern Iberian Peninsula from 3800 to 3000 cal. BP (1850 – 1050 BCE). These are reflected in the annual reconstructions (Video S4), but clearly forced by decreasing winter precipitation (Video S5). This decrease in winter precipitation is likely related to the drying trend during the Holocene and, thus, is very different from the two earlier events.

During the first event, which occurred between 4400 and 4000 cal. BP (2450 – 2050 BCE), the whole Iberian Peninsula faced cooler annual conditions (Fig 6.4). Contrastingly, the alkenone record of GeoB5901-2 from the Gulf of Cádiz suggests distinctly warmer annual sea surface temperatures by 2 °C. But, this may be rather a result of a shift in the growing season of the alkenone producers in response to altered seasonality and nutrient conditions [*Schirrmacher et al.*, 2019]. Seasonal temperature data based on pollen and planktonic foraminiferal assemblages implies that the annual cooling was likely a result of cooler winter conditions, while summer temperatures were relatively constant (Videos S2 and S3). Altogether, this suggests a decrease in seasonality during this event. Paralleling the winter cooling between 4400 and 4000 cal. BP (2450 – 2050 BCE), hydroclimatic conditions across the Iberian Peninsula were rather stable indicating no event-like features (Fig 6.4). Decreasing annual or winter precipitation as suggested by two offshore marine records based on *n*-alkane concentrations or localized pollen data between 4200 and 4000 cal. BP (2250 – 2050 BCE) rather mirror altered sediment transport pathways into the marine realm or anthropogenic forest clearance, respectively.

Thus, the period from 4400 to 4000 cal. BP (2450 – 2050 BCE) is characterized by a winter cooling event, which is contemporaneous with a major ice-berg discharge in the North Atlantic – the so-called Bond Event 3 [*Bond et al.*, 2001]. This, further, corroborates the hypothesis by *Schirrmacher et al.* [2019] that cooling during Bond Event 3 close to the Iberian Atlantic coast was a winter phenomenon. Our data also indicates that Bond Event 3 was not associated with a regional decrease in precipitation on the Iberian Peninsula.

Having discussed the first climatic event of the period between 4400 and 3400 cal. BP (2450 – 1450 BCE), we can now turn to the second event, which abruptly occurred between 4000 and 3800 cal. BP (2050 – 1850 BCE). During this period, the hydroclimatic data points to a sharp

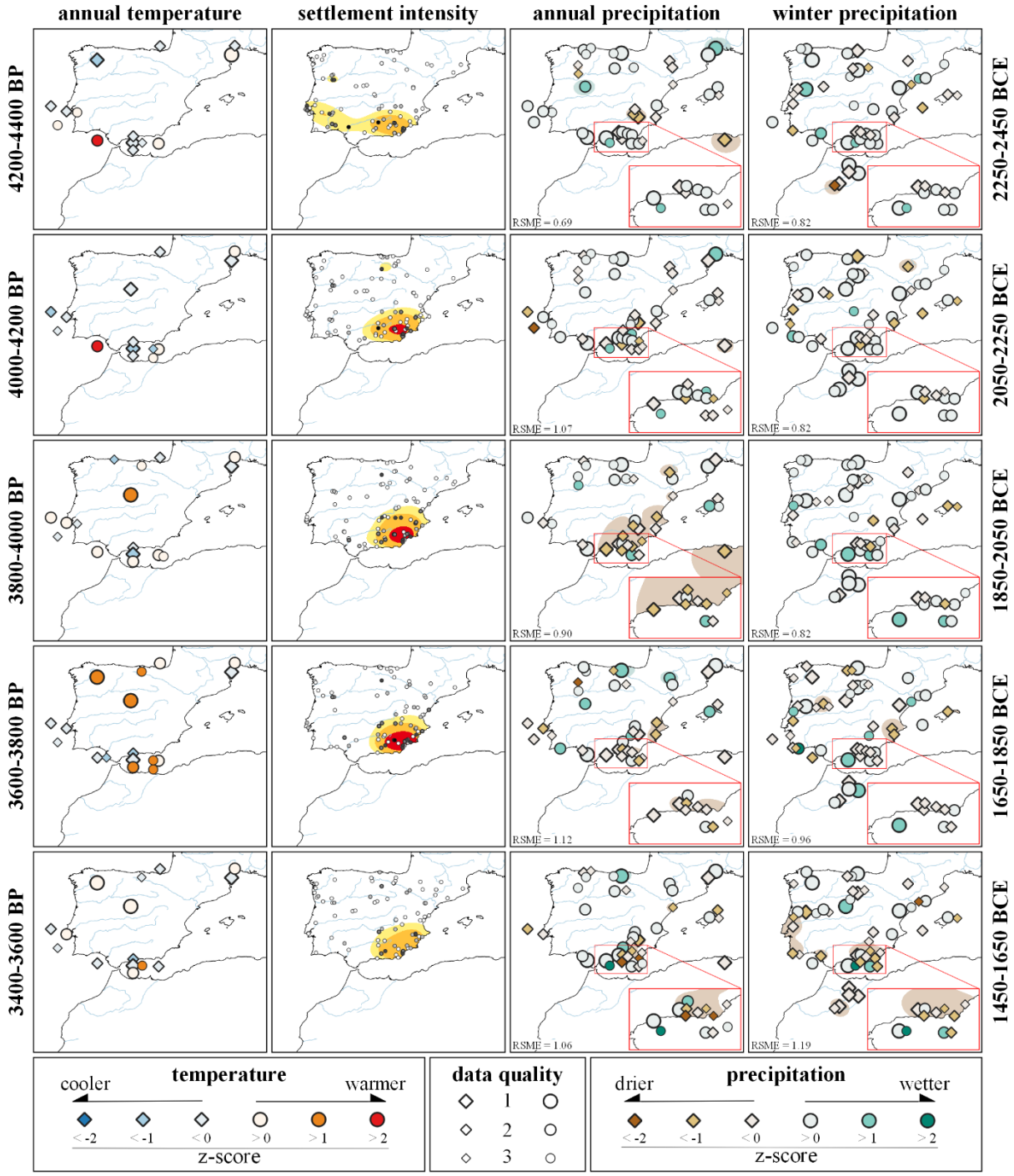

Figure 6.4 Climatic and archaeological proxy data for the time slices between 4400 to 3400 cal. BP (2450 – 1450 BCE). *From left to right: annual temperatures, settlement intensities, annual precipitation and winter precipitation reconstructions. The heatmap in the settlement intensity column (from yellow to red colours) were calculated using the settlement density as well as the SPD data of each settlement. The brown and green shadings in the annual and winter precipitation data highlight areas of profound regional change towards drier or wetter conditions, respectively, based in inverse distance weighted interpolation of the z-score data.*

decrease in annual precipitation in the SE, while winter precipitation in the area remains relatively constant or even increased (Fig 6.4). This leads to the conclusion that this event was probably driven by a sharp decrease in summer precipitation or an elongation of the summer

dry period. Despite just two compiled archives are indicative of summer precipitation variability, a regional decrease in summer precipitation in the SE is suggested by pollen-based MAT reconstruction in marine sediment core MD95-2043 from the Alboran Sea (Video S6) [*Bini et al.*, 2019]. Thus, this event noticeably differs from the drying trend, which is evident afterwards and characterized by a decrease in winter precipitation (Fig 6.4; Video S5). At the same time, the western and northern Atlantic coasts faced stable annual precipitation levels, pointing to a strong Atlantic – Mediterranean gradient and a potential Mediterranean forcing of the summer dry event between 4000 and 3800 cal. BP (2050 – 1850 BCE).

In light of the 4.2 ka BP drought event, which is described for the period between 4300 to 3800 cal. BP (2350 – 1850 BCE) in the Central and Eastern Mediterranean [*Bini et al.*, 2019; *Kaniewski et al.*, 2018], we suggest that this event had a shorter duration (4000 – 3800 cal. BP; 2050 – 1850 BCE) and just affected the Mediterranean coast – the SE in particular – of Iberian Peninsula. Moreover, the 4.2 ka BP drought event in the area was likely restricted to the summer season.

The 4.2 ka BP drought event is known for contributing to social collapse and large-scale population displacements in the Near East [*Weiss*, 2017; *Welc and Marks*, 2014]. Therefore, it is interesting to note that social developments, among them the large-scale abandonment of settlement sites on the southern Iberian Peninsula around 4200 cal. BP (2250 BCE), are indicative of a collapse as well [*Lull et al.*, 2015; *Valera*, 2015]. But, from our paleo-climatic data it appears that the 4.2 ka BP event was not directly affecting societies in the SW and the SE at that time. On the southern Iberian Peninsula, the 4.2 ka BP event occurred later (4000 – 3800 cal. BP; 2050 – 1850 BCE) and had likely not impacted the SW at all (Fig 6.4). This is corroborated by *Valera et al.* [2015], who proposed that the abandonment of ditched enclosures in the SW was not driven by climatic factors. The SE, on the other hand, even featured the boom of the El Argar culture at that time [*Lull et al.*, 2011] despite the dry summer conditions associated with the regional manifestation of the 4.2 ka BP event and the abandonment of Chalcolithic sites. Multiple lines of evidence suggest that the Argaric people were able to deal with dry summer conditions during the 4.2 ka BP event as indicated by agricultural practises, which are based on dry farming, monoculture [*Castro et al.*, 1999; *Delgado-Raack and Risch*, 2015], and/or irrigation techniques [*Benítez de Lugo Enrich and Mejías*, 2017; *Mora-González et al.*, 2016]. In addition, our paleo-climatic data suggests that the stable or increased winter precipitation during this phase supported people in maintaining the intensive agricultural production (Fig 6.4).

Interestingly, during the collapse of the Argaric society between 3600 and 3500 cal. BP (1650 – 1550 BCE) [*Lull et al.*, 2013b] an over-regional decrease in winter precipitation across the southern Iberian Peninsula becomes evident from various terrestrial and marine pollen records as well as speleothem data (Fig 6.4). So far, it has been suggested that the collapse of the Argaric society was caused by the extensive over-exploitation of the environment including intense woodland clearance [*Castro et al.*, 1999; *Lull et al.*, 2013a, 2013b]. This may account for the decrease in winter precipitations mirrored by some localized pollen data from the SE between 3600 and 3400 cal. BP (1650 – 1450 BCE). But, a decrease in winter precipitation is also suggested from speleothem data and marine pollen records. Furthermore, pollen data from the SW, where human activity was limited according to our SPD analysis, also imply dry winter conditions. Altogether, a regional-wide decrease in winter precipitation across the southern Iberian Peninsula is suggested already after 3800 cal. BP (1850 BCE). Accordingly, we conclude that during the boom of the Argaric culture its society was increasingly dependent on winter precipitation in order to maintain the intense agriculture. Thus, a significant decrease in winter precipitation after 3800 cal. BP (1850 BCE) likely contributed to the collapse of the El Argar culture by hampering the intense agricultural practises.

6.5 Conclusion

In order to fill important knowledge gaps concerning a potential link between climate change and social developments during the Chalcolithic and the Bronze Age on the Iberian Peninsula, we compiled paleo-climatic and archaeological data from the time period between 6000 to 3000 cal. BP (4050 – 1050 BCE) from the Iberian Peninsula. The paleo-climate was analysed for seasonal (summer and winter) and annual variability in precipitation as well as temperature. Sum-calibrated probability densities (SPDs) of AMS ^{14}C data served as proxy for settlement intensity.

The results of the SPD analysis indicate an increase in settlement intensity in the southwest (SW) of the Iberian Peninsula after 5600 cal. BP (3650 BCE) and a subsequent rise in settlement density in the adjacent southeast (SE) after 4800 cal. BP (2850 BCE), which is associated with the Los Millares culture. While settlement intensity in the SW sharply declined around 4200 cal. BP (2250 BCE), increasing settlement activity related to the emerging El Argar culture is indicated for the SE until ca. 3600 cal. BP (1650 BCE).

The paleo-climatic analysis resolved the long-term Holocene aridification trend on the Iberian Peninsula. This trend is primarily associated with a gradual decrease in winter precipitation and culminates after ca. 3800 cal. BP (1850 BCE), when particularly the southern Iberian Peninsula faced dry winter conditions. The aridification trend is superimposed by the 4.2 ka BP climate event from 4000 to 3800 cal. BP (2050 – 1850 BCE). During the event the SE was affected by an abrupt decrease in summer precipitation or an elongation of the summer dry period, while winter precipitation remained rather constant. With respect to temperature, the Iberian Peninsula experienced winter cooling between 4400 and 4000 cal. BP (2450 – 2050 BCE) in phase with Bond Event 3.

Comparing settlement patterns and the distribution of precipitation, we found no direct link between the large-scale abandonment of settlement sites in the SW around 4200 cal. BP (2250 BCE) and the 4.2 ka BP climate event. But, we noticed that the Chalcolithic and Bronze Age societies of the southern Iberian Peninsula were highly dependent on winter precipitation to maintain their agricultural practises. For instance, the decline in settlement intensity in the SW around 4800 cal. BP (2850 BCE) was preceded by a reduce in winter precipitation in the area. Furthermore, a sharp decrease in winter precipitation also coincides with the bust of the El Argar culture in the SE after 3600 cal. BP (1650 BCE). Before, between 4000 and 3800 cal. BP (2050 – 1850 BCE), the Argaric society boomed during the enhanced summer drought associated with the regional manifestation of the 4.2 ka BP event. This further highlights the dependence on winter precipitation of the southern Iberian societies during the Chalcolithic and Bronze Age.

6.6 Outlook

Apart from the results and conclusions, this study has also highlighted the need of much more well-dated, high-resolution paleo-climate data. Especially, seasonal data have an insufficient spatial resolution, but also in the annual data some regions, for example the Alentejo, Extremadura, and Algarve are not well researched. In the marine realm, the northern Atlantic and western Mediterranean coasts are clearly underrepresented. From the archaeological perspective surely more fieldwork should be carried out in the northern part of the Iberian Peninsula, in order to better understand why these regions are characterized by relative stability during the Chalcolithic and the Bronze Age. Also, there is a need for detailed archaeo-botanical and dietary studies to significantly improve the knowledge of agricultural practises in the past.

This knowledge will be needed for better comparability of social and paleo-climatological variability on the Iberian Peninsula.

6.7 Acknowledgements

This research was performed in the framework of the CRC 1266 “Scales of transformation” (project number: 2901391021) funded by the DFG (German Research Foundation). The authors acknowledge the tremendous work of the databases (European Pollen Database, Pangaea, NOAA Paleo Data Search, SISAL, and IDEArq) from which the data for this study have been compiled. In this respect, we also want to thank Gianni Zanchetta and Monica Bini for providing data. We are also grateful for help with the archaeological analysis by Jan-Eric Schlicht and Ingo Feeser. Additionally, we thank Eileen Kücükkaraca for editing and improving the English language.

6.8 Supplement

The supplementary videos S1 to S7 showing animations of the time slices of each paleo-climatological and archaeological parameter of this study are available online at https://www.sciencedirect.com/science/article/abs/pii/S0277379119310182.

Table 6.3 Supplementary table S6.1. *New AMS ^{14}C dates from sediment cores ODP-161-976A and GeoB5901-2.*

Lab No.	depth (cm)	material	AMS ^{14}C age (yr BP)	error (yr)
ODP-161-976A				
KIA-54017	100.0 – 100.5	*G. ruber w+p*	3930	±40
KIA-54210	108.5 – 109.0	*G. ruber w+p*	3590	±35
KIA-54211	110.0 – 110.5	*G. ruber w+p*	3680	±30
KIA-54018	116.5 – 117.0	*G. ruber w+p*	4565	±35
KIA-54019	148.0 – 148.5	*G. ruber w+p*	5350	±55
GeoB5901-2				
KIA-54011	9.0 – 9.5	*G. ruber w+p*	2833	±26
KIA-54012	20.5 – 21.0	*G. ruber w+p*	4138	±29
KIA-54013	21.0 – 21.5	*G. ruber w+p*	4225	±28
KIA-54014	21.5 – 22.0	*G. ruber w+p*	4384	±28
KIA-54015	31.0 – 31.5	*G. ruber w+p*	5139	±29
KIA-54016	49.0 – 49.5	*G. ruber w+p*	5680	±35

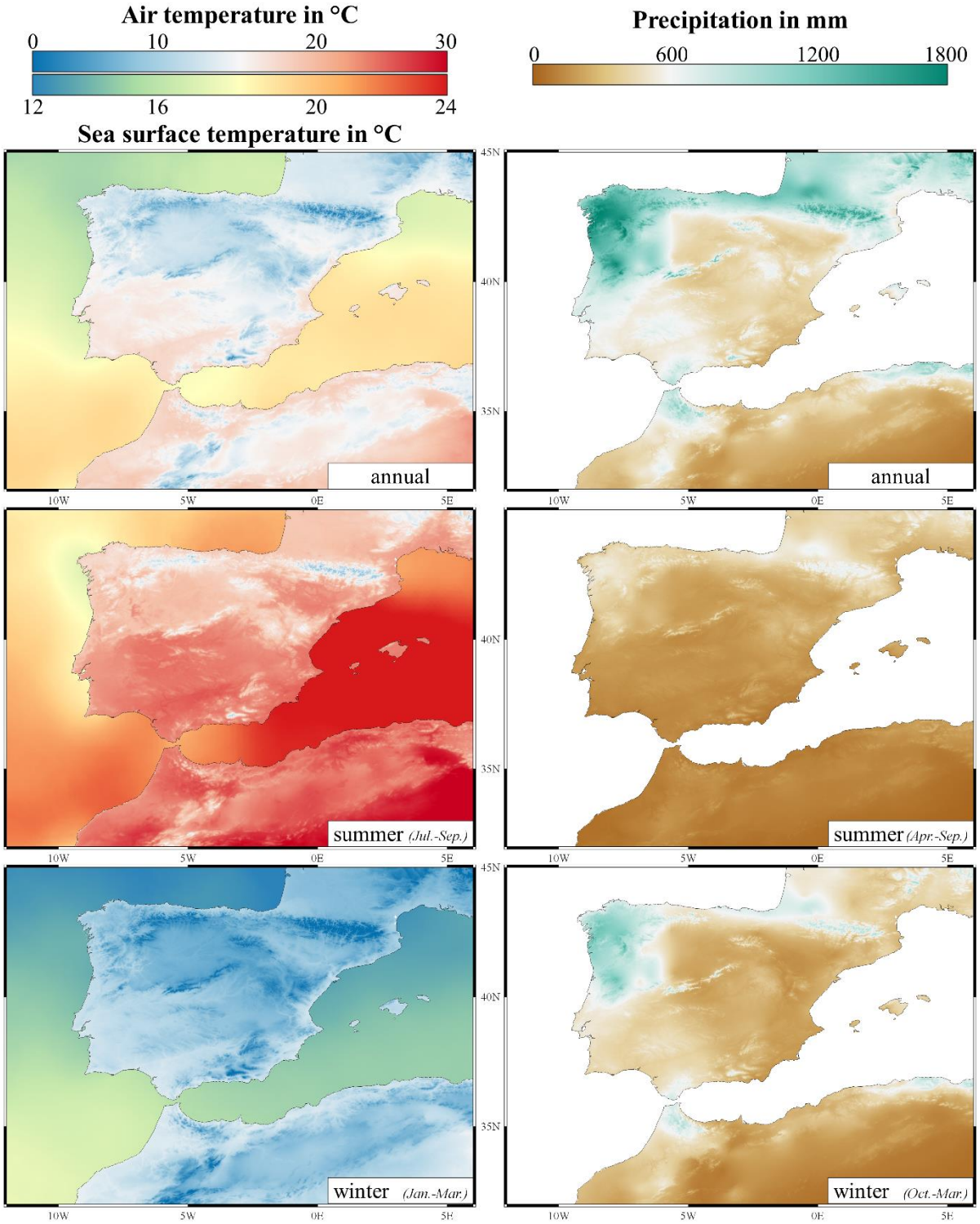

Figure 6.5 Supplementary figure S6.1. *Recent annual and seasonal air temperature as well as sea surface temperature (left) and precipitation (right) at the Iberian Peninsula. Temperatures are averages, while precipitation is displayed as total amount. Precipitation and air temperatures are based on monthly averages (1970 – 2000) and were downloaded from WorldClim V2 [Fick and Hijmans, 2017]. Sea surface temperature data are averaged for the period from 1955 – 2017 and was provided by World Ocean Atlas 18 [Locarnini et al., 2019].*

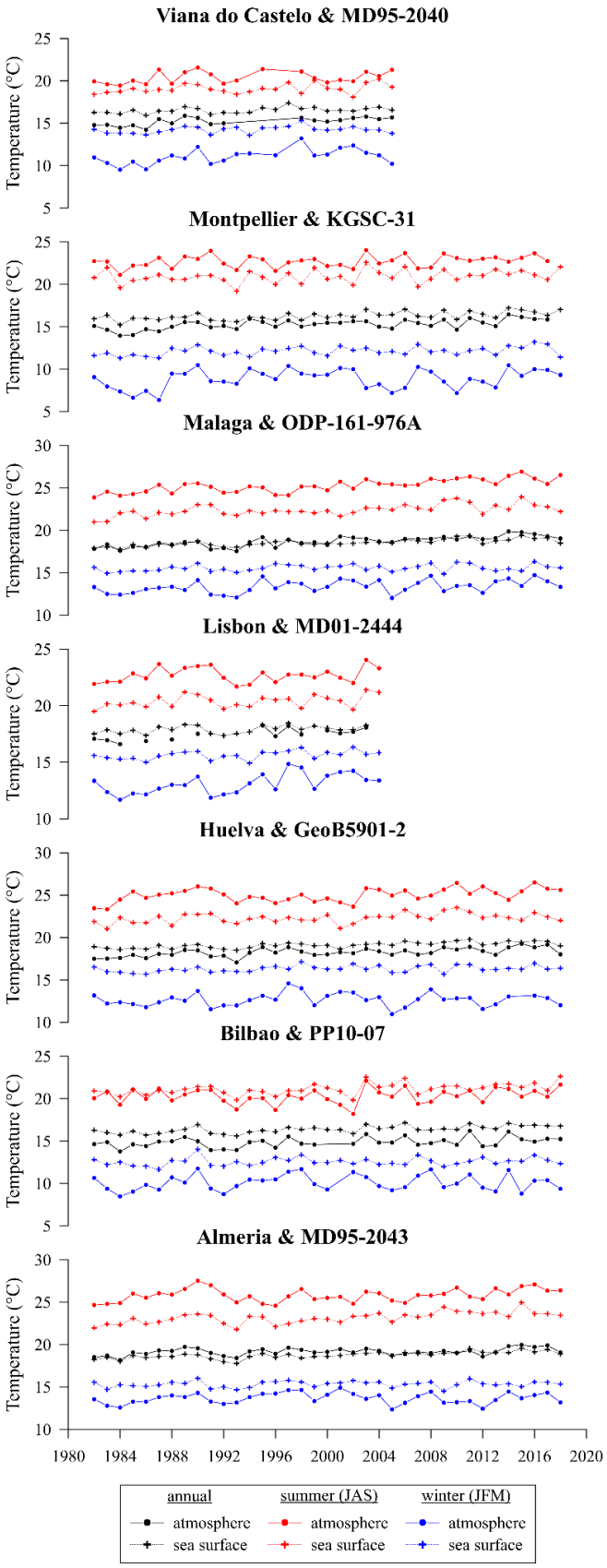

Figure 6.6 Supplementary figure S6.2. *Averaged seasonal (winter and summer) and annual sea surface temperatures from chosen locations of marine sedimentary archives as well as the according air temperatures from the closest station on land. Sea surface temperature data were provided by NOAA OISST V2 High Resolution Dataset. Air temperatures have been collected from the Spanish State Meteorological Agency (AEMET) and European Climate Assessment & Dataset (ECAD).*

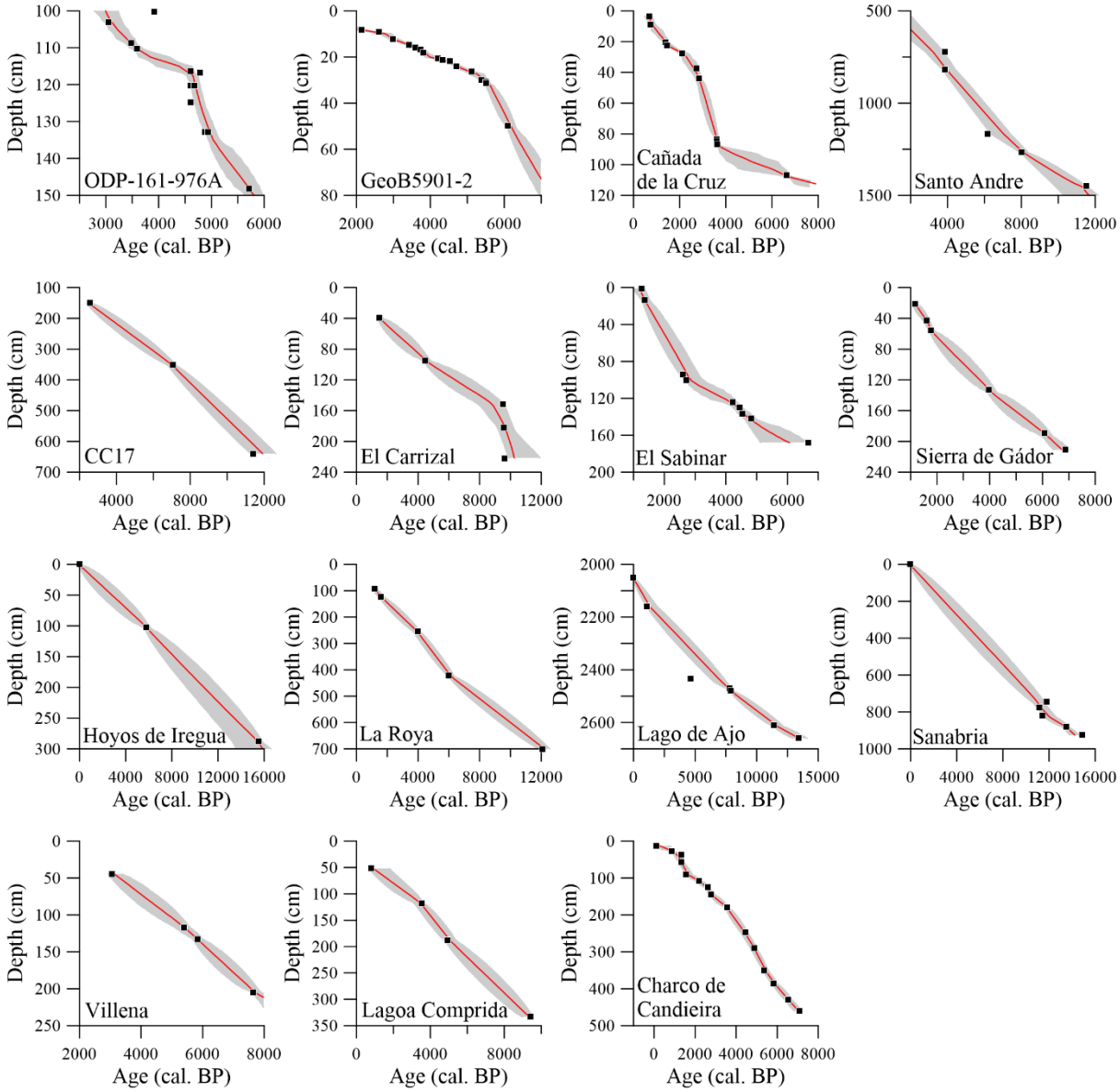

Figure 6.7 Supplementary figure S6.3. *Updated or calculated age models for all paleo-climatic archives. The source of the AMS ^{14}C data is referenced in Tab 6.1 within the original publication.*

6.9 References

Allen, J. R. M., B. Huntley, and W. A. Watts (1996), The vegetation and climate of northwest Iberia over the last 14,000 years, *J. Quaternary Sci.*, *11*(2), 125–147.

Aranda, G., S. Fernández, M. Haro, F. Molina, T. Nájera, and M. Sánchez (2008), Water control and cereal management on the Bronze Age Iberian Peninsula: La motilla del Azuer, *Oxford Journal of Archaeology*, *27*(3), 241–259, doi:10.1111/j.1468-0092.2008.00306.x.

Atsawawaranunt, K., S. Harrison, and L. Comas-Bru (2019), SISAL (Speleothem Isotopes Synthesis and AnaLysis Working Group) database version 1b.

Ausín, B., J. A. Flores, F. J. Sierro, I. Cacho, I. Hernández-Almeida, B. Martrat, and J. O. Grimalt (2015), Atmospheric patterns driving Holocene productivity in the Alboran Sea (Western Mediterranean): A multiproxy approach, *The Holocene*, *25*(4), 583–595, doi:10.1177/0959683614565952.

Bartelheim, M., and M. Pearce (2015), Early Metallurgy in Iberia and the Western Mediterranean, in *The Oxford Handbook of Neolithic Europe*, *Oxford handbooks*, edited by C. Fowler et al., Oxford University Press, Oxford.

Benítez de Lugo Enrich, L., and M. Mejías (2017), The hydrogeological and paleoclimatic factors in the Bronze Age Motillas Culture of La Mancha (Spain): The first hydraulic culture in Europe, *Hydrogeol J*, *25*(7), 1931–1950, doi:10.1007/s10040-017-1607-z.

Bevan, A., and E. R. Crema (2018), *rcarbon: Methods for calibrating and analysing radiocarbon dates*.

Bini, M., G. Zanchetta, A. Perşoiu, R. Cartier, A. Català, I. Cacho, J. R. Dean, F. Di Rita, R. N. Drysdale, M. Finnè, I. Isola, B. Jalali, F. Lirer, D. Magri, A. Masi, L. Marks, A. M. Mercuri, O. Peyron, L. Sadori, M.-A. Sicre, F. Welc, C. Zielhofer, and E. Brisset (2019), The 4.2 ka BP Event in the Mediterranean region: An overview, *Clim. Past*, *15*(2), 555–577, doi:10.5194/cp-15-555-2019.

Blaauw, M., and J. A. Christen (2011), Flexible paleoclimate age-depth models using an autoregressive gamma process, *Bayesian Anal.*, *6*(3), 457–474, doi:10.1214/11-BA618.

Blanco-González, A., K. T. Lillios, J. A. López-Sáez, and B. L. Drake (2018), Cultural, Demographic and Environmental Dynamics of the Copper and Early Bronze Age in Iberia (3300–1500 BC): Towards an Interregional Multiproxy Comparison at the Time of the 4.2 ky BP Event, *J World Prehist*, *31*(1), 1–79, doi:10.1007/s10963-018-9113-3.

Bond, G., B. Kromer, J. Beer, R. Muscheler, M. N. Evans, W. Showers, S. Hoffmann, R. Lotti-Bond, I. Hajdas, and G. Bonani (2001), Persistent solar influence on North Atlantic climate during the Holocene, *Science (New York, N.Y.)*, *294*(5549), 2130–2136, doi:10.1126/science.1065680.

Burjachs, F., S. Giralt, J. R. Roca, G. Seret, and R. Julià (1997), Palinología holocénica y desertización en el Mediterráneo occidental., in *El paisaje mediterráneo a través del espacio y del tiempo.: Implicaiones en la desertificación.*, edited by J. J. Ibañez et al., pp. 379–394, Geoforma Editores, Logroño.

Cacho, I., J. O. Grimalt, M. Canals, L. Sbaffi, N. J. Shackleton, J. Schönfeld, and R. Zahn (2001), Variability of the western Mediterranean Sea surface temperature during the last 25,000 years and its connection with the Northern Hemisphere climatic changes, *Paleoceanography*, *16*(1), 40–52, doi:10.1029/2000PA000502.

Campbell, J. F. E., W. J. Fletcher, S. Joannin, P. D. Hughes, M. Rhanem, and C. Zielhofer (2017), Environmental Drivers of Holocene Forest Development in the Middle Atlas, Morocco, *Front. Ecol. Evol.*, *5*, 201, doi:10.3389/fevo.2017.00113.

Cariñanos, P., C. Galan, P. Alcázar, and E. Domínguez (2004), Airborne pollen records response to climatic conditions in arid areas of the Iberian Peninsula, *Environmental and Experimental Botany*, *52*(1), 11–22, doi:10.1016/j.envexpbot.2003.11.008.

Carrión, J. S. (2002), Patterns and processes of Late Quaternary environmental change in a montane region of southwestern Europe, *Quaternary Science Reviews*, *21*(18-19), 2047–2066, doi:10.1016/S0277-3791(02)00010-0.

Carrión, J. S., A. Andrade, K. D. Bennett, C. Navarro, and M. Munuera (2001a), Crossing forest thresholds: inertia and collapse in a Holocene sequence from south-central Spain, *The Holocene*, *11*(6), 635–653.

Carrión, J. S., M. Munuera, M. Dupré, and A. Andrade (2001b), Abrupt vegetation changes in the Segura Mountains of southern Spain throughout the Holocene, *J Ecol*, *89*(5), 783–797, doi:10.1046/j.0022-0477.2001.00601.x.

Carrión, J. S., E. I. Yll, K. J. Willis, and P. Sánchez (2004), Holocene forest history of the eastern plateaux in the Segura Mountains (Murcia, southeastern Spain), *Review of Palaeobotany and Palynology*, *132*(3-4), 219–236, doi:10.1016/j.revpalbo.2004.07.002.

Castro, P. V., R. W. Chapman, S. Gili, V. Lull, R. Micó, C. Rihuete, R. Risch, and M. E. Sanahuja (1999), Agricultural production and social change in the Bronze Age of southeast Spain: The Gatas Project, *Antiquity*, *73*(282), 846–856, doi:10.1017/S0003598X00065583.

Català, A., I. Cacho, J. Frigola, L. D. Pena, and F. Lirer (2019), Holocene hydrography evolution in the Alboran Sea: A multi-record and multi-proxy comparison, *Clim. Past*, *15*(3), 927–942, doi:10.5194/cp-15-927-2019.

Chabaud, L., M. F. Sánchez Goñi, S. Desprat, and L. Rossignol (2014), Land–sea climatic variability in the eastern North Atlantic subtropical region over the last 14,200 years: Atmospheric and oceanic processes at different timescales, *The Holocene*, *24*(7), 787–797, doi:10.1177/0959683614530439.

Chapman, R. (2008), Producing Inequalities: Regional Sequences in Later Prehistoric Southern Spain, *J World Prehist*, *21*(3-4), 195–260, doi:10.1007/s10963-008-9014-y.

Cheng, H., A. Sinha, S. Verheyden, F. H. Nader, X. L. Li, P. Z. Zhang, J. J. Yin, L. Yi, Y. B. Peng, Z. G. Rao, Y. F. Ning, and R. L. Edwards (2015), The climate variability in northern Levant over the past 20,000 years, *Geophysical Research Letters*, *42*(20), 8641–8650, doi:10.1002/2015GL065397.

Clark-Carter, D. (2014), z Scores, in *Wiley StatsRef: Statistics Reference Online*, edited by N. Balakrishnan, p. 44, Wiley, [Erscheinungsort nicht ermittelbar].

Comendador Rey, B., J. Millos, and P. Álvarez-Iglesias (2014), Provenance of the prehistoric silver set of Antas de Ulla, north-western Iberia, using lead stable isotope ratios, in *Metalle der Macht - frühes Gold und Silber: 6. Mitteldeutscher Archäologentag vom 17. bis 19. Oktober 2013 in Halle (Saale) = Metals of power - early gold and silver*, *Tagungen des Landesmuseums für Vorgeschichte Halle*, vol. 11,2, edited by H. Meller et al., pp. 285–308, Landesamt für Denkmalpflege und Archäologie Sachsen-Anhalt Landesmuseum für Vorgeschichte, Halle (Saale).

Contreras, D. A., and J. Meadows (2014), Summed radiocarbon calibrations as a population proxy: A critical evaluation using a realistic simulation approach, *Journal of Archaeological Science*, *52*, 591–608, doi:10.1016/j.jas.2014.05.030.

Crema, E. R., A. Bevan, and S. Shennan (2017), Spatio-temporal approaches to archaeological radiocarbon dates, *Journal of Archaeological Science*, *87*, 1–9, doi:10.1016/j.jas.2017.09.007.

Davis, B. A. S., and A. C. Stevenson (2007), The 8.2ka event and Early–Mid Holocene forests, fires and flooding in the Central Ebro Desert, NE Spain, *Quaternary Science Reviews*, *26*(13-14), 1695–1712, doi:10.1016/j.quascirev.2007.04.007.

Davis, B.A.S., S. Brewer, A. C. Stevenson, and J. Guiot (2003), The temperature of Europe during the Holocene reconstructed from pollen data, *Quaternary Science Reviews*, *22*(15-17), 1701–1716, doi:10.1016/S0277-3791(03)00173-2.

Delgado-Raack, S., V. Lull, K. Martin, R. Micó, C. Rihuete Herrada, and R. Risch (2014), Die Silberschmiede von Tira del Lienzo, Totana, Prov. Murcia, im Kontext der El Argar Metallurgie, in *Metalle der Macht - frühes Gold und Silber: 6. Mitteldeutscher Archäologentag vom 17. bis 19. Oktober 2013 in Halle (Saale) = Metals of power - early gold and silver*, *Tagungen des Landesmuseums für Vorgeschichte Halle*, vol. 11,2, edited by H. Meller et al., pp. 577–592, Landesamt für Denkmalpflege und Archäologie Sachsen-Anhalt Landesmuseum für Vorgeschichte, Halle (Saale).

Delgado-Raack, S., and R. Risch (2015), Social Change and Subsistence Production on the Iberian Peninsula during the 3rd and 2nd Millennia BCE, in *The Third Food Revolution?: Setting the Bronze Age table : common trends in economic and subsistence strategies in Bronze Age Europe : proceedings of the International Workshop "Socio-Environmental Dynamics over the Last 12,000 Years: the Creation of Landscapes III (15th-18th April 2013)" in Kiel*, edited by J. Kneisel et al., pp. 21–46, Verlag Dr. Rudolph Habelt GmbH, Bonn.

Díaz-Zorita Bonilla, M. (2013), *The Copper Age in south-west Spain: A bioarchaeological approach to prehistoric social organisation*, 502 pp., vol. 2013, Durham.

Díaz-Zorita Bonilla, M., J. Beck, H. Bocherens, and P. Díaz-del-Río (2018), Isotopic evidence for mobility at large-scale human aggregations in Copper Age Iberia: The mega-site of Marroquíes, *Antiquity*, *92*(364), 991–1007, doi:10.15184/aqy.2018.33.

Drake, B. L., A. Blanco-González, and K. T. Lillios (2017), Regional Demographic Dynamics in the Neolithic Transition in Iberia: Results from Summed Calibrated Date Analysis, *J Archaeol Method Theory*, *24*(3), 796–812, doi:10.1007/s10816-016-9286-y.

Faust, D., and D. Wolf (2017), Interpreting drivers of change in fluvial archives of the Western Mediterranean - A critical view, *Earth-Science Reviews*, *174*, 53–83, doi:10.1016/j.earscirev.2017.09.011.

Fick, S. E., and R. J. Hijmans (2017), WorldClim 2: New 1-km spatial resolution climate surfaces for global land areas, *Int. J. Climatol.*, *37*(12), 4302–4315, doi:10.1002/joc.5086.

Fletcher, W. J., M. F. Sanchez Goñi, O. Peyron, and I. Dormoy (2010), Abrupt climate changes of the last deglaciation detected in a Western Mediterranean forest record, *Clim. Past*, *6*(2), 245–264, doi:10.5194/cp-6-245-2010.

Franco-Múgica, F., M. García-Antón, J. Maldonado-Ruiz, C. Morla-Juaristi, and H. Sainz-Ollerol (2001), The Holocene history of Pinus forests in the Spanish Northern Meseta, *The Holocene*, *11*(3), 343–358, doi:10.1191/095968301669474913.

Frigola, J., A. Moreno, I. Cacho, M. Canals, F. J. Sierro, J. A. Flores, and J. O. Grimalt (2008), Evidence of abrupt changes in Western Mediterranean Deep Water circulation during the last 50kyr: A high-resolution marine record from the Balearic Sea, *Quaternary International*, *181*(1), 88–104, doi:10.1016/j.quaint.2007.06.016.

Fyfe, R. M., J. Woodbridge, A. Palmisano, A. Bevan, S. Shennan, F. Burjachs, B. Legarra Herrero, O. García Puchol, J.-S. Carrión, J. Revelles, and C. N. Roberts (2019), Prehistoric palaeodemographics and regional land cover change in eastern Iberia, *The Holocene*, *29*(5), 799–815, doi:10.1177/0959683619826643.

García Sanjuán, L., M. d. C. Moreno Escobar, J. Márquez Pérez, and D. W. Wheatley (2016), The Copper Age in the lands of Antequera (Málaga): Introduction to the settlement patterns and social dynamics, *Zephyrus*, *78*, 35–65, doi:10.14201/zephyrus2016783565.

García Sanjuán, L., C. Scarre, and D. W. Wheatley (2017), The Mega-Site of Valencina de la Concepción (Seville, Spain): Debating Settlement Form, Monumentality and Aggregation in Southern Iberian Copper Age Societies, *J World Prehist*, *30*(3), 239–257, doi:10.1007/s10963-017-9107-6.

García Sanjuán, L., J. M. Vargas Jiménez, L. M. Cáceres Puro, M. E. Costa Caramé, M. Díaz-Guardamino Uribe, M. Díaz-Zorita Bonilla, Á. Fernández Flores, V. Hurtado Pérez, P. M. López Aldana, E. Méndez Izquierdo, A. Pajuelo Pando, J. Rodríguez Vidal, D. Wheatley, C. Bronk Ramsey, A. Delgado-Huertas, E. Dunbar, A. Mora González, A. Bayliss, N. Beavan, D. Hamilton, and A. Whittle (2018), Assembling the Dead, Gathering the Living: Radiocarbon Dating and Bayesian Modelling for Copper Age Valencina de la Concepción (Seville, Spain), *Journal of world prehistory*, *31*(2), 179–313, doi:10.1007/s10963-018-9114-2.

Giorgi, F., and P. Lionello (2008), Climate change projections for the Mediterranean region, *Global and Planetary Change*, *63*(2-3), 90–104, doi:10.1016/j.gloplacha.2007.09.005.

Gouveia, C., R. M. Trigo, C. C. DaCamara, R. Libonati, and J. M. C. Pereira (2008), The North Atlantic Oscillation and European vegetation dynamics, *Int. J. Climatol.*, *28*(14), 1835–1847, doi:10.1002/joc.1682.

Haynes, R., E. D. Barton, and I. Pilling (1993), Development, persistence, and variability of upwelling filaments off the Atlantic coast of the Iberian Peninsula, *J. Geophys. Res.*, *98*(C12), 22681, doi:10.1029/93JC02016.

Hernández, A., R. M. Trigo, S. Pla-Rabes, B. L. Valero-Garcés, S. Jerez, M. Rico-Herrero, J. C. Vega, M. Jambrina-Enríquez, and S. Giralt (2015), Sensitivity of two Iberian lakes to North Atlantic atmospheric circulation modes, *Clim Dyn*, *45*(11-12), 3403–3417, doi:10.1007/s00382-015-2547-8.

Hijmans, R. J. (2019), *raster: Geographic Data Analysis and Modeling*.

Hinz, M., I. Feeser, K.-G. Sjögren, and J. Müller (2012a), Demography and the intensity of cultural activities: An evaluation of Funnel Beaker Societies (4200–2800 cal BC), *Journal of Archaeological Science*, *39*(10), 3331–3340, doi:10.1016/j.jas.2012.05.028.

Hinz, M., M. Furholt, J. Müller, D. Raetzel-Fabian, C. Rinne, K.-G. Sjögren, and H.-P. Wotza (2012b), RADON - Radiocarbon dates online 2012: Central European database of 14C dates for the Neolithic and Early Bronze Age.

Hinz, M., J. Schirrmacher, J. Kneisel, C. Rinne, and M. Weinelt (2019), The Chalcolithic–Bronze Age transition in southern Iberia under the influence of the 4.2 kyr event?: A correlation of climatological and demographic proxies, *Journal of Neolithic Archaeology*, *21*, 1–26, doi:10.12766/jna.2019.1.

Hurrell, J. W. (1995), Decadal trends in the north atlantic oscillation: regional temperatures and precipitation, *Science*, *269*(5224), 676–679, doi:10.1126/science.269.5224.676.

IDEArq, IDEArq: Infraestructura de Datos Espaciales de Investigación Arqueológica, http://www.idearqueologia.org/.

Ilvonen, L., J. A. López-Sáez, L. Holmström, F. Alba-Sánchez, S. Pérez-Díaz, J. S. Carrión, and H. Seppä (2019), Quantitative reconstruction of precipitation changes in the Iberian Peninsula during the Late Pleistocene and the Holocene, *Clim. Past Discuss.*, 1–30, doi:10.5194/cp-2019-33.

Jalali, B., M.-A. Sicre, M.-A. Bassetti, and N. Kallel (2016), Holocene climate variability in the North-Western Mediterranean Sea (Gulf of Lions), *Climate of the Past*, *12*(1), 91–101, doi:10.5194/cp-12-91-2016.

Jalut, G., J. J. Dedoubat, M. Fontugne, and T. Otto (2009), Holocene circum-Mediterranean vegetation changes: Climate forcing and human impact, *Quaternary International*, *200*(1-2), 4–18, doi:10.1016/j.quaint.2008.03.012.

Jiménez-Moreno, G., A. Rodríguez-Ramírez, J. N. Pérez-Asensio, J. S. Carrión, J. A. López-Sáez, J. Villarías-Robles, JR, S. Celestino-Pérez, E. Cerrillo-Cuenca, Á. León, and C. Contreras (2015), Impact of late-Holocene

aridification trend, climate variability and geodynamic control on the environment from a coastal area in SW Spain, *The Holocene*, *25*(4), 607–617, doi:10.1177/0959683614565955.

Kaniewski, D., N. Marriner, R. Cheddadi, J. Guiot, and E. van Campo (2018), The 4.2 ka BP event in the Levant, *Clim. Past*, *14*(10), 1529–1542, doi:10.5194/cp-14-1529-2018.

Kneisel, J., M. Hinz, and C. Rinne (2013), Radon-B, http://radon-b.ufg.uni-kiel.de.

Kovats, R. S., R. Valentini, L. M. Bouwer, E. Georgopoulou, D. Jacob, E. Martin, M. Rounsevell, and J.-F. Soussana (2014), Europe, in *Climate Change 2014: Impacts, Adaptation, and Vulnerability. Part B: Regional Aspects.Contribution of Working Group II to the Fifth Assessment Report of the Intergovernmental Panel on Climate Change*, edited by V. R. Barros et al., pp. 1267–1326, Cambridge, United Kingdom and New York, NY, USA.

Kunst, M., and N. Lutz (2008), Zambujal (Torres Vedras, Portugal): Zur Präzision der absoluten Chronologie durch die Untersuchungen an der vierten Befestigungslinie, in *Madrider Mitteilungen*, vol. 49, edited by Deutsches Archäologisches Institut, pp. 29–63, Ludwig Reichert Verlag, Wiesbaden.

Lamb, H. F., and S. van der Kaars (1995), Vegetational response to Holocene climatic change: Pollen and palaeolimnological data from the Middle Atlas, Morocco, *The Holocene*, *5*(4), 400–408, doi:10.1177/095968369500500402.

Lillios, K. T., A. Blanco-González, B. L. Drake, and J. A. López-Sáez (2016), Mid-late Holocene climate, demography, and cultural dynamics in Iberia: A multi-proxy approach, *Quaternary Science Reviews*, *135*, 138–153, doi:10.1016/j.quascirev.2016.01.011.

Lionello, P. (Ed.) (2012), *The climate of the Mediterranean region: From the past to the future*, 1st ed., 502 pp., *Elsevier insights*, Elsevier Science, Amsterdam.

Locarnini, R. A., A. V. Mishonov, O. K. Baranova, T. P. Boyer, M. M. Zweng, H. E. Garcia, J. R. Reagan, D. Seidov, K. Weathers, C. R. Paver, and I. Smolyar (2019), World Ocean Atlas 2018, Volume 1: Temperature, 52 pp., NOAA Atlas NESDIS 81.

López Saez, J. A., A. Blanco González, S. Pérez Díaz, F. Alba Sánchez, R. Luelmo Lautenschlaeger, A. Glais, and S. Núñez de la Fuente (2017), Landscapes, Human Activities and Climate Dynamics in the South Meseta of the Iberian Peninsula During the 3rd and 2nd Millennia calBC, in *Key resources and socio-cultural developments in the Iberian Chalcolithic*, 1st ed., *RessourcenKulturen*, Band 6, edited by M. Bartelheim et al., pp. 129–142, Eberhard Karls Universität Tübingen Tübingen Library Publishing, Tübingen.

López-Sáez, J. A., D. Abel-Schaad, S. Pérez-Díaz, A. Blanco-González, F. Alba-Sánchez, M. Dorado, B. Ruiz-Zapata, M. J. Gil-García, C. Gómez-González, and F. Franco-Múgica (2014), Vegetation history, climate and human impact in the Spanish Central System over the last 9000 years, *Quaternary International*, *353*, 98–122, doi:10.1016/j.quaint.2013.06.034.

López-Sáez, J. A., S. Pérez-Díaz, A. Rodríguez-Ramírez, A. Blanco-González, J. J.R. Villarías-Robles, R. Luelmo-Lautenschlaeger, G. Jiménez-Moreno, S. Celestino-Pérez, E. Cerrillo-Cuenca, J. N. Pérez-Asensio, and Á. León (2018), Mid-late Holocene environmental and cultural dynamics at the south-west tip of Europe (Doñana National Park, SW Iberia, Spain), *Journal of Archaeological Science: Reports*, *22*, 58–78, doi:10.1016/j.jasrep.2018.09.014.

Lull, V., R. Micó, C. Rihuete Herrada, and R. Risch (2011), El Argar and the Beginning of Class Society in the Western Mediterranean, in *Sozialarchäologische Perspektiven: Gesellschaftlicher Wandel 5000 - 1500 v. Chr. zwischen Atlantik und Kaukasus: Internationale Tagung, 15. - 18. Oktober 2007 in Kiel*, *Archäologie in Eurasien*, vol. 24, edited by S. Hansen and J. Müller, pp. 381–414, von Zabern, Mainz.

Lull, V., R. Micó, C. Rihuete Herrada, and R. Risch (2013a), Bronze Age Iberia, in *The Oxford Handbook of the European Bronze Age*, edited by H. Fokkens and A. Harding, Oxford University Press.

Lull, V., R. Micó, C. Rihuete Herrada, and R. Risch (2013b), Political collapse and social change at the end of El Argar, in *1600 - Kultureller Umbruch im Schatten des Thera-Ausbruchs?: 4. Mitteldeutscher Archäologentag vom 14. bis 16. Oktober 2011 in Halle (Saale)*, Band 9, edited by H. Meller et al., pp. 283–302, Landesamt für Denkmalpflege und Archäologie Sachsen-Anhalt, Landesmuseum für Vorgeschichte, Halle (Saale).

Lull, V., R. Micó, C. Rihuete Herrada, and R. Risch (2015), Transition and conflict at the end of the 3rd millennium BC in south Iberia, in *2200 BC - ein Klimasturz als Ursache für den Zerfall der alten Welt?: 7. Mitteldeutscher Archäologentag vom 23. bis 26. Oktober 2014 in Halle (Saale)*, *Tagungen des Landesmuseums für Vorgeschichte Halle*, Band 12,1, edited by H. Meller et al., pp. 365–408, Landesamt für Denkmalpflege und Archäologie Sachsen-Anhalt, Landesmuseum für Vorgeschichte, Halle (Saale).

Mariscal, B. (1993), Variacion de la Vegetation Holocena (4300-280 B.P.): De Cantabria a traves del analisis polinico de la Turbera del Alsa, *Estud. geol.*, *49*(1-2), 63–68, doi:10.3989/egeol.93491-2338.

Molina González, F., J. A. Camara Serrano, J. Capel Martínez, T. Nájera Colino, and L. Sáez Pérez (2004), Los Millares y la periodización de la prehistoria reciente del sureste, in *II -III Simposios de prehistoria Cueva de Nerja*, edited by M. Pellicer Catalán and A. Arribas, pp. 142–158, Fundación Cueva de Nerja, Nerja.

Mora-González, A., A. Delgado-Huertas, A. Granados-Torres, F. Contreras Cortés, F. J. Jover Maestre, and J. A. López Padilla (2016), The isotopic footprint of irrigation in the western Mediterranean basin during the Bronze Age: The settlement of Terlinques, southeast Iberian Peninsula, *Veget Hist Archaeobot*, *25*(5), 459–468, doi:10.1007/s00334-016-0560-4.

Mora-González, A., A. Delgado-Huertas, A. Granados-Torres, F. Contreras Cortés, I. Pavón Soldevila, and D. Duque Espino (2018), Complex agriculture during the second millennium BC: Isotope composition of carbon studies (δ13C) in archaeological plants of the settlement Cerro del Castillo de Alange (SW Iberian Peninsula, Spain), *Veget Hist Archaeobot*, *27*(3), 453-462, doi:10.1007/s00334-017-0634-y.

Morellón, M., B. Valero-Garcés, T. Vegas-Vilarrúbia, P. González-Sampériz, Ó. Romero, A. Delgado-Huertas, P. Mata, A. Moreno, M. Rico, and J. P. Corella (2009), Lateglacial and Holocene palaeohydrology in the western Mediterranean region: The Lake Estanya record (NE Spain), *Quaternary Science Reviews*, *28*(25-26), 2582–2599, doi:10.1016/j.quascirev.2009.05.014.

Müller, J., and S. van Willigen (2001), New radiocarbon evidence for european Bell Beakers and the consequences for the diffusion of the Bell Beaker Phenomenon, in *Bell beakers today: Pottery, people, culture, symbols in prehistoric Europe; proceedings of the International colloquium, Riva del Garda (Trento, Italy), 11-16 May 1998*, edited by F. Nicolis, pp. 59–80, Provincia autonoma di Trento Servizio beni culturali Ufficio beni archeologici, Trento.

Palumbo, E., J. A. Flores, C. Perugia, D. Emanuele, Z. Petrillo, T. Rodrigues, A. H. L. Voelker, and F. O. Amore (2013), Abrupt variability of the last 24 ka BP recorded by coccolithophore assemblages off the Iberian Margin (core MD03-2699), *J. Quaternary Sci.*, *28*(3), 320–328, doi:10.1002/jqs.2623.

Pantaléon-Cano, J., E.-I. Yll, R. Pérez-Obiol, and J. M. Roure (2003), Palynological evidence for vegetational history in semi-arid areas of the western Mediterranean (Almería, Spain), *The Holocene*, *13*(1), 109–119, doi:10.1191/0959683603hl598rp.

Pebesma, E. J. (2004), Multivariable geostatistics in S: The gstat package, *Computers & Geosciences*, *30*(7), 683–691, doi:10.1016/j.cageo.2004.03.012.

Peliz, Á., J. Dubert, A. M. P. Santos, P. B. Oliveira, and B. Le Cann (2005), Winter upper ocean circulation in the Western Iberian Basin—Fronts, Eddies and Poleward Flows: An overview, *Deep Sea Research Part I: Oceanographic Research Papers*, *52*(4), 621–646, doi:10.1016/j.dsr.2004.11.005.

Peliz, Á., T. L. Rosa, A.M. P. Santos, and J. L. Pissarra (2002), Fronts, jets, and counter-flows in the Western Iberian upwelling system, *Journal of Marine Systems*, *35*(1-2), 61–77, doi:10.1016/S0924-7963(02)00076-3.

Pérez-Obiol, R., G. Jalut, R. Julià, A. Pèlachs, M. J. Iriarte, T. Otto, and B. Hernández-Beloqui (2011), Mid-Holocene vegetation and climatic history of the Iberian Peninsula, *The Holocene*, *21*(1), 75–93, doi:10.1177/0959683610384161.

Pérez-Sanz, A., P. González-Sampériz, A. Moreno, B. Valero-Garcés, G. Gil-Romera, M. Rieradevall, P. Tarrats, L. Lasheras-Álvarez, M. Morellón, A. Belmonte, C. Sancho, M. Sevilla-Callejo, and A. Navas (2013), Holocene climate variability, vegetation dynamics and fire regime in the central Pyrenees: The Basa de la Mora sequence (NE Spain), *Quaternary Science Reviews*, *73*, 149–169, doi:10.1016/j.quascirev.2013.05.010.

Peyron, O., N. Combourieu-Nebout, D. Brayshaw, S. Goring, V. Andrieu-Ponel, S. Desprat, W. Fletcher, B. Gambin, C. Ioakim, S. Joannin, U. Kotthoff, K. Kouli, V. Montade, J. Pross, L. Sadori, and M. Magny (2017), Precipitation changes in the Mediterranean basin during the Holocene from terrestrial and marine pollen records: A model–data comparison, *Climate of the Past*, *13*(3), 249–265, doi:10.5194/cp-13-249-2017.

R Core Team (2019), *R: A Language and Environment for Statistical Computing*, R Foundation for Statistical Computing, Vienna, Austria.

Ramos-Román, M. J., G. Jiménez-Moreno, J. Camuera, A. García-Alix, R. Scott Anderson, F. J. Jiménez-Espejo, D. Sachse, J. L. Toney, J. S. Carrión, C. Webster, and Y. Yanes (2018), Millennial-scale cyclical environment and climate variability during the Holocene in the western Mediterranean region deduced from a new multi-proxy analysis from the Padul record (Sierra Nevada, Spain), *Global and Planetary Change*, *168*, 35–53, doi:10.1016/j.gloplacha.2018.06.003.

Reimer, P. J., E. Bard, A. Bayliss, J. W. Beck, P. G. Blackwell, C. B. Ramsey, C. E. Buck, H. Cheng, R. L. Edwards, M. Friedrich, P. M. Grootes, T. P. Guilderson, H. Haflidason, I. Hajdas, C. Hatté, T. J. Heaton, D. L. Hoffmann, A. G. Hogg, K. A. Hughen, K. F. Kaiser, B. Kromer, S. W. Manning, M. Niu, R. W. Reimer, D. A. Richards, E. M. Scott, J. R. Southon, R. A. Staff, C. S. M. Turney, and J. van der Plicht (2013), IntCal13 and Marine13 Radiocarbon Age Calibration Curves 0–50,000 Years cal BP, *Radiocarbon*, *55*(04), 1869–1887, doi:10.2458/azu_js_rc.55.16947.

Rodrigues, T., J. O. Grimalt, F. G. Abrantes, J. A. Flores, and S. M. Lebreiro (2009), Holocene interdependences of changes in sea surface temperature, productivity, and fluvial inputs in the Iberian continental shelf (Tagus mud patch), *Geochemistry, Geophysics, Geosystems*, *10*(7), n/a-n/a, doi:10.1029/2008GC002367.

Ruan, J., F. Kherbouche, D. Genty, D. Blamart, H. Cheng, F. Dewilde, S. Hachi, R. L. Edwards, E. Régnier, and J.-L. Michelot (2016), Evidence of a prolonged drought ca. 4200 yr BP correlated with prehistoric settlement abandonment from the Gueldaman GLD1 Cave, Northern Algeria, *Climate of the Past*, *12*(1), 1–14, doi:10.5194/cp-12-1-2016.

Sabatier, P., L. Dezileau, C. Colin, L. Briqueu, F. Bouchette, P. Martinez, G. Siani, O. Raynal, and U. von Grafenstein (2012), 7000 years of paleostorm activity in the NW Mediterranean Sea in response to Holocene climate events, *Quat. res.*, *77*(01), 1–11, doi:10.1016/j.yqres.2011.09.002.

Sánchez Goñi, M. F., and G. E. Hannon (1999), High-altitude vegetational pattern on the Iberian Mountain Chain (north-central Spain) during the Holocene, *The Holocene*, *9*(1), 39–57.

Santos, L., and M. F. Sánchez Goñi (2003), Lateglacial and Holocene environmental changes in Portuguese coastal lagoons 3: Vegetation history of the Santo Andre coastal area, *The Holocene*, *13*(3), 459–464, doi:10.1191/0959683603hl638rp.

Sarhan, T., J. G. Lafuente, M. Vargas, J. M. Vargas, and F. Plaza (2000), Upwelling mechanisms in the northwestern Alboran Sea, *Journal of Marine Systems*, *23*(4), 317–331, doi:10.1016/S0924-7963(99)00068-8.

Schirrmacher, J., M. Weinelt, T. Blanz, N. Andersen, E. Salgueiro, and R. R. Schneider (2019), Multi-decadal atmospheric and marine climate variability in southern Iberia during the mid- to late-Holocene, *Clim. Past*, *15*(2), 617–634, doi:10.5194/cp-15-617-2019.

Schneider, H., D. Höfer, C. Trog, S. Busch, M. Schneider, J. Baade, G. Daut, and R. Mäusbacher (2010), Holocene estuary development in the Algarve Region (Southern Portugal) – A reconstruction of sedimentological and ecological evolution, *Quaternary International*, *221*(1-2), 141–158, doi:10.1016/j.quaint.2009.10.004.

Schneider, H., D. Höfer, C. Trog, and R. Mäusbacher (2016), Holocene landscape development along the Portuguese Algarve coast – A high resolution palynological approach, *Quaternary International*, *407*, 47–63, doi:10.1016/j.quaint.2016.02.039.

Schuhmacher, T. X. (2017), Ivory Exchange Networks in the Chalcolithic of the Western Mediterranean, in *Key resources and socio-cultural developments in the Iberian Chalcolithic*, 1st ed., *RessourcenKulturen*, Band 6, edited by M. Bartelheim et al., pp. 291–312, Eberhard Karls Universität Tübingen Tübingen Library Publishing, Tübingen.

Schulz Paulsson, B. (2019), Radiocarbon dates and Bayesian modeling support maritime diffusion model for megaliths in Europe, *Proceedings of the National Academy of Sciences of the United States of America*, *116*(9), 3460–3465, doi:10.1073/pnas.1813268116.

Smith, A. C., P. M. Wynn, P. A. Barker, M. J. Leng, S. R. Noble, and W. Tych (2016), North Atlantic forcing of moisture delivery to Europe throughout the Holocene, *Scientific reports*, *6*, 24745, doi:10.1038/srep24745.

Soares, A. M. M., J. Soares, and C. Tavares da Silva (2007), A datação pelo radiocarbono das fases de ocupação do Porto das Carretas: algumas reflexões sobre a cronologia do Campaniforme, *Revista Portuguesa de Arqueologia*, *10*(2), 127–134.

Trigo, R. M., D. Pozo-Vázquez, T. J. Osborn, Y. Castro-Díez, S. Gámiz-Fortis, and M. J. Esteban-Parra (2004), North Atlantic oscillation influence on precipitation, river flow and water resources in the Iberian Peninsula, *Int. J. Climatol*, *24*(8), 925–944, doi:10.1002/joc.1048.

Valera, A. C. (2015), Social change in the late 3rd millennium BC in Portugal: the twilight of enclosures, in *2200 BC - ein Klimasturz als Ursache für den Zerfall der alten Welt?: 7. Mitteldeutscher Archäologentag vom 23. bis 26. Oktober 2014 in Halle (Saale)*, *Tagungen des Landesmuseums für Vorgeschichte Halle*, Band 12,1, edited by H. Meller et al., pp. 409–428, Landesamt für Denkmalpflege und Archäologie Sachsen-Anhalt, Landesmuseum für Vorgeschichte, Halle (Saale).

Walsh, K., J.-F. Berger, C. N. Roberts, B. Vanniere, M. Ghilardi, A. G. Brown, J. Woodbridge, L. Lespez, J. Estrany, A. Glais, A. Palmisano, M. Finné, and G. Verstraeten (2019), Holocene demographic fluctuations, climate and erosion in the Mediterranean: A meta data-analysis, *The Holocene*, *29*(5), 864–885, doi:10.1177/0959683619826637.

Warden, L., M. Moros, T. Neumann, S. Shennan, A. Timpson, K. Manning, M. Sollai, L. Wacker, K. Perner, K. Häusler, T. Leipe, L. Zillén, A. Kotilainen, E. Jansen, R. R. Schneider, R. Oeberst, H. Arz, and J. S. Sinninghe Damsté (2017), Climate induced human demographic and cultural change in northern Europe during the mid-Holocene, *Scientific reports*, *7*(1), 15251, doi:10.1038/s41598-017-14353-5.

Wassenburg, J. A., S. Dietrich, J. Fietzke, J. Fohlmeister, K. P. Jochum, D. Scholz, D. K. Richter, A. Sabaoui, C. Spötl, G. Lohmann, M. O. Andreae, and A. Immenhauser (2016), Reorganization of the North Atlantic Oscillation during early Holocene deglaciation, *Nature Geoscience*, *9*(8), 602–605, doi:10.1038/ngeo2767.

Weinelt, M., C. Schwab, J. Kneisel, and M. Hinz (2015), Climate and societal change in the western Mediterranean area around 4.2 ka BP, in *2200 BC - ein Klimasturz als Ursache für den Zerfall der alten Welt?: 7. Mitteldeutscher Archäologentag vom 23. bis 26. Oktober 2014 in Halle (Saale)*, *Tagungen des Landesmuseums für Vorgeschichte Halle*, Band 12,1, edited by H. Meller et al., pp. 461–480, Landesamt für Denkmalpflege und Archäologie Sachsen-Anhalt, Landesmuseum für Vorgeschichte, Halle (Saale).

Weiss, H. (2017), 4.2 ka BP Megadrought and the Akkadian Collapse, in *Megadrought and collapse: From early agriculture to angkor*, edited by H. Weiss, pp. 93–161, Oxford University Press, New York, NY.

Welc, F., and L. Marks (2014), Climate change at the end of the Old Kingdom in Egypt around 4200 BP: New geoarchaeological evidence, *Quaternary International*, *324*, 124–133, doi:10.1016/j.quaint.2013.07.035.

Weninger, B., L. Clare, O. Jöris, R. Jung, and K. Edinborough (2015), Quantum theory of radiocarbon calibration, *World Archaeology*, *47*(4), 543–566, doi:10.1080/00438243.2015.1064022.

Williams, A. N. (2012), The use of summed radiocarbon probability distributions in archaeology: A review of methods, *Journal of Archaeological Science*, *39*(3), 578–589, doi:10.1016/j.jas.2011.07.014.

Yll, E.-I., R. Perez-Obiol, J. Pantaleon-Cano, and J. M. Roure (1997), Palynological Evidence for Climatic Change and Human Activity during the Holocene on Minorca (Balearic Islands), *Quat. res.*, *48*(03), 339–347, doi:10.1006/qres.1997.1925.

Zanchetta, G., E. Regattieri, I. Isola, R. N. Drysdale, M. Bini, I. Baneschi, and J. C. Hellstrom (2016), The so-called "4.2 event" in the Central Mediterranean and its climatic teleconnections, *Alpine and Mediterranean Quaternary*, *29*(1), 5–17.

Zielhofer, C., W. J. Fletcher, S. Mischke, M. de Batist, J. F.E. Campbell, S. Joannin, R. Tjallingii, N. El Hamouti, A. Junginger, A. Stele, J. Bussmann, B. Schneider, T. Lauer, K. Spitzer, M. Strupler, T. Brachert, and A. Mikdad (2017), Atlantic forcing of Western Mediterranean winter rain minima during the last 12,000 years, *Quaternary Science Reviews*, *157*, 29–51, doi:10.1016/j.quascirev.2016.11.037.

Zielhofer, C., A. Köhler, S. Mischke, A. Benkaddour, A. Mikdad, and W. J. Fletcher (2019), Western Mediterranean hydro-climatic consequences of Holocene ice-rafted debris (Bond) events, *Clim. Past*, *15*(2), 463–475, doi:10.5194/cp-15-463-2019.

Zorita, E., V. Kharin, and H. von Storch (1992), The Atmospheric Circulation and Sea Surface Temperature in the North Atlantic Area in Winter: Their Interaction and Relevance for Iberian Precipitation, *Journal of Climate*, *5*(10), 1097–1108, doi:10.1175/1520-0442(1992)005<1097:TACASS>2.0.CO;2.

Chapter 7

Fossil leaf wax hydrogen isotopes reveal variability of North Atlantic climate forcing on the southeast Iberian Peninsula between 3000 to 6000 cal. BP

Julien Schirrmacher, Nils Andersen, Ralph R. Schneider, and Mara Weinelt (to be submitted to PlosOne): Fossil leaf wax hydrogen isotopes reveal variability of North Atlantic climate forcing on the southeast Iberian Peninsula between 3000 to 6000 cal. BP

7 Fossil leaf wax hydrogen isotopes reveal variability of North Atlantic climate forcing on the southeast Iberian Peninsula between 3000 to 6000 cal. BP

7.1 Abstract

Many recently published papers have investigated the spatial and temporal manifestation of the 4.2 ka BP climate event at regional and global scales. However, questions with regard to the potential drivers of the associated climate change remain open. Here, we investigate the interaction between Atlantic and Mediterranean climate forcing on the south-eastern Iberian Peninsula during the Mid- to Late Holocene using compound-specific hydrogen isotopes from *n*-alkanes preserved in marine sediments. Variability of hydrogen isotope values in the study area is related to changes in the precipitation source and indicates three phases of increased Mediterranean sourced precipitation from 3250 to 3400 cal. BP, from 4300 to 5150 cal. BP, and from 5350 to 5450 cal. BP. These phases are in good agreement with times of a prevailing positive mode of the North Atlantic Oscillation, reduced storm activity in the Mediterranean, and an increase in summer precipitation over southeast Iberia. Instead, as suggested by a major decrease in hydrogen isotope values of the *n*-C_{33} *n*-alkane, the 4.2 ka BP event on the south-eastern Iberian Peninsula was characterized by rapid reductions in summer precipitation indicating a decrease of Mediterranean sourced moisture influence.

7.2 Introduction

In recent years much effort has been made in reconstructing and understanding the socio-environmental dynamics associated with the 4.2 ka BP event. Initially, the 4.2 ka BP event was described as an "archaeological event" in the Near East, where the Akkadian Empire collapsed due to an increase in regional aridity [*Weiss et al.*, 1993]. Similar climatic related collapses or transformations within ancient societies around 4.2 ka BP have also been documented in different regions across the northern hemisphere [*Liu and Feng*, 2012; *Staubwasser et al.*, 2003; *Welc and Marks*, 2014] including southern Iberia [*Schirrmacher et al.*, 2020; *Valera*, 2015]. Accordingly, the narrative of a megadrought affecting ancient societies across Asia, the Mediterranean, and northeast Africa arose [*Weiss*, 2015, 2016].

Such a first evidence of climate related collapses or transformations in ancient societies have promoted intense investigations of the "climatic" 4.2 ka BP event, which resulted in a variety of associated paleo-climatic studies from the Mediterranean area [*Bini et al.*, 2019; *Kaniewski et al.*, 2018; *Schirrmacher et al.*, 2019; *Schirrmacher et al.*, 2020], Asia [*Giesche et al.*, 2019; *Kathayat et al.*, 2018; *Zhang et al.*, 2018], North America [*Booth et al.*, 2005], the northern North Atlantic region [*Bradley and Bakke*, 2019; *Geirsdóttir et al.*, 2019; *Jalali et al.*, 2019], and the southern hemisphere as well [*Li et al.*, 2018; *Railsback et al.*, 2018]. Altogether, paleo-climatic studies point to a series of climatic anomalies between 3800 and 4400 cal. BP, which across the Mediterranean region are often registered as dry and cool events [*Bini et al.*, 2019; *Schirrmacher et al.*, 2020].

However, potential drivers of the more widespread drier and cooler climate periods across the mid-latitudes of the northern hemisphere are not yet understood. Since the North Atlantic Oscillation (NAO) is modulating winter precipitation across large parts of the Mediterranean region, in particular the Western Mediterranean [*Lionello*, 2012; *Trigo et al.*, 2004], it is often regarded as one important driver for drought associated with the 4.2 ka BP event [*Ramos-Román et al.*, 2018; *Schirrmacher et al.*, 2019; *Zielhofer et al.*, 2017]. At that time, a major NAO-like forcing is also suggested by modelling studies [*Yan and Liu*, 2019]. On the other hand, recent studies have indicated that the 4.2 ka BP event in the Mediterranean region could have been more pronounced during the summer season [*Baldini et al.*, 2019; *Bini et al.*, 2019; *Schirrmacher et al.*, 2020]. Thus, the search for a potential driver of the climatic 4.2 ka BP event particularly in the Western Mediterranean region has to include seasonal variability with Atlantic winter versus Mediterranean summer forcing.

To shade further light on the potential driver of climate variability around 4.2 ka BP, we investigate the temporal variability of the interaction between Atlantic and Mediterranean climatic regimes. Therefore, we analysed compound-specific hydrogen and carbon isotopes from land-derived *n*-alkanes as tracer of past atmospheric circulation patterns in a well-suited marine sediment core from the Alboran Sea – an area actually located at the interface of Atlantic and Mediterranean climate regimes (Fig 7.1).

7.2.1 Study area

Modern climate at the Iberian Peninsula is characterized by a large seasonality in both, atmospheric temperature and precipitation. In the southeast, annual mean atmospheric temperature ranges between 2.5 and 20 °C depending on the altitude, while summer

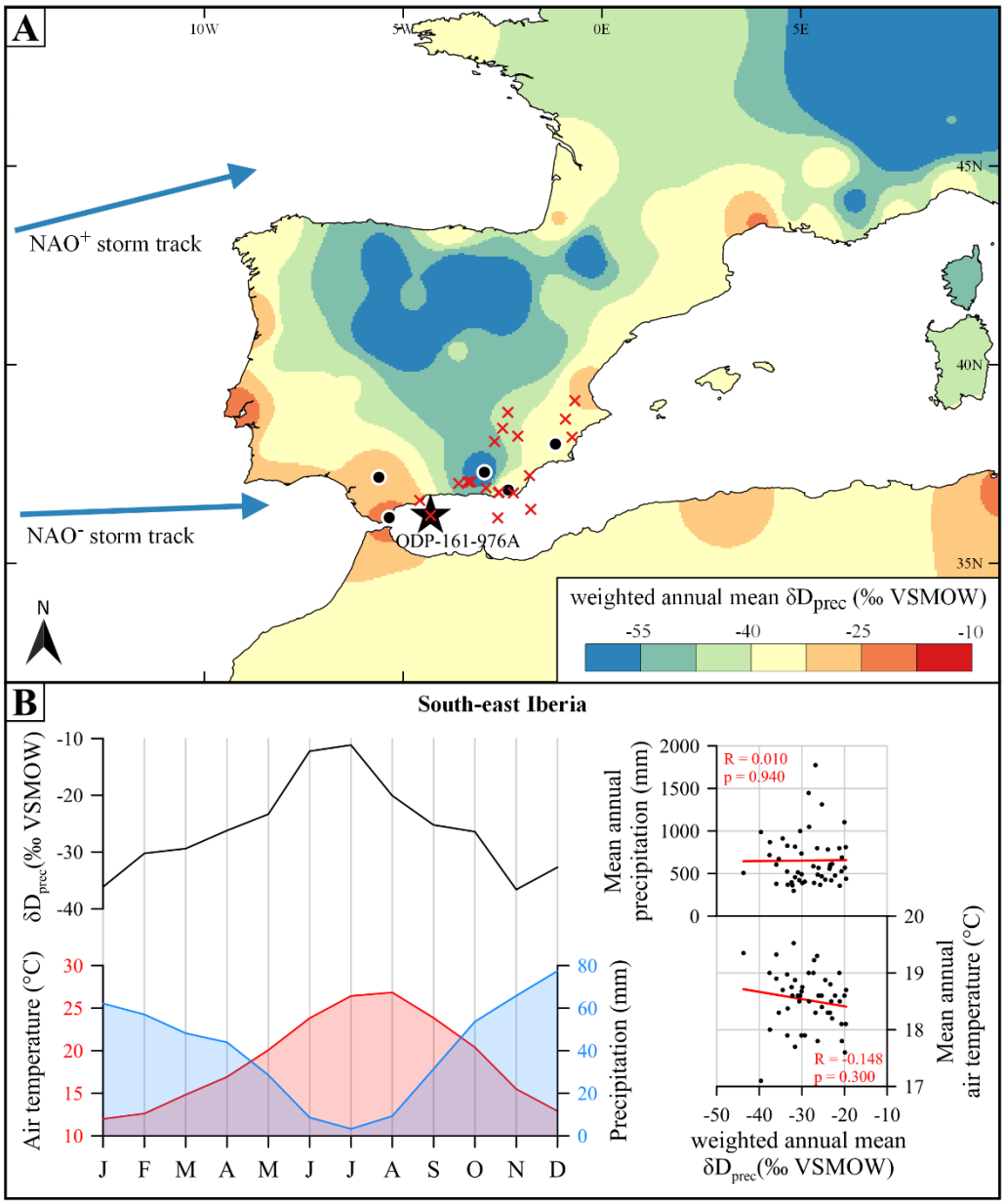

Figure 7.1 Study area. *A) Map showing the spatial distribution of weighted long-term (1961-2016) annual mean hydrogen isotopic composition of precipitation (δD_{prec}). The raw data was downloaded from the Global Network of Isotopes in Precipitation (GNIP) database and interpolated using an inverse distance weighted (IDW) approach (unlimited search radius and power value = 3.0). Black dots show locations of weather stations used for calculation of regional southeast Iberian climate parameters shown below. Star indicates the location of marine sediment core ODP-161-976A and red crosses locations of additional archives used for regional paleo-climatological analysis (see Tab 7.1 for more detailed information): Navarrés [Ilvonen et al., 2019], Villaverde [Carrión et al., 2001a], Villena [Jones et al., 2018], Siles [Carrión, 2002], El Sabinar [Carrión et al., 2004], Elx [Burjachs et al., 1997], Cañada de la Cruz [Carrión et al., 2001b], Antas [Pantaléon-Cano et al., 2003], Borreguil de la Virgen [Jiménez-Moreno and Anderson, 2012], Laguna Hondera [Mesa-Fernández et al., 2018], Laguna de Río Seco [Anderson et al., 2011], Padul [Ramos-Román et al., 2018], Sierra de Gádor [Carrión et al., 2003], Roquetas de Mar [Pantaléon-Cano et al., 2003], San Rafael [Pantaléon-Cano et al., 2003], Cabo de Gata [Burjachs and Expósito, 2015], El Refugio [Walczak et al., 2015], TTR14-300G [Cortés-Sánchez et al., 2011], ODP-161-976A [Combourieu Nebout et al., 2009; Schirrmacher et al., 2019] and, MD95-2043 [Bini et al., 2019; Fletcher and Sánchez Goñi, 2008; Fletcher et al., 2010; Peyron et al., 2017]. Blue arrows indicate the main storm track of the westerlies during positive (NAO^+) and negative North Atlantic Oscillation (NAO^-) B) Average seasonal air temperature, precipitation and, δD_{prec} of southeast Iberia (left) as well as the correlation of their annual means (right).*

temperatures range between 8 and 28 °C and winter temperatures vary between -5 and 15 °C [*Fick and Hijmans*, 2017]. Annual precipitation in the area fluctuates between 150 mm at Cabo de Gata and 1900 mm at Gibraltar [*Fick and Hijmans*, 2017]. Summer precipitation ranges from 0 to 50 mm per month and winter precipitation from 15 to 300 mm per month [*Fick and Hijmans*, 2017]. The spatial distribution of precipitation at the Iberian Peninsula is driven by the interaction of the Atlantic and Mediterranean atmospheric regimes with regions dominated by the Mediterranean regime experiencing significantly less precipitation [*Lionello*, 2012]. This is particularly true for the Sierra Nevada region in the southeast adjacent to the Alboran Sea, which, recently is the driest area of whole Europe. The temporal variability of precipitation on the entire Iberian Peninsula, on the other hand, is mainly controlled by the North Atlantic Oscillation (NAO), which primarily transports moisture from the Atlantic during the winter season [*Hernández et al.*, 2015; *Hurrell*, 1995; *Trigo et al.*, 2004]. During positive NAO (NAO+; i.e. a high difference in sea level pressure between the Azores and Iceland) most of the Iberian Peninsula, including the southeast, experiences drier conditions, because the main storm track of the westerlies lead towards northern and central Europe (Fig 7.1), and *vice versa*. The scarce precipitation during the summer season, when the NAO driven influence is less pronounced [*Barnston and Livezey*, 1987], is mainly driven by mesoscale synoptic patterns and local convective systems [*Araguas-Araguas and Diaz Teijeiro*, 2005]. These are responsible for short torrential rainfall events, which are particularly evident along the Mediterranean coast during times of a high land-sea temperature contrast [*Araguas-Araguas and Diaz Teijeiro*, 2005].

These two precipitation sources (Atlantic and Mediterranean) are also reflected in the spatial distribution of the hydrogen isotopic composition within the weighted long-term annual mean precipitation (δD_{prec}; Fig 7.1). In the Atlantic dominated areas weighted annual mean δD_{prec} values are typically below -40 ‰ VSMOW, while coastal areas, which are more intensely affected by Mediterranean precipitation sources, vary between -15 and -35 ‰ VSMOW. Moreover, southeast Iberian δD_{prec} values show no significant correlation with precipitation amount or temperature on the annual scale (Fig 7.1). However, on the monthly scale δD_{prec} values are highly correlated with precipitation amount ($R = -0.928$; $p < 0.001$) and temperature ($R = 0.852$; $p < 0.001$) (not shown). This is because the precipitation source, which varies on a seasonal scale (Atlantic winter and Mediterranean summer), is responsible for the observed seasonal variability of δD_{prec} values in southeast Iberia [*Araguas-Araguas and Diaz Teijeiro*, 2005].

7.2.2 Compound-specific isotopes as paleo-climatic proxy

Isotopic analyses of individual *n*-alkanes have been used extensively during the last years in tropical [*Kuechler et al.*, 2013; *Niedermeyer et al.*, 2010; Niedermeyer et al., 2016; *Schefuß et al.*, 2005] but also in Mediterranean regions [*Schäfer et al.*, 2018; *Schemmel et al.*, 2016; *Taylor et al.*, 2018] in order to assess terrestrial environmental and climatic parameters.

Analysing individual *n*-alkane homologues for carbon isotopes ($\delta^{13}C_{Cx}$) provides important information on the distribution of C3 and C4 plants [*Diefendorf and Freimuth*, 2017]. Due to their different photosynthetic pathway, C4 plants typically exhibit elevated $\delta^{13}C_{Cx}$ values varying between -20 to -15 ‰ VPDB compared to C3 plants, which vary between -45 to -30 ‰ VPDB [*Diefendorf and Freimuth*, 2017; *Schwab et al.*, 2015].

Moreover, the $\delta^{13}C_{Cx}$ values are needed for potential correction of the hydrogen isotopic data of the individual *n*-alkanes (δD_{Cx}) [*Gamarra et al.*, 2016; *Wang et al.*, 2013]. Despite of potential alteration through the vegetation type, the δD_{Cx} data is highly correlated with that of the water source, i.e. precipitation (δD_{prec}) during the plants growing season [*Sachse et al.*, 2012]. Additional factors controlling δD_{prec} and, thus, also δD_{Cx} are atmospheric temperature, the amount of rainfall, and evaporation [*Sachse et al.*, 2012; *Wirth and Sessions*, 2016]. Furthermore, δD_{Cx} data helps to differentiate between local precipitation sources with high δD_{prec} values and distant precipitation sources (low δD_{prec} values) [*Araguas-Araguas and Diaz Teijeiro*, 2005].

7.3 Materials and methods

7.3.1 Sediment core and age model

Sediment core ODP-161-976A (36°12.320’ N; 4°18.760’ W; 1108 m water depth) was retrieved in the Alboran Sea during the JOIDES RESOLUTION cruise in 1995 [*Comas et al.*, 1996]. The sampling of this sediment core was already described in a previous paper [*Schirrmacher et al.*, 2019]. To achieve multi-decadal resolution, the section from 100.0 to 149.0 cm was continuously sampled at 0.5 cm distances in the IODP (International Ocean Discovery Program) core repository at MARUM (Center for Marine Environmental Sciences) in Bremen (Germany). Also, the age model of sediment core ODP-161-976A has already been published in earlier publications [*Schirrmacher et al.*, 2019; *Schirrmacher et al.*, 2020]. The final age model of ODP-161-976A is based on 11 AMS ^{14}C dates. The sediment core

encompasses an analysed time period between ca. 3000 to 5750 cal. BP with a temporal resolution varying between 8 and 114 years for ODP-161-976A.

7.3.2 Sample preparation

The sample preparation of sediment core ODP-161-976A followed the protocol of the biomarker laboratory at Kiel University and has already been described in an earlier study [*Schirrmacher et al.*, 2019]. In short, *n*-alkanes were extracted from the freeze-dried and finely ground sediment samples with an accelerated solvent extractor (ASE-200, Dionex) at 100 bar and 100 °C using a 9:1 (v=v) mixture of dichloromethane (DCM) and methanol. After extraction samples were de-sulfured by stirring for 30 minutes with activated copper. The de-sulfured *n*-alkanes were subsequently separated by silica gel column chromatography using activated silica gel and hexane. *n*-Alkanes were further separated using silver nitrate ($AgNO_3$) coated silica gel. Subsequently, individual *n*-alkane homologues have been identified with an Agilent 6890N gas chromatograph equipped with a Restek XTI-5 capillary column (30 m x 320 µm x 0.25 µm) based on the comparison of their retention times with an external standard containing a series of *n*-alkane homologues of known concentration. On this basis, *n*-alkanes were also quantified using the FID peak areas calibrated against the external standard.

7.3.3 Compound-specific isotope analysis

After quantification, terrestrial-sourced *n*-alkane homologues of sufficient concentration (i.e. *n*-C_{29}, *n*-C_{31}, and *n*-C_{33}) have been analysed by gas chromatography-isotope ratio mass spectrometry (GC-IRMS) for δD and $\delta^{13}C$ at the Leibniz Laboratory for Radiometric Dating and Stable Isotope Research at Kiel University. Samples have been measured on an Agilent 6890 gas chromatograph equipped with a Gerstel KAS 4 PTV injector and an Agilent DB-5 capillary column (30 m x 250 µm x 0.25 µm) coupled to a Thermo Scientific MAT 253 isotope ratio mass spectrometer (IRMS). Depending on the *n*-alkane concentration, between 5 and 30 µl of each sample has been injected 2-4 times in order to achieve a statistically robust analytical error for each *n*-alkane homologue. The δD and $\delta^{13}C$ values are reported relative to Vienna Standard Mean Ocean Water (‰ VSMOW) based on Arndt Schimmelmann's A6 reference mixture from 2015 and Vienna Pee Dee Belemnite (‰ VPDB) scales using Arndt Schimmelmann's A7 reference mixture from 2017, respectively. Long-term measurements of internal *n*-alkane standards yielded an analytical precision of ±3.0 ‰ for δD and ±0.3 ‰ for $\delta^{13}C$.

Table 7.4 Dataset used for the regional precipitation analysis.

Site	Season	Archive	Proxy	Reference
Antas	annual	terrestrial	Xerophytes	[*Pantaléon-Cano et al.*, 2003]
Borreguil de la Virgen	annual	lake	Artemisia	[*Jiménez-Moreno and Anderson*, 2012]
Cañada de la Cruz	annual	lake	Xerophytes	[*Carrión et al.*, 2001b]
El Refugio Cave	annual	speleothem	Stalagmite density	[*Walczak et al.*, 2015]
El Sabinar	annual	terrestrial	Xerophytes	[*Carrión et al.*, 2004]
Elx	annual	terrestrial	Xerophytes	[*Burjachs et al.*, 1997]
Laguna de Río Seco	annual	lake	Artemisia	[*Anderson et al.*, 2011]
Laguna Hondera	annual	lake	Ca/Ti ratio	[*Mesa-Fernández et al.*, 2018]
MD95-2043	annual	marine	MAT on pollen	[*Bini et al.*, 2019; *Fletcher and Sánchez Goñi*, 2008; *Fletcher et al.*, 2010; *Peyron et al.*, 2017]
MD95-2043	annual	marine	Xerophytes	[*Fletcher and Sánchez Goñi*, 2008]
Navarrés	annual	terrestrial	WAPLS on pollen	[*Ilvonen et al.*, 2019]
ODP-161-976A	annual	marine	MAT on pollen	[*Combourieu Nebout et al.*, 2009; *Schirrmacher et al.*, 2020]
Padul	annual	terrestrial	Xerophytes	[*Ramos-Román et al.*, 2018]
Roquetas de Mar	annual	terrestrial	Xerophytes	[*Pantaléon-Cano et al.*, 2003]
San Rafael	annual	terrestrial	Xerophytes	[*Pantaléon-Cano et al.*, 2003]
San Rafael	annual	terrestrial	WAPLS on pollen	[*Ilvonen et al.*, 2019]
Sierra de Gádor	annual	lake	Xerophytes	[*Carrión et al.*, 2003]
Siles	annual	lake	Xerophytes	[*Carrión*, 2002]
TTR14-300G	annual	marine	La/Lu ratio	[*Cortés-Sánchez et al.*, 2011]
Villaverde	annual	terrestrial	Xerophytes	[*Carrión et al.*, 2001a]
Antas	winter	terrestrial	arboreal pollen	[*Pantaléon-Cano et al.*, 2003]
Borreguil de la Virgen	winter	lake	arboreal pollen	[*Jiménez-Moreno and Anderson*, 2012]
Cañada de la Cruz	winter	lake	arboreal pollen	[*Carrión et al.*, 2001b]
Cabo de Gata	winter	terrestrial	arboreal pollen	[*Burjachs and Expósito*, 2015]
Elx	winter	terrestrial	arboreal pollen	[*Burjachs et al.*, 1997]
Laguna de Río Seco	winter	lake	arboreal pollen	[*Anderson et al.*, 2011]
MD95-2043	winter	marine	MAT on pollen	[*Bini et al.*, 2019; *Fletcher and Sánchez Goñi*, 2008; *Fletcher et al.*, 2010; *Peyron et al.*, 2017]
MD95-2043	winter	marine	arboreal pollen	[*Fletcher and Sánchez Goñi*, 2008]
ODP-161-976A	winter	marine	n-C_{C27-33}	[*Schirrmacher et al.*, 2019; *Schirrmacher et al.*, 2020]
ODP-161-976A	winter	marine	MAT on pollen	[*Combourieu Nebout et al.*, 2009; *Schirrmacher et al.*, 2020]
Padul	winter	terrestrial	arboreal pollen	[*Ramos-Román et al.*, 2018]
Roquetas de Mar	winter	terrestrial	arboreal pollen	[*Pantaléon-Cano et al.*, 2003]
San Rafael	winter	terrestrial	arboreal pollen	[*Pantaléon-Cano et al.*, 2003]
Sierra de Gádor	winter	lake	arboreal pollen	[*Carrión et al.*, 2003]
Villaverde	winter	terrestrial	arboreal pollen	[*Carrión et al.*, 2001a]
Villena	winter	terrestrial	pollen aridity ratio	[*Jones et al.*, 2018]

7.3.4 Regional analysis

The regional analysis of the past seasonal precipitation development is based on a compilation of various climatic proxies from speleothems, marine, lacustrine, and terrestrial archives from

the Iberian Peninsula published in a previous paper [*Schirrmacher et al.*, 2020]. Here, this compilation has been regionally subsampled for the southeast of the Iberian Peninsula with 20 records reflecting annual and 16 records reflecting winter precipitation variability (Tab 7.1; Fig 7.1). The z-scores [*Clark-Carter*, 2014] of all paleo-climatic proxies reflecting either annual or winter precipitation have been combined to a regional time-series of qualitative annual and winter precipitation change. Prior to analysis the speleothem data of El Refugio Cave [*Walczak et al.*, 2015], which has an average temporal resolution of 3 years, has been downscaled to a temporal resolution of 50 years. The calculation of 50-year means prevents the over-representation of this archive in the regional time-series since it had a much higher temporal resolution compared to all other archives. The regional time-series have then been smoothed using a symmetric LOESS smooth with a 2nd order polynomial and a smoothing parameter of 0.1. In order to acquire also a measure of qualitative summer precipitation changes, the difference between the annual and the winter smoothed time-series has been calculated.

7.4 Results

Cumulative concentrations of odd terrestrial *n*-alkanes (*n*-C_{27}, *n*-C_{29}, *n*-C_{31}, and *n*-C_{33}) have been analysed for variability in winter precipitation amount (*n*-C_{C27-33}) (Fig 7.2). The *n*-C_{C27-33} concentration reveals no long-term trend and varies between 713.5 and 66.6 ng/ g sediment. Altogether, four periods of *n*-C_{C27-33} concentration below 250 ng/ g sediment have been identified around 3500, 4800, 5000, and 5700 cal. BP.

Carbon and hydrogen isotopic data of three *n*-alkane homologues (*n*-C_{29}, *n*-C_{31}, and *n*-C_{33}) are presented for the period between ca. 3000 and 5800 cal. BP. In this interval, the carbon isotopic values of the *n*-C_{29} homologue ($\delta^{13}C_{C29}$) vary between -31.4 and -32.3 ‰ VPDB (Fig 7.2). $\delta^{13}C_{C31}$ values vary between -30.5 and -31.7 ‰ VPDB, while $\delta^{13}C_{C33}$ values range from -29.5 to -31.6 ‰ VPDB. There is no obvious trend in any of the carbon isotopic time series, but average values progressively increase with increasing chain length. $\delta^{13}C_{C29}$ values exhibit an average of -31.9 ‰ VPDB, while $\delta^{13}C_{C31}$ values vary around a mean of -31.3 ‰ VPDB and $\delta^{13}C_{C33}$ values are on average -30.5 ‰ VPDB (Fig 7.2).

Within the studied timespan, the hydrogen isotopic values vary between -137.3 and -157.5 ‰ VSMOW for the *n*-C_{29} homologue (δD_{C29}), between -141.7 and -160.8 ‰ VSMOW for δD_{C31}, and between -113.8 and -139.9 ‰ VSMOW for δD_{C33} (Fig 7.2). While the absolute values and the amplitude of δDC_{29} and δD_{C31} are similar, δD_{C33} values are slightly higher and their

variability is of larger amplitude. Apart from these differences, hydrogen isotopic values of all three homologues covary in the analysed period. Due to the larger amplitude in variability within the δD_{C33} data, periods of high and low isotopic values can be distinguished. High δD_{C33} values (-125.9 ‰ VSMOW on average) are evident at 3000, from 3300 to 3400, from 4300 to 5100, and around 5400 cal. BP. In contrast, low δD_{C33} values averaging -132.6 ‰ VSMOW are noticed from 3400 to 4200, at 5300, and at 5500 cal. BP.

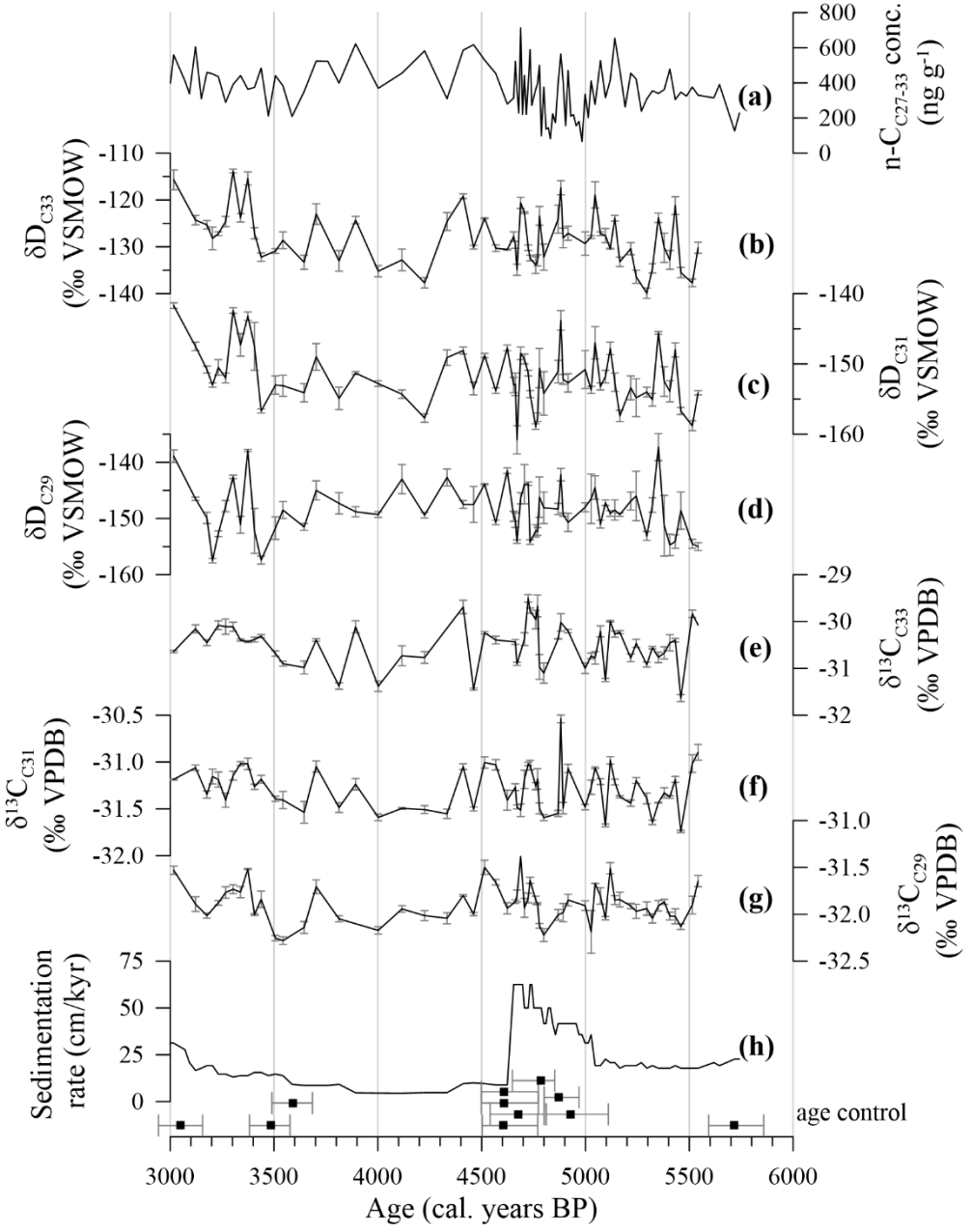

Figure 7.2 Molecular and isotopic n-alkane data from ODP-161-976A. *(a) Terrestrial n-alkane concentration (n-C_{C27-33}), hydrogen isotopic data of individual n-alkane homologues (b) δD_{C33}, (c) δD_{C31}, and (d) δD_{C29}, carbon isotopic data of individual n-alkane homologues (e) $\delta^{13}C_{C33}$, (f) $\delta^{13}C_{C31}$, and (g) $\delta^{13}C_{C29}$, and (h) sedimentation rate. Black squares show calibrated AMS ^{14}C dates and their according uncertainties.*

7.5 Discussion

7.5.1 Drivers of hydrogen isotopic variability

Variability of hydrogen isotopic data from individual *n*-alkane homologues is potentially driven by five major parameters, which are changes in (1) vegetation types, (2) precipitation amount, (3) atmospheric temperature, (4) evaporation, and (5) precipitation source [*Gamarra et al.*, 2016; *Sachse et al.*, 2012; *Wirth and Sessions*, 2016]. In the following, we conclude that the variability of hydrogen isotopic values from individual *n*-alkanes originating from southeast Iberia and deposited in marine sediment core ODP-161-976A is primarily driven by changes in the source of precipitation.

Several studies have highlighted the dependence of *n*-alkane hydrogen isotopic composition on the distribution of C3 and C4 plants in modern [*Garcin et al.*, 2012] and paleo-climatic studies [*Collins et al.*, 2013; *Nelson et al.*, 2013; *Wang et al.*, 2013]. This is due to the different photosynthetic regulatory pathways of these plant types, which results in a different apparent fractionation between the hydrogen isotopic value of precipitation (δD_{prec}) and that of *n*-alkanes (δD_{Cx}) [*Gamarra et al.*, 2016]. Any variation in the C3 vs. C4 plant distribution can be tested in parallel through *n*-alkane $\delta^{13}C$ values. Typically, C4 plants exhibit $\delta^{13}C_{Cx}$ values between -20 to -15 ‰ VPDB, while $\delta^{13}C_{Cx}$ values of C3 plants vary between -45 to -30 ‰ VPDB [*Diefendorf and Freimuth*, 2017; *Schwab et al.*, 2015]. In our case, the similarity and very low variability in absolute values for all three compound-specific carbon isotopic data ($\delta^{13}C_{C29}$, $\delta^{13}C_{C31}$, and $\delta^{13}C_{C33}$) in sediment core ODP-161-976A suggest a dominant C3 vegetation cover throughout the entire period (Fig 7.2). This is in line with various pollen records from southeast Iberia, which show a dominance of C3 vegetation and no major change towards increased C4 vegetation between 3000 and 6000 cal. BP [*Combourieu Nebout et al.*, 2009; *Fletcher and Sánchez Goñi*, 2008; *Ramos-Román et al.*, 2018]. Furthermore, $\delta^{13}C$ and δD values within each *n*-alkane homologue are not correlated at significant level, with the exception of the *n*-C_{31} homologue revealing a significant but moderate correlation (Tab 7.2). This rules out any significant changes in plant types that may have affected the hydrogen isotopic data at the core site.

Other crucial parameters driving the hydrogen isotopic signal of *n*-alkanes are changes in atmospheric temperature and precipitation amount [*Sachse et al.*, 2012]. Meteorological data from the southeast Iberian Peninsula implies a general connection of δD_{prec} values to modern changes in the amount of precipitation and atmospheric temperature on a monthly scale (Fig 7.1). However, no significant statistical correlation of δD_{prec} values with precipitation amount

(R = 0.01, p = 0.94) and atmospheric temperature (R = -0.15, p = 0.30) exists during modern times on the annual scale (Fig 7.1). Moreover, there is also no significant correlation between all three compound-specific hydrogen isotope records and their concentration as well as with other ODP-161-976A data such as the cumulative *n*-C_{C27-33} concentrations (reflecting changes in winter precipitation amount) and alkenone-based annual mean SST (Tab 7.2), which are closely coupled to atmospheric temperature variability in southeast Iberia [*Schirrmacher et al.*, 2020]. The only exception are δD_{C33} values that show a significant moderate correlation with *n*-C_{33} concentrations (Tab 7.2).

Table 7.5 Correlation of paleo-climatological parameters from ODP-161-976A. *Correlation indices are given for the hydrogen isotopes of every individual n-alkane and their carbon isotopic values, their individual concentrations, cumulative concentration of long-chained odd n-alkanes, and the alkenone-based SST. Cross-plots of each individual parameter are provided in the supplement of this article.*

	δD_{C29}	**δD_{C31}**	**δD_{C33}**
n-C_x conc.	R = 0.045; p = 0.725	R = 0.084; p = 0.529	R = 0.367; p = 0.004
$\delta^{13}C_{Cx}$	R = 0.176; p = 0.196	R = 0.363; p = 0.005	R = 0.245, p = 0.073
n-C_{C27-33} conc.	R = 0.032; p = 0.860	R = 0.089; p = 0.501	R = 0.226; p = 0.083
alkenone SST	R = 0.184; p = 0.160	R = 0.114; p = 0.382	R = 0.100; p = 0.440

Another potential effect related to precipitation amount and temperature, which may alter δD_{Cx} values, is evaporation [*Gamarra et al.*, 2016]. Under the semi-arid climate in southeast Iberia evaporation potentially is an important parameter to be considered, when interpreting δD_{Cx} data. Therefore, it is interesting to note that there is an offset in absolute δD_{Cx} values between the *n*-C_{33} homologue and the *n*-C_{29} and *n*-C_{31} homologues of ca. 25 ‰ VSMOW (Fig 7.2). It is also obvious that the $\delta^{13}C_{Cx}$ values progressively increase by on average 1.5 ‰ VPDB from the *n*-C_{29} to the *n*-C_{33} homologue (Fig 7.2), suggesting that an overall higher C4 plant proportion within the *n*-C_{33} alkane might account for the higher δD_{C33} values [*Garcin et al.*, 2012]. In addition, the *n*-C_{33} alkane is dominantly produced by grasses, while the *n*-C_{29} alkane is dominant in trees [*Bush and McInerney*, 2013; *Kirkels et al.*, 2013]. As grasses have shallower rooting systems compared to trees, they are much more affected by evaporation from the soils, which also may increase their hydrogen isotopic values [*Dawson and Pate*, 1996; *Sachse et al.*, 2012]. But, the high covariation of all three δD_{Cx} records suggests that evaporation exerted no major impact on the centennial-scale variability. It may be a reason for the observed offset in average hydrogen isotopic values between the *n*-C_{33} *n*-alkane and the other two homologues, though.

Thus, we assume that precipitation amount, atmospheric temperature, and related evaporation have not been dominant drivers for the observed *n*-alkane hydrogen variability in ODP-161-976A during the analysed period. Another potential driver is the source of precipitation [*Wirth and Sessions*, 2016]. Indeed, modern analyses of meteorological data from the Western Mediterranean indicate that δD_{prec} values in the area depend on the source of precipitation with Atlantic derived precipitation exhibiting significantly lower δD_{prec} values compared to more Mediterranean derived precipitation [*Araguas-Araguas and Diaz Teijeiro*, 2005; *Ouda et al.*, 2005]. Since Atlantic sourced precipitation on the Iberian Peninsula is much more prominent during the winter season [*Araguas-Araguas and Diaz Teijeiro*, 2005; *Fick and Hijmans*, 2017], changes in precipitation source likely account for the apparent correlation of monthly δD_{prec} values with the monthly variability of atmospheric temperature and precipitation amount (Fig 7.1). *n*-Alkane δD values were also considered to reflect changes in the precipitation source by previous paleo-climatic studies from the Iberian Peninsula [*Schäfer et al.*, 2018; *Taylor et al.*, 2018]. Accordingly, we conclude that the dominant parameter driving hydrogen isotopic variability of individual *n*-alkanes in marine sediment core ODP-161-976A is the source of precipitation with low δD_{Cx} values reflecting increasing Atlantic derived precipitation and high δD_{Cx} values reflecting an increase in Mediterranean sourced precipitation.

Moreover, we have shown that evaporation and related climatic parameters are unlikely to be responsible for the observed centennial-scale variability in δD_{Cx} values. Thus, we attribute the high amplitude variability in hydrogen isotopic values of the *n*-C_{33} alkane to a higher sensitivity to short-term paleo-climatic variability due to the shallower rooting systems of grasses compared to trees [*Dawson and Pate*, 1996]. Thus, for further comparison we focus on the δD_{C33} data due to its higher sensitivity.

7.5.2 Over-regional driver of climate variability

Based on high δD_{C33} values we define three major periods of enhanced Mediterranean sourced precipitation (Fig 7.3). These range from 3250 to 3400 cal. BP, from 4300 to 5150 cal. BP, and from 5350 to 5450 cal. BP. These periods of enhanced Mediterranean sourced precipitation well correspond to times of positive modes of the North Atlantic Oscillation (NAO^+) [*Olsen et al.*, 2012] and reduced Western Mediterranean storminess [*Dezileau et al.*, 2016; *Sabatier et al.*, 2012] (Fig 7.3). NAO^+ conditions would have favoured a northward shift of the Atlantic storm track towards northern and central Europe [*Hurrell*, 1995] (Fig 7.1). Consequently, this resulted in reduced storminess across the Western Mediterranean as evidenced by a clay mineral

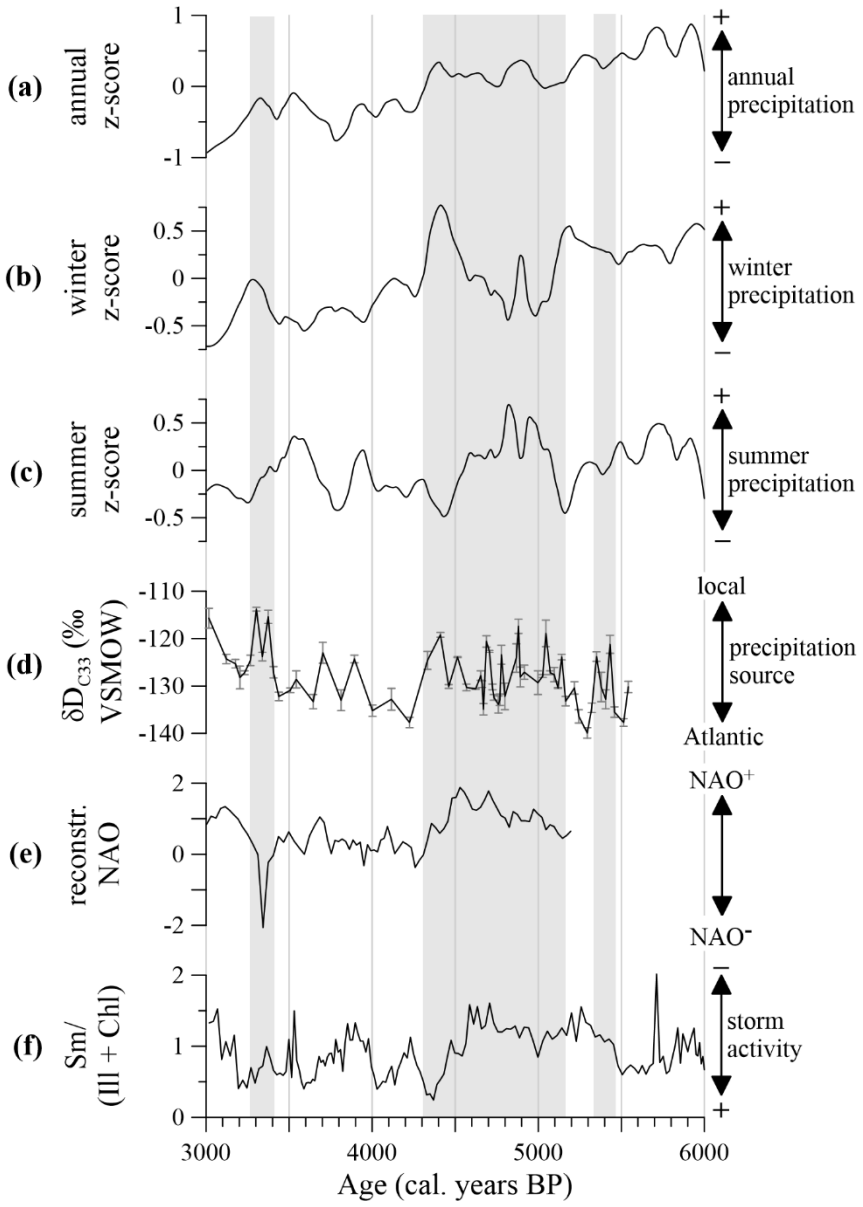

Figure 7.3 Atlantic versus Mediterranean influence. *(a) Regional z-score of annual precipitation variability, (b) regional z-score of winter precipitation variability, (c) regional z-score of summer precipitation variability, (d) hydrogen isotopes of the n-C_{33} n-alkane homologue, (e) reconstructed NAO from lake SS1200 in Greenland [Olsen et al., 2012], and (f) clay mineral ratio of Smectite (Sm), Illite (Ill), and Chlorite (Chl) from Gulf of Lions sediment core PB06 indicative of Western Mediterranean storminess [Sabatier et al., 2012]. Vertical grey bars indicate periods of increased Mediterranean precipitation in southeast Iberia based on the hydrogen isotopic data from ODP-161-976A.*

ratio from the Gulf of Lions [*Sabatier et al.*, 2012]. Along with the northward displacement of the Atlantic storm track the majority of Atlantic sourced precipitation was shifted to northern and central Europe [*Trigo et al.*, 2002]. This results in high δD_{C33} values as Atlantic sourced precipitation in southeast Iberia was reduced and the Mediterranean sourced precipitation gained more importance. The only exception is the period from 3250 to 3400 cal. BP, when the NAO reconstruction indicates a prominent change to a negative mode (NAO^-).

This overall relationship can be applied in more detail to the period of the climatic 4.2 ka BP event, which encompasses the period from 3800 to 4400 cal. BP. At around 4300/4400 cal. BP, the most prominent shift from a long-lasting period of increased Mediterranean sourced precipitation to an increase in Atlantic sourced precipitation is observed (Fig 7.3). Taken into account the uncertainties in the age models of the individual records, this shift is coincident with a change to more negative NAO conditions [*Olsen et al.*, 2012] and increased storminess in the Western Mediterranean [*Dezileau et al.*, 2016; *Sabatier et al.*, 2012]. Based on the modern precipitation seasonality and atmospheric circulation, the increase in Atlantic sourced precipitation after 4300 cal. BP would further imply an increased proportion of winter precipitation on the Iberian Peninsula [*Hernández et al.*, 2015; *Trigo et al.*, 2004]. Indeed, the overall decreasing trend in the regional winter precipitation over southeast Iberia is superimposed by a short-term increase around 4400 cal. BP (Fig 7.3). But, after 4300 cal. BP regional winter precipitation again followed the general trend towards drier conditions. Despite of this drying trend, winter precipitation between 3400 and 4300 cal. BP was rather stable revealing no high amplitude variability implying a stable Atlantic influence during winter. This stability is corroborated by the persistent low δD_{C33} values between 3400 and 4300 cal. BP.

But still, the rather stable regional winter precipitation cannot be the main reason for the sudden decrease in δD_{C33} values after 4400 cal. BP. Another option to increase the proportion of the winter precipitation and, thus, to decrease the δD_{C33} values is to significantly reduce the summer precipitation. Therefore, it is interesting to note that from our regional precipitation analysis a decrease in summer precipitation between 3800 and 4400 cal. BP culminating around 3800 and 4400 cal. BP is suggested (Fig 7.3). A significant decrease in summer precipitation around 3800 and 4400 cal. BP is corroborated by stalagmite records from northern Iberia [*Baldini et al.*, 2019]. Altogether, this implies a weakening of the Mediterranean influence during summer and, thus an increase in seasonality, which resulted in the sudden decrease of the δD_{C33} data observed at 4300/4400 cal. BP.

A potential large-scale atmospheric driver of summer precipitation variability might be the summer monsoon systems, in particular the West African Summer Monsoon (WASM). Dry conditions associated with the 4.2 ka BP event linked to a weakening of the summer monsoons were observed in Egypt [*Welc and Marks*, 2014], the Indus river valley [*Dutt et al.*, 2018; *Giesche et al.*, 2019], India [*Kathayat et al.*, 2018], and China [*Zhang et al.*, 2018]. But, a dramatic weakening of the WASM is already observed earlier at around 5000 cal. BP and not during the period of the 4.2 ka BP event [*deMenocal et al.*, 2000; *Weldeab et al.*, 2007]. Furthermore, modelling studies suggest that the WASM did not reach as far north as the Iberian

Peninsula during the Mid- Holocene [*Messori et al.*, 2018; *Patricola and Cook*, 2007; *Pausata et al.*, 2016]. However, all modelling studies agree with each other that the northward shift of the WASM belt and the regional increase in summer precipitation during the Mid- Holocene is underestimated by the climate models [*Pausata et al.*, 2016; *Perez-Sanz et al.*, 2014]. Accordingly, a potential impact of a WASM weakening associated with summer dry conditions during the 4.2 ka BP event on the south-eastern Iberian Peninsula may seem unlikely, but needs further investigation.

7.6 Conclusion

In order to investigate the interaction between Atlantic and Mediterranean climate at the south-eastern Iberian Peninsula during the Mid- to Late Holocene, compound-specific hydrogen (δD_{Cx}) and carbon isotopic records ($\delta^{13}C_{Cx}$) from *n*-alkanes have been analysed. Detailed comparison with $\delta^{13}C_{Cx}$ values, sea surface temperature variability, and changes in precipitation amount indicate that δD_{Cx} values analysed in this study are related to changes in the precipitation source. While low δD_{Cx} values are indicative of increased Atlantic origin, high δD_{Cx} values indicate a Mediterranean precipitation source.

Overall, δD_{Cx} variability appears closely related to the North Atlantic Oscillation (NAO) between 3000 and 6000 cal. BP with positive NAO modes resulting in reduced storm activity across the Western Mediterranean and an increase of Mediterranean sourced precipitation in southeast Iberia. During these phases, which occurred from 3250 to 3400 cal. BP, from 4300 to 5150 cal. BP, and from 5350 to 5450 cal. BP, also the amount of summer precipitation increased in southeast Iberia. According to this general relationship it can be concluded that the period of the 4.2 ka BP event (3800 to 4400 cal. BP) on the southeast of the Iberian Peninsula was a time of major centennial-scale climate variability including rapid changes towards reduced summer precipitation. These reductions in summer precipitation were related to a reduction of the Mediterranean influence during summer. While it is indicated that the NAO was at least not directly responsible for the reduced summer precipitation, a potential influence of the West African Summer Monsoon during this time needs further investigation.

7.7 Acknowledgements

This research was performed in the framework of the CRC 1266 “Scales of transformation”. Sample material has been provided by the IODP Core Repository at the MARUM – Center for Marine Environmental Sciences, University of Bremen, Germany. We thank Karsten Gramenz and Philipp Schindler for their enormous lab-work.

7.8 Supplement

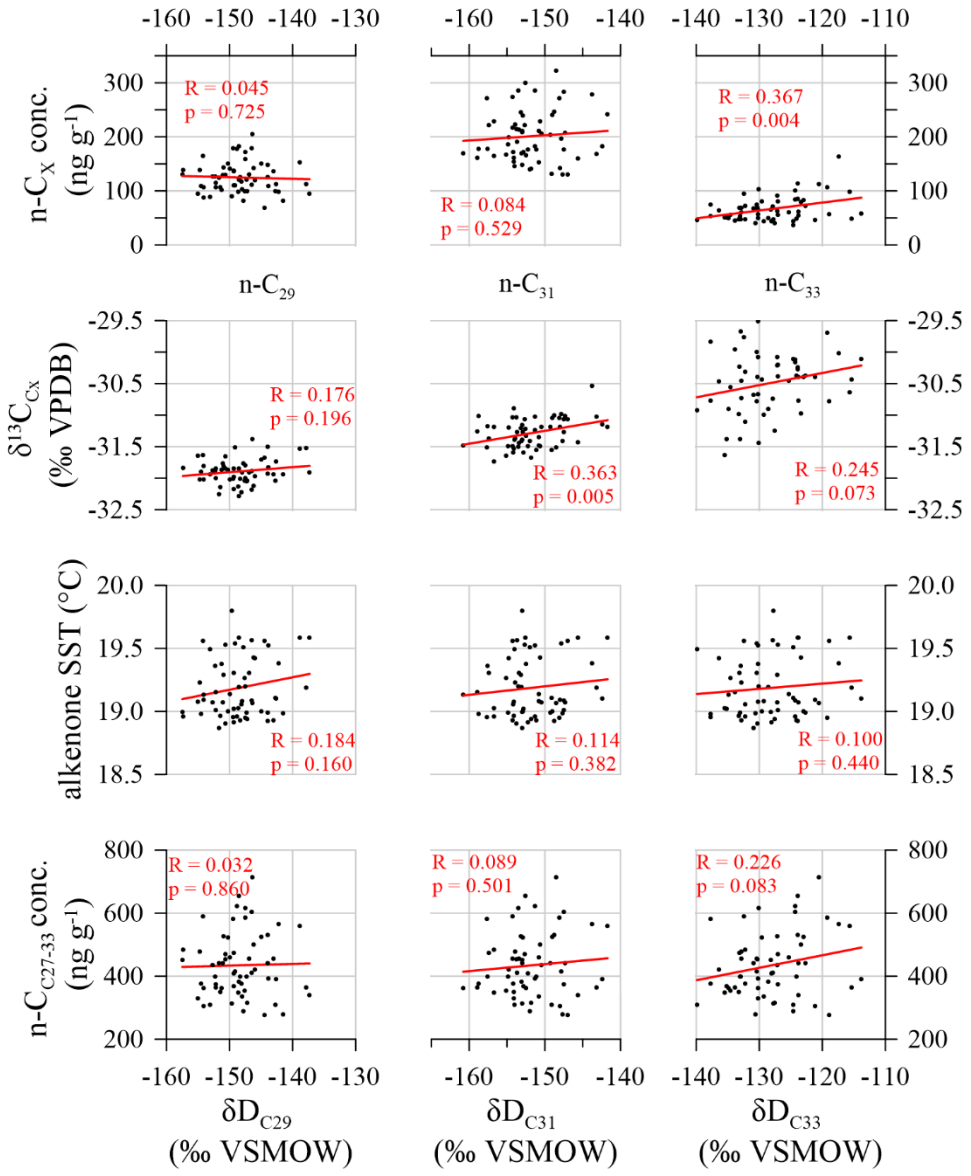

Figure 7.4 Supplementary figure S7.1. *Cross-plots and correlations of paleo-climatic parameters from sediment core ODP-161-976A.*

7.9 References

Anderson, R. S., G. Jiménez-Moreno, J. S. Carrión, and C. Pérez-Martínez (2011), Postglacial history of alpine vegetation, fire, and climate from Laguna de Río Seco, Sierra Nevada, southern Spain, *Quaternary Science Reviews*, *30*(13-14), 1615–1629, doi:10.1016/j.quascirev.2011.03.005.

Araguas-Araguas, L. J., and M. F. Diaz Teijeiro (2005), Isotope composition of precipitation and water vapour in the Iberian Peninsula, in *Isotopic composition of precipitation in the Mediterranean basin in relation to air circulation patterns and climate: Final report of a coordinated research project 2000-2004*, *IAEA-TECDOC*, vol. 1453, edited by International Atomic Energy Agency, pp. 173–190, IAEA, Vienna.

Baldini, L. M., J. U.L. Baldini, F. McDermott, P. Arias, M. Cueto, I. J. Fairchild, D. L. Hoffmann, D. P. Mattey, W. Müller, D. C. Nita, R. Ontañón, C. Garciá-Moncó, and D. A. Richards (2019), North Iberian temperature and rainfall seasonality over the Younger Dryas and Holocene, *Quaternary Science Reviews*, *226*, 105998, doi:10.1016/j.quascirev.2019.105998.

Barnston, A. G., and R. E. Livezey (1987), Classification, Seasonality and Persistence of Low-Frequency Atmospheric Circulation Patterns, *Mon. Wea. Rev.*, *115*(6), 1083–1126, doi:10.1175/1520-0493(1987)115<1083:CSAPOL>2.0.CO;2.

Bini, M., G. Zanchetta, A. Perşoiu, R. Cartier, A. Català, I. Cacho, J. R. Dean, F. Di Rita, R. N. Drysdale, M. Finnè, I. Isola, B. Jalali, F. Lirer, D. Magri, A. Masi, L. Marks, A. M. Mercuri, O. Peyron, L. Sadori, M.-A. Sicre, F. Welc, C. Zielhofer, and E. Brisset (2019), The 4.2 ka BP Event in the Mediterranean region: An overview, *Clim. Past*, *15*(2), 555–577, doi:10.5194/cp-15-555-2019.

Booth, R. K., S. T. Jackson, S. L. Forman, J. E. Kutzbach, E. A. Bettis, J. Kreigs, and D. K. Wright (2005), A severe centennial-scale drought in midcontinental North America 4200 years ago and apparent global linkages, *The Holocene*, *15*(3), 321–328, doi:10.1191/0959683605hl825ft.

Bradley, R. S., and J. Bakke (2019), Is there evidence for a 4.2 ka BP event in the northern North Atlantic region?, *Clim. Past*, *15*(5), 1665–1676, doi:10.5194/cp-15-1665-2019.

Burjachs, F., and I. Expósito (2015), Charcoal and pollen analysis: Examples of Holocene fire dynamics in Mediterranean Iberian Peninsula, *CATENA*, *135*, 340–349, doi:10.1016/j.catena.2014.10.006.

Burjachs, F., S. Giralt, J. R. Roca, G. Seret, and R. Julià (1997), Palinología holocénica y desertización en el Mediterráneo occidental., in *El paisaje mediterráneo a través del espacio y del tiempo.: Implicaiones en la desertificación.*, edited by J. J. Ibañez et al., pp. 379–394, Geoforma Editores, Logroño.

Bush, R. T., and F. A. McInerney (2013), Leaf wax n-alkane distributions in and across modern plants: Implications for paleoecology and chemotaxonomy, *Geochimica et Cosmochimica Acta*, *117*, 161–179, doi:10.1016/j.gca.2013.04.016.

Carrión, J. S. (2002), Patterns and processes of Late Quaternary environmental change in a montane region of southwestern Europe, *Quaternary Science Reviews*, *21*(18-19), 2047–2066, doi:10.1016/S0277-3791(02)00010-0.

Carrión, J. S., A. Andrade, K. D. Bennett, C. Navarro, and M. Munuera (2001a), Crossing forest thresholds: inertia and collapse in a Holocene sequence from south-central Spain, *The Holocene*, *11*(6), 635–653.

Carrión, J. S., M. Munuera, M. Dupré, and A. Andrade (2001b), Abrupt vegetation changes in the Segura Mountains of southern Spain throughout the Holocene, *J Ecol*, *89*(5), 783–797, doi:10.1046/j.0022-0477.2001.00601.x.

Carrión, J. S., P. Sánchez-Gómez, J. F. Mota, R. Yll, and C. Chaín (2003), Holocene vegetation dynamics, fire and grazing in the Sierra de Gádor, southern Spain, *The Holocene*, *13*(6), 839–849, doi:10.1191/0959683603hl662rp.

Carrión, J. S., E. I. Yll, K. J. Willis, and P. Sánchez (2004), Holocene forest history of the eastern plateaux in the Segura Mountains (Murcia, southeastern Spain), *Review of Palaeobotany and Palynology*, *132*(3-4), 219–236, doi:10.1016/j.revpalbo.2004.07.002.

Clark-Carter, D. (2014), z Scores, in *Wiley StatsRef: Statistics Reference Online*, edited by N. Balakrishnan, p. 44, Wiley, [Erscheinungsort nicht ermittelbar].

Collins, J. A., E. Schefuß, S. Mulitza, M. Prange, M. Werner, T. Tharammal, A. Paul, and G. Wefer (2013), Estimating the hydrogen isotopic composition of past precipitation using leaf-waxes from western Africa, *Quaternary Science Reviews*, *65*, 88–101, doi:10.1016/j.quascirev.2013.01.007.

Comas, M. C., R. Zahn, and A. Klaus (Eds.) (1996), *Proceedings of the Ocean Drilling Program, 161 Initial Reports*, *Proceedings of the Ocean Drilling Program*, vol. 161, Ocean Drilling Program.

Combourieu Nebout, N., O. Peyron, I. Dormoy, S. Desprat, C. Beaudouin, U. Kotthoff, and F. Marret (2009), Rapid climatic variability in the west Mediterranean during the last 25 000 years from high resolution pollen data, *Clim. Past*, *5*(1), 671–707, doi:10.5194/cpd-5-671-2009.

Cortés-Sánchez, M., A. Morales-Muñiz, M. D. Simón-Vallejo, M. C. Lozano-Francisco, J. L. Vera-Peláez, C. Finlayson, J. Rodríguez-Vidal, A. Delgado-Huertas, F. J. Jiménez-Espejo, F. Martínez-Ruiz, M. A. Martínez-Aguirre, A. J. Pascual-Granged, M. M. Bergadà-Zapata, J. F. Gibaja-Bao, J. A. Riquelme-Cantal, J. A. López-Sáez, M. Rodrigo-Gámiz, S. Sakai, S. Sugisaki, G. Finlayson, D. A. Fa, and N. F. Bicho (2011), Earliest known use of marine resources by Neanderthals, *PloS one*, *6*(9), e24026, doi:10.1371/journal.pone.0024026.

Dawson, T. E., and J. S. Pate (1996), Seasonal water uptake and movement in root systems of Australian phraeatophytic plants of dimorphic root morphology: A stable isotope investigation, *Oecologia*, *107*(1), 13–20, doi:10.1007/BF00582230.

deMenocal, P., J. Ortiz, T. Guilderson, J. Adkins, M. Sarnthein, L. Baker, and M. Yarusinsky (2000), Abrupt onset and termination of the African Humid Period, *Quaternary Science Reviews*, *19*(1-5), 347–361, doi:10.1016/S0277-3791(99)00081-5.

Dezileau, L., A. Pérez-Ruzafa, P. Blanchemanche, J.-P. Degeai, O. Raji, P. Martinez, C. Marcos, and U. von Grafenstein (2016), Extreme storms during the last 6500 years from lagoonal sedimentary archives in the Mar Menor (SE Spain), *Clim. Past*, *12*(6), 1389–1400, doi:10.5194/cp-12-1389-2016.

Diefendorf, A. F., and E. J. Freimuth (2017), Extracting the most from terrestrial plant-derived n -alkyl lipids and their carbon isotopes from the sedimentary record: A review, *Organic Geochemistry*, *103*, 1–21, doi:10.1016/j.orggeochem.2016.10.016.

Dutt, S., A. K. Gupta, B. Wünnemann, and D. Yan (2018), A long arid interlude in the Indian summer monsoon during ~4,350 to 3,450 cal. yr BP contemporaneous to displacement of the Indus valley civilization, *Quaternary International*, *482*, 83–92, doi:10.1016/j.quaint.2018.04.005.

Fick, S. E., and R. J. Hijmans (2017), WorldClim 2: New 1-km spatial resolution climate surfaces for global land areas, *Int. J. Climatol.*, *37*(12), 4302–4315, doi:10.1002/joc.5086.

Fletcher, W. J., M. F. Sanchez Goñi, O. Peyron, and I. Dormoy (2010), Abrupt climate changes of the last deglaciation detected in a Western Mediterranean forest record, *Clim. Past*, *6*(2), 245–264, doi:10.5194/cp-6-245-2010.

Fletcher, W. J., and M. F. Sánchez Goñi (2008), Orbital- and sub-orbital-scale climate impacts on vegetation of the western Mediterranean basin over the last 48,000 yr, *Quat. res.*, *70*(03), 451–464, doi:10.1016/j.yqres.2008.07.002.

Gamarra, B., D. Sachse, and A. Kahmen (2016), Effects of leaf water evaporative ^{2}H-enrichment and biosynthetic fractionation on leaf wax n-alkane δ^{2}H values in C3 and C4 grasses, *Plant, Cell and Environment*, *39*(11), 2390–2403, doi:10.1111/pce.12789.

Garcin, Y., V. F. Schwab, G. Gleixner, A. Kahmen, G. Todou, O. Séné, J.-M. Onana, G. Achoundong, and D. Sachse (2012), Hydrogen isotope ratios of lacustrine sedimentary n-alkanes as proxies of tropical African hydrology: Insights from a calibration transect across Cameroon, *Geochimica et Cosmochimica Acta*, *79*, 106–126, doi:10.1016/j.gca.2011.11.039.

Geirsdóttir, Á., G. H. Miller, J. T. Andrews, D. J. Harning, L. S. Anderson, C. Florian, D. J. Larsen, and T. Thordarson (2019), The onset of neoglaciation in Iceland and the 4.2 ka event, *Clim. Past*, *15*(1), 25–40, doi:10.5194/cp-15-25-2019.

Giesche, A., M. Staubwasser, C. A. Petrie, and D. A. Hodell (2019), Indian winter and summer monsoon strength over the 4.2 ka BP event in foraminifer isotope records from the Indus River delta in the Arabian Sea, *Clim. Past*, *15*(1), 73–90, doi:10.5194/cp-15-73-2019.

Hernández, A., R. M. Trigo, S. Pla-Rabes, B. L. Valero-Garcés, S. Jerez, M. Rico-Herrero, J. C. Vega, M. Jambrina-Enríquez, and S. Giralt (2015), Sensitivity of two Iberian lakes to North Atlantic atmospheric circulation modes, *Clim Dyn*, *45*(11-12), 3403–3417, doi:10.1007/s00382-015-2547-8.

Hurrell, J. W. (1995), Decadal trends in the north atlantic oscillation: regional temperatures and precipitation, *Science*, *269*(5224), 676–679, doi:10.1126/science.269.5224.676.

Ilvonen, L., J. A. López-Sáez, L. Holmström, F. Alba-Sánchez, S. Pérez-Díaz, J. S. Carrión, and H. Seppä (2019), Quantitative reconstruction of precipitation changes in the Iberian Peninsula during the Late Pleistocene and the Holocene, *Clim. Past Discuss.*, 1–30, doi:10.5194/cp-2019-33.

Jalali, B., M.-A. Sicre, J. Azuara, V. Pellichero, and N. Combourieu-Nebout (2019), Influence of the North Atlantic subpolar gyre circulation on the 4.2 ka BP event, *Clim. Past*, *15*(2), 701–711, doi:10.5194/cp-15-701-2019.

Jiménez-Moreno, G., and R. S. Anderson (2012), Holocene vegetation and climate change recorded in alpine bog sediments from the Borreguiles de la Virgen, Sierra Nevada, southern Spain, *Quat. res.*, *77*(01), 44–53, doi:10.1016/j.yqres.2011.09.006.

Jones, S. E., F. Burjachs, C. Ferrer-García, S. Giralt, L. Schulte, and J. Fernández-López de Pablo (2018), A multi-proxy approach to understanding complex responses of salt-lake catchments to climate variability and human pressure: A Late Quaternary case study from south-eastern, Spain, *Quaternary Science Reviews*, *184*, 201–223, doi:10.1016/j.quascirev.2017.12.015.

Kaniewski, D., N. Marriner, R. Cheddadi, J. Guiot, and E. van Campo (2018), The 4.2 ka BP event in the Levant, *Clim. Past*, *14*(10), 1529–1542, doi:10.5194/cp-14-1529-2018.

Kathayat, G., H. Cheng, A. Sinha, M. Berkelhammer, H. Zhang, P. Duan, H. Li, X. Li, Y. Ning, and R. L. Edwards (2018), Evaluating the timing and structure of the 4.2 ka event in the Indian summer monsoon domain from an annually resolved speleothem record from Northeast India, *Clim. Past*, *14*(12), 1869–1879, doi:10.5194/cp-14-1869-2018.

Kirkels, F. M., B. Jansen, and K. Kalbitz (2013), Consistency of plant-specific n-alkane patterns in plaggen ecosystems: A review, *The Holocene*, *23*(9), 1355–1368, doi:10.1177/0959683613486943.

Kuechler, R. R., E. Schefuß, B. Beckmann, L. Dupont, and G. Wefer (2013), NW African hydrology and vegetation during the Last Glacial cycle reflected in plant-wax-specific hydrogen and carbon isotopes, *Quaternary Science Reviews*, *82*, 56–67, doi:10.1016/j.quascirev.2013.10.013.

Li, H., H. Cheng, A. Sinha, G. Kathayat, C. Spötl, A. A. André, A. Meunier, J. Biswas, P. Duan, Y. Ning, and R. L. Edwards (2018), Speleothem Evidence for Megadroughts in the SW Indian Ocean during the Late Holocene, *Clim. Past Discuss.*, 1–23, doi:10.5194/cp-2018-100.

Lionello, P. (Ed.) (2012), *The climate of the Mediterranean region: From the past to the future*, 1st ed., 502 pp., *Elsevier insights*, Elsevier Science, Amsterdam.

Liu, F., and Z. Feng (2012), A dramatic climatic transition at ~4000 cal. yr BP and its cultural responses in Chinese cultural domains, *The Holocene*, *22*(10), 1181–1197, doi:10.1177/0959683612441839.

Mesa-Fernández, J. M., G. Jiménez-Moreno, M. Rodrigo-Gámiz, A. García-Alix, F. J. Jiménez-Espejo, F. Martínez-Ruiz, R. S. Anderson, J. Camuera, and M. J. Ramos-Román (2018), Vegetation and geochemical responses to Holocene rapid climate change in the Sierra Nevada (southeastern Iberia): The Laguna Hondera record, *Clim. Past*, *14*(11), 1687–1706, doi:10.5194/cp-14-1687-2018.

Messori, G., M. Gaetani, Q. Zhang, Q. Zhang, and F. S. R. Pausata (2018), The water cycle of the mid-Holocene West African monsoon: The role of vegetation and dust emission changes, *Int. J. Climatol*, *39*(4), 1927–1939, doi:10.1002/joc.5924.

Nelson, D. M., A. K. Henderson, Y. Huang, and F. S. Hu (2013), Influence of terrestrial vegetation on leaf wax δD of Holocene lake sediments, *Organic Geochemistry*, *56*, 106–110, doi:10.1016/j.orggeochem.2012.12.010.

Niedermeyer, E. M., M. Forrest, B. Beckmann, A. L. Sessions, A. Mulch, and E. Schefuß (2016), The stable hydrogen isotopic composition of sedimentary plant waxes as quantitative proxy for rainfall in the West African Sahel, *Geochimica et Cosmochimica Acta*, *184*, 55–70, doi:10.1016/j.gca.2016.03.034.

Niedermeyer, E. M., E. Schefuß, A. L. Sessions, S. Mulitza, G. Mollenhauer, M. Schulz, and G. Wefer (2010), Orbital- and millennial-scale changes in the hydrologic cycle and vegetation in the western African Sahel: Insights from individual plant wax δD and $\delta^{13}C$, *Quaternary Science Reviews*, *29*(23-24), 2996–3005, doi:10.1016/j.quascirev.2010.06.039.

Olsen, J., N. J. Anderson, and M. F. Knudsen (2012), Variability of the North Atlantic Oscillation over the past 5,200 years, *Nature Geoscience*, *5*(11), 808–812, doi:10.1038/ngeo1589.

Ouda, B., M. El Hamdaoui, and M. Ibn Majah (2005), Isotopic composition of precipitation at three Moroccan stations influenced by Oceanic and Mediterranean air masses, in *Isotopic composition of precipitation in the Mediterranean basin in relation to air circulation patterns and climate: Final report of a coordinated research project 2000-2004*, *IAEA-TECDOC*, vol. 1453, edited by International Atomic Energy Agency, pp. 125–140, IAEA, Vienna.

Pantaléon-Cano, J., E.-I. Yll, R. Pérez-Obiol, and J. M. Roure (2003), Palynological evidence for vegetational history in semi-arid areas of the western Mediterranean (Almería, Spain), *The Holocene*, *13*(1), 109–119, doi:10.1191/0959683603hl598rp.

Patricola, C. M., and K. H. Cook (2007), Dynamics of the West African Monsoon under Mid-Holocene Precessional Forcing: Regional Climate Model Simulations, *J. Climate*, *20*(4), 694–716, doi:10.1175/JCLI4013.1.

Pausata, F. S.R., G. Messori, and Q. Zhang (2016), Impacts of dust reduction on the northward expansion of the African monsoon during the Green Sahara period, *Earth and Planetary Science Letters*, *434*, 298–307, doi:10.1016/j.epsl.2015.11.049.

Perez-Sanz, A., G. Li, P. González-Sampériz, and S. P. Harrison (2014), Evaluation of modern and mid-Holocene seasonal precipitation of the Mediterranean and northern Africa in the CMIP5 simulations, *Clim. Past*, *10*(2), 551–568, doi:10.5194/cp-10-551-2014.

Peyron, O., N. Combourieu-Nebout, D. Brayshaw, S. Goring, V. Andrieu-Ponel, S. Desprat, W. Fletcher, B. Gambin, C. Ioakim, S. Joannin, U. Kotthoff, K. Kouli, V. Montade, J. Pross, L. Sadori, and M. Magny (2017), Precipitation changes in the Mediterranean basin during the Holocene from terrestrial and marine pollen records: A model–data comparison, *Climate of the Past*, *13*(3), 249–265, doi:10.5194/cp-13-249-2017.

Railsback, L. B., F. Liang, G. A. Brook, N. R. G. Voarintsoa, H. R. Sletten, E. Marais, B. Hardt, H. Cheng, and R. L. Edwards (2018), The timing, two-pulsed nature, and variable climatic expression of the 4.2 ka event: A review and new high-resolution stalagmite data from Namibia, *Quaternary Science Reviews*, *186*, 78–90, doi:10.1016/j.quascirev.2018.02.015.

Ramos-Román, M. J., G. Jiménez-Moreno, J. Camuera, A. García-Alix, R. S. Anderson, F. J. Jiménez-Espejo, and J. S. Carrión (2018), Holocene climate aridification trend and human impact interrupted by millennial- and centennial-scale climate fluctuations from a new sedimentary record from Padul (Sierra Nevada, southern Iberian Peninsula), *Clim. Past*, *14*(1), 117–137, doi:10.5194/cp-14-117-2018.

Sabatier, P., L. Dezileau, C. Colin, L. Briqueu, F. Bouchette, P. Martinez, G. Siani, O. Raynal, and U. von Grafenstein (2012), 7000 years of paleostorm activity in the NW Mediterranean Sea in response to Holocene climate events, *Quat. res.*, *77*(01), 1–11, doi:10.1016/j.yqres.2011.09.002.

Sachse, D., I. Billault, G. J. Bowen, Y. Chikaraishi, T. E. Dawson, S. J. Feakins, K. H. Freeman, C. R. Magill, F. A. McInerney, M. T.J. van der Meer, P. Polissar, R. J. Robins, J. P. Sachs, H.-L. Schmidt, A. L. Sessions, J. W.C. White, J. B. West, and A. Kahmen (2012), Molecular Paleohydrology: Interpreting the Hydrogen-Isotopic Composition of Lipid Biomarkers from Photosynthesizing Organisms, *Annual Review of Earth and Planetary Sciences*, *40*(1), 221–249, doi:10.1146/annurev-earth-042711-105535.

Schäfer, I. K., M. Bliedtner, D. Wolf, T. Kolb, J. Zech, D. Faust, and R. Zech (2018), A δ 13 C and δ 2 H leaf wax record from the Late Quaternary loess-paleosoil sequence El Paraíso, Central Spain, *Palaeogeography, Palaeoclimatology, Palaeoecology*, *507*, 52–59, doi:10.1016/j.palaeo.2018.06.039.

Schefuß, E., S. Schouten, and R. R. Schneider (2005), Climatic controls on central African hydrology during the past 20,000 years, *Nature*, *437*(7061), 1003–1006, doi:10.1038/nature03945.

Schemmel, F., E. M. Niedermeyer, V. F. Schwab, G. Gleixner, J. Pross, and A. Mulch (2016), Plant wax δD values record changing Eastern Mediterranean atmospheric circulation patterns during the 8.2 kyr B.P. climatic event, *Quaternary Science Reviews*, *133*, 96–107, doi:10.1016/j.quascirev.2015.12.019.

Schirrmacher, J., J. Kneisel, D. Knitter, W. Hamer, M. Hinz, R. R. Schneider, and M. Weinelt (2020), Spatial patterns of temperature, precipitation, and settlement dynamics on the Iberian Peninsula during the Chalcolithic and the Bronze Age, *Quaternary Science Reviews*, *233*, doi:10.1016/j.quascirev.2020.106220.

Schirrmacher, J., M. Weinelt, T. Blanz, N. Andersen, E. Salgueiro, and R. R. Schneider (2019), Multi-decadal atmospheric and marine climate variability in southern Iberia during the mid- to late-Holocene, *Clim. Past*, *15*(2), 617–634, doi:10.5194/cp-15-617-2019.

Schwab, V. F., Y. Garcin, D. Sachse, G. Todou, O. Séné, J.-M. Onana, G. Achoundong, and G. Gleixner (2015), Effect of aridity on $\delta^{13}C$ and δD values of C_3 plant- and C_4 graminoid-derived leaf wax lipids from soils along an environmental gradient in Cameroon (Western Central Africa), *Organic Geochemistry*, *78*, 99–109, doi:10.1016/j.orggeochem.2014.09.007.

Staubwasser, M., F. Sirocko, P. M. Grootes, and M. Segl (2003), Climate change at the 4.2 ka BP termination of the Indus valley civilization and Holocene south Asian monsoon variability, *Geophysical Research Letters*, *30*(8), 155, doi:10.1029/2002GL016822.

Taylor, A. K., M. M. Benedetti, J. A. Haws, and C. S. Lane (2018), Mid-Holocene Iberian hydroclimate variability and paleoenvironmental change: Molecular and isotopic insights from Praia Rei Cortiço, Portugal, *J. Quaternary Sci.*, *33*(1), 79–92, doi:10.1002/jqs.3000.

Trigo, R. M., T. J. Osborn, and J. M. Corte-Real (2002), The North Atlantic Oscillation influence on Europe: Climate impacts and associated physical mechanisms, *Clim. Res.*, *20*, 9–17, doi:10.3354/cr020009.

Trigo, R. M., D. Pozo-Vázquez, T. J. Osborn, Y. Castro-Díez, S. Gámiz-Fortis, and M. J. Esteban-Parra (2004), North Atlantic oscillation influence on precipitation, river flow and water resources in the Iberian Peninsula, *Int. J. Climatol*, *24*(8), 925–944, doi:10.1002/joc.1048.

Valera, A. C. (2015), Social change in the late 3rd millennium BC in Portugal: the twilight of enclosures, in *2200 BC - ein Klimasturz als Ursache für den Zerfall der alten Welt?: 7. Mitteldeutscher Archäologentag vom 23. bis 26. Oktober 2014 in Halle (Saale)*, *Tagungen des Landesmuseums für Vorgeschichte Halle*, Band 12,1, edited by H. Meller et al., pp. 409–428, Landesamt für Denkmalpflege und Archäologie Sachsen-Anhalt, Landesmuseum für Vorgeschichte, Halle (Saale).

Walczak, I. W., J. U.L. Baldini, L. M. Baldini, F. McDermott, S. Marsden, C. D. Standish, D. A. Richards, B. Andreo, and J. Slater (2015), Reconstructing high-resolution climate using CT scanning of unsectioned stalagmites: A case study identifying the mid-Holocene onset of the Mediterranean climate in southern Iberia, *Quaternary Science Reviews*, *127*, 117–128, doi:10.1016/j.quascirev.2015.06.013.

Wang, Y. V., T. Larsen, G. Leduc, N. Andersen, T. Blanz, and R. R. Schneider (2013), What does leaf wax δD from a mixed C3/C4 vegetation region tell us?, *Geochimica et Cosmochimica Acta*, *111*, 128–139, doi:10.1016/j.gca.2012.10.016.

Weiss, H. (2015), Megadrought, collapse, and resilience in late 3rd millennium BC Mesopotamia, in *2200 BC - ein Klimasturz als Ursache für den Zerfall der alten Welt?: 7. Mitteldeutscher Archäologentag vom 23. bis 26. Oktober 2014 in Halle (Saale)*, *Tagungen des Landesmuseums für Vorgeschichte Halle*, Band 12,1, edited by H. Meller et al., pp. 35–52, Landesamt für Denkmalpflege und Archäologie Sachsen-Anhalt, Landesmuseum für Vorgeschichte, Halle (Saale).

Weiss, H. (2016), Global megadrought, societal collapse and resilience at 4.2-3.9 ka BP across the Mediterranean and west Asia, *PAGES Mag*, *24*(2), 62–63, doi:10.22498/pages.24.2.62.

Weiss, H., M. A. Courty, W. Wetterstrom, F. Guichard, L. Senior, R. Meadow, and A. Curnow (1993), The genesis and collapse of third millennium north mesopotamian civilization, *Science (New York, N.Y.)*, *261*(5124), 995–1004, doi:10.1126/science.261.5124.995.

Welc, F., and L. Marks (2014), Climate change at the end of the Old Kingdom in Egypt around 4200 BP: New geoarchaeological evidence, *Quaternary International*, *324*, 124–133, doi:10.1016/j.quaint.2013.07.035.

Weldeab, S., D. W. Lea, R. R. Schneider, and N. Andersen (2007), 155,000 years of West African monsoon and ocean thermal evolution, *Science (New York, N.Y.)*, *316*(5829), 1303–1307, doi:10.1126/science.1140461.

Wirth, S. B., and A. L. Sessions (2016), Plant-wax D/H ratios in the southern European Alps record multiple aspects of climate variability, *Quaternary Science Reviews*, *148*, 176–191, doi:10.1016/j.quascirev.2016.07.020.

Yan, M., and J. Liu (2019), Physical processes of cooling and mega-drought during the 4.2 ka BP event: Results from TraCE-21ka simulations, *Clim. Past*, *15*(1), 265–277, doi:10.5194/cp-15-265-2019.

Zhang, H., H. Cheng, Y. Cai, C. Spötl, G. Kathayat, A. Sinha, R. L. Edwards, and L. Tan (2018), Hydroclimatic variations in southeastern China during the 4.2 ka event reflected by stalagmite records, *Clim. Past*, *14*(11), 1805–1817, doi:10.5194/cp-14-1805-2018.

Zielhofer, C., W. J. Fletcher, S. Mischke, M. de Batist, J. F.E. Campbell, S. Joannin, R. Tjallingii, N. El Hamouti, A. Junginger, A. Stele, J. Bussmann, B. Schneider, T. Lauer, K. Spitzer, M. Strupler, T. Brachert, and A. Mikdad (2017), Atlantic forcing of Western Mediterranean winter rain minima during the last 12,000 years, *Quaternary Science Reviews*, *157*, 29–51, doi:10.1016/j.quascirev.2016.11.037.

Chapter 8

Conclusions and outlook

8 Conclusions and outlook

8.1 Conclusions

By studying the paleo-climatic variability and its potential impact on ancient societies, this thesis tries to contribute to the discussion on the ongoing global warming and its potential environmental and human impacts on a regional scale. In more detail, this thesis aims to decipher the spatio-temporal manifestation of paleo-climatic variability on the Iberian Peninsula during the Mid- to Late Holocene with a particular focus on the 4.2 ka BP event. Paleo-climatic and paleo-environmental variables, which have been considered important, were atmospheric temperature and sea surface temperature (SST) as well as precipitation. Also, much emphasis has been paid to reconstructing the seasonal variability of these variables.

In order to reconstruct the paleo-climatic variability of the Iberian Peninsula two main approaches have been pursued. The first one was the reconstruction of annual SSTs and of precipitation patterns based on alkenones and *n*-alkanes in two marine sediment cores from the Gulf of Cádiz (GeoB5901-2) and the Alboran Sea (ODP-161-976A), respectively. While the investigation of alkenones provides information on a local scale at the marine coring sites, the *n*-alkane based proxies spatially integrate over riverine catchment areas, and thus, provide paleo-climatic information on a regional scale. In particular, the investigation of compound-specific hydrogen and carbon isotopes from individual *n*-alkanes represents a novel approach to study atmospheric precipitation patterns in the study area. This approach was complemented by the reconstruction of seasonal (summer and winter) SSTs from planktonic foraminiferal assemblages within both sediment cores. The second approach is based on a compilation of paleo-climatic proxies from the Iberian Peninsula and adjacent marine and terrestrial areas, which was used for analysing spatially coherent patterns of the aforementioned paleo-climatic variables.

The reconstructed paleo-climatological variability, and the 4.2 ka BP event in particular, has been further be compared to changes in human activities of the Iberian Peninsula. Here, a focus was laid on the comparison to changes in settlement intensity as reconstructed from summed probability densities (SPDs) and aoristic analysis.

Paleo-climatic reconstructions revealed well known long-term cooling and drying trends on the Iberian Peninsula during the Holocene. More precisely, the seasonal reconstructions of this thesis showed that the long-term cooling and drying trends were mainly associated with winter conditions. Moreover, the SST cooling trends seems to be restricted to the Atlantic realm at site

GeoB5901-2 from the Gulf of Cádiz, whereas more stable conditions prevailed in the Alboran Sea where no cooling trends was reported in sediment core ODP-161-976A.

The long-term development of SST and precipitation was superimposed by pronounced seasonal SST and precipitation events, which aappear uncoupled due to their different timing and likely were responses to different forcings. For instance, winter cooling events in the Gulf of Cádiz of up to 2 °C correlate with ice-rafted debris (IRD) discharge during Bond Events. This is particularly true for Bond Event 3 that occurred between 4400 and 4000 cal. BP. Here, a major winter cooling is observed on the Iberian Peninsula. In contrast, SST variations in the Alboran Sea appear as rather local phenomena and show similarities with the North Atlantic Oscillation (NAO) patterns.

In parallel, the NAO was contributing to variability in winter precipitation amount and changes in the seasonal precipitation source on the southern Iberian Peninsula. Positive NAO conditions are generally considered to favour winter dry events and, consequently, an increased proportion of summer precipitation with local Mediterranean origin. However, this thesis suggests that the NAO likely had no impact on the 4.2 ka BP event on the Iberian Peninsula, which was manifested as a series of summer dry events between 4400 and 3800 cal. BP restricted to the south east (SE) of the Iberian Peninsula.

Based on a comparison with reconstructed settlement intensities, it could be further shown that the El Argar society in the SE of the Iberian Peninsula were well able to cope with reduced summer precipitation during the 4.2 ka BP event. But generally, the contemporaneity of winter dry conditions and reductions in settlement intensities in the same area implies a high dependency of (agrarian) economy of Iberian societies on winter precipitation. For instance, a spatial shift in settlement intensity from the south west (SW) to the SE of the Iberian Peninsula is evident at around 4800 cal. BP under dry winter conditions. Similarly, a later sharp decline in settlement intensity in the SE at around 3600 cal. BP also coincided with the onset of dry winter conditions and here, likely contributed to the collapse of the ca. 700-year lasting boom phase of the El Argar society.

Altogether, this relationship suggests that also the modern society might well be able to cope with the projected increase in summer heat waves. But despite being more resilient compared to ancient societies, modern society may also struggle much more in scenarios, when winter precipitation will be severly reduced due to ongoing global warming.

8.2 Outlook

This thesis significantly helped to improve the understanding of the Mid- to Late Holocene climate variability on the Iberian Peninsula and further, provides new insights into the 4.2 ka BP event. In addition to these important results, this thesis also highlighted various aspects, which need further research in future.

One aspect is dealing with the marine sediment cores investigated within this thesis. They provide new data and knowledge on a regional scale and on decadal to multi-decadal temporal resolution. But, surely there do exist marine archives, which are even more suitable to study the Holocene climate variability in much more detail. In this regard, future studies should concentrate on near-shore archives from the riverine mudbelts. Those archives would increase the temporal resolution. They would, further, enable to differentiate between the riverine basins and thus, allow even better investigation of regional differences in climate change. This will, on the one hand, improve the comparison to other local paleo-climatic archives and archaeological site data and, on the other hand, allow the recognition of potential spatial heterogeneity between different river catchments. Another advantage of those archives is the higher concentration of terrestrial-derived material, e.g. *n*-alkanes. The marine sediment cores analysed in this thesis contained relatively low amounts of *n*-alkanes, which even requires the improvement of the analytical setup in order to allow the measurement of the hydrogen isotopic composition. Still, some of the samples could not be analysed due to their low *n*-alkane concentration. Instead, near-shore archives from the riverine mudbelts will likely allow for a continuous measurement of the compound-specific isotopic composition of individual *n*-alkanes.

Another crucial issue, which was noticed during this thesis, concerns the radiocarbon dating of marine archives. Both archives analysed in this thesis were densely dated and provide a robust chronological age model. But still, there is uncertainty due to the global marine reservoir age of 400 years and potential local reservoir effects. This impedes the comparison with terrestrial archives and archaeological data. Thus, more attention should be paid to the linkage of marine and terrestrial records. One interesting approach, for example, could be the direct dating of terrestrial long-chain *n*-alkanes, even individually. Admittedly, this would not produce an age model applicable to sea surface temperature estimates, but it will provide important insights into the depositional history of *n*-alkanes and the terrestrial input. In the end, it will produce a "true" age model for every paleo-climatic parameter based on *n*-alkanes.

The third major aspect, which needs further research in future, is the linkage between paleo-climatic and archaeological data. One point is the already mentioned chronological issue, but also potential causal relationships between climate events or variability and archaeological transformations need further research. The comparison of climate variability and settlement patterns as applied in this thesis provides important information, but the establishment of causal relationships is hardly possible. Climatic events affect the crops in first place and, thus, the agricultural practises of past societies. Accordingly, more archaeo-botanical and dietary studies from the Iberian Peninsula are needed in order to improve the comparability of paleo-climatological and archaeological data and maybe allow for the establishment of causal relationships.

Minor aspects have been highlighted by the paleo-climatic compilation acquired during this thesis. As also stated within the respective chapter, the compilation highlighted the need for more paleo-climatic records in the study area. In general, the overall low temporal resolution just allows a calculation of 200-year time slices. More well-dated archives with decadal resolution would enable the calculation of 100-year time slices or even less. Moreover, some areas of the Iberian Pennsula remain underrepresented and new records are needed from these regions, in particular. For instance, the interior of the Iberian Peninsula including the Meseta, the Extremadura, the Alentejo, Galicia, and the Algarve are lacking Holocene paleo-climatic records. In addition, more Holocene marine records are needed from the northern coasts and the Bay of Biscay, the Gulf of Cádiz, and the Valencian and Catalonian coasts. Furthermore, much more seasonal paleo-climatic records, particularly from the summer season, are needed to improve the knowledge on seasonality. This will not only be important for the climate models but is also crucial for comparison with archaeological data since past societies organized their way of life around the large seasonal contrast on the Iberian Peninsula with humid winters and summer drought. Consequently, more detailed knowledge on the past development and variability of seasonality is not just important for paleo-climatological research.

Appendix

Table A1 Age versus depth of ODP-161-976A.

Depth (cm)	Interval (cm)	Median age (cal. years BP)	Minimum age (cal. years BP)	Maximum age (cal. years BP)	Sedimentation rate (cm/ kyr)
100.25	100.0-100.5	3001	2800	3237	31.25
100.75	100.5-101.0	3017	2836	3249	31.25
102.25	102.0-102.5	3071	2920	3292	27.78
102.75	102.5-103.0	3093	2952	3307	20.83
103.25	103.0-103.5	3122	2989	3324	16.67
103.75	103.5-104.0	3150	3014	3342	17.86
104.25	104.0-104.5	3177	3032	3360	19.23
104.75	104.5-105.0	3204	3047	3398	19.23
105.25	105.0-105.5	3232	3078	3426	14.71
105.75	105.5-106.0	3267	3117	3442	14.71
106.25	106.0-106.5	3303	3146	3461	13.16
106.75	106.5-107.0	3339	3169	3485	13.89
107.25	107.0-107.5	3374	3188	3521	13.89
107.75	107.5-108.0	3406	3232	3551	15.63
108.25	108.0-108.5	3438	3301	3564	15.63
108.75	108.5-109.0	3473	3362	3582	13.89
109.25	109.0-109.5	3507	3405	3610	14.71
109.75	109.5-110.0	3543	3434	3654	13.89
110.25	110.0-110.5	3587	3492	3707	9.26
110.75	110.5-111.0	3645	3546	3782	8.62
111.25	111.0-111.5	3703	3579	3890	8.62
111.75	111.5-112.0	3759	3598	4017	8.62
112.25	112.0-112.5	3813	3617	4147	9.26
112.75	112.5-113.0	3893	3683	4238	4.72
113.25	113.0-113.5	4002	3774	4293	4.55
113.75	113.5-114.0	4116	3836	4355	4.46
114.25	114.0-114.5	4225	3890	4443	4.81
114.75	114.5-115.0	4333	3934	4560	4.81
115.25	115.0-115.5	4411	4025	4636	9.62
115.75	115.5-116.0	4461	4161	4648	10.00
116.25	116.0-116.5	4514	4294	4660	9.62
116.75	116.5-117.0	4568	4424	4680	8.93
117.25	117.0-117.5	4623	4504	4712	8.93
117.75	117.5-118.0	4654	4535	4748	62.50
118.25	118.0-118.5	4662	4553	4754	62.50
118.75	118.5-119.0	4670	4567	4761	62.50
119.25	119.0-119.5	4679	4580	4770	62.50
119.75	119.5-120.0	4688	4589	4780	62.50
120.25	120.0-120.5	4697	4602	4789	62.50
120.75	120.5-121.0	4706	4614	4796	50.00
121.25	121.0-121.5	4715	4624	4803	50.00
121.75	121.5-122.0	4724	4633	4811	50.00
122.25	122.0-122.5	4733	4641	4823	62.50
122.75	122.5-123.0	4741	4649	4832	62.50
123.25	123.0-123.5	4751	4656	4838	50.00
123.75	123.5-124.0	4760	4664	4847	50.00
124.25	124.0-124.5	4769	4670	4856	50.00
124.75	124.5-125.0	4778	4677	4866	50.00
125.25	125.0-125.5	4787	4686	4877	50.00
125.75	125.5-126.0	4799	4698	4885	41.67
126.25	126.0-126.5	4810	4708	4896	41.67
126.75	126.5-127.0	4821	4716	4912	50.00
127.25	127.0-127.5	4831	4724	4931	50.00
127.75	127.5-128.0	4842	4734	4945	41.67
128.25	128.0-128.5	4855	4748	4958	35.71
128.75	128.5-129.0	4868	4760	4971	41.67
129.25	129.0-129.5	4881	4767	4986	41.67
129.75	129.5-130.0	4892	4776	5006	41.67

Depth (cm)	Interval (cm)	Median age (cal. years BP)	Minimum age (cal. years BP)	Maximum age (cal. years BP)	Sedimentation rate (cm/ kyr)
130.25	130.0-130.5	4904	4791	5023	41.67
130.75	130.5-131.0	4916	4811	5031	41.67
131.25	131.0-131.5	4929	4826	5043	41.67
131.75	131.5-132.0	4942	4837	5058	41.67
132.25	132.0-132.5	4955	4847	5076	41.67
132.75	132.5-133.0	4969	4866	5090	35.71
133.25	133.0-133.5	4983	4891	5103	35.71
133.75	133.5-134.0	4998	4910	5116	31.25
134.25	134.0-134.5	5013	4925	5131	31.25
134.75	134.5-135.0	5027	4936	5151	35.71
135.25	135.0-135.5	5046	4951	5180	19.23
135.75	135.5-136.0	5072	4967	5212	19.23
136.25	136.0-136.5	5096	4978	5258	22.73
136.75	136.5-137.0	5119	4988	5315	20.83
137.25	137.0-137.5	5141	4996	5379	20.83
137.75	137.5-138.0	5165	5013	5418	17.86
138.25	138.0-138.5	5191	5033	5439	19.23
138.75	138.5-139.0	5218	5051	5468	19.23
139.25	139.0-139.5	5244	5065	5500	19.23
139.75	139.5-140.0	5269	5077	5537	20.83
140.25	140.0-140.5	5295	5097	5567	17.86
140.75	140.5-141.0	5322	5120	5590	19.23
141.25	141.0-141.5	5351	5138	5612	17.86
141.75	141.5-142.0	5379	5157	5638	17.86
142.25	142.0-142.5	5406	5171	5671	17.86
142.75	142.5-143.0	5432	5196	5700	19.23
143.25	143.0-143.5	5459	5223	5717	17.86
143.75	143.5-144.0	5486	5246	5735	17.86
144.25	144.0-144.5	5514	5264	5758	17.86
144.75	144.5-145.0	5542	5282	5789	17.86
146.25	146.0-146.5	5618	5380	5842	20.83
146.75	146.5-147.0	5645	5403	5863	19.23
148.25	148.0-148.5	5718	5511	5921	22.73
148.75	148.5-149.0	5741	5560	5937	22.73

Table A2 n-Alkane raw data and molecular proxies from ODP-161-976A.

Depth (cm)	Weight (g)	Area (pA*s)											Concentration (ng/g)					CPI 27-33	ACL 27-33	Norm 33
		n-C_{25}	*n*-C_{26}	*n*-C_{27}	*n*-C_{28}	*n*-C_{29}	*n*-C_{30}	*n*-C_{31}	*n*-C_{32}	*n*-C_{33}	*n*-C_{34}	*n*-C_{35}	*n*-C_{27}	*n*-C_{29}	*n*-C_{31}	*n*-C_{33}	*n*-C_{27-33}			
100.25	4.339	26.5	20.4	44.0	26.6	98.6	33.2	143.5	40.1	69.0	27.5	28.1	41.18	110.31	176.13	71.11	398.72	2.87	30.34	0.41
100.75	3.917	34.2	27.0	59.9	34.1	117.8	42.3	170.6	50.7	82.4	33.7	33.3	66.29	152.45	242.30	97.91	558.96	2.74	30.28	0.41
102.25	4.834	30.9	24.1	50.2	30.7	110.8	39.1	160.1	47.1	77.4	32.4	32.0	43.35	114.45	181.33	73.46	412.60	2.75	30.33	0.41
102.75	4.764	25.6	18.8	41.4	24.7	93.5	31.4	135.6	38.3	65.1	26.5	26.1	34.84	94.08	149.44	60.32	338.68	2.87	30.34	0.41
103.25	9.144	70.6	44.6	105.2	41.0	265.6	48.3	393.8	45.3	144.7	22.0	37.8	56.73	179.49	283.77	84.45	604.44	5.44	30.27	0.35
103.75	6.462	26.0	17.4	44.4	19.4	115.8	23.0	169.3	22.5	67.3	14.6	20.4	27.95	90.46	145.47	46.31	310.20	4.91	30.31	0.37
104.25	8.210	63.2	36.7	82.0	34.8	199.7	38.4	278.1	32.3	102.3	16.5	26.8	46.43	140.73	211.33	61.03	459.52	5.04	30.21	0.34
104.75	5.528	42.8	27.5	56.4	24.2	137.4	27.8	201.3	27.8	78.6	16.5	23.3	43.66	130.93	211.10	65.46	451.15	4.67	30.28	0.36
105.25	6.244	45.6	28.0	59.3	24.3	147.2	29.9	217.5	27.8	83.9	16.4	24.7	41.08	126.36	205.74	62.80	435.98	4.89	30.28	0.36
105.75	8.052	23.8	16.6	47.1	19.8	127.5	25.7	195.1	26.6	76.9	17.4	24.2	24.09	81.86	139.39	43.75	289.10	5.01	30.35	0.38
106.25	6.546	40.1	24.2	57.7	23.7	139.9	29.2	205.4	31.6	81.3	17.9	25.4	37.91	113.09	182.79	57.63	391.42	4.59	30.28	0.37
106.75	6.739	45.4	29.5	65.8	26.8	159.5	29.5	233.1	28.1	87.8	15.4	23.7	43.20	129.46	207.65	61.54	441.85	5.13	30.26	0.36
107.25	6.413	22.5	18.5	53.2	21.0	136.8	25.9	188.8	24.9	69.8	14.8	20.5	35.06	112.24	167.99	48.79	364.09	5.07	30.23	0.34
107.75	6.340	39.3	23.5	53.1	22.3	130.4	26.7	194.9	29.0	76.5	17.2	23.0	35.38	106.93	176.80	55.21	374.33	4.63	30.30	0.37
108.25	6.196	48.2	30.9	64.3	27.8	157.8	33.8	235.4	35.8	92.9	20.9	27.8	45.69	138.93	228.59	71.76	484.97	4.47	30.30	0.37
108.75	7.147	25.9	16.7	35.3	16.1	88.2	22.7	135.1	26.3	57.7	17.0	19.2	19.14	58.35	99.15	34.72	211.36	3.86	30.36	0.40
109.25	7.361	48.1	32.6	67.8	31.6	165.8	37.2	251.4	36.0	101.1	20.2	29.4	41.02	124.41	208.56	67.08	441.07	4.48	30.32	0.38
109.75	7.034	36.5	24.4	67.9	26.2	156.6	32.4	204.4	30.1	76.6	18.4	24.8	43.01	121.21	169.08	49.85	383.15	4.59	30.15	0.33
110.25	8.029	19.5	13.4	36.8	15.2	97.7	20.3	148.7	22.9	60.1	15.5	19.4	17.92	58.94	99.52	32.47	208.86	4.71	30.35	0.38
110.75	6.370	30.8	19.4	53.1	19.9	131.0	24.6	181.6	24.2	67.2	15.0	20.4	35.22	107.04	161.11	46.90	350.26	5.04	30.21	0.34
111.25	5.696	44.8	30.6	64.1	30.5	157.6	39.8	229.5	44.2	97.2	30.1	35.2	49.51	150.88	241.01	82.56	523.95	3.79	30.31	0.38
111.75	6.309	39.4	27.4	64.9	30.9	166.6	44.2	251.8	52.2	111.1	36.1	40.8	45.38	146.03	243.81	87.99	523.21	3.74	30.38	0.40

Depth (cm)	Weight (g)	Area (pA*s)											Concentration (ng/g)					CPI 27-33	ACL 27-33	Norm 33
		n-C_{25}	*n*-C_{26}	*n*-C_{27}	*n*-C_{28}	*n*-C_{29}	*n*-C_{30}	*n*-C_{31}	*n*-C_{32}	*n*-C_{33}	*n*-C_{34}	*n*-C_{35}	*n*-C_{27}	*n*-C_{29}	*n*-C_{31}	*n*-C_{33}	*n*-C_{27-33}			
112.25	6.824	34.1	23.1	61.8	24.6	152.1	27.3	215.4	24.7	78.8	13.4	21.4	39.53	120.46	186.00	53.20	399.19	5.37	30.22	0.34
112.75	7.232	61.2	38.5	90.6	38.7	217.4	51.1	321.7	61.7	137.7	42.7	49.7	59.61	177.53	285.15	100.35	622.65	4.00	30.32	0.39
113.25	6.809	32.4	22.1	56.5	23.5	141.4	26.8	202.3	25.0	76.0	14.8	21.3	35.52	110.18	172.44	51.00	369.15	5.09	30.25	0.35
113.75	6.510	34.8	23.5	63.4	24.8	161.2	28.8	234.6	25.4	83.8	14.1	22.8	42.74	135.80	216.66	60.14	455.35	5.56	30.25	0.34
114.25	8.598	55.5	36.8	100.8	39.5	251.6	42.5	357.9	36.6	125.5	18.8	31.7	57.21	178.73	271.21	75.16	582.31	5.73	30.22	0.33
114.75	7.342	40.3	28.5	68.8	25.0	138.4	24.8	173.5	23.0	61.2	14.8	20.4	41.87	99.48	132.03	36.30	309.68	4.70	30.03	0.31
115.25	7.468	49.6	32.2	79.4	37.3	204.0	60.5	317.0	78.9	149.0	57.6	62.4	49.06	158.87	271.43	107.27	586.63	3.39	30.43	0.42
115.75	6.807	52.6	36.8	81.9	37.2	202.3	52.8	306.2	63.2	133.7	43.3	49.6	55.92	172.49	285.88	102.76	617.05	3.75	30.36	0.40
116.25	6.661	45.6	31.1	73.0	32.1	176.0	43.1	266.2	51.2	113.3	36.5	41.8	49.62	148.15	247.08	85.40	530.25	3.92	30.34	0.39
116.75	7.064	39.5	26.3	65.1	29.2	165.8	41.9	248.6	43.6	99.7	25.5	31.9	40.68	129.64	214.37	68.70	453.39	4.12	30.32	0.38
117.25	7.163	24.4	17.0	45.1	18.2	116.2	23.8	169.0	25.0	66.0	15.9	20.3	25.70	81.96	130.95	40.80	279.40	4.75	30.29	0.36
117.75	8.071	28.7	20.7	53.3	21.4	137.8	28.6	205.5	30.5	82.6	20.2	26.2	27.92	90.00	148.35	47.66	313.93	4.75	30.32	0.37
118.25	7.933	58.6	40.2	88.3	39.1	205.3	48.3	299.6	55.4	124.4	35.7	43.7	52.64	150.74	239.06	80.57	523.02	3.97	30.28	0.38
118.75	5.574	26.3	19.9	47.8	18.7	117.8	21.7	169.6	20.0	63.1	12.2	18.0	35.43	107.13	169.02	49.63	361.22	5.22	30.25	0.35
119.25	6.927	26.5	18.6	43.3	19.0	98.9	23.5	133.1	25.7	54.6	18.2	19.8	25.30	69.36	100.41	33.50	228.57	3.81	30.21	0.36
119.75	7.407	77.4	52.0	107.8	46.3	249.7	59.6	366.2	71.3	153.9	47.5	57.3	72.19	205.55	323.09	112.63	713.45	3.87	30.29	0.38
120.25	7.477	20.9	13.9	38.5	16.1	99.0	20.5	143.7	22.6	57.5	16.0	19.9	20.33	64.34	102.39	33.05	220.10	4.57	30.30	0.37
120.75	6.652	40.3	26.6	61.8	27.9	153.8	40.7	227.0	49.7	99.3	35.2	39.2	40.55	125.31	203.60	72.59	442.05	3.64	30.34	0.39
121.25	7.900	25.1	16.4	35.9	19.3	93.2	37.1	148.3	49.1	77.6	35.6	34.2	17.68	56.51	100.81	45.09	220.09	2.71	30.51	0.45
121.75	8.174	47.2	29.4	65.5	30.7	162.3	44.2	245.7	49.7	108.1	34.4	39.8	35.42	109.08	182.62	65.64	392.77	3.72	30.36	0.40
122.25	7.519	68.5	43.3	88.7	38.6	211.6	50.6	321.1	58.4	136.0	39.7	49.3	55.85	165.13	273.67	95.03	589.68	4.01	30.33	0.39
122.75	6.038	25.2	16.3	40.3	16.6	98.4	21.1	143.4	21.9	57.0	14.0	18.0	26.61	79.07	126.46	40.49	272.63	4.54	30.28	0.37
123.25	6.229	24.4	16.3	43.6	18.4	113.2	22.3	170.9	22.4	68.0	14.6	21.3	28.37	91.22	152.70	48.66	320.95	5.04	30.33	0.38
123.75	8.442	42.4	31.7	76.9	31.1	173.8	34.9	228.4	29.7	81.5	18.2	26.4	41.73	115.07	161.65	44.82	363.27	4.66	30.12	0.32

Depth (cm)	Weight (g)	Area (pA*s)											Concentration (ng/g)					CPI 27-33	ACL 27-33	Norm 33
		n-C_{25}	*n*-C_{26}	*n*-C_{27}	*n*-C_{28}	*n*-C_{29}	*n*-C_{30}	*n*-C_{31}	*n*-C_{32}	*n*-C_{33}	*n*-C_{34}	*n*-C_{35}	*n*-C_{27}	*n*-C_{29}	*n*-C_{31}	*n*-C_{33}	*n*-C_{27-33}			
124.25	8.998	49.9	32.1	87.3	33.3	198.1	36.0	259.6	29.0	90.1	16.0	25.8	45.76	127.13	177.42	47.58	397.89	5.21	30.11	0.31
124.75	6.934	57.1	36.7	76.0	36.7	175.9	44.6	257.8	49.6	111.0	34.9	42.4	50.08	142.22	228.29	79.97	500.56	3.72	30.30	0.39
125.25	7.100	15.7	8.6	18.7	9.8	46.3	17.4	68.9	22.3	36.0	17.4	17.4	8.76	26.76	43.38	19.73	98.64	2.73	30.44	0.44
125.75	7.250	38.9	25.0	65.1	25.4	156.1	29.7	211.7	26.7	76.0	15.7	22.1	39.64	117.13	171.35	47.90	376.02	4.99	30.17	0.33
126.25	7.309	32.5	17.2	29.8	14.3	66.5	20.3	90.5	21.9	40.9	15.4	16.5	15.23	40.35	58.90	22.38	136.86	3.13	30.25	0.38
126.75	5.090	13.0	8.8	19.4	10.1	49.6	18.4	72.5	22.1	34.9	16.2	15.6	12.81	40.58	64.39	26.51	144.29	2.81	30.39	0.41
127.25	8.663	17.7	9.6	19.2	9.6	44.7	15.3	70.9	19.1	36.9	13.7	14.4	7.43	21.02	36.82	16.67	81.93	3.09	30.46	0.45
127.75	6.843	20.8	13.8	36.0	15.5	92.7	20.7	137.1	20.9	53.9	12.7	17.1	20.48	64.80	105.48	33.38	224.14	4.54	30.31	0.37
128.25	7.836	31.9	17.9	35.0	16.0	81.9	20.6	119.0	24.0	55.0	17.9	22.1	17.28	48.58	77.18	29.88	172.91	3.71	30.33	0.40
128.75	7.556	50.4	37.3	77.6	28.8	171.2	35.5	224.9	32.8	79.7	20.3	27.1	47.15	126.16	177.20	48.72	399.23	4.42	30.11	0.32
129.25	6.751	36.0	19.8	40.8	25.1	128.5	72.9	297.6	122.8	192.7	101.7	97.2	24.15	98.60	278.69	163.70	565.14	2.39	30.95	0.60
129.75	7.087	43.6	28.7	78.2	29.7	174.5	33.7	212.6	27.3	70.0	16.1	21.9	50.74	137.76	176.22	44.31	409.03	4.75	30.03	0.29
130.25	7.719	28.9	15.1	28.0	13.3	76.4	18.9	112.8	20.1	45.0	13.7	16.0	13.36	45.28	73.29	23.78	155.71	3.93	30.33	0.37
130.75	6.597	41.5	25.0	59.3	25.5	156.5	40.4	241.5	47.9	107.3	34.2	42.2	38.88	129.14	221.55	80.58	470.15	3.94	30.41	0.41
131.25	8.613	39.4	21.7	42.8	19.3	108.1	26.3	154.2	26.6	60.1	16.8	19.8	20.06	62.30	97.09	30.27	209.72	4.00	30.27	0.36
131.75	6.678	28.0	18.3	41.9	17.8	92.1	25.4	123.3	31.1	54.1	23.2	25.0	25.22	65.88	94.66	34.36	220.11	3.28	30.22	0.37
132.25	6.972	30.1	18.3	33.2	15.3	73.8	18.0	97.0	19.1	39.6	13.7	15.5	18.21	48.05	67.28	22.56	156.09	3.57	30.17	0.35
132.75	5.316	11.3	7.7	20.7	9.5	57.1	18.8	93.2	24.3	47.4	18.9	20.2	13.32	46.09	83.98	36.78	180.16	3.34	30.53	0.45
133.25	8.887	26.0	12.9	23.4	9.5	45.2	11.7	55.6	14.3	24.6	11.5	12.3	9.30	20.77	26.69	9.89	66.65	3.12	30.09	0.35
133.75	7.499	37.0	25.8	61.6	26.0	144.7	30.2	199.1	26.6	72.3	16.2	21.8	35.83	102.98	153.50	43.56	335.86	4.61	30.18	0.33
134.25	6.128	26.7	14.3	27.1	14.7	72.8	24.2	111.0	31.6	58.8	25.8	27.1	16.17	53.76	90.49	41.43	201.85	2.99	30.49	0.45
134.75	7.268	49.8	33.6	62.5	28.6	149.8	41.2	232.0	50.5	105.0	36.2	41.6	37.62	110.96	191.42	71.20	411.21	3.54	30.38	0.41
135.25	7.559	21.3	14.2	37.8	18.4	106.0	34.9	175.9	47.6	90.9	38.1	40.9	19.67	69.27	130.46	57.26	276.66	3.26	30.56	0.46
135.75	7.297	55.9	35.5	73.3	36.5	184.5	52.7	285.9	61.7	128.9	42.6	49.3	45.53	143.45	245.79	91.57	526.34	3.54	30.40	0.41

Depth (cm)	Weight (g)	Area (pA*s)											Concentration (ng/g)					CPI	ACL	Norm
		n-C_{25}	*n*-C_{26}	*n*-C_{27}	*n*-C_{28}	*n*-C_{29}	*n*-C_{30}	*n*-C_{31}	*n*-C_{32}	*n*-C_{33}	*n*-C_{34}	*n*-C_{35}	*n*-C_{27}	*n*-C_{29}	*n*-C_{31}	*n*-C_{33}	*n*-C_{27-33}	27-33	27-33	33
136.25	8.066	37.6	27.1	64.1	26.4	149.2	32.1	197.8	29.8	71.4	17.6	22.7	34.96	99.48	141.55	39.88	315.88	4.37	30.15	0.32
136.75	6.935	NA	27.3	55.2	28.1	143.2	43.7	228.1	52.6	105.4	36.6	NA	33.91	109.91	196.46	74.97	415.25	3.40	30.44	0.42
137.25	7.241	73.0	43.8	88.9	41.4	222.3	58.2	336.3	71.4	152.2	51.3	58.8	58.16	182.27	299.87	113.62	653.91	3.66	30.38	0.41
137.75	7.354	48.9	29.6	75.6	30.7	178.2	36.7	264.5	36.3	103.7	22.7	33.8	46.92	136.29	222.06	69.29	474.56	4.79	30.27	0.37
138.25	7.619	24.1	16.3	40.8	17.6	108.0	26.0	172.0	31.1	76.0	21.5	26.7	21.40	70.34	125.85	45.58	263.17	4.24	30.43	0.41
138.75	7.750	46.0	28.4	73.4	30.7	179.1	37.3	267.3	37.4	107.0	22.9	33.5	42.94	130.14	213.42	68.36	454.86	4.79	30.30	0.37
139.25	8.032	43.5	28.1	69.4	30.1	172.2	36.9	260.0	36.1	104.8	21.4	31.9	38.68	119.55	199.13	64.28	421.64	4.75	30.32	0.38
139.75	7.432	21.3	15.5	38.0	17.9	98.8	24.8	154.9	28.6	68.3	20.1	25.0	20.13	64.57	113.16	41.00	238.86	4.04	30.41	0.41
140.25	8.357	36.7	24.3	56.1	24.3	139.9	29.6	207.8	28.5	83.4	17.7	26.4	28.69	88.58	145.26	46.58	309.12	4.72	30.31	0.37
140.75	7.984	37.1	25.3	58.9	25.5	148.4	32.0	224.3	32.9	93.6	20.1	29.9	31.87	99.83	167.15	56.21	355.05	4.65	30.34	0.39
141.25	6.319	34.5	21.2	47.7	20.9	118.3	26.8	179.4	27.3	74.9	17.6	25.2	31.18	95.00	159.95	53.98	340.11	4.45	30.34	0.39
141.75	7.733	54.4	34.0	63.9	27.9	147.2	33.7	217.9	37.5	92.0	22.6	31.2	36.33	102.03	166.50	56.81	361.67	4.10	30.30	0.38
142.25	8.052	71.1	44.4	82.8	36.5	193.9	40.0	286.3	37.1	111.2	18.5	32.9	47.91	138.32	223.12	69.02	478.37	4.69	30.26	0.36
142.75	7.922	47.4	27.8	55.7	23.6	132.4	32.3	195.2	36.5	79.3	21.8	27.4	30.01	87.22	141.77	46.18	305.18	3.95	30.29	0.37
143.25	8.618	57.0	32.9	63.7	27.8	156.2	31.8	236.6	30.8	91.8	17.6	28.1	32.47	98.61	165.38	50.84	347.31	4.76	30.30	0.37
143.75	6.648	43.4	24.3	47.9	20.9	117.6	29.1	180.0	32.2	76.3	20.9	26.6	29.78	89.63	152.67	52.49	324.58	4.03	30.35	0.39
144.25	8.383	55.8	33.4	67.8	28.3	165.4	33.7	245.0	32.9	93.9	17.2	28.5	36.02	108.91	177.45	53.75	376.13	4.78	30.28	0.36
144.75	7.325	48.1	30.3	56.1	24.1	132.4	29.5	195.6	29.7	78.4	18.6	26.8	32.74	94.33	153.71	49.25	330.03	4.31	30.28	0.37
146.25	2.495	22.1	16.4	25.4	19.2	50.1	25.1	71.6	32.3	40.6	22.7	19.6	36.66	83.79	129.38	64.97	314.80	1.95	30.36	0.45
146.75	4.690	34.4	26.4	49.1	32.0	104.0	39.8	145.8	48.7	74.1	33.2	31.7	43.50	109.04	166.22	71.78	390.54	2.48	30.31	0.42
148.25	3.763	12.4	8.3	14.5	10.1	31.1	16.3	48.0	22.7	30.4	17.2	15.7	11.82	31.17	52.75	30.31	126.05	2.02	30.52	0.49
148.75	6.118	28.2	19.0	37.2	22.2	81.7	27.1	120.4	32.5	59.0	22.3	24.0	23.83	62.03	100.30	41.67	227.83	2.91	30.35	0.42

Table A 3 Compound-specific hydrogen and carbon isotope data from ODP-161-976A. *SEM = standard error of the mean*

Depth (cm)	δD *n*-C_{29} (‰VSMOW)			δD *n*-C_{31} (‰VSMOW)			δD *n*-C_{33} (‰VSMOW)			$\delta^{13}C$ *n*-C_{29} (‰VPDB)			$\delta^{13}C$ *n*-C_{31} (‰VPDB)			$\delta^{13}C$ *n*-C_{33} (‰VPDB)		
	n	mean	SEM	n	mean	SEM	n	mean	SEM	n	mean	SEM	n	mean	SEM	n	mean	SEM
100.75	3	-138.9	1.1	3	-141.7	0.4	3	-115.7	2.1	3	-31.53	0.04	3	-31.19	0.01	3	-30.64	0.03
103.25	4	-146.5	0.3	4	-147.5	0.6	4	-124.3	1.0	3	-31.89	0.08	3	-31.06	0.03	3	-30.16	0.08
104.25	4	-149.9	1.0	4	-150.8	0.5	4	-125.3	0.9	3	-32.01	0.03	3	-31.35	0.04	3	-30.45	0.06
104.75	3	-157.5	0.4	3	-153.0	0.3	3	-128.2	2.4				3	-31.15	0.08			
105.25	3	-152.7	0.5	3	-150.5	1.1	3	-127.2	0.4	2	-31.88	0.02	2	-31.19	0.08	2	-30.08	0.09
105.75	3	-147.8	1.0	3	-152.0	0.7	3	-124.6	1.1	3	-31.77	0.06	3	-31.41	0.08	3	-30.11	0.16
106.25	3	-142.6	0.3	3	-142.4	0.4	3	-113.8	0.4	2	-31.73	0.05	2	-31.14	0.05	2	-30.11	0.10
106.75	2	-151.1	1.5	3	-147.3	1.6	2	-123.8	0.9	3	-31.76	0.06	3	-31.02	0.02	3	-30.40	0.02
107.25	3	-137.9	0.2	3	-143.2	0.6	3	-115.4	1.4	2	-31.52	0.01	2	-31.02	0.06	2	-30.43	0.02
107.75	3	-152.2	4.0	3	-147.5	3.4	2	-127.1	1.2	3	-32.00	0.01	3	-31.26	0.03	3	-30.38	0.05
108.25	3	-157.4	0.7	3	-156.7	0.3	3	-132.2	0.9	3	-31.84	0.09	3	-31.18	0.04	3	-30.31	0.03
109.25	4	-151.7	2.0	4	-153.0	1.3	4	-130.9	0.5	3	-32.25	0.03	3	-31.39	0.03	3	-30.68	0.06
109.75	3	-148.5	1.5	3	-153.1	1.5	3	-128.6	1.8	3	-32.28	0.04	3	-31.41	0.09	3	-30.90	0.05
110.75	2	-151.5	0.6	2	-154.1	1.3	2	-133.3	1.5	3	-32.14	0.06	3	-31.54	0.12	3	-30.98	0.14
111.25	3	-145.0	1.7	3	-149.0	1.9	3	-123.0	2.2	3	-31.71	0.07	3	-31.05	0.06	3	-30.40	0.03
112.25	3	-147.3	1.9	3	-154.9	1.6	3	-133.0	2.2	3	-32.05	0.03	3	-31.49	0.05	3	-31.38	0.07
112.75	4	-148.8	0.9	4	-151.3	0.2	4	-124.3	0.8				3	-31.24	0.06	3	-30.11	0.13
113.25	3	-149.3	0.5	3	-152.8	0.4	3	-135.2	1.2	3	-32.17	0.04	3	-31.59	0.04	3	-31.38	0.11
113.75	3	-143.0	2.6	2	-154.3	0.6	2	-132.8	2.3	3	-31.94	0.03	3	-31.49	0.01	3	-30.73	0.21
114.25	4	-149.4	0.5	4	-157.7	0.6	4	-137.7	1.1	4	-32.01	0.05	4	-31.51	0.04	4	-30.77	0.12
114.75	3	-142.7	1.5	3	-149.1	1.1	3	-124.6	1.9	3	-32.04	0.06	3	-31.55	0.05			
115.25	4	-147.5	0.7	4	-148.1	0.5	4	-119.2	0.5	3	-31.80	0.01	3	-31.05	0.03	3	-29.69	0.14
115.75	4	-147.5	3.2	3	-153.5	0.9	3	-130.1	0.4	3	-32.00	0.02	3	-31.50	0.02	3	-31.44	0.02
116.25	3	-143.9	0.1	3	-148.8	0.3	3	-123.9	0.1	2	-31.50	0.08	3	-31.01	0.06	2	-30.24	0.03
116.75	3	-150.7	0.4	3	-153.8	0.4	3	-130.3	0.7	3	-31.66	0.03	3	-31.03	0.06	3	-30.39	0.08
117.25	2	-141.5	0.5	3	-147.7	0.4	2	-130.6	0.1	3	-31.94	0.06	3	-31.41	0.11			
117.75	3	-149.6	0.9	3	-153.0	1.1	3	-127.8	1.0	3	-31.87	0.02	3	-31.27	0.04	3	-30.44	0.05
118.25	4	-150.3	1.3	4	-152.9	1.6	4	-129.6	0.7	3	-31.80	0.06	2	-31.48	0.02	2	-30.90	0.03
118.75	3	-154.1	0.3	3	-160.8	2.0	3	-134.9	1.2	1	-31.38		2	-31.51	0.07			
119.75	4	-146.4	1.0	4	-148.5	0.9	4	-120.6	1.2	3	-31.93	0.10	3	-31.19	0.10	3	-30.38	0.14
120.75	3	-143.9	3.5	2	-149.3	0.7	2	-122.7	0.2	3	-31.83	0.05	3	-31.02	0.02	3	-29.51	0.08
121.75	3	-143.8	0.3	3	-151.3	0.4	3	-130.2	0.6	3	-31.64	0.03	3	-31.03	0.05	3	-29.77	0.06
122.25	4	-154.2	0.4	4	-154.3	0.5	4	-132.4	0.6	3	-31.85	0.04	3	-31.26	0.04	3	-29.96	0.20
123.75	2	-152.2	1.1	2	-158.9	0.4	2	-133.9	1.8	3	-31.53	0.04	3	-31.19	0.01	3	-30.64	0.03

Depth (cm)	δD *n*-C_{29} (‰VSMOW)			δD *n*-C_{31} (‰VSMOW)			δD *n*-C_{33} (‰VSMOW)			$\delta^{13}C$ *n*-C_{29} (‰VPDB)			$\delta^{13}C$ *n*-C_{31} (‰VPDB)			$\delta^{13}C$ *n*-C_{33} (‰VPDB)		
	n	mean	SEM	n	mean	SEM	n	mean	SEM	n	mean	SEM	n	mean	SEM	n	mean	SEM
124.25	4	-152.3	0.7	4	-157.6	0.6	4	-132.9	1.2	3	-31.89	0.01	3	-31.18	0.11	3	-29.67	0.23
124.75	3	-146.2	3.6	3	-150.6	2.8	3	-123.4	2.0	3	-32.12	0.02	3	-31.49	0.06	3	-30.97	0.26
125.75	3	-148.1	2.8	3	-154.2	3.1	3	-132.2	2.8	3	-32.22	0.07	3	-31.59	0.03	3	-31.10	0.22
128.75	2	-148.3	1.0	3	-151.1	1.6	3	-124.1	3.0	3	-32.01	0.06	3	-31.55	0.03	2	-30.37	0.01
129.25	3	-142.2	1.1	3	-143.8	1.4	3	-117.4	1.5				3	-30.54	0.04	3	-30.02	0.19
129.75	3	-149.3	0.3	3	-152.2	0.7	3	-128.1	2.1	3	-31.98	0.10	3	-31.49	0.06			
130.75	3	-150.7	1.6	3	-152.7	1.3	3	-127.1	1.5	3	-31.85	0.06	3	-31.07	0.04	3	-30.20	0.04
133.75	2	-148.0	0.8	2	-150.8	2.7	2	-129.3	2.5	3	-31.91	0.05	3	-31.48	0.03	3	-31.00	0.11
134.75	3	-146.5	4.4	2	-153.7	0.5	2	-127.9	0.3	3	-32.19	0.23	3	-31.27	0.08	2	-30.73	0.06
135.25	3	-144.5	2.1	3	-147.0	2.3	3	-118.9	2.8	3	-31.67	0.00	3	-31.06	0.01	3	-30.78	0.13
135.75	4	-151.0	0.7	4	-153.2	0.5	4	-127.2	0.4	3	-31.80	0.09	3	-31.21	0.03	3	-30.21	0.12
136.25	3	-147.2	0.5	3	-151.8	0.9	3	-127.6	1.5	3	-32.04	0.02	3	-31.68	0.02	3	-31.25	0.04
136.75	2	-149.1	0.5	3	-147.8	0.9	2	-130.4	0.1	3	-31.51	0.06	3	-30.98	0.04	3	-29.99	0.01
137.25	4	-148.5	1.8	4	-152.6	1.3	4	-123.9	0.6	3	-31.85	0.05	3	-31.21	0.03	3	-30.27	0.07
137.75	4	-149.3	0.3	4	-157.4	0.8	4	-133.2	1.0	3	-31.84	0.08	3	-31.37	0.01	3	-30.23	0.03
138.75	4	-146.9	1.6	4	-153.4	1.7	4	-130.4	1.3	3	-31.91	0.03	3	-31.44	0.03	3	-30.78	0.08
139.25	3	-146.0	4.4	3	-154.8	2.7	2	-136.4	1.4	3	-31.97	0.08	3	-31.20	0.03	3	-30.47	0.09
140.25	2	-153.1	0.8	2	-154.0	0.7	2	-139.9	1.1	3	-31.94	0.07	3	-31.39	0.06	3	-30.92	0.05
140.75	3	-147.6	1.3	3	-155.1	0.9	3	-134.6	1.0	3	-32.04	0.05	3	-31.64	0.02	3	-30.56	0.03
141.25	3	-137.3	2.4	2	-145.6	0.2	2	-123.8	1.0	3	-31.91	0.06	3	-31.43	0.00	3	-30.76	0.11
141.75	3	-151.3	5.4	3	-152.5	2.1	3	-130.2	3.1	3	-31.87	0.03	3	-31.33	0.05	3	-30.67	0.13
142.25	4	-154.7	1.9	4	-153.9	1.5	4	-132.8	2.0	2	-32.02	0.04	2	-31.37	0.01	2	-30.45	0.17
142.75	3	-154.1	1.2	3	-148.0	1.0	3	-121.2	1.9	3	-32.02	0.08	3	-31.19	0.03	3	-30.40	0.04
143.25	3	-148.6	3.3	2	-156.7	0.5	2	-135.5	1.1	3	-32.13	0.03	3	-31.74	0.01	3	-31.64	0.07
144.25	3	-154.5	0.8	3	-158.8	0.7	3	-137.7	0.8	3	-31.90	0.10	3	-31.02	0.09	3	-29.83	0.08
144.75	3	-155.0	0.7	3	-154.1	0.3	3	-130.2	1.2	3	-31.65	0.06	3	-30.90	0.08	1	-30.07	

Table A 4 Alkenone data from ODP-161-976A.

Depth (cm)	Weight (g)	soluted in (µl)	C37:2		C37:3		$\sum C_{37}$ (ng/g)	$U^{K'}_{37}$	Sea surface temperature (°C)			
			Area (pA*s)	Conc. (ng/g)	Area (pA*s)	Conc. (ng/g)			*Müller et al.* [1998]	*Ternois et al.* [1997]	*Conte et al.* [2006]	*Prahl et al.* [1988]
100.25	4.339	400	55.16	235.3	24.98	106.6	341.9	0.6883	19.5	21.9	20.7	19.1
100.75	3.917	400	47.63	225.1	21.37	101.0	326.1	0.6903	19.6	22.0	20.7	19.2
102.25	4.834	400	55.85	213.9	25.82	98.9	312.8	0.6839	19.4	21.8	20.6	19.0
102.75	4.764	400	54.52	211.9	24.39	94.8	306.6	0.6910	19.6	22.0	20.7	19.2
103.25	9.144	400	137.37	235.5	66.46	114.0	349.5	0.6739	19.1	21.6	20.3	18.7
103.75	6.462	400	113.74	261.7	55.94	128.7	390.4	0.6703	19.0	21.5	20.3	18.6
104.25	8.210	400	129.14	246.6	62.00	118.4	365.0	0.6756	19.1	21.6	20.4	18.7
104.75	5.528	400	91.41	259.3	44.84	127.2	386.4	0.6709	19.0	21.5	20.3	18.6
105.25	6.244	400	98.30	246.8	47.70	119.8	366.6	0.6733	19.1	21.5	20.3	18.7
105.75	8.052	400	128.21	249.6	58.20	113.3	363.0	0.6878	19.5	21.9	20.6	19.1
106.25	6.546	400	99.76	238.9	48.17	115.4	354.3	0.6744	19.1	21.6	20.3	18.7
106.75	6.739	400	103.20	240.1	50.07	116.5	356.6	0.6733	19.1	21.5	20.3	18.7
107.25	6.413	400	114.84	245.5	54.72	117.0	362.5	0.6773	19.2	21.6	20.4	18.8
107.75	6.340	400	100.10	247.5	49.01	121.2	368.7	0.6713	19.0	21.5	20.3	18.6
108.25	6.196	400	101.02	255.6	49.82	126.1	381.7	0.6697	19.0	21.5	20.2	18.6
108.75	7.147	400	118.26	259.4	59.03	129.5	388.9	0.6671	18.9	21.4	20.2	18.5
109.25	7.361	400	127.86	272.3	63.94	136.2	408.5	0.6666	18.9	21.4	20.2	18.5
109.75	7.034	400	137.53	290.7	65.48	138.4	429.1	0.6775	19.2	21.6	20.4	18.8
110.25	8.029	400	136.15	265.9	63.49	124.0	389.8	0.6820	19.3	21.8	20.5	18.9
110.75	6.370	400	118.92	277.6	58.60	136.8	414.3	0.6699	19.0	21.5	20.3	18.6
111.25	5.696	400	94.22	259.3	46.18	127.1	386.4	0.6711	19.0	21.5	20.3	18.6
111.75	6.309	400	99.76	247.9	48.85	121.4	369.3	0.6713	19.0	21.5	20.3	18.6
112.25	6.824	400	131.43	286.4	64.54	140.6	427.0	0.6707	19.0	21.5	20.3	18.6
112.75	7.232	400	124.06	268.9	61.18	132.6	401.6	0.6697	19.0	21.5	20.2	18.6
113.25	6.809	400	133.05	290.5	65.03	142.0	432.5	0.6717	19.0	21.5	20.3	18.6
113.75	6.510	400	128.88	294.3	63.87	145.9	440.2	0.6686	18.9	21.4	20.2	18.5
114.25	8.598	400	164.30	284.1	81.12	140.3	424.4	0.6695	19.0	21.5	20.2	18.5
114.75	7.342	400	134.64	272.7	64.96	131.5	404.2	0.6746	19.1	21.6	20.4	18.7
115.25	7.468	400	115.56	242.6	57.08	119.8	362.4	0.6694	19.0	21.4	20.2	18.5
115.75	6.807	400	108.19	249.2	51.47	118.6	367.7	0.6776	19.2	21.6	20.4	18.8
116.25	6.661	400	108.08	254.4	53.61	126.2	380.6	0.6685	18.9	21.4	20.2	18.5
116.75	7.064	400	112.77	250.3	56.11	124.5	374.8	0.6678	18.9	21.4	20.2	18.5
117.25	7.163	400	131.24	272.4	64.50	133.9	406.3	0.6705	19.0	21.5	20.3	18.6
117.75	8.071	400	130.28	253.1	56.53	109.8	362.9	0.6974	19.8	22.1	20.9	19.4
118.25	7.933	400	127.31	251.6	62.44	123.4	375.0	0.6709	19.0	21.5	20.3	18.6
118.75	5.574	400	98.03	261.5	47.12	125.7	387.2	0.6754	19.1	21.6	20.4	18.7
119.25	6.927	400	120.11	257.8	59.16	127.0	384.8	0.6700	19.0	21.5	20.3	18.6
119.75	7.407	400	112.29	258.1	54.50	125.3	383.4	0.6732	19.1	21.5	20.3	18.7
120.25	7.477	400	115.44	262.9	53.20	121.1	384.0	0.6845	19.4	21.8	20.6	19.0
120.75	6.652	400	104.35	267.1	51.22	131.1	398.2	0.6707	19.0	21.5	20.3	18.6
121.25	7.900	400	108.18	246.0	50.25	114.3	360.2	0.6828	19.4	21.8	20.5	18.9
121.75	8.174	400	112.31	246.8	50.86	111.8	358.6	0.6883	19.5	21.9	20.7	19.1
122.25	7.519	400	101.63	242.8	45.77	109.3	352.1	0.6895	19.6	21.9	20.7	19.1
122.75	6.038	400	105.00	238.4	50.12	113.8	352.3	0.6769	19.2	21.6	20.4	18.8
123.25	6.229	400	107.60	256.8	52.40	125.1	381.9	0.6725	19.0	21.5	20.3	18.6
123.75	8.442	400	135.60	273.5	64.99	131.1	404.6	0.6760	19.2	21.6	20.4	18.7
124.25	8.998	400	154.88	255.9	71.88	118.8	374.7	0.6830	19.4	21.8	20.5	18.9
124.75	6.934	400	91.92	238.1	42.25	109.5	347.6	0.6851	19.4	21.8	20.6	19.0
125.25	7.100	400	86.12	154.2	38.75	69.4	223.5	0.6897	19.6	21.9	20.7	19.1
125.75	7.250	400	123.97	254.2	60.28	123.6	377.9	0.6728	19.1	21.5	20.3	18.6
126.25	7.309	400	102.10	207.7	46.75	95.1	302.8	0.6859	19.5	21.9	20.6	19.0
126.75	5.090	400	75.42	252.3	36.73	122.9	375.1	0.6725	19.0	21.5	20.3	18.6
127.25	8.663	400	113.99	195.6	49.85	85.5	281.2	0.6958	19.8	22.1	20.8	19.3
127.75	6.843	400	96.54	240.2	41.51	103.3	343.5	0.6993	19.9	22.2	20.9	19.4
128.25	7.836	400	111.10	210.8	51.16	97.1	307.9	0.6847	19.4	21.8	20.6	19.0
128.75	7.556	400	114.95	259.0	56.95	128.3	387.3	0.6687	18.9	21.4	20.2	18.5

Depth (cm)	Weight (g)	soluted in (µl)	C37:2		C37:3		$\sum C_{37}$ (ng/g)	$U^{K'}_{37}$	Sea surface temperature (°C)			
			Area (pA*s)	Conc. (ng/g)	Area (pA*s)	Conc. (ng/g)			*Müller et al.* [1998]	*Ternois et al.* [1997]	*Conte et al.* [2006]	*Prahl et al.* [1988]
129.25	6.751	400	104.40	196.6	48.34	91.0	287.6	0.6835	19.4	21.8	20.5	19.0
129.75	7.087	400	110.28	264.9	54.77	131.6	396.5	0.6681	18.9	21.4	20.2	18.5
130.25	7.719	400	101.68	224.3	45.59	100.5	324.8	0.6905	19.6	22.0	20.7	19.2
130.75	6.597	400	91.44	249.0	41.37	112.6	361.6	0.6885	19.5	21.9	20.7	19.1
131.25	8.613	400	112.67	222.7	49.69	98.2	321.0	0.6940	19.7	22.0	20.8	19.3
131.75	6.678	400	109.97	280.4	54.20	138.2	418.6	0.6699	19.0	21.5	20.3	18.6
132.25	6.972	400	106.52	227.2	48.59	103.6	330.8	0.6868	19.5	21.9	20.6	19.1
132.75	5.316	400	85.16	272.7	35.91	115.0	387.8	0.7034	20.0	22.3	21.0	19.5
133.25	8.887	400	126.79	212.1	57.49	96.2	308.3	0.6880	19.5	21.9	20.6	19.1
133.75	7.499	400	120.13	272.7	58.16	132.1	404.8	0.6738	19.1	21.6	20.3	18.7
134.25	6.128	400	97.42	202.1	45.62	94.6	296.7	0.6811	19.3	21.7	20.5	18.9
134.75	7.268	400	100.51	248.4	45.23	111.8	360.2	0.6897	19.6	21.9	20.7	19.1
135.25	7.559	400	117.09	263.7	52.74	118.8	382.5	0.6895	19.6	21.9	20.7	19.1
135.75	7.297	400	102.81	253.1	48.24	118.7	371.8	0.6807	19.3	21.7	20.5	18.9
136.25	8.066	400	121.24	255.9	59.98	126.6	382.5	0.6690	18.9	21.4	20.2	18.5
136.75	6.935	400	92.66	240.0	41.87	108.4	348.5	0.6888	19.5	21.9	20.7	19.1
137.25	7.241	400	95.10	235.9	42.67	105.9	341.8	0.6903	19.6	22.0	20.7	19.2
137.75	7.354	400	96.43	233.2	45.14	109.2	342.4	0.6811	19.3	21.7	20.5	18.9
138.25	7.619	400	116.07	259.4	52.16	116.6	375.9	0.6900	19.6	22.0	20.7	19.1
138.75	7.750	400	100.34	230.3	46.99	107.8	338.2	0.6811	19.3	21.7	20.5	18.9
139.25	8.032	400	101.57	224.9	46.71	103.4	328.4	0.6850	19.4	21.8	20.6	19.0
139.75	7.432	400	106.62	244.3	47.86	109.6	353.9	0.6902	19.6	22.0	20.7	19.2
140.25	8.357	400	97.70	208.0	44.45	94.6	302.6	0.6873	19.5	21.9	20.6	19.1
140.75	7.984	400	94.43	210.4	44.47	99.1	309.4	0.6798	19.3	21.7	20.5	18.8
141.25	6.319	400	69.99	197.0	31.41	88.4	285.5	0.6902	19.6	22.0	20.7	19.2
141.75	7.733	400	91.22	209.8	42.25	97.2	307.0	0.6835	19.4	21.8	20.5	19.0
142.25	8.052	400	105.89	233.9	50.14	110.8	344.7	0.6786	19.2	21.7	20.4	18.8
142.75	7.922	400	109.38	242.0	52.89	117.0	358.9	0.6741	19.1	21.6	20.3	18.7
143.25	8.618	400	112.41	228.6	54.92	111.7	340.2	0.6718	19.0	21.5	20.3	18.6
143.75	6.648	400	90.66	239.0	44.71	117.8	356.8	0.6697	19.0	21.5	20.2	18.6
144.25	8.383	400	108.65	227.1	53.42	111.7	338.8	0.6704	19.0	21.5	20.3	18.6
144.75	7.325	400	93.92	224.7	45.52	108.9	333.6	0.6736	19.1	21.6	20.3	18.7
146.25	2.495	400	26.24	194.7	11.40	84.6	279.3	0.6971	19.8	22.1	20.8	19.4
146.75	4.690	400	50.69	200.1	22.94	90.5	290.6	0.6885	19.5	21.9	20.7	19.1
148.25	3.763	400	40.34	198.5	18.27	89.9	288.3	0.6883	19.5	21.9	20.7	19.1
148.75	6.118	400	67.77	205.1	30.55	92.4	297.5	0.6893	19.6	21.9	20.7	19.1

Table A 5 Planktonic foraminiferal assemblage-based sea surface temperatures from ODP-161-976A.

Depth (cm)	Similarity index	non-distance weighed sea surface temperatures (°C)							
		winter (JFM)	JFM standard deviation	spring (AMJ)	AMJ standard deviation	summer (JAS)	JAS standard deviation	fall (OND)	OND standard deviation
100.25	0.99	15.0	0.4	17.5	0.2	22.6	1.3	18.5	0.4
100.75	0.97	15.2	1.0	17.5	0.3	22.7	1.3	18.8	0.9
102.25	0.98	15.0	0.6	17.6	0.3	22.8	1.3	18.8	0.7
104.25	0.97	15.8	0.8	17.7	0.4	22.0	1.3	19.2	0.6
104.75	0.97	15.4	0.8	17.7	0.4	22.5	1.3	19.0	0.7
106.25	0.97	15.9	1.1	17.8	0.4	22.3	1.3	19.4	0.5
106.75	0.98	15.0	0.4	17.5	0.2	22.8	1.4	18.7	0.7
108.25	0.98	15.0	0.6	17.6	0.3	22.8	1.3	18.8	0.7
108.75	0.97	15.7	0.7	17.5	0.5	21.4	1.3	19.0	0.5
110.25	0.98	15.1	0.6	17.5	0.3	22.5	1.3	18.6	0.5
110.75	0.99	14.9	0.4	17.6	0.2	22.8	1.3	18.5	0.4
112.25	0.98	15.1	0.6	17.5	0.3	22.7	1.4	18.8	0.7
112.75	0.97	15.0	0.6	17.6	0.3	23.0	1.3	18.9	0.6
114.25	0.98	14.9	0.4	17.5	0.2	23.0	1.2	18.7	0.7
114.75	0.97	15.0	0.6	17.5	0.3	23.0	1.3	18.9	0.7
116.25	0.98	15.2	0.7	17.6	0.3	22.8	1.4	18.9	0.7
116.75	0.97	15.8	0.9	17.7	0.5	21.9	1.2	19.2	0.4
118.25	0.98	15.3	1.0	17.6	0.3	23.0	1.3	19.1	0.9
118.75	0.98	15.0	0.4	17.5	0.2	22.8	1.4	18.7	0.7
120.25	0.98	15.1	0.6	17.5	0.3	22.7	1.4	18.8	0.7
120.75	0.97	15.7	0.9	17.7	0.5	22.3	1.5	19.3	0.5
122.25	0.98	15.0	0.4	17.5	0.2	22.8	1.4	18.7	0.7
124.75	0.98	15.0	0.4	17.5	0.2	22.8	1.4	18.7	0.7
126.25	0.98	15.3	1.0	17.6	0.3	23.0	1.3	19.1	0.9
128.75	0.98	15.0	0.4	17.5	0.2	22.8	1.4	18.7	0.7
128.75	0.98	15.0	0.6	17.6	0.3	22.8	1.3	18.8	0.7
128.75	0.98	15.0	0.4	17.5	0.2	22.8	1.4	18.7	0.7
130.25	0.98	15.0	0.4	17.5	0.2	22.8	1.4	18.7	0.7
132.75	0.99	15.0	0.4	17.5	0.2	22.8	1.4	18.7	0.7
134.25	0.97	15.8	1.1	17.8	0.5	22.2	1.5	19.4	0.6
136.75	0.98	14.9	0.4	17.5	0.2	22.7	1.3	18.5	0.4
142.25	0.98	15.0	0.4	17.5	0.2	22.5	1.4	18.5	0.4
144.25	0.98	14.9	0.4	17.5	0.2	22.9	1.3	18.7	0.7

Table A 6 Age versus depth of GeoB5901-2.

Depth (cm)	Interval (cm)	Median age (cal. years BP)	Minimum age (cal. years BP)	Maximum age (cal. years BP)	Sedimentation rate (cm/ kyr)
1.25	1.0-1.5	1376	1250	1549	20.83
6.25	6.0-6.5	1742	1553	1979	10.00
6.75	6.5-7.0	1792	1591	2005	10.00
7.25	7.0-7.5	1839	1623	2047	12.50
7.75	7.5-8.0	1951	1757	2139	2.72
8.25	8.0-8.5	2136	2000	2262	2.69
8.75	8.5-9.0	2323	2215	2416	2.69
9.25	9.0-9.5	2508	2380	2612	2.75
9.75	9.5-10.0	2692	2518	2842	2.75
10.25	10.0-10.5	2808	2624	2975	10.87
10.75	10.5-11.0	2856	2703	3005	10.87
11.25	11.0-11.5	2904	2773	3041	10.42
11.75	11.5-12.0	2952	2834	3086	10.42
12.25	12.0-12.5	3000	2875	3144	10.42
12.75	12.5-13.0	3068	2949	3210	5.68

Depth (cm)	Interval (cm)	Median age (cal. years BP)	Minimum age (cal. years BP)	Maximum age (cal. years BP)	Sedimentation rate (cm/ kyr)
13.25	13.0-13.5	3157	3058	3270	5.56
13.75	13.5-14.0	3246	3161	3342	5.81
14.25	14.0-14.5	3333	3251	3432	5.81
14.75	14.5-15.0	3420	3332	3534	5.81
15.25	15.0-15.5	3497	3412	3608	7.35
15.75	15.5-16.0	3565	3496	3651	7.35
16.25	16.0-16.5	3634	3566	3704	7.58
16.75	16.5-17.0	3701	3622	3776	7.14
17.25	17.0-17.5	3770	3665	3861	7.35
17.75	17.5-18.0	3822	3718	3916	13.89
18.25	18.0-18.5	3858	3770	3949	13.89
18.75	18.5-19.0	3893	3800	3995	13.89
19.25	19.0-19.5	3928	3823	4062	14.71
19.75	19.5-20.0	3963	3840	4138	15.63
20.25	20.0-20.5	4041	3927	4213	3.97
20.75	20.5-21.0	4167	4082	4291	3.97
21.25	21.0-21.5	4294	4224	4376	3.97
21.75	21.5-22.0	4419	4349	4483	4.10
22.25	22.0-22.5	4542	4450	4624	4.10
22.75	22.5-23.0	4628	4528	4720	10.42
23.25	23.0-23.5	4676	4581	4760	9.62
23.75	23.5-24.0	4727	4620	4813	9.62
24.25	24.0-24.5	4777	4646	4874	10.00
24.75	24.5-25.0	4827	4669	4945	10.00
25.25	25.0-25.5	4893	4741	5012	6.10
25.75	25.5-26.0	4975	4850	5082	5.95
26.25	26.0-26.5	5058	4931	5174	5.81
26.75	26.5-27.0	5144	4983	5278	5.95
27.25	27.0-27.5	5228	5032	5397	5.68
27.75	27.5-28.0	5291	5091	5466	13.16
28.25	28.0-28.5	5330	5163	5482	12.50
28.75	28.5-29.0	5369	5228	5500	11.90
29.25	29.0-29.5	5410	5275	5523	11.90
29.75	29.5-30.0	5451	5308	5560	13.16
30.25	30.0-30.5	5486	5357	5591	16.67
30.75	30.5-31.0	5517	5415	5604	15.63
31.25	31.0-31.5	5549	5446	5621	16.67
31.75	31.5-32.0	5580	5471	5645	16.67
32.75	32.5-33.0	5634	5503	5734	31.25
34.75	34.5-35.0	5693	5562	5838	35.71
35.25	35.0-35.5	5708	5576	5863	27.78
38.75	38.5-39.0	5824	5666	5996	31.25
41.75	41.5-42.0	5921	5749	6094	35.71
43.25	43.0-43.5	5968	5792	6138	35.71
44.25	44.0-44.5	6000	5819	6167	31.25
44.75	44.5-45.0	6016	5831	6183	27.78
45.25	45.0-45.5	6032	5848	6198	35.71
45.75	45.5-46.0	6046	5869	6205	31.25
48.25	48.0-48.5	6123	5969	6264	31.25
49.75	49.5-50.0	6170	6028	6297	31.25

Table A7 n-Alkane raw data and molecular proxies from GeoB5901-2.

Depth (cm)	Weight (g)	Area (pA*s)											Concentration (ng/g)					CPI	ACL	Norm
		n-C_{25}	*n*-C_{26}	*n*-C_{27}	*n*-C_{28}	*n*-C_{29}	*n*-C_{30}	*n*-C_{31}	*n*-C_{32}	*n*-C_{33}	*n*-C_{34}	*n*-C_{35}	*n*-C_{27}	*n*-C_{29}	*n*-C_{31}	*n*-C_{33}	*n*-C_{27-33}	27-33	27-33	33
1.25	3.024	21.3	14.7	26.5	17.2	62.8	23.5	90.8	31.3	53.2	27.4	28.2	31.87	90.96	142.94	74.35	340.13	2.52	30.46	0.46
12.75	9.625	66.0	52.7	111.0	64.0	230.3	71.9	317.2	76.5	138.6	48.2	51.8	57.61	143.24	210.76	76.02	487.63	3.03	30.21	0.38
13.25	9.389	44.9	38.6	82.5	50.5	173.7	56.2	246.9	59.5	111.2	37.6	41.1	40.91	103.39	159.94	59.19	363.43	3.01	30.26	0.39
13.75	5.632	55.1	47.2	82.6	56.5	158.9	62.8	214.5	66.1	102.2	41.9	41.7	68.30	154.17	224.21	88.85	535.53	2.43	30.20	0.39
14.25	8.062	39.8	34.7	66.1	44.0	129.7	49.9	179.3	54.4	88.6	37.1	37.7	36.31	83.53	125.28	52.02	297.14	2.52	30.25	0.41
14.75	5.113	55.7	43.7	70.4	48.2	134.1	53.8	183.0	59.2	89.6	38.2	37.8	61.84	137.31	202.65	83.16	484.97	2.36	30.22	0.40
15.25	11.728	54.0	43.1	92.1	50.0	195.7	56.0	277.6	62.0	122.6	41.0	46.1	37.51	96.06	147.62	53.52	334.71	3.28	30.25	0.39
15.75	11.093	61.2	50.6	103.6	61.1	205.7	65.6	270.5	67.4	114.7	41.6	42.2	45.88	108.06	151.27	52.07	357.28	2.89	30.14	0.36
16.25	9.339	51.3	42.7	85.6	51.3	174.8	56.7	242.2	61.8	108.7	39.8	41.8	43.04	104.77	157.06	57.85	362.71	2.90	30.22	0.38
16.75	10.121	9.0	7.5	13.9	9.3	27.4	13.3	42.8	19.6	28.2	15.7	14.9	4.15	9.92	17.07	10.28	41.42	2.10	30.52	0.51
17.25	9.327	68.9	56.5	116.5	74.9	246.1	88.7	316.3	90.5	149.5	64.0	78.3	63.14	160.37	216.77	86.25	526.53	2.64	30.20	0.38
17.25	4.049	7.6	4.3	8.9	4.2	16.6	7.3	21.3	10.4	13.7	8.9	8.0	5.33	13.16	18.13	10.17	46.79	2.14	30.32	0.45
17.75	15.457	91.8	49.2	115.0	49.8	279.7	53.0	361.1	56.5	135.7	27.7	49.8	37.49	113.02	152.39	46.10	349.01	4.52	30.16	0.33
18.25	10.623	65.9	30.6	78.3	38.2	173.8	39.8	226.2	43.6	87.1	22.9	38.4	33.91	91.45	126.94	38.65	290.95	3.81	30.14	0.33
18.75	12.733	72.2	40.9	100.8	44.6	222.6	43.0	286.6	46.5	101.5	21.7	38.2	38.63	103.83	141.27	38.97	322.70	4.32	30.09	0.31
19.25	9.779	73.4	38.7	91.0	44.4	208.1	56.2	272.9	65.7	118.6	36.8	52.7	44.32	124.36	173.43	61.58	403.70	3.38	30.21	0.36
19.75	12.292	60.8	30.5	87.7	36.9	204.4	46.3	267.2	52.5	104.7	25.7	40.4	33.69	96.76	134.50	41.95	306.90	4.05	30.17	0.34
20.25	6.771	37.0	20.4	43.3	21.8	98.5	29.4	133.3	33.3	56.2	21.3	22.1	25.88	70.60	102.92	35.49	234.89	3.14	30.22	0.36
20.75	6.278	47.0	24.4	47.1	22.0	108.1	26.1	145.3	30.5	59.4	16.1	21.7	30.90	85.47	123.65	40.94	280.96	3.65	30.21	0.35
21.25	5.812	33.6	19.5	42.0	18.2	98.0	26.6	132.1	29.0	58.1	18.6	25.1	29.06	81.74	118.55	43.05	272.40	3.56	30.25	0.37
21.75	7.011	25.6	13.9	22.5	12.0	43.3	17.5	56.8	21.8	31.0	15.5	15.3	11.22	24.99	34.72	16.66	87.60	2.33	30.25	0.42
22.25	13.303	55.8	32.2	63.5	27.1	132.4	30.0	163.3	29.5	62.8	15.6	22.4	20.96	51.94	67.54	20.68	161.12	3.84	30.07	0.32

Depth (cm)	Weight (g)	Area (pA*s)											Concentration (ng/g)					CPI 27-33	ACL 27-33	Norm 33
		n-C_{25}	*n*-C_{26}	*n*-C_{27}	*n*-C_{28}	*n*-C_{29}	*n*-C_{30}	*n*-C_{31}	*n*-C_{32}	*n*-C_{33}	*n*-C_{34}	*n*-C_{35}	*n*-C_{27}	*n*-C_{29}	*n*-C_{31}	*n*-C_{33}	*n*-C_{27-33}			
22.75	6.974	61.9	28.1	62.6	35.0	141.3	34.0	196.4	32.7	77.8	20.9	33.5	39.29	107.48	162.27	51.24	360.28	3.79	30.21	0.36
23.25	11.227	69.1	39.6	89.8	34.5	206.5	41.9	274.1	41.7	105.7	22.5	40.1	37.98	107.29	151.86	46.48	343.61	4.55	30.17	0.34
23.75	12.764	57.8	33.2	73.1	26.9	160.6	32.6	199.1	27.1	75.4	17.3	24.8	25.94	68.94	90.18	26.94	212.01	4.57	30.09	0.32
24.25	9.987	10.0	6.4	13.6	7.0	27.4	11.7	39.1	17.4	23.6	14.5	13.5	4.08	10.06	15.51	8.36	38.00	2.24	30.40	0.46
24.75	6.250	16.7	10.5	23.3	11.3	43.5	11.8	53.5	12.8	23.4	9.7	10.4	13.15	28.19	36.22	13.22	90.78	3.12	30.07	0.35
25.25	10.155	31.4	19.5	42.1	19.1	78.4	18.0	92.7	20.4	37.6	15.6	16.8	16.68	35.53	43.67	14.54	110.42	3.34	30.00	0.32
25.75	26.559	8.5	6.1	11.8	7.3	20.3	9.2	24.9	12.4	15.6	10.3	9.4	1.26	2.60	3.36	1.85	9.06	1.96	30.22	0.43
26.25	12.906	31.8	21.7	40.7	25.3	57.0	21.1	59.4	22.5	30.2	18.0	19.2	12.60	18.94	19.92	8.77	60.22	2.11	29.84	0.35
26.75	10.558	72.5	49.3	98.5	55.6	190.1	47.6	242.5	43.1	94.2	27.0	33.1	45.28	102.92	139.13	42.84	330.17	3.40	30.06	0.33
27.25	15.852	56.1	38.2	96.1	43.8	203.0	37.6	265.8	33.9	95.6	19.6	28.4	29.25	74.39	103.63	29.06	236.33	4.60	30.09	0.32
27.75	7.649	9.9	7.0	14.8	7.2	28.7	7.6	36.7	9.0	16.6	6.9	7.3	5.98	13.90	18.75	6.97	45.59	3.15	30.14	0.37
28.25	15.182	106.6	61.6	129.4	62.5	258.2	48.8	327.5	45.1	115.9	25.8	36.2	44.23	104.46	138.69	38.54	325.93	4.19	30.03	0.31
28.75	11.113	65.4	39.5	78.1	41.1	147.1	33.3	174.3	33.2	65.8	22.3	25.9	32.31	70.94	87.73	26.20	217.17	3.37	29.98	0.31
29.25	12.623	43.1	31.6	69.4	36.2	137.8	40.6	182.6	46.6	79.5	30.4	31.9	24.61	57.55	81.86	29.07	193.09	3.04	30.16	0.37
48.25	3.036	31.1	16.4	36.2	19.7	84.3	26.1	121.0	30.2	57.9	21.4	24.3	46.46	129.91	203.38	82.07	461.83	3.16	30.34	0.41

Table A 8 Alkenone data from GeoB5901-2.

Depth (cm)	Weight (g)	soluted in (µl)	C37:2		C37:3		$\sum C_{37}$ (ng/g)	$U^{K'}_{37}$	Sea surface temperature (°C)			
			Area (pA*s)	Conc. (ng/g)	Area (pA*s)	Conc. (ng/g)			*Müller et al.* [1998]	*Ternois et al.* [1997]	*Conte et al.* [2006]	*Prahl et al.* [1988]
1.25	3.024	200	25.3	78.37	10.2	31.60	109.97	0.7127	20.3	22.5	21.2	19.8
12.75	9.625	500	67.5	164.24	25.2	61.32	225.55	0.7282	20.7	22.9	21.5	20.3
13.25	9.389	500	53.1	132.45	18.9	47.14	179.59	0.7375	21.0	23.1	21.8	20.5
13.75	5.632	400	46.5	154.69	16.6	55.22	209.91	0.7369	21.0	23.1	21.7	20.5
14.25	8.062	500	71.3	209.97	28.7	84.52	294.49	0.7130	20.3	22.5	21.2	19.8
14.75	5.113	400	57.0	211.74	22.2	82.47	294.21	0.7197	20.5	22.7	21.4	20.0
15.25	11.728	500	97.9	198.18	40.6	82.19	280.37	0.7069	20.1	22.4	21.1	19.6
15.75	11.093	500	87.3	186.84	36.9	78.97	265.82	0.7029	20.0	22.3	21.0	19.5
16.25	9.339	500	72.8	185.07	28.4	72.20	257.27	0.7194	20.5	22.7	21.3	20.0
16.75	10.121	500	60.6	146.18	24.0	57.89	204.07	0.7163	20.4	22.6	21.3	19.9
17.25	9.327	500	86.6	226.68	35.3	92.40	319.08	0.7104	20.2	22.4	21.1	19.7
17.75	15.457	1000	60.7	191.75	24.4	77.08	268.83	0.7133	20.3	22.5	21.2	19.8
18.25	10.623	500	74.2	170.53	24.1	55.39	225.92	0.7548	21.5	23.5	22.2	21.1
18.75	12.733	500	106.0	189.20	37.9	67.65	256.85	0.7366	21.0	23.1	21.7	20.5
19.25	9.779	500	87.9	204.29	28.8	66.93	271.22	0.7532	21.5	23.5	22.1	21.0
19.75	12.292	500	99.4	183.79	36.6	67.67	251.46	0.7309	20.8	22.9	21.6	20.3
20.25	6.771	400	66.4	178.30	20.2	54.24	232.54	0.7667	21.9	23.8	22.4	21.4
20.25	3.018	200	59.8	180.13	23.8	71.69	251.82	0.7153	20.3	22.6	21.3	19.9
20.75	6.278	400	56.0	160.14	16.5	47.19	207.33	0.7724	22.1	24.0	22.6	21.6
21.25	5.812	400	46.7	144.26	12.1	37.38	181.63	0.7942	22.7	24.5	23.1	22.2
21.75	7.011	500	49.3	157.81	16.8	53.78	211.58	0.7458	21.3	23.3	21.9	20.8
22.25	13.303	500	99.5	167.85	37.9	63.94	231.79	0.7242	20.6	22.8	21.5	20.2
22.75	6.974	400	72.2	185.87	25.0	64.36	250.22	0.7428	21.2	23.2	21.9	20.7
23.25	11.227	500	102.0	198.28	37.2	72.31	270.60	0.7328	20.9	23.0	21.6	20.4
23.75	12.764	500	112.8	192.87	44.3	75.75	268.62	0.7180	20.4	22.6	21.3	20.0
24.25	9.987	500	85.4	186.62	33.9	74.08	260.71	0.7158	20.4	22.6	21.3	19.9
24.75	6.250	400	73.3	204.77	29.7	82.97	287.73	0.7117	20.2	22.5	21.2	19.8
25.25	10.155	500	81.7	175.58	33.9	72.86	248.44	0.7067	20.1	22.4	21.1	19.6
25.75	26.559	1500	60.5	155.17	22.7	58.22	213.40	0.7272	20.7	22.9	21.5	20.2
26.25	12.906	500	90.8	159.75	36.2	63.69	223.44	0.7150	20.3	22.6	21.2	19.9
26.75	10.558	500	88.9	191.19	34.2	73.55	264.75	0.7222	20.6	22.7	21.4	20.1
27.25	15.852	500	63.0	90.24	25.7	36.81	127.06	0.7103	20.2	22.4	21.1	19.7
27.75	7.649	500	60.7	180.19	24.5	72.73	252.92	0.7124	20.3	22.5	21.2	19.8
28.25	15.182	1000	67.3	199.41	27.6	81.78	281.19	0.7092	20.2	22.4	21.1	19.7
28.75	11.113	500	101.4	205.23	42.7	86.42	291.65	0.7037	20.0	22.3	21.0	19.5
29.25	12.623	500	132.3	235.74	55.7	99.25	334.99	0.7037	20.0	22.3	21.0	19.6
29.75	8.473	500	87.1	231.21	36.1	95.83	327.04	0.7070	20.1	22.4	21.1	19.6
48.25	3.036	200	76.7	227.29	30.1	89.20	316.49	0.7182	20.4	22.6	21.3	20.0

Table A 9 Planktonic foraminiferal assemblage-based sea surface temperatures from GeoB5901-2.

Depth (cm)	Similarity index	non-distance weighed sea surface temperatures (°C)							
		winter (JFM)	JFM standard deviation	spring (AMJ)	AMJ standard deviation	summer (JAS)	JAS standard deviation	fall (OND)	OND standard deviation
6.25	0.98	16.5	0.9	18.1	0.3	21.8	0.8	19.7	0.3
6.75	0.98	16.8	0.4	18.3	0.1	21.6	0.3	19.8	0.2
7.25	0.98	16.8	0.5	18.2	0.1	21.5	0.3	19.7	0.2
7.75	0.98	16.7	1.1	18.2	0.5	21.7	0.8	19.8	0.6
8.25	0.98	16.8	0.4	18.3	0.1	21.6	0.4	19.8	0.2
8.75	0.99	16.7	1.1	18.2	0.5	21.7	0.8	19.8	0.6
9.25	0.98	17.1	0.7	18.4	0.3	21.6	0.3	19.9	0.6

Depth (cm)	Similarity index	non-distance weighed sea surface temperatures (°C)							
		winter (JFM)	JFM standard deviation	spring (AMJ)	AMJ standard deviation	summer (JAS)	JAS standard deviation	fall (OND)	OND standard deviation
9.75	0.99	16.7	0.6	18.1	0.4	21.3	0.6	19.6	0.4
10.25	0.98	16.6	0.5	18.1	0.4	21.4	0.6	19.6	0.4
10.75	0.98	16.7	0.5	18.2	0.1	21.5	0.3	19.7	0.3
11.25	0.99	16.7	1.1	18.2	0.5	21.7	0.8	19.8	0.6
11.75	0.98	16.9	0.5	18.3	0.1	21.5	0.4	19.8	0.2
12.25	0.98	16.8	1.1	18.3	0.5	21.8	0.8	19.9	0.6
12.75	0.98	16.7	1.1	18.2	0.5	21.7	0.8	19.8	0.6
13.25	0.96	17.0	0.7	18.3	0.5	21.7	0.3	20.1	0.5
13.75	0.98	17.0	0.4	18.3	0.1	21.5	0.3	19.9	0.2
14.25	0.98	16.7	1.1	18.2	0.5	21.7	0.8	19.8	0.6
14.75	0.98	16.8	1.1	18.3	0.5	21.8	0.8	19.9	0.6
15.25	0.97	17.0	0.6	18.3	0.2	21.6	0.4	20.0	0.4
15.75	0.98	16.9	1.1	18.3	0.5	21.7	0.8	19.9	0.6
16.25	0.98	17.1	0.6	18.4	0.3	21.5	0.4	20.0	0.5
16.75	0.98	16.8	1.1	18.3	0.5	21.7	0.8	19.9	0.6
17.25	0.98	17.0	0.4	18.3	0.1	21.5	0.4	19.9	0.2
17.75	0.98	16.7	1.1	18.3	0.5	21.8	0.8	19.9	0.6
18.25	0.98	16.6	1.3	18.2	0.6	22.0	1.0	19.8	0.7
18.75	0.97	16.6	0.9	18.1	0.3	21.7	0.8	19.7	0.3
19.25	0.97	16.5	1.3	18.2	0.6	22.0	1.0	19.8	0.7
19.75	0.98	16.8	1.1	18.3	0.5	21.8	0.8	19.8	0.6
20.25	0.97	15.7	1.5	17.8	0.5	22.7	1.4	19.5	0.5
20.75	0.97	16.6	0.9	18.1	0.4	21.8	0.8	19.8	0.4
21.25	0.98	16.7	1.1	18.2	0.5	21.8	0.8	19.8	0.6
21.75	0.98	16.9	0.7	18.3	0.3	21.5	0.3	19.9	0.5
22.25	0.98	16.6	1.0	18.2	0.5	21.8	0.8	19.8	0.6
22.75	0.98	16.4	1.3	18.1	0.6	22.0	1.0	19.7	0.7
23.25	0.98	16.7	1.1	18.3	0.5	21.8	0.8	19.9	0.6
23.75	0.97	15.7	1.5	17.8	0.5	22.7	1.4	19.5	0.5
24.25	0.97	16.5	1.4	18.1	0.6	21.8	0.9	19.6	0.9
24.75	0.98	16.7	1.1	18.2	0.5	21.8	0.8	19.8	0.6
25.25	0.98	16.4	1.3	18.1	0.5	22.0	1.0	19.7	0.7
25.75	0.98	16.3	1.1	18.1	0.4	22.0	1.0	19.6	0.4
26.25	0.97	16.0	1.7	18.0	0.6	22.3	1.2	19.5	1.0
26.75	0.97	15.8	1.5	17.9	0.5	22.6	1.3	19.5	0.5
27.25	0.98	16.4	1.3	18.1	0.6	22.0	1.0	19.7	0.7
27.75	0.98	16.4	1.1	18.1	0.4	22.1	1.0	19.7	0.5
28.25	0.97	16.0	1.5	17.9	0.5	22.5	1.3	19.6	0.5
28.75	0.98	16.5	1.3	18.2	0.6	22.0	1.0	19.8	0.6
29.25	0.97	16.1	1.3	18.0	0.5	22.2	1.2	19.6	0.4
29.75	0.98	16.3	1.1	18.1	0.4	22.0	1.0	19.6	0.4
30.25	0.97	14.6	0.8	17.5	0.3	23.9	0.8	19.2	0.3
30.75	0.97	14.6	0.8	17.5	0.3	23.9	0.8	19.2	0.3
31.25	0.98	16.5	1.3	18.1	0.5	22.0	1.0	19.7	0.7
31.75	0.98	16.5	1.3	18.2	0.6	22.0	1.0	19.8	0.7
32.75	0.98	16.5	0.9	18.1	0.3	21.7	0.8	19.6	0.4
34.75	0.98	16.3	1.1	18.1	0.4	22.0	1.0	19.6	0.4
35.25	0.97	15.7	1.4	17.8	0.5	22.6	1.4	19.4	0.4
38.75	0.97	14.9	1.1	17.6	0.4	23.6	1.1	19.3	0.4
41.75	0.97	15.5	1.5	17.7	0.5	22.9	1.4	19.4	0.5
43.25	0.98	16.1	1.3	18.0	0.5	22.2	1.2	19.5	0.4
44.25	0.97	15.5	1.5	17.8	0.5	23.0	1.4	19.5	0.5
44.75	0.97	16.0	1.4	17.8	0.5	22.4	1.4	19.6	0.5
45.25	0.97	14.6	0.9	17.7	0.4	23.8	1.0	19.0	0.9
45.75	0.98	14.6	0.8	17.5	0.3	23.9	0.8	19.2	0.3
48.25	0.97	15.7	1.5	17.8	0.5	22.7	1.4	19.5	0.5
49.75	0.98	16.1	1.2	18.0	0.5	22.2	1.2	19.5	0.4

Table A 10 z-Scores of compiled paleo-climatic variables at 200 year time slices. *T = temperature; P = precipitation*

ID	Site	Var	Season	Latitude	Longitude	Median z-score of 200 year time slices (cal. BP)														
						3000 - 3200	3200 - 3400	3400 - 3600	3600 - 3800	3800 - 4000	4000 - 4200	4200 - 4400	4400 - 4600	4600 - 4800	4800 - 5000	5000 - 5200	5200 - 5400	5400 - 5600	5600 - 5800	5800 - 6000
1	Grotte de Clamouse	T	annual	43.710000	3.550000	0.37	1.54	0.96	0.63	0.57	0.01	-0.09	-1.13	-2.17	-1.00	-0.15	-0.44	-0.22	0.01	-0.90
2	PP10-07	T	annual	43.677000	-2.228000	-0.02	-0.12	-0.22	0.09	-0.02	-0.42	-0.22	-0.02	-0.22	-0.22	0.39	-0.02	-0.42	0.19	1.41
3	PP10-07	T	winter	43.677000	-2.228000	-0.19	-0.09	-0.29	0.20	-0.09	-0.29	-0.09	0.10	-0.49	-0.09	0.30	-0.09	-0.29	-0.09	1.28
4	PP10-07	T	summer	43.677000	-2.228000	0.11	0.11	-0.28	-0.08	-0.08	-0.47	-0.47	-0.08	-0.08	-0.28	0.49	0.11	-0.47	0.49	1.26
5	Monte Areo	P	annual	43.528889	-5.768889	NA	NA	-0.37	NA	NA	NA	0.70	NA	NA	NA	1.03	NA	-1.76	0.47	-0.07
6	Monte Areo	T	annual	43.528889	-5.768889	0.62	NA	NA	NA	-1.15	NA	NA	NA	0.13	NA	NA	NA	-1.32	0.68	1.04
7	PB06	P	annual	43.506604	3.875170	-0.65	0.67	0.85	0.43	-0.53	1.01	1.04	0.01	-1.25	-1.07	-0.78	-1.01	0.54	0.56	-0.20
8	Cuadramón	P	winter	43.474167	-7.534722	NA	-1.68	NA	NA	0.24	NA	0.41	NA	NA	0.05	NA	NA	0.98	NA	NA
9	Pedrido	P	winter	43.450278	-7.529167	1.22	-0.48	0.34	-0.40	0.17	0.02	0.29	1.55	0.12	-0.73	0.13	-0.85	NA	NA	NA
10	Alto de la Espina	P	annual	43.381111	-6.327222	0.23	-0.40	-0.82	0.96	-0.80	-0.19	0.47	-0.70	-1.33	0.30	1.25	-0.23	-0.13	NA	0.53
11	Cueva de Asiul	P	winter	43.316842	-3.591200	-0.47	-0.32	0.45	0.71	0.09	-1.14	-0.27	0.25	-1.06	0.04	0.81	0.73	0.09	-0.01	0.27
12	SU92-03	T	summer	43.195800	-10.113000	0.15	NA	NA	NA	NA	NA	0.91	NA	NA	NA	NA	NA	-1.07	NA	NA
13	Zalama	P	annual	43.135000	-3.409722	0.44	-0.43	1.22	1.58	0.06	0.17	0.20	0.90	0.18	-0.47	-1.46	-0.41	-1.22	-0.65	-1.23
14	Alsa	P	winter	43.117778	-4.016667	0.25	0.29	0.45	-1.41	0.22	-0.04	0.24	NA	NA	NA	NA	NA	NA	NA	NA
15	Alsa	P	annual	43.117778	-4.016667	-0.02	0.32	0.39	-1.47	0.34	0.32	0.24	NA	NA	NA	NA	NA	NA	NA	NA
16	Avellanosa	P	winter	43.116667	-4.364167	-1.35	-0.13	-0.80	-1.09	0.09	0.68	0.99	0.67	1.25	0.91	-0.51	1.04	-0.52	0.75	-1.97
17	Lago de Ajo	P	annual	43.050000	-6.150000	0.07	0.07	0.55	0.55	0.55	0.55	0.55	-2.35	-1.86	NA	-0.41	1.04	0.07	1.04	-0.41
18	Lago de Ajo	T	winter	43.050000	-6.150000	0.07	-0.36	-0.49	-0.36	0.03	-0.29	-0.80	0.03	2.96	NA	-1.00	0.36	-0.58	1.08	-0.64

ID	Site	Var	Season	Latitude	Longitude	Median z-score of 200 year time slices (cal. BP)														
						3000 - 3200	3200 - 3400	3400 - 3600	3600 - 3800	3800 - 4000	4000 - 4200	4200 - 4400	4400 - 4600	4600 - 4800	4800 - 5000	5000 - 5200	5200 - 5400	5400 - 5600	5600 - 5800	5800 - 6000
19	Kaite Cave	T	annual	43.033333	-3.650000	-0.63	-0.28	-0.45	1.01	0.75	NA	NA	NA	NA	NA	NA	NA	NA	NA	NA
20	KGSC-31	P	annual	43.006389	3.298889	0.00	0.03	-0.13	-0.54	0.27	-0.11	0.41	-0.11	-0.33	0.63	1.09	0.46	-0.67	-0.84	-0.89
21	KGSC-31	T	annual	43.006389	3.298889	-0.28	-0.41	-0.39	-0.03	-0.50	-0.23	0.29	0.51	0.05	0.41	-0.28	0.77	0.81	-0.15	-0.03
22	Cova da Arcoia	T	annual	42.610000	-7.090000	0.09	0.69	0.67	1.05	NA	NA	-1.11	-1.74	-1.13	-0.45	NA	-0.51	-0.41	-0.32	-0.32
23	Cova da Arcoia	P	winter	42.610000	-7.090000	0.70	0.99	0.30	-0.64	NA	NA	0.99	0.18	0.06	-0.23	NA	-0.85	-0.13	0.57	-1.82
24	Basa de la Mora	P	winter	42.533333	0.316667	0.70	-0.10	-0.09	0.02	-0.89	-1.63	-0.57	-1.48	0.57	0.75	NA	1.37	0.73	1.48	1.20
25	Basa de la Mora	P	annual	42.533333	0.316667	0.17	0.26	0.29	1.23	-1.39	-0.72	-0.53	-0.68	-1.31	NA	-0.21	1.27	1.57	0.48	0.26
26	Basa de la Mora	T	summer	42.533333	0.316667	-1.05	0.64	-1.42	0.81	-0.28	0.55	NA	-0.98	NA	NA	NA	NA	NA	1.18	NA
27	PRD-4	P	winter	42.533333	-8.516667	NA	-2.52	-0.86	0.00	0.96	0.09	NA	0.56	1.09	0.23	NA	0.63	NA	-0.09	-0.09
28	OMEXII-9K	T	summer	42.343000	-10.051000	NA	NA	0.65	NA	-0.06	NA	NA	-0.24	NA	0.65	NA	NA	0.83	NA	-1.84
29	Castelló d'Empúries	P	winter	42.281389	3.120278	-1.45	-2.44	-0.35	NA	0.47	0.21	0.41	NA	0.19	0.40	0.29	NA	1.14	0.31	0.83
30	Laguna de la Roya	P	annual	42.216667	-6.766667	-2.13	NA	0.55	-2.13	0.55	0.55	-0.34	-0.34	0.55	0.55	0.55	0.55	0.55	0.55	0.55
31	Laguna de la Roya	T	winter	42.216667	-6.766667	0.06	NA	1.99	1.99	-0.95	-0.55	0.89	-0.53	-0.59	-0.65	-0.55	-0.55	0.07	-0.54	-0.66
32	MD03-2697	T	summer	42.150000	-9.700000	NA	NA	NA	NA	0.46	NA	NA	NA	NA	NA	-1.15	NA	NA	NA	0.69
33	Sanabria	T	winter	42.100000	-6.733333	-1.25	-0.45	NA	-1.11	-0.82	0.13	0.63	-0.41	NA	NA	2.45	0.94	-0.52	0.46	1.15
34	Sanabria	P	annual	42.100000	-6.733333	-1.06	0.67	NA	0.67	1.02	-0.37	-1.75	-0.37	NA	NA	0.67	-0.71	0.67	-0.19	-0.37
35	Las Pardillas	P	winter	42.045556	-3.045278	NA	1.02	-0.92	0.59	0.20	-0.46	NA	0.97	1.00	0.99	-0.73	1.00	NA	-1.47	-1.48
36	Las Pardillas	P	annual	42.045556	-3.045278	NA	0.47	-0.49	-0.04	0.92	-0.47	NA	0.54	-0.77	1.58	0.57	-0.52	NA	-1.27	-0.95
37	Estanya	P	annual	42.027139	0.530434	-1.14	0.86	0.30	0.58	0.32	-0.04	-0.31	-0.86	-2.00	0.27	0.58	-0.55	-0.15	-0.64	-0.66

ID	Site	Var	Season	Latitude	Longitude	Median z-score of 200 year time slices (cal. BP)														
						3000 - 3200	3200 - 3400	3400 - 3600	3600 - 3800	3800 - 4000	4000 - 4200	4200 - 4400	4400 - 4600	4600 - 4800	4800 - 5000	5000 - 5200	5200 - 5400	5400 - 5600	5600 - 5800	5800 - 6000
38	Quintanar de la Sierra	P	annual	42.025278	-3.026111	NA	-0.66	NA	NA	-0.84	NA	0.25	NA	-0.32	-0.32	NA	1.89	NA	NA	NA
39	Hoyos de Iregua	P	winter	42.023889	-2.750000	-1.31	-0.29	NA	-0.93	-0.96	NA	-1.09	0.13	0.74	NA	0.77	0.23	NA	1.80	0.90
40	Espinosa de Cerrato	P	winter	41.956667	-3.935000	0.02	0.06	-0.92	-0.61	0.78	0.67	-0.52	-2.72	0.65	0.56	0.60	0.96	0.49	0.88	0.42
41	Espinosa de Cerrato	P	annual	41.956667	-3.935000	0.63	0.45	0.63	0.63	0.63	0.63	0.04	-2.19	-0.19	0.04	-1.04	-0.19	0.19	0.14	-0.04
42	Tubilla del Lago	P	winter	41.808417	-3.572675	0.78	0.80	-0.05	0.28	-0.12	0.30	0.94	0.00	0.57	-0.61	-0.29	-1.89	NA	-0.37	-0.72
43	PO200-10-28-1	T	summer	41.488000	-9.721000	NA	NA	0.94	NA	NA	NA	NA	NA	NA	NA	0.11	NA	NA	NA	-1.05
44	Hoya del Castillo	P	winter	41.481944	-0.158333	NA	NA	NA	NA	NA	NA	NA	NA	-1.46	-0.50	-0.72	-0.16	0.94	1.41	0.48
45	Hoya del Castillo	P	annual	41.481944	-0.158333	NA	NA	NA	NA	NA	NA	NA	NA	-1.29	-0.42	-1.06	0.13	1.22	1.22	0.21
46	El Carrizal	P	winter	41.320028	-4.146972	-2.62	1.21	0.32	0.99	-0.62	0.54	0.20	0.54	NA	-0.35	-0.47	NA	-0.20	0.44	NA
47	Cubelles	P	winter	41.200278	1.675000	0.61	0.62	0.71	0.50	0.86	0.78	0.24	-0.25	-1.18	-1.53	NA	0.18	0.33	-0.65	-1.98
48	Creixell	P	winter	41.155556	1.433889	-0.89	NA	-2.29	0.44	-0.30	0.32	1.21	NA	0.57	0.22	0.05	-0.30	-0.57	NA	1.53
49	Molinos Cave	T	annual	40.792500	-4.492000	NA	-0.51	0.51	1.45	1.14	-0.91	NA	NA	NA	-0.35	0.30	0.09	0.02	-0.68	-0.61
50	Molinos Cave	P	winter	40.792500	-4.492000	NA	0.47	1.12	-0.05	0.11	0.29	NA	NA	NA	-1.39	-1.48	-2.66	-1.75	-1.62	-1.70
51	Amposta	P	annual	40.706669	0.574036	-0.61	NA	-1.70	-0.24	-0.97	0.49	-0.73	0.24	0.97	NA	0.49	0.24	1.21	1.21	NA
52	Amposta	P	winter	40.706669	0.574036	-0.17	NA	0.09	1.06	0.36	-0.08	-1.84	-1.84	0.80	NA	1.06	1.33	-0.17	-0.43	NA
53	MD95-2040	T	summer	40.581833	-9.861167	-0.12	0.91	NA	0.63	-1.70	0.63	NA	-0.58	0.82	0.72	NA	-1.80	0.82	0.54	-0.86
54	El Maíllo	P	annual	40.546667	-6.209722	0.46	0.58	0.25	1.25	NA	0.95	1.71	0.84	NA	0.77	NA	NA	-0.97	-0.52	0.43
55	El Maíllo	P	winter	40.546667	-6.209722	NA	-0.32	0.25	-1.85	NA	-0.38	-0.62	NA	-0.32	-0.99	1.36	NA	-0.42	0.28	1.35
56	MD99-2343	P	annual	40.497333	4.028167	-0.37	-0.37	-1.35	-0.37	-0.37	-0.37	0.60	-0.37	-0.37	-0.37	-0.37	1.58	1.58	-0.37	1.58

ID	Site	Var	Season	Latitude	Longitude	Median z-score of 200 year time slices (cal. BP)													
						3000 - 3200	3200 - 3400	3400 - 3600	3600 - 3800	3800 - 4000	4000 - 4200	4200 - 4400	4400 - 4600	4600 - 4800	4800 - 5000	5000 - 5200	5200 - 5400	5400 - 5600	5600 - 5800	5800 - 6000
57	Ejulve Cave	P	winter	40.450000	-0.350000	0.67	0.12	0.24	-0.80	0.60	0.73	0.13	0.57	0.59	-0.73	-0.13	-1.68	-0.17	-0.29	0.55
58	Peña Negra	P	winter	40.334722	-5.792222	1.47	0.73	-0.22	-0.42	-0.85	-1.43	NA	NA	NA	NA	NA	NA	NA	NA	NA
59	El Payo	P	winter	40.253333	-6.771111	1.24	-0.24	0.84	-0.94	-0.90	NA	NA	NA	NA	NA	NA	NA	NA	NA	NA
60	Algendar	P	winter	39.940556	3.958611	2.19	-1.28	0.86	-1.55	-1.12	0.43	-0.50	0.09	0.14	-0.46	-0.11	0.17	0.25	-0.18	0.15
61	Algendar	P	annual	39.940556	3.958611	-0.10	0.72	0.89	1.04	1.09	0.89	0.83	0.45	-0.14	0.27	0.19	0.28	-0.64	-0.71	-0.53
62	Hort Timoner	P	winter	39.875000	4.126389	-0.22	NA	-1.58	NA	-1.58	-1.51	-0.25	2.16	-0.56	0.93	-0.18	0.32	0.02	-0.64	0.84
63	Hort Timoner	P	annual	39.875000	4.126389	0.11	NA	-0.38	NA	0.71	0.51	-0.02	0.28	0.73	0.59	-0.83	0.40	0.45	-0.01	0.13
64	Navarrés	P	annual	39.093333	-0.683333	-0.64	-1.30	0.04	-1.05	-1.14	0.03	0.06	1.21	0.54	0.01	0.90	2.07	0.31	-0.56	0.45
65	CC-17	P	winter	39.083333	-3.866667	1.33	1.07	NA	NA	0.63	1.17	0.20	NA	0.58	NA	-1.08	NA	-1.16	-0.87	0.35
66	MD03-2699	T	annual	39.036700	-10.660500	-1.24	-0.83	-0.35	-0.41	0.51	-1.09	-0.45	-0.02	1.10	1.53	1.22	0.69	0.89	-0.41	-1.80
67	MD03-2699	P	annual	39.036700	-10.660500	-0.20	-0.01	-1.04	-0.27	0.36	-1.14	0.02	0.52	0.40	1.14	0.77	0.90	1.27	-0.95	-2.66
68	Eivissa	P	winter	38.915833	1.435000	0.15	1.39	-0.76	0.91	-0.54	-1.62	-1.71	0.00	1.20	0.62	0.39	0.30	0.71	-1.20	NA
69	Villaverde	P	winter	38.800000	-2.366667	-1.08	-0.04	-0.22	-0.29	-1.67	-0.32	0.30	-0.01	-0.08	-0.03	0.08	1.50	0.53	0.18	0.80
70	Villaverde	P	annual	38.800000	-2.366667	-1.16	-1.07	0.03	0.96	0.17	-0.33	-0.48	-1.55	-0.92	-1.01	-0.30	0.96	0.96	0.96	0.96
71	D13882	T	annual	38.634500	-9.454200	-1.50	-1.50	0.25	-0.92	0.68	-0.63	-0.19	0.54	0.98	-0.34	0.39	-0.04	-0.63	1.71	0.98
72	D13882	P	annual	38.634500	-9.454200	-1.27	-1.13	-0.53	-1.02	-0.47	0.41	0.25	0.31	-0.37	-0.26	0.95	0.84	0.89	1.51	1.71
73	Villena	P	winter	38.629667	-0.919889	NA	NA	0.66	-1.94	0.25	0.50	0.60	0.53	-0.16	0.04	0.98	0.56	0.45	-1.72	-0.81
74	D13902	T	annual	38.554000	-9.335500	NA	-0.89	NA	NA	-0.84	NA	0.81	0.92	NA	NA	NA	NA	NA	NA	NA
75	D13902	P	annual	38.554000	-9.335500	NA	-1.45	NA	NA	0.20	NA	0.45	0.80	NA	NA	NA	NA	NA	NA	NA

ID	Site	Var	Season	Latitude	Longitude	Median z-score of 200 year time slices (cal. BP)													
						3000 - 3200	3200 - 3400	3400 - 3600	3600 - 3800	3800 - 4000	4000 - 4200	4200 - 4400	4400 - 4600	4600 - 4800	4800 - 5000	5000 - 5200	5200 - 5400	5400 - 5600	5600 - 5800	5800 - 6000
76	Siles	P	annual	38.400000	-2.500000	-0.09	-0.28	0.27	-0.57	-1.73	0.06	-1.41	0.43	-1.18	0.92	-0.51	0.92	1.34	1.38	1.63
77	El Sabinar	P	annual	38.200000	-2.116667	-1.17	-1.43	-1.09	-0.50	-0.68	-1.37	-1.47	0.25	0.55	0.80	0.86	1.07	0.90	1.07	1.07
78	Elx	P	winter	38.174444	-0.752778	NA	NA	NA	-1.15	-0.63	-1.01	-0.05	1.05	1.23	0.48	NA	0.63	0.41	-0.12	-0.53
79	Elx	P	annual	38.174444	-0.752778	NA	NA	NA	-1.51	-0.12	-0.23	-0.11	0.94	1.04	0.05	NA	0.51	0.01	-0.94	-1.28
80	Santo Andre	P	winter	38.083333	-8.783333	NA	-0.54	NA	-0.27	NA	-1.32	NA	-0.23	NA	NA	1.35	NA	1.01	NA	NA
81	Santo Andre	P	annual	38.083333	-8.783333	NA	-1.92	NA	-0.09	NA	0.96	NA	0.34	NA	NA	0.34	NA	0.38	NA	NA
82	Cañada de la Cruz	P	annual	38.066667	-2.700000	-0.68	-0.46	-0.75	1.37	NA	0.91	NA	NA	NA	1.01	NA	NA	NA	NA	1.59
83	Cañada de la Cruz	P	winter	38.066667	-2.700000	-0.69	-0.22	-0.83	1.34	NA	0.91	NA	NA	NA	0.94	NA	NA	NA	NA	1.62
84	MD95-2041	T	summer	37.833333	-9.510833	NA	0.83	NA	NA	-0.21	NA	NA	-1.60	NA	NA	0.14	NA	NA	0.83	NA
85	MD95-2042	T	summer	37.799833	-10.166500	-0.93	NA	-0.65	NA	-1.34	NA	-0.65	NA	0.58	NA	0.72	NA	1.27	NA	1.00
86	MD95-2042	P	winter	37.799833	-10.166500	NA	-0.43	NA	-0.26	NA	0.45	0.45	0.14	NA	-0.40	0.36	-1.60	1.98	-0.57	0.78
87	MD95-2042	T	winter	37.799833	-10.166500	NA	-0.89	NA	-2.02	NA	-1.71	-0.47	-0.65	NA	-0.14	0.58	0.18	1.57	0.58	0.88
88	MD95-2042	P	annual	37.799833	-10.166500	NA	-0.61	NA	-0.68	NA	-2.48	0.98	-1.17	NA	0.57	1.19	0.01	-0.47	0.64	0.29
89	MD01-2444	T	annual	37.561333	-10.142167	-0.43	-0.80	-0.21	-0.43	-0.06	-0.65	0.27	-0.69	0.96	0.16	-1.53	1.33	1.77	0.30	0.96
90	Antas	P	winter	37.208333	-1.823611	1.60	NA	-0.80	NA	0.16	NA	NA	-1.12	NA	-0.95	NA	0.64	NA	0.46	NA
91	Antas	P	annual	37.208333	-1.823611	-0.71	NA	-0.16	NA	-1.05	NA	NA	0.93	NA	1.07	NA	-1.12	NA	1.05	NA
92	Borreguil de la Virgen	P	winter	37.054167	-3.377778	-1.03	-0.60	-1.67	-0.38	0.09	-1.00	0.14	1.09	-0.19	1.36	-0.66	-0.14	-0.05	0.31	0.73
93	Borreguil de la Virgen	P	annual	37.054167	-3.377778	-2.75	-1.16	-2.96	-0.26	-1.06	-1.06	-0.04	-0.03	0.57	0.83	0.52	0.31	0.41	0.92	0.83
94	Laguna Hondera	P	annual	37.048000	-3.294333	-1.03	0.13	1.54	0.51	-1.67	-0.64	NA	0.13	0.13	NA	1.67	0.13	0.51	0.00	-0.90

ID	Site	Var	Season	Latitude	Longitude	Median z-score of 200 year time slices (cal. BP)													
						3000 - 3200	3200 - 3400	3400 - 3600	3600 - 3800	3800 - 4000	4000 - 4200	4200 - 4400	4400 - 4600	4600 - 4800	4800 - 5000	5000 - 5200	5200 - 5400	5400 - 5600	5600 - 5800	5800 - 6000
95	Laguna de Río Seco	P	winter	37.040500	-3.342833	-1.59	NA	0.08	-0.37	-0.91	-0.81	-0.70	-0.39	0.74	-0.28	1.40	1.18	0.61	0.87	1.27
96	Laguna de Río Seco	P	annual	37.040500	-3.342833	-0.80	NA	-1.94	-1.04	0.14	0.61	0.61	0.58	1.21	0.43	1.21	-0.16	-1.53	0.38	0.56
97	Padul	P	winter	37.011047	-3.603906	-1.07	-1.05	-0.84	-0.81	-0.81	0.01	-0.06	0.39	0.72	2.15	1.80	NA	0.26	0.98	0.96
98	Padul	P	annual	37.011047	-3.603906	-0.72	-1.13	0.03	-0.96	-0.38	0.12	-0.09	0.53	0.45	1.53	0.16	-1.05	1.03	0.95	1.94
99	Donana	P	winter	36.941667	-6.413333	-1.02	-0.03	-1.15	0.08	1.15	-0.52	1.34	NA	0.97	NA	1.70	NA	NA	NA	NA
100	Donana	P	annual	36.941667	-6.413333	-1.39	-0.01	0.87	-0.91	-0.25	-0.20	0.98	NA	2.03	NA	1.36	NA	NA	NA	NA
101	Sierra de Gádor	P	annual	36.900000	-2.916667	-1.58	-0.17	-0.59	-0.80	-0.33	0.13	0.26	-0.37	-0.28	0.13	-0.57	0.77	1.25	1.74	1.64
102	Sierra de Gádor	P	winter	36.900000	-2.916667	-1.17	-0.83	-0.96	-0.67	0.41	-0.03	0.53	0.34	-0.42	0.60	0.20	0.69	1.02	1.43	1.11
103	Roquetas de Mar	P	winter	36.794444	-2.588889	-0.93	NA	NA	-0.87	-1.62	0.40	-0.53	-0.12	-0.02	-0.09	0.99	0.89	1.59	0.64	-1.35
104	Roquetas de Mar	P	annual	36.794444	-2.588889	-1.13	NA	NA	-0.96	-1.63	0.61	0.15	-0.11	0.08	-0.02	0.59	1.07	1.47	0.82	-1.43
105	San Rafael	P	winter	36.773611	-2.601389	NA	-1.07	-1.77	NA	NA	-0.65	NA	-1.54	NA	-0.60	-0.51	0.16	0.07	1.12	0.77
106	San Rafael	P	annual	36.773611	-2.601389	NA	1.47	-1.73	NA	NA	1.81	NA	-0.27	NA	-0.66	-0.98	-0.55	-0.36	0.55	0.92
107	San Rafael	P	annual	36.773611	-2.601389	NA	-0.90	-2.70	NA	NA	-1.46	NA	-1.60	1.29	1.48	-0.26	-0.34	-0.06	0.48	0.56
108	Cabo de Gata	P	winter	36.771389	-2.228611	-1.82	0.00	-1.08	0.23	0.75	0.67	0.12	-0.49	0.83	0.81	0.63	0.79	0.29	-0.41	-2.01
109	Lake Medina	P	annual	36.617778	-6.053611	0.32	0.53	0.34	0.46	0.54	0.53	0.14	0.53	0.53	-0.20	0.53	0.52	-0.45	0.53	-1.36
110	El Refugio Cave	P	annual	36.583333	-4.583333	1.55	0.17	0.72	-0.05	-1.36	-0.74	0.28	-0.28	-0.40	0.30	0.29	0.99	-0.04	0.79	0.86
111	Gueldaman Cave	P	annual	36.433300	4.566700	-0.74	-0.22	-0.09	-0.38	-1.35	-0.80	-1.29	0.09	1.45	1.65	1.41	1.34	0.45	1.12	NA
112	GeoB5901-2	P	winter	36.380000	-7.071333	1.21	1.15	0.73	-1.45	0.49	0.04	0.14	-0.90	0.18	-1.14	-0.40	-0.18	-0.42	NA	NA
113	GeoB5901-2	T	annual	36.380000	-7.071333	0.30	-0.06	-0.90	-0.47	0.48	2.01	3.15	0.40	-0.05	-0.68	-0.36	-0.77	-0.98	NA	NA

ID	Site	Var	Season	Latitude	Longitude	Median z-score of 200 year time slices (cal. BP)														
						3000 - 3200	3200 - 3400	3400 - 3600	3600 - 3800	3800 - 4000	4000 - 4200	4200 - 4400	4400 - 4600	4600 - 4800	4800 - 5000	5000 - 5200	5200 - 5400	5400 - 5600	5600 - 5800	5800 - 6000
114	GeoB5901-2	T	summer	36.380000	-7.071333	-0.69	-0.86	-0.69	-1.04	-0.52	0.26	-0.52	-0.78	-0.35	-0.17	0.60	-0.09	0.00	-0.17	1.47
115	GeoB5901-2	T	winter	36.380000	-7.071333	0.76	0.84	0.92	1.09	0.42	-0.33	0.59	0.67	0.17	0.09	-0.75	0.09	-0.25	-0.08	-1.42
116	M39008-3	T	annual	36.380000	-7.071667	NA	NA	NA	-1.30	NA	NA	NA	-0.10	NA	-0.58	NA	NA	1.11	NA	0.87
117	HER_GC_T1	T	annual	36.370146	-4.299015	-1.29	-0.96	-1.11	-1.00	-0.87	-0.62	-0.64	0.39	0.18	0.44	0.33	0.24	0.56	1.54	2.31
118	TTR14-300G	P	annual	36.358867	-1.791783	NA	-2.14	0.27	-0.92	NA	-0.42	-0.96	NA	0.79	NA	0.32	0.72	NA	0.56	1.09
119	ODP-161-976A	P	winter	36.205333	-4.312667	0.33	0.34	0.09	1.14	1.05	0.33	0.58	1.40	-0.03	-1.10	0.32	-0.08	-0.20	-0.69	NA
120	ODP-161-976A	T	annual	36.205333	-4.312667	0.49	-0.61	-0.97	-0.92	-1.01	-1.01	-0.81	-1.15	-0.32	0.65	1.03	0.60	-0.74	1.03	NA
121	ODP-161-976A	T	summer	36.205333	-4.312667	0.01	-0.41	-0.41	0.43	0.58	NA	1.00	-0.83	0.43	0.43	-0.55	NA	0.15	NA	NA
122	ODP-161-976A	T	winter	36.205333	-4.312667	-0.26	0.70	-0.26	-0.90	-0.42	NA	-0.74	1.02	-0.42	-0.58	0.54	NA	-0.74	NA	NA
123	ODP-161-976A	P	annual	36.205333	-4.312667	NA	-0.05	2.03	NA	NA	NA	1.38	NA	-0.64	-0.74	-0.80	-0.89	0.40	NA	-0.06
124	ODP-161-976A	P	summer	36.205333	-4.312667	NA	-1.10	1.79	NA	NA	NA	1.08	NA	-0.15	-0.04	-0.08	-1.06	0.90	NA	-1.19
125	ODP-161-976A	P	winter	36.205333	-4.312667	NA	-0.11	2.06	NA	NA	NA	1.39	NA	-0.74	-0.74	-0.98	0.00	0.24	NA	-0.39
126	ODP-161-976A	T	annual	36.205333	-4.312667	NA	0.02	1.59	NA	NA	NA	-0.25	NA	-0.98	-0.89	-0.89	1.59	0.40	NA	0.40
127	ODP-161-976A	T	summer	36.205333	-4.312667	NA	0.40	1.80	NA	NA	NA	0.30	NA	-1.07	-1.15	-0.89	0.35	0.45	NA	0.87
128	ODP-161-976A	T	winter	36.205333	-4.312667	NA	-0.72	0.14	NA	NA	NA	-1.09	NA	-0.18	-0.18	0.09	2.64	-0.39	NA	-0.13
129	TTR-17_434G	T	summer	36.205220	-4.312250	1.72	0.84	-0.12	-0.38	-0.29	-0.03	-0.21	0.06	1.11	0.49	-0.47	-0.56	-1.26	0.49	-0.82
130	TTR-17_434G	T	annual	36.205220	-4.312250	1.92	0.55	0.29	1.23	0.20	-0.83	-0.48	1.14	0.72	-0.14	-0.83	-1.34	-0.83	-0.65	-0.83
131	TTR-12_293G	T	summer	36.173567	-2.754667	NA	0.44	NA	0.19	NA	1.94	NA	0.19	0.19	NA	-0.81	NA	-1.06	NA	-1.06
132	TTR-12_293G	T	annual	36.173567	-2.754667	NA	0.21	NA	1.22	NA	-1.47	NA	-0.13	-0.46	NA	-1.14	NA	0.55	NA	1.22

ID	Site	Var	Season	Latitude	Longitude	Median z-score of 200 year time slices (cal. BP)													
						3000 - 3200	3200 - 3400	3400 - 3600	3600 - 3800	3800 - 4000	4000 - 4200	4200 - 4400	4400 - 4600	4600 - 4800	4800 - 5000	5000 - 5200	5200 - 5400	5400 - 5600	5600 - 5800	5800 - 6000
133	TTR-12_293G	T	annual	36.173567	-2.754667	NA	0.63	NA	1.23	NA	0.79	NA	-0.10	0.53	NA	-0.20	NA	-1.47	NA	-1.41
134	MD95-2043	P	winter	36.143333	-2.621167	1.63	0.84	1.03	0.52	1.54	0.38	0.86	0.05	-2.07	0.60	-0.12	-0.58	-0.65	-0.58	-0.32
135	MD95-2043	P	summer	36.143333	-2.621167	-0.58	-0.61	-0.96	-1.06	-0.75	-1.29	0.01	0.01	1.66	-0.09	0.42	0.91	-0.43	-0.25	0.92
136	MD95-2043	P	annual	36.143333	-2.621167	1.23	0.45	0.41	0.01	1.05	-0.24	0.69	0.51	-1.99	0.21	-0.25	-0.94	0.54	0.04	0.07
137	MD95-2043	T	annual	36.143333	-2.621167	-0.22	-0.36	-0.63	0.58	0.44	0.18	0.58	0.31	1.78	-0.63	0.04	-1.29	-1.29	-0.63	1.25
138	MD95-2043	P	annual	36.143333	-2.621167	0.99	0.76	-0.44	-1.53	-0.05	-0.18	0.94	0.01	-0.98	-0.50	-0.55	0.28	0.00	1.18	1.09
139	MD95-2043	P	winter	36.143333	-2.621167	-1.50	-1.12	-1.29	-0.82	0.02	0.18	0.59	0.04	-0.37	-0.69	0.02	-0.09	1.77	1.45	0.24
140	ODP-161-977	T	annual	36.031700	-1.955283	-1.43	NA	NA	NA	0.12	NA	NA	0.86	NA	NA	NA	0.45	NA	NA	NA
141	MD99-2339	T	summer	35.885500	-7.527833	-1.21	-1.41	NA	NA	1.08	NA	NA	NA	1.08	NA	0.09	NA	NA	NA	0.29
142	Chaara Cave	P	winter	33.950000	-4.246000	-0.48	-0.63	-0.28	0.54	0.70	-0.02	-0.42	-0.43	NA	-0.11	-0.57	-1.11	0.84	0.84	0.14
143	Chaara Cave	P	winter	33.950000	-4.246000	-0.75	-1.87	-0.83	-0.91	0.27	0.14	0.21	0.14	0.43	1.01	0.58	-0.52	0.00	-0.06	-0.06
144	Grotte de Piste	P	winter	33.840000	-4.090000	0.04	-0.19	-0.26	1.42	0.43	0.63	0.61	0.45	-0.49	-0.90	-0.24	-0.24	-0.85	-0.85	0.20
145	Lake Sidi Ali	P	winter	33.050000	-5.000000	-0.93	-0.38	-0.86	-0.56	-0.02	0.33	-0.38	0.40	0.16	0.21	0.09	-0.26	0.39	2.59	0.39
146	Lake Sidi Ali	T	summer	33.050000	-5.000000	-0.11	-0.59	-0.80	-0.87	-0.82	-1.10	0.29	0.87	-0.07	1.29	1.39	1.74	1.59	1.71	1.80
147	Tigalmamine	T	summer	32.900000	-5.350000	-2.49	-1.42	-1.39	-0.41	-0.07	0.28	0.35	0.25	0.11	0.72	0.74	0.66	0.95	0.88	0.80
148	Tigalmamine	P	winter	32.900000	-5.350000	-3.01	0.47	-0.37	0.44	0.47	0.37	-2.09	-1.34	0.52	0.45	0.56	0.36	0.47	0.40	0.29
149	ADP 01/06	P	winter	37.110503	-8.345146	-0.35	0.22	NA	-1.75	-0.66	NA	NA	0.84	NA	NA	NA	1.16	NA	NA	0.53
150	VDL PB2	P	winter	37.055965	-8.074490	0.40	-0.20	-0.31	NA	NA	NA	NA	NA	NA	NA	NA	NA	NA	NA	NA
151	P01-5	P	winter	37.085105	-8.138509	0.46	0.03	NA	2.01	NA	0.90	NA	-0.58	-0.15	0.50	-1.32	NA	NA	NA	NA

ID	Site	Var	Season	Latitude	Longitude	Median z-score of 200 year time slices (cal. BP)													
						3000 - 3200	3200 - 3400	3400 - 3600	3600 - 3800	3800 - 4000	4000 - 4200	4200 - 4400	4400 - 4600	4600 - 4800	4800 - 5000	5000 - 5200	5200 - 5400	5400 - 5600	5600 - 5800	5800 - 6000
152	P01-5	P	annual	37.085105	-8.138509	1.23	1.31	NA	1.23	NA	0.99	NA	-0.55	0.01	-0.76	-1.16	NA	NA	NA	NA
153	ABI 05/07	P	winter	37.152416	-8.594227	-0.36	-0.51	-1.51	-0.11	0.42	1.36	-1.05	0.07	-1.15	-0.98	0.89	0.42	0.50	1.39	0.50
154	Lagoa Comprida	P	winter	40.362778	-7.636111	-1.44	-0.50	0.02	-0.49	0.79	-0.86	-0.20	0.55	-1.04	-0.67	-0.26	0.54	0.82	1.53	0.97
155	Charco de Candieira	P	winter	40.341667	-7.576389	-1.39	-1.47	-1.26	0.21	0.39	0.78	1.11	1.05	1.02	-0.69	-0.28	0.42	-0.14	-0.24	0.33
156	ALP III	P	winter	39.221083	-8.568478	-1.41	-0.82	-0.75	-1.19	-0.64	-1.17	-0.46	-0.07	1.37	0.85	1.43	0.43	0.37	0.75	0.96
157	501.029	P	winter	39.387519	-8.532257	-0.89	-1.24	-1.03	1.04	1.32	NA	-0.34	-0.96	-0.43	NA	1.76	0.41	NA	-0.08	0.97

Table A 11 LOESS interpolated seasonal precipitation data from the SE of the Iberian Peninsula based on compiled paleo-climatic data.

Age (cal. BP)	SE Iberian precipitation (z-score)		
	annual	winter	summer
3000	NA	NA	NA
3001	NA	-0.72	NA
3002	NA	-0.72	NA
3003	NA	-0.72	NA
3004	NA	-0.72	NA
3005	NA	-0.72	NA
3006	NA	-0.72	NA
3007	-0.93	-0.72	-0.21
3008	-0.93	-0.72	-0.21
3009	-0.93	-0.72	-0.21
3010	-0.92	-0.72	-0.21
3011	-0.92	-0.72	-0.21
3012	-0.92	-0.72	-0.20
3013	-0.92	-0.72	-0.20
3014	-0.92	-0.72	-0.20
3015	-0.92	-0.72	-0.20
3016	-0.91	-0.72	-0.20
3017	-0.91	-0.72	-0.20
3018	-0.91	-0.72	-0.19
3019	-0.91	-0.72	-0.19
3020	-0.91	-0.72	-0.19
3021	-0.91	-0.72	-0.19
3022	-0.90	-0.72	-0.19
3023	-0.90	-0.72	-0.19
3024	-0.90	-0.72	-0.18
3025	-0.90	-0.72	-0.18
3026	-0.90	-0.71	-0.18
3027	-0.89	-0.71	-0.18
3028	-0.89	-0.71	-0.18
3029	-0.89	-0.71	-0.18
3030	-0.89	-0.71	-0.18
3031	-0.89	-0.71	-0.17
3032	-0.89	-0.71	-0.17
3033	-0.88	-0.71	-0.17
3034	-0.88	-0.71	-0.17
3035	-0.88	-0.71	-0.17
3036	-0.88	-0.71	-0.17
3037	-0.88	-0.71	-0.17
3038	-0.87	-0.71	-0.17
3039	-0.87	-0.71	-0.16
3040	-0.87	-0.71	-0.16
3041	-0.87	-0.71	-0.16
3042	-0.87	-0.71	-0.16
3043	-0.87	-0.71	-0.16
3044	-0.86	-0.70	-0.16
3045	-0.86	-0.70	-0.16
3046	-0.86	-0.70	-0.16
3047	-0.86	-0.70	-0.16
3048	-0.86	-0.70	-0.16
3049	-0.86	-0.70	-0.16
3050	-0.85	-0.70	-0.16
3051	-0.85	-0.70	-0.15
3052	-0.85	-0.70	-0.15
3053	-0.85	-0.70	-0.15
3054	-0.85	-0.69	-0.15
3055	-0.85	-0.69	-0.15
3056	-0.84	-0.69	-0.15
3057	-0.84	-0.69	-0.15
3058	-0.84	-0.69	-0.15
3059	-0.84	-0.69	-0.15
3060	-0.84	-0.69	-0.15
3061	-0.84	-0.69	-0.15
3062	-0.84	-0.68	-0.15
3063	-0.83	-0.68	-0.15
3064	-0.83	-0.68	-0.15
3065	-0.83	-0.68	-0.15
3066	-0.83	-0.68	-0.15
3067	-0.83	-0.68	-0.15
3068	-0.83	-0.68	-0.15
3069	-0.82	-0.67	-0.15
3070	-0.82	-0.67	-0.15
3071	-0.82	-0.67	-0.15
3072	-0.82	-0.67	-0.15
3073	-0.82	-0.67	-0.15
3074	-0.82	-0.67	-0.15
3075	-0.82	-0.66	-0.15
3076	-0.81	-0.66	-0.15
3077	-0.81	-0.66	-0.15
3078	-0.81	-0.66	-0.15
3079	-0.81	-0.66	-0.15
3080	-0.81	-0.65	-0.15
3081	-0.81	-0.65	-0.15
3082	-0.81	-0.65	-0.16
3083	-0.81	-0.65	-0.16
3084	-0.80	-0.65	-0.16
3085	-0.80	-0.65	-0.16
3086	-0.80	-0.64	-0.16
3087	-0.80	-0.64	-0.16
3088	-0.80	-0.64	-0.16
3089	-0.80	-0.64	-0.16
3090	-0.80	-0.63	-0.16
3091	-0.79	-0.63	-0.16
3092	-0.79	-0.63	-0.16
3093	-0.79	-0.63	-0.16
3094	-0.79	-0.63	-0.16
3095	-0.79	-0.62	-0.16
3096	-0.79	-0.62	-0.16
3097	-0.79	-0.62	-0.17
3098	-0.78	-0.62	-0.17
3099	-0.78	-0.62	-0.17
3100	-0.78	-0.61	-0.17
3101	-0.78	-0.61	-0.17
3102	-0.78	-0.61	-0.17
3103	-0.78	-0.61	-0.17
3104	-0.77	-0.60	-0.17
3105	-0.77	-0.60	-0.17
3106	-0.77	-0.60	-0.17
3107	-0.77	-0.60	-0.17
3108	-0.77	-0.59	-0.17
3109	-0.77	-0.59	-0.17
3110	-0.77	-0.59	-0.18
3111	-0.76	-0.59	-0.18
3112	-0.76	-0.58	-0.18
3113	-0.76	-0.58	-0.18
3114	-0.76	-0.58	-0.18
3115	-0.76	-0.58	-0.18
3116	-0.76	-0.57	-0.18
3117	-0.75	-0.57	-0.18
3118	-0.75	-0.57	-0.18
3119	-0.75	-0.57	-0.18
3120	-0.75	-0.56	-0.18
3121	-0.75	-0.56	-0.18
3122	-0.74	-0.56	-0.18
3123	-0.74	-0.56	-0.18
3124	-0.74	-0.55	-0.19
3125	-0.74	-0.55	-0.19
3126	-0.74	-0.55	-0.19
3127	-0.73	-0.55	-0.19
3128	-0.73	-0.54	-0.19
3129	-0.73	-0.54	-0.19
3130	-0.73	-0.54	-0.19
3131	-0.73	-0.53	-0.19
3132	-0.72	-0.53	-0.19
3133	-0.72	-0.53	-0.20
3134	-0.72	-0.52	-0.20
3135	-0.72	-0.52	-0.20
3136	-0.72	-0.52	-0.20
3137	-0.72	-0.51	-0.20
3138	-0.71	-0.51	-0.20
3139	-0.71	-0.51	-0.20
3140	-0.71	-0.50	-0.21
3141	-0.71	-0.50	-0.21
3142	-0.71	-0.50	-0.21

Age (cal. BP)	SE Iberian precipitation (z-score)		
	annual	winter	summer
3143	-0.71	-0.49	-0.21
3144	-0.70	-0.49	-0.21
3145	-0.70	-0.49	-0.22
3146	-0.70	-0.48	-0.22
3147	-0.70	-0.48	-0.22
3148	-0.70	-0.47	-0.22
3149	-0.69	-0.47	-0.22
3150	-0.69	-0.47	-0.23
3151	-0.69	-0.46	-0.23
3152	-0.69	-0.46	-0.23
3153	-0.69	-0.45	-0.23
3154	-0.69	-0.45	-0.24
3155	-0.68	-0.45	-0.24
3156	-0.68	-0.44	-0.24
3157	-0.68	-0.44	-0.24
3158	-0.68	-0.43	-0.24
3159	-0.68	-0.43	-0.25
3160	-0.67	-0.43	-0.25
3161	-0.67	-0.42	-0.25
3162	-0.67	-0.42	-0.25
3163	-0.67	-0.41	-0.25
3164	-0.67	-0.41	-0.26
3165	-0.66	-0.40	-0.26
3166	-0.66	-0.40	-0.26
3167	-0.66	-0.40	-0.26
3168	-0.66	-0.39	-0.26
3169	-0.65	-0.39	-0.27
3170	-0.65	-0.38	-0.27
3171	-0.65	-0.38	-0.27
3172	-0.65	-0.38	-0.27
3173	-0.64	-0.37	-0.27
3174	-0.64	-0.37	-0.28
3175	-0.64	-0.36	-0.28
3176	-0.64	-0.36	-0.28
3177	-0.63	-0.35	-0.28
3178	-0.63	-0.35	-0.28
3179	-0.63	-0.35	-0.28
3180	-0.63	-0.34	-0.28
3181	-0.62	-0.34	-0.28
3182	-0.62	-0.33	-0.29
3183	-0.62	-0.33	-0.29
3184	-0.61	-0.33	-0.29
3185	-0.61	-0.32	-0.29
3186	-0.61	-0.32	-0.29
3187	-0.61	-0.31	-0.29
3188	-0.60	-0.31	-0.29
3189	-0.60	-0.31	-0.29
3190	-0.60	-0.30	-0.29
3191	-0.59	-0.30	-0.29
3192	-0.59	-0.30	-0.29
3193	-0.59	-0.29	-0.29
3194	-0.58	-0.29	-0.30
3195	-0.58	-0.29	-0.30
3196	-0.58	-0.28	-0.30
3197	-0.57	-0.28	-0.30
3198	-0.57	-0.27	-0.30
3199	-0.57	-0.27	-0.30
3200	-0.56	-0.27	-0.30
3201	-0.56	-0.26	-0.30
3202	-0.56	-0.26	-0.30
3203	-0.55	-0.26	-0.30
3204	-0.55	-0.26	-0.30
3205	-0.55	-0.25	-0.30
3206	-0.55	-0.25	-0.30
3207	-0.54	-0.25	-0.30
3208	-0.54	-0.24	-0.30
3209	-0.54	-0.24	-0.30
3210	-0.53	-0.23	-0.30
3211	-0.53	-0.23	-0.30
3212	-0.53	-0.23	-0.30
3213	-0.52	-0.22	-0.30
3214	-0.52	-0.22	-0.30
3215	-0.52	-0.22	-0.30
3216	-0.51	-0.21	-0.30

Age (cal. BP)	SE Iberian precipitation (z-score)		
	annual	winter	summer
3217	-0.51	-0.21	-0.30
3218	-0.51	-0.20	-0.30
3219	-0.50	-0.20	-0.30
3220	-0.50	-0.20	-0.30
3221	-0.50	-0.19	-0.31
3222	-0.49	-0.19	-0.31
3223	-0.49	-0.18	-0.31
3224	-0.49	-0.18	-0.31
3225	-0.48	-0.17	-0.31
3226	-0.48	-0.17	-0.31
3227	-0.48	-0.16	-0.31
3228	-0.48	-0.16	-0.31
3229	-0.47	-0.16	-0.32
3230	-0.47	-0.15	-0.32
3231	-0.47	-0.15	-0.32
3232	-0.46	-0.14	-0.32
3233	-0.46	-0.14	-0.32
3234	-0.46	-0.13	-0.32
3235	-0.46	-0.13	-0.33
3236	-0.45	-0.12	-0.33
3237	-0.45	-0.12	-0.33
3238	-0.45	-0.12	-0.33
3239	-0.44	-0.11	-0.33
3240	-0.44	-0.11	-0.33
3241	-0.44	-0.10	-0.34
3242	-0.44	-0.10	-0.34
3243	-0.43	-0.10	-0.34
3244	-0.43	-0.09	-0.34
3245	-0.43	-0.09	-0.34
3246	-0.42	-0.08	-0.34
3247	-0.42	-0.08	-0.34
3248	-0.42	-0.08	-0.34
3249	-0.41	-0.07	-0.34
3250	-0.41	-0.07	-0.34
3251	-0.41	-0.06	-0.34
3252	-0.40	-0.06	-0.34
3253	-0.40	-0.06	-0.34
3254	-0.40	-0.05	-0.34
3255	-0.39	-0.05	-0.34
3256	-0.39	-0.05	-0.34
3257	-0.38	-0.05	-0.34
3258	-0.38	-0.04	-0.34
3259	-0.38	-0.04	-0.34
3260	-0.37	-0.04	-0.34
3261	-0.37	-0.03	-0.33
3262	-0.37	-0.03	-0.33
3263	-0.36	-0.03	-0.33
3264	-0.36	-0.03	-0.33
3265	-0.35	-0.03	-0.33
3266	-0.35	-0.02	-0.32
3267	-0.34	-0.02	-0.32
3268	-0.34	-0.02	-0.32
3269	-0.34	-0.02	-0.32
3270	-0.33	-0.02	-0.31
3271	-0.33	-0.02	-0.31
3272	-0.32	-0.02	-0.31
3273	-0.32	-0.02	-0.30
3274	-0.32	-0.01	-0.30
3275	-0.31	-0.01	-0.30
3276	-0.31	-0.01	-0.29
3277	-0.30	-0.01	-0.29
3278	-0.30	-0.01	-0.29
3279	-0.29	-0.01	-0.28
3280	-0.29	-0.01	-0.28
3281	-0.29	-0.01	-0.27
3282	-0.28	-0.01	-0.27
3283	-0.28	-0.01	-0.27
3284	-0.27	-0.01	-0.26
3285	-0.27	-0.01	-0.26
3286	-0.27	-0.01	-0.25
3287	-0.26	-0.01	-0.25
3288	-0.26	-0.01	-0.25
3289	-0.25	-0.01	-0.24
3290	-0.25	-0.01	-0.24

Age (cal. BP)	SE Iberian precipitation (z-score)		
	annual	winter	summer
3291	-0.25	-0.02	-0.23
3292	-0.24	-0.02	-0.23
3293	-0.24	-0.02	-0.22
3294	-0.24	-0.02	-0.22
3295	-0.23	-0.02	-0.21
3296	-0.23	-0.02	-0.21
3297	-0.23	-0.02	-0.20
3298	-0.22	-0.02	-0.20
3299	-0.22	-0.02	-0.20
3300	-0.22	-0.03	-0.19
3301	-0.21	-0.03	-0.19
3302	-0.21	-0.03	-0.18
3303	-0.21	-0.03	-0.18
3304	-0.20	-0.03	-0.17
3305	-0.20	-0.03	-0.17
3306	-0.20	-0.03	-0.16
3307	-0.20	-0.04	-0.16
3308	-0.19	-0.04	-0.15
3309	-0.19	-0.04	-0.15
3310	-0.19	-0.04	-0.15
3311	-0.19	-0.04	-0.14
3312	-0.18	-0.05	-0.14
3313	-0.18	-0.05	-0.13
3314	-0.18	-0.05	-0.13
3315	-0.18	-0.05	-0.13
3316	-0.18	-0.05	-0.12
3317	-0.17	-0.06	-0.12
3318	-0.17	-0.06	-0.11
3319	-0.17	-0.06	-0.11
3320	-0.17	-0.06	-0.11
3321	-0.17	-0.06	-0.10
3322	-0.17	-0.07	-0.10
3323	-0.17	-0.07	-0.10
3324	-0.17	-0.07	-0.10
3325	-0.16	-0.07	-0.09
3326	-0.16	-0.07	-0.09
3327	-0.16	-0.08	-0.09
3328	-0.16	-0.08	-0.08
3329	-0.16	-0.08	-0.08
3330	-0.16	-0.08	-0.08
3331	-0.17	-0.09	-0.08
3332	-0.17	-0.09	-0.08
3333	-0.17	-0.09	-0.08
3334	-0.17	-0.09	-0.08
3335	-0.17	-0.10	-0.07
3336	-0.17	-0.10	-0.07
3337	-0.17	-0.10	-0.07
3338	-0.18	-0.10	-0.07
3339	-0.18	-0.10	-0.07
3340	-0.18	-0.11	-0.07
3341	-0.18	-0.11	-0.07
3342	-0.18	-0.11	-0.07
3343	-0.19	-0.12	-0.07
3344	-0.19	-0.12	-0.07
3345	-0.19	-0.12	-0.07
3346	-0.20	-0.13	-0.07
3347	-0.20	-0.13	-0.07
3348	-0.20	-0.14	-0.06
3349	-0.20	-0.14	-0.06
3350	-0.21	-0.15	-0.06
3351	-0.21	-0.15	-0.06
3352	-0.21	-0.16	-0.06
3353	-0.22	-0.16	-0.06
3354	-0.22	-0.17	-0.05
3355	-0.22	-0.17	-0.05
3356	-0.23	-0.18	-0.05
3357	-0.23	-0.18	-0.05
3358	-0.23	-0.19	-0.04
3359	-0.24	-0.19	-0.04
3360	-0.24	-0.20	-0.04
3361	-0.24	-0.21	-0.03
3362	-0.24	-0.21	-0.03
3363	-0.25	-0.22	-0.03
3364	-0.25	-0.22	-0.03

Age (cal. BP)	SE Iberian precipitation (z-score)		
	annual	winter	summer
3365	-0.25	-0.23	-0.02
3366	-0.25	-0.24	-0.02
3367	-0.26	-0.24	-0.01
3368	-0.26	-0.25	-0.01
3369	-0.26	-0.25	-0.01
3370	-0.26	-0.26	0.00
3371	-0.27	-0.27	0.00
3372	-0.27	-0.27	0.00
3373	-0.27	-0.28	0.01
3374	-0.27	-0.28	0.01
3375	-0.27	-0.29	0.02
3376	-0.27	-0.30	0.02
3377	-0.28	-0.30	0.03
3378	-0.28	-0.31	0.03
3379	-0.28	-0.31	0.03
3380	-0.28	-0.32	0.03
3381	-0.28	-0.32	0.04
3382	-0.29	-0.33	0.04
3383	-0.29	-0.33	0.04
3384	-0.29	-0.33	0.04
3385	-0.30	-0.34	0.04
3386	-0.30	-0.34	0.04
3387	-0.31	-0.35	0.04
3388	-0.31	-0.35	0.04
3389	-0.32	-0.35	0.04
3390	-0.32	-0.35	0.03
3391	-0.32	-0.36	0.03
3392	-0.33	-0.36	0.03
3393	-0.33	-0.36	0.03
3394	-0.34	-0.37	0.03
3395	-0.35	-0.37	0.02
3396	-0.35	-0.37	0.02
3397	-0.36	-0.37	0.02
3398	-0.36	-0.38	0.02
3399	-0.37	-0.38	0.01
3400	-0.37	-0.38	0.01
3401	-0.38	-0.39	0.01
3402	-0.38	-0.39	0.01
3403	-0.39	-0.39	0.01
3404	-0.39	-0.40	0.00
3405	-0.40	-0.40	0.00
3406	-0.40	-0.40	0.00
3407	-0.41	-0.41	0.00
3408	-0.41	-0.41	0.00
3409	-0.42	-0.41	-0.01
3410	-0.42	-0.41	-0.01
3411	-0.43	-0.42	-0.01
3412	-0.43	-0.42	-0.01
3413	-0.43	-0.42	-0.01
3414	-0.44	-0.43	-0.01
3415	-0.44	-0.43	-0.01
3416	-0.44	-0.43	-0.01
3417	-0.45	-0.43	-0.01
3418	-0.45	-0.44	-0.01
3419	-0.45	-0.44	-0.01
3420	-0.46	-0.44	-0.01
3421	-0.46	-0.45	-0.01
3422	-0.46	-0.45	-0.01
3423	-0.46	-0.45	-0.01
3424	-0.46	-0.45	-0.01
3425	-0.46	-0.46	-0.01
3426	-0.46	-0.46	0.00
3427	-0.46	-0.46	0.00
3428	-0.46	-0.46	0.00
3429	-0.46	-0.46	0.01
3430	-0.46	-0.47	0.01
3431	-0.45	-0.47	0.01
3432	-0.45	-0.47	0.02
3433	-0.45	-0.47	0.02
3434	-0.45	-0.47	0.03
3435	-0.44	-0.48	0.03
3436	-0.44	-0.48	0.04
3437	-0.43	-0.48	0.05
3438	-0.43	-0.48	0.05

Age (cal. BP)	SE Iberian precipitation (z-score)		
	annual	winter	summer
3439	-0.42	-0.48	0.06
3440	-0.42	-0.48	0.06
3441	-0.41	-0.48	0.07
3442	-0.41	-0.48	0.07
3443	-0.40	-0.48	0.08
3444	-0.40	-0.48	0.08
3445	-0.39	-0.48	0.09
3446	-0.38	-0.48	0.09
3447	-0.38	-0.48	0.10
3448	-0.37	-0.48	0.10
3449	-0.37	-0.47	0.11
3450	-0.36	-0.47	0.11
3451	-0.36	-0.47	0.11
3452	-0.35	-0.47	0.12
3453	-0.34	-0.46	0.12
3454	-0.34	-0.46	0.12
3455	-0.33	-0.46	0.12
3456	-0.33	-0.46	0.13
3457	-0.32	-0.45	0.13
3458	-0.32	-0.45	0.13
3459	-0.31	-0.45	0.13
3460	-0.31	-0.44	0.13
3461	-0.31	-0.44	0.13
3462	-0.30	-0.44	0.13
3463	-0.30	-0.43	0.13
3464	-0.30	-0.43	0.13
3465	-0.29	-0.43	0.13
3466	-0.29	-0.42	0.13
3467	-0.29	-0.42	0.13
3468	-0.29	-0.42	0.13
3469	-0.28	-0.42	0.13
3470	-0.28	-0.41	0.13
3471	-0.28	-0.41	0.13
3472	-0.27	-0.41	0.14
3473	-0.27	-0.41	0.14
3474	-0.27	-0.41	0.14
3475	-0.26	-0.41	0.14
3476	-0.26	-0.40	0.15
3477	-0.26	-0.40	0.15
3478	-0.25	-0.40	0.15
3479	-0.25	-0.40	0.16
3480	-0.24	-0.40	0.16
3481	-0.24	-0.40	0.16
3482	-0.24	-0.41	0.17
3483	-0.23	-0.41	0.17
3484	-0.23	-0.41	0.18
3485	-0.22	-0.41	0.18
3486	-0.22	-0.41	0.19
3487	-0.21	-0.41	0.19
3488	-0.21	-0.41	0.20
3489	-0.20	-0.41	0.21
3490	-0.20	-0.41	0.21
3491	-0.20	-0.41	0.22
3492	-0.19	-0.41	0.22
3493	-0.19	-0.41	0.23
3494	-0.18	-0.41	0.23
3495	-0.18	-0.42	0.24
3496	-0.17	-0.42	0.24
3497	-0.17	-0.42	0.25
3498	-0.17	-0.42	0.25
3499	-0.16	-0.42	0.26
3500	-0.16	-0.42	0.26
3501	-0.15	NA	NA
3502	-0.15	-0.42	0.27
3503	-0.15	-0.42	0.28
3504	-0.14	-0.42	0.28
3505	-0.14	-0.42	0.29
3506	-0.13	-0.43	0.29
3507	-0.13	-0.43	0.30
3508	-0.12	-0.43	0.30
3509	-0.12	-0.43	0.31
3510	-0.12	-0.43	0.31
3511	-0.11	-0.43	0.32
3512	-0.11	-0.43	0.32

Age (cal. BP)	SE Iberian precipitation (z-score)		
	annual	winter	summer
3513	-0.11	-0.43	0.32
3514	-0.11	-0.43	0.33
3515	-0.10	-0.44	0.33
3516	-0.10	-0.44	0.33
3517	-0.10	-0.44	0.34
3518	-0.10	-0.44	0.34
3519	-0.10	-0.44	0.34
3520	-0.10	-0.44	0.34
3521	-0.09	-0.44	0.35
3522	-0.09	-0.44	0.35
3523	-0.09	-0.44	0.35
3524	-0.09	-0.44	0.35
3525	-0.09	-0.45	0.35
3526	-0.09	-0.45	0.36
3527	-0.09	-0.45	0.36
3528	-0.09	-0.45	0.36
3529	-0.09	-0.45	0.36
3530	-0.09	-0.45	0.36
3531	-0.09	-0.45	0.36
3532	-0.09	-0.45	0.36
3533	-0.10	-0.45	0.36
3534	-0.10	-0.45	0.36
3535	-0.10	-0.46	0.36
3536	-0.10	-0.46	0.36
3537	-0.10	-0.46	0.36
3538	-0.10	-0.46	0.35
3539	-0.10	-0.46	0.35
3540	-0.11	-0.46	0.35
3541	-0.11	-0.46	0.35
3542	-0.11	-0.46	0.35
3543	-0.11	-0.46	0.35
3544	-0.12	-0.46	0.35
3545	-0.12	-0.46	0.34
3546	-0.12	-0.46	0.34
3547	-0.12	-0.46	0.34
3548	-0.13	-0.46	0.34
3549	-0.13	-0.47	0.34
3550	-0.13	-0.47	0.34
3551	-0.13	-0.47	0.34
3552	-0.14	-0.47	0.33
3553	-0.14	-0.47	0.33
3554	-0.14	-0.47	0.33
3555	-0.15	-0.48	0.33
3556	-0.15	-0.48	0.33
3557	-0.15	-0.48	0.33
3558	-0.15	-0.48	0.33
3559	-0.16	-0.49	0.33
3560	-0.16	-0.49	0.33
3561	-0.16	-0.49	0.33
3562	-0.17	-0.50	0.33
3563	-0.17	-0.50	0.33
3564	-0.17	-0.50	0.33
3565	-0.18	-0.50	0.33
3566	-0.18	-0.51	0.33
3567	-0.18	-0.51	0.33
3568	-0.18	-0.51	0.33
3569	-0.19	-0.52	0.33
3570	-0.19	-0.52	0.33
3571	-0.19	-0.52	0.33
3572	-0.19	-0.52	0.33
3573	-0.20	-0.53	0.33
3574	-0.20	-0.53	0.33
3575	-0.20	-0.53	0.33
3576	-0.20	-0.54	0.33
3577	-0.20	-0.54	0.33
3578	-0.21	-0.54	0.33
3579	-0.21	-0.54	0.33
3580	-0.21	-0.54	0.33
3581	-0.21	-0.55	0.33
3582	-0.21	-0.55	0.33
3583	-0.22	-0.55	0.33
3584	-0.22	-0.55	0.33
3585	-0.22	-0.55	0.33
3586	-0.22	-0.55	0.33

Age (cal. BP)	SE Iberian precipitation (z-score)		
	annual	winter	summer
3587	-0.22	-0.55	0.33
3588	-0.23	-0.55	0.33
3589	-0.23	-0.55	0.32
3590	-0.23	-0.55	0.32
3591	-0.23	-0.55	0.32
3592	-0.24	-0.55	0.32
3593	-0.24	-0.55	0.31
3594	-0.24	-0.55	0.31
3595	-0.24	-0.55	0.31
3596	-0.25	-0.55	0.30
3597	-0.25	-0.55	0.30
3598	-0.25	-0.55	0.30
3599	-0.26	-0.55	0.29
3600	-0.26	-0.55	0.29
3601	-0.26	-0.55	0.29
3602	-0.26	-0.55	0.28
3603	-0.27	-0.55	0.28
3604	-0.27	-0.54	0.27
3605	-0.27	-0.54	0.27
3606	-0.28	-0.54	0.27
3607	-0.28	-0.54	0.26
3608	-0.28	-0.54	0.26
3609	-0.29	-0.54	0.25
3610	-0.29	-0.54	0.25
3611	-0.29	-0.53	0.24
3612	-0.29	-0.53	0.24
3613	-0.30	-0.53	0.23
3614	-0.30	-0.53	0.23
3615	-0.30	-0.53	0.22
3616	-0.31	-0.53	0.22
3617	-0.31	-0.52	0.21
3618	-0.31	-0.52	0.21
3619	-0.32	-0.52	0.20
3620	-0.32	-0.52	0.20
3621	-0.32	-0.52	0.19
3622	-0.32	-0.51	0.19
3623	-0.33	-0.51	0.19
3624	-0.33	-0.51	0.18
3625	-0.33	-0.51	0.18
3626	-0.33	-0.51	0.17
3627	-0.34	-0.50	0.17
3628	-0.34	-0.50	0.16
3629	-0.34	-0.50	0.16
3630	-0.35	-0.50	0.15
3631	-0.35	-0.49	0.15
3632	-0.35	-0.49	0.14
3633	-0.35	-0.49	0.14
3634	-0.35	-0.49	0.13
3635	-0.36	-0.49	0.13
3636	-0.36	-0.48	0.12
3637	-0.36	-0.48	0.12
3638	-0.36	-0.48	0.12
3639	-0.37	-0.48	0.11
3640	-0.37	-0.47	0.11
3641	-0.37	-0.47	0.10
3642	-0.37	-0.47	0.10
3643	-0.37	-0.47	0.09
3644	-0.38	-0.47	0.09
3645	-0.38	-0.46	0.09
3646	-0.38	-0.46	0.08
3647	-0.38	-0.46	0.08
3648	-0.39	-0.46	0.07
3649	-0.39	-0.46	0.07
3650	-0.39	-0.45	0.06
3651	-0.39	-0.45	0.06
3652	-0.39	-0.45	0.05
3653	-0.40	-0.44	0.05
3654	-0.40	-0.44	0.04
3655	-0.40	-0.44	0.03
3656	-0.40	-0.43	0.03
3657	-0.40	-0.43	0.02
3658	-0.41	-0.42	0.02
3659	-0.41	-0.42	0.01
3660	-0.41	-0.42	0.01

Age (cal. BP)	SE Iberian precipitation (z-score)		
	annual	winter	summer
3661	-0.41	-0.41	0.00
3662	-0.42	-0.41	-0.01
3663	-0.42	-0.40	-0.01
3664	-0.42	-0.40	-0.02
3665	-0.42	-0.40	-0.02
3666	-0.42	-0.39	-0.03
3667	-0.43	-0.39	-0.04
3668	-0.43	-0.38	-0.04
3669	-0.43	-0.38	-0.05
3670	-0.43	-0.38	-0.05
3671	-0.43	-0.37	-0.06
3672	-0.43	-0.37	-0.06
3673	-0.44	-0.37	-0.07
3674	-0.44	-0.36	-0.07
3675	-0.44	-0.36	-0.08
3676	-0.44	-0.36	-0.08
3677	-0.44	-0.36	-0.09
3678	-0.45	-0.35	-0.09
3679	-0.45	-0.35	-0.09
3680	-0.45	-0.35	-0.10
3681	-0.45	-0.35	-0.10
3682	-0.45	-0.35	-0.10
3683	-0.45	-0.35	-0.11
3684	-0.45	-0.34	-0.11
3685	-0.46	-0.34	-0.11
3686	-0.46	-0.34	-0.12
3687	-0.46	-0.34	-0.12
3688	-0.46	-0.34	-0.12
3689	-0.46	-0.34	-0.12
3690	-0.46	-0.33	-0.13
3691	-0.46	-0.33	-0.13
3692	-0.46	-0.33	-0.13
3693	-0.46	-0.33	-0.13
3694	-0.47	-0.33	-0.14
3695	-0.47	-0.33	-0.14
3696	-0.47	-0.33	-0.14
3697	-0.47	-0.33	-0.14
3698	-0.47	-0.32	-0.14
3699	-0.47	-0.32	-0.15
3700	-0.47	-0.32	-0.15
3701	-0.47	-0.32	-0.15
3702	-0.47	-0.32	-0.15
3703	-0.47	-0.32	-0.15
3704	-0.47	-0.32	-0.16
3705	-0.48	-0.32	-0.16
3706	-0.48	-0.32	-0.16
3707	-0.48	-0.32	-0.16
3708	-0.48	-0.32	-0.16
3709	-0.48	-0.31	-0.16
3710	-0.48	-0.31	-0.17
3711	-0.48	-0.31	-0.17
3712	-0.48	-0.31	-0.17
3713	-0.48	-0.31	-0.17
3714	-0.48	-0.31	-0.17
3715	-0.49	-0.31	-0.18
3716	-0.49	-0.31	-0.18
3717	-0.49	-0.31	-0.18
3718	-0.49	-0.31	-0.18
3719	-0.49	-0.31	-0.18
3720	-0.49	-0.31	-0.18
3721	-0.49	-0.31	-0.19
3722	-0.50	-0.31	-0.19
3723	-0.50	-0.31	-0.19
3724	-0.50	-0.31	-0.19
3725	-0.50	-0.31	-0.19
3726	-0.50	-0.31	-0.20
3727	-0.50	-0.31	-0.20
3728	-0.51	-0.31	-0.20
3729	-0.51	-0.31	-0.20
3730	-0.51	-0.30	-0.21
3731	-0.51	-0.30	-0.21
3732	-0.52	-0.30	-0.21
3733	-0.52	-0.30	-0.21
3734	-0.52	-0.30	-0.22

Age (cal. BP)	SE Iberian precipitation (z-score)		
	annual	winter	summer
3735	-0.52	-0.30	-0.22
3736	-0.53	-0.30	-0.22
3737	-0.53	-0.30	-0.22
3738	-0.53	-0.30	-0.23
3739	-0.53	-0.30	-0.23
3740	-0.54	-0.30	-0.24
3741	-0.54	-0.30	-0.24
3742	-0.55	-0.30	-0.25
3743	-0.55	-0.30	-0.25
3744	-0.56	-0.30	-0.26
3745	-0.57	-0.30	-0.26
3746	-0.57	-0.30	-0.27
3747	-0.58	-0.30	-0.28
3748	-0.59	-0.30	-0.28
3749	-0.59	-0.30	-0.29
3750	-0.60	-0.30	-0.30
3751	-0.61	-0.30	-0.31
3752	-0.62	-0.30	-0.31
3753	-0.63	-0.30	-0.32
3754	-0.63	-0.30	-0.33
3755	-0.64	-0.30	-0.34
3756	-0.65	-0.31	-0.34
3757	-0.66	-0.31	-0.35
3758	-0.67	-0.31	-0.36
3759	-0.67	-0.31	-0.36
3760	-0.68	-0.31	-0.37
3761	-0.69	-0.32	-0.37
3762	-0.70	-0.32	-0.38
3763	-0.70	-0.32	-0.38
3764	-0.71	-0.32	-0.39
3765	-0.72	-0.33	-0.39
3766	-0.72	-0.33	-0.39
3767	-0.73	-0.33	-0.40
3768	-0.73	-0.33	-0.40
3769	-0.74	-0.34	-0.40
3770	-0.74	-0.34	-0.40
3771	-0.75	-0.34	-0.41
3772	-0.75	-0.34	-0.41
3773	-0.75	-0.34	-0.41
3774	-0.76	-0.34	-0.41
3775	-0.76	-0.35	-0.41
3776	-0.76	-0.35	-0.41
3777	-0.76	-0.35	-0.41
3778	-0.76	-0.35	-0.42
3779	-0.76	-0.35	-0.42
3780	-0.76	-0.35	-0.42
3781	-0.76	-0.35	-0.42
3782	-0.76	-0.34	-0.42
3783	-0.76	-0.34	-0.42
3784	-0.76	-0.34	-0.42
3785	-0.76	-0.34	-0.42
3786	-0.76	-0.34	-0.42
3787	-0.76	-0.34	-0.42
3788	-0.76	-0.34	-0.42
3789	-0.76	-0.34	-0.42
3790	-0.76	-0.34	-0.42
3791	-0.76	-0.34	-0.42
3792	-0.76	-0.34	-0.42
3793	-0.76	-0.34	-0.42
3794	-0.76	-0.33	-0.42
3795	-0.75	-0.33	-0.42
3796	-0.75	-0.33	-0.42
3797	-0.75	-0.33	-0.42
3798	-0.75	-0.33	-0.42
3799	-0.75	-0.33	-0.42
3800	-0.75	-0.33	-0.42
3801	-0.74	-0.33	-0.42
3802	-0.74	-0.33	-0.42
3803	-0.74	-0.32	-0.42
3804	-0.74	-0.32	-0.42
3805	-0.74	-0.32	-0.41
3806	-0.73	-0.32	-0.41
3807	-0.73	-0.32	-0.41
3808	-0.73	-0.32	-0.41

Age (cal. BP)	SE Iberian precipitation (z-score)		
	annual	winter	summer
3809	-0.73	-0.32	-0.41
3810	-0.73	-0.32	-0.41
3811	-0.72	-0.32	-0.41
3812	-0.72	-0.31	-0.41
3813	-0.72	-0.31	-0.40
3814	-0.72	-0.31	-0.40
3815	-0.71	-0.31	-0.40
3816	-0.71	-0.31	-0.40
3817	-0.71	-0.31	-0.40
3818	-0.71	-0.31	-0.39
3819	-0.70	-0.31	-0.39
3820	-0.70	-0.31	-0.39
3821	-0.70	-0.31	-0.39
3822	-0.70	-0.31	-0.39
3823	-0.69	-0.31	-0.38
3824	-0.69	-0.31	-0.38
3825	-0.69	-0.31	-0.38
3826	-0.69	-0.31	-0.37
3827	-0.68	-0.31	-0.37
3828	-0.68	-0.31	-0.37
3829	-0.68	-0.31	-0.36
3830	-0.68	-0.31	-0.36
3831	-0.67	-0.32	-0.36
3832	-0.67	-0.32	-0.35
3833	-0.67	-0.32	-0.35
3834	-0.66	-0.32	-0.34
3835	-0.66	-0.32	-0.34
3836	-0.65	-0.32	-0.34
3837	-0.65	-0.32	-0.33
3838	-0.65	-0.32	-0.33
3839	-0.64	-0.32	-0.32
3840	-0.64	-0.32	-0.32
3841	-0.63	-0.32	-0.31
3842	-0.63	-0.32	-0.31
3843	-0.63	-0.32	-0.30
3844	-0.62	-0.33	-0.30
3845	-0.62	-0.33	-0.29
3846	-0.61	-0.33	-0.29
3847	-0.61	-0.33	-0.28
3848	-0.61	-0.33	-0.28
3849	-0.60	-0.33	-0.27
3850	-0.60	-0.33	-0.27
3851	-0.60	-0.33	-0.26
3852	-0.59	-0.33	-0.26
3853	-0.59	-0.33	-0.25
3854	-0.58	-0.33	-0.25
3855	-0.58	-0.34	-0.24
3856	-0.57	-0.34	-0.24
3857	-0.57	-0.34	-0.23
3858	-0.56	-0.34	-0.22
3859	-0.55	-0.34	-0.21
3860	-0.55	-0.34	-0.21
3861	-0.54	-0.34	-0.20
3862	-0.53	-0.34	-0.19
3863	-0.53	-0.34	-0.18
3864	-0.52	-0.34	-0.18
3865	-0.51	-0.35	-0.17
3866	-0.51	-0.35	-0.16
3867	-0.50	-0.35	-0.15
3868	-0.49	-0.35	-0.14
3869	-0.48	-0.35	-0.13
3870	-0.48	-0.35	-0.13
3871	-0.47	-0.35	-0.12
3872	-0.46	-0.35	-0.11
3873	-0.45	-0.35	-0.10
3874	-0.44	-0.35	-0.09
3875	-0.44	-0.36	-0.08
3876	-0.43	-0.36	-0.07
3877	-0.42	-0.36	-0.06
3878	-0.41	-0.36	-0.05
3879	-0.41	-0.36	-0.04
3880	-0.40	-0.37	-0.03
3881	-0.39	-0.37	-0.03
3882	-0.39	-0.37	-0.02

Age (cal. BP)	SE Iberian precipitation (z-score)		
	annual	winter	summer
3883	-0.38	-0.37	-0.01
3884	-0.37	-0.37	0.00
3885	-0.37	-0.38	0.01
3886	-0.36	-0.38	0.02
3887	-0.36	-0.38	0.03
3888	-0.35	-0.38	0.03
3889	-0.34	-0.39	0.04
3890	-0.34	-0.39	0.05
3891	-0.34	-0.39	0.05
3892	-0.33	-0.39	0.06
3893	-0.33	-0.39	0.07
3894	-0.32	-0.40	0.07
3895	-0.32	-0.40	0.08
3896	-0.32	-0.40	0.08
3897	-0.31	-0.40	0.09
3898	-0.31	-0.40	0.09
3899	-0.31	-0.41	0.10
3900	-0.30	-0.41	0.10
3901	-0.30	-0.41	0.11
3902	-0.30	-0.41	0.11
3903	-0.29	-0.41	0.12
3904	-0.29	-0.41	0.12
3905	-0.29	-0.41	0.12
3906	-0.29	-0.41	0.13
3907	-0.28	-0.41	0.13
3908	-0.28	-0.41	0.13
3909	-0.28	-0.41	0.14
3910	-0.28	-0.42	0.14
3911	-0.28	-0.42	0.14
3912	-0.27	-0.42	0.15
3913	-0.27	-0.42	0.15
3914	-0.27	-0.42	0.15
3915	-0.27	-0.42	0.16
3916	-0.27	-0.42	0.16
3917	-0.26	-0.43	0.16
3918	-0.26	-0.43	0.16
3919	-0.26	-0.43	0.17
3920	-0.26	-0.43	0.17
3921	-0.26	-0.43	0.17
3922	-0.26	-0.43	0.18
3923	-0.26	-0.44	0.18
3924	-0.26	-0.44	0.18
3925	-0.25	-0.44	0.18
3926	-0.25	-0.44	0.19
3927	-0.25	-0.44	0.19
3928	-0.25	-0.44	0.19
3929	-0.25	-0.45	0.19
3930	-0.25	-0.45	0.20
3931	-0.25	-0.45	0.20
3932	-0.25	-0.45	0.20
3933	-0.25	-0.45	0.20
3934	-0.25	-0.45	0.20
3935	-0.25	-0.45	0.21
3936	-0.25	-0.46	0.21
3937	-0.25	-0.46	0.21
3938	-0.25	-0.46	0.21
3939	-0.25	-0.46	0.21
3940	-0.25	-0.46	0.21
3941	-0.25	-0.46	0.21
3942	-0.25	-0.46	0.21
3943	-0.25	-0.46	0.21
3944	-0.25	-0.46	0.21
3945	-0.25	-0.46	0.21
3946	-0.25	-0.46	0.21
3947	-0.25	-0.46	0.21
3948	-0.25	-0.46	0.21
3949	-0.25	-0.46	0.21
3950	-0.25	-0.46	0.21
3951	-0.26	-0.46	0.21
3952	-0.26	-0.46	0.20
3953	-0.26	-0.46	0.20
3954	-0.26	-0.46	0.20
3955	-0.27	-0.46	0.19
3956	-0.27	-0.46	0.19

Age (cal. BP)	SE Iberian precipitation (z-score)		
	annual	winter	summer
3957	-0.27	-0.45	0.18
3958	-0.28	-0.45	0.18
3959	-0.28	-0.45	0.17
3960	-0.28	-0.45	0.16
3961	-0.29	-0.44	0.16
3962	-0.29	-0.44	0.15
3963	-0.30	-0.44	0.14
3964	-0.30	-0.44	0.13
3965	-0.31	-0.43	0.13
3966	-0.31	-0.43	0.12
3967	-0.31	-0.43	0.11
3968	-0.32	-0.42	0.10
3969	-0.32	-0.42	0.10
3970	-0.33	-0.41	0.09
3971	-0.33	-0.41	0.08
3972	-0.33	-0.41	0.07
3973	-0.34	-0.40	0.07
3974	-0.34	-0.40	0.06
3975	-0.34	-0.39	0.05
3976	-0.34	-0.39	0.04
3977	-0.35	-0.38	0.04
3978	-0.35	-0.38	0.03
3979	-0.35	-0.38	0.03
3980	-0.35	-0.37	0.02
3981	-0.35	-0.37	0.01
3982	-0.35	-0.36	0.01
3983	-0.36	-0.36	0.00
3984	-0.36	-0.35	0.00
3985	-0.36	-0.35	-0.01
3986	-0.36	-0.34	-0.02
3987	-0.36	-0.34	-0.02
3988	-0.36	-0.34	-0.03
3989	-0.37	-0.33	-0.04
3990	-0.37	-0.33	-0.04
3991	-0.37	-0.32	-0.05
3992	-0.37	-0.32	-0.06
3993	-0.38	-0.31	-0.06
3994	-0.38	-0.31	-0.07
3995	-0.38	-0.31	-0.07
3996	-0.38	-0.30	-0.08
3997	-0.39	-0.30	-0.09
3998	-0.39	-0.29	-0.09
3999	-0.39	-0.29	-0.10
4000	-0.39	-0.29	-0.11
4001	-0.40	-0.28	-0.11
4002	-0.40	-0.28	-0.12
4003	-0.40	-0.28	-0.12
4004	-0.40	-0.28	-0.13
4005	-0.41	-0.27	-0.13
4006	-0.41	-0.27	-0.14
4007	-0.41	-0.27	-0.14
4008	-0.41	-0.27	-0.15
4009	-0.42	-0.26	-0.15
4010	-0.42	-0.26	-0.16
4011	-0.42	-0.26	-0.16
4012	-0.42	-0.26	-0.16
4013	-0.42	-0.25	-0.17
4014	-0.42	-0.25	-0.17
4015	-0.43	-0.25	-0.18
4016	-0.43	-0.25	-0.18
4017	-0.43	-0.24	-0.18
4018	-0.43	-0.24	-0.19
4019	-0.43	-0.24	-0.19
4020	-0.43	-0.24	-0.19
4021	-0.43	-0.23	-0.20
4022	-0.43	-0.23	-0.20
4023	-0.43	-0.23	-0.20
4024	-0.43	-0.22	-0.21
4025	-0.43	-0.22	-0.21
4026	-0.43	-0.22	-0.21
4027	-0.43	-0.22	-0.21
4028	-0.43	-0.21	-0.21
4029	-0.42	-0.21	-0.21
4030	-0.42	-0.21	-0.22

Age (cal. BP)	SE Iberian precipitation (z-score)		
	annual	winter	summer
4031	-0.42	-0.20	-0.22
4032	-0.42	-0.20	-0.22
4033	-0.42	-0.20	-0.22
4034	-0.41	-0.20	-0.22
4035	-0.41	-0.19	-0.22
4036	-0.41	-0.19	-0.22
4037	-0.41	-0.19	-0.22
4038	-0.40	-0.18	-0.22
4039	-0.40	-0.18	-0.22
4040	-0.40	-0.18	-0.22
4041	-0.39	-0.17	-0.22
4042	-0.39	-0.17	-0.22
4043	-0.39	-0.17	-0.22
4044	-0.38	-0.17	-0.22
4045	-0.38	-0.16	-0.21
4046	-0.37	-0.16	-0.21
4047	-0.37	-0.16	-0.21
4048	-0.37	-0.15	-0.21
4049	-0.36	-0.15	-0.21
4050	-0.36	-0.15	-0.21
4051	-0.35	-0.15	-0.21
4052	-0.35	-0.14	-0.21
4053	-0.34	-0.14	-0.20
4054	-0.34	-0.14	-0.20
4055	-0.33	-0.13	-0.20
4056	-0.33	-0.13	-0.20
4057	-0.33	-0.13	-0.20
4058	-0.32	-0.13	-0.20
4059	-0.32	-0.12	-0.19
4060	-0.31	-0.12	-0.19
4061	-0.31	-0.12	-0.19
4062	-0.30	-0.12	-0.19
4063	-0.30	-0.11	-0.19
4064	-0.30	-0.11	-0.18
4065	-0.29	-0.11	-0.18
4066	-0.29	-0.11	-0.18
4067	-0.28	-0.10	-0.18
4068	-0.28	-0.10	-0.18
4069	-0.27	-0.10	-0.18
4070	-0.27	-0.10	-0.17
4071	-0.27	-0.09	-0.17
4072	-0.26	-0.09	-0.17
4073	-0.26	-0.09	-0.17
4074	-0.26	-0.09	-0.17
4075	-0.25	-0.08	-0.17
4076	-0.25	-0.08	-0.17
4077	-0.25	-0.08	-0.16
4078	-0.24	-0.08	-0.16
4079	-0.24	-0.08	-0.16
4080	-0.24	-0.08	-0.16
4081	-0.23	-0.07	-0.16
4082	-0.23	-0.07	-0.16
4083	-0.23	-0.07	-0.16
4084	-0.23	-0.07	-0.16
4085	-0.23	-0.07	-0.16
4086	-0.22	-0.06	-0.16
4087	-0.22	-0.06	-0.16
4088	-0.22	-0.06	-0.16
4089	-0.22	-0.06	-0.16
4090	-0.22	-0.06	-0.16
4091	-0.22	-0.05	-0.16
4092	-0.22	-0.05	-0.17
4093	-0.22	-0.05	-0.17
4094	-0.22	-0.05	-0.17
4095	-0.22	-0.05	-0.17
4096	-0.21	-0.05	-0.17
4097	-0.21	-0.04	-0.17
4098	-0.21	-0.04	-0.17
4099	-0.21	-0.04	-0.17
4100	-0.21	-0.04	-0.17
4101	-0.21	-0.04	-0.17
4102	-0.21	-0.03	-0.17
4103	-0.21	-0.03	-0.17
4104	-0.21	-0.03	-0.17

Age (cal. BP)	SE Iberian precipitation (z-score)		
	annual	winter	summer
4105	-0.20	-0.03	-0.18
4106	-0.20	-0.03	-0.18
4107	-0.20	-0.03	-0.18
4108	-0.20	-0.02	-0.18
4109	-0.20	-0.02	-0.18
4110	-0.20	-0.02	-0.18
4111	-0.20	-0.02	-0.18
4112	-0.20	-0.02	-0.18
4113	-0.20	-0.02	-0.18
4114	-0.20	-0.02	-0.18
4115	-0.19	-0.01	-0.18
4116	-0.19	-0.01	-0.18
4117	-0.19	-0.01	-0.18
4118	-0.19	-0.01	-0.18
4119	-0.19	-0.01	-0.18
4120	-0.19	-0.01	-0.18
4121	-0.19	-0.01	-0.18
4122	-0.19	-0.01	-0.18
4123	-0.19	-0.01	-0.18
4124	-0.19	0.00	-0.18
4125	-0.19	0.00	-0.18
4126	-0.19	0.00	-0.18
4127	-0.18	0.00	-0.18
4128	-0.18	0.00	-0.18
4129	-0.18	0.00	-0.18
4130	-0.18	0.00	-0.18
4131	-0.18	0.00	-0.18
4132	-0.18	0.00	-0.18
4133	-0.18	0.00	-0.18
4134	-0.18	0.00	-0.18
4135	-0.18	0.00	-0.18
4136	-0.18	0.00	-0.18
4137	-0.18	0.00	-0.18
4138	-0.18	0.00	-0.18
4139	-0.18	0.00	-0.18
4140	-0.18	0.00	-0.18
4141	-0.18	0.00	-0.18
4142	-0.18	-0.01	-0.18
4143	-0.18	-0.01	-0.18
4144	-0.18	-0.01	-0.18
4145	-0.18	-0.01	-0.18
4146	-0.19	-0.01	-0.18
4147	-0.19	-0.01	-0.18
4148	-0.19	-0.01	-0.18
4149	-0.19	-0.01	-0.18
4150	-0.19	-0.01	-0.18
4151	-0.19	-0.01	-0.18
4152	-0.20	-0.01	-0.18
4153	-0.20	-0.02	-0.18
4154	-0.20	-0.02	-0.19
4155	-0.20	-0.02	-0.19
4156	-0.21	-0.02	-0.19
4157	-0.21	-0.02	-0.19
4158	-0.21	-0.02	-0.19
4159	-0.22	-0.02	-0.19
4160	-0.22	-0.02	-0.20
4161	-0.22	-0.03	-0.20
4162	-0.23	-0.03	-0.20
4163	-0.23	-0.03	-0.20
4164	-0.23	-0.03	-0.20
4165	-0.24	-0.03	-0.21
4166	-0.24	-0.03	-0.21
4167	-0.25	-0.03	-0.21
4168	-0.25	-0.03	-0.21
4169	-0.25	-0.04	-0.22
4170	-0.26	-0.04	-0.22
4171	-0.26	-0.04	-0.22
4172	-0.26	-0.04	-0.22
4173	-0.27	-0.04	-0.23
4174	-0.27	-0.04	-0.23
4175	-0.28	-0.04	-0.23
4176	-0.28	-0.05	-0.23
4177	-0.28	-0.05	-0.24
4178	-0.29	-0.05	-0.24

Age (cal. BP)	SE Iberian precipitation (z-score)		
	annual	winter	summer
4179	-0.29	-0.05	-0.24
4180	-0.29	-0.05	-0.24
4181	-0.30	-0.05	-0.25
4182	-0.30	-0.05	-0.25
4183	-0.31	-0.05	-0.25
4184	-0.31	-0.06	-0.25
4185	-0.31	-0.06	-0.26
4186	-0.32	-0.06	-0.26
4187	-0.32	-0.06	-0.26
4188	-0.32	-0.06	-0.26
4189	-0.32	-0.06	-0.26
4190	-0.33	-0.06	-0.27
4191	-0.33	-0.06	-0.27
4192	-0.33	-0.06	-0.27
4193	-0.34	-0.06	-0.27
4194	-0.34	-0.06	-0.27
4195	-0.34	-0.07	-0.27
4196	-0.34	-0.07	-0.28
4197	-0.34	-0.07	-0.28
4198	-0.35	-0.07	-0.28
4199	-0.35	-0.07	-0.28
4200	-0.35	-0.07	-0.28
4201	-0.35	-0.07	-0.28
4202	-0.35	-0.07	-0.28
4203	-0.35	-0.07	-0.28
4204	-0.35	-0.07	-0.28
4205	-0.35	-0.07	-0.28
4206	-0.35	-0.07	-0.28
4207	-0.35	-0.07	-0.28
4208	-0.35	-0.07	-0.28
4209	-0.35	-0.07	-0.28
4210	-0.35	-0.07	-0.28
4211	-0.35	-0.08	-0.28
4212	-0.36	-0.08	-0.28
4213	-0.36	-0.08	-0.28
4214	-0.36	-0.08	-0.27
4215	-0.36	-0.08	-0.27
4216	-0.36	-0.09	-0.27
4217	-0.36	-0.09	-0.27
4218	-0.36	-0.09	-0.27
4219	-0.36	-0.09	-0.26
4220	-0.36	-0.10	-0.26
4221	-0.36	-0.10	-0.26
4222	-0.36	-0.10	-0.26
4223	-0.36	-0.11	-0.25
4224	-0.36	-0.11	-0.25
4225	-0.36	-0.11	-0.25
4226	-0.36	-0.12	-0.24
4227	-0.36	-0.12	-0.24
4228	-0.36	-0.12	-0.24
4229	-0.36	-0.13	-0.23
4230	-0.36	-0.13	-0.23
4231	-0.36	-0.13	-0.23
4232	-0.36	-0.14	-0.22
4233	-0.36	-0.14	-0.22
4234	-0.36	-0.14	-0.22
4235	-0.36	-0.15	-0.21
4236	-0.36	-0.15	-0.21
4237	-0.36	-0.15	-0.21
4238	-0.36	-0.16	-0.20
4239	-0.36	-0.16	-0.20
4240	-0.36	-0.16	-0.20
4241	-0.36	-0.17	-0.19
4242	-0.36	-0.17	-0.19
4243	-0.36	-0.17	-0.19
4244	-0.36	-0.17	-0.18
4245	-0.36	-0.18	-0.18
4246	-0.35	-0.18	-0.17
4247	-0.35	-0.18	-0.17
4248	-0.35	-0.18	-0.17
4249	-0.35	-0.19	-0.16
4250	-0.35	-0.19	-0.16
4251	-0.35	-0.19	-0.16
4252	-0.34	-0.19	-0.16

Age (cal. BP)	SE Iberian precipitation (z-score)		
	annual	winter	summer
4253	-0.34	-0.19	-0.15
4254	-0.34	-0.19	-0.15
4255	-0.34	-0.19	-0.15
4256	-0.34	-0.19	-0.14
4257	-0.33	-0.19	-0.14
4258	-0.33	-0.19	-0.14
4259	-0.33	-0.19	-0.14
4260	-0.33	-0.19	-0.13
4261	-0.32	-0.19	-0.13
4262	-0.32	-0.19	-0.13
4263	-0.32	-0.19	-0.13
4264	-0.31	-0.19	-0.13
4265	-0.31	-0.18	-0.13
4266	-0.30	-0.18	-0.12
4267	-0.30	-0.18	-0.12
4268	-0.30	-0.18	-0.12
4269	-0.29	-0.17	-0.12
4270	-0.29	-0.17	-0.12
4271	-0.28	-0.17	-0.12
4272	-0.28	-0.16	-0.12
4273	-0.27	-0.16	-0.11
4274	-0.27	-0.15	-0.11
4275	-0.26	-0.15	-0.11
4276	-0.26	-0.14	-0.11
4277	-0.25	-0.14	-0.11
4278	-0.24	-0.14	-0.11
4279	-0.24	-0.13	-0.11
4280	-0.23	-0.13	-0.11
4281	-0.23	-0.12	-0.11
4282	-0.22	-0.11	-0.10
4283	-0.21	-0.11	-0.10
4284	-0.21	-0.10	-0.10
4285	-0.20	-0.10	-0.10
4286	-0.19	-0.09	-0.10
4287	-0.19	-0.09	-0.10
4288	-0.18	-0.08	-0.10
4289	-0.17	-0.08	-0.10
4290	-0.17	-0.07	-0.10
4291	-0.16	-0.06	-0.10
4292	-0.16	-0.06	-0.10
4293	-0.15	-0.05	-0.10
4294	-0.14	-0.05	-0.10
4295	-0.14	-0.04	-0.10
4296	-0.13	-0.03	-0.10
4297	-0.13	-0.03	-0.10
4298	-0.12	-0.02	-0.10
4299	-0.11	-0.02	-0.10
4300	-0.11	-0.01	-0.10
4301	-0.10	-0.01	-0.10
4302	-0.10	0.00	-0.10
4303	-0.09	0.00	-0.10
4304	-0.09	0.01	-0.10
4305	-0.08	0.01	-0.10
4306	-0.08	0.02	-0.10
4307	-0.07	0.02	-0.10
4308	-0.07	0.03	-0.10
4309	-0.06	0.03	-0.10
4310	-0.06	0.04	-0.10
4311	-0.05	0.05	-0.10
4312	-0.05	0.06	-0.10
4313	-0.04	0.07	-0.11
4314	-0.04	0.07	-0.11
4315	-0.03	0.08	-0.11
4316	-0.02	0.09	-0.12
4317	-0.02	0.10	-0.12
4318	-0.01	0.11	-0.12
4319	0.00	0.13	-0.13
4320	0.00	0.14	-0.13
4321	0.01	0.15	-0.14
4322	0.02	0.16	-0.14
4323	0.03	0.17	-0.15
4324	0.03	0.19	-0.15
4325	0.04	0.20	-0.16
4326	0.05	0.21	-0.16

Age (cal. BP)	SE Iberian precipitation (z-score)		
	annual	winter	summer
4327	0.06	0.23	-0.17
4328	0.06	0.24	-0.17
4329	0.07	0.25	-0.18
4330	0.08	0.26	-0.19
4331	0.09	0.28	-0.19
4332	0.09	0.29	-0.20
4333	0.10	0.30	-0.20
4334	0.11	0.32	-0.21
4335	0.12	0.33	-0.21
4336	0.12	0.34	-0.22
4337	0.13	0.36	-0.23
4338	0.14	0.37	-0.23
4339	0.14	0.38	-0.24
4340	0.15	0.39	-0.24
4341	0.16	0.41	-0.25
4342	0.16	0.42	-0.25
4343	0.17	0.43	-0.26
4344	0.18	0.44	-0.26
4345	0.18	0.45	-0.27
4346	0.19	0.46	-0.27
4347	0.19	0.47	-0.28
4348	0.20	0.48	-0.28
4349	0.20	0.48	-0.28
4350	0.21	0.49	-0.29
4351	0.21	0.50	-0.29
4352	0.21	0.51	-0.29
4353	0.22	0.51	-0.30
4354	0.22	0.52	-0.30
4355	0.22	0.53	-0.30
4356	0.23	0.53	-0.31
4357	0.23	0.54	-0.31
4358	0.24	0.55	-0.31
4359	0.24	0.55	-0.31
4360	0.24	0.56	-0.32
4361	0.25	0.57	-0.32
4362	0.25	0.57	-0.32
4363	0.25	0.58	-0.33
4364	0.26	0.59	-0.33
4365	0.26	0.59	-0.33
4366	0.26	0.60	-0.33
4367	0.27	0.60	-0.34
4368	0.27	0.61	-0.34
4369	0.27	0.62	-0.34
4370	0.28	0.62	-0.34
4371	0.28	0.63	-0.35
4372	0.28	0.63	-0.35
4373	0.29	0.64	-0.35
4374	0.29	0.65	-0.35
4375	0.29	0.65	-0.36
4376	0.30	0.66	-0.36
4377	0.30	0.66	-0.36
4378	0.30	0.67	-0.36
4379	0.31	0.67	-0.37
4380	0.31	0.68	-0.37
4381	0.31	0.68	-0.37
4382	0.31	0.69	-0.37
4383	0.32	0.69	-0.38
4384	0.32	0.70	-0.38
4385	0.32	0.70	-0.38
4386	0.32	0.70	-0.38
4387	0.32	0.71	-0.39
4388	0.33	0.71	-0.39
4389	0.33	0.72	-0.39
4390	0.33	0.72	-0.39
4391	0.33	0.73	-0.39
4392	0.33	0.73	-0.40
4393	0.33	0.73	-0.40
4394	0.34	0.74	-0.40
4395	0.34	0.74	-0.40
4396	0.34	0.74	-0.40
4397	0.34	0.75	-0.41
4398	0.34	0.75	-0.41
4399	0.34	0.75	-0.41
4400	0.34	0.75	-0.41

Age (cal. BP)	SE Iberian precipitation (z-score)		
	annual	winter	summer
4401	0.34	0.76	-0.42
4402	0.34	0.76	-0.42
4403	0.34	0.76	-0.42
4404	0.34	0.76	-0.42
4405	0.34	0.76	-0.42
4406	0.34	0.77	-0.43
4407	0.34	0.77	-0.43
4408	0.33	0.77	-0.43
4409	0.33	0.77	-0.44
4410	0.33	0.77	-0.44
4411	0.33	0.77	-0.44
4412	0.32	0.77	-0.45
4413	0.32	0.77	-0.45
4414	0.32	0.77	-0.46
4415	0.31	0.77	-0.46
4416	0.31	0.77	-0.46
4417	0.31	0.77	-0.46
4418	0.30	0.77	-0.47
4419	0.30	0.77	-0.47
4420	0.29	0.77	-0.47
4421	0.29	0.76	-0.47
4422	0.28	0.76	-0.48
4423	0.28	0.76	-0.48
4424	0.28	0.76	-0.48
4425	0.27	0.75	-0.48
4426	0.27	0.75	-0.48
4427	0.26	0.75	-0.49
4428	0.26	0.75	-0.49
4429	0.26	0.74	-0.49
4430	0.25	0.74	-0.49
4431	0.25	0.74	-0.49
4432	0.25	0.73	-0.49
4433	0.24	0.73	-0.49
4434	0.24	0.73	-0.49
4435	0.24	0.72	-0.49
4436	0.24	0.72	-0.48
4437	0.23	0.72	-0.48
4438	0.23	0.72	-0.48
4439	0.23	0.71	-0.48
4440	0.23	0.71	-0.48
4441	0.23	0.71	-0.48
4442	0.22	0.70	-0.48
4443	0.22	0.70	-0.48
4444	0.22	0.70	-0.48
4445	0.22	0.69	-0.48
4446	0.21	0.69	-0.47
4447	0.21	0.68	-0.47
4448	0.21	0.68	-0.47
4449	0.20	0.67	-0.47
4450	0.20	0.66	-0.46
4451	0.20	0.66	-0.46
4452	0.19	0.65	-0.46
4453	0.19	0.65	-0.46
4454	0.19	0.64	-0.45
4455	0.19	0.63	-0.45
4456	0.18	0.63	-0.45
4457	0.18	0.62	-0.44
4458	0.18	0.61	-0.44
4459	0.17	0.61	-0.43
4460	0.17	0.60	-0.43
4461	0.17	0.59	-0.43
4462	0.17	0.59	-0.42
4463	0.16	0.58	-0.42
4464	0.16	0.57	-0.41
4465	0.16	0.56	-0.41
4466	0.16	0.56	-0.40
4467	0.15	0.55	-0.40
4468	0.15	0.54	-0.39
4469	0.15	0.53	-0.39
4470	0.15	0.53	-0.38
4471	0.15	0.52	-0.37
4472	0.14	0.51	-0.37
4473	0.14	0.51	-0.36
4474	0.14	0.50	-0.36

Age (cal. BP)	SE Iberian precipitation (z-score)		
	annual	winter	summer
4475	0.14	0.49	-0.35
4476	0.14	0.49	-0.35
4477	0.14	0.48	-0.34
4478	0.14	0.47	-0.33
4479	0.14	0.47	-0.33
4480	0.14	0.46	-0.32
4481	0.14	0.45	-0.31
4482	0.14	0.45	-0.31
4483	0.14	0.44	-0.30
4484	0.14	0.43	-0.30
4485	0.14	0.43	-0.29
4486	0.14	0.42	-0.28
4487	0.14	0.42	-0.28
4488	0.14	0.41	-0.27
4489	0.14	0.41	-0.27
4490	0.14	0.41	-0.26
4491	0.14	0.40	-0.26
4492	0.15	0.40	-0.25
4493	0.15	0.39	-0.25
4494	0.15	0.39	-0.24
4495	0.15	0.38	-0.23
4496	0.15	0.38	-0.23
4497	0.15	0.38	-0.22
4498	0.15	0.37	-0.22
4499	0.15	0.37	-0.21
4500	0.16	0.36	-0.21
4501	0.16	0.36	-0.20
4502	0.16	NA	NA
4503	0.16	0.35	-0.19
4504	0.16	0.35	-0.19
4505	0.16	0.35	-0.18
4506	0.17	0.34	-0.17
4507	0.17	0.34	-0.17
4508	0.17	0.33	-0.16
4509	0.17	0.33	-0.16
4510	0.17	0.32	-0.15
4511	0.17	0.32	-0.15
4512	0.17	0.32	-0.14
4513	0.17	0.31	-0.14
4514	0.18	0.31	-0.13
4515	0.18	0.30	-0.13
4516	0.18	0.30	-0.12
4517	0.18	0.29	-0.12
4518	0.18	0.29	-0.11
4519	0.18	0.29	-0.11
4520	0.18	0.28	-0.10
4521	0.18	0.28	-0.10
4522	0.18	0.27	-0.09
4523	0.18	0.27	-0.09
4524	0.18	0.27	-0.09
4525	0.18	0.26	-0.08
4526	0.18	0.26	-0.08
4527	0.18	0.25	-0.08
4528	0.18	0.25	-0.07
4529	0.17	0.24	-0.07
4530	0.17	0.24	-0.07
4531	0.17	0.23	-0.06
4532	0.17	0.23	-0.06
4533	0.17	0.23	-0.06
4534	0.17	0.22	-0.05
4535	0.17	0.22	-0.05
4536	0.17	0.21	-0.05
4537	0.16	0.21	-0.04
4538	0.16	0.20	-0.04
4539	0.16	0.20	-0.04
4540	0.16	0.20	-0.04
4541	0.16	0.19	-0.03
4542	0.16	0.19	-0.03
4543	0.15	0.18	-0.03
4544	0.15	0.18	-0.02
4545	0.15	0.17	-0.02
4546	0.15	0.17	-0.02
4547	0.15	0.16	-0.01
4548	0.15	0.16	-0.01

Age (cal. BP)	SE Iberian precipitation (z-score)		
	annual	winter	summer
4549	0.14	0.15	0.00
4550	0.14	0.14	0.00
4551	0.14	0.14	0.00
4552	0.14	0.13	0.01
4553	0.14	0.13	0.01
4554	0.14	0.12	0.02
4555	0.14	0.11	0.02
4556	0.14	0.11	0.03
4557	0.14	0.10	0.03
4558	0.13	0.10	0.04
4559	0.13	0.09	0.04
4560	0.13	0.08	0.05
4561	0.13	0.08	0.06
4562	0.13	0.07	0.06
4563	0.13	0.07	0.07
4564	0.13	0.06	0.07
4565	0.13	0.05	0.08
4566	0.13	0.05	0.09
4567	0.13	0.04	0.09
4568	0.14	0.04	0.10
4569	0.14	0.03	0.10
4570	0.14	0.03	0.11
4571	0.14	0.02	0.12
4572	0.14	0.02	0.12
4573	0.14	0.01	0.13
4574	0.14	0.01	0.13
4575	0.14	0.00	0.14
4576	0.14	0.00	0.14
4577	0.14	0.00	0.15
4578	0.15	-0.01	0.15
4579	0.15	-0.01	0.16
4580	0.15	-0.01	0.16
4581	0.15	-0.02	0.17
4582	0.15	-0.02	0.17
4583	0.15	-0.02	0.17
4584	0.15	-0.02	0.17
4585	0.15	-0.02	0.18
4586	0.16	-0.02	0.18
4587	0.16	-0.02	0.18
4588	0.16	-0.02	0.18
4589	0.16	-0.02	0.18
4590	0.16	-0.02	0.18
4591	0.16	-0.02	0.19
4592	0.16	-0.02	0.19
4593	0.17	-0.02	0.19
4594	0.17	-0.02	0.19
4595	0.17	-0.02	0.18
4596	0.17	-0.02	0.18
4597	0.17	-0.01	0.18
4598	0.17	-0.01	0.18
4599	0.17	-0.01	0.18
4600	0.17	-0.01	0.18
4601	0.17	0.00	0.18
4602	0.17	0.00	0.18
4603	0.17	0.00	0.17
4604	0.17	0.00	0.17
4605	0.17	0.01	0.17
4606	0.17	0.01	0.17
4607	0.18	0.01	0.16
4608	0.18	0.01	0.16
4609	0.18	0.02	0.16
4610	0.18	0.02	0.16
4611	0.18	0.02	0.16
4612	0.18	0.02	0.16
4613	0.18	0.02	0.15
4614	0.18	0.03	0.15
4615	0.18	0.03	0.15
4616	0.18	0.03	0.15
4617	0.18	0.03	0.15
4618	0.18	0.03	0.15
4619	0.18	0.03	0.15
4620	0.18	0.03	0.15
4621	0.18	0.03	0.15
4622	0.18	0.03	0.15

Age (cal. BP)	SE Iberian precipitation (z-score)		
	annual	winter	summer
4623	0.18	0.03	0.15
4624	0.18	0.03	0.15
4625	0.18	0.03	0.15
4626	0.18	0.03	0.15
4627	0.18	0.03	0.15
4628	0.18	0.03	0.15
4629	0.19	0.03	0.16
4630	0.19	0.03	0.16
4631	0.19	0.03	0.16
4632	0.19	0.03	0.16
4633	0.19	0.03	0.16
4634	0.19	0.03	0.16
4635	0.19	0.03	0.16
4636	0.19	0.03	0.16
4637	0.19	0.03	0.16
4638	0.19	0.03	0.16
4639	0.19	0.03	0.16
4640	0.19	0.03	0.16
4641	0.19	0.03	0.16
4642	0.19	0.03	0.16
4643	0.18	0.03	0.16
4644	0.18	0.03	0.16
4645	0.18	0.02	0.16
4646	0.18	0.02	0.16
4647	0.18	0.02	0.16
4648	0.18	0.02	0.16
4649	0.18	0.02	0.16
4650	0.18	0.02	0.16
4651	0.18	0.02	0.16
4652	0.18	0.02	0.16
4653	0.18	0.02	0.16
4654	0.17	0.02	0.15
4655	0.17	0.02	0.15
4656	0.17	0.02	0.15
4657	0.17	0.02	0.15
4658	0.17	0.02	0.15
4659	0.17	0.02	0.15
4660	0.16	0.02	0.15
4661	0.16	0.02	0.15
4662	0.16	0.01	0.14
4663	0.16	0.01	0.14
4664	0.15	0.01	0.14
4665	0.15	0.01	0.14
4666	0.15	0.01	0.14
4667	0.14	0.01	0.14
4668	0.14	0.01	0.13
4669	0.14	0.01	0.13
4670	0.13	0.00	0.13
4671	0.13	0.00	0.13
4672	0.13	0.00	0.13
4673	0.12	0.00	0.13
4674	0.12	0.00	0.12
4675	0.12	-0.01	0.12
4676	0.11	-0.01	0.12
4677	0.11	-0.01	0.12
4678	0.11	-0.02	0.12
4679	0.10	-0.02	0.12
4680	0.10	-0.02	0.12
4681	0.10	-0.03	0.13
4682	0.09	-0.03	0.13
4683	0.09	-0.04	0.13
4684	0.09	-0.04	0.13
4685	0.09	-0.05	0.13
4686	0.08	-0.05	0.13
4687	0.08	-0.06	0.14
4688	0.08	-0.06	0.14
4689	0.08	-0.07	0.14
4690	0.07	-0.07	0.14
4691	0.07	-0.08	0.15
4692	0.07	-0.08	0.15
4693	0.07	-0.09	0.16
4694	0.07	-0.09	0.16
4695	0.07	-0.10	0.16
4696	0.07	-0.10	0.17

Age (cal. BP)	SE Iberian precipitation (z-score)		
	annual	winter	summer
4697	0.06	-0.11	0.17
4698	0.06	-0.11	0.18
4699	0.06	-0.12	0.18
4700	0.06	-0.12	0.18
4701	0.06	-0.13	0.19
4702	0.06	-0.13	0.19
4703	0.06	-0.14	0.20
4704	0.06	-0.14	0.20
4705	0.05	-0.15	0.20
4706	0.05	-0.15	0.20
4707	0.05	-0.16	0.21
4708	0.05	-0.16	0.21
4709	0.05	-0.16	0.21
4710	0.05	-0.17	0.21
4711	0.05	-0.17	0.22
4712	0.04	-0.17	0.22
4713	0.04	-0.18	0.22
4714	0.04	-0.18	0.22
4715	0.04	-0.18	0.22
4716	0.04	-0.18	0.22
4717	0.04	-0.18	0.21
4718	0.04	-0.18	0.21
4719	0.03	-0.18	0.21
4720	0.03	-0.17	0.21
4721	0.03	-0.17	0.20
4722	0.03	-0.17	0.20
4723	0.03	-0.17	0.19
4724	0.03	-0.16	0.19
4725	0.02	-0.16	0.18
4726	0.02	-0.16	0.18
4727	0.02	-0.15	0.17
4728	0.02	-0.15	0.17
4729	0.02	-0.15	0.16
4730	0.02	-0.14	0.16
4731	0.02	-0.14	0.15
4732	0.01	-0.14	0.15
4733	0.01	-0.13	0.15
4734	0.01	-0.13	0.14
4735	0.01	-0.13	0.14
4736	0.01	-0.13	0.14
4737	0.01	-0.13	0.14
4738	0.01	-0.13	0.13
4739	0.01	-0.13	0.13
4740	0.00	-0.13	0.13
4741	0.00	-0.13	0.13
4742	0.00	-0.13	0.14
4743	0.00	-0.14	0.14
4744	0.00	-0.14	0.14
4745	0.00	-0.14	0.14
4746	0.00	-0.14	0.14
4747	0.00	-0.14	0.14
4748	0.00	-0.15	0.14
4749	0.00	-0.15	0.15
4750	0.00	-0.15	0.15
4751	0.00	-0.15	0.15
4752	0.00	-0.15	0.15
4753	0.00	-0.16	0.15
4754	0.00	-0.16	0.15
4755	0.00	-0.16	0.16
4756	0.00	-0.16	0.16
4757	0.00	-0.16	0.16
4758	0.00	-0.16	0.16
4759	0.00	-0.17	0.17
4760	0.00	-0.17	0.17
4761	0.00	-0.17	0.17
4762	0.00	-0.17	0.17
4763	0.00	-0.17	0.18
4764	0.00	-0.18	0.18
4765	0.00	-0.18	0.18
4766	0.01	-0.18	0.18
4767	0.01	-0.18	0.19
4768	0.01	-0.18	0.19
4769	0.01	-0.19	0.20
4770	0.01	-0.19	0.20

Age (cal. BP)	SE Iberian precipitation (z-score)		
	annual	winter	summer
4771	0.01	-0.19	0.20
4772	0.02	-0.19	0.21
4773	0.02	-0.19	0.21
4774	0.02	-0.20	0.22
4775	0.03	-0.20	0.23
4776	0.03	-0.20	0.23
4777	0.03	-0.20	0.24
4778	0.04	-0.21	0.25
4779	0.04	-0.21	0.25
4780	0.05	-0.21	0.26
4781	0.05	-0.21	0.27
4782	0.06	-0.22	0.28
4783	0.06	-0.22	0.29
4784	0.07	-0.22	0.29
4785	0.08	-0.23	0.30
4786	0.08	-0.23	0.31
4787	0.09	-0.23	0.32
4788	0.09	-0.24	0.33
4789	0.10	-0.24	0.34
4790	0.11	-0.25	0.35
4791	0.11	-0.26	0.37
4792	0.12	-0.26	0.38
4793	0.12	-0.27	0.40
4794	0.13	-0.28	0.41
4795	0.14	-0.29	0.43
4796	0.14	-0.30	0.44
4797	0.15	-0.31	0.46
4798	0.16	-0.32	0.47
4799	0.16	-0.33	0.49
4800	0.17	-0.34	0.50
4801	0.17	-0.35	0.52
4802	0.18	-0.36	0.54
4803	0.19	-0.37	0.55
4804	0.19	-0.37	0.57
4805	0.20	-0.38	0.58
4806	0.20	-0.39	0.60
4807	0.21	-0.40	0.61
4808	0.21	-0.41	0.62
4809	0.22	-0.42	0.63
4810	0.22	-0.42	0.64
4811	0.23	-0.43	0.65
4812	0.23	-0.43	0.66
4813	0.23	-0.44	0.67
4814	0.24	-0.44	0.67
4815	0.24	-0.44	0.68
4816	0.24	-0.44	0.68
4817	0.25	-0.44	0.69
4818	0.25	-0.44	0.69
4819	0.25	-0.44	0.69
4820	0.25	-0.44	0.69
4821	0.26	-0.44	0.69
4822	0.26	-0.43	0.69
4823	0.26	-0.43	0.69
4824	0.26	-0.43	0.69
4825	0.27	-0.42	0.69
4826	0.27	-0.42	0.69
4827	0.27	-0.42	0.69
4828	0.27	-0.41	0.69
4829	0.28	-0.41	0.68
4830	0.28	-0.40	0.68
4831	0.28	-0.40	0.68
4832	0.28	-0.39	0.68
4833	0.29	-0.39	0.67
4834	0.29	-0.38	0.67
4835	0.29	-0.37	0.66
4836	0.29	-0.37	0.66
4837	0.29	-0.36	0.65
4838	0.30	-0.35	0.65
4839	0.30	-0.35	0.64
4840	0.30	-0.34	0.64
4841	0.30	-0.33	0.63
4842	0.30	-0.32	0.63
4843	0.31	-0.32	0.62
4844	0.31	-0.31	0.62

Age (cal. BP)	SE Iberian precipitation (z-score)		
	annual	winter	summer
4845	0.31	-0.30	0.61
4846	0.31	-0.29	0.61
4847	0.31	-0.29	0.60
4848	0.32	-0.28	0.59
4849	0.32	-0.27	0.59
4850	0.32	-0.26	0.58
4851	0.32	-0.26	0.58
4852	0.32	-0.25	0.57
4853	0.32	-0.24	0.56
4854	0.32	-0.23	0.56
4855	0.33	-0.23	0.55
4856	0.33	-0.22	0.54
4857	0.33	-0.21	0.54
4858	0.33	-0.20	0.53
4859	0.33	-0.19	0.52
4860	0.33	-0.18	0.51
4861	0.33	-0.16	0.50
4862	0.34	-0.15	0.48
4863	0.34	-0.13	0.47
4864	0.34	-0.12	0.46
4865	0.34	-0.10	0.44
4866	0.34	-0.09	0.43
4867	0.34	-0.07	0.41
4868	0.34	-0.05	0.40
4869	0.34	-0.04	0.38
4870	0.34	-0.02	0.36
4871	0.35	0.00	0.35
4872	0.35	0.01	0.33
4873	0.35	0.03	0.32
4874	0.35	0.05	0.30
4875	0.35	0.06	0.29
4876	0.35	0.08	0.27
4877	0.35	0.10	0.26
4878	0.35	0.11	0.24
4879	0.36	0.13	0.23
4880	0.36	0.14	0.21
4881	0.36	0.16	0.20
4882	0.36	0.17	0.19
4883	0.36	0.18	0.18
4884	0.36	0.19	0.17
4885	0.36	0.20	0.16
4886	0.36	0.21	0.15
4887	0.36	0.22	0.14
4888	0.36	0.23	0.14
4889	0.37	0.23	0.13
4890	0.37	0.24	0.13
4891	0.37	0.24	0.13
4892	0.37	0.24	0.13
4893	0.37	0.24	0.13
4894	0.37	0.24	0.13
4895	0.37	0.24	0.13
4896	0.37	0.24	0.13
4897	0.37	0.24	0.13
4898	0.37	0.24	0.13
4899	0.37	0.24	0.13
4900	0.37	0.24	0.13
4901	0.37	0.23	0.13
4902	0.37	0.23	0.13
4903	0.37	0.23	0.14
4904	0.36	0.23	0.14
4905	0.36	0.22	0.14
4906	0.36	0.22	0.14
4907	0.36	0.21	0.15
4908	0.36	0.20	0.16
4909	0.36	0.20	0.16
4910	0.36	0.19	0.17
4911	0.36	0.18	0.18
4912	0.36	0.16	0.19
4913	0.36	0.15	0.21
4914	0.35	0.14	0.22
4915	0.35	0.12	0.23
4916	0.35	0.11	0.25
4917	0.35	0.09	0.26
4918	0.35	0.07	0.27

Age (cal. BP)	SE Iberian precipitation (z-score)		
	annual	winter	summer
4919	0.35	0.06	0.29
4920	0.35	0.04	0.30
4921	0.34	0.02	0.32
4922	0.34	0.01	0.34
4923	0.34	-0.01	0.35
4924	0.34	-0.03	0.37
4925	0.34	-0.05	0.38
4926	0.33	-0.07	0.40
4927	0.33	-0.08	0.41
4928	0.33	-0.10	0.43
4929	0.33	-0.12	0.44
4930	0.33	-0.13	0.46
4931	0.32	-0.15	0.47
4932	0.32	-0.16	0.48
4933	0.32	-0.18	0.50
4934	0.32	-0.19	0.51
4935	0.31	-0.20	0.52
4936	0.31	-0.21	0.53
4937	0.31	-0.22	0.53
4938	0.31	-0.23	0.54
4939	0.30	-0.24	0.55
4940	0.30	-0.25	0.55
4941	0.30	-0.26	0.55
4942	0.29	-0.26	0.55
4943	0.29	-0.27	0.56
4944	0.29	-0.27	0.56
4945	0.28	-0.28	0.56
4946	0.28	-0.28	0.56
4947	0.27	-0.29	0.56
4948	0.27	-0.29	0.56
4949	0.26	-0.30	0.56
4950	0.26	-0.30	0.56
4951	0.25	-0.31	0.56
4952	0.25	-0.31	0.56
4953	0.24	-0.32	0.56
4954	0.23	-0.32	0.56
4955	0.23	-0.33	0.56
4956	0.22	-0.33	0.56
4957	0.22	-0.34	0.55
4958	0.21	-0.34	0.55
4959	0.20	-0.35	0.55
4960	0.20	-0.35	0.55
4961	0.19	-0.35	0.54
4962	0.19	-0.36	0.54
4963	0.18	-0.36	0.54
4964	0.17	-0.36	0.54
4965	0.17	-0.37	0.53
4966	0.16	-0.37	0.53
4967	0.16	-0.37	0.53
4968	0.15	-0.37	0.53
4969	0.15	-0.38	0.52
4970	0.14	-0.38	0.52
4971	0.14	-0.38	0.52
4972	0.13	-0.38	0.52
4973	0.13	-0.39	0.51
4974	0.12	-0.39	0.51
4975	0.12	-0.39	0.51
4976	0.12	-0.39	0.51
4977	0.11	-0.39	0.51
4978	0.11	-0.39	0.50
4979	0.11	-0.39	0.50
4980	0.11	-0.39	0.50
4981	0.11	-0.40	0.50
4982	0.10	-0.40	0.50
4983	0.10	-0.40	0.50
4984	0.10	-0.40	0.49
4985	0.10	-0.40	0.49
4986	0.09	-0.40	0.49
4987	0.09	-0.39	0.48
4988	0.09	-0.39	0.48
4989	0.09	-0.39	0.48
4990	0.08	-0.39	0.47
4991	0.08	-0.38	0.46
4992	0.08	-0.38	0.46

Age (cal. BP)	SE Iberian precipitation (z-score)		
	annual	winter	summer
4993	0.07	-0.38	0.45
4994	0.07	-0.37	0.45
4995	0.07	-0.37	0.44
4996	0.07	-0.37	0.43
4997	0.06	-0.36	0.42
4998	0.06	-0.36	0.42
4999	0.06	-0.35	0.41
5000	0.06	-0.35	0.40
5001	0.05	-0.34	0.39
5002	0.05	-0.34	0.39
5003	0.05	-0.33	0.38
5004	0.04	-0.33	0.37
5005	0.04	-0.32	0.36
5006	0.04	-0.32	0.35
5007	0.04	-0.31	0.35
5008	0.03	-0.30	0.34
5009	0.03	-0.30	0.33
5010	0.03	-0.29	0.32
5011	0.02	-0.29	0.31
5012	0.02	-0.29	0.31
5013	0.02	-0.28	0.30
5014	0.02	-0.28	0.29
5015	0.01	-0.27	0.29
5016	0.01	-0.27	0.28
5017	0.01	-0.26	0.27
5018	0.01	-0.26	0.27
5019	0.00	-0.26	0.26
5020	0.00	-0.26	0.26
5021	0.00	-0.25	0.25
5022	0.00	-0.25	0.25
5023	0.00	-0.25	0.25
5024	-0.01	-0.25	0.24
5025	-0.01	-0.25	0.24
5026	-0.01	-0.25	0.24
5027	-0.01	-0.24	0.23
5028	-0.01	-0.24	0.23
5029	-0.01	-0.24	0.23
5030	-0.02	-0.24	0.23
5031	-0.02	-0.24	0.22
5032	-0.02	-0.24	0.22
5033	-0.02	-0.24	0.22
5034	-0.02	-0.24	0.22
5035	-0.02	-0.24	0.22
5036	-0.02	-0.24	0.22
5037	-0.02	-0.24	0.22
5038	-0.02	-0.24	0.22
5039	-0.02	-0.24	0.22
5040	-0.02	-0.24	0.22
5041	-0.02	-0.24	0.22
5042	-0.02	-0.24	0.22
5043	-0.02	-0.24	0.22
5044	-0.02	-0.24	0.22
5045	-0.02	-0.24	0.22
5046	-0.02	-0.24	0.22
5047	-0.02	-0.24	0.22
5048	-0.02	-0.24	0.22
5049	-0.02	-0.24	0.22
5050	-0.02	-0.24	0.22
5051	-0.02	-0.24	0.22
5052	-0.02	-0.24	0.22
5053	-0.02	-0.24	0.22
5054	-0.02	-0.24	0.22
5055	-0.02	-0.24	0.22
5056	-0.01	-0.24	0.22
5057	-0.01	-0.24	0.22
5058	-0.01	-0.23	0.22
5059	-0.01	-0.23	0.22
5060	-0.01	-0.23	0.22
5061	-0.01	-0.23	0.22
5062	-0.01	-0.22	0.21
5063	-0.01	-0.22	0.21
5064	-0.01	-0.22	0.21
5065	-0.01	-0.21	0.21
5066	0.00	-0.21	0.20

Age (cal. BP)	SE Iberian precipitation (z-score)		
	annual	winter	summer
5067	0.00	-0.20	0.20
5068	0.00	-0.20	0.19
5069	0.00	-0.19	0.19
5070	0.00	-0.18	0.18
5071	0.00	-0.18	0.18
5072	0.00	-0.17	0.17
5073	0.00	-0.16	0.16
5074	0.00	-0.15	0.16
5075	0.00	-0.15	0.15
5076	0.00	-0.14	0.14
5077	0.00	-0.13	0.13
5078	0.01	-0.12	0.12
5079	0.01	-0.11	0.12
5080	0.01	-0.10	0.11
5081	0.01	-0.09	0.10
5082	0.01	-0.08	0.09
5083	0.01	-0.07	0.08
5084	0.01	-0.06	0.07
5085	0.01	-0.05	0.06
5086	0.01	-0.04	0.05
5087	0.01	-0.03	0.04
5088	0.01	-0.02	0.03
5089	0.01	-0.01	0.02
5090	0.01	0.00	0.01
5091	0.01	0.02	0.00
5092	0.02	0.03	-0.01
5093	0.02	0.04	-0.02
5094	0.02	0.05	-0.03
5095	0.02	0.06	-0.04
5096	0.02	0.07	-0.05
5097	0.02	0.08	-0.06
5098	0.02	0.09	-0.07
5099	0.02	0.10	-0.08
5100	0.02	0.11	-0.09
5101	0.02	0.12	-0.10
5102	0.02	0.13	-0.11
5103	0.02	0.14	-0.12
5104	0.02	0.15	-0.12
5105	0.03	0.16	-0.13
5106	0.03	0.16	-0.14
5107	0.03	0.17	-0.15
5108	0.03	0.18	-0.15
5109	0.03	0.19	-0.16
5110	0.03	0.19	-0.16
5111	0.03	0.20	-0.17
5112	0.03	0.21	-0.18
5113	0.03	0.21	-0.18
5114	0.03	0.22	-0.19
5115	0.03	0.23	-0.20
5116	0.03	0.24	-0.20
5117	0.04	0.25	-0.21
5118	0.04	0.25	-0.22
5119	0.04	0.26	-0.23
5120	0.04	0.27	-0.23
5121	0.04	0.28	-0.24
5122	0.04	0.29	-0.25
5123	0.04	0.30	-0.26
5124	0.04	0.31	-0.27
5125	0.04	0.32	-0.28
5126	0.04	0.33	-0.29
5127	0.05	0.34	-0.29
5128	0.05	0.35	-0.30
5129	0.05	0.36	-0.31
5130	0.05	0.37	-0.32
5131	0.05	0.38	-0.33
5132	0.05	0.39	-0.34
5133	0.05	0.39	-0.34
5134	0.05	0.40	-0.35
5135	0.05	0.41	-0.36
5136	0.05	0.42	-0.37
5137	0.05	0.43	-0.37
5138	0.05	0.43	-0.38
5139	0.05	0.44	-0.39
5140	0.05	0.44	-0.39

Age (cal. BP)	SE Iberian precipitation (z-score)		
	annual	winter	summer
5141	0.05	0.45	-0.40
5142	0.05	0.45	-0.40
5143	0.05	0.46	-0.41
5144	0.05	0.46	-0.41
5145	0.05	0.47	-0.42
5146	0.05	0.47	-0.42
5147	0.05	0.48	-0.42
5148	0.05	0.48	-0.43
5149	0.05	0.48	-0.43
5150	0.05	0.49	-0.43
5151	0.05	0.49	-0.44
5152	0.05	0.49	-0.44
5153	0.06	0.50	-0.44
5154	0.06	0.50	-0.44
5155	0.06	0.50	-0.45
5156	0.06	0.51	-0.45
5157	0.06	0.51	-0.45
5158	0.06	0.51	-0.45
5159	0.06	0.51	-0.45
5160	0.07	0.52	-0.45
5161	0.07	0.52	-0.45
5162	0.07	0.52	-0.45
5163	0.07	0.52	-0.45
5164	0.07	0.53	-0.45
5165	0.08	0.53	-0.45
5166	0.08	0.53	-0.45
5167	0.08	0.53	-0.45
5168	0.09	0.53	-0.44
5169	0.09	0.53	-0.44
5170	0.10	0.54	-0.44
5171	0.10	0.54	-0.44
5172	0.10	0.54	-0.43
5173	0.11	0.54	-0.43
5174	0.11	0.54	-0.43
5175	0.12	0.54	-0.42
5176	0.12	0.54	-0.42
5177	0.13	0.54	-0.42
5178	0.13	0.55	-0.41
5179	0.14	0.55	-0.41
5180	0.14	0.55	-0.41
5181	0.15	0.55	-0.40
5182	0.15	0.55	-0.40
5183	0.16	0.55	-0.39
5184	0.16	0.55	-0.39
5185	0.17	0.55	-0.38
5186	0.17	0.55	-0.38
5187	0.18	0.55	-0.38
5188	0.18	0.55	-0.37
5189	0.19	0.55	-0.37
5190	0.19	0.55	-0.36
5191	0.20	0.55	-0.36
5192	0.20	0.55	-0.35
5193	0.20	0.55	-0.34
5194	0.21	0.54	-0.34
5195	0.21	0.54	-0.33
5196	0.22	0.54	-0.32
5197	0.22	0.54	-0.31
5198	0.23	0.53	-0.31
5199	0.23	0.53	-0.30
5200	0.23	0.53	-0.29
5201	0.24	0.52	-0.28
5202	0.24	0.52	-0.28
5203	0.24	0.51	-0.27
5204	0.25	0.51	-0.26
5205	0.25	0.50	-0.25
5206	0.25	0.50	-0.25
5207	0.26	0.49	-0.24
5208	0.26	0.49	-0.23
5209	0.26	0.48	-0.22
5210	0.26	0.48	-0.22
5211	0.27	0.48	-0.21
5212	0.27	0.47	-0.20
5213	0.27	0.47	-0.19
5214	0.28	0.46	-0.19

Age (cal. BP)	SE Iberian precipitation (z-score)		
	annual	winter	summer
5215	0.28	0.46	-0.18
5216	0.28	0.45	-0.17
5217	0.28	0.45	-0.16
5218	0.29	0.45	-0.16
5219	0.29	0.44	-0.15
5220	0.29	0.44	-0.14
5221	0.30	0.44	-0.14
5222	0.30	0.43	-0.13
5223	0.30	0.43	-0.13
5224	0.31	0.43	-0.12
5225	0.31	0.43	-0.12
5226	0.31	0.43	-0.11
5227	0.32	0.42	-0.11
5228	0.32	0.42	-0.10
5229	0.32	0.42	-0.10
5230	0.33	0.42	-0.09
5231	0.33	0.42	-0.09
5232	0.34	0.42	-0.08
5233	0.34	0.42	-0.08
5234	0.34	0.42	-0.07
5235	0.35	0.41	-0.07
5236	0.35	0.41	-0.06
5237	0.35	0.41	-0.06
5238	0.36	0.41	-0.06
5239	0.36	0.41	-0.05
5240	0.36	0.41	-0.05
5241	0.37	0.41	-0.04
5242	0.37	0.41	-0.04
5243	0.37	0.41	-0.03
5244	0.38	0.41	-0.03
5245	0.38	0.41	-0.03
5246	0.38	0.40	-0.02
5247	0.39	0.40	-0.02
5248	0.39	0.40	-0.01
5249	0.39	0.40	-0.01
5250	0.39	0.40	-0.01
5251	0.40	0.40	0.00
5252	0.40	0.40	0.00
5253	0.40	0.40	0.00
5254	0.41	0.40	0.01
5255	0.41	0.40	0.01
5256	0.41	0.40	0.01
5257	0.41	0.40	0.02
5258	0.42	0.39	0.02
5259	0.42	0.39	0.02
5260	0.42	0.39	0.03
5261	0.42	0.39	0.03
5262	0.42	0.39	0.03
5263	0.43	0.39	0.04
5264	0.43	0.39	0.04
5265	0.43	0.39	0.04
5266	0.43	0.39	0.04
5267	0.43	0.39	0.05
5268	0.43	0.39	0.05
5269	0.44	0.39	0.05
5270	0.44	0.38	0.05
5271	0.44	0.38	0.05
5272	0.44	0.38	0.06
5273	0.44	0.38	0.06
5274	0.44	0.38	0.06
5275	0.44	0.38	0.06
5276	0.44	0.38	0.06
5277	0.44	0.38	0.06
5278	0.44	0.38	0.06
5279	0.44	0.38	0.07
5280	0.44	0.37	0.07
5281	0.44	0.37	0.07
5282	0.44	0.37	0.07
5283	0.44	0.37	0.07
5284	0.44	0.37	0.07
5285	0.44	0.37	0.07
5286	0.44	0.37	0.07
5287	0.44	0.37	0.08
5288	0.44	0.37	0.08

Age (cal. BP)	SE Iberian precipitation (z-score)		
	annual	winter	summer
5289	0.44	0.36	0.08
5290	0.44	0.36	0.08
5291	0.44	0.36	0.08
5292	0.44	0.36	0.08
5293	0.44	0.36	0.08
5294	0.44	0.36	0.08
5295	0.44	0.36	0.08
5296	0.44	0.36	0.08
5297	0.44	0.36	0.08
5298	0.44	0.35	0.08
5299	0.44	0.35	0.08
5300	0.44	0.35	0.08
5301	0.44	0.35	0.09
5302	0.44	0.35	0.09
5303	0.44	0.35	0.09
5304	0.43	0.35	0.09
5305	0.43	0.35	0.09
5306	0.43	0.35	0.09
5307	0.43	0.34	0.09
5308	0.43	0.34	0.09
5309	0.43	0.34	0.09
5310	0.43	0.34	0.09
5311	0.43	0.34	0.09
5312	0.43	0.34	0.09
5313	0.43	0.34	0.09
5314	0.42	0.34	0.09
5315	0.42	0.34	0.09
5316	0.42	0.34	0.09
5317	0.42	0.33	0.09
5318	0.42	0.33	0.09
5319	0.42	0.33	0.09
5320	0.42	0.33	0.08
5321	0.42	0.33	0.08
5322	0.41	0.33	0.08
5323	0.41	0.33	0.08
5324	0.41	0.33	0.08
5325	0.41	0.33	0.08
5326	0.41	0.33	0.08
5327	0.41	0.33	0.08
5328	0.41	0.33	0.08
5329	0.40	0.33	0.08
5330	0.40	0.33	0.08
5331	0.40	0.33	0.07
5332	0.40	0.33	0.07
5333	0.40	0.33	0.07
5334	0.40	0.33	0.07
5335	0.40	0.33	0.07
5336	0.40	0.33	0.07
5337	0.39	0.33	0.07
5338	0.39	0.32	0.07
5339	0.39	0.32	0.07
5340	0.39	0.32	0.07
5341	0.39	0.32	0.07
5342	0.39	0.32	0.07
5343	0.39	0.32	0.07
5344	0.39	0.32	0.07
5345	0.39	0.32	0.06
5346	0.38	0.32	0.06
5347	0.38	0.32	0.06
5348	0.38	0.32	0.06
5349	0.38	0.32	0.06
5350	0.37	0.32	0.06
5351	0.37	0.32	0.05
5352	0.37	0.32	0.05
5353	0.37	0.32	0.05
5354	0.36	0.32	0.05
5355	0.36	0.32	0.04
5356	0.36	0.32	0.04
5357	0.35	0.31	0.04
5358	0.35	0.31	0.03
5359	0.34	0.31	0.03
5360	0.34	0.31	0.03
5361	0.34	0.31	0.02
5362	0.33	0.31	0.02

Age (cal. BP)	SE Iberian precipitation (z-score)		
	annual	winter	summer
5363	0.33	0.31	0.02
5364	0.32	0.31	0.01
5365	0.32	0.31	0.01
5366	0.32	0.31	0.01
5367	0.31	0.31	0.00
5368	0.31	0.31	0.00
5369	0.30	0.31	0.00
5370	0.30	0.31	-0.01
5371	0.30	0.31	-0.01
5372	0.29	0.31	-0.01
5373	0.29	0.31	-0.02
5374	0.28	0.31	-0.02
5375	0.28	0.30	-0.02
5376	0.28	0.30	-0.03
5377	0.27	0.30	-0.03
5378	0.27	0.30	-0.03
5379	0.27	0.30	-0.03
5380	0.27	0.30	-0.04
5381	0.26	0.30	-0.04
5382	0.26	0.30	-0.04
5383	0.26	0.30	-0.04
5384	0.26	0.30	-0.04
5385	0.26	0.30	-0.04
5386	0.25	0.30	-0.04
5387	0.25	0.30	-0.04
5388	0.25	0.30	-0.04
5389	0.25	0.30	-0.04
5390	0.25	0.29	-0.04
5391	0.25	0.29	-0.04
5392	0.25	0.29	-0.04
5393	0.25	0.29	-0.04
5394	0.25	0.29	-0.04
5395	0.25	0.29	-0.04
5396	0.25	0.29	-0.04
5397	0.26	0.29	-0.03
5398	0.26	0.29	-0.03
5399	0.26	0.29	-0.03
5400	0.26	0.29	-0.03
5401	0.26	0.29	-0.03
5402	0.26	0.28	-0.02
5403	0.26	0.28	-0.02
5404	0.26	0.28	-0.02
5405	0.27	0.28	-0.02
5406	0.27	0.28	-0.01
5407	0.27	0.28	-0.01
5408	0.27	0.28	-0.01
5409	0.27	0.28	0.00
5410	0.28	0.28	0.00
5411	0.28	0.28	0.00
5412	0.28	0.28	0.00
5413	0.28	0.28	0.01
5414	0.28	0.28	0.01
5415	0.29	0.28	0.01
5416	0.29	0.28	0.01
5417	0.29	0.28	0.01
5418	0.29	0.28	0.02
5419	0.30	0.28	0.02
5420	0.30	0.28	0.02
5421	0.30	0.28	0.02
5422	0.30	0.28	0.03
5423	0.30	0.28	0.03
5424	0.31	0.28	0.03
5425	0.31	0.28	0.03
5426	0.31	0.28	0.03
5427	0.31	0.28	0.04
5428	0.31	0.27	0.04
5429	0.32	0.27	0.04
5430	0.32	0.27	0.04
5431	0.32	0.27	0.05
5432	0.32	0.27	0.05
5433	0.32	0.27	0.05
5434	0.33	0.27	0.06
5435	0.33	0.27	0.06
5436	0.33	0.26	0.07

Age (cal. BP)	SE Iberian precipitation (z-score)		
	annual	winter	summer
5437	0.33	0.26	0.07
5438	0.34	0.26	0.08
5439	0.34	0.26	0.08
5440	0.34	0.26	0.09
5441	0.35	0.25	0.09
5442	0.35	0.25	0.10
5443	0.35	0.25	0.10
5444	0.35	0.25	0.11
5445	0.36	0.24	0.11
5446	0.36	0.24	0.12
5447	0.36	0.24	0.12
5448	0.36	0.23	0.13
5449	0.37	0.23	0.14
5450	0.37	0.23	0.14
5451	0.37	0.22	0.15
5452	0.38	0.22	0.15
5453	0.38	0.22	0.16
5454	0.38	0.21	0.17
5455	0.38	0.21	0.17
5456	0.38	0.21	0.18
5457	0.39	0.20	0.18
5458	0.39	0.20	0.19
5459	0.39	0.20	0.19
5460	0.39	0.20	0.20
5461	0.40	0.19	0.20
5462	0.40	0.19	0.21
5463	0.40	0.19	0.21
5464	0.40	0.18	0.22
5465	0.40	0.18	0.22
5466	0.40	0.18	0.23
5467	0.40	0.17	0.23
5468	0.41	0.17	0.23
5469	0.41	0.17	0.24
5470	0.41	0.17	0.24
5471	0.41	0.16	0.25
5472	0.41	0.16	0.25
5473	0.41	0.16	0.25
5474	0.42	0.16	0.26
5475	0.42	0.16	0.26
5476	0.42	0.15	0.26
5477	0.42	0.15	0.27
5478	0.42	0.15	0.27
5479	0.43	0.15	0.27
5480	0.43	0.15	0.28
5481	0.43	0.15	0.28
5482	0.43	0.15	0.28
5483	0.43	0.15	0.29
5484	0.44	0.15	0.29
5485	0.44	0.15	0.29
5486	0.44	0.15	0.29
5487	0.44	0.15	0.29
5488	0.45	0.15	0.30
5489	0.45	0.15	0.30
5490	0.45	0.15	0.30
5491	0.45	0.15	0.30
5492	0.45	0.16	0.30
5493	0.46	0.16	0.30
5494	0.46	0.16	0.30
5495	0.46	0.16	0.30
5496	0.46	0.16	0.30
5497	0.46	0.16	0.30
5498	0.46	0.17	0.30
5499	0.47	0.17	0.30
5500	0.47	0.17	0.29
5501	0.47	0.17	0.29
5502	0.47	0.18	0.29
5503	0.47	NA	NA
5504	0.47	0.18	0.29
5505	0.47	0.18	0.29
5506	0.47	0.18	0.28
5507	0.47	0.19	0.28
5508	0.47	0.19	0.28
5509	0.47	0.19	0.27
5510	0.47	0.20	0.27

Age (cal. BP)	SE Iberian precipitation (z-score)		
	annual	winter	summer
5511	0.47	0.20	0.27
5512	0.47	0.20	0.26
5513	0.46	0.21	0.26
5514	0.46	0.21	0.25
5515	0.46	0.21	0.25
5516	0.46	0.22	0.24
5517	0.46	0.22	0.24
5518	0.46	0.22	0.24
5519	0.46	0.23	0.23
5520	0.45	0.23	0.23
5521	0.45	0.23	0.22
5522	0.45	0.23	0.22
5523	0.45	0.24	0.21
5524	0.45	0.24	0.21
5525	0.44	0.24	0.20
5526	0.44	0.25	0.20
5527	0.44	0.25	0.19
5528	0.44	0.25	0.19
5529	0.44	0.25	0.18
5530	0.43	0.26	0.18
5531	0.43	0.26	0.17
5532	0.43	0.26	0.17
5533	0.43	0.26	0.17
5534	0.43	0.27	0.16
5535	0.42	0.27	0.16
5536	0.42	0.27	0.15
5537	0.42	0.27	0.15
5538	0.42	0.27	0.15
5539	0.42	0.27	0.14
5540	0.41	0.27	0.14
5541	0.41	0.28	0.14
5542	0.41	0.28	0.13
5543	0.41	0.28	0.13
5544	0.41	0.28	0.13
5545	0.41	0.28	0.13
5546	0.41	0.28	0.13
5547	0.40	0.28	0.13
5548	0.40	0.28	0.12
5549	0.40	0.28	0.12
5550	0.40	0.28	0.12
5551	0.40	0.28	0.12
5552	0.40	0.28	0.12
5553	0.40	0.28	0.12
5554	0.40	0.28	0.12
5555	0.40	0.28	0.12
5556	0.40	0.28	0.12
5557	0.40	0.28	0.12
5558	0.40	0.28	0.12
5559	0.40	0.28	0.11
5560	0.39	0.28	0.11
5561	0.39	0.28	0.11
5562	0.39	0.28	0.11
5563	0.39	0.28	0.11
5564	0.39	0.28	0.11
5565	0.39	0.28	0.11
5566	0.39	0.28	0.10
5567	0.39	0.29	0.10
5568	0.39	0.29	0.10
5569	0.39	0.29	0.10
5570	0.38	0.29	0.10
5571	0.38	0.29	0.09
5572	0.38	0.29	0.09
5573	0.38	0.29	0.09
5574	0.38	0.29	0.09
5575	0.38	0.30	0.09
5576	0.38	0.30	0.08
5577	0.38	0.30	0.08
5578	0.38	0.30	0.08
5579	0.38	0.30	0.08
5580	0.38	0.30	0.08
5581	0.38	0.31	0.07
5582	0.38	0.31	0.07
5583	0.38	0.31	0.07
5584	0.38	0.31	0.07

Age (cal. BP)	SE Iberian precipitation (z-score)		
	annual	winter	summer
5585	0.38	0.31	0.07
5586	0.38	0.31	0.07
5587	0.38	0.32	0.07
5588	0.39	0.32	0.07
5589	0.39	0.32	0.07
5590	0.39	0.32	0.07
5591	0.39	0.32	0.07
5592	0.39	0.32	0.07
5593	0.39	0.33	0.07
5594	0.40	0.33	0.07
5595	0.40	0.33	0.07
5596	0.40	0.33	0.07
5597	0.40	0.33	0.07
5598	0.40	0.33	0.07
5599	0.41	0.34	0.07
5600	0.41	0.34	0.07
5601	0.41	0.34	0.07
5602	0.42	0.34	0.08
5603	0.42	0.34	0.08
5604	0.42	0.34	0.08
5605	0.42	0.34	0.08
5606	0.43	0.34	0.08
5607	0.43	0.34	0.09
5608	0.43	0.35	0.09
5609	0.44	0.35	0.09
5610	0.44	0.35	0.09
5611	0.44	0.35	0.09
5612	0.45	0.35	0.10
5613	0.45	0.35	0.10
5614	0.45	0.35	0.10
5615	0.46	0.35	0.10
5616	0.46	0.35	0.11
5617	0.46	0.35	0.11
5618	0.47	0.35	0.11
5619	0.47	0.35	0.12
5620	0.47	0.35	0.12
5621	0.48	0.35	0.12
5622	0.48	0.35	0.12
5623	0.48	0.36	0.13
5624	0.48	0.36	0.13
5625	0.49	0.36	0.13
5626	0.49	0.36	0.14
5627	0.50	0.36	0.14
5628	0.50	0.36	0.14
5629	0.51	0.36	0.15
5630	0.51	0.36	0.15
5631	0.52	0.36	0.16
5632	0.52	0.36	0.16
5633	0.53	0.36	0.17
5634	0.53	0.36	0.18
5635	0.54	0.36	0.18
5636	0.55	0.36	0.19
5637	0.55	0.36	0.20
5638	0.56	0.36	0.20
5639	0.57	0.36	0.21
5640	0.58	0.36	0.22
5641	0.58	0.36	0.23
5642	0.59	0.36	0.23
5643	0.60	0.36	0.24
5644	0.60	0.36	0.25
5645	0.61	0.35	0.26
5646	0.62	0.35	0.27
5647	0.63	0.35	0.27
5648	0.64	0.35	0.28
5649	0.64	0.35	0.29
5650	0.65	0.35	0.30
5651	0.66	0.35	0.31
5652	0.66	0.35	0.31
5653	0.67	0.35	0.32
5654	0.68	0.35	0.33
5655	0.68	0.35	0.33
5656	0.69	0.35	0.34
5657	0.70	0.35	0.35
5658	0.70	0.35	0.35

Age (cal. BP)	SE Iberian precipitation (z-score)		
	annual	winter	summer
5659	0.71	0.35	0.36
5660	0.71	0.35	0.37
5661	0.72	0.35	0.37
5662	0.72	0.35	0.38
5663	0.73	0.35	0.38
5664	0.73	0.35	0.38
5665	0.73	0.35	0.39
5666	0.74	0.35	0.39
5667	0.74	0.34	0.40
5668	0.74	0.34	0.40
5669	0.75	0.34	0.40
5670	0.75	0.34	0.41
5671	0.75	0.34	0.41
5672	0.76	0.34	0.41
5673	0.76	0.34	0.42
5674	0.76	0.34	0.42
5675	0.77	0.34	0.42
5676	0.77	0.34	0.43
5677	0.77	0.34	0.43
5678	0.77	0.34	0.43
5679	0.78	0.34	0.43
5680	0.78	0.34	0.44
5681	0.78	0.34	0.44
5682	0.78	0.34	0.44
5683	0.79	0.34	0.44
5684	0.79	0.34	0.45
5685	0.79	0.34	0.45
5686	0.79	0.34	0.45
5687	0.80	0.34	0.45
5688	0.80	0.34	0.46
5689	0.80	0.34	0.46
5690	0.80	0.34	0.46
5691	0.81	0.34	0.46
5692	0.81	0.34	0.46
5693	0.81	0.35	0.46
5694	0.81	0.35	0.47
5695	0.81	0.35	0.47
5696	0.81	0.35	0.47
5697	0.82	0.35	0.47
5698	0.82	0.35	0.47
5699	0.82	0.35	0.47
5700	0.82	0.35	0.47
5701	0.82	0.35	0.47
5702	0.82	0.35	0.48
5703	0.83	0.35	0.48
5704	0.83	0.35	0.48
5705	0.83	0.35	0.48
5706	0.83	0.35	0.48
5707	0.83	0.35	0.48
5708	0.83	0.35	0.48
5709	0.83	0.35	0.48
5710	0.83	0.35	0.49
5711	0.83	0.35	0.49
5712	0.83	0.35	0.49
5713	0.83	0.34	0.49
5714	0.83	0.34	0.49
5715	0.83	0.34	0.49
5716	0.83	0.34	0.49
5717	0.83	0.34	0.49
5718	0.83	0.34	0.49
5719	0.83	0.34	0.49
5720	0.83	0.34	0.49
5721	0.83	0.34	0.49
5722	0.83	0.34	0.49
5723	0.83	0.34	0.49
5724	0.83	0.33	0.49
5725	0.83	0.33	0.49
5726	0.82	0.33	0.49
5727	0.82	0.33	0.49
5728	0.82	0.33	0.49
5729	0.82	0.33	0.49
5730	0.82	0.33	0.49
5731	0.82	0.32	0.49
5732	0.81	0.32	0.49

Age (cal. BP)	SE Iberian precipitation (z-score)		
	annual	winter	summer
5733	0.81	0.32	0.49
5734	0.81	0.32	0.49
5735	0.81	0.32	0.49
5736	0.81	0.32	0.49
5737	0.80	0.31	0.49
5738	0.80	0.31	0.49
5739	0.80	0.31	0.49
5740	0.80	0.31	0.49
5741	0.79	0.31	0.49
5742	0.79	0.31	0.49
5743	0.79	0.30	0.48
5744	0.79	0.30	0.48
5745	0.78	0.30	0.48
5746	0.78	0.30	0.48
5747	0.78	0.29	0.48
5748	0.77	0.29	0.48
5749	0.77	0.29	0.48
5750	0.77	0.29	0.48
5751	0.76	0.28	0.48
5752	0.76	0.28	0.48
5753	0.76	0.28	0.48
5754	0.75	0.27	0.48
5755	0.75	0.27	0.48
5756	0.74	0.26	0.48
5757	0.74	0.26	0.48
5758	0.73	0.26	0.47
5759	0.72	0.25	0.47
5760	0.72	0.25	0.47
5761	0.71	0.24	0.47
5762	0.70	0.24	0.46
5763	0.69	0.24	0.46
5764	0.69	0.23	0.45
5765	0.68	0.23	0.45
5766	0.67	0.22	0.45
5767	0.66	0.22	0.44
5768	0.65	0.22	0.44
5769	0.65	0.21	0.43
5770	0.64	0.21	0.43
5771	0.63	0.21	0.42
5772	0.62	0.20	0.42
5773	0.61	0.20	0.41
5774	0.61	0.19	0.41
5775	0.60	0.19	0.41
5776	0.59	0.19	0.40
5777	0.58	0.18	0.40
5778	0.58	0.18	0.40
5779	0.57	0.18	0.39
5780	0.56	0.18	0.39
5781	0.56	0.17	0.39
5782	0.55	0.17	0.38
5783	0.55	0.17	0.38
5784	0.55	0.17	0.38
5785	0.54	0.16	0.38
5786	0.54	0.16	0.38
5787	0.54	0.16	0.38
5788	0.54	0.16	0.38
5789	0.53	0.16	0.37
5790	0.53	0.16	0.37
5791	0.53	0.16	0.37
5792	0.52	0.16	0.37
5793	0.52	0.16	0.36
5794	0.52	0.16	0.36
5795	0.51	0.16	0.35
5796	0.51	0.16	0.35
5797	0.50	0.16	0.34
5798	0.50	0.16	0.34
5799	0.50	0.16	0.33
5800	0.49	0.17	0.33
5801	0.49	0.17	0.32
5802	0.48	0.17	0.31
5803	0.48	0.18	0.31
5804	0.48	0.18	0.30
5805	0.47	0.18	0.29
5806	0.47	0.19	0.28

Age (cal. BP)	SE Iberian precipitation (z-score)		
	annual	winter	summer
5807	0.46	0.19	0.27
5808	0.46	0.19	0.27
5809	0.46	0.20	0.26
5810	0.45	0.20	0.25
5811	0.45	0.21	0.24
5812	0.45	0.21	0.23
5813	0.44	0.22	0.22
5814	0.44	0.22	0.22
5815	0.44	0.23	0.21
5816	0.43	0.23	0.20
5817	0.43	0.24	0.19
5818	0.43	0.24	0.18
5819	0.43	0.25	0.18
5820	0.42	0.26	0.17
5821	0.42	0.26	0.16
5822	0.42	0.27	0.15
5823	0.42	0.27	0.15
5824	0.42	0.28	0.14
5825	0.42	0.28	0.14
5826	0.42	0.29	0.13
5827	0.42	0.29	0.13
5828	0.42	0.30	0.12
5829	0.42	0.30	0.12
5830	0.42	0.30	0.11
5831	0.42	0.31	0.11
5832	0.42	0.31	0.11
5833	0.43	0.32	0.11
5834	0.43	0.32	0.11
5835	0.43	0.32	0.11
5836	0.44	0.33	0.11
5837	0.44	0.33	0.11
5838	0.44	0.33	0.11
5839	0.45	0.33	0.12
5840	0.46	0.34	0.12
5841	0.46	0.34	0.12
5842	0.47	0.34	0.12
5843	0.47	0.35	0.13
5844	0.48	0.35	0.13
5845	0.49	0.35	0.14
5846	0.49	0.35	0.14
5847	0.50	0.36	0.14
5848	0.51	0.36	0.15
5849	0.52	0.36	0.15
5850	0.52	0.37	0.16
5851	0.53	0.37	0.16
5852	0.54	0.37	0.17
5853	0.55	0.38	0.17
5854	0.56	0.38	0.18
5855	0.56	0.38	0.18
5856	0.57	0.39	0.19
5857	0.58	0.39	0.19
5858	0.59	0.39	0.20
5859	0.60	0.39	0.20
5860	0.60	0.40	0.21
5861	0.61	0.40	0.21
5862	0.62	0.40	0.21
5863	0.63	0.41	0.22
5864	0.63	0.41	0.22
5865	0.64	0.41	0.23
5866	0.65	0.42	0.23
5867	0.65	0.42	0.23
5868	0.66	0.42	0.24
5869	0.67	0.43	0.24
5870	0.67	0.43	0.24
5871	0.68	0.43	0.24
5872	0.68	0.43	0.25
5873	0.69	0.44	0.25
5874	0.69	0.44	0.25
5875	0.69	0.44	0.25
5876	0.70	0.45	0.25
5877	0.70	0.45	0.25
5878	0.71	0.45	0.25
5879	0.71	0.46	0.25
5880	0.71	0.46	0.26

Age (cal. BP)	SE Iberian precipitation (z-score)		
	annual	winter	summer
5881	0.72	0.46	0.26
5882	0.72	0.46	0.26
5883	0.73	0.47	0.26
5884	0.73	0.47	0.26
5885	0.74	0.47	0.27
5886	0.74	0.47	0.27
5887	0.75	0.48	0.27
5888	0.75	0.48	0.27
5889	0.76	0.48	0.28
5890	0.76	0.48	0.28
5891	0.77	0.49	0.28
5892	0.77	0.49	0.29
5893	0.78	0.49	0.29
5894	0.78	0.49	0.29
5895	0.79	0.50	0.29
5896	0.80	0.50	0.30
5897	0.80	0.50	0.30
5898	0.81	0.50	0.30
5899	0.81	0.50	0.31
5900	0.82	0.50	0.31
5901	0.82	0.51	0.31
5902	0.83	0.51	0.32
5903	0.83	0.51	0.32
5904	0.83	0.51	0.32
5905	0.84	0.51	0.33
5906	0.84	0.51	0.33
5907	0.85	0.52	0.33
5908	0.85	0.52	0.33
5909	0.85	0.52	0.33
5910	0.86	0.52	0.33
5911	0.86	0.52	0.34
5912	0.86	0.53	0.34
5913	0.87	0.53	0.34
5914	0.87	0.53	0.34
5915	0.87	0.53	0.34
5916	0.87	0.53	0.34
5917	0.87	0.54	0.34
5918	0.87	0.54	0.34
5919	0.87	0.54	0.34
5920	0.88	0.54	0.33
5921	0.88	0.54	0.33
5922	0.87	0.54	0.33
5923	0.87	0.55	0.33
5924	0.87	0.55	0.33
5925	0.87	0.55	0.32
5926	0.87	0.55	0.32
5927	0.87	0.55	0.31
5928	0.86	0.55	0.31
5929	0.86	0.56	0.31
5930	0.86	0.56	0.30
5931	0.86	0.56	0.30
5932	0.85	0.56	0.29
5933	0.85	0.56	0.29
5934	0.85	0.56	0.28
5935	0.84	0.56	0.28
5936	0.84	0.57	0.27
5937	0.84	0.57	0.27
5938	0.83	0.57	0.26
5939	0.83	0.57	0.26
5940	0.83	0.57	0.25
5941	0.82	0.57	0.25
5942	0.82	0.57	0.24
5943	0.81	0.57	0.24
5944	0.81	0.57	0.23
5945	0.80	0.57	0.23
5946	0.80	0.58	0.22
5947	0.79	0.58	0.22
5948	0.79	0.58	0.21
5949	0.78	0.58	0.21
5950	0.78	0.58	0.20
5951	0.77	0.58	0.19
5952	0.76	0.58	0.19
5953	0.76	0.58	0.18
5954	0.75	0.58	0.18

Age (cal. BP)	SE Iberian precipitation (z-score)		
	annual	winter	summer
5955	0.75	0.58	0.17
5956	0.74	0.58	0.16
5957	0.73	0.58	0.15
5958	0.72	0.58	0.15
5959	0.72	0.58	0.14
5960	0.71	0.58	0.13
5961	0.70	0.57	0.12
5962	0.69	0.57	0.12
5963	0.68	0.57	0.11
5964	0.67	0.57	0.10
5965	0.66	0.57	0.09
5966	0.66	0.57	0.08
5967	0.65	0.57	0.08
5968	0.64	0.57	0.07
5969	0.63	0.57	0.06
5970	0.62	0.57	0.05
5971	0.61	0.57	0.04
5972	0.59	0.57	0.03
5973	0.58	0.56	0.02
5974	0.57	0.56	0.01
5975	0.56	0.56	0.00
5976	0.55	0.56	-0.01
5977	0.54	0.56	-0.02
5978	0.53	0.56	-0.03
5979	0.52	0.56	-0.04
5980	0.50	0.56	-0.05
5981	0.49	0.55	-0.06
5982	0.48	0.55	-0.07
5983	0.47	0.55	-0.09
5984	0.45	0.55	-0.10
5985	0.44	0.55	-0.11
5986	0.43	0.55	-0.12
5987	0.41	0.54	-0.13
5988	0.40	0.54	-0.14
5989	0.38	0.54	-0.16
5990	0.37	0.54	-0.17
5991	0.36	0.54	-0.18
5992	0.34	0.53	-0.19
5993	0.33	0.53	-0.20
5994	0.31	0.53	-0.22
5995	0.30	0.53	-0.23
5996	0.28	0.53	-0.24
5997	0.27	0.52	-0.26
5998	0.25	0.52	-0.27
5999	0.24	0.52	-0.28
6000	0.22	0.52	-0.30

Table A 12 Summed probability densities of Iberian settlement sites at 200 year time slices between 6000 and 3000 cal. BP.

Site	Lat	Lon	SPD of Iberian settlement sites at 200 year time slices (cal. BP)														
			6000-5800	5800-5600	5600-5400	5400-5200	5200-5000	5000-4800	4800-4600	4600-4400	4400-4200	4200-4000	4000-3800	3800-3600	3600-3400	3400-3200	3200-3000
Abauntz	43.01	-1.64	0.00020	0.00000	0.00000	0.00042	0.00179	0.00712	0.00224	0.00090	0.00010	0.00000	0.00000	0.00000	0.00000	0.00000	0.00000
Abrigo 6 del Humo	36.71	-4.32	0.00000	0.00000	0.00000	0.00000	0.00000	0.00000	0.00000	0.00000	0.00000	0.00000	0.00000	0.00000	0.00000	0.00000	0.00000
Abrunheiro	38.71	-9.30	0.00000	0.00000	0.00000	0.00000	0.00000	0.00000	0.00000	0.00000	0.00000	0.00000	0.00000	0.00000	0.00000	0.00000	0.00000
Acequión (El)	39.03	-2.03	0.00219	0.00248	0.00055	0.00003	0.00000	0.00000	0.00117	0.00462	0.01755	0.04614	0.05830	0.02443	0.00030	0.00363	0.00314
Achadizo (O)	42.61	-8.89	0.00000	0.00000	0.00000	0.00000	0.00000	0.00000	0.00000	0.00000	0.00000	0.00000	0.00000	0.00000	0.00000	0.00001	0.00743
Acinipo	36.84	-5.24	0.00000	0.00000	0.00000	0.00000	0.00000	0.00000	0.00000	0.00000	0.00063	0.01207	0.01945	0.00244	0.00009	0.00266	0.00531
Agroal	39.68	-8.43	0.00000	0.00000	0.00000	0.00000	0.00000	0.00000	0.00004	0.00018	0.00088	0.00262	0.00440	0.00382	0.00122	0.00012	0.00002
Aguiar. Castelo de	41.47	-7.68	0.00000	0.00009	0.00340	0.00141	0.00050	0.00014	0.00112	0.00192	0.00212	0.00129	0.00044	0.00007	0.00000	0.00014	0.00087
Aizpea	42.94	-1.26	0.00000	0.00000	0.00000	0.00000	0.00000	0.00000	0.00000	0.00000	0.00000	0.00028	0.00611	0.00011	0.00000	0.00000	0.00000
Alarcón	36.73	-4.12	0.00000	0.00000	0.00000	0.00000	0.00000	0.00000	0.00000	0.00000	0.00000	0.00000	0.00000	0.00000	0.00000	0.00000	0.00239
Alarcos	38.95	-4.02	0.00000	0.00000	0.00000	0.00000	0.00000	0.00000	0.00000	0.00000	0.00000	0.00000	0.00000	0.00000	0.00000	0.00000	0.00000
Albalate	37.87	-4.22	0.00000	0.00000	0.00000	0.00000	0.00000	0.00007	0.00594	0.00944	0.00909	0.00412	0.00040	0.00000	0.00000	0.00000	0.00000
Albardeiros. Monte Novo dos	38.37	-7.45	0.00000	0.00000	0.00000	0.00000	0.00000	0.00000	0.00302	0.00434	0.00238	0.00353	0.00121	0.00005	0.00000	0.00000	0.00000
Alcácer do Sal. Castelo de	38.38	-8.52	0.00000	0.00000	0.00000	0.00000	0.00000	0.00000	0.00000	0.00000	0.00000	0.00000	0.00000	0.00000	0.00417	0.00009	0.00000
Alcáçova de Santarém	39.23	-8.68	0.00000	0.00000	0.00000	0.00000	0.00000	0.00000	0.00000	0.00000	0.00000	0.00000	0.00000	0.00000	0.00000	0.00000	0.00000
Alcalar 7	37.20	-8.59	0.00000	0.00000	0.00000	0.00350	0.00820	0.01125	0.00347	0.00308	0.01103	0.00552	0.00123	0.00000	0.00817	0.00000	0.00000
Alcazaba de Loja	37.17	-4.15	0.00000	0.00000	0.00000	0.00000	0.00000	0.00000	0.00000	0.00077	0.00613	0.00023	0.00000	0.00000	0.00000	0.00000	0.00000
Aldeagordillo	40.66	-4.66	0.00000	0.00000	0.00000	0.00002	0.00028	0.00404	0.01415	0.00328	0.00017	0.00627	0.00542	0.00429	0.00004	0.00000	0.00000
Aldovesta	40.95	0.49	0.00000	0.00000	0.00000	0.00000	0.00000	0.00000	0.00000	0.00000	0.00000	0.00000	0.00000	0.00000	0.00000	0.00000	0.00000
Alegrios	40.06	-7.13	0.00102	0.00000	0.00000	0.00000	0.00000	0.00000	0.00000	0.00000	0.00009	0.00264	0.00579	0.00671	0.00593	0.00660	0.00109
Almaraz. Quinta do	38.69	-9.15	0.00000	0.00000	0.00000	0.00111	0.00990	0.00537	0.00000	0.00000	0.00000	0.00000	0.00000	0.00000	0.00023	0.04755	0.03246
Almendricos. El Rincón de	37.48	-1.79	0.00000	0.00000	0.00000	0.00000	0.00000	0.00000	0.00000	0.00001	0.00057	0.00328	0.00300	0.00035	0.00000	0.00000	0.00000
Almizaraque	37.27	-1.79	0.00000	0.00003	0.00370	0.00519	0.00479	0.01528	0.03796	0.05770	0.04710	0.00384	0.00014	0.00000	0.00000	0.00000	0.00000
Almoloya (La)	37.96	-1.51	0.00000	0.00000	0.00000	0.00000	0.00000	0.00000	0.00000	0.00000	0.00000	0.01310	0.00002	0.00000	0.00000	0.00000	0.00000
Almonda	39.51	-8.62	0.00000	0.00000	0.00000	0.00000	0.00000	0.00000	0.00000	0.00000	0.01362	0.00845	0.00000	0.00103	0.01275	0.00000	0.00000
Alonso Norte	41.01	-0.16	0.00002	0.00016	0.00167	0.00204	0.00200	0.00092	0.00004	0.00000	0.00000	0.00000	0.00000	0.00000	0.00000	0.00000	0.00000
Alt de Benamaquia	38.82	0.08	0.00000	0.00000	0.00000	0.00000	0.00000	0.00000	0.00000	0.00000	0.00000	0.00000	0.00000	0.00000	0.00000	0.00000	0.00000
Alto de la Garma	43.43	-3.67	0.00000	0.00000	0.00000	0.00000	0.00000	0.00000	0.00000	0.00000	0.00000	0.00000	0.00000	0.00000	0.00000	0.00000	0.00000
Alto de Santa Ana	41.77	-7.45	0.00000	0.00000	0.00000	0.00000	0.00000	0.00000	0.00000	0.00000	0.00000	0.00000	0.00000	0.00000	0.00000	0.00036	0.00507
Alto del Arenal	41.82	-3.07	0.00000	0.00000	0.00000	0.00000	0.00000	0.00000	0.00000	0.00000	0.00000	0.00000	0.00000	0.00000	0.00000	0.00000	0.00000
Alto del Quemado	40.58	-5.50	0.00000	0.00000	0.00002	0.00015	0.00024	0.00052	0.00401	0.00794	0.00961	0.00852	0.00280	0.00132	0.00055	0.00013	0.00004
Alto do Castelo	39.25	-8.58	0.00000	0.00008	0.00253	0.00000	0.00000	0.00000	0.00000	0.00000	0.00000	0.00000	0.00000	0.00000	0.00000	0.00000	0.00000

Site	Lat	Lon	SPD of Iberian settlement sites at 200 year time slices (cal. BP)														
			6000-5800	5800-5600	5600-5400	5400-5200	5200-5000	5000-4800	4800-4600	4600-4400	4400-4200	4200-4000	4000-3800	3800-3600	3600-3400	3400-3200	3200-3000
Alto do Castro	42.63	-8.55	0.00000	0.00000	0.00000	0.00000	0.00000	0.00000	0.00000	0.00000	0.00000	0.00000	0.00000	0.00000	0.00000	0.00000	0.00000
Alto do Dafundo	38.71	-9.24	0.00000	0.00000	0.00365	0.00041	0.00001	0.00000	0.00000	0.00000	0.00000	0.00000	0.00000	0.00000	0.00000	0.00000	0.00000
Amarejo (El)	38.85	-1.35	0.00000	0.00000	0.00000	0.00000	0.00000	0.00000	0.00000	0.00000	0.00000	0.00000	0.00000	0.00000	0.00002	0.00514	0.00192
Amarguillo 2	37.16	-5.69	0.00000	0.00000	0.00000	0.00000	0.00000	0.00000	0.00489	0.00971	0.00049	0.00000	0.00000	0.00000	0.00000	0.00000	0.00000
Ameal VI	40.45	-7.94	0.00000	0.00000	0.00004	0.00381	0.00568	0.00005	0.00781	0.00383	0.00238	0.00036	0.00001	0.00000	0.00000	0.00000	0.00000
Amoladeras (Las)	37.64	-0.71	0.00000	0.00005	0.00504	0.00009	0.00000	0.00000	0.00000	0.00000	0.00000	0.00000	0.00000	0.00000	0.00000	0.00000	0.00000
Amoreira. Cabeço de	39.11	-8.68	0.00131	0.00000	0.00000	0.00000	0.00000	0.00000	0.00000	0.00005	0.00552	0.00000	0.00000	0.00000	0.00000	0.00000	0.00000
Amoreiras. Cabeço das	38.25	-8.37	0.00000	0.00000	0.00000	0.00000	0.00000	0.00000	0.00000	0.00000	0.00000	0.00000	0.00000	0.00000	0.00000	0.00000	0.00000
Amorim. Quinta de	41.57	-8.40	0.00000	0.00000	0.00000	0.00000	0.00000	0.00000	0.00000	0.00000	0.00000	0.00000	0.00000	0.00035	0.00376	0.00000	0.00000
Ampla. Cova	38.81	0.09	0.00000	0.00000	0.00000	0.00000	0.00000	0.00000	0.00000	0.00000	0.00000	0.00000	0.00000	0.00000	0.00000	0.00000	0.00000
Andrés. Tozal de	41.93	0.03	0.00000	0.00000	0.00000	0.00000	0.00000	0.00000	0.00000	0.00000	0.00000	0.00000	0.00000	0.00000	0.00000	0.00139	0.00618
Ángel 1. Abrigo del	40.71	-0.42	0.00061	0.00000	0.00000	0.00000	0.00000	0.00000	0.00000	0.00000	0.00000	0.00000	0.00000	0.00000	0.00000	0.00000	0.00000
Ángel 2. Abrigo del	40.71	-0.42	0.00000	0.00000	0.00000	0.00000	0.00000	0.00000	0.00000	0.00000	0.00000	0.00000	0.00000	0.00000	0.00000	0.00000	0.00000
Angosturas. Las	37.39	-2.99	0.00195	0.00213	0.00160	0.00271	0.00400	0.00851	0.01343	0.01117	0.00760	0.00406	0.00224	0.00196	0.00135	0.00036	0.00010
Anton Koba	42.97	-2.40	0.00000	0.00000	0.00000	0.00008	0.00024	0.00126	0.00289	0.00272	0.00410	0.00155	0.00010	0.00011	0.00306	0.00148	0.00006
Arangas. Cueva de	43.33	-4.80	0.00000	0.00000	0.00794	0.00667	0.00590	0.00910	0.00146	0.00000	0.00000	0.00000	0.00310	0.01005	0.00000	0.00000	0.00000
Arcos. Ermita de Nuestra Señora de los	42.40	-2.71	0.00000	0.00000	0.00000	0.00000	0.00000	0.00000	0.00000	0.00000	0.00000	0.00000	0.00000	0.00000	0.00000	0.00000	0.00000
Ardales. Cueva de	36.99	-4.84	0.00000	0.00000	0.00000	0.00000	0.00000	0.00000	0.00000	0.00000	0.01000	0.02064	0.01035	0.00000	0.00000	0.00000	0.00000
Arenaza I	43.25	-3.10	0.00160	0.00245	0.00865	0.00695	0.00423	0.00077	0.00000	0.00024	0.01612	0.02041	0.00876	0.00736	0.00290	0.00529	0.00005
Arenillas	43.40	-4.62	0.00000	0.00000	0.00000	0.00000	0.00000	0.00000	0.00000	0.00000	0.00000	0.00000	0.00000	0.00000	0.00000	0.00000	0.00000
Arenillas. Cueva de	43.39	-3.31	0.00000	0.00000	0.00000	0.00000	0.00000	0.00000	0.00000	0.00000	0.00000	0.00000	0.00000	0.00000	0.00000	0.00000	0.00000
Arevalillo	41.18	-3.87	0.00000	0.00000	0.00000	0.00000	0.00000	0.00000	0.00000	0.00000	0.00006	0.00063	0.00234	0.01109	0.00988	0.00001	0.00000
Argar (El)	37.25	-1.92	0.00000	0.00000	0.00000	0.00000	0.00000	0.00000	0.00000	0.00000	0.00002	0.01950	0.00831	0.00866	0.00667	0.00000	0.00000
Armação Nova/Rocha das Gaivotas	37.03	-8.99	0.00000	0.00000	0.00000	0.00000	0.00000	0.00000	0.00000	0.00000	0.00000	0.00000	0.00000	0.00000	0.00000	0.00000	0.00000
Arrikrutz	43.00	-2.42	0.00000	0.00000	0.00000	0.00000	0.00000	0.00000	0.00000	0.00256	0.00299	0.00000	0.00000	0.00000	0.00504	0.00005	0.00000
Arruda. Cabeço da	39.12	-8.67	0.00128	0.00112	0.00055	0.00327	0.00599	0.00187	0.00514	0.00073	0.00000	0.00000	0.00000	0.00000	0.00000	0.00000	0.00000
Asno. Cueva del	41.71	-2.46	0.00000	0.00000	0.00000	0.00000	0.00000	0.00000	0.00001	0.00059	0.00461	0.00170	0.00007	0.00249	0.00148	0.00000	0.00000
Assentada. Quinta da	40.63	-7.53	0.00000	0.00000	0.00000	0.00000	0.00000	0.00000	0.00000	0.00000	0.00000	0.00000	0.00000	0.00000	0.00012	0.00113	0.00284
Assut. L´	40.92	0.49	0.00000	0.00000	0.00000	0.00000	0.00000	0.00000	0.00000	0.00000	0.00000	0.00000	0.00000	0.00000	0.00000	0.00000	0.00000
Atalaya (La)	39.36	-6.23	0.00000	0.00000	0.00000	0.00000	0.00000	0.00000	0.01215	0.00425	0.00000	0.00000	0.00000	0.00000	0.00000	0.00000	0.00000
Atxa	42.87	-2.71	0.00000	0.00000	0.00000	0.00000	0.00000	0.00000	0.00000	0.00000	0.00000	0.00000	0.00000	0.00000	0.00000	0.00000	0.00000
Atxoste	42.76	-2.47	0.00000	0.00000	0.00620	0.00362	0.00301	0.00088	0.00000	0.00000	0.00004	0.00665	0.00014	0.00065	0.00201	0.00000	0.00000
Ayllón. Castillo de	41.42	-3.37	0.00000	0.00000	0.00000	0.00000	0.00000	0.00000	0.00000	0.00000	0.00000	0.00000	0.00000	0.00000	0.00000	0.00000	0.00000

Site	Lat	Lon	SPD of Iberian settlement sites at 200 year time slices (cal. BP)														
			6000-5800	5800-5600	5600-5400	5400-5200	5200-5000	5000-4800	4800-4600	4600-4400	4400-4200	4200-4000	4000-3800	3800-3600	3600-3400	3400-3200	3200-3000
Azuer (El)	39.05	-3.50	0.00000	0.00000	0.00000	0.00000	0.00000	0.00018	0.00509	0.01028	0.01495	0.02682	0.05919	0.04863	0.02353	0.00755	0.00026
Azután	39.78	-5.15	0.00437	0.00286	0.00118	0.00341	0.00260	0.00026	0.00000	0.00000	0.00000	0.00000	0.00000	0.00000	0.00000	0.00000	0.00000
Balconcillo (El)	41.75	-3.07	0.00000	0.00000	0.00000	0.00000	0.00000	0.00000	0.00000	0.00000	0.00000	0.00000	0.00011	0.00459	0.00041	0.00000	0.00000
Baldio	39.07	-7.25	0.00000	0.00000	0.00000	0.00000	0.00000	0.00000	0.00000	0.00000	0.00000	0.00000	0.00000	0.00000	0.00000	0.00000	0.00000
Barahones (Los)	42.74	-4.20	0.00000	0.00000	0.00000	0.00000	0.00000	0.00000	0.00000	0.00000	0.00000	0.00000	0.00000	0.00000	0.00349	0.00021	0.00000
Barbudo	41.66	-8.46	0.00000	0.00000	0.00000	0.00000	0.00000	0.00000	0.00000	0.00000	0.00000	0.00000	0.00000	0.00000	0.00000	0.00000	0.00004
Barranc d´en Fabra	40.74	0.56	0.00000	0.00000	0.00000	0.00000	0.00000	0.00000	0.00000	0.00000	0.00000	0.00000	0.00000	0.00000	0.00000	0.00000	0.00000
Barranc de Gàfols	41.04	0.63	0.00000	0.00000	0.00000	0.00000	0.00000	0.00000	0.00000	0.00000	0.00000	0.00000	0.00000	0.00000	0.00000	0.00000	0.00003
Barranco de la Pilona	41.31	-2.14	0.00000	0.00000	0.00000	0.00000	0.00000	0.00000	0.00000	0.00000	0.00000	0.00000	0.00000	0.00000	0.00000	0.00000	0.00000
Barranco de la Viuda	37.67	-1.56	0.00000	0.00000	0.00000	0.00000	0.00000	0.00000	0.00000	0.00000	0.00000	0.00000	0.00000	0.02071	0.00008	0.00000	0.00000
Barranco Tuerto	38.64	-0.84	0.00000	0.00000	0.00000	0.00000	0.00000	0.00000	0.00000	0.00000	0.00000	0.00000	0.00249	0.00390	0.00000	0.00000	0.00000
Barrocal Alto	41.27	-6.55	0.00090	0.00444	0.00009	0.00002	0.00025	0.00824	0.01138	0.00526	0.00000	0.00000	0.00000	0.00031	0.00338	0.00123	0.00007
Barrocal Tenreiro	40.94	-7.06	0.00000	0.00000	0.00000	0.00000	0.00000	0.00000	0.00008	0.00615	0.00007	0.00000	0.00000	0.00000	0.00000	0.00000	0.00000
Barrosinha	38.41	-8.77	0.00000	0.00000	0.00626	0.00625	0.00312	0.00684	0.00000	0.00000	0.00000	0.00000	0.00000	0.00000	0.00000	0.00000	0.00000
Barruecos (Los)	39.42	-6.48	0.00000	0.00000	0.00103	0.00199	0.00013	0.00000	0.00080	0.00472	0.00208	0.00452	0.00213	0.00004	0.00000	0.00000	0.00000
Basagain	43.17	-2.08	0.00000	0.00000	0.00000	0.00000	0.00000	0.00000	0.00000	0.00000	0.00000	0.00000	0.00000	0.00000	0.00000	0.00000	0.00000
Bastida (La)	37.76	-1.56	0.00000	0.00000	0.00000	0.00000	0.00000	0.00000	0.00001	0.00140	0.00069	0.07584	0.04167	0.05713	0.01883	0.00006	0.00000
Berniollo	42.82	-2.90	0.00000	0.00000	0.00002	0.00024	0.00045	0.00112	0.00238	0.00367	0.00448	0.00117	0.00007	0.00000	0.00000	0.00000	0.00000
Berreaga	43.31	-2.85	0.00000	0.00000	0.00000	0.00000	0.00000	0.00000	0.00000	0.00000	0.00000	0.00000	0.00000	0.00000	0.00000	0.00000	0.00000
Berroberría	43.28	-1.52	0.00000	0.00000	0.00000	0.00000	0.00000	0.00000	0.00000	0.00000	0.00000	0.00000	0.00000	0.00000	0.00000	0.00000	0.00000
Berrueco (El)	36.45	-6.03	0.00000	0.00000	0.00000	0.00000	0.00000	0.00000	0.00000	0.00000	0.00003	0.00157	0.00437	0.00205	0.00444	0.00007	0.00000
Bitarados	41.69	-8.60	0.00000	0.00000	0.00000	0.00000	0.00000	0.00000	0.01639	0.01049	0.00000	0.00000	0.00000	0.00000	0.00000	0.00000	0.00000
Boluntxo	43.27	-1.83	0.00000	0.00000	0.00000	0.00000	0.00000	0.00000	0.00000	0.00000	0.00000	0.00000	0.00000	0.00000	0.00000	0.00000	0.00000
Bon Jaumet	41.50	1.60	0.00000	0.00000	0.00000	0.00000	0.00000	0.00000	0.00000	0.00000	0.00000	0.00000	0.00000	0.00000	0.00000	0.00000	0.00000
Bonete. Castillejo del	38.60	-2.86	0.00000	0.00000	0.00000	0.00000	0.00000	0.00000	0.00000	0.00000	0.01031	0.01011	0.00211	0.00162	0.00028	0.00000	0.00000
Bonica. Cova	41.37	1.89	0.00000	0.00000	0.00000	0.00000	0.00000	0.00000	0.00275	0.00000	0.00000	0.00000	0.00000	0.00000	0.00000	0.00000	0.00000
Borneiro	43.20	-8.96	0.00000	0.00000	0.00000	0.00000	0.00000	0.00000	0.00000	0.00000	0.00000	0.00000	0.00000	0.00000	0.00000	0.00000	0.00000
Botiquería dels Moros	41.06	0.11	0.00000	0.00000	0.00000	0.00000	0.00000	0.00000	0.00000	0.00000	0.00000	0.00000	0.00000	0.00000	0.00000	0.00000	0.00000
Bouça do Frade	41.17	-8.05	0.00000	0.00000	0.00000	0.00000	0.00000	0.00000	0.00003	0.00611	0.00546	0.00000	0.00002	0.00917	0.00010	0.00000	0.00000
Boucinhas	41.69	-8.60	0.00000	0.00026	0.00390	0.00002	0.00000	0.00000	0.00000	0.00000	0.00020	0.00618	0.00027	0.00000	0.00000	0.00000	0.00000
Bricia. Cueva de	43.43	-4.85	0.00000	0.00000	0.00000	0.00000	0.00000	0.00000	0.00000	0.00000	0.00000	0.00000	0.00000	0.00000	0.00000	0.00000	0.00000
Brics d´Ardèvol	41.87	1.54	0.00000	0.00000	0.00000	0.00000	0.00000	0.00000	0.00009	0.00353	0.00271	0.00001	0.00000	0.00000	0.00000	0.00000	0.00000
Bruixes. Cova de les	40.62	0.20	0.00000	0.00000	0.00000	0.00000	0.00000	0.00024	0.00417	0.00034	0.00000	0.00000	0.00000	0.00000	0.00000	0.00000	0.00000
Brujas. Cerro de las	40.23	-3.69	0.00000	0.00000	0.00000	0.00000	0.00000	0.00000	0.00000	0.00000	0.00000	0.00000	0.00000	0.00000	0.00000	0.00000	0.00000
Brunos. Loma de los	41.13	-0.02	0.00000	0.00000	0.00000	0.00000	0.00000	0.00000	0.00000	0.00000	0.00000	0.00000	0.00000	0.00000	0.00000	0.00000	0.00000

Site	Lat	Lon	SPD of Iberian settlement sites at 200 year time slices (cal. BP)														
			6000-5800	5800-5600	5600-5400	5400-5200	5200-5000	5000-4800	4800-4600	4600-4400	4400-4200	4200-4000	4000-3800	3800-3600	3600-3400	3400-3200	3200-3000
Bú. Cerro del	39.85	-4.02	0.00000	0.00000	0.00000	0.00000	0.00000	0.00000	0.00099	0.00397	0.00615	0.00301	0.00033	0.00000	0.00000	0.00000	0.00000
Buraca da Moura	39.34	-8.97	0.00000	0.00000	0.00001	0.00220	0.00408	0.00313	0.00000	0.00000	0.00000	0.00000	0.00000	0.00000	0.00000	0.00000	0.00000
Buraca Grande	39.98	-8.55	0.00019	0.00124	0.00440	0.00218	0.00495	0.00000	0.00000	0.00000	0.00000	0.00000	0.00000	0.00000	0.00000	0.00000	0.00000
Buraco da Moura de São Romão	40.39	-7.70	0.00000	0.00000	0.00042	0.00325	0.00371	0.00119	0.00000	0.00000	0.00000	0.00000	0.00000	0.00000	0.00000	0.00064	0.00700
Buraco da Pala	41.46	-7.29	0.00418	0.00364	0.00384	0.00793	0.00818	0.01355	0.05509	0.04782	0.01392	0.00075	0.00010	0.00000	0.00000	0.00000	0.00000
Buxu. Cueva del	43.36	-5.10	0.00000	0.00000	0.00000	0.00000	0.00000	0.00000	0.00000	0.00000	0.00001	0.00161	0.00448	0.00031	0.00000	0.00000	0.00000
Ca n´Isach	42.31	3.14	0.00387	0.00294	0.00284	0.00524	0.00555	0.00207	0.00000	0.00000	0.00000	0.00000	0.00000	0.00000	0.00000	0.00000	0.00000
Cabanas	41.57	-8.42	0.00000	0.00000	0.00000	0.00000	0.00000	0.00000	0.00000	0.00000	0.00000	0.00000	0.00000	0.00000	0.00000	0.00000	0.00000
Cabecicos Negros	37.21	-1.83	0.00000	0.00000	0.00000	0.00000	0.00000	0.00000	0.00000	0.00000	0.00000	0.00000	0.00000	0.00000	0.00000	0.00000	0.00000
Cabezo Negro	37.57	-1.48	0.00000	0.00000	0.00000	0.00000	0.00000	0.00000	0.00000	0.00000	0.00000	0.00043	0.00300	0.00385	0.00709	0.00183	0.00005
Cabezo Pardo	38.16	-0.84	0.00000	0.00000	0.00000	0.00000	0.00000	0.00000	0.00000	0.00037	0.00590	0.00056	0.02418	0.05009	0.02135	0.00000	0.00000
Cabezo Redondo	38.64	-0.89	0.00000	0.00000	0.00000	0.00000	0.00000	0.00000	0.00000	0.00000	0.00000	0.00002	0.00447	0.01611	0.07463	0.03198	0.00174
Cabo Blanco	43.57	-6.85	0.00000	0.00000	0.00000	0.00000	0.00000	0.00000	0.00000	0.00000	0.00000	0.00000	0.00000	0.00000	0.00000	0.00000	0.00000
Cabranosa	37.04	-8.96	0.00000	0.00000	0.00000	0.00000	0.00000	0.00000	0.00000	0.00000	0.00000	0.00000	0.00000	0.00000	0.00000	0.00000	0.00000
Cabrerizas	39.40	-6.00	0.00000	0.00000	0.00000	0.00000	0.00000	0.00000	0.00300	0.00405	0.00050	0.00000	0.00000	0.00000	0.00000	0.00000	0.00000
Cachouça	39.98	-7.24	0.00000	0.00000	0.00000	0.00000	0.00000	0.00000	0.00000	0.00000	0.00000	0.00000	0.00000	0.00000	0.00000	0.00906	0.00425
Caldeirão	39.65	-8.42	0.00041	0.00482	0.00012	0.00000	0.00000	0.00000	0.00000	0.00000	0.00000	0.00000	0.00000	0.00000	0.00003	0.00012	0.00024
Calle Colón 3	38.39	-0.77	0.00000	0.00000	0.00000	0.00000	0.00000	0.00000	0.00000	0.00000	0.00000	0.00000	0.00000	0.00000	0.00000	0.00000	0.00000
Calle San Miguel	37.30	-3.14	0.00000	0.00000	0.00000	0.00000	0.00000	0.00000	0.00000	0.00000	0.00000	0.00000	0.00000	0.00000	0.00000	0.00000	0.00004
Calor. Cueva del	38.09	-1.81	0.00000	0.00000	0.00000	0.00000	0.00000	0.00000	0.00000	0.00000	0.00000	0.00214	0.00438	0.00000	0.00000	0.00000	0.00000
Calvari. Serra del	41.41	0.35	0.00000	0.00000	0.00000	0.00000	0.00000	0.00000	0.00000	0.00000	0.00000	0.00000	0.00000	0.00000	0.00000	0.00000	0.00000
Cameixa	42.42	-8.15	0.00000	0.00000	0.00000	0.00000	0.00000	0.00000	0.00000	0.00000	0.00053	0.00521	0.00000	0.00000	0.00000	0.00000	0.00000
Camoca. Castillo de	43.46	-5.47	0.00000	0.00000	0.00000	0.00000	0.00000	0.00000	0.00000	0.00000	0.00000	0.00000	0.00000	0.00000	0.00000	0.00000	0.00000
Camp dels Moros de la Codina	41.94	1.35	0.00000	0.00000	0.00000	0.00000	0.00000	0.00000	0.00000	0.00000	0.00000	0.00000	0.00000	0.00000	0.00000	0.00040	0.00379
Campa Torres. La	43.57	-5.70	0.00000	0.00000	0.00000	0.00000	0.00000	0.00000	0.00000	0.00000	0.00000	0.00000	0.00000	0.00000	0.00000	0.00000	0.00352
Campana. Cerro de la	38.60	-1.14	0.00000	0.00000	0.00000	0.00000	0.00000	0.00000	0.00000	0.00000	0.00000	0.00000	0.00000	0.00056	0.02351	0.00000	0.00000
Campo de Golf	42.30	-8.69	0.00000	0.00000	0.00000	0.00000	0.00000	0.00000	0.00000	0.00000	0.00000	0.00000	0.00000	0.00689	0.00000	0.00000	0.00000
Campón. El	43.52	-5.36	0.00000	0.00000	0.00000	0.00000	0.00000	0.00000	0.00000	0.00000	0.00000	0.00000	0.00000	0.00000	0.00000	0.00000	0.00000
Campos	37.30	-1.87	0.00000	0.00000	0.00000	0.00000	0.00000	0.00000	0.00146	0.02510	0.00681	0.00000	0.00000	0.00000	0.00000	0.00000	0.00000
Can Ballester	39.83	-0.25	0.00000	0.00000	0.00000	0.00000	0.00000	0.00000	0.00000	0.00000	0.00000	0.00000	0.00004	0.00127	0.00385	0.00021	0.00000
Can Barraca	42.20	2.69	0.00000	0.00000	0.00000	0.00000	0.00000	0.00000	0.00000	0.00000	0.00000	0.00000	0.00000	0.00000	0.00002	0.00588	0.00059
Can Perramón	42.33	1.05	0.00000	0.00000	0.00000	0.00000	0.00000	0.00000	0.00000	0.00000	0.00000	0.00000	0.00000	0.00000	0.00000	0.00000	0.00000
Can Sadurní	41.35	1.91	0.00990	0.00068	0.00000	0.00045	0.00353	0.00766	0.01216	0.00794	0.00135	0.00025	0.00126	0.00470	0.00420	0.00247	0.00401
Can Xac	42.22	2.65	0.00000	0.00000	0.00000	0.00000	0.00000	0.00000	0.00000	0.00000	0.00000	0.00000	0.00000	0.00000	0.00000	0.00000	0.00002

Site	Lat	Lon	SPD of Iberian settlement sites at 200 year time slices (cal. BP)														
			6000-5800	5800-5600	5600-5400	5400-5200	5200-5000	5000-4800	4800-4600	4600-4400	4400-4200	4200-4000	4000-3800	3800-3600	3600-3400	3400-3200	3200-3000
Canaleja 1	39.75	-5.72	0.00405	0.00041	0.00000	0.00000	0.00000	0.00000	0.00000	0.00000	0.00000	0.00000	0.00000	0.00000	0.00000	0.00000	0.00000
Canaleja 2	39.75	-5.72	0.00000	0.00000	0.00000	0.00000	0.00000	0.00000	0.00000	0.00000	0.00000	0.00000	0.00000	0.00000	0.00000	0.00000	0.00000
Cancho Enamorado	40.46	-5.56	0.00000	0.00000	0.00000	0.00000	0.00000	0.00000	0.00001	0.00340	0.00234	0.00475	0.00006	0.00157	0.00928	0.00110	0.00000
Cancho Roano	38.70	-5.69	0.00000	0.00000	0.00000	0.00000	0.00000	0.00000	0.00000	0.00000	0.00000	0.00000	0.00000	0.00000	0.00000	0.00000	0.00061
Canedotes	40.88	-7.76	0.00000	0.00000	0.00000	0.00000	0.00000	0.00000	0.00000	0.00000	0.00000	0.00000	0.00000	0.00000	0.00014	0.00203	0.00508
Canes. Cueva de los	43.33	-4.80	0.00000	0.00000	0.00000	0.00000	0.00000	0.00000	0.00000	0.00000	0.00000	0.00000	0.00000	0.00000	0.00000	0.00000	0.00000
Cantallops. Forat de	40.45	-0.12	0.00000	0.00000	0.00000	0.00000	0.00000	0.00000	0.00000	0.00012	0.00443	0.00261	0.00004	0.00000	0.00000	0.00000	0.00000
Cantera de las Hálagas	40.66	-4.76	0.00000	0.00000	0.00000	0.00000	0.00000	0.00000	0.00208	0.00475	0.00043	0.00000	0.00000	0.00000	0.00000	0.00000	0.00000
Capellanía. Cerro de la	36.90	-4.18	0.00000	0.00000	0.00000	0.00041	0.00124	0.00402	0.00494	0.00128	0.00187	0.00310	0.00161	0.00018	0.00000	0.00000	0.00000
Capitán (El)	37.81	-1.88	0.00081	0.00246	0.00162	0.00021	0.00015	0.00071	0.00281	0.00205	0.00051	0.00005	0.00000	0.00000	0.00000	0.00000	0.00000
Carabassí. Playa de	38.24	-0.52	0.00160	0.00398	0.00001	0.00000	0.00000	0.00000	0.00000	0.00000	0.00000	0.00000	0.00000	0.00000	0.00000	0.00000	0.00395
Carabión	43.35	-3.51	0.00000	0.00000	0.00000	0.00000	0.00000	0.00000	0.00000	0.00000	0.00000	0.00000	0.00000	0.00000	0.00000	0.00000	0.00000
Carambolo (El)	37.39	-6.04	0.00000	0.00000	0.00000	0.00000	0.00000	0.00000	0.00000	0.00000	0.00000	0.00000	0.00000	0.00000	0.00000	0.00469	0.00146
Caramoro II	38.29	-0.70	0.00000	0.00000	0.00000	0.00000	0.00000	0.00000	0.00000	0.00000	0.00000	0.00000	0.00000	0.00000	0.00000	0.00000	0.00056
Caravia	43.45	-5.19	0.00000	0.00000	0.00000	0.00000	0.00000	0.00000	0.00000	0.00000	0.00000	0.00000	0.00000	0.00000	0.00000	0.00000	0.00000
Carigüela (La)	37.44	-3.43	0.00000	0.00000	0.00000	0.00000	0.00000	0.00000	0.00000	0.00000	0.00000	0.00000	0.00000	0.00000	0.00000	0.00000	0.00000
Carmona. calle Juan de Ortega	37.48	-5.63	0.00000	0.00000	0.00000	0.00000	0.00000	0.00000	0.00000	0.00000	0.00000	0.00000	0.00000	0.00000	0.00000	0.00000	0.00000
Carrascal	38.72	-9.28	0.00000	0.00000	0.00000	0.00046	0.00373	0.01229	0.00055	0.00094	0.00563	0.00002	0.00000	0.00000	0.00000	0.00000	0.00000
Carretelà	41.49	0.45	0.00000	0.00000	0.00000	0.00000	0.00000	0.00000	0.00000	0.00000	0.00000	0.00000	0.00000	0.00000	0.00016	0.00770	0.00570
Carril de Caldereros	37.68	-1.70	0.00000	0.00000	0.00000	0.00075	0.00582	0.00221	0.00955	0.00164	0.00000	0.00000	0.00000	0.00000	0.00000	0.00000	0.00000
Cartimil	42.67	-8.24	0.00000	0.00000	0.00000	0.00000	0.00000	0.00000	0.00000	0.00000	0.00000	0.00000	0.00000	0.00000	0.00000	0.00000	0.00000
Casa Branca 7	37.99	-7.62	0.00000	0.00000	0.00000	0.00000	0.00000	0.00000	0.00000	0.00000	0.00000	0.00046	0.00467	0.00000	0.00000	0.00000	0.00000
Casa Novas	38.98	-8.46	0.00000	0.00000	0.00000	0.00000	0.00000	0.00000	0.00000	0.00000	0.00000	0.00000	0.00000	0.00000	0.00000	0.00000	0.00000
Casal da Cerca	38.57	-8.90	0.00000	0.00000	0.00000	0.00000	0.00000	0.00000	0.00000	0.00000	0.00000	0.00000	0.00000	0.00000	0.00000	0.00000	0.00000
Cascajos (Los)	42.45	-2.99	0.00000	0.00000	0.00000	0.00000	0.00000	0.00000	0.00452	0.00068	0.00000	0.00000	0.00000	0.00000	0.00000	0.00000	0.00000
Caserna de Sant Pau del Camp	41.38	2.17	0.00314	0.00164	0.00039	0.00026	0.00023	0.00017	0.00009	0.00006	0.00003	0.00002	0.00001	0.00000	0.00000	0.00000	0.00000
Castanheiro do Vento	41.07	-7.32	0.00000	0.00000	0.00000	0.00039	0.00221	0.00570	0.03658	0.10162	0.07535	0.04186	0.01302	0.03380	0.01235	0.00000	0.00041
Castañuelo (El)	37.93	-6.57	0.00000	0.00000	0.00000	0.00000	0.00000	0.00000	0.00000	0.00000	0.00000	0.00000	0.00000	0.00000	0.00000	0.00000	0.00000
Castelejo	40.34	-7.17	0.00000	0.00000	0.00000	0.00000	0.00000	0.00000	0.00000	0.00000	0.00000	0.00000	0.00000	0.00000	0.00000	0.00000	0.00000
Castelejo	37.10	-8.94	0.00000	0.00000	0.00000	0.00000	0.00000	0.00000	0.00000	0.00000	0.00000	0.00000	0.00000	0.00000	0.00000	0.00000	0.00000
Castellar (El)	37.89	-1.39	0.00000	0.00000	0.00000	0.00000	0.00000	0.00000	0.00000	0.00000	0.00000	0.00000	0.00000	0.00000	0.00000	0.00000	0.00000
Castellón Alto	37.74	-2.57	0.00000	0.00000	0.00000	0.00000	0.00000	0.00000	0.00000	0.00006	0.00532	0.00640	0.03930	0.07992	0.00292	0.00006	0.00000
Castellones de Ceal	37.72	-3.05	0.00000	0.00000	0.00000	0.00000	0.00000	0.00000	0.00000	0.00000	0.00000	0.00000	0.00000	0.00000	0.00000	0.00000	0.00000

Site	Lat	Lon	SPD of Iberian settlement sites at 200 year time slices (cal. BP)														
			6000-5800	5800-5600	5600-5400	5400-5200	5200-5000	5000-4800	4800-4600	4600-4400	4400-4200	4200-4000	4000-3800	3800-3600	3600-3400	3400-3200	3200-3000
Castellones. Cerro de los	37.45	-3.28	0.00000	0.00000	0.00000	0.00000	0.00000	0.00000	0.00000	0.00007	0.00085	0.01015	0.00518	0.00377	0.00085	0.00002	0.00000
Castellot (El)	42.42	1.89	0.00000	0.00000	0.00000	0.00000	0.00000	0.00000	0.00000	0.00000	0.00000	0.00000	0.00000	0.00000	0.00000	0.00000	0.00000
Castelo Belinho	37.20	-8.55	0.00000	0.00000	0.00000	0.00000	0.00000	0.00000	0.00000	0.00000	0.00000	0.00000	0.00000	0.00000	0.00000	0.00000	0.00000
Castelo Velho	41.07	-7.19	0.00188	0.00339	0.00025	0.00003	0.00002	0.00058	0.02260	0.04982	0.06073	0.01440	0.01728	0.01798	0.02336	0.01147	0.00131
Castelos de Beijós	40.51	-7.96	0.00000	0.00000	0.00000	0.00000	0.00000	0.00000	0.00000	0.00000	0.00000	0.00000	0.00000	0.00000	0.00000	0.00078	0.01212
Castil de Cabras	40.57	-5.99	0.00000	0.00000	0.00000	0.00000	0.00000	0.00000	0.00000	0.00000	0.00000	0.00041	0.00821	0.00318	0.00000	0.00000	0.00000
Castillejo (El)	36.88	-4.51	0.00000	0.00000	0.00000	0.00000	0.00000	0.00000	0.00495	0.00774	0.00226	0.00006	0.00000	0.00000	0.00000	0.00000	0.00000
Castillejo (El)	39.84	-2.21	0.00000	0.00000	0.00000	0.00000	0.00000	0.00000	0.00015	0.00057	0.00180	0.00374	0.00511	0.00280	0.00331	0.00137	0.00013
Castillejo (El)	40.00	-4.21	0.00002	0.00509	0.00000	0.00000	0.00000	0.00000	0.00825	0.00546	0.00416	0.00773	0.00198	0.00001	0.00000	0.00000	0.00000
Castillejo (El)	41.82	-2.45	0.00000	0.00000	0.00000	0.00000	0.00000	0.00000	0.00018	0.00098	0.00285	0.00244	0.00069	0.00005	0.00000	0.00000	0.00000
Castillejos (Los)	37.33	-3.97	0.00014	0.00351	0.00924	0.00730	0.01545	0.00049	0.00002	0.00357	0.01764	0.00783	0.00355	0.00106	0.00005	0.00000	0.00000
Castillejos (Los)	40.66	-4.87	0.00000	0.00000	0.00000	0.00000	0.00000	0.00000	0.00000	0.00008	0.00260	0.00693	0.00406	0.00045	0.00000	0.00000	0.00000
Castillejos (Los)	38.20	-6.32	0.00000	0.00000	0.00000	0.00000	0.00000	0.00000	0.00000	0.00000	0.00000	0.00000	0.00000	0.00000	0.00000	0.00000	0.00000
Castillejos (Los)	41.29	-2.18	0.00000	0.00000	0.00000	0.00000	0.00000	0.00000	0.00000	0.00000	0.00000	0.00000	0.00000	0.00000	0.00000	0.00000	0.00000
Castillejos de Alcorrín (Los)	36.34	-5.26	0.00000	0.00000	0.00000	0.00000	0.00000	0.00000	0.00000	0.00000	0.00000	0.00000	0.00000	0.00000	0.00000	0.00000	0.00000
Castillico (El)	37.43	-2.23	0.00000	0.00000	0.00000	0.00000	0.00000	0.00000	0.00000	0.00000	0.00000	0.00000	0.00009	0.00402	0.00158	0.00000	0.00000
Castillo	40.54	-1.04	0.00000	0.00000	0.00000	0.00000	0.00000	0.00000	0.00111	0.00517	0.00038	0.00000	0.00000	0.00000	0.00000	0.00000	0.00000
Castillo (El)	39.91	-1.88	0.00000	0.00000	0.00000	0.00000	0.00000	0.00000	0.00000	0.00000	0.00019	0.00128	0.00283	0.00211	0.00029	0.00000	0.00000
Castillo (El)	40.34	-1.61	0.00000	0.00000	0.00000	0.00000	0.00000	0.00000	0.00000	0.00000	0.00000	0.00377	0.02844	0.00832	0.00076	0.00000	0.00000
Castillo (El)	42.34	-3.70	0.00000	0.00000	0.00000	0.00000	0.00000	0.00000	0.00000	0.00000	0.00000	0.00000	0.00000	0.00003	0.00407	0.00155	0.00364
Castillo (Manzanal de Abajo)	41.98	-6.28	0.00000	0.00000	0.00000	0.00000	0.00000	0.00000	0.00000	0.00000	0.00000	0.00000	0.00000	0.00000	0.00000	0.00000	0.00000
Castillo. Cerro del	41.91	-4.90	0.00000	0.00000	0.00000	0.00000	0.00000	0.00000	0.00000	0.00000	0.00000	0.00000	0.00000	0.00000	0.00000	0.00000	0.00000
Castilnegro	43.37	-3.80	0.00000	0.00000	0.00000	0.00000	0.00000	0.00000	0.00000	0.00000	0.00000	0.00000	0.00000	0.00000	0.00000	0.00000	0.00000
Castro (Fresno de la Carballeda). El	41.98	-6.34	0.00000	0.00000	0.00000	0.00027	0.00156	0.00529	0.00002	0.00000	0.00000	0.00000	0.00000	0.00000	0.00000	0.00000	0.00000
Castro Grande de Neixón	42.66	-8.84	0.00000	0.00000	0.00000	0.00000	0.00000	0.00000	0.00000	0.00000	0.00000	0.00000	0.00000	0.00369	0.00022	0.00000	0.00000
Castro Marim (Castelo)	37.22	-7.44	0.00000	0.00000	0.00000	0.00000	0.00000	0.00000	0.00000	0.00002	0.00004	0.00667	0.00086	0.00872	0.00043	0.00058	0.00080
Castro Real de As Corredoiras	43.02	-8.11	0.00000	0.00000	0.00000	0.00000	0.00000	0.00000	0.00000	0.00000	0.00000	0.00000	0.00000	0.00000	0.00000	0.00000	0.00000
Castromaior	42.83	-7.72	0.00000	0.00000	0.00000	0.00000	0.00000	0.00000	0.00000	0.00000	0.00000	0.00000	0.00000	0.00000	0.00000	0.00000	0.00000
Castromao	42.16	-7.97	0.00000	0.00000	0.00000	0.00000	0.00000	0.00000	0.00000	0.00000	0.00000	0.00000	0.00000	0.00000	0.00000	0.00000	0.00000
Castros (Os)	43.02	-7.96	0.00000	0.00000	0.00000	0.00000	0.00000	0.00000	0.00000	0.00000	0.00000	0.00000	0.00000	0.00000	0.00000	0.00000	0.00000
Castros de Lastra	42.86	-3.07	0.00000	0.00000	0.00000	0.00000	0.00000	0.00000	0.00000	0.00000	0.00000	0.00000	0.00000	0.00000	0.00001	0.00330	0.00824

Site	Lat	Lon	SPD of Iberian settlement sites at 200 year time slices (cal. BP)														
			6000-5800	5800-5600	5600-5400	5400-5200	5200-5000	5000-4800	4800-4600	4600-4400	4400-4200	4200-4000	4000-3800	3800-3600	3600-3400	3400-3200	3200-3000
Castros. Os	43.36	-7.11	0.00000	0.00000	0.00000	0.00000	0.00000	0.00000	0.00000	0.00000	0.00000	0.00000	0.00000	0.00000	0.00002	0.00115	0.00307
Castrovite	42.75	-8.34	0.00000	0.00000	0.00000	0.00000	0.00000	0.00000	0.00000	0.00000	0.00000	0.00000	0.00000	0.00000	0.00000	0.00000	0.00000
Catalão	37.06	-8.95	0.00000	0.00000	0.00000	0.00000	0.00000	0.00000	0.00031	0.00315	0.00335	0.00018	0.00000	0.00000	0.00000	0.00000	0.00000
Catí Forada	38.51	-0.69	0.00000	0.00000	0.00000	0.00000	0.00000	0.00000	0.00000	0.00000	0.00012	0.00074	0.00210	0.00254	0.00096	0.00005	0.00000
Catujal	38.81	-9.13	0.00000	0.00000	0.00000	0.00000	0.00000	0.00000	0.00000	0.00000	0.00000	0.00000	0.00466	0.00050	0.00000	0.00000	0.00000
Cava 16-17. Calle	37.68	-1.70	0.00000	0.00000	0.00000	0.00000	0.00000	0.00000	0.00000	0.00000	0.00000	0.00088	0.00361	0.00000	0.00000	0.00000	0.00000
Cava 35. Calle	37.68	-1.70	0.00000	0.00000	0.00000	0.00000	0.00000	0.00000	0.00000	0.00000	0.00482	0.00102	0.00000	0.00000	0.00000	0.00000	0.00000
Celti	37.71	-5.35	0.00000	0.00000	0.00000	0.00000	0.00000	0.00000	0.00000	0.00000	0.00000	0.00000	0.00000	0.00000	0.00000	0.00000	0.00010
Cementerio. Cerro del	41.22	-4.53	0.00000	0.00000	0.00000	0.00000	0.00000	0.00000	0.00000	0.00000	0.00000	0.00000	0.00000	0.00000	0.00000	0.00000	0.00000
Cendres. Cova de les	38.68	0.15	0.00307	0.00486	0.01069	0.00324	0.00223	0.00395	0.00849	0.00282	0.00174	0.00972	0.00250	0.00000	0.00000	0.00000	0.00000
Ceñuela (La)	37.67	-1.41	0.00000	0.00000	0.00000	0.00000	0.00000	0.00000	0.00251	0.00470	0.00031	0.00056	0.00483	0.00101	0.00000	0.00000	0.00000
Cepo	42.25	-7.90	0.00000	0.00000	0.00000	0.00000	0.00000	0.00000	0.00000	0.00000	0.00000	0.00000	0.00000	0.00000	0.00000	0.00000	0.00000
Cerco (El)	41.73	-6.47	0.00000	0.00000	0.00000	0.00000	0.00000	0.00000	0.00000	0.00000	0.00000	0.00000	0.00000	0.00000	0.00000	0.00000	0.00000
Cereixo. Chan do	42.07	-8.78	0.00635	0.00393	0.00137	0.00002	0.00000	0.00000	0.00000	0.00000	0.00000	0.00000	0.00000	0.00000	0.00000	0.00000	0.00000
Ceremeño (El)	40.89	-1.97	0.00000	0.00000	0.00000	0.00000	0.00000	0.00000	0.00000	0.00000	0.00000	0.00000	0.00000	0.00000	0.00000	0.00102	0.00424
Cerro Borreguero	36.67	-5.76	0.00000	0.00000	0.00000	0.00000	0.00000	0.00000	0.00000	0.00000	0.00000	0.00000	0.00000	0.00000	0.00000	0.00000	0.00000
Cerro Hervero	40.66	-4.67	0.00000	0.00000	0.00000	0.00000	0.00000	0.00000	0.00000	0.00052	0.00536	0.00000	0.00000	0.00000	0.00000	0.00000	0.00000
Cerrón (El)	40.11	-3.88	0.00000	0.00000	0.00000	0.00000	0.00000	0.00000	0.00000	0.00000	0.00000	0.00000	0.00000	0.00000	0.00000	0.00000	0.00000
Chano	42.89	-6.67	0.00000	0.00000	0.00000	0.00000	0.00000	0.00000	0.00000	0.00000	0.00000	0.00000	0.00000	0.00000	0.00000	0.00000	0.00000
Chao Samartín	43.20	-6.93	0.00000	0.00000	0.00000	0.00000	0.00000	0.00023	0.00005	0.00000	0.00000	0.00000	0.00000	0.00000	0.00000	0.00434	0.00175
Chaves	42.23	-0.15	0.00112	0.00093	0.00046	0.00018	0.00013	0.00006	0.00000	0.00000	0.00000	0.00000	0.00000	0.00000	0.00000	0.00000	0.00000
Chibanes	38.56	-8.92	0.00000	0.00000	0.00000	0.00000	0.00000	0.00077	0.01293	0.01857	0.02191	0.00050	0.00000	0.00000	0.00000	0.00000	0.00000
Chinflón	37.60	-6.64	0.00000	0.00000	0.00000	0.00000	0.00000	0.00000	0.00000	0.00000	0.00000	0.00002	0.00028	0.00175	0.00292	0.00062	0.00524
Chora (La)	43.34	-3.51	0.00000	0.00000	0.00000	0.00000	0.00000	0.00000	0.00000	0.00000	0.00000	0.00000	0.00000	0.00000	0.00000	0.00000	0.00000
Ciavieja	36.78	-2.80	0.00000	0.00000	0.00000	0.00000	0.00002	0.00096	0.02042	0.01762	0.00278	0.00008	0.00000	0.00000	0.00000	0.00000	0.00000
Cidá (A)	41.94	-7.63	0.00000	0.00000	0.00000	0.00000	0.00000	0.00000	0.00000	0.00000	0.00000	0.00000	0.00000	0.00000	0.00000	0.00000	0.00000
Cinc. Abric de les	39.75	-0.22	0.00000	0.00000	0.00000	0.00000	0.00000	0.00000	0.00000	0.00000	0.00000	0.00000	0.00000	0.00000	0.00000	0.00102	0.00420
Cipreses (Los)	37.64	-1.73	0.00000	0.00000	0.00000	0.00000	0.00000	0.00000	0.00000	0.00000	0.00000	0.00018	0.00873	0.03465	0.00021	0.00232	0.00434
Ciquilines 4	42.10	-0.35	0.00000	0.00000	0.00000	0.00000	0.00000	0.00000	0.00000	0.00000	0.00000	0.00000	0.00021	0.00224	0.00747	0.00021	0.00000
Cobatillas la Vieja	38.06	-1.06	0.00000	0.00000	0.00000	0.00000	0.00000	0.00000	0.00000	0.00000	0.00000	0.00000	0.00000	0.00000	0.00000	0.00690	0.00712
Cocina. Abric de la	39.25	-0.73	0.00000	0.00000	0.00000	0.00000	0.00000	0.00000	0.00000	0.00000	0.00000	0.00000	0.00000	0.00000	0.00000	0.00000	0.00000
Cofresnedo. Cueva de	43.32	-3.59	0.00000	0.00000	0.00000	0.00000	0.00000	0.00000	0.00000	0.00000	0.00000	0.00000	0.00000	0.00501	0.00042	0.00304	0.00439
Coiro. Chan do	42.29	-8.76	0.00000	0.00000	0.00000	0.00000	0.00000	0.00000	0.00000	0.00026	0.00411	0.00274	0.00010	0.00000	0.00000	0.00000	0.00000
Colina del Castillo	37.48	-4.58	0.00000	0.00000	0.00000	0.00006	0.00016	0.00071	0.00246	0.00210	0.00080	0.00018	0.00056	0.00304	0.00492	0.00611	0.00268
Colomera	42.08	0.69	0.00000	0.00000	0.00000	0.00311	0.01036	0.00000	0.00000	0.00000	0.00000	0.00068	0.00884	0.00007	0.01342	0.00000	0.00000

Site	Lat	Lon	SPD of Iberian settlement sites at 200 year time slices (cal. BP)														
			6000-5800	5800-5600	5600-5400	5400-5200	5200-5000	5000-4800	4800-4600	4600-4400	4400-4200	4200-4000	4000-3800	3800-3600	3600-3400	3400-3200	3200-3000
Coma d´Espòs	42.51	1.00	0.00000	0.00000	0.00000	0.00000	0.00000	0.00000	0.00580	0.00000	0.00000	0.00000	0.00000	0.00000	0.00000	0.00000	0.00000
Conímbriga	40.10	-8.49	0.00000	0.00000	0.00000	0.00000	0.00000	0.00000	0.00000	0.00000	0.00000	0.00000	0.00000	0.00000	0.00000	0.00000	0.00000
Conjunt del Mig	42.67	1.08	0.00000	0.00000	0.00000	0.00000	0.00000	0.00000	0.00000	0.00000	0.00000	0.00000	0.00000	0.00005	0.00613	0.00000	0.00000
Consejo Consultativo	41.50	-5.76	0.00000	0.00000	0.00000	0.00000	0.00000	0.00000	0.00000	0.00000	0.00000	0.00000	0.00000	0.00000	0.00000	0.00941	0.00692
Convento de las Franciscanas	36.23	-5.96	0.00000	0.00000	0.00000	0.00000	0.00000	0.00000	0.00000	0.00000	0.00000	0.00000	0.00000	0.00000	0.00000	0.00000	0.00000
Coquino. Cueva del	37.19	-4.16	0.00000	0.00000	0.00000	0.00000	0.00000	0.00000	0.00000	0.00000	0.00000	0.00003	0.00050	0.00253	0.00262	0.00017	0.00000
Corno do Cunho	41.29	-6.53	0.00000	0.00000	0.00000	0.00000	0.00000	0.00000	0.00000	0.00000	0.00000	0.00000	0.00000	0.00000	0.00000	0.00000	0.00000
Corolla. La	43.45	-5.48	0.00000	0.00000	0.00728	0.00000	0.00000	0.00000	0.00000	0.00000	0.00000	0.00000	0.00000	0.00000	0.00000	0.00000	0.00000
Corona (La)	42.32	-6.45	0.00000	0.00000	0.00000	0.00000	0.00000	0.00000	0.00000	0.00000	0.00000	0.00000	0.00000	0.00000	0.00000	0.00000	0.00000
Coronilla (La)	40.80	-1.78	0.00000	0.00000	0.00000	0.00000	0.00000	0.00000	0.00000	0.00000	0.00000	0.00000	0.00000	0.00000	0.00000	0.00068	0.00386
Correio-Mor	38.82	-9.18	0.00000	0.00000	0.00000	0.00033	0.00662	0.00060	0.00020	0.00000	0.00000	0.00000	0.00000	0.00000	0.00000	0.00000	0.00000
Cortegada	42.67	-8.23	0.00000	0.00000	0.00000	0.00000	0.00000	0.00000	0.00000	0.00000	0.00000	0.00000	0.00000	0.00000	0.00000	0.00000	0.00000
Cortijo de la Torre	37.90	-4.01	0.00000	0.00000	0.00000	0.00000	0.00000	0.00000	0.00003	0.00059	0.00352	0.00271	0.00033	0.00000	0.00000	0.00000	0.00000
Corvera (La)	40.42	-5.77	0.00000	0.00000	0.00000	0.00000	0.00000	0.00000	0.00000	0.00000	0.00000	0.00000	0.00000	0.00002	0.00926	0.00000	0.00000
Coscojar. Cueva del	40.29	-0.68	0.00000	0.00000	0.00000	0.00000	0.00000	0.00000	0.00000	0.00012	0.00197	0.00351	0.00121	0.00005	0.00000	0.00000	0.00000
Cossourado	41.92	-8.64	0.00000	0.00000	0.00000	0.00000	0.00000	0.00000	0.00000	0.00000	0.00000	0.00000	0.00000	0.00000	0.00000	0.00000	0.00000
Costa do Pereiro	39.58	-8.54	0.00206	0.00003	0.00000	0.00040	0.00256	0.00546	0.00000	0.00000	0.00000	0.00000	0.00000	0.00000	0.00000	0.00000	0.00000
Costalena	41.12	0.20	0.00000	0.00000	0.00000	0.00000	0.00000	0.00000	0.00000	0.00000	0.00000	0.00000	0.00000	0.00000	0.00000	0.00000	0.00000
Costeras (Las)	40.27	-0.86	0.00000	0.00000	0.00000	0.00000	0.00000	0.00000	0.00000	0.00000	0.00000	0.00680	0.00639	0.00000	0.00000	0.00000	0.00000
Coto da Pena	41.86	-8.83	0.00000	0.00000	0.00000	0.00000	0.00000	0.00000	0.00000	0.00000	0.00000	0.00000	0.00000	0.00000	0.00003	0.00316	0.00715
Coto do Mosteiro	42.48	-8.06	0.00000	0.00000	0.00000	0.00000	0.00000	0.00000	0.00000	0.00000	0.00000	0.00000	0.00000	0.00000	0.00000	0.00000	0.00000
Cotorros (Los)	41.63	-3.42	0.00000	0.00000	0.00000	0.00000	0.00000	0.00000	0.00000	0.00000	0.00000	0.00062	0.00772	0.00484	0.00000	0.00000	0.00000
Cova 120	42.28	2.61	0.00000	0.00000	0.00000	0.00000	0.00000	0.00096	0.00210	0.00006	0.00000	0.00000	0.00002	0.00037	0.00232	0.00208	0.00053
Cova Fonda	41.24	1.34	0.00000	0.00000	0.00000	0.00000	0.00000	0.00000	0.00000	0.00000	0.00000	0.00000	0.00000	0.00249	0.00148	0.00000	0.00000
Cova Negra	38.82	-0.42	0.00000	0.00000	0.00000	0.00000	0.00000	0.00000	0.00000	0.00000	0.00000	0.00000	0.00000	0.00000	0.00000	0.00000	0.00000
Covachos. Cueva de los	37.88	-6.08	0.00000	0.00000	0.00000	0.00000	0.00000	0.00000	0.00482	0.00363	0.00078	0.00711	0.00357	0.00016	0.00000	0.00000	0.00000
Covetes (Les)	42.56	0.90	0.00000	0.00000	0.00000	0.00000	0.00000	0.00000	0.00000	0.00140	0.00053	0.00000	0.00000	0.00000	0.00000	0.00000	0.00000
Crastoeiro	41.42	-7.93	0.00000	0.00000	0.00000	0.00000	0.00000	0.00000	0.00000	0.00000	0.00000	0.00000	0.00000	0.00000	0.00000	0.00000	0.00000
Cristelo	41.90	-8.55	0.00000	0.00000	0.00000	0.00000	0.00000	0.00000	0.00000	0.00000	0.00000	0.00000	0.00000	0.00000	0.00000	0.00000	0.00000
Cristo de San Esteban	41.53	-5.97	0.00000	0.00000	0.00000	0.00000	0.00000	0.00000	0.00000	0.00000	0.00000	0.00000	0.00000	0.00000	0.00000	0.00000	0.00000
Croas (As)	42.40	-8.65	0.00000	0.00000	0.00000	0.00000	0.00000	0.00000	0.00000	0.00000	0.00000	0.00000	0.00000	0.00000	0.00000	0.00000	0.00000
Cruito	41.14	-8.04	0.00000	0.00000	0.00000	0.00000	0.00000	0.00000	0.00000	0.00000	0.00000	0.00000	0.00000	0.00000	0.00000	0.00000	0.00000
Cruz. Cabezo de la	41.49	-1.07	0.00000	0.00000	0.00000	0.00000	0.00000	0.00000	0.00000	0.00000	0.00000	0.00000	0.00000	0.00000	0.00000	0.00000	0.00000
Cruz. Cabezo de la	38.20	-1.56	0.00000	0.00000	0.00000	0.00000	0.00000	0.00000	0.00000	0.00000	0.00000	0.00006	0.00322	0.00336	0.00002	0.00000	0.00000

Site	Lat	Lon	SPD of Iberian settlement sites at 200 year time slices (cal. BP)														
			6000-5800	5800-5600	5600-5400	5400-5200	5200-5000	5000-4800	4800-4600	4600-4400	4400-4200	4200-4000	4000-3800	3800-3600	3600-3400	3400-3200	3200-3000
Cuatro Vientos	42.25	-0.35	0.00000	0.00000	0.00000	0.00000	0.00000	0.00000	0.00000	0.00000	0.00000	0.00000	0.00000	0.00000	0.00000	0.00572	0.00009
Cubío Redondo	43.32	-3.62	0.00000	0.00000	0.00000	0.00000	0.00000	0.00000	0.00000	0.00000	0.00000	0.00000	0.00000	0.00000	0.00000	0.00000	0.00000
Cuchillo. Cerro del	38.87	-1.27	0.00000	0.00000	0.00000	0.00000	0.00000	0.00000	0.00000	0.00000	0.00003	0.00136	0.00983	0.01594	0.00457	0.00001	0.00000
Cuco (El)	39.39	-1.94	0.00000	0.00000	0.00000	0.00000	0.00000	0.00000	0.00000	0.00000	0.00000	0.00000	0.00000	0.00612	0.00502	0.01400	0.01385
Cuervo. Cabezo del	41.04	-0.12	0.00000	0.00000	0.00000	0.00000	0.00000	0.00000	0.00000	0.00000	0.00000	0.00005	0.00251	0.01774	0.02199	0.00263	0.00009
Cuesta de la Encina A	43.37	-3.70	0.00000	0.00000	0.00000	0.00000	0.00000	0.00000	0.00046	0.00168	0.00426	0.00475	0.00309	0.00644	0.00006	0.00000	0.00000
Cuesta de la Encina B	43.37	-3.70	0.00000	0.00000	0.00000	0.00000	0.00000	0.00000	0.00000	0.00000	0.00000	0.00000	0.00000	0.00000	0.00000	0.00023	0.00081
Cuesta de la Iglesia A	41.99	-1.42	0.00000	0.00000	0.00000	0.00000	0.00000	0.00000	0.00000	0.00000	0.00000	0.00000	0.00000	0.00000	0.00178	0.00000	0.00000
Cuesta de San Cayetano	38.02	-1.10	0.00000	0.00000	0.00000	0.00000	0.00000	0.00000	0.00000	0.00000	0.00000	0.00000	0.00000	0.00501	0.00409	0.00003	0.00000
Cuesta del Negro	37.33	-3.24	0.00000	0.00000	0.00000	0.00000	0.00000	0.00000	0.00000	0.00000	0.00000	0.00004	0.03272	0.09396	0.08212	0.01403	0.00000
Cuesta del Viso	41.46	-5.60	0.00000	0.00000	0.00000	0.00000	0.00000	0.00000	0.00000	0.00000	0.00000	0.00000	0.00000	0.00000	0.00000	0.00000	0.00000
Cueva Blanca	38.47	-1.56	0.00000	0.00000	0.00000	0.00000	0.00000	0.00000	0.00000	0.00000	0.00004	0.00665	0.00005	0.00000	0.00000	0.00000	0.00000
Dehesilla. Cueva de la	36.67	-5.64	0.00000	0.00000	0.00000	0.00000	0.00000	0.00000	0.00000	0.00000	0.00000	0.00000	0.00006	0.00038	0.00144	0.00212	0.00139
Dessobriga	42.40	-4.32	0.00000	0.00000	0.00000	0.00000	0.00000	0.00000	0.00000	0.00000	0.00000	0.00000	0.00000	0.00000	0.00000	0.00000	0.00737
Devesa do Rei	42.78	-8.46	0.00064	0.00000	0.00000	0.00000	0.00000	0.00000	0.00000	0.00000	0.00000	0.00000	0.00338	0.00102	0.00000	0.00160	0.00544
Dornajos (Los)	39.73	-2.42	0.00000	0.00000	0.00000	0.00000	0.00000	0.00000	0.00000	0.00000	0.00000	0.00000	0.00718	0.02302	0.00596	0.00000	0.00000
Dou (La)	42.12	2.47	0.00000	0.00000	0.00000	0.00000	0.00000	0.00000	0.00000	0.00000	0.00000	0.00000	0.00000	0.00000	0.00000	0.00000	0.00000
Draga (La)	42.13	2.76	0.00004	0.00003	0.00001	0.00000	0.00000	0.00000	0.00000	0.00000	0.00000	0.00000	0.00000	0.00000	0.00000	0.00000	0.00000
Drólica. Cueva	42.30	0.00	0.00000	0.00000	0.00000	0.00000	0.00000	0.00000	0.00683	0.01201	0.00767	0.00624	0.00019	0.00460	0.00000	0.00000	0.00000
Ekain	43.23	-2.27	0.00044	0.00503	0.00001	0.00000	0.00000	0.00000	0.00000	0.00000	0.00000	0.00000	0.00000	0.00000	0.00000	0.00000	0.00000
Emparetá. Coveta	38.76	-0.58	0.00000	0.00000	0.00000	0.00000	0.00000	0.00000	0.00000	0.00000	0.00000	0.00000	0.00000	0.00000	0.00059	0.00000	0.00000
Encaños (Los)	40.05	-2.45	0.00000	0.00000	0.00000	0.00000	0.00000	0.00000	0.00000	0.00000	0.00000	0.00000	0.00000	0.00000	0.00000	0.00000	0.00000
Encantada. Cerro de la	38.82	-3.73	0.00000	0.00000	0.00000	0.00000	0.00000	0.00000	0.00000	0.00000	0.01665	0.00019	0.00825	0.03361	0.04042	0.00004	0.00000
Encina. Cerro de la	37.14	-3.55	0.00000	0.00000	0.00000	0.00000	0.00000	0.00000	0.00000	0.00002	0.00065	0.00586	0.03989	0.03867	0.03429	0.00456	0.00020
Encosta de Sant'Ana	38.71	-9.14	0.00243	0.00144	0.00005	0.00000	0.00000	0.00000	0.00000	0.00000	0.00000	0.00000	0.00000	0.00000	0.00000	0.00000	0.00000
Enebralejos. Cueva de los	41.14	-3.68	0.00000	0.00000	0.00000	0.00000	0.00000	0.00000	0.00338	0.00478	0.00290	0.00417	0.00004	0.00000	0.00000	0.00000	0.00000
Eras del Alcázar	38.01	-3.36	0.00000	0.00026	0.00419	0.00686	0.01916	0.02044	0.08107	0.02677	0.01712	0.01687	0.02596	0.00665	0.00000	0.00000	0.00000
Ereta del Pedregal (La)	39.08	-0.69	0.00000	0.00000	0.00000	0.00007	0.00013	0.00033	0.01161	0.00156	0.00156	0.00120	0.00069	0.00027	0.00006	0.00000	0.00000
Eretas (Las)	42.53	-1.83	0.00000	0.00000	0.00000	0.00000	0.00000	0.00000	0.00000	0.00000	0.00000	0.00000	0.00000	0.00000	0.00000	0.00000	0.00000
Ermidas	41.46	-8.52	0.00000	0.00000	0.00000	0.00000	0.00000	0.00000	0.00000	0.00000	0.00000	0.00000	0.00000	0.00000	0.00000	0.00000	0.00020
Ermitons (Els)	42.28	2.59	0.00000	0.00000	0.00105	0.00266	0.00284	0.00101	0.00000	0.00000	0.00000	0.00000	0.00000	0.00000	0.00000	0.00000	0.00000
Escoba. Cerro de la	38.69	-0.91	0.00000	0.00000	0.00000	0.00000	0.00000	0.00000	0.00000	0.00000	0.00407	0.00075	0.00101	0.00369	0.00506	0.00002	0.00000
Escoural. Povoado do	38.55	-8.14	0.00000	0.00000	0.00000	0.00008	0.00070	0.00834	0.00876	0.00953	0.00528	0.00046	0.00000	0.00000	0.00000	0.00000	0.00000

Site	Lat	Lon	SPD of Iberian settlement sites at 200 year time slices (cal. BP)														
			6000-5800	5800-5600	5600-5400	5400-5200	5200-5000	5000-4800	4800-4600	4600-4400	4400-4200	4200-4000	4000-3800	3800-3600	3600-3400	3400-3200	3200-3000
Espina del Gallego	43.18	-3.97	0.00000	0.00000	0.00000	0.00000	0.00000	0.00000	0.00000	0.00000	0.00000	0.00000	0.00000	0.00000	0.00000	0.00000	0.00000
Espinos (Los)	42.75	-4.27	0.00000	0.00000	0.00000	0.00042	0.00135	0.00394	0.00038	0.00001	0.00000	0.00000	0.00000	0.00000	0.00090	0.00374	0.00285
Esplugón	42.39	-0.29	0.00000	0.00000	0.00000	0.00000	0.00000	0.00000	0.00000	0.00000	0.00000	0.00000	0.00000	0.00000	0.00000	0.00000	0.00000
Estany de la Coveta. Abric de l´	42.54	1.03	0.00000	0.00000	0.00000	0.00061	0.00738	0.00009	0.00000	0.00000	0.00000	0.00000	0.00000	0.00000	0.00000	0.00000	0.00000
ETAR de Vilanova de Milfontes	37.72	-8.80	0.00000	0.00000	0.00000	0.00438	0.00729	0.00038	0.00000	0.00000	0.00000	0.00000	0.00000	0.00000	0.00000	0.00000	0.00000
Falguera. Abrigo de la	38.67	-0.56	0.00000	0.00000	0.00000	0.00007	0.00115	0.00698	0.00326	0.00213	0.00032	0.00001	0.00000	0.00000	0.00000	0.00000	0.00000
Feixa del Moro	42.44	1.49	0.01341	0.00792	0.00152	0.00027	0.00013	0.00002	0.00000	0.00000	0.00000	0.00000	0.00000	0.00000	0.00000	0.00000	0.00000
Fiais	37.59	-8.67	0.00000	0.00000	0.00000	0.00000	0.00000	0.00000	0.00000	0.00000	0.00000	0.00000	0.00000	0.00000	0.00000	0.00000	0.00000
Fixón (O)	42.27	-8.84	0.00021	0.00143	0.00270	0.00030	0.00008	0.00000	0.00018	0.00098	0.01292	0.00244	0.00069	0.00005	0.00000	0.00000	0.00000
Floridablanca. Calle	37.68	-1.70	0.00000	0.00000	0.00004	0.00067	0.00006	0.00006	0.00617	0.00180	0.00046	0.00064	0.00080	0.00091	0.00091	0.00073	0.00057
Fonollera (La)	42.02	3.18	0.00000	0.00000	0.00000	0.00000	0.00000	0.00000	0.00000	0.00000	0.00000	0.00003	0.00065	0.00314	0.00214	0.00005	0.00000
Font Major. Cova de la	41.40	1.10	0.00000	0.00000	0.00000	0.00000	0.00000	0.00000	0.00000	0.00000	0.00000	0.00000	0.00000	0.00000	0.00000	0.00000	0.00000
Font. Tossal de la	40.11	-0.06	0.00000	0.00005	0.00504	0.00009	0.00002	0.00027	0.00389	0.00210	0.00014	0.00000	0.00000	0.00000	0.00000	0.00000	0.00000
Fonte Quente	39.61	-8.42	0.00000	0.00000	0.00000	0.00000	0.00000	0.00000	0.00005	0.00048	0.00252	0.00306	0.00102	0.00008	0.00000	0.00000	0.00000
Fonteta	38.10	-0.65	0.00000	0.00000	0.00000	0.00000	0.00000	0.00000	0.00000	0.00000	0.00000	0.00000	0.00000	0.00000	0.00000	0.00000	0.00000
Foradà. Cova	38.88	-0.10	0.00000	0.00000	0.00000	0.00000	0.00000	0.00000	0.00000	0.00000	0.00000	0.00000	0.00000	0.00000	0.00000	0.00000	0.00000
Foradada. Cova	38.81	0.17	0.00000	0.00000	0.00000	0.00000	0.00000	0.00000	0.00000	0.00000	0.00000	0.00000	0.00000	0.00000	0.00000	0.00003	0.00148
Forcas 2. Peña de las	42.19	0.34	0.00000	0.00000	0.00000	0.00000	0.00000	0.00457	0.00000	0.00005	0.00552	0.00000	0.00000	0.00000	0.00000	0.00000	0.00000
Forno da Telha	39.34	-8.96	0.00000	0.00000	0.00012	0.00224	0.00300	0.00004	0.00000	0.00000	0.00000	0.00000	0.00000	0.00000	0.00000	0.00000	0.00000
Forte do Passo	38.99	-9.12	0.00000	0.00000	0.00000	0.00000	0.00000	0.00005	0.00660	0.00798	0.00112	0.00007	0.00000	0.00000	0.00000	0.00000	0.00000
Fosca. Cova	40.42	-0.11	0.00016	0.00001	0.00000	0.00000	0.00000	0.00000	0.00000	0.00000	0.00000	0.00000	0.00000	0.00000	0.00000	0.00456	0.00277
Fosca. Cova	38.81	-0.17	0.00000	0.00000	0.00000	0.00000	0.00000	0.00000	0.00000	0.00000	0.00000	0.00000	0.00000	0.00000	0.00000	0.00000	0.00000
Fotenla (A)	42.29	-8.66	0.00000	0.00000	0.00000	0.00015	0.00206	0.00604	0.00000	0.00000	0.00000	0.00000	0.00000	0.00000	0.00000	0.00000	0.00000
Fozara	42.22	-8.51	0.00000	0.00000	0.00000	0.00000	0.00000	0.00000	0.00000	0.00000	0.00000	0.00000	0.00000	0.00000	0.00000	0.00000	0.00000
Fraga d´Aia	41.06	-7.50	0.00439	0.00251	0.00420	0.00079	0.00014	0.00000	0.00000	0.00000	0.00000	0.00000	0.00000	0.00000	0.00000	0.00000	0.00000
Fraga da Pena	40.72	-7.46	0.00000	0.00000	0.00000	0.00000	0.00000	0.00000	0.00000	0.00000	0.00015	0.00561	0.00151	0.00000	0.00000	0.00002	0.00249
Fragua (La)	43.44	-3.43	0.00000	0.00000	0.00000	0.00000	0.00000	0.00000	0.00000	0.00000	0.00000	0.00000	0.00000	0.00000	0.00000	0.00000	0.00000
Frare. Cova del	41.64	2.02	0.00142	0.00434	0.00009	0.00230	0.00360	0.00297	0.00134	0.00400	0.00601	0.00858	0.00713	0.00169	0.00002	0.00000	0.00000
Freiria	38.72	-9.32	0.00000	0.00000	0.00000	0.00000	0.00000	0.00000	0.00000	0.00000	0.00033	0.00556	0.00536	0.00000	0.00000	0.00000	0.00000
Fuensaúco. El Castillejo de	41.76	-2.33	0.00000	0.00000	0.00000	0.00000	0.00000	0.00000	0.00000	0.00000	0.00000	0.00000	0.00000	0.00000	0.00000	0.00000	0.00023
Fuente Álamo	37.33	-1.86	0.00000	0.00000	0.00000	0.00000	0.00000	0.00000	0.00076	0.00468	0.00924	0.05305	0.09420	0.09492	0.04533	0.01263	0.00849
Fuente Amarga	37.76	-2.60	0.00000	0.00000	0.00000	0.00000	0.00000	0.00000	0.00000	0.00000	0.00005	0.00108	0.00360	0.00190	0.00006	0.00000	0.00000

Site	Lat	Lon	SPD of Iberian settlement sites at 200 year time slices (cal. BP)														
			6000-5800	5800-5600	5600-5400	5400-5200	5200-5000	5000-4800	4800-4600	4600-4400	4400-4200	4200-4000	4000-3800	3800-3600	3600-3400	3400-3200	3200-3000
Fuente Amarguilla/Cortijo Nuevo	36.83	-2.24	0.00000	0.00000	0.00000	0.00000	0.00000	0.00000	0.00000	0.00000	0.00000	0.00000	0.00000	0.00059	0.00808	0.00000	0.00000
Fuente de la Mota	39.66	-2.06	0.00000	0.00000	0.00000	0.00000	0.00000	0.00000	0.00000	0.00000	0.00000	0.00000	0.00000	0.00000	0.00001	0.00005	0.00010
Fuente de las Pocillas	41.75	-4.77	0.00000	0.00000	0.00000	0.00000	0.00000	0.00005	0.00078	0.00159	0.00220	0.00165	0.00069	0.00014	0.00000	0.00000	0.00000
Fuente Estaca	40.96	-1.70	0.00000	0.00000	0.00000	0.00000	0.00000	0.00000	0.00000	0.00000	0.00000	0.00000	0.00000	0.00000	0.00000	0.00000	0.00044
Fuente Flores	39.49	-1.13	0.00000	0.00000	0.00000	0.00000	0.00000	0.00000	0.00465	0.00302	0.00000	0.00000	0.00000	0.00000	0.00000	0.00000	0.00000
Fuente Hoz	42.80	-2.90	0.00483	0.00111	0.00000	0.00000	0.00000	0.00000	0.00000	0.00000	0.00000	0.00000	0.00000	0.00000	0.00000	0.00000	0.00000
Fuente Lirio	40.64	-4.81	0.00000	0.00000	0.00000	0.00000	0.00000	0.00117	0.00126	0.00203	0.00377	0.00099	0.00004	0.00000	0.00000	0.00000	0.00000
Fuente Salina	41.86	-5.55	0.00000	0.00000	0.00000	0.00000	0.00000	0.00000	0.00000	0.00000	0.00000	0.00000	0.00000	0.00000	0.00000	0.00000	0.00000
Fumo	40.99	-7.08	0.00000	0.00000	0.00000	0.00000	0.00000	0.00000	0.00000	0.00000	0.00000	0.00062	0.00859	0.00331	0.00000	0.00000	0.00000
Fumo. Lapa do	38.44	-9.14	0.00230	0.00230	0.00045	0.00030	0.00245	0.00524	0.00000	0.00000	0.00000	0.00000	0.00000	0.00000	0.00000	0.00000	0.00000
Gamelas 3	38.71	-9.30	0.00000	0.00000	0.00000	0.00000	0.00000	0.00000	0.00000	0.00000	0.00000	0.00000	0.00000	0.00000	0.00000	0.00000	0.00000
Gándara (A)	42.16	-8.64	0.00000	0.00000	0.00000	0.00000	0.00000	0.00000	0.00535	0.00268	0.00000	0.00000	0.00000	0.00000	0.00000	0.00000	0.00000
Garma A (La)	43.43	-3.67	0.00000	0.00000	0.00000	0.00000	0.00000	0.00020	0.02131	0.00599	0.00204	0.00004	0.00199	0.00863	0.01832	0.00000	0.00000
Gatas	37.13	-1.89	0.00000	0.00000	0.00002	0.00007	0.00009	0.00019	0.00615	0.00247	0.01134	0.04684	0.09472	0.08857	0.07799	0.03106	0.00574
Gato 2. Cueva del	41.61	-1.42	0.00000	0.00000	0.00000	0.00000	0.00000	0.00000	0.00000	0.00000	0.00000	0.00000	0.00000	0.00000	0.00000	0.00000	0.00000
Gavín-Sepulcro	41.66	-0.87	0.00000	0.00000	0.00000	0.00000	0.00000	0.00000	0.00000	0.00000	0.00000	0.00000	0.00000	0.00000	0.00000	0.00000	0.00000
Genó	41.47	0.47	0.00000	0.00000	0.00000	0.00000	0.00000	0.00000	0.00000	0.00000	0.00000	0.00000	0.00000	0.00000	0.00000	0.00144	0.00899
Giraldo. Castelo do	38.54	-8.04	0.00000	0.00000	0.00000	0.00000	0.00000	0.00000	0.00000	0.00000	0.00000	0.00000	0.00000	0.00000	0.00000	0.00000	0.00000
Gitanos (Los)	43.36	-3.25	0.00349	0.00096	0.00012	0.00125	0.00189	0.00284	0.00483	0.00039	0.00001	0.00000	0.00000	0.00000	0.00000	0.00000	0.00000
Glorieta de San Vicente	37.68	-1.70	0.00000	0.00000	0.00000	0.00000	0.00000	0.00000	0.00184	0.01099	0.00000	0.00000	0.00000	0.00000	0.00000	0.00000	0.00000
Goldra	37.11	-8.00	0.00117	0.00122	0.00093	0.00050	0.00038	0.00020	0.00004	0.00001	0.00000	0.00000	0.00000	0.00000	0.00000	0.00000	0.00000
Grajas. Cueva de las	43.32	-3.58	0.00000	0.00000	0.00000	0.00000	0.00000	0.00000	0.00000	0.00000	0.00015	0.00561	0.00151	0.00000	0.00000	0.00000	0.00000
Grajos. Los / Grajos. Barranco de los (Abrigo Grande)	38.26	-1.38	0.00064	0.00063	0.00053	0.00042	0.00039	0.00031	0.00018	0.00014	0.00009	0.00005	0.00003	0.00002	0.00000	0.00000	0.00000
Graña (A)	42.97	-7.98	0.00000	0.00000	0.00000	0.00000	0.00000	0.00000	0.00000	0.00000	0.00000	0.00000	0.00000	0.00000	0.00000	0.00000	0.00005
Griera. Balma de la	41.23	1.58	0.00016	0.00000	0.00006	0.00376	0.00493	0.00050	0.00000	0.00000	0.00000	0.00000	0.00000	0.00000	0.00000	0.00000	0.00000
Grioteres (Les)	41.98	2.37	0.00336	0.00275	0.00122	0.00018	0.00008	0.00000	0.00000	0.00000	0.00000	0.00000	0.00000	0.00000	0.00000	0.00012	0.00045
Guaya	40.68	-4.60	0.00334	0.00376	0.00000	0.00378	0.00841	0.00002	0.00000	0.00000	0.00000	0.00000	0.00000	0.00000	0.00000	0.00817	0.00854
Guidoiro Areoso	42.54	-8.89	0.00000	0.00000	0.00000	0.00000	0.00000	0.00000	0.00016	0.00620	0.00003	0.00000	0.00000	0.00000	0.00000	0.00000	0.00000
Guineu. Cueva de la	41.43	1.57	0.00004	0.00000	0.00000	0.00403	0.00909	0.01106	0.02217	0.00112	0.00000	0.00000	0.00000	0.00025	0.00533	0.00410	0.01212
Güixas. Cueva de las	42.69	-0.53	0.00000	0.00000	0.00000	0.00000	0.00000	0.00000	0.00000	0.00000	0.00000	0.00000	0.00000	0.00000	0.00579	0.00000	0.00000
Guixeres de Vilobí (Les)	41.39	1.65	0.00000	0.00000	0.00000	0.00000	0.00000	0.00000	0.00000	0.00000	0.00000	0.00000	0.00000	0.00000	0.00000	0.00000	0.00000

Site	Lat	Lon	SPD of Iberian settlement sites at 200 year time slices (cal. BP)														
			6000-5800	5800-5600	5600-5400	5400-5200	5200-5000	5000-4800	4800-4600	4600-4400	4400-4200	4200-4000	4000-3800	3800-3600	3600-3400	3400-3200	3200-3000
Haltzerreka	42.95	-2.23	0.00000	0.00000	0.00000	0.00000	0.00000	0.00000	0.00000	0.00007	0.00369	0.00856	0.00063	0.00000	0.00000	0.00000	0.00000
Henayo. Castillo de	42.85	-2.50	0.00000	0.00000	0.00000	0.00000	0.00000	0.00000	0.00000	0.00000	0.00000	0.00000	0.00000	0.00002	0.00089	0.00637	0.00833
Herriko Barra	43.29	-2.17	0.00076	0.00340	0.00085	0.00038	0.00051	0.00268	0.00131	0.00013	0.00000	0.00000	0.00000	0.00000	0.00000	0.00000	0.00000
Higuera. Cueva de la	40.86	-3.51	0.00000	0.00000	0.00000	0.00000	0.00000	0.00000	0.00000	0.00000	0.00000	0.00000	0.00000	0.00000	0.00000	0.00000	0.00000
Horca. Cerro de la	37.77	-3.73	0.00000	0.00000	0.00000	0.00000	0.00000	0.00000	0.00000	0.00000	0.00000	0.00145	0.00115	0.00000	0.00000	0.00000	0.00000
Horca. Cerro de la	39.38	-6.04	0.00000	0.00000	0.00000	0.00001	0.00009	0.00114	0.00301	0.00069	0.00002	0.00000	0.00000	0.00000	0.00000	0.00000	0.00000
Horts de Can Torras	41.62	2.09	0.00000	0.00001	0.00140	0.00000	0.00000	0.00000	0.00000	0.00000	0.00000	0.00000	0.00000	0.00000	0.00000	0.00000	0.00000
Hostal Guadalupe. Cueva del	36.62	-4.50	0.00000	0.00000	0.00000	0.00000	0.00000	0.00000	0.00000	0.00000	0.00000	0.00000	0.00000	0.00000	0.00000	0.00000	0.00000
Hoya (La)	42.57	-2.59	0.00000	0.00000	0.00000	0.00000	0.00000	0.00000	0.00000	0.00000	0.00003	0.00012	0.00079	0.00493	0.00790	0.01403	0.01393
Hoya Quemada	40.25	-0.73	0.00000	0.00000	0.00000	0.00008	0.00018	0.00059	0.00196	0.00203	0.00127	0.00062	0.01362	0.01218	0.00637	0.00076	0.00003
Hoyas del Castillo	39.95	-1.70	0.00000	0.00000	0.00000	0.00000	0.00000	0.00000	0.00003	0.00239	0.00397	0.00003	0.00113	0.01224	0.00758	0.00822	0.00101
Hoyo de la Mina	36.72	-4.33	0.00000	0.00000	0.00000	0.00000	0.00000	0.00000	0.00000	0.00000	0.00000	0.00000	0.00000	0.00000	0.00000	0.00000	0.00000
Huerto Raso	42.21	0.04	0.00000	0.00000	0.00000	0.00000	0.00000	0.00000	0.00000	0.00000	0.00000	0.00000	0.00000	0.00000	0.00000	0.00000	0.00000
Hundidero-Gato	36.73	-5.24	0.00000	0.00000	0.00000	0.00000	0.00000	0.00000	0.00000	0.00000	0.00000	0.00000	0.00000	0.00000	0.00000	0.00000	0.00000
Husos I (Los)	42.60	-2.55	0.00001	0.00050	0.00699	0.00191	0.00062	0.00002	0.00036	0.00776	0.01006	0.00820	0.00840	0.00994	0.00517	0.00211	0.00647
Husos II (Los)	42.60	-2.55	0.00086	0.00884	0.00593	0.00087	0.00002	0.00000	0.00000	0.00000	0.00000	0.00000	0.00000	0.00000	0.00000	0.00000	0.00000
Ibne Ahmmar	37.15	-8.50	0.00000	0.00000	0.00000	0.00000	0.00000	0.00000	0.00000	0.00000	0.00000	0.00000	0.00000	0.00000	0.00000	0.00000	0.00000
Ifre	37.55	-1.43	0.00000	0.00000	0.00000	0.00000	0.00000	0.00000	0.00000	0.00000	0.00002	0.00129	0.00448	0.00085	0.00000	0.00000	0.00000
Igreja do Carmo	38.71	-9.14	0.00000	0.00000	0.00000	0.00000	0.00000	0.00000	0.00000	0.00000	0.00000	0.00000	0.00000	0.00000	0.00000	0.00000	0.00000
Igreja Velha de São Jorge	37.95	-7.30	0.00000	0.00000	0.00003	0.00383	0.00490	0.00016	0.00000	0.00000	0.00000	0.00000	0.00000	0.00000	0.00000	0.00000	0.00000
Illa d´en Reixac	42.01	3.09	0.00000	0.00000	0.00000	0.00000	0.00000	0.00000	0.00000	0.00000	0.00000	0.00000	0.00000	0.00000	0.00000	0.00012	0.00377
Illeta dels Banyets	38.43	-0.38	0.00000	0.00000	0.00000	0.00002	0.00129	0.00655	0.00000	0.00000	0.00000	0.00739	0.02450	0.03166	0.02150	0.00000	0.00000
Infantes. Cerro de los	37.27	-3.77	0.00000	0.00000	0.00000	0.00000	0.00000	0.00000	0.00000	0.00000	0.00000	0.00000	0.00000	0.00000	0.00000	0.00102	0.00458
Intxur	43.12	-2.15	0.00000	0.00000	0.00000	0.00000	0.00000	0.00000	0.00000	0.00000	0.00000	0.00000	0.00000	0.00000	0.00000	0.00000	0.00010
Iritegi	42.98	-2.41	0.00022	0.00204	0.00202	0.00078	0.00069	0.00246	0.00425	0.00516	0.00427	0.00259	0.00124	0.00201	0.00371	0.00301	0.00157
Itueros (Los)	40.61	-4.93	0.00007	0.00016	0.00051	0.00093	0.00109	0.00165	0.00475	0.00741	0.00782	0.00280	0.00033	0.00004	0.00000	0.00000	0.00000
Jarama 2	40.95	-3.32	0.00000	0.00000	0.00000	0.00000	0.00000	0.00000	0.00530	0.00007	0.00000	0.00000	0.00000	0.00000	0.00000	0.00000	0.00000
Jardinero (El)	39.38	-7.18	0.00000	0.00000	0.00000	0.00000	0.00000	0.00000	0.00000	0.00000	0.00000	0.00000	0.00000	0.00000	0.00000	0.00000	0.00000
Jou´l Llobu	43.34	-4.92	0.00000	0.00000	0.00000	0.00041	0.00360	0.00427	0.00323	0.00499	0.00000	0.00000	0.00000	0.00000	0.00000	0.00000	0.00000
Juan Climaco. Cabezo de	37.76	-1.57	0.00000	0.00000	0.00000	0.00000	0.00000	0.00000	0.00000	0.00000	0.00000	0.00000	0.00000	0.00000	0.00000	0.00004	0.00064
Judiciária	37.02	-7.93	0.00000	0.00000	0.00000	0.00000	0.00000	0.00000	0.00000	0.00000	0.00000	0.00000	0.00000	0.00000	0.00000	0.00000	0.00002
Junta de los Ríos	37.66	-7.35	0.00000	0.00000	0.00000	0.00000	0.00001	0.00064	0.00969	0.04578	0.03151	0.00012	0.00000	0.00000	0.00000	0.00000	0.00000
Juré. Cabezo	37.56	-7.09	0.00000	0.00000	0.00000	0.00012	0.00222	0.02226	0.03299	0.08028	0.03743	0.01217	0.00618	0.00087	0.00000	0.00000	0.00000

Site	Lat	Lon	SPD of Iberian settlement sites at 200 year time slices (cal. BP)														
			6000-5800	5800-5600	5600-5400	5400-5200	5200-5000	5000-4800	4800-4600	4600-4400	4400-4200	4200-4000	4000-3800	3800-3600	3600-3400	3400-3200	3200-3000
Kanpanoste	42.76	-2.47	0.00000	0.00000	0.00000	0.00008	0.00032	0.00193	0.00220	0.00047	0.00001	0.00000	0.00004	0.00187	0.00772	0.00078	0.00002
Kanpanoste Goikoa	42.76	-2.47	0.00000	0.00000	0.00000	0.00304	0.00448	0.00638	0.00352	0.00106	0.00003	0.00000	0.00011	0.00459	0.00041	0.00000	0.00000
Kobaederra	43.34	-2.62	0.00426	0.00481	0.00004	0.00021	0.00205	0.00606	0.00000	0.00077	0.00615	0.00370	0.00755	0.00240	0.00000	0.00000	0.00000
Kobeaga II	43.35	-2.57	0.00000	0.00000	0.00000	0.00017	0.00046	0.00181	0.00228	0.00080	0.00007	0.00000	0.00000	0.00000	0.00000	0.00000	0.00000
Kosmoaga	43.32	-2.69	0.00000	0.00000	0.00000	0.00000	0.00000	0.00000	0.00000	0.00000	0.00000	0.00000	0.00000	0.00000	0.00000	0.00000	0.00000
Kukuma	42.89	-2.30	0.00000	0.00000	0.00000	0.00000	0.00000	0.00000	0.00000	0.00000	0.00000	0.00000	0.00000	0.00000	0.00000	0.00000	0.00000
Labradas	42.10	-5.91	0.00000	0.00000	0.00000	0.00000	0.00000	0.00000	0.00000	0.00000	0.00000	0.00000	0.00000	0.00000	0.00000	0.00000	0.00000
Lac Major de Saboredo 2	42.62	0.97	0.00000	0.00000	0.00000	0.00000	0.00000	0.00000	0.00008	0.00615	0.00007	0.00000	0.00000	0.00000	0.00000	0.00000	0.00000
Lagoa (A)	42.99	-7.98	0.00000	0.00000	0.00000	0.00000	0.00000	0.00000	0.00002	0.00117	0.01013	0.00579	0.00001	0.00000	0.00012	0.00878	0.00205
Lagos (Los)	42.99	-4.32	0.00000	0.00000	0.00000	0.00000	0.00000	0.00000	0.00054	0.00360	0.00262	0.00009	0.00000	0.00017	0.00511	0.00013	0.00000
Lagrimal. Cueva del	38.51	-1.02	0.00000	0.00000	0.00000	0.00000	0.00000	0.00000	0.00000	0.00000	0.00000	0.00000	0.00000	0.00000	0.00000	0.00000	0.00000
Laias. Castelo de	42.33	-8.02	0.00000	0.00000	0.00000	0.00000	0.00000	0.00000	0.00000	0.00000	0.00000	0.00000	0.00000	0.00000	0.00000	0.00000	0.00000
Lamas de Abade	42.86	-8.53	0.00000	0.00000	0.00000	0.00000	0.00000	0.00000	0.00465	0.00950	0.01000	0.00004	0.00193	0.00222	0.00000	0.00000	0.00661
Lameira	38.57	-7.29	0.00000	0.00000	0.00000	0.00000	0.00000	0.00000	0.00716	0.00000	0.00000	0.00000	0.00000	0.00000	0.00000	0.00000	0.00000
Langatxo	43.28	-2.37	0.00000	0.00000	0.00000	0.00000	0.00000	0.00000	0.00000	0.00026	0.00367	0.00308	0.00020	0.00000	0.00000	0.00000	0.00000
Lapías das Lameiras	38.85	-9.35	0.00000	0.00000	0.00000	0.00000	0.00000	0.00000	0.00000	0.00000	0.00000	0.00000	0.00000	0.00000	0.00000	0.00000	0.00000
Lavapés	42.28	-8.83	0.00000	0.00000	0.00000	0.00000	0.00000	0.00000	0.00074	0.00792	0.00309	0.00098	0.00009	0.00000	0.00000	0.00000	0.00000
Lavra	41.85	-8.71	0.00000	0.00000	0.00000	0.00000	0.00000	0.00000	0.00000	0.00000	0.00000	0.00000	0.00000	0.00000	0.00622	0.00004	0.00000
Leceia	38.72	-9.28	0.00000	0.00000	0.00235	0.01614	0.02428	0.04239	0.06989	0.06729	0.04536	0.01362	0.00794	0.00083	0.00008	0.00000	0.00000
Librilla. Rambla de	37.87	-1.34	0.00038	0.00034	0.00226	0.00906	0.01016	0.00706	0.00012	0.00045	0.00638	0.00042	0.00000	0.00000	0.00000	0.00000	0.00000
Linatzeta	43.24	-2.32	0.00000	0.00000	0.00000	0.00000	0.00000	0.00000	0.00000	0.00000	0.00000	0.00000	0.00000	0.00000	0.00000	0.00000	0.00000
Llagú	43.33	-5.90	0.00000	0.00000	0.00000	0.00000	0.00000	0.00000	0.00000	0.00000	0.00000	0.00000	0.00000	0.00000	0.00000	0.00000	0.00000
Llanete de los Moros	38.02	-4.38	0.00000	0.00000	0.00000	0.00000	0.00000	0.00000	0.00000	0.00000	0.00000	0.00000	0.00000	0.00002	0.00078	0.03488	0.03222
Llano de la Virgen	36.65	-4.79	0.00000	0.00000	0.00000	0.00000	0.00000	0.00000	0.00135	0.00438	0.00138	0.00430	0.00923	0.00344	0.00157	0.00002	0.00000
Lloma de Betxi	39.53	-0.51	0.00000	0.00000	0.00000	0.00000	0.00000	0.00000	0.00000	0.00000	0.00031	0.01200	0.03730	0.02581	0.00127	0.00000	0.00000
Lloma Redona	38.41	-0.71	0.00000	0.00000	0.00000	0.00000	0.00000	0.00000	0.00000	0.00000	0.00000	0.00000	0.00151	0.00513	0.00001	0.00000	0.00000
Llop. Cova del	41.07	0.13	0.00004	0.00010	0.00036	0.00072	0.00085	0.00106	0.00114	0.00100	0.00071	0.00044	0.00023	0.00010	0.00003	0.00000	0.00000
Lloseta. Cueva de la	43.46	-5.08	0.00038	0.00044	0.00054	0.00058	0.00059	0.00058	0.00053	0.00048	0.00041	0.00034	0.00027	0.00020	0.00013	0.00007	0.00005
Lobosandos. Castro de	42.36	-8.01	0.00000	0.00000	0.00000	0.00000	0.00000	0.00000	0.00000	0.00000	0.00000	0.00000	0.00000	0.00000	0.00000	0.00000	0.00000
Lóbrega. Cueva	42.24	-2.64	0.00000	0.00000	0.00000	0.00308	0.00586	0.00145	0.00000	0.00000	0.00000	0.00000	0.00000	0.00000	0.00286	0.00020	0.00000
Loulé Velho	37.05	-8.08	0.00000	0.00000	0.00000	0.00000	0.00000	0.00000	0.00000	0.00000	0.00000	0.00000	0.00000	0.00000	0.00000	0.00000	0.00000
Lugarico Viejo	37.25	-1.96	0.00000	0.00000	0.00000	0.00000	0.00000	0.00000	0.00000	0.00000	0.00000	0.00548	0.00000	0.00000	0.00000	0.00000	0.00000
Lumentxa	43.36	-2.51	0.00616	0.00162	0.00000	0.00000	0.00000	0.00000	0.00000	0.00000	0.00000	0.00000	0.00000	0.00000	0.00000	0.00000	0.00000
Lunas (Las)	40.03	-3.88	0.00000	0.00000	0.00000	0.00000	0.00000	0.00000	0.00000	0.00000	0.00000	0.00000	0.00000	0.00000	0.00000	0.00000	0.00265
Macarullo. Tozal de	41.82	0.09	0.00000	0.00000	0.00000	0.00000	0.00000	0.00000	0.00000	0.00000	0.00000	0.00000	0.00000	0.00000	0.00000	0.00000	0.00120

Site	Lat	Lon	SPD of Iberian settlement sites at 200 year time slices (cal. BP)														
			6000-5800	5800-5600	5600-5400	5400-5200	5200-5000	5000-4800	4800-4600	4600-4400	4400-4200	4200-4000	4000-3800	3800-3600	3600-3400	3400-3200	3200-3000
Macerado	41.78	-0.57	0.00000	0.00000	0.00000	0.00000	0.00000	0.00000	0.00000	0.00000	0.00000	0.00000	0.00000	0.00000	0.00000	0.00010	0.01746
Madres Mercedarias	37.68	-1.70	0.00000	0.00000	0.00000	0.00000	0.00000	0.00000	0.00000	0.00000	0.00496	0.00368	0.00724	0.01136	0.00000	0.00000	0.00000
Magoito	38.87	-9.45	0.00016	0.01000	0.00921	0.00060	0.00004	0.00000	0.00000	0.00000	0.00000	0.00000	0.00000	0.00000	0.00000	0.00000	0.00139
Maja. Cueva	41.72	-2.89	0.00000	0.00000	0.00000	0.00000	0.00000	0.00000	0.00000	0.00000	0.00000	0.00482	0.00536	0.00000	0.00000	0.00000	0.00000
Malagón (El)	37.56	-2.42	0.00055	0.00075	0.00165	0.00237	0.00243	0.00263	0.00660	0.01676	0.02578	0.01097	0.00023	0.00011	0.00007	0.00004	0.00002
Malhada	40.68	-7.47	0.00000	0.00000	0.00000	0.00000	0.00000	0.00008	0.00757	0.01021	0.00315	0.00006	0.00000	0.00000	0.00000	0.00000	0.00000
Malhadas	38.55	-8.95	0.00000	0.00000	0.00000	0.00000	0.00000	0.00003	0.00605	0.00610	0.00204	0.00002	0.00000	0.00000	0.00000	0.00000	0.00000
Malhoeira. Cabeço de	40.23	-7.25	0.00000	0.00000	0.00000	0.00000	0.00000	0.00000	0.00574	0.00009	0.00000	0.00000	0.00000	0.00000	0.00000	0.00000	0.00000
Mar 3. Cueva del	43.46	-4.94	0.00000	0.00000	0.00000	0.00000	0.00000	0.00000	0.00000	0.00000	0.00000	0.00000	0.00000	0.00000	0.00000	0.00000	0.00000
Marcelo. Quinta do	38.68	-9.17	0.00000	0.00000	0.00000	0.00000	0.00000	0.00000	0.00000	0.00000	0.00000	0.00000	0.00000	0.00292	0.01292	0.00166	0.00130
Marco	42.67	-8.24	0.00000	0.00000	0.00000	0.00000	0.00000	0.00000	0.00000	0.00000	0.00000	0.00000	0.00000	0.00000	0.00000	0.00000	0.00000
Marge del Moro. Coveta del	41.35	1.94	0.00000	0.00000	0.00000	0.00000	0.00000	0.00028	0.00427	0.00149	0.00004	0.00000	0.00000	0.00000	0.00000	0.00000	0.00000
Margineda. Balma de la	42.48	1.49	0.00000	0.00000	0.00000	0.00000	0.00000	0.00000	0.00000	0.00000	0.00000	0.00000	0.00000	0.00000	0.00000	0.00000	0.00000
Marianela	37.68	-1.70	0.00000	0.00000	0.00000	0.00000	0.00000	0.00000	0.00008	0.00443	0.00000	0.00000	0.00000	0.00000	0.00000	0.00000	0.00000
Marijuan 1	42.13	-1.56	0.00000	0.00000	0.00000	0.00000	0.00000	0.00000	0.00000	0.00000	0.00003	0.00077	0.00331	0.00237	0.00010	0.00000	0.00000
Marizulo	43.22	-1.97	0.00175	0.00003	0.00073	0.00233	0.00261	0.00016	0.00000	0.00000	0.00000	0.00000	0.00000	0.00000	0.00000	0.00000	0.00000
Mármoles. Cueva de los	37.46	-4.13	0.00000	0.00000	0.00000	0.00000	0.00000	0.00000	0.00000	0.00000	0.00000	0.00000	0.00000	0.00000	0.00000	0.00000	0.00000
Marroquíes Bajos	37.78	-3.78	0.00225	0.00152	0.00021	0.00044	0.00049	0.00000	0.01658	0.03733	0.14979	0.13909	0.04262	0.00564	0.00568	0.00183	0.00198
Marueleza	43.31	-2.61	0.00000	0.00000	0.00000	0.00000	0.00000	0.00000	0.00000	0.00000	0.00000	0.00000	0.00000	0.00000	0.00000	0.00000	0.00000
Mas Castellar	42.20	2.90	0.00000	0.00000	0.00000	0.00000	0.00000	0.00000	0.00000	0.00000	0.00000	0.00000	0.00000	0.00000	0.00000	0.00000	0.00000
Mas Cremat. Cingle de	40.50	-0.29	0.00000	0.00000	0.00000	0.00000	0.00000	0.00000	0.00837	0.00078	0.00000	0.00000	0.00000	0.00000	0.00000	0.00000	0.00000
Mas d´Abad	40.38	0.09	0.00000	0.00000	0.00000	0.00000	0.00000	0.00000	0.00000	0.00000	0.00000	0.00000	0.00044	0.00381	0.00175	0.00188	0.00433
Mas d´Is	38.68	-0.39	0.00000	0.00000	0.00000	0.00000	0.00000	0.00000	0.00000	0.00000	0.00000	0.00000	0.00000	0.00000	0.00000	0.00000	0.00000
Mas de Valero	40.28	-0.86	0.00000	0.00000	0.00000	0.00000	0.00000	0.00000	0.00000	0.00000	0.00000	0.00000	0.00000	0.00000	0.00000	0.00000	0.00000
Mas del Corral	38.70	-0.59	0.00000	0.00000	0.00000	0.00000	0.00000	0.00000	0.00000	0.00000	0.00159	0.00973	0.00189	0.00000	0.00000	0.00000	0.00000
Mas Nou. Cingle de	40.42	-0.11	0.00000	0.00000	0.00000	0.00000	0.00000	0.00000	0.00000	0.00000	0.00000	0.00000	0.00000	0.00000	0.00000	0.00000	0.00000
Masada de Ratón	41.49	0.38	0.00000	0.00000	0.00000	0.00000	0.00000	0.00000	0.00002	0.00008	0.00029	0.00071	0.00127	0.00165	0.00183	0.00405	0.00314
Mata (La)	38.87	-5.67	0.00000	0.00000	0.00000	0.00000	0.00000	0.00000	0.00000	0.00000	0.00000	0.00000	0.00000	0.00000	0.00000	0.00000	0.00000
Mata del Castillo (La)	40.59	-6.08	0.00000	0.00000	0.00000	0.00000	0.00000	0.00000	0.00000	0.00000	0.00000	0.00000	0.00000	0.00000	0.00000	0.00000	0.00000
Matos. Castelo de	41.17	-7.99	0.00000	0.00000	0.00000	0.00000	0.00000	0.00000	0.00000	0.00000	0.00000	0.00000	0.00000	0.00000	0.00000	0.00000	0.00032
Mayor de Atapuerca. Cueva (El Portalón)	42.35	-3.52	0.00432	0.00352	0.00000	0.00065	0.00452	0.01070	0.00003	0.00149	0.00669	0.08906	0.08694	0.06840	0.03796	0.00975	0.02510
Mazaculos 2	43.39	-4.58	0.00300	0.00274	0.00013	0.00000	0.00000	0.00000	0.00000	0.00000	0.00000	0.00000	0.00000	0.00000	0.00000	0.00000	0.00000

Site	Lat	Lon	SPD of Iberian settlement sites at 200 year time slices (cal. BP)														
			6000-5800	5800-5600	5600-5400	5400-5200	5200-5000	5000-4800	4800-4600	4600-4400	4400-4200	4200-4000	4000-3800	3800-3600	3600-3400	3400-3200	3200-3000
Mazo (El)	43.40	-4.70	0.00000	0.00000	0.00000	0.00000	0.00000	0.00000	0.00000	0.00000	0.00000	0.00000	0.00000	0.00000	0.00000	0.00000	0.00000
Medellín. Castro de	38.96	-5.95	0.00000	0.00000	0.00000	0.00000	0.00000	0.00000	0.00000	0.00000	0.00000	0.00000	0.00000	0.00000	0.00000	0.00000	0.00000
Mediona 2	41.47	1.66	0.00000	0.00000	0.00000	0.00000	0.00000	0.00000	0.00000	0.00000	0.00022	0.00470	0.00000	0.00000	0.00000	0.00000	0.00000
Medo Tojeiro	37.63	-8.81	0.00024	0.00003	0.00000	0.00000	0.00000	0.00000	0.00000	0.00000	0.00000	0.00000	0.00000	0.00000	0.00000	0.00000	0.00000
Mejorada 1	39.95	-4.09	0.00000	0.00000	0.00000	0.00000	0.00000	0.00000	0.00000	0.00066	0.00654	0.00495	0.00000	0.00000	0.00000	0.00000	0.00000
Mendandia	42.73	-2.60	0.00000	0.00000	0.00000	0.00000	0.00000	0.00000	0.00000	0.00000	0.00000	0.00000	0.00000	0.00000	0.00000	0.00000	0.00000
Mercador	38.42	-7.34	0.00000	0.00000	0.00000	0.00000	0.00000	0.00000	0.00000	0.00000	0.00300	0.01030	0.00411	0.00003	0.00000	0.00000	0.00000
Mesa. Cerro de la	39.78	-5.08	0.00000	0.00000	0.00000	0.00000	0.00000	0.00000	0.00000	0.00000	0.00000	0.00000	0.00000	0.00000	0.00000	0.00000	0.00000
Mesas (Las)	38.58	-6.50	0.00000	0.00000	0.00000	0.00000	0.00000	0.00034	0.00042	0.00000	0.00000	0.00000	0.00000	0.00000	0.00000	0.00000	0.00000
Mezquitilla. Morro de	36.74	-4.04	0.00005	0.00012	0.00037	0.00070	0.00081	0.00100	0.00109	0.00097	0.00073	0.00048	0.00027	0.00013	0.00038	0.00288	0.00929
Miel. Cerro de la	37.20	-3.98	0.00000	0.00000	0.00000	0.00000	0.00000	0.00000	0.00000	0.00000	0.00000	0.00000	0.00000	0.00000	0.00024	0.00331	0.00270
Miguens 3	38.48	-7.33	0.00000	0.00000	0.00000	0.00000	0.00000	0.00000	0.00000	0.00043	0.01181	0.00000	0.00000	0.00000	0.00000	0.00000	0.00000
Millares (Los). Fortín 1	36.96	-2.53	0.00000	0.00000	0.00000	0.00000	0.00000	0.00000	0.00080	0.01355	0.02752	0.00239	0.00000	0.00000	0.00000	0.00000	0.00000
Millares (Los). Fortín 4	36.96	-2.52	0.00000	0.00000	0.00000	0.00000	0.00000	0.00000	0.00000	0.00012	0.00443	0.00261	0.00004	0.00000	0.00000	0.00000	0.00000
Millares (Los). Fortín 5	36.96	-2.52	0.00000	0.00000	0.00000	0.00000	0.00000	0.00000	0.00000	0.00019	0.01031	0.00343	0.00002	0.00000	0.00000	0.00000	0.00000
Millares (Los). Poblado	36.96	-2.52	0.00000	0.00000	0.00000	0.00138	0.00615	0.01511	0.03178	0.02484	0.01004	0.00051	0.00002	0.00000	0.00000	0.00000	0.00000
Mirador (El)	40.96	-4.11	0.00000	0.00000	0.00000	0.00000	0.00000	0.00000	0.00000	0.00000	0.00000	0.00046	0.00428	0.00000	0.00000	0.00000	0.00000
Mirador. Cueva del	42.35	-3.51	0.00682	0.00923	0.00514	0.00000	0.00000	0.00000	0.00000	0.00010	0.01264	0.00673	0.00287	0.00369	0.00022	0.00638	0.00077
Miranda. Castillo de	41.71	-0.93	0.00000	0.00000	0.00000	0.00000	0.00000	0.00000	0.00000	0.00000	0.00000	0.00000	0.00000	0.00000	0.00000	0.00000	0.00000
Mirón. Cueva del	43.24	-3.46	0.00420	0.00527	0.00455	0.00083	0.00009	0.00012	0.00786	0.00302	0.00331	0.01062	0.00362	0.00075	0.00382	0.00002	0.00000
Mocegueira	41.86	-8.38	0.00000	0.00000	0.00000	0.00000	0.00000	0.00000	0.00000	0.00000	0.00000	0.00000	0.00000	0.00175	0.00041	0.00000	0.00000
Mohías	43.55	-6.75	0.00000	0.00000	0.00000	0.00000	0.00000	0.00000	0.00000	0.00000	0.00000	0.00000	0.00000	0.00000	0.00000	0.00000	0.00000
Moinho de Valadares	38.36	-7.39	0.00000	0.00000	0.00000	0.00000	0.00000	0.00000	0.00873	0.00000	0.00000	0.00674	0.00003	0.00012	0.00601	0.00008	0.00747
Moinho Novo de Baixo 1	38.51	-7.32	0.00000	0.00000	0.00000	0.00000	0.00000	0.00000	0.00000	0.00626	0.00000	0.00000	0.00000	0.00000	0.00000	0.00000	0.00000
Moita da Ladra	38.89	-9.07	0.00000	0.00000	0.00000	0.00000	0.00027	0.01293	0.02668	0.02286	0.00852	0.01484	0.00431	0.00395	0.00071	0.00000	0.00000
Moita do Sebastião	39.11	-8.69	0.00000	0.00000	0.00000	0.00000	0.00000	0.00000	0.00000	0.00000	0.00000	0.00000	0.00000	0.00000	0.00000	0.00000	0.00000
Mola d'Agres	38.79	-0.50	0.00000	0.00000	0.00000	0.00000	0.00000	0.00000	0.00000	0.00000	0.00102	0.01068	0.00074	0.00000	0.00000	0.00000	0.00000
Molinet. Tossal del	41.68	0.88	0.00000	0.00000	0.00000	0.00000	0.00000	0.00000	0.00000	0.00000	0.00000	0.00000	0.00000	0.00000	0.00000	0.00000	0.00000
Molinicos (Los)	38.21	-1.85	0.00000	0.00000	0.00000	0.00000	0.00000	0.00000	0.00000	0.00000	0.00000	0.00000	0.00000	0.00000	0.00000	0.00000	0.00000
Molinot. Cova del	41.42	1.51	0.00000	0.00004	0.00520	0.00511	0.00255	0.00020	0.00000	0.00000	0.00000	0.00000	0.00000	0.00000	0.00000	0.00000	0.00000
Moncín	41.86	-1.58	0.00000	0.00000	0.00000	0.00000	0.00000	0.00000	0.00000	0.00010	0.00838	0.00927	0.01428	0.01028	0.02485	0.02543	0.00535
Monleón. Cabezo de	41.21	0.02	0.00000	0.00000	0.00000	0.00000	0.00000	0.00000	0.00000	0.00000	0.00000	0.00000	0.00000	0.00000	0.00000	0.00000	0.00040

Site	Lat	Lon	SPD of Iberian settlement sites at 200 year time slices (cal. BP)														
			6000-5800	5800-5600	5600-5400	5400-5200	5200-5000	5000-4800	4800-4600	4600-4400	4400-4200	4200-4000	4000-3800	3800-3600	3600-3400	3400-3200	3200-3000
Montaz	42.65	-8.23	0.00000	0.00000	0.00000	0.00000	0.00000	0.00000	0.00000	0.00000	0.00000	0.00000	0.00000	0.00000	0.00000	0.00000	0.00000
Monte Aguilar	42.03	-1.35	0.00000	0.00000	0.00000	0.00000	0.00000	0.00000	0.00000	0.00000	0.00003	0.00129	0.02112	0.02297	0.01998	0.00000	0.00000
Monte Aguilar 2	42.02	-1.35	0.00000	0.00000	0.00000	0.00000	0.00000	0.00000	0.00000	0.00000	0.00000	0.00010	0.00161	0.00370	0.00076	0.00000	0.00000
Monte Buruntza	43.24	-2.01	0.00000	0.00000	0.00000	0.00000	0.00000	0.00000	0.00000	0.00000	0.00000	0.00000	0.00000	0.00000	0.00000	0.00310	0.00583
Monte Cantabria	42.48	-2.43	0.00000	0.00000	0.00000	0.00000	0.00000	0.00000	0.00000	0.00000	0.00000	0.00000	0.00000	0.00000	0.00000	0.00000	0.00000
Monte Castrelo de Pelóu	43.16	-6.91	0.00000	0.00000	0.00000	0.00000	0.00000	0.00000	0.00000	0.00000	0.00000	0.00000	0.00000	0.00000	0.00047	0.00664	0.00521
Monte do Castelo	38.72	-9.29	0.00000	0.00000	0.00044	0.00631	0.01305	0.00208	0.00030	0.00548	0.00001	0.00000	0.00000	0.00000	0.00000	0.00000	0.00000
Monte do Frade	40.14	-7.13	0.00000	0.00004	0.00489	0.00000	0.00000	0.00000	0.00000	0.00000	0.00000	0.00000	0.00142	0.00465	0.00000	0.00013	0.00892
Monte do Trigo	39.93	-7.19	0.00004	0.00023	0.00183	0.00304	0.00309	0.00293	0.00155	0.00070	0.00015	0.00002	0.00000	0.00000	0.00000	0.00711	0.03625
Monte Ornedo	42.91	-4.18	0.00000	0.00000	0.00000	0.00000	0.00000	0.00000	0.00000	0.00000	0.00000	0.00000	0.00000	0.00000	0.00000	0.00000	0.00000
Montecristo. Cerro de	36.75	-3.01	0.00000	0.00000	0.00000	0.00000	0.00000	0.00000	0.00000	0.00000	0.00000	0.00000	0.00000	0.00000	0.00000	0.00000	0.00000
Montes de Baixo	37.44	-8.79	0.00000	0.00000	0.00000	0.00306	0.00427	0.00002	0.00000	0.00000	0.00000	0.00000	0.00000	0.00000	0.00000	0.00000	0.00000
Montgròs. Turó del	41.80	2.27	0.00000	0.00000	0.00000	0.00000	0.00000	0.00000	0.00000	0.00000	0.00000	0.00000	0.00000	0.00000	0.00000	0.00583	0.00927
Mora. Cerro de la	37.20	-3.98	0.00000	0.00000	0.00000	0.00000	0.00000	0.00000	0.00000	0.00001	0.00129	0.00786	0.00520	0.00142	0.00280	0.00953	0.01707
Moreirinha	40.06	-7.12	0.00000	0.00000	0.00000	0.00000	0.00000	0.00000	0.00000	0.00000	0.00000	0.00000	0.00000	0.00000	0.00000	0.00014	0.01488
Morente. Cerro	37.32	-2.92	0.00545	0.00203	0.00000	0.00000	0.00000	0.00000	0.00000	0.00000	0.00000	0.00000	0.00000	0.00000	0.00000	0.00000	0.00000
Moriyón. Picu Castiellu de	43.50	-5.39	0.00000	0.00000	0.00000	0.00000	0.00000	0.00000	0.00000	0.00000	0.00000	0.00000	0.00000	0.00000	0.00000	0.00000	0.00000
Moro. Cueva del	42.11	0.27	0.00305	0.00037	0.00000	0.00000	0.00000	0.00000	0.00000	0.00000	0.00000	0.00006	0.00322	0.00785	0.00002	0.00643	0.00046
Moros. Cueva de los	42.02	0.32	0.00000	0.00000	0.00000	0.00000	0.00000	0.00000	0.00000	0.00000	0.00000	0.00000	0.00000	0.00000	0.00497	0.00000	0.00000
Mort. Cova del	42.09	0.69	0.00000	0.00181	0.00844	0.00000	0.00000	0.00000	0.00000	0.00000	0.00000	0.00081	0.00462	0.00086	0.00851	0.00774	0.00006
Moru	43.21	-2.43	0.00000	0.00000	0.00000	0.00000	0.00000	0.00000	0.00000	0.00000	0.00000	0.00000	0.00000	0.00000	0.00000	0.00000	0.00009
Mota (La)	41.31	-4.91	0.00000	0.00000	0.00000	0.00000	0.00000	0.00000	0.00000	0.00000	0.00000	0.00000	0.00000	0.00000	0.00000	0.00000	0.00000
Mota del Marqués	41.63	-5.17	0.00000	0.00000	0.00000	0.00000	0.00000	0.00000	0.00000	0.00000	0.00000	0.00000	0.00000	0.00000	0.00000	0.00000	0.00000
Moura. Casa da	39.33	-9.25	0.00804	0.01316	0.03057	0.00394	0.00222	0.00024	0.02596	0.00000	0.00000	0.00000	0.00000	0.00000	0.00000	0.00000	0.00000
Moura. Cova da	39.09	-9.24	0.00000	0.00080	0.01603	0.00117	0.00067	0.00692	0.00067	0.00609	0.00333	0.00002	0.00000	0.00000	0.00000	0.00000	0.00000
Muela de Sabucar	40.52	-1.08	0.00000	0.00000	0.00000	0.00000	0.00000	0.00000	0.00000	0.00000	0.00520	0.00719	0.00007	0.00000	0.00000	0.00000	0.00000
Munoaundi	43.16	-2.30	0.00000	0.00000	0.00000	0.00000	0.00000	0.00000	0.00000	0.00000	0.00000	0.00000	0.00000	0.00000	0.00000	0.00000	0.00000
Muntanya Assolada	39.14	-0.38	0.00000	0.00000	0.00000	0.00000	0.00000	0.00000	0.00000	0.00000	0.00035	0.00942	0.00165	0.00490	0.00020	0.00000	0.00000
Muradellas (As)	42.02	-6.92	0.00000	0.00000	0.00000	0.00000	0.00000	0.00003	0.00020	0.00040	0.00078	0.00115	0.00135	0.00128	0.00086	0.00032	0.00014
Murciélago. Cueva del	39.82	-0.59	0.00000	0.00000	0.00000	0.00000	0.00000	0.00000	0.00000	0.00000	0.00000	0.00022	0.00283	0.00347	0.00050	0.00331	0.00270
Murciélagos. Cueva de los	37.54	-4.30	0.00318	0.00228	0.00098	0.00003	0.00000	0.00000	0.00000	0.00000	0.00000	0.00000	0.00000	0.00000	0.00000	0.00000	0.00000
Murciélagos. Cueva de los	43.37	-3.72	0.00000	0.00000	0.00000	0.00000	0.00000	0.00000	0.00000	0.00000	0.00000	0.00000	0.00000	0.00000	0.00000	0.00016	0.00631
Murganho 2	40.53	-7.84	0.00000	0.00000	0.00000	0.00000	0.00002	0.00473	0.00000	0.00000	0.00000	0.00000	0.00000	0.00000	0.00000	0.00000	0.00000

Site	Lat	Lon	SPD of Iberian settlement sites at 200 year time slices (cal. BP)														
			6000-5800	5800-5600	5600-5400	5400-5200	5200-5000	5000-4800	4800-4600	4600-4400	4400-4200	4200-4000	4000-3800	3800-3600	3600-3400	3400-3200	3200-3000
Muricecs	42.05	0.89	0.00000	0.00000	0.00000	0.00000	0.00000	0.00000	0.00000	0.00000	0.00000	0.00000	0.00000	0.00000	0.00000	0.00000	0.00000
Murviedro	37.68	-1.71	0.00000	0.00000	0.00000	0.00000	0.00000	0.00000	0.00000	0.00000	0.00000	0.00000	0.00000	0.00000	0.00000	0.01117	0.00235
Nacimiento. Cueva del	38.09	-2.70	0.00003	0.00000	0.00000	0.00000	0.00000	0.00002	0.00152	0.00302	0.00217	0.00040	0.00002	0.00000	0.00000	0.00000	0.00000
Navas	42.16	-8.80	0.00000	0.00000	0.00000	0.00000	0.00000	0.00000	0.00000	0.00000	0.00000	0.00000	0.00000	0.00000	0.00000	0.00000	0.00000
Negret (El)	38.46	-0.63	0.00000	0.00000	0.00000	0.00000	0.00000	0.00000	0.00000	0.00000	0.00000	0.00000	0.00000	0.00005	0.00619	0.00384	0.00647
Nerja. Cueva de	36.76	-3.84	0.01841	0.00654	0.00180	0.00430	0.00847	0.00186	0.00876	0.00005	0.00000	0.00312	0.00320	0.00504	0.00005	0.00000	0.00000
Niebla	37.36	-6.68	0.00000	0.00000	0.00000	0.00000	0.00000	0.00000	0.00000	0.00000	0.00000	0.00000	0.00000	0.00000	0.00000	0.00000	0.00000
Niño. Cueva del	38.54	-2.15	0.00000	0.00000	0.00000	0.00000	0.00000	0.00000	0.00000	0.00000	0.00000	0.00000	0.00000	0.00000	0.00000	0.00000	0.00000
Noville	43.46	-8.23	0.00000	0.00000	0.00000	0.00000	0.00000	0.00000	0.00000	0.00000	0.00000	0.00000	0.00000	0.00000	0.00000	0.00000	0.00000
Numancia	41.81	-2.45	0.00000	0.00000	0.00000	0.00000	0.00000	0.00000	0.00000	0.00000	0.00000	0.00000	0.00000	0.00000	0.00000	0.00000	0.00000
Obagues de Ratera. Abric de les	42.60	0.97	0.00000	0.00000	0.00000	0.00000	0.00000	0.00000	0.00904	0.00002	0.00000	0.00000	0.00000	0.00000	0.00000	0.00000	0.00000
Oficio (El)	37.33	-1.75	0.00000	0.00000	0.00000	0.00000	0.00000	0.00000	0.00000	0.00000	0.00000	0.00139	0.00822	0.00728	0.00140	0.00000	0.00000
Olelas	38.84	-9.28	0.00000	0.00013	0.00799	0.00528	0.00416	0.01525	0.00398	0.00495	0.00024	0.00000	0.00000	0.00000	0.00000	0.00000	0.00000
Or. Cova de l´	38.85	-0.36	0.00000	0.00000	0.00000	0.00000	0.00072	0.01533	0.00000	0.00000	0.01172	0.00000	0.00000	0.00000	0.00000	0.00000	0.00000
Orcillas 1. Cueva de las	42.67	-2.23	0.00000	0.00000	0.00000	0.00287	0.00831	0.00020	0.00000	0.00000	0.00000	0.00000	0.00000	0.00000	0.00000	0.00000	0.00000
Orelas (As)	42.66	-8.21	0.00000	0.00000	0.00000	0.00000	0.00000	0.00000	0.00000	0.00000	0.00000	0.00000	0.00000	0.00000	0.00000	0.00000	0.00000
Orpesa la Vella	40.08	0.13	0.00001	0.00042	0.00632	0.00280	0.00113	0.00007	0.00001	0.00020	0.00333	0.01226	0.02425	0.03414	0.01091	0.00352	0.00034
Ourantes	42.36	-8.01	0.00000	0.00000	0.00000	0.00000	0.00000	0.00000	0.00000	0.00000	0.00000	0.00000	0.00000	0.00000	0.00000	0.00000	0.00000
Outeiro da Cerca	41.95	-7.86	0.00000	0.00000	0.00000	0.00000	0.00000	0.00000	0.00000	0.00000	0.00000	0.00000	0.00000	0.00000	0.00000	0.00000	0.00000
Outeiro Redondo	38.45	-9.11	0.00000	0.00000	0.00648	0.01953	0.02340	0.07383	0.03059	0.03820	0.00716	0.01349	0.00286	0.00003	0.00000	0.00000	0.00000
Pacencia. Cueva	42.28	-0.09	0.00000	0.00000	0.00000	0.00000	0.00000	0.00000	0.00000	0.00000	0.00000	0.00000	0.00000	0.00000	0.00000	0.00000	0.00000
Paco Pons	42.39	-0.89	0.00000	0.00000	0.00000	0.00000	0.00000	0.00000	0.00006	0.00085	0.00370	0.00223	0.00021	0.00000	0.00000	0.00000	0.00000
Padrão 1	37.06	-8.89	0.00000	0.00000	0.00000	0.00000	0.00000	0.00000	0.00000	0.00000	0.00000	0.00000	0.00000	0.00000	0.00000	0.00000	0.00000
Padre Areso	42.69	-1.14	0.00005	0.00000	0.00000	0.00000	0.00000	0.00000	0.00000	0.00000	0.00000	0.00000	0.00000	0.00000	0.00000	0.00353	0.00147
Pala da Vella	42.49	-6.83	0.00012	0.00101	0.00299	0.00411	0.00983	0.00003	0.00000	0.00000	0.00000	0.00000	0.00011	0.00117	0.00312	0.00085	0.00009
Palacio Quemado	38.70	-6.30	0.00000	0.00000	0.00000	0.00000	0.00000	0.00010	0.00758	0.00570	0.00100	0.00095	0.00347	0.00214	0.00008	0.00024	0.00160
Palacios (Los)	38.98	-3.64	0.00000	0.00000	0.00000	0.00000	0.00000	0.00000	0.00000	0.00003	0.00037	0.00150	0.00290	0.00366	0.00336	0.00053	0.00005
Palermo 3/4	41.21	-0.16	0.00000	0.00000	0.00000	0.00000	0.00000	0.00000	0.00000	0.00000	0.00000	0.00004	0.00012	0.00033	0.00078	0.00134	0.00141
Palheirão Furado	37.73	-8.80	0.00000	0.00000	0.00000	0.00000	0.00000	0.00012	0.00404	0.00012	0.00000	0.00000	0.00000	0.00000	0.00000	0.00000	0.00000
Palheiros	41.41	-7.38	0.00000	0.00000	0.00000	0.00000	0.00000	0.00000	0.01803	0.03546	0.02768	0.00758	0.00083	0.00590	0.00624	0.00000	0.00068
Palomar	41.01	-0.67	0.00000	0.00000	0.00000	0.00000	0.00000	0.00000	0.00000	0.00000	0.00000	0.00000	0.00000	0.00000	0.00000	0.00000	0.00000
Palomas. Cueva de las	36.99	-4.88	0.00189	0.00021	0.00000	0.00000	0.00000	0.00000	0.00030	0.00547	0.00000	0.00000	0.00000	0.00000	0.00000	0.00000	0.00000
Papa Uvas	37.27	-7.04	0.00217	0.00685	0.03054	0.02311	0.03725	0.02308	0.00881	0.00418	0.00140	0.00057	0.00014	0.00002	0.00000	0.00000	0.00000
Papúa (La)	37.95	-6.44	0.00000	0.00000	0.00000	0.00000	0.00000	0.00000	0.00000	0.00000	0.00000	0.00006	0.00668	0.00002	0.00000	0.00000	0.00000

Site	Lat	Lon	SPD of Iberian settlement sites at 200 year time slices (cal. BP)														
			6000-5800	5800-5600	5600-5400	5400-5200	5200-5000	5000-4800	4800-4600	4600-4400	4400-4200	4200-4000	4000-3800	3800-3600	3600-3400	3400-3200	3200-3000
Parazuelos	37.53	-1.44	0.00000	0.00000	0.00000	0.00020	0.00102	0.00456	0.00017	0.00000	0.00000	0.00000	0.00000	0.00000	0.00000	0.00000	0.00000
Parco	41.92	0.94	0.00000	0.00000	0.00000	0.00000	0.00000	0.00000	0.00000	0.00000	0.00000	0.00000	0.00000	0.00000	0.00000	0.00000	0.00000
Pardo. Cova d´en	38.82	-0.29	0.00456	0.00962	0.00478	0.01241	0.01601	0.00566	0.00033	0.00000	0.00000	0.00000	0.00000	0.00000	0.00000	0.00850	0.00526
Parede	38.69	-9.36	0.00000	0.00000	0.00000	0.00000	0.00000	0.00005	0.00192	0.00000	0.00000	0.00000	0.00000	0.00000	0.00000	0.00000	0.00000
Pareko Landa	43.38	-2.75	0.00000	0.00000	0.00000	0.00000	0.00000	0.00000	0.00000	0.00000	0.00000	0.00000	0.00000	0.00000	0.00000	0.00000	0.00000
Parpantique (El)	41.38	-2.56	0.00000	0.00000	0.00000	0.00000	0.00000	0.00000	0.00000	0.00000	0.00000	0.01347	0.00006	0.00000	0.00000	0.00000	0.00000
Partelapeña	42.35	-2.20	0.00000	0.00000	0.00000	0.00000	0.00000	0.00000	0.00000	0.00000	0.00000	0.00000	0.00000	0.00000	0.00000	0.00000	0.00000
Pastora 1. Cueva de la	37.36	-2.74	0.00000	0.00000	0.00000	0.00000	0.00000	0.00000	0.00000	0.00000	0.00000	0.00000	0.00000	0.00000	0.00000	0.00000	0.00000
Pastoria	41.73	-7.56	0.00000	0.00000	0.00000	0.00000	0.00000	0.00000	0.00000	0.00000	0.00000	0.00000	0.00000	0.00003	0.00060	0.00274	0.00227
Patio de las Catedrales	40.96	-5.66	0.00000	0.00000	0.00000	0.00000	0.00000	0.00000	0.00000	0.00000	0.00000	0.00000	0.00000	0.00000	0.00000	0.00000	0.00000
Pau 4. Cova d´en	42.16	2.75	0.00109	0.00297	0.00113	0.00064	0.00079	0.00252	0.00153	0.00030	0.00001	0.00011	0.00135	0.00462	0.00572	0.00001	0.00000
Pé de Erra	38.99	-8.47	0.00000	0.00000	0.00000	0.00000	0.00000	0.00004	0.00199	0.00000	0.00000	0.00000	0.00000	0.00000	0.00000	0.00000	0.00000
Pedreira de Salemas	38.87	-9.20	0.00000	0.00000	0.00000	0.00000	0.00000	0.00000	0.00000	0.00000	0.00000	0.00000	0.00000	0.00000	0.00000	0.00000	0.00000
Pedroses. Cueva de les	43.46	-5.10	0.00000	0.00000	0.00000	0.00000	0.00000	0.00000	0.00000	0.00000	0.00000	0.00000	0.00000	0.00000	0.00000	0.00000	0.00000
Pedroso (El)	41.75	-6.55	0.00000	0.00000	0.00000	0.00000	0.00000	0.00000	0.00043	0.00584	0.00262	0.00955	0.00016	0.00000	0.00000	0.00000	0.00000
Pego	41.49	-8.52	0.00000	0.00000	0.00000	0.00000	0.00000	0.00000	0.00000	0.00000	0.00000	0.00001	0.00364	0.00464	0.00565	0.00696	0.00201
Pena d´Água. Abrigo da	39.58	-8.55	0.00337	0.00240	0.00052	0.00007	0.00003	0.00044	0.00080	0.00000	0.00000	0.00000	0.00000	0.00349	0.00000	0.00000	0.00000
Peña del Castro	42.83	-5.23	0.00000	0.00000	0.00000	0.00000	0.00000	0.00000	0.00000	0.00000	0.00000	0.00000	0.00000	0.00000	0.00000	0.00000	0.00000
Peña Dorada	40.50	-1.03	0.00000	0.00000	0.00000	0.00000	0.00000	0.00000	0.00000	0.00000	0.00000	0.00801	0.00826	0.00000	0.00000	0.00000	0.00000
Peña Larga	42.61	-2.51	0.00085	0.00787	0.00101	0.01263	0.01436	0.00274	0.00085	0.00591	0.00000	0.00000	0.00000	0.00000	0.00000	0.00000	0.00000
Peña Negra	38.27	-0.83	0.00000	0.00000	0.00000	0.00000	0.00000	0.00000	0.00000	0.00000	0.00000	0.00000	0.00001	0.00034	0.00255	0.00242	0.00214
Peña Oviedo	43.15	-4.73	0.00008	0.00000	0.00176	0.00000	0.00000	0.00000	0.00000	0.00000	0.00000	0.00000	0.00000	0.00000	0.00000	0.00519	0.00000
Peña. Abrigo de la	42.63	-2.45	0.00000	0.00000	0.00000	0.00020	0.00102	0.00456	0.00017	0.00000	0.00015	0.00632	0.00798	0.00031	0.00000	0.00002	0.00186
Penalba	42.54	-8.55	0.00000	0.00000	0.00000	0.00000	0.00000	0.00004	0.00185	0.00314	0.00184	0.00046	0.00087	0.00250	0.00580	0.01274	0.00787
Peñalosa	38.17	-3.80	0.00000	0.00000	0.00000	0.00000	0.00000	0.00000	0.00000	0.00001	0.00246	0.01148	0.01432	0.02099	0.00959	0.00008	0.00000
Penarrubia	43.02	-7.61	0.00000	0.00000	0.00000	0.00000	0.00000	0.00000	0.00000	0.00000	0.00000	0.00000	0.00000	0.00000	0.00000	0.00000	0.00000
Peñas (Las)	42.01	-5.86	0.00000	0.00000	0.00000	0.00000	0.00000	0.00000	0.00950	0.01589	0.00000	0.00000	0.00000	0.00000	0.00000	0.00000	0.00000
Pendo (El)	43.39	-3.91	0.00018	0.00021	0.00027	0.00031	0.00033	0.00035	0.00039	0.00040	0.00041	0.00040	0.00040	0.00220	0.00243	0.00030	0.00027
Peneda del Viso	42.32	-8.59	0.00000	0.00000	0.00000	0.00000	0.00000	0.00000	0.00000	0.00000	0.00000	0.00000	0.00000	0.00000	0.00000	0.00000	0.00000
Penedo do Lexim	38.89	-9.32	0.00000	0.00000	0.00000	0.00000	0.00000	0.00000	0.01332	0.01293	0.01172	0.01440	0.01146	0.00002	0.00000	0.00000	0.00000
Penedo dos Mouros	40.53	-7.63	0.00000	0.00000	0.00000	0.00000	0.00000	0.00000	0.00000	0.00000	0.00000	0.00000	0.00165	0.00005	0.00000	0.00000	0.00000
Penedos do Castro	42.42	-7.69	0.00000	0.00000	0.00000	0.00000	0.00000	0.00000	0.00000	0.00000	0.00000	0.00000	0.00000	0.00000	0.00000	0.00000	0.00000
Penedos Grandes	41.85	-8.38	0.00000	0.00000	0.00000	0.00000	0.00033	0.00796	0.00000	0.00000	0.00000	0.00000	0.00000	0.00000	0.00000	0.00793	0.00002
Penha Verde	38.79	-9.40	0.00000	0.00000	0.00000	0.00000	0.00000	0.00000	0.00023	0.01611	0.01568	0.01252	0.00341	0.00194	0.00160	0.00046	0.00012
Penha. Monte da	41.43	-8.27	0.00000	0.00000	0.00000	0.00000	0.00000	0.00000	0.00000	0.00000	0.00000	0.00000	0.00000	0.00000	0.00000	0.00008	0.00369

Site	Lat	Lon	SPD of Iberian settlement sites at 200 year time slices (cal. BP)														
			6000-5800	5800-5600	5600-5400	5400-5200	5200-5000	5000-4800	4800-4600	4600-4400	4400-4200	4200-4000	4000-3800	3800-3600	3600-3400	3400-3200	3200-3000
Penices	41.41	-8.61	0.00000	0.00000	0.00000	0.00000	0.00000	0.00000	0.00000	0.00000	0.00000	0.00000	0.00000	0.00000	0.00000	0.00000	0.00000
Percevejo. Quinta do	38.67	-9.20	0.00000	0.00000	0.00000	0.00000	0.00000	0.00000	0.00000	0.00000	0.00000	0.00000	0.00000	0.00148	0.00171	0.00056	0.00559
Perdigões	38.45	-7.55	0.00000	0.00429	0.00002	0.00877	0.02648	0.04192	0.02585	0.09228	0.09149	0.01995	0.00143	0.00155	0.00196	0.00101	0.00038
Pericos (Os)	42.52	-9.04	0.00000	0.00000	0.00000	0.00000	0.00000	0.00000	0.00000	0.00000	0.00000	0.00000	0.00000	0.00000	0.00000	0.00000	0.00458
Pesadero (El)	42.04	-5.74	0.00000	0.00000	0.00000	0.00000	0.00000	0.00000	0.00000	0.00000	0.00000	0.00000	0.00000	0.00000	0.00000	0.00000	0.00000
Petrolí. Cova de	40.17	0.10	0.00000	0.00000	0.00000	0.00002	0.00006	0.00054	0.00302	0.00223	0.00063	0.00552	0.00002	0.00000	0.00000	0.00000	0.00000
Pez. Cabeço do	38.25	-8.34	0.00001	0.00000	0.00000	0.00000	0.00000	0.00000	0.00000	0.00000	0.00000	0.00002	0.00433	0.00092	0.00000	0.00000	0.00000
Pialfor	41.89	0.11	0.00000	0.00000	0.00000	0.00000	0.00000	0.00000	0.00000	0.00000	0.00000	0.00000	0.00000	0.00000	0.00000	0.00095	0.00647
Pic de les Moreres	38.26	-0.82	0.00000	0.00000	0.00000	0.00000	0.00003	0.00027	0.00251	0.00268	0.00113	0.00019	0.00001	0.00000	0.00000	0.00000	0.00000
Pic dels Corbs	39.71	-0.27	0.00000	0.00000	0.00000	0.00000	0.00000	0.00000	0.00000	0.00000	0.00001	0.00044	0.00306	0.00627	0.00710	0.00857	0.00722
Picacho (El)	37.49	-2.23	0.00000	0.00000	0.00000	0.00000	0.00000	0.00000	0.00000	0.00000	0.00000	0.00022	0.00304	0.01409	0.00551	0.00014	0.00000
Picareiro. Lapa do	39.53	-8.65	0.00000	0.00000	0.00000	0.00000	0.00000	0.00000	0.00000	0.00000	0.00000	0.00000	0.00000	0.00000	0.00000	0.00000	0.00000
Pico (El)	41.79	-2.48	0.00000	0.00000	0.00000	0.00000	0.00000	0.00000	0.00000	0.00000	0.00000	0.00000	0.00000	0.00000	0.00000	0.00000	0.00000
Pico Buitre	40.89	-3.05	0.00000	0.00000	0.00000	0.00000	0.00000	0.00000	0.00000	0.00000	0.00000	0.00000	0.00000	0.00000	0.00040	0.00743	0.00961
Pico del Castro (El)	41.62	-4.27	0.00000	0.00000	0.00000	0.00000	0.00000	0.00000	0.00000	0.00000	0.00072	0.00504	0.00040	0.00000	0.00000	0.00000	0.00000
Pico Ramos	43.33	-3.12	0.00010	0.00088	0.00320	0.00041	0.00025	0.00138	0.00630	0.00381	0.00053	0.00002	0.00000	0.00000	0.00000	0.00000	0.00000
Pico Romero	41.60	-3.55	0.00000	0.00000	0.00000	0.00000	0.00000	0.00000	0.00000	0.00000	0.00067	0.00743	0.00589	0.00052	0.00000	0.00000	0.00000
Picos (Los)	40.00	-4.21	0.00000	0.00000	0.00000	0.00000	0.00000	0.00000	0.00562	0.01633	0.00003	0.00000	0.00000	0.00000	0.00000	0.00000	0.00000
Picuezo (El)	40.62	-4.97	0.00000	0.00000	0.00000	0.00000	0.00000	0.00004	0.00527	0.00028	0.00000	0.00000	0.00000	0.00000	0.00000	0.00000	0.00000
Pijotilla (La)	38.80	-6.66	0.00000	0.00000	0.00000	0.00000	0.00027	0.00716	0.02341	0.00724	0.00674	0.00143	0.00000	0.00000	0.00000	0.00000	0.00000
Pilas (Las)	37.15	-1.85	0.00000	0.00000	0.00000	0.00000	0.00000	0.00000	0.03623	0.01522	0.05765	0.00806	0.00001	0.00000	0.00000	0.00000	0.00000
Pileta. Cueva de la	36.69	-5.27	0.00000	0.00000	0.00021	0.00242	0.00315	0.00256	0.00010	0.00001	0.00100	0.00470	0.00056	0.00308	0.00238	0.00000	0.00000
Pinhal da Carneira	39.35	-8.93	0.00128	0.00043	0.00001	0.00010	0.00042	0.00245	0.00151	0.00017	0.00000	0.00000	0.00000	0.00000	0.00000	0.00000	0.00000
Pixarelles. Cova de les	41.99	2.40	0.00000	0.00000	0.00000	0.00000	0.00002	0.00010	0.00075	0.00139	0.00224	0.00270	0.00283	0.00281	0.00285	0.00479	0.00720
Plano del Pulido	41.14	-0.03	0.00312	0.00293	0.00000	0.00000	0.00000	0.00000	0.00000	0.00000	0.00000	0.00000	0.00000	0.00000	0.00000	0.00000	0.00000
Plansallosa	42.25	2.60	0.00116	0.00412	0.00025	0.00000	0.00000	0.00000	0.00000	0.00000	0.00000	0.00000	0.00000	0.00000	0.00000	0.00000	0.00000
Plaza (La)	41.53	-4.40	0.00000	0.00000	0.00000	0.00000	0.00000	0.00000	0.00000	0.00000	0.00000	0.00000	0.00000	0.00000	0.01752	0.00000	0.00000
Plaza de Armas (Puente Tablas) . La	37.81	-3.75	0.00000	0.00000	0.00000	0.00000	0.00000	0.00000	0.00000	0.00000	0.00000	0.00000	0.00269	0.00294	0.00000	0.00000	0.00007
Plaza de las Monjas	37.26	-6.95	0.00000	0.00000	0.00000	0.00000	0.00000	0.00000	0.00000	0.00000	0.00000	0.00000	0.00000	0.00000	0.00000	0.00000	0.00000
Plaza de Moros	39.85	-3.33	0.00000	0.00000	0.00000	0.00000	0.00000	0.00000	0.00000	0.00000	0.00000	0.00000	0.00000	0.00000	0.00000	0.00000	0.00000
Plaza del Castillo	41.40	-4.32	0.00000	0.00000	0.00000	0.00000	0.00000	0.00000	0.00000	0.00000	0.00000	0.00000	0.00000	0.00000	0.00000	0.00000	0.00000
Plaza Mayor 17	41.59	-4.82	0.00000	0.00000	0.00000	0.00000	0.00000	0.00000	0.00000	0.00000	0.00000	0.00000	0.00000	0.00000	0.00000	0.00000	0.00000
Plomo. Cabezo del	37.57	-1.30	0.00398	0.00352	0.00099	0.00003	0.00000	0.00000	0.00000	0.00000	0.00000	0.00000	0.00000	0.00000	0.00000	0.00000	0.00000
Poças de São Bento	38.25	-8.44	0.00000	0.00000	0.00000	0.00000	0.00000	0.00000	0.00000	0.00000	0.00000	0.00000	0.00000	0.00000	0.00000	0.00000	0.00000
Polovar. Cabezo del	38.61	-0.90	0.00000	0.00000	0.00000	0.00000	0.00000	0.00000	0.00000	0.00000	0.00000	0.00000	0.00007	0.00539	0.00241	0.00000	0.00000

Site	Lat	Lon	SPD of Iberian settlement sites at 200 year time slices (cal. BP)														
			6000-5800	5800-5600	5600-5400	5400-5200	5200-5000	5000-4800	4800-4600	4600-4400	4400-4200	4200-4000	4000-3800	3800-3600	3600-3400	3400-3200	3200-3000
Pompeya	41.19	-0.41	0.00000	0.00000	0.00000	0.00000	0.00000	0.00000	0.00000	0.00000	0.00000	0.00000	0.00000	0.00000	0.00000	0.00000	0.00000
Ponta da Passadeira	38.67	-9.04	0.00000	0.00004	0.01452	0.01881	0.01564	0.00657	0.00038	0.00000	0.00000	0.00000	0.00000	0.00000	0.00000	0.00000	0.00000
Pontal	38.40	-8.77	0.00003	0.00513	0.00001	0.00000	0.00000	0.00000	0.00000	0.00000	0.00000	0.00000	0.00000	0.00000	0.00000	0.00000	0.00000
Pontes (As)	43.36	-7.49	0.00000	0.00000	0.00115	0.00059	0.00000	0.00000	0.00000	0.00000	0.00000	0.00000	0.00000	0.00000	0.00000	0.00000	0.00000
Pontes do Marchil	37.03	-7.95	0.00000	0.00000	0.00000	0.00000	0.00000	0.00000	0.00000	0.00000	0.00000	0.00000	0.00000	0.00061	0.00341	0.00000	0.00000
Pontet	41.09	0.13	0.00067	0.00036	0.00007	0.00001	0.00000	0.00000	0.00000	0.00000	0.00000	0.00000	0.00000	0.00000	0.00000	0.00000	0.00000
Portarró	42.58	0.97	0.00000	0.00000	0.00000	0.00000	0.00000	0.00018	0.00023	0.00000	0.00000	0.00000	0.00000	0.00000	0.00000	0.00000	0.00000
Portecelo	41.95	-8.87	0.00000	0.00000	0.00000	0.00000	0.00000	0.00000	0.00000	0.00000	0.00000	0.00000	0.00000	0.00000	0.00000	0.00655	0.00101
Portes (Les)	42.10	1.51	0.00000	0.00000	0.00000	0.00000	0.00000	0.00000	0.00251	0.00470	0.00031	0.00070	0.00502	0.00003	0.00000	0.00445	0.01272
Porto das Carretas	38.38	-7.40	0.00000	0.00000	0.00000	0.00000	0.00004	0.00071	0.02128	0.00751	0.01952	0.00199	0.00000	0.00000	0.00000	0.00000	0.00000
Porto Marinho. Cabeço de	39.36	-8.94	0.00000	0.00000	0.00000	0.00000	0.00000	0.00000	0.00000	0.00000	0.00000	0.00154	0.00491	0.00084	0.00247	0.00157	0.00045
Possanco	38.40	-8.78	0.00000	0.00000	0.00000	0.00000	0.00000	0.00090	0.00033	0.00000	0.00000	0.00000	0.00000	0.00000	0.00000	0.00000	0.00000
Pousada (A)	42.85	-8.53	0.00000	0.00000	0.00131	0.00008	0.00000	0.00000	0.00000	0.00000	0.00000	0.00000	0.00000	0.00000	0.00000	0.00000	0.00000
Poyos del Molinillo	36.79	-3.90	0.00000	0.00000	0.00000	0.00000	0.00000	0.00000	0.00000	0.00000	0.00000	0.00010	0.00638	0.00000	0.00000	0.00000	0.00000
Pozas (Las)	41.43	-5.66	0.00000	0.00000	0.00000	0.00002	0.00323	0.00765	0.00248	0.00591	0.00283	0.00108	0.00014	0.00000	0.00000	0.00000	0.00000
Pozo. Abrigos del	38.24	-1.62	0.00000	0.00000	0.00000	0.00000	0.00000	0.00000	0.00000	0.00000	0.00000	0.00690	0.00042	0.00000	0.00000	0.00000	0.00000
Prado (El)	38.46	-1.32	0.00000	0.00000	0.00000	0.00298	0.01098	0.01357	0.02596	0.00837	0.00319	0.00118	0.00025	0.00002	0.00000	0.00000	0.00000
Prado do Inferno	43.46	-7.72	0.00000	0.00000	0.00000	0.00000	0.00004	0.00051	0.00326	0.00213	0.00032	0.00001	0.00000	0.00000	0.00000	0.00000	0.00000
Pragança	39.20	-9.05	0.00000	0.00000	0.00000	0.00000	0.00000	0.00000	0.00937	0.00755	0.00013	0.00000	0.00000	0.00000	0.00000	0.00000	0.00000
Praia da Foz 1	37.89	-8.80	0.00000	0.00000	0.00001	0.00012	0.00022	0.00057	0.00163	0.00178	0.00139	0.00073	0.00026	0.00006	0.00000	0.00000	0.00000
Praia da Oliveirinha	37.89	-8.80	0.00000	0.00000	0.00000	0.00000	0.00000	0.00000	0.00000	0.00000	0.00000	0.00000	0.00015	0.00560	0.00002	0.00000	0.00000
Praia do Forte Novo	37.06	-8.09	0.00000	0.00000	0.00083	0.00555	0.00596	0.00361	0.00504	0.00155	0.00002	0.00000	0.00000	0.00000	0.00000	0.00000	0.00000
Praia Ladeira	42.62	-8.86	0.00000	0.00000	0.00000	0.00000	0.00000	0.00000	0.00000	0.00002	0.00904	0.00728	0.00607	0.00000	0.00000	0.00000	0.00000
Praileaitz 1	43.28	-2.37	0.00000	0.00000	0.00000	0.00000	0.00000	0.00000	0.00000	0.00593	0.00000	0.00000	0.00000	0.00000	0.00000	0.00000	0.00000
Praileaitz 2	43.28	-2.37	0.00000	0.00000	0.00000	0.00000	0.00000	0.00000	0.00000	0.00000	0.00000	0.00000	0.00000	0.00000	0.00000	0.00000	0.00000
Prazo	41.07	-7.24	0.00000	0.00000	0.00572	0.00522	0.00449	0.00340	0.00000	0.00000	0.00000	0.00000	0.00000	0.00000	0.00000	0.00000	0.00000
Prunera (La)	42.19	2.52	0.00000	0.00000	0.00000	0.00027	0.00126	0.00466	0.00012	0.00000	0.00000	0.00000	0.00019	0.00448	0.00096	0.00000	0.00000
Puente de la Aldehuela	40.31	-3.58	0.00000	0.00000	0.00000	0.00000	0.00000	0.00000	0.00000	0.00000	0.00000	0.00000	0.00000	0.00000	0.00000	0.00000	0.00026
Puig Mascaró	42.02	3.17	0.00000	0.00000	0.00000	0.00000	0.00004	0.00080	0.00343	0.00081	0.00002	0.00000	0.00000	0.00000	0.00000	0.00000	0.00000
Puig Roig del Roget	41.16	0.73	0.00000	0.00000	0.00000	0.00000	0.00000	0.00000	0.00000	0.00000	0.00000	0.00000	0.00000	0.00000	0.00001	0.00490	0.00260
Punta de los Gavilanes	37.56	-1.28	0.00000	0.00000	0.00000	0.00000	0.00000	0.00000	0.00000	0.00000	0.00926	0.03515	0.08682	0.09431	0.02432	0.00026	0.00107
Punta de Muros	43.36	-8.50	0.00000	0.00000	0.00000	0.00000	0.00000	0.00000	0.00000	0.00000	0.00000	0.00000	0.00000	0.00000	0.00000	0.00000	0.00000
Punta Farisa	41.50	0.38	0.00000	0.00000	0.00000	0.00000	0.00000	0.00000	0.00000	0.00000	0.00000	0.00000	0.00005	0.00237	0.00329	0.00001	0.00000
Puntal dels Llops	39.71	-0.54	0.00000	0.00000	0.00000	0.00000	0.00000	0.00000	0.00000	0.00000	0.00000	0.00000	0.00000	0.00002	0.00629	0.00000	0.00000

Site	Lat	Lon	SPD of Iberian settlement sites at 200 year time slices (cal. BP)														
			6000-5800	5800-5600	5600-5400	5400-5200	5200-5000	5000-4800	4800-4600	4600-4400	4400-4200	4200-4000	4000-3800	3800-3600	3600-3400	3400-3200	3200-3000
Puntassa. Cova	40.71	0.08	0.00000	0.00000	0.00039	0.00324	0.00356	0.00169	0.00001	0.00000	0.00000	0.00000	0.00000	0.00000	0.00000	0.00000	0.00000
Puy Águila	42.28	-1.39	0.00000	0.00000	0.00000	0.00000	0.00000	0.00000	0.00000	0.00000	0.00000	0.00000	0.00014	0.01470	0.00000	0.00000	0.00000
Puyascada	42.46	0.31	0.00000	0.00000	0.00038	0.00304	0.00353	0.00035	0.00000	0.00000	0.00000	0.00000	0.00000	0.00000	0.00000	0.00000	0.00000
Queimada. Quinta da	37.13	-8.66	0.00000	0.00000	0.00000	0.00000	0.00000	0.00000	0.00000	0.00000	0.00000	0.00000	0.00000	0.00000	0.00000	0.00000	0.00000
Quintanar. Morra del	39.02	-2.46	0.00000	0.00000	0.00000	0.00000	0.00000	0.00000	0.00026	0.00378	0.01800	0.02822	0.05902	0.04357	0.02281	0.00060	0.00007
Rabas (Las)	42.95	-4.13	0.00000	0.00000	0.00000	0.00000	0.00000	0.00000	0.00000	0.00000	0.00000	0.00000	0.00000	0.00000	0.00000	0.00000	0.00000
Raboses (Les)	39.69	-0.35	0.00000	0.00000	0.00000	0.00000	0.00000	0.00000	0.00000	0.00000	0.00000	0.00029	0.00741	0.00631	0.00045	0.00425	0.00007
Ramalha 2	38.67	-9.17	0.00208	0.00061	0.00001	0.00000	0.00000	0.00000	0.00000	0.00000	0.00000	0.00000	0.00000	0.00000	0.00000	0.00000	0.00000
Rambla Castellarda	39.67	-0.75	0.00000	0.00000	0.00000	0.00000	0.00000	0.00000	0.00606	0.00001	0.00000	0.00000	0.00000	0.00000	0.00000	0.00000	0.00000
Rambla de Legunova	41.35	-0.94	0.00000	0.00000	0.00000	0.00316	0.00468	0.00001	0.00000	0.00000	0.00000	0.00000	0.00000	0.00000	0.00000	0.00000	0.00000
Rapido. Quinta do	41.50	-8.63	0.00000	0.00000	0.00000	0.00000	0.00000	0.00000	0.00000	0.00000	0.00000	0.00000	0.00000	0.00049	0.00308	0.00000	0.00000
Raso (El)	40.19	-5.36	0.00000	0.00000	0.00000	0.00000	0.00000	0.00000	0.00000	0.00000	0.00000	0.00000	0.00000	0.00005	0.00061	0.00256	0.00266
Ratinhos. Castro dos	38.20	-7.49	0.00000	0.00000	0.00000	0.00000	0.00000	0.00000	0.00000	0.00000	0.00000	0.00000	0.00000	0.00000	0.00000	0.00008	0.00180
Rebanadilla (La)	36.72	-4.55	0.00000	0.00000	0.00000	0.00000	0.00000	0.00000	0.00000	0.00000	0.00000	0.00000	0.00000	0.00000	0.00000	0.00000	0.00006
Recambra. Cova de la	38.98	-0.22	0.00001	0.00000	0.00000	0.00000	0.00000	0.00001	0.00048	0.00136	0.00242	0.00198	0.00078	0.00013	0.00000	0.00000	0.00000
Recarea	42.87	-9.05	0.00000	0.00000	0.00000	0.00000	0.00000	0.00000	0.00000	0.00000	0.00000	0.00000	0.00000	0.00000	0.00000	0.00000	0.00000
Recouso	43.04	-8.38	0.00000	0.00000	0.00000	0.00000	0.00000	0.00000	0.00000	0.00000	0.00000	0.00000	0.00000	0.00000	0.00000	0.00000	0.00000
Recuenco (El)	39.76	-2.42	0.00000	0.00000	0.00000	0.00000	0.00000	0.00000	0.00000	0.00015	0.00263	0.00704	0.01059	0.00455	0.00551	0.00098	0.00004
Reina Mora. Cueva de la	41.19	-2.32	0.00005	0.00059	0.00500	0.00394	0.00251	0.00059	0.00000	0.00000	0.00000	0.00000	0.00000	0.00000	0.00000	0.00000	0.00013
Reiro (O)	43.30	-8.57	0.00000	0.00000	0.00000	0.00000	0.00000	0.00000	0.00000	0.00000	0.00000	0.00000	0.00000	0.00000	0.00000	0.00000	0.00000
Renke Norte (La)	42.69	-2.80	0.00549	0.00090	0.00325	0.01521	0.01754	0.01933	0.00688	0.00227	0.00016	0.00000	0.00000	0.00000	0.00000	0.00000	0.00000
Requeán	42.96	-7.98	0.00000	0.00000	0.00000	0.00001	0.00006	0.00081	0.00733	0.00141	0.00009	0.00000	0.00000	0.00000	0.00000	0.00000	0.00000
Retamar (El)	36.53	-6.16	0.00000	0.00000	0.00000	0.00000	0.00000	0.00000	0.00000	0.00000	0.00000	0.00000	0.00000	0.00000	0.00000	0.00000	0.00000
Ria De Guernica	43.32	-2.68	0.00000	0.00737	0.00142	0.00000	0.00000	0.00000	0.00000	0.00066	0.00453	0.00000	0.00000	0.00000	0.00000	0.00000	0.00000
Ribeira de Alcantarilha	37.13	-8.35	0.00000	0.00000	0.00000	0.00000	0.00000	0.00000	0.00000	0.00000	0.00000	0.00000	0.00000	0.00000	0.00000	0.00000	0.00000
Riera Masarac	42.33	2.93	0.00000	0.00000	0.00000	0.00000	0.00000	0.00002	0.00074	0.00186	0.00262	0.00153	0.00039	0.00004	0.00000	0.00000	0.00000
Riera. Cueva de la	43.43	-4.85	0.00000	0.00000	0.00000	0.00000	0.00000	0.00000	0.00000	0.00000	0.00000	0.00000	0.00000	0.00000	0.00000	0.00000	0.00000
Riereta 37-37bis. Carrer de la	41.38	2.17	0.00000	0.00000	0.00009	0.00388	0.00476	0.00108	0.00000	0.00000	0.00000	0.00000	0.00193	0.00222	0.00000	0.00000	0.00072
Rincón de Olvera	38.13	-3.29	0.00000	0.00000	0.00000	0.00000	0.00000	0.00000	0.00000	0.00000	0.00000	0.00006	0.00121	0.00885	0.00647	0.00123	0.00105
Roca Chica	36.62	-4.50	0.00000	0.00000	0.00000	0.00000	0.00000	0.00000	0.00000	0.00000	0.00000	0.00000	0.00000	0.00000	0.00000	0.00000	0.00000
Roca Roja	40.09	0.11	0.00000	0.00000	0.00000	0.00000	0.00000	0.00000	0.00000	0.00000	0.00000	0.00003	0.00050	0.00253	0.00262	0.00017	0.00000
Rocha Branca	37.18	-8.46	0.00000	0.00000	0.00000	0.00000	0.00000	0.00000	0.00000	0.00000	0.00000	0.00000	0.00466	0.00050	0.00000	0.00321	0.00756
Rocha do Vigio 1	38.38	-7.40	0.00000	0.00000	0.00000	0.00000	0.00000	0.00000	0.00000	0.00000	0.00000	0.00000	0.00000	0.00000	0.00000	0.00000	0.00000

Site	Lat	Lon	SPD of Iberian settlement sites at 200 year time slices (cal. BP)													
			6000-5800	5800-5600	5600-5400	5400-5200	5200-5000	5000-4800	4800-4600	4600-4400	4400-4200	4200-4000	4000-3800	3800-3600	3600-3400	3400-3200	3200-3000
Rodiles (Los)	40.90	-1.78	0.00000	0.00000	0.00000	0.00000	0.00000	0.00000	0.00000	0.00000	0.00000	0.00000	0.00000	0.00000	0.00000	0.00000	0.00000
Romarigães	41.87	-8.64	0.00000	0.00000	0.00000	0.00000	0.00000	0.00000	0.00000	0.00000	0.00000	0.00000	0.00000	0.00000	0.00000	0.00000	0.00000
Romariz	40.94	-8.46	0.00000	0.00000	0.00000	0.00000	0.00000	0.00000	0.00000	0.00000	0.00000	0.00000	0.00000	0.00000	0.00000	0.00000	0.00000
Romeros (Los)	39.15	-3.30	0.00000	0.00000	0.00000	0.00000	0.00000	0.00000	0.00000	0.00000	0.00038	0.00299	0.00640	0.00489	0.00360	0.00069	0.00006
Ronda (Casco urbano)	36.74	-5.16	0.00000	0.00000	0.00000	0.00000	0.00000	0.00000	0.00000	0.00000	0.00000	0.00000	0.00000	0.00000	0.00000	0.00000	0.00006
Roques del Sarró	41.67	0.63	0.00000	0.00002	0.00537	0.00152	0.00026	0.00000	0.00220	0.00825	0.00344	0.00032	0.00000	0.00075	0.00515	0.00514	0.00192
Ros. Font del	42.09	1.85	0.00000	0.00000	0.00000	0.00000	0.00000	0.00000	0.00000	0.00000	0.00000	0.00000	0.00000	0.00000	0.00000	0.00000	0.00000
Rosas. Quinta das	40.68	-7.47	0.00000	0.00000	0.00000	0.00000	0.00000	0.00000	0.00000	0.00000	0.00000	0.00000	0.00000	0.00000	0.00000	0.00000	0.00006
Rotura	38.54	-8.92	0.00000	0.00000	0.00000	0.00000	0.00000	0.00000	0.01014	0.00698	0.00722	0.00569	0.00000	0.00000	0.00000	0.00000	0.00000
Royo (El)	41.91	-2.69	0.00000	0.00000	0.00000	0.00000	0.00000	0.00000	0.00000	0.00000	0.00000	0.00000	0.00000	0.00000	0.00000	0.00000	0.00000
Rozas (As)	42.57	-8.56	0.00241	0.00132	0.00004	0.00000	0.00000	0.00000	0.00084	0.00000	0.00000	0.00000	0.00000	0.00000	0.00000	0.00000	0.00000
Rubia. Cueva	42.75	-4.25	0.00006	0.00571	0.00008	0.00339	0.00428	0.00010	0.00000	0.00000	0.00000	0.00000	0.00000	0.00000	0.00610	0.00000	0.00000
Rubira 12. Calle	37.68	-1.70	0.00000	0.00000	0.00000	0.00000	0.00000	0.00000	0.00000	0.00012	0.00197	0.00351	0.00121	0.00005	0.00000	0.00000	0.00000
Salas 1	38.11	-7.64	0.00000	0.00000	0.00047	0.00981	0.01217	0.00614	0.00392	0.00210	0.00014	0.00000	0.00000	0.00000	0.00000	0.00000	0.00000
Salemas	38.87	-9.20	0.00000	0.00000	0.00333	0.00000	0.00000	0.00000	0.00000	0.00000	0.00000	0.00000	0.00000	0.00000	0.00000	0.00000	0.00000
Saltés	37.21	-6.98	0.00000	0.00000	0.00000	0.00000	0.00000	0.00000	0.00000	0.00000	0.00000	0.00000	0.00932	0.00645	0.00000	0.00000	0.00000
Salud (La)	37.72	-1.64	0.00000	0.00000	0.00000	0.00008	0.00032	0.00193	0.00220	0.00047	0.00001	0.00000	0.00000	0.00000	0.00000	0.00000	0.00000
Samitiel	42.27	-0.73	0.00011	0.00000	0.00000	0.00000	0.00000	0.00000	0.00000	0.00000	0.00000	0.00000	0.00000	0.00000	0.00000	0.00000	0.00000
Samouqueira I	37.87	-8.80	0.00242	0.00080	0.00000	0.00000	0.00000	0.00000	0.00000	0.00000	0.00000	0.00000	0.00000	0.00000	0.00000	0.00000	0.00000
San Blas	38.55	-7.29	0.00000	0.00000	0.00000	0.00490	0.00544	0.01070	0.00032	0.01462	0.00679	0.00165	0.00000	0.00000	0.00000	0.00000	0.00000
San Chuis	43.23	-6.60	0.00000	0.00000	0.00000	0.00009	0.00148	0.00637	0.00000	0.00000	0.00000	0.00000	0.00000	0.00000	0.00000	0.00000	0.00000
San Cibrán de Lás	42.36	-8.03	0.00000	0.00000	0.00000	0.00000	0.00000	0.00000	0.00000	0.00000	0.00000	0.00000	0.00000	0.00000	0.00000	0.00000	0.00000
San Cristóbal	42.60	-2.61	0.00471	0.01099	0.00002	0.00280	0.00514	0.00348	0.03226	0.03806	0.00149	0.00033	0.00005	0.00000	0.00502	0.00485	0.00000
San Jorge	40.99	-0.85	0.00000	0.00000	0.00000	0.00000	0.00000	0.00000	0.00000	0.00000	0.00000	0.00000	0.00000	0.00000	0.00000	0.00000	0.00003
San Juan. Cerro de	37.29	-6.05	0.00000	0.00000	0.00000	0.00000	0.00000	0.00000	0.00000	0.00000	0.00000	0.00252	0.03902	0.01806	0.00000	0.00000	0.00000
San Miguel de Irura	43.17	-2.07	0.00000	0.00000	0.00000	0.00000	0.00000	0.00024	0.00002	0.00000	0.00736	0.00344	0.00000	0.00000	0.00000	0.00000	0.00000
San Pelayo	42.04	-4.82	0.00000	0.00000	0.00000	0.00000	0.00000	0.00000	0.00000	0.00000	0.00000	0.00000	0.00000	0.00000	0.00000	0.00000	0.00000
San Pelayo. Cerro de	40.79	-5.57	0.00000	0.00000	0.00000	0.00000	0.00000	0.00000	0.00000	0.00000	0.00000	0.00000	0.00000	0.00000	0.00008	0.00142	0.00275
San Vicente. Cerro de	40.96	-5.67	0.00000	0.00000	0.00000	0.00000	0.00000	0.00000	0.00000	0.00000	0.00000	0.00000	0.00000	0.00000	0.00000	0.00000	0.00000
Sant Jaume-Mas d´en Serra	40.57	0.52	0.00000	0.00000	0.00000	0.00000	0.00000	0.00000	0.00000	0.00000	0.00000	0.00000	0.00000	0.00000	0.00000	0.00000	0.00000
Sant Llorenç. Cova de	41.25	1.83	0.00000	0.00067	0.00005	0.00000	0.00000	0.00000	0.00000	0.00034	0.00208	0.00000	0.00000	0.00000	0.00000	0.00000	0.00000
Sant Martí d´Empúries	42.14	3.12	0.00000	0.00000	0.00000	0.00000	0.00000	0.00000	0.00000	0.00000	0.00000	0.00000	0.00000	0.00000	0.00001	0.00252	0.00411
Sant Martí. Cova de	38.45	-0.63	0.00000	0.00000	0.00000	0.00000	0.00000	0.00000	0.00000	0.00000	0.00000	0.00000	0.00000	0.00000	0.00000	0.00000	0.00000
Sant Miquel d´Olèrdola	41.30	1.71	0.00000	0.00000	0.00000	0.00000	0.00000	0.00000	0.00129	0.00503	0.00031	0.00000	0.00000	0.00000	0.00000	0.00000	0.00000

Site	Lat	Lon	SPD of Iberian settlement sites at 200 year time slices (cal. BP)														
			6000-5800	5800-5600	5600-5400	5400-5200	5200-5000	5000-4800	4800-4600	4600-4400	4400-4200	4200-4000	4000-3800	3800-3600	3600-3400	3400-3200	3200-3000
Santa Catarina	41.43	-8.27	0.00000	0.00000	0.00000	0.00000	0.00000	0.00000	0.00000	0.00000	0.00000	0.00000	0.00000	0.00000	0.00000	0.00000	0.00025
Santa Coloma. Cueva de	42.84	-2.89	0.00000	0.00000	0.00000	0.00000	0.00000	0.00000	0.00000	0.00000	0.00000	0.00000	0.00000	0.00000	0.00000	0.00000	0.00000
Santa Comba	43.55	-8.29	0.00000	0.00000	0.00000	0.00000	0.00000	0.00000	0.00000	0.00000	0.00000	0.00000	0.00000	0.00000	0.00000	0.00000	0.00000
Santa Eulàlia	42.40	1.13	0.00000	0.00000	0.00000	0.00000	0.00000	0.00000	0.00000	0.00000	0.00000	0.00000	0.00000	0.00000	0.00000	0.00000	0.00000
Santa Justa. Castelo de	37.42	-7.70	0.00215	0.00111	0.00047	0.00393	0.00607	0.01020	0.01301	0.01649	0.01654	0.00736	0.00152	0.00015	0.00000	0.00000	0.00000
Santa Llúcia	40.26	0.27	0.00000	0.00000	0.00000	0.00000	0.00000	0.00000	0.00000	0.00000	0.00000	0.00000	0.00000	0.00000	0.00000	0.00000	0.00000
Santa Luzia	40.70	-7.92	0.00000	0.00000	0.00000	0.00000	0.00000	0.00000	0.00000	0.00000	0.00000	0.00000	0.00000	0.00003	0.00028	0.00338	0.01560
Santa Maira. Coves de	38.73	-0.20	0.00000	0.00000	0.00000	0.00000	0.00000	0.00000	0.00000	0.00000	0.00000	0.00000	0.00000	0.00000	0.00000	0.00000	0.00000
Santa María del Retamar	39.06	-3.03	0.00000	0.00000	0.00000	0.00000	0.00000	0.00000	0.00000	0.00000	0.00000	0.00014	0.00752	0.00445	0.00000	0.00000	0.00000
Santa Olaia	40.17	-8.72	0.00000	0.00000	0.00000	0.00000	0.00000	0.00000	0.00000	0.00000	0.00000	0.00000	0.00000	0.00000	0.00000	0.00000	0.00233
Santa Vitória	39.00	-7.09	0.00003	0.00013	0.00071	0.00145	0.00160	0.00170	0.01487	0.01014	0.00340	0.00559	0.00301	0.00053	0.00007	0.00000	0.00000
Santa. Cova	38.80	-0.89	0.00339	0.00278	0.00017	0.00016	0.00017	0.00021	0.00027	0.00031	0.00035	0.00038	0.00041	0.00043	0.00044	0.00044	0.00055
Santiago. Castro de	40.64	-7.48	0.00000	0.00000	0.00000	0.00000	0.00007	0.00695	0.00280	0.00000	0.00000	0.00000	0.00000	0.00000	0.00000	0.00000	0.00420
Santiago. Cueva Chica de	38.03	-5.92	0.00294	0.00195	0.00004	0.00000	0.00000	0.00000	0.00000	0.00000	0.00000	0.00000	0.00000	0.00000	0.00000	0.00000	0.00000
Santiagomendi	43.28	-1.93	0.00000	0.00000	0.00000	0.00000	0.00000	0.00000	0.00000	0.00000	0.00000	0.00000	0.00000	0.00000	0.00000	0.00000	0.00000
Santimamiñe	43.34	-2.63	0.00700	0.00828	0.00000	0.00000	0.00000	0.00000	0.00000	0.00000	0.00000	0.00690	0.00042	0.00000	0.00000	0.00000	0.00020
Santinha	41.63	-8.34	0.00000	0.00000	0.00000	0.00000	0.00000	0.00000	0.00000	0.00000	0.00000	0.00000	0.00000	0.00000	0.00000	0.00000	0.00862
Santo Estevão	41.72	-8.64	0.00000	0.00000	0.00000	0.00000	0.00000	0.00000	0.00000	0.00000	0.00000	0.00000	0.00000	0.00000	0.00000	0.00000	0.00000
São Brás 1	37.90	-7.62	0.00000	0.00000	0.00017	0.00475	0.00810	0.00420	0.00045	0.00007	0.00000	0.00000	0.00000	0.00000	0.00000	0.00000	0.00000
São Bráz	41.27	-8.42	0.00000	0.00000	0.00000	0.00000	0.00002	0.00008	0.00080	0.00147	0.00198	0.00162	0.00083	0.00024	0.00003	0.00000	0.00000
São João de Rei	41.62	-8.29	0.00000	0.00000	0.00000	0.00000	0.00000	0.00000	0.00000	0.00000	0.00000	0.00000	0.00000	0.00000	0.00000	0.00000	0.00000
São Julião	38.93	-9.42	0.00000	0.00000	0.00000	0.00000	0.00000	0.00000	0.00000	0.00000	0.00000	0.00000	0.00000	0.00000	0.00000	0.00000	0.00000
São Julião de Caldelas	41.69	-8.39	0.00000	0.00000	0.00000	0.00000	0.00000	0.00000	0.00000	0.00000	0.00248	0.00171	0.00000	0.00000	0.00003	0.01672	0.04622
São Lourenço	41.56	-8.77	0.00000	0.00000	0.00000	0.00000	0.00000	0.00000	0.00000	0.00000	0.00000	0.00000	0.00000	0.00000	0.00000	0.00000	0.00000
São Lourenço	41.72	-7.42	0.00001	0.00000	0.00000	0.00000	0.00000	0.00009	0.00234	0.00000	0.00000	0.00000	0.00000	0.00000	0.00000	0.00000	0.00000
São Pedro	38.65	-7.55	0.00000	0.00000	0.00000	0.00018	0.00069	0.00324	0.03617	0.00574	0.00096	0.00003	0.00000	0.00000	0.00000	0.00000	0.00000
São Pedro de Canaferrim	38.79	-9.39	0.00000	0.00000	0.00000	0.00000	0.00000	0.00000	0.00000	0.00000	0.00000	0.00000	0.00000	0.00000	0.00000	0.00000	0.00000
São Romão. Cabeço do Castro de	40.39	-7.70	0.00000	0.00000	0.00000	0.00000	0.00000	0.00000	0.00000	0.00000	0.00000	0.00000	0.00000	0.00000	0.00000	0.00018	0.01323
Sardo de Boí 2	42.55	0.91	0.00000	0.00000	0.00000	0.00028	0.00652	0.00023	0.00000	0.00000	0.00000	0.00000	0.00000	0.00000	0.00000	0.00000	0.00000
Sardo de Boí. Cova del	42.55	0.91	0.00922	0.01203	0.01166	0.01069	0.01000	0.00085	0.00683	0.00248	0.00000	0.00000	0.00000	0.00000	0.00000	0.00000	0.00000
Sarradé. Cova de	42.56	0.90	0.00000	0.00000	0.00000	0.00000	0.00000	0.00000	0.00000	0.00095	0.00220	0.00000	0.00000	0.00000	0.00000	0.00000	0.00000
Sarsa. Cova de la	38.76	-0.58	0.00000	0.00000	0.00000	0.00147	0.00433	0.00000	0.00079	0.00395	0.00000	0.00000	0.00045	0.00002	0.00000	0.00000	0.00000

Site	Lat	Lon	SPD of Iberian settlement sites at 200 year time slices (cal. BP)														
			6000-5800	5800-5600	5600-5400	5400-5200	5200-5000	5000-4800	4800-4600	4600-4400	4400-4200	4200-4000	4000-3800	3800-3600	3600-3400	3400-3200	3200-3000
Seada. Castelo da	39.72	-8.21	0.00000	0.00000	0.00000	0.00000	0.00000	0.00000	0.00000	0.00000	0.00000	0.00000	0.00000	0.00000	0.00000	0.00039	0.00583
Segóvia	38.97	-7.11	0.00000	0.00000	0.00000	0.00000	0.00000	0.00000	0.00000	0.00000	0.00000	0.00000	0.00000	0.00000	0.00000	0.00000	0.00014
Sellado. Cabezo	41.17	-0.20	0.00000	0.00000	0.00000	0.00000	0.00000	0.00000	0.00000	0.00001	0.00043	0.00255	0.00693	0.01174	0.00002	0.00747	0.00000
Senhora da Guia	40.76	-8.09	0.00000	0.00000	0.00000	0.00000	0.00000	0.00000	0.00000	0.00000	0.00000	0.00000	0.00000	0.00000	0.00000	0.00002	0.00024
Serra (La)	42.12	2.46	0.00000	0.00000	0.00000	0.00000	0.00000	0.00000	0.00000	0.00000	0.00000	0.00000	0.00000	0.00000	0.00000	0.00000	0.00069
Serra Grossa	38.36	-0.45	0.00000	0.00000	0.00000	0.00000	0.00000	0.00000	0.00002	0.00044	0.00324	0.00305	0.00045	0.00000	0.00000	0.00000	0.00000
Serrat del Pont. Bauma del	42.25	2.60	0.00004	0.00005	0.00008	0.00680	0.01577	0.01983	0.01014	0.00813	0.00594	0.00308	0.00356	0.00356	0.00223	0.00314	0.00078
Setefilla. La Mesa de	37.73	-5.49	0.00000	0.00000	0.00000	0.00000	0.00000	0.00000	0.00000	0.00000	0.00000	0.00035	0.00435	0.00750	0.00088	0.00067	0.01703
Silla del Moro	36.80	-5.25	0.00000	0.00000	0.00000	0.00000	0.00000	0.00868	0.00000	0.00000	0.00000	0.00000	0.00000	0.00000	0.00000	0.00000	0.00000
Sima del Ruidor	40.28	-1.02	0.00000	0.00000	0.00000	0.00000	0.00000	0.00000	0.00000	0.00000	0.00000	0.00000	0.00031	0.02113	0.00386	0.01582	0.00213
Sola	41.58	-8.42	0.00001	0.00000	0.00000	0.00000	0.00000	0.00007	0.00277	0.00332	0.00095	0.00006	0.00010	0.01146	0.01775	0.00038	0.00002
Solacueva de Lakozmonte	42.87	-2.94	0.00000	0.00000	0.00000	0.00000	0.00000	0.00000	0.00000	0.00003	0.00097	0.00375	0.00230	0.00018	0.00000	0.00000	0.00000
Solana (La)	40.42	-5.79	0.00000	0.00000	0.00000	0.00000	0.00000	0.00000	0.00153	0.00531	0.00000	0.00000	0.00000	0.00000	0.00000	0.00000	0.00000
Sorbán	42.30	-1.98	0.00000	0.00000	0.00000	0.00000	0.00000	0.00000	0.00000	0.00000	0.00000	0.00000	0.00000	0.00000	0.00000	0.00000	0.00000
Sorrera (La)	41.65	2.24	0.00000	0.00000	0.00000	0.00000	0.00000	0.00000	0.00000	0.00000	0.00000	0.00000	0.00027	0.00331	0.00231	0.00001	0.00000
Soto de Medinilla	41.68	-4.71	0.00000	0.00000	0.00000	0.00000	0.00000	0.00000	0.00000	0.00000	0.00000	0.00000	0.00000	0.00000	0.00000	0.00000	0.00029
Soto de Tovilla	41.60	-4.52	0.00000	0.00000	0.00000	0.00000	0.00000	0.00000	0.00139	0.00460	0.00000	0.00000	0.00000	0.00000	0.00000	0.00000	0.00000
Tabayá (El)	38.33	-0.72	0.00000	0.00000	0.00000	0.00000	0.00000	0.00000	0.00000	0.00000	0.00000	0.00000	0.00134	0.00206	0.00425	0.00000	0.00000
Tàbegues. Cova de les	40.40	0.08	0.00000	0.00000	0.00000	0.00297	0.00656	0.00000	0.00000	0.00000	0.00000	0.00000	0.00000	0.00000	0.00000	0.00000	0.00000
Tapada da Ajuda	38.71	-9.19	0.00000	0.00000	0.00000	0.00000	0.00000	0.00000	0.00000	0.00000	0.00000	0.00000	0.00001	0.01875	0.00679	0.00488	0.01559
Tapado da Caldeira	41.17	-8.05	0.00000	0.00000	0.00000	0.00000	0.00000	0.00000	0.00000	0.00000	0.00000	0.00000	0.00000	0.00009	0.00948	0.00337	0.00535
Tarajal (El)	36.85	-2.20	0.00000	0.00000	0.00000	0.00000	0.00000	0.00019	0.03116	0.03873	0.01070	0.00421	0.00003	0.00000	0.00000	0.00000	0.00000
Tarragona	41.12	1.26	0.00000	0.00000	0.00000	0.00000	0.00000	0.00000	0.00000	0.00000	0.00000	0.00000	0.00000	0.00000	0.00000	0.00000	0.00000
Tarrerón	43.22	-3.44	0.00000	0.00000	0.00000	0.00000	0.00000	0.00000	0.00000	0.00000	0.00000	0.00000	0.00000	0.00000	0.00000	0.00000	0.00000
Terlinques	38.60	-0.90	0.00000	0.00000	0.00000	0.00000	0.00000	0.00000	0.00005	0.00051	0.00317	0.03420	0.04358	0.02909	0.02231	0.00164	0.00013
Terrera del Reloj	37.60	-3.01	0.00000	0.00000	0.00000	0.00000	0.00000	0.00000	0.00000	0.00000	0.00000	0.00000	0.00070	0.01106	0.00009	0.00000	0.00000
Terrera Ventura	37.04	-2.40	0.00102	0.00100	0.00374	0.01431	0.01864	0.02473	0.05035	0.02829	0.00481	0.00027	0.00013	0.00227	0.00764	0.00053	0.00000
Tesoro. Cerro del	37.53	-2.17	0.00000	0.00000	0.00000	0.00000	0.00000	0.00000	0.00000	0.00000	0.00000	0.00001	0.00020	0.00127	0.00280	0.00099	0.00017
Teta (La)	40.42	-5.62	0.00000	0.00000	0.00000	0.00000	0.00001	0.00590	0.00050	0.00377	0.00236	0.00005	0.00000	0.00000	0.00000	0.00000	0.00000
Tío Melón. Rambla del	37.56	-2.86	0.00000	0.00000	0.00000	0.00000	0.00000	0.00000	0.00000	0.00124	0.01194	0.00024	0.00000	0.00000	0.00000	0.00000	0.00000
Tira del Lienzo	37.79	-1.49	0.00000	0.00000	0.00000	0.00000	0.00000	0.00000	0.01330	0.00470	0.00000	0.00302	0.01184	0.02369	0.00000	0.00000	0.00000
Tito Bustillo	43.46	-5.06	0.00000	0.00000	0.00000	0.00000	0.00000	0.00003	0.00395	0.00003	0.00000	0.00003	0.00642	0.00003	0.00000	0.00000	0.00000
Titulcia	40.14	-3.56	0.00000	0.00000	0.00000	0.00000	0.00000	0.00000	0.00000	0.00000	0.00000	0.00000	0.00000	0.00000	0.00000	0.00000	0.00000

Site	Lat	Lon	SPD of Iberian settlement sites at 200 year time slices (cal. BP)														
			6000-5800	5800-5600	5600-5400	5400-5200	5200-5000	5000-4800	4800-4600	4600-4400	4400-4200	4200-4000	4000-3800	3800-3600	3600-3400	3400-3200	3200-3000
Toll. Cova del	41.81	2.14	0.01524	0.00319	0.00003	0.00051	0.00104	0.00237	0.00161	0.00113	0.00270	0.00311	0.00516	0.01203	0.00202	0.00000	0.00000
Tolmos (Los)	41.37	-3.08	0.00000	0.00000	0.00000	0.00000	0.00000	0.00000	0.00000	0.00000	0.00000	0.00088	0.01033	0.02626	0.01152	0.00550	0.00356
Toral 3	43.40	-4.72	0.00000	0.00000	0.00226	0.00000	0.00000	0.00000	0.00000	0.00000	0.00000	0.00000	0.00000	0.00000	0.00000	0.00000	0.00000
Toro. Cueva del	36.96	-4.54	0.00769	0.00341	0.00535	0.00042	0.00023	0.00040	0.00326	0.00245	0.00045	0.00002	0.00000	0.00006	0.00097	0.00297	0.00510
Torojones (Los)	41.48	-3.19	0.00000	0.00000	0.00000	0.00000	0.00000	0.00000	0.00000	0.00000	0.00003	0.00157	0.00437	0.00067	0.00000	0.00000	0.00000
Toros. Cueva de los	40.53	-0.44	0.00000	0.00000	0.00000	0.00000	0.00000	0.00000	0.00041	0.00347	0.00299	0.00013	0.00000	0.00000	0.00000	0.00000	0.00000
Torraza (La)	41.82	0.07	0.00000	0.00000	0.00000	0.00000	0.00000	0.00000	0.00000	0.00000	0.00000	0.00000	0.00000	0.00000	0.00000	0.00520	0.00205
Torrazas (Las)	41.04	-0.19	0.00000	0.00000	0.00000	0.00000	0.00000	0.00000	0.00000	0.00000	0.00000	0.00000	0.00000	0.00000	0.00504	0.00005	0.00000
Torre de Codes (La)	41.07	-2.17	0.00000	0.00000	0.00000	0.00000	0.00000	0.00000	0.00000	0.00000	0.00000	0.00000	0.00000	0.00000	0.00000	0.00000	0.00000
Torre do Esporão	38.39	-7.56	0.00000	0.00000	0.00000	0.00000	0.00000	0.00000	0.00068	0.00530	0.00066	0.00000	0.00000	0.00000	0.00000	0.00000	0.00000
Torrelló	39.99	-0.19	0.00000	0.00000	0.00000	0.00000	0.00000	0.00000	0.00000	0.00000	0.00000	0.00000	0.00002	0.00144	0.00830	0.00071	0.00000
Torrelló del Boverot	39.97	-0.15	0.00000	0.00000	0.00000	0.00000	0.00000	0.00000	0.00000	0.00000	0.00000	0.00000	0.00000	0.00000	0.00000	0.00000	0.00219
Torroso	42.20	-8.63	0.00000	0.00000	0.00000	0.00000	0.00000	0.00000	0.00000	0.00000	0.00000	0.00001	0.00041	0.00593	0.01055	0.00298	0.00345
Toscanos	36.73	-4.12	0.00000	0.00000	0.00000	0.00000	0.00000	0.00000	0.00000	0.00000	0.00000	0.00000	0.00000	0.00000	0.00000	0.00001	0.00028
Toscas (Las)	40.43	-1.08	0.00000	0.00000	0.00000	0.00000	0.00000	0.00000	0.00722	0.00132	0.00887	0.00004	0.00000	0.00003	0.00136	0.00323	0.00062
Tourão da Ramila	40.94	-7.16	0.00000	0.00000	0.00000	0.00042	0.00548	0.00180	0.00000	0.00000	0.00000	0.00000	0.00000	0.00000	0.00000	0.00000	0.00000
Tragalamocha	36.77	-3.87	0.00000	0.00000	0.00000	0.00000	0.00000	0.00000	0.00000	0.00000	0.00000	0.00000	0.00000	0.00134	0.00695	0.00000	0.00000
Trastejón	37.93	-6.39	0.00000	0.00000	0.00000	0.00000	0.00000	0.00000	0.00000	0.00005	0.00234	0.00431	0.01176	0.03702	0.01892	0.00162	0.01113
Trecha (La)	43.40	-3.32	0.00036	0.00017	0.00003	0.00000	0.00000	0.00000	0.00000	0.00000	0.00000	0.00000	0.00000	0.00000	0.00000	0.00000	0.00000
Trocs. Cova de les	42.45	0.55	0.00028	0.00690	0.00000	0.00444	0.01247	0.00655	0.00000	0.00000	0.00000	0.00000	0.00000	0.00000	0.00000	0.00000	0.00000
Troña	42.21	-8.49	0.00000	0.00000	0.00000	0.00000	0.00000	0.00000	0.00000	0.00000	0.00000	0.00017	0.00171	0.00341	0.00170	0.00620	0.00432
Truchiro (El)	43.43	-3.65	0.00000	0.00000	0.00000	0.00000	0.00000	0.00050	0.00144	0.00000	0.00000	0.00000	0.00000	0.00000	0.00000	0.00000	0.00000
Tumba. Monte da	38.28	-8.23	0.00000	0.00005	0.00152	0.00829	0.01144	0.02690	0.01118	0.00122	0.00006	0.00000	0.00000	0.00000	0.00000	0.00000	0.00000
Ulaña (La)	42.66	-4.07	0.00000	0.00000	0.00000	0.00000	0.00000	0.00000	0.00000	0.00000	0.00000	0.00000	0.00000	0.00000	0.00000	0.00000	0.00000
Umbría del Cerro del Castillo	38.79	-6.26	0.00000	0.00000	0.00000	0.00000	0.00000	0.00000	0.00000	0.00000	0.00001	0.00109	0.00698	0.00490	0.00043	0.00419	0.00148
Uña. Cueva de la	43.06	-5.14	0.00000	0.00000	0.00000	0.00000	0.00000	0.00000	0.00000	0.00000	0.00000	0.00000	0.00000	0.00000	0.00000	0.00000	0.00000
Urratxa III	43.05	-2.79	0.00000	0.00000	0.00000	0.00000	0.00000	0.00000	0.00000	0.00000	0.00000	0.00002	0.00153	0.01149	0.00484	0.00000	0.00000
Urtiaga	43.28	-2.32	0.00000	0.00000	0.00000	0.00039	0.00090	0.00242	0.00158	0.00040	0.00003	0.00041	0.00400	0.00991	0.00373	0.00003	0.00000
Valada do Mato	38.61	-7.99	0.00000	0.00000	0.00000	0.00000	0.00000	0.00000	0.00000	0.00000	0.00000	0.00000	0.00000	0.00000	0.00000	0.00000	0.00000
Valcervera	41.33	-0.96	0.00000	0.00000	0.00092	0.00134	0.00004	0.00000	0.00000	0.00000	0.00000	0.00000	0.00000	0.00000	0.00000	0.00000	0.00000
Valdavara	42.85	-7.14	0.00000	0.00000	0.00000	0.00287	0.00831	0.00020	0.00000	0.00000	0.00000	0.00000	0.00000	0.00000	0.01196	0.00000	0.00000
Vale Boi	37.09	-8.80	0.00000	0.00000	0.00000	0.00000	0.00000	0.00000	0.00000	0.00000	0.00000	0.00000	0.00000	0.00000	0.00000	0.00000	0.00000
Vale da Fonte da Moça 1	39.15	-8.66	0.00000	0.00000	0.00000	0.00000	0.00000	0.00000	0.00000	0.00000	0.00000	0.00000	0.00000	0.00000	0.00000	0.00000	0.00000
Vale de Lobos	38.84	-9.29	0.00000	0.00000	0.00000	0.00287	0.00831	0.00151	0.00002	0.00000	0.00000	0.00000	0.00000	0.00000	0.00000	0.00000	0.00000

Site	Lat	Lon	SPD of Iberian settlement sites at 200 year time slices (cal. BP)														
			6000-5800	5800-5600	5600-5400	5400-5200	5200-5000	5000-4800	4800-4600	4600-4400	4400-4200	4200-4000	4000-3800	3800-3600	3600-3400	3400-3200	3200-3000
Vale de Rodrigo 2	38.50	-8.06	0.00275	0.00343	0.00020	0.00000	0.00000	0.00000	0.00004	0.00146	0.00494	0.00052	0.00000	0.00000	0.00000	0.00000	0.00000
Vale de Rodrigo 3	38.50	-8.07	0.00005	0.00213	0.00000	0.00000	0.00000	0.00000	0.00000	0.00000	0.00000	0.00000	0.00000	0.00000	0.00000	0.00000	0.00000
Vale Pincel 1	37.95	-8.85	0.00000	0.00000	0.00000	0.00000	0.00000	0.00000	0.00000	0.00000	0.00000	0.00000	0.00000	0.00000	0.00000	0.00000	0.00000
Vale Santo 1	37.04	-8.96	0.00000	0.00000	0.00000	0.00000	0.00000	0.00000	0.00000	0.00000	0.00000	0.00000	0.00000	0.00000	0.00000	0.00000	0.00000
Valencina de la Concepción	37.42	-6.07	0.00000	0.00005	0.00326	0.02834	0.08413	0.12144	0.07538	0.09797	0.11664	0.01868	0.01245	0.00301	0.00700	0.00058	0.00004
Valmayor 11. Cingle del	41.32	0.14	0.00000	0.00000	0.00000	0.00000	0.00000	0.00000	0.00000	0.00000	0.00000	0.00000	0.00000	0.00000	0.00000	0.00000	0.00000
Vaquera. Cueva de la	41.09	-4.06	0.00071	0.00451	0.00928	0.00867	0.00654	0.00291	0.00061	0.00000	0.00000	0.00000	0.00000	0.00025	0.00539	0.00530	0.00155
Vasconcelos	41.58	-8.37	0.00000	0.00000	0.00000	0.00000	0.00000	0.00000	0.00000	0.00000	0.00000	0.00000	0.00000	0.00000	0.00000	0.00000	0.00000
Velilla (La)	42.42	-4.39	0.00720	0.00396	0.01468	0.02336	0.02202	0.04393	0.00000	0.00000	0.00000	0.00000	0.00000	0.00000	0.00000	0.00000	0.00000
Ventana. Cueva de la	40.85	-3.52	0.00000	0.00000	0.00000	0.00000	0.00000	0.00044	0.00080	0.00000	0.00000	0.00000	0.00000	0.00000	0.00000	0.00000	0.00000
Verdelpino	40.14	-2.10	0.00506	0.00277	0.00218	0.00316	0.00318	0.00331	0.00106	0.00021	0.00000	0.00000	0.00000	0.00000	0.00000	0.00007	0.00118
Vermoim	41.43	-8.46	0.00000	0.00000	0.00000	0.00000	0.00000	0.00000	0.00000	0.00000	0.00000	0.00000	0.00000	0.00000	0.00000	0.00000	0.00005
Víboras. Cerro de las	38.24	-2.07	0.00000	0.00000	0.00000	0.00002	0.00011	0.00105	0.00456	0.00680	0.01091	0.00787	0.00276	0.00245	0.00327	0.00010	0.00000
Vidigal	37.82	-8.77	0.00058	0.00040	0.00015	0.00005	0.00004	0.00002	0.00000	0.00000	0.00000	0.00000	0.00000	0.00000	0.00000	0.00000	0.00000
Vidre. Cova del	40.77	0.31	0.00000	0.00000	0.00000	0.00000	0.00000	0.00000	0.00000	0.00000	0.00000	0.00000	0.00000	0.00000	0.00000	0.00000	0.00000
Vila Cova-à-Coelheira	40.86	-7.80	0.00000	0.00000	0.00000	0.00000	0.00000	0.00000	0.00000	0.00000	0.00000	0.00000	0.00000	0.00000	0.00000	0.00000	0.00016
Vila Velha de Alvor	37.13	-8.59	0.00000	0.00000	0.00000	0.00000	0.00000	0.00000	0.00000	0.00000	0.00000	0.00000	0.00000	0.00000	0.00000	0.00000	0.00000
Vila. Tossal de la	40.28	-0.35	0.00000	0.00000	0.00000	0.00000	0.00000	0.00000	0.00000	0.00000	0.00000	0.00000	0.00000	0.00000	0.00000	0.00000	0.00000
Viladonga	43.16	-7.39	0.00000	0.00000	0.00000	0.00000	0.00000	0.00000	0.00000	0.00000	0.00000	0.00000	0.00000	0.00000	0.00000	0.00000	0.00000
Vilars (Els)	41.56	0.96	0.00000	0.00000	0.00000	0.00000	0.00000	0.00000	0.00000	0.00000	0.00000	0.00000	0.00000	0.00000	0.00000	0.00000	0.00000
Vilches IV	38.52	-1.58	0.00000	0.00000	0.00003	0.00095	0.00181	0.00316	0.01068	0.00313	0.00357	0.00000	0.00000	0.00000	0.00000	0.00000	0.00000
Vilela	42.68	-7.77	0.00000	0.00000	0.00000	0.00000	0.00000	0.00000	0.00000	0.00000	0.00000	0.00000	0.00000	0.00000	0.00000	0.00000	0.00000
Villarrabines	42.18	-5.57	0.00000	0.00000	0.00000	0.00000	0.00000	0.00000	0.00000	0.00000	0.00000	0.00000	0.00014	0.00140	0.00314	0.00059	0.00004
Villasviejas del Tamuja	39.37	-6.09	0.00000	0.00000	0.00000	0.00000	0.00000	0.00000	0.00000	0.00000	0.00000	0.00000	0.00000	0.00000	0.00000	0.00000	0.00000
Villavieja	37.26	-4.23	0.00000	0.00000	0.00000	0.00000	0.00000	0.00000	0.00004	0.00489	0.00000	0.00000	0.00000	0.00000	0.00000	0.00000	0.00000
Vilot de Montagut	41.63	0.49	0.00000	0.00000	0.00000	0.00000	0.00000	0.00000	0.00000	0.00000	0.00000	0.00000	0.00000	0.00005	0.00453	0.00641	0.00127
Viña de Esteban García	40.59	-5.58	0.00000	0.00000	0.00000	0.00000	0.00000	0.00009	0.00428	0.00284	0.00281	0.00354	0.00074	0.00002	0.00000	0.00000	0.00000
Viñas. Cerro de las	37.93	-1.82	0.00000	0.00000	0.00000	0.00000	0.00000	0.00000	0.00000	0.00000	0.00000	0.00015	0.00607	0.00000	0.00000	0.00000	0.00000
Vincamet	41.51	0.36	0.00000	0.00000	0.00000	0.00000	0.00000	0.00000	0.00000	0.00000	0.00000	0.00000	0.00000	0.00000	0.00000	0.00007	0.01461
Vinha da Soutilha	41.82	-7.36	0.00007	0.00061	0.00492	0.00515	0.00454	0.00356	0.00075	0.00014	0.00000	0.00000	0.00000	0.00000	0.00000	0.00000	0.00000
Virgen del Espino	38.97	-3.36	0.00000	0.00000	0.00000	0.00000	0.00000	0.00000	0.00000	0.00000	0.00000	0.00009	0.00102	0.00306	0.00180	0.00006	0.00000
Virgen. Cerro de la	37.73	-2.51	0.00000	0.00000	0.00000	0.00000	0.00000	0.00000	0.00096	0.00888	0.06082	0.04758	0.04121	0.10256	0.02598	0.00005	0.00000
Virtud. Cerro	37.27	-1.79	0.00087	0.00009	0.00000	0.00000	0.00000	0.00000	0.00000	0.00000	0.00000	0.00000	0.00000	0.00000	0.00000	0.00000	0.00000

Site	Lat	Lon	SPD of Iberian settlement sites at 200 year time slices (cal. BP)														
			6000-5800	5800-5600	5600-5400	5400-5200	5200-5000	5000-4800	4800-4600	4600-4400	4400-4200	4200-4000	4000-3800	3800-3600	3600-3400	3400-3200	3200-3000
Viveiro 2 (O)	42.28	-8.65	0.00000	0.00000	0.00000	0.00000	0.00000	0.00000	0.00000	0.00000	0.00000	0.00170	0.00191	0.00000	0.00000	0.00000	0.00000
Vixil	43.27	-7.69	0.00000	0.00000	0.00000	0.00000	0.00000	0.00000	0.00000	0.00000	0.00000	0.00000	0.00000	0.00000	0.00000	0.00000	0.00000
Xammar. Carrer d´en	41.54	2.44	0.00000	0.00000	0.00000	0.00000	0.00000	0.00000	0.00000	0.00000	0.00000	0.00000	0.00000	0.00000	0.00000	0.00000	0.00000
Yacimiento 129	37.04	-4.71	0.00000	0.00000	0.00000	0.00000	0.00000	0.00000	0.00000	0.00000	0.00000	0.00000	0.00000	0.00000	0.00000	0.00000	0.00003
Zaforas	41.20	-0.15	0.00000	0.00000	0.00000	0.00000	0.00000	0.00000	0.00000	0.00000	0.00000	0.00000	0.00000	0.00000	0.00000	0.00000	0.00817
Zájara	37.28	-1.85	0.00000	0.00000	0.00000	0.00000	0.00000	0.00000	0.00032	0.00169	0.00704	0.00887	0.00341	0.00025	0.00000	0.00000	0.00000
Zambujal	39.08	-9.29	0.00000	0.00000	0.00000	0.00006	0.00413	0.00248	0.06117	0.10376	0.06302	0.00822	0.00929	0.01791	0.00003	0.00000	0.00045
Zapata	37.54	-1.49	0.00000	0.00000	0.00000	0.00000	0.00000	0.00000	0.00000	0.00000	0.00000	0.00000	0.00021	0.00528	0.00008	0.00000	0.00000
Zapatería 9. Calle	37.68	-1.70	0.00000	0.00000	0.00000	0.00000	0.00000	0.00000	0.00000	0.00000	0.00009	0.00515	0.00196	0.00000	0.00000	0.00000	0.00000
Zarra de Xoacín	42.63	-8.13	0.00000	0.00000	0.00000	0.00000	0.00000	0.00000	0.00039	0.00079	0.00526	0.00000	0.00000	0.00000	0.00000	0.00000	0.00000
Zarranzano. Castro del	41.90	-2.47	0.00000	0.00000	0.00000	0.00000	0.00000	0.00000	0.00000	0.00000	0.00000	0.00000	0.00000	0.00000	0.00000	0.00000	0.00000
Zatoya	42.91	-1.17	0.00000	0.00000	0.00000	0.00000	0.00000	0.00000	0.00000	0.00000	0.00000	0.00000	0.00000	0.00000	0.00000	0.00000	0.00000
Zimbreira. Castelo Velho de	39.57	-7.83	0.00000	0.00000	0.00000	0.00000	0.00000	0.00000	0.00000	0.00000	0.00000	0.00000	0.00000	0.00000	0.00000	0.00000	0.00000
Zoñán	43.43	-7.40	0.00000	0.00000	0.00000	0.00000	0.00000	0.00000	0.00000	0.00000	0.00000	0.00000	0.00000	0.00000	0.00000	0.00000	0.00000
Zorra. Peñón de la	38.68	-0.86	0.00000	0.00000	0.00000	0.00000	0.00000	0.00000	0.00000	0.00010	0.01846	0.00578	0.03302	0.01841	0.00023	0.00000	0.00000